OCS Study
MMS 98-0036

Texas-Louisiana Shelf Circulation and Transport Processes Study: Synthesis Report

Volume II: Appendices

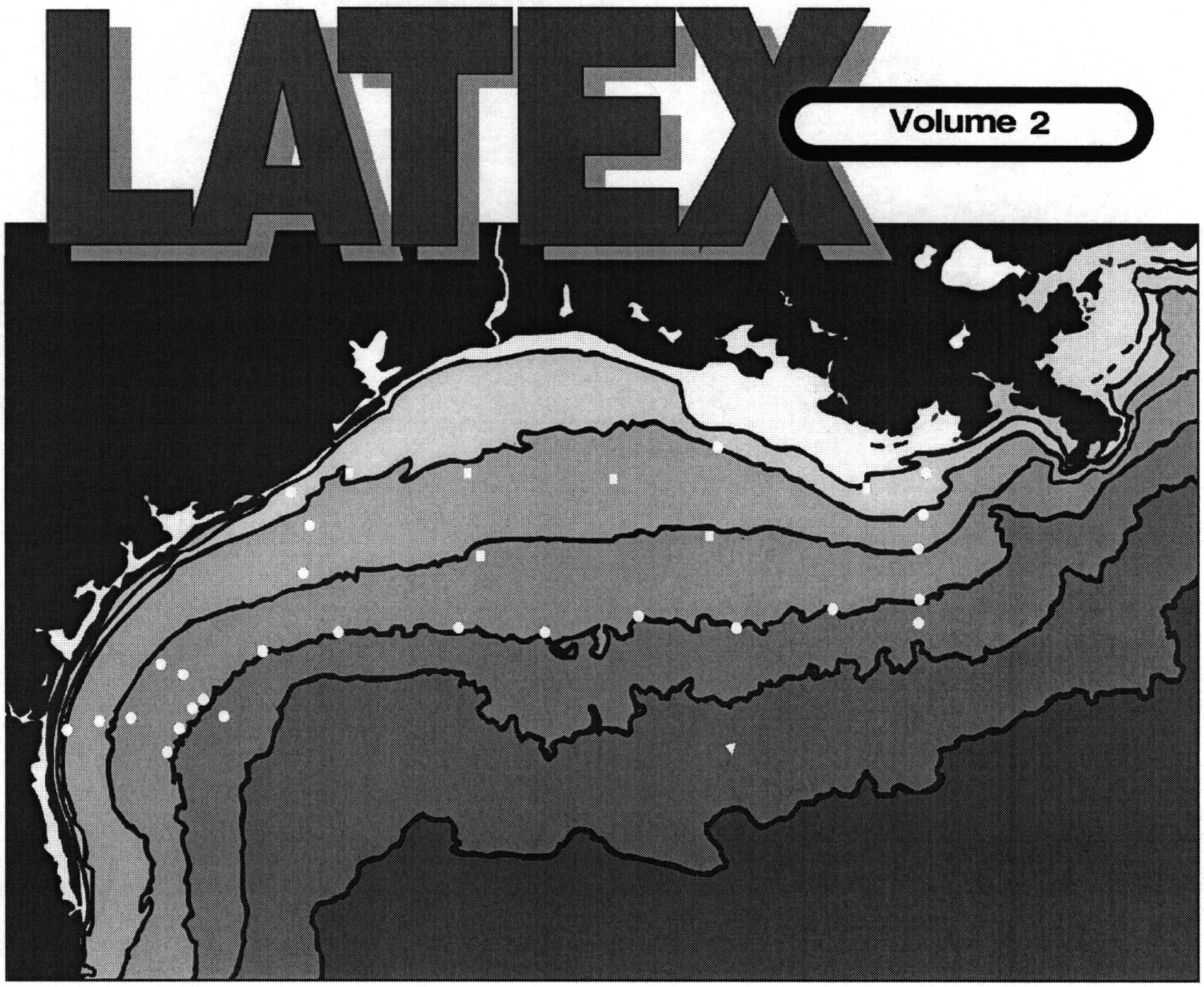

U.S. Department of the Interior
Minerals Management Service
Gulf of Mexico OCS Region

OCS Study
MMS 98-0036

Texas-Louisiana Shelf Circulation and Transport Processes Study: Synthesis Report

Volume II: Appendices

Authors

W.D. Nowlin, Jr.
A.E. Jochens
R.O. Reid
S.F. DiMarco

Prepared under MMS Contract
14-35-0001-30509
by
Texas A&M University
College Station, Texas 77843-3146

Published by

U.S. Department of the Interior
Minerals Management Service
Gulf of Mexico OCS Region

New Orleans
September 1998

DISCLAIMER

REPORT AVAILABILITY

Extra copies of the report may be obtained from the Public Information Office (Mail Stop 5034) at the following address:

U.S. Department of the Interior
Minerals Management Service
Gulf of Mexico OCS Region
Public Information Office (MS 5034)
1201 Elmwood Park Boulevard
New Orleans, Louisiana 70123-2394

Telephone Number: 1-800-200-GULF or
504-736-2519

CITATION

Suggested citation:

Nowlin, W.D. Jr., A.E. Jochens, R.O. Reid, and S.F. DiMarco. 1998. Texas-Louisiana Shelf Circulation and Transport Processes Study: Synthesis Report, Volume II: Appendices. OCS Study MMS 98-0036. U.S. Dept. of the Interior, Minerals Mgmt Service, Gulf of Mexico OCS Region, New Orleans, LA. 288 pp.

ABOUT THE COVER

The cover art, by Karen Glenn, shows the LATEX study area, with LATEX A's mooring locations superimposed over the bathymetry.

TABLE OF CONTENTS

VOLUME II

APPENDIX A: WINTER CYCLOGENSIS

A.1 Event analysis

Cyclogenesis is defined as a development or strengthening of cyclonic circulation in the atmosphere (Hsu 1988). Many winter storms originate and strengthen in Gulf of Mexico waters, creating havoc along the Gulf coast (Hsu 1993). In certain coastal regions such as the Texas-Louisiana shelf, cyclogenesis is an important phenomenon to shipping and drilling interests as well as coastal residents and businesses.

Gulf storms are sometimes described as "a swollen belly of water surrounded by pouring rain"—the ocean surface bulges upward beneath a whirling, forward moving, low pressure system. High waves, stirred by high winds form atop this bulge. The worst storms are meteorological bombs, i.e., they form quickly and exhibit pressure drops of 12 mb or more in 24 hr in these latitudes. They are accompanied by waves of up to 5 m or more, floods, and strong winds. It is helpful to classify this cyclogenesis on the basis of minimum pressures and related maximum wind speeds. Pressure variations are significant, especially in the tropics where they are normally minor compared to those in higher latitudes. Over the Texas-Louisiana shelf pressure observations are plentiful thanks to NDBC buoys and C-MAN (Coastal-Marine Automated Network) stations, and reports from ships and other platforms in the Voluntary Observing Ship program.

In a 40-year climatology of western Gulf cyclones prepared by Saucier (1949), an average of 9.7 cyclones per year developed across the region, with an average of 11 years between peaks. The majority of these storms developed between 25° and 30°N, from 90° to 99°W. Using 1972-1982 as a control period, an average of 10.4 winter cyclones developed each year over the Gulf of Mexico, and in half of them central pressures dipped to 1010 mb or below (Johnson et al. 1984). From November 1982 through March 1983, a total of 26 surface cyclones affected the Gulf region. Five of those met the criteria for meteorological bombs (Murty et al. 1983). During these intensification periods the mean subtropical jet stream was about 5° farther south than normal over the Gulf of Mexico (Quirox 1983). This southward displacement of the mean jet stream, particularly during El Niño years, is an important factor in the formation of upper level disturbances. When upper level lows move over the surface weather front along the shelf break, the cyclogenesis and deepening process is enhanced; i.e., there is a good chance for the rapid development or intensification of a coastal storm (Hsu 1988).

Examples of cyclogenesis

A classic example of cyclogenesis over the Gulf of Mexico and its effect on shelf waters occurred on 16 February 1983 (Figure A.1-1). This storm was one of the top five cyclones

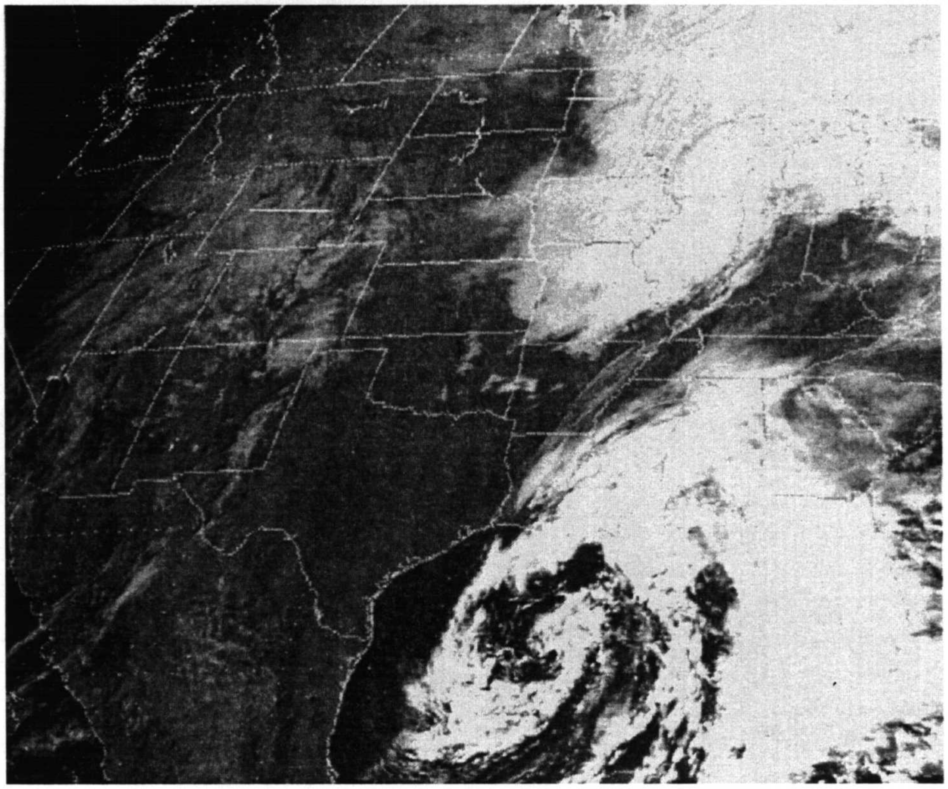

Figure A.1-1. A GOES satellite image showing an example of cyclogenesis which took place over the Gulf of Mexico on 16 February 1983. Note the comma shaped whirlpool cloud pattern and also that this system is not linked to other larger scale systems.

that developed over the Gulf during the 1982-1983 El Niño year (Johnson et al. 1984). This storm qualified as a meteorological bomb when its central pressure fell 12 mb within a 24-hr period. Its minimum pressure was 996 mb with a reported maximum wind of 20 $m \cdot s^{-1}$ (Figure A.1-2). At a platform on the shelf off Louisiana, the lowest pressure recorded was 1001 mb, with a maximum wind of 15 $m \cdot s^{-1}$ and a significant wave height of 4.3 m. The time series of the pressure, winds, and waves for this storm are similar to those of a hurricane. The maximum wind speed does not usually occur at the time of lowest pressure, but, in general, the lower the pressure, the stronger the wind will be. These particular time series (Figure A.1-2) very much resemble typical tropical cyclone plots, for which the wind speed would be expected to drop off dramatically in the eye or center of lowest pressure.

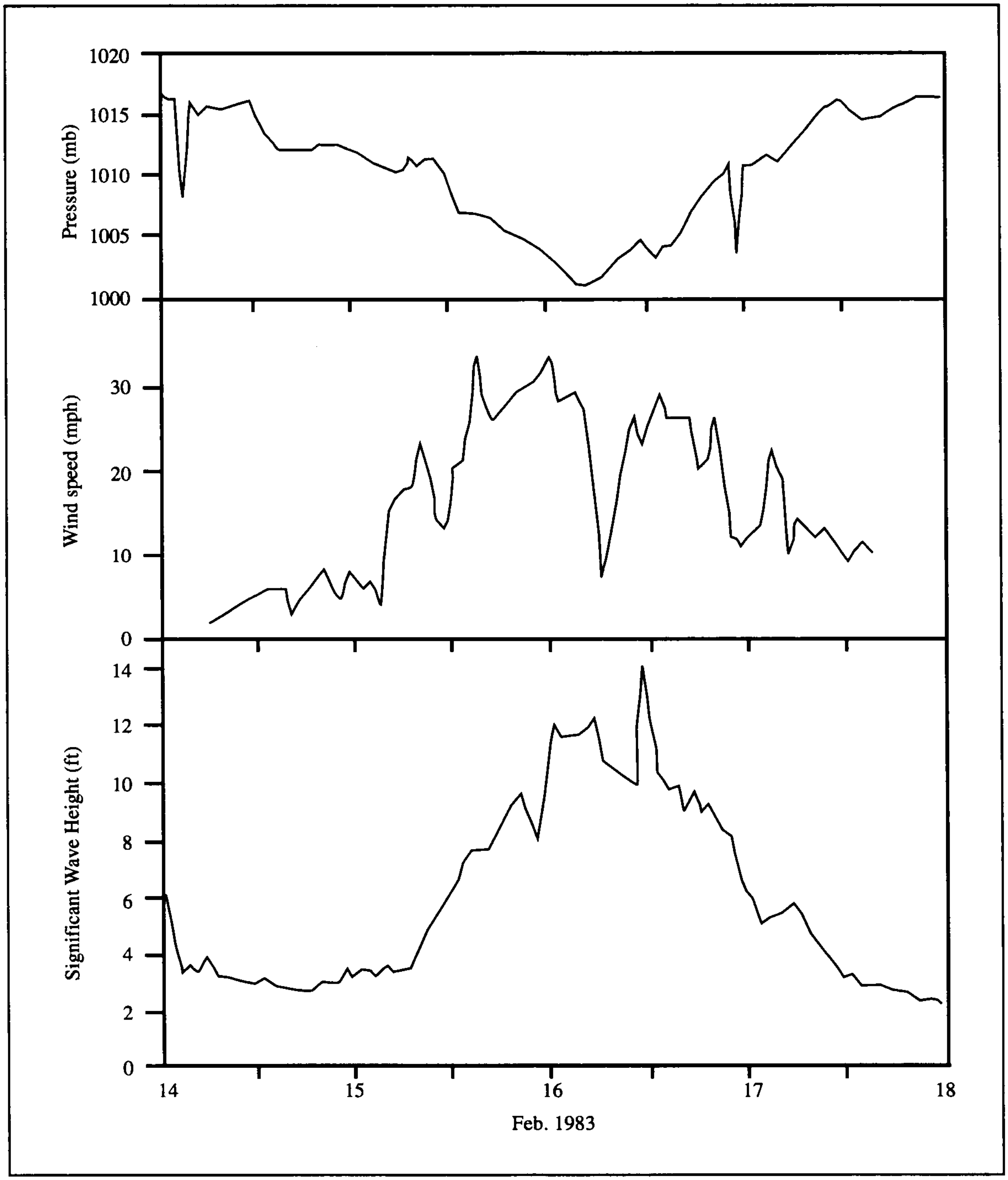

Figure A.1-2. Time series of atmospheric pressure, wind speed, and significant wave height for the 16 February 1983 storm (Figure A.1-1) from 28.4°N, 92.0°W. Note the relationship between pressure and winds.

A second example of a meteorological bomb in the Gulf of Mexico occurred on 27 February 1983. This storm generated seas and tides that caused extensive erosion and property damage on Grand Isle, Louisiana. February 1983 also provided a fine example of a nor'easter that had its origins in the Gulf. A storm that developed near the mouth of the Mississippi River on 10 February moved to off Wilmington, North Carolina, the following day, where the ship *John Cabot* reported 32 $m \cdot s^{-1}$ winds in 6-m seas. This nor'easter was generating hurricane-force winds by 13 February, and it devastated the eastern seaboard with a snowfall of up to 89 cm. New York City measured 51 cm, Baltimore had 61 cm, and 66 cm buried Washington, D.C. At least 69 deaths were attributed to this storm (Hsu 1993).

A third recent example is shown in Figures A.1-3 and A.1-4. During the period 12-13 March 1993, a combination of upper-level dynamics and an existing baroclinic zone in the western Gulf of Mexico produced an intense extratropical cyclone. This system was comparable in strength to a category 1 hurricane, and was dubbed by many as the "Storm of the Century" (also see Appendix B). Along the storm's path, winds reached 40 $m \cdot s^{-1}$, generating seas more than 7 m high and producing storm surges of more than 3 m along parts of the northeastern Gulf coast (Figure A.1-3; see Schumann et al. 1995). For brevity, we concentrate our description of this cyclogenesis near the sea surface, inasmuch as the upper air dynamics are discussed in detail in Schumann et al. (1995). Figure A.1-5a shows the stationary front over the northern Gulf of Mexico, which had persisted for several days. Surface cyclogenesis became evident at 1200 UTC when a closed, 1002-mb low moved into the Gulf from the Texas coast (Figure A.1-5b). Southeast winds near the low were approaching 23 $m \cdot s^{-1}$, with seas of 2-3 m in the northwestern Gulf. The strength of the surface cold outbreak advancing southward was well indicated with cold, 1000-mb temperatures moving south across the mid-west and a 1044-mb high center moving southward over Wyoming. Figure A.1-5c shows a pressure fall of 10 mb in 12 hours (compared to Figure A.1-5b) associated with the surface low (992 mb at 0000 UTC on 13 March). On the northwest side of the low, offshore oil rigs approximately 30 m above the water surface reported sustained winds near 40 $m \cdot s^{-1}$ (see also Figure A.1-4). Sea heights increased to 4.5-6 m over a large area of the northwestern Gulf. Minimum pressure at Moisant International Airport (MSY) in New Orleans reached 1003.6 mb, with winds around the metropolitan area gusting to 32 $m \cdot s^{-1}$ for several hours. Twelve hours later, at 1200 UTC on 13 March, the surface low was over southeast Georgia with a pressure of 976 mb, and the cold front was crossing Florida (Figure A.1-5d). During the previous 24 hours, the storm's central pressure at the surface fell 26 mb. When the bitter cold surge entered the less frictional northern Gulf, the wind force showed incredible strength again—the buoy data indicated northerly winds of 29-40 $m \cdot s^{-1}$ from 90°W eastward to Florida. Seas reached 9 m at NDBC buoy 42001 (25.9°N, 89.7°W), and there were numerous buoy and C-MAN reports of 6-7.5 m seas over the north-central and eastern Gulf.

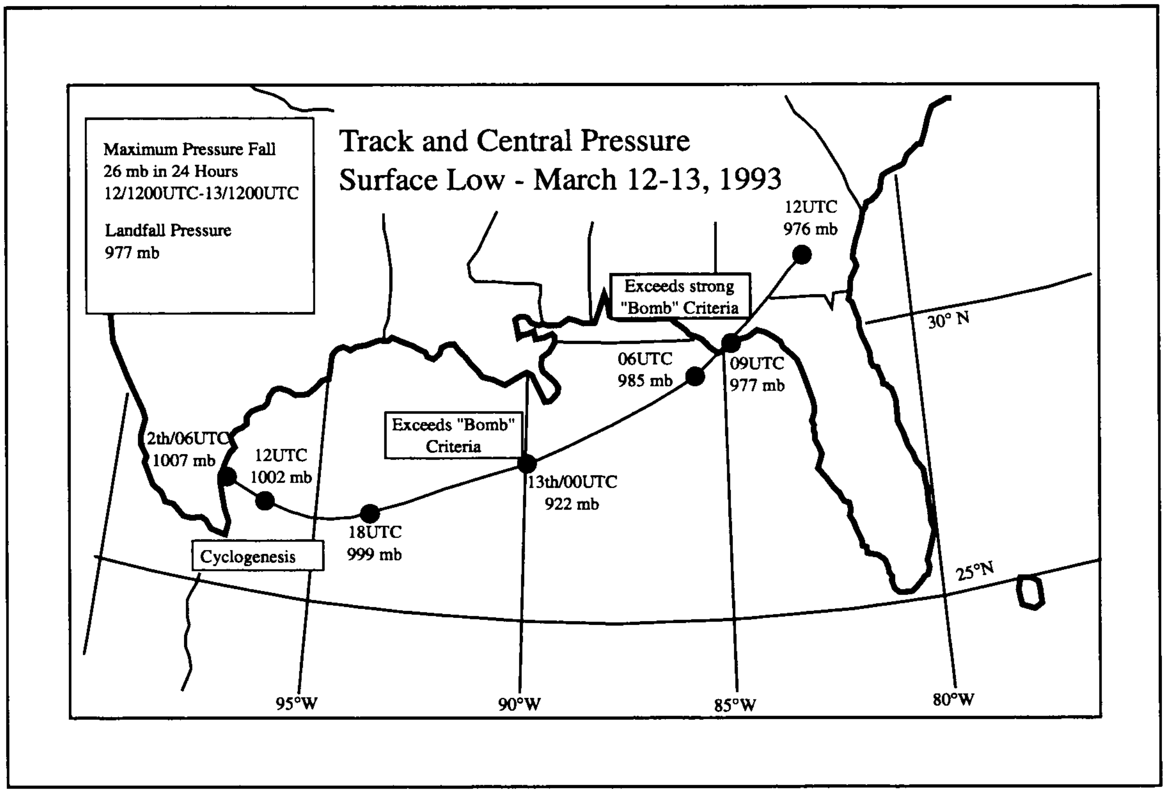

Figure A.1-3. Surface low center track across the Gulf of Mexico (from Schumann et al. 1995).

A classification of winter cyclogenesis over the Gulf of Mexico

Winter storms in the Gulf of Mexico are important both to maritime interests in that basin and along the east coast. A classification scheme is needed to compare the intensity of these systems, and using the relationship of maximum winds to minimum pressures is a theoretically sound and simple way of achieving this. The classification scheme shown in Figure A.1-6 is based on Hsu (1993).

Because airflow around the centers of these winter storms in the Gulf is nearly circular (e.g., Figure A.1-1) to a first approximation, the cyclostrophic equation (see, e.g., Hsu 1988) may be applicable, such that the centrifugal force and the pressure gradient are in balance, as

$$\frac{V_{\max}^2}{R} = \frac{1}{\rho}\frac{\partial P}{\partial R} = \frac{1}{\rho}\frac{(P_{ambient} - P_0)}{(R - 0)}, \qquad \text{A.1.1}$$

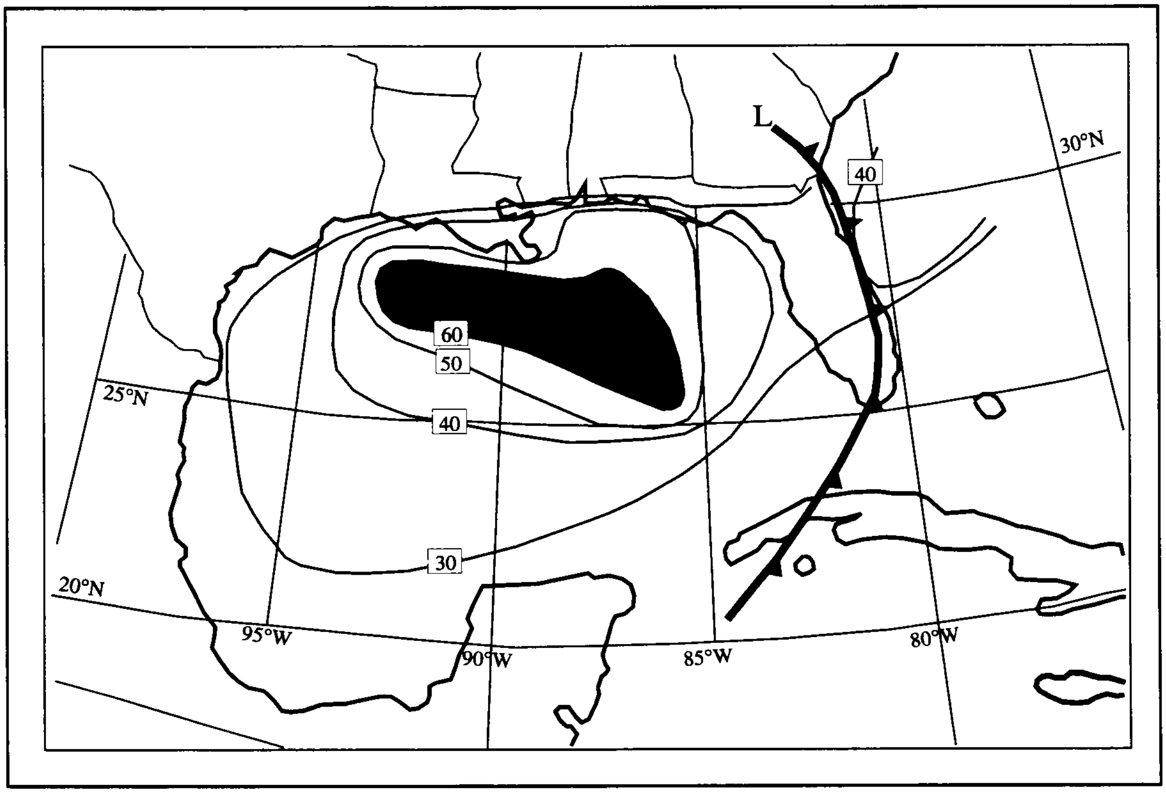

Figure A.1-4. Surface wind analysis (isotachs in kt; from low to high, these are 15.4, 20.6, 25.7, and 30.9 m·s^{-1}) for 1200 UTC 13 March 1993 (from NWS Forecast Office, New Orleans).

or

$$V_{max}^2 = \frac{1}{\rho}(P_{ambient} - P_0), \qquad \text{A.1.2}$$

where V_{max} is the maximum wind speed; R is the radius to V_{max}; ρ is the air density; $P_{ambient}$ is the ambient pressure, which equals 1016 mb for the annual climatological average over the northwestern Gulf of Mexico; P_0 is the minimum pressure of the storm; and (R - 0) is an effective scale. For statistical analysis, equation (A.1.2) may be written

$$V_{max} = A + B\,(1016 - P_0)^{.5}, \qquad \text{A.1.3}$$

when A and B are determined in the data.

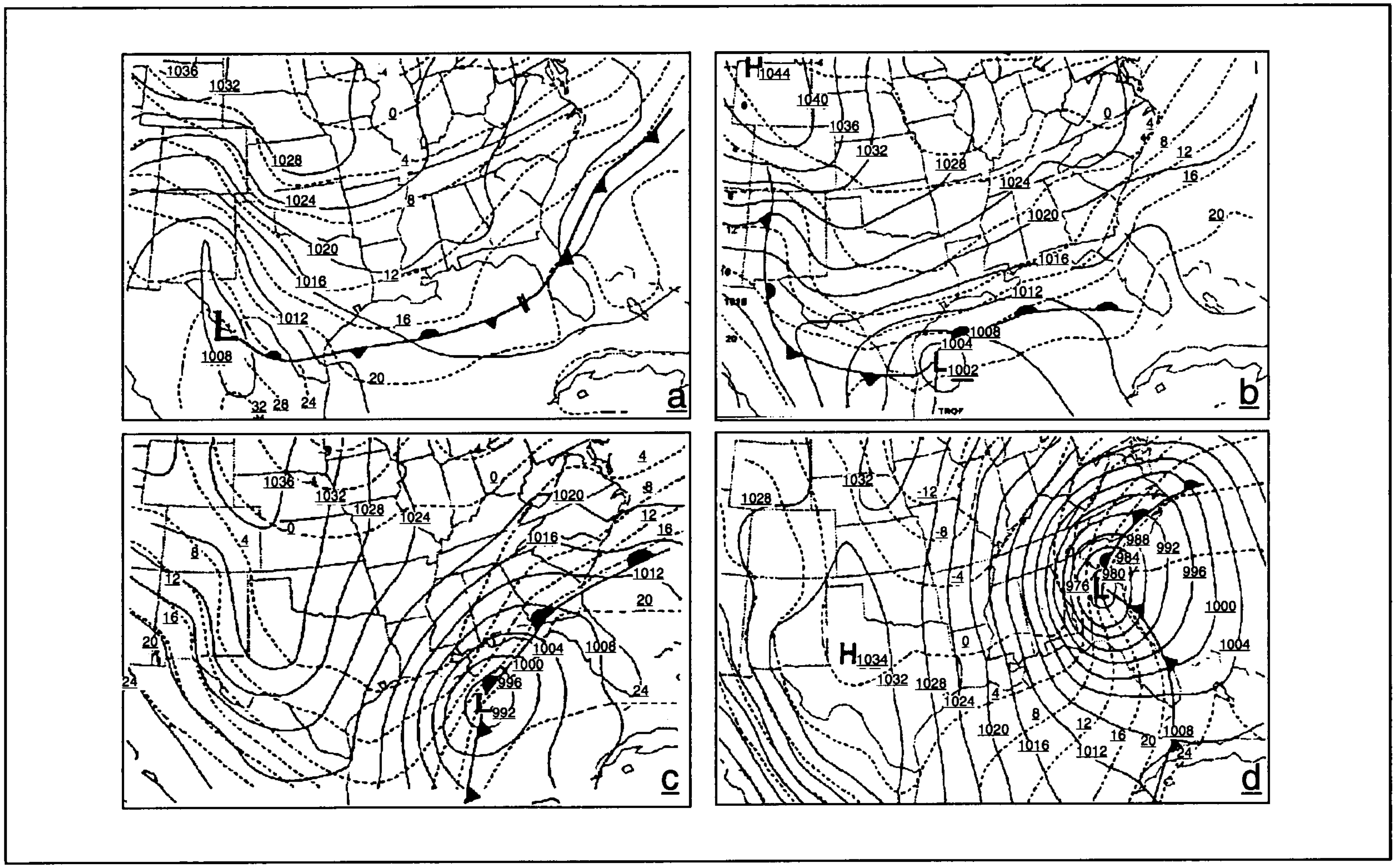

Figure A.1-5. (a) Surface fronts (heavy solid), isobars (solid; mb), and 1000-mb temperatures (dashed; °C) for 0000 UTC 12 March 1993. (b) Same as (a) for 1200 UTC 12 March 1993. (c) Same as (a) for 0000 UTC 13 March 1993. (d) Same as (a) for 1200 UTC 13 March 1993.

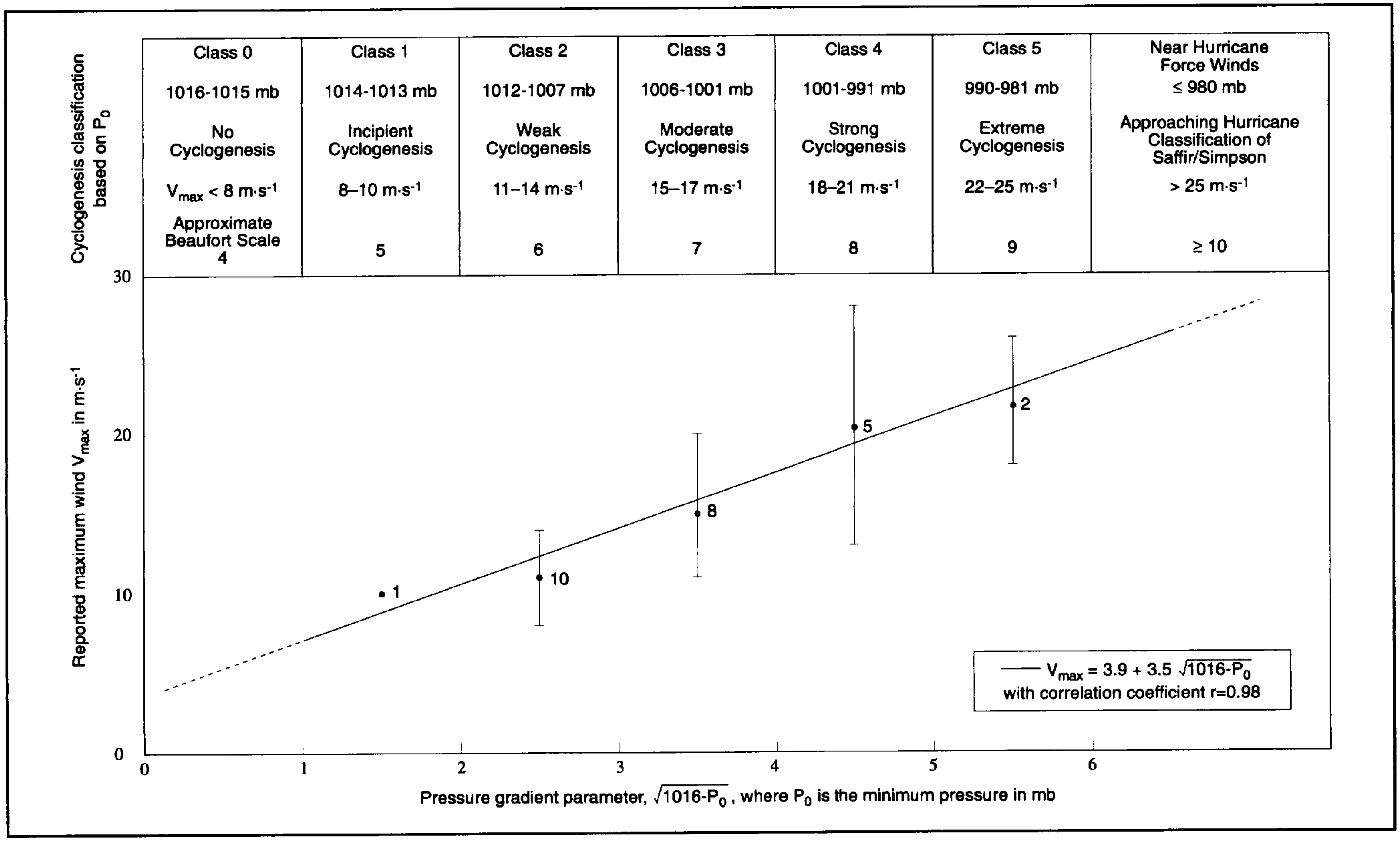

Figure A.1-6. Cyclogenesis classification (upper) is based on the minimum pressure of winter storms in the Gulf of Mexico. The graph (lower) shows the number of storms of each class studied and the relationship between the pressure gradient parameter and the reported maximum winds. Vertical bars indicate one standard deviation around means. (After Hsu 1993).

On the basis of 26 winter cyclones studied (Johnson et al. 1984), it was verified that

$$V_{max} = 3.9 + 3.5\,(1016 - P_0)^{.5}, \tag{A.1.4}$$

where V_{max} is in $m{\cdot}s^{-1}$ and P_0 is in mb. Equation (A.1.4) has a correlation coefficient 0.98 (as shown in Figure A.1-6) and is recommended for practical use such as the cyclogenesis classification. This storm ranking scheme has two constraints:

1) when $P_0 \geq 1015$ mb, no cyclogenesis is observed, and
2) when $P_0 \leq 980$ mb, the minimum (or central) pressure approaches the hurricane classification scheme of Saffir/Simpson (Simpson and Riehl 1981).

Taking the above conditions along with the interval analysis suggested by Panofsky and Brier (1968) and the winter storm classification suggested by Dolan and Davis (1992), five classes for the winter cyclogenesis are proposed. For ease of classification, we use numerical intervals of $(1016 - P_0)^{.5}$, which range from 1 to 6 with five classes in between.

Equation (A.1.4) may be applied to relate maximum wind speed in $m{\cdot}s^{-1}$ to the storm's central pressure in mb. For example, if the storm's central pressure is 991 mb, then the maximum wind speed works out to $3.9 + 3.5(25)^{.5}$ or 21.4 $m{\cdot}s^{-1}$. Using the classification table, this puts the storm in Class 4, indicating strong cyclogenesis. The suggested classification of Gulf of Mexico winter storms range from Class 0 to Class 5, or from no cyclogenesis to extreme cyclogenesis. The corresponding pressure values and approximate wind speeds are indicated in Figure A.1-6. The Dolan/Davis classification scheme is based upon storm effect (beach erosion), while this one is based upon storm pressure. Despite this difference, they are in reasonable agreement.

If the lowest pressure in the "Storm of the Century" is 972 mb, as is now estimated, then the classification equation would give maximum winds of 27 $m{\cdot}s^{-1}$, which, in Figure A.1-6, is greater than Class 5, or approaching hurricane status—an unusual occurrence in the Gulf of Mexico.

A.2 30-year climatology of cyclogenesis events

Presented here are the results of a detailed analysis of the frequency of occurrence of cyclogenesis over the Texas-Louisiana shelf region.

A 30-year record of the NOAA series Daily Weather Maps, extending from 1966 to 1996, was examined for incidences of cyclone formation over the Texas-Louisiana shelf region, specifically between 25° to 30°N and 90° to 100°W (NOAA 1996). The winter season was defined as the months of November through May; after May, hurricane season begins with the dominance of tropical systems. The winter cyclones were further classified using the scheme described in Section A.1. Therefore, any atmospheric low pressure center having a minimum central pressure ≤ 1014 mb was included. Table A.2-1 shows the total number of cyclogenesis events in our region for each month of the winter seasons studied.

Figure A.2-1 shows cyclogenesis events over the northwestern Gulf of Mexico by season and category of strength. There appears to be a relationship between the number of cyclones per winter season and the influence of the El Niño/La Niña phenomenon. There were El Niño episodes in 1972-1973, 1976-1977, 1982-1983, 1986-1987, and 1991-1995. At least the latter three of these were accompanied by higher cyclogenetic activity over the northwestern Gulf, and in 1972-1973, 1982-1983, and 1991-1993 a greater number of the cyclones formed intensified into Category 3 and 4 storms. The longest consecutive El Niño event on record was from 1991-1995 (Trenberth and Hoar 1996). This is clearly reflected in our data, with those five years each having six or more strong cyclogenesis cases. Note also that there is a marked decrease in both the frequency and strength of cyclogenesis associated with the La Niña periods of 1970-1971, 1973-1975, and 1988-1989.

Table A.2-1. Monthly totals of cyclogenesis events from 1966-1967 through 1995-1996 winter seasons.

Month	No. of Events
November	12
December	19
January	25
February	20
March	12
April	9
May	10

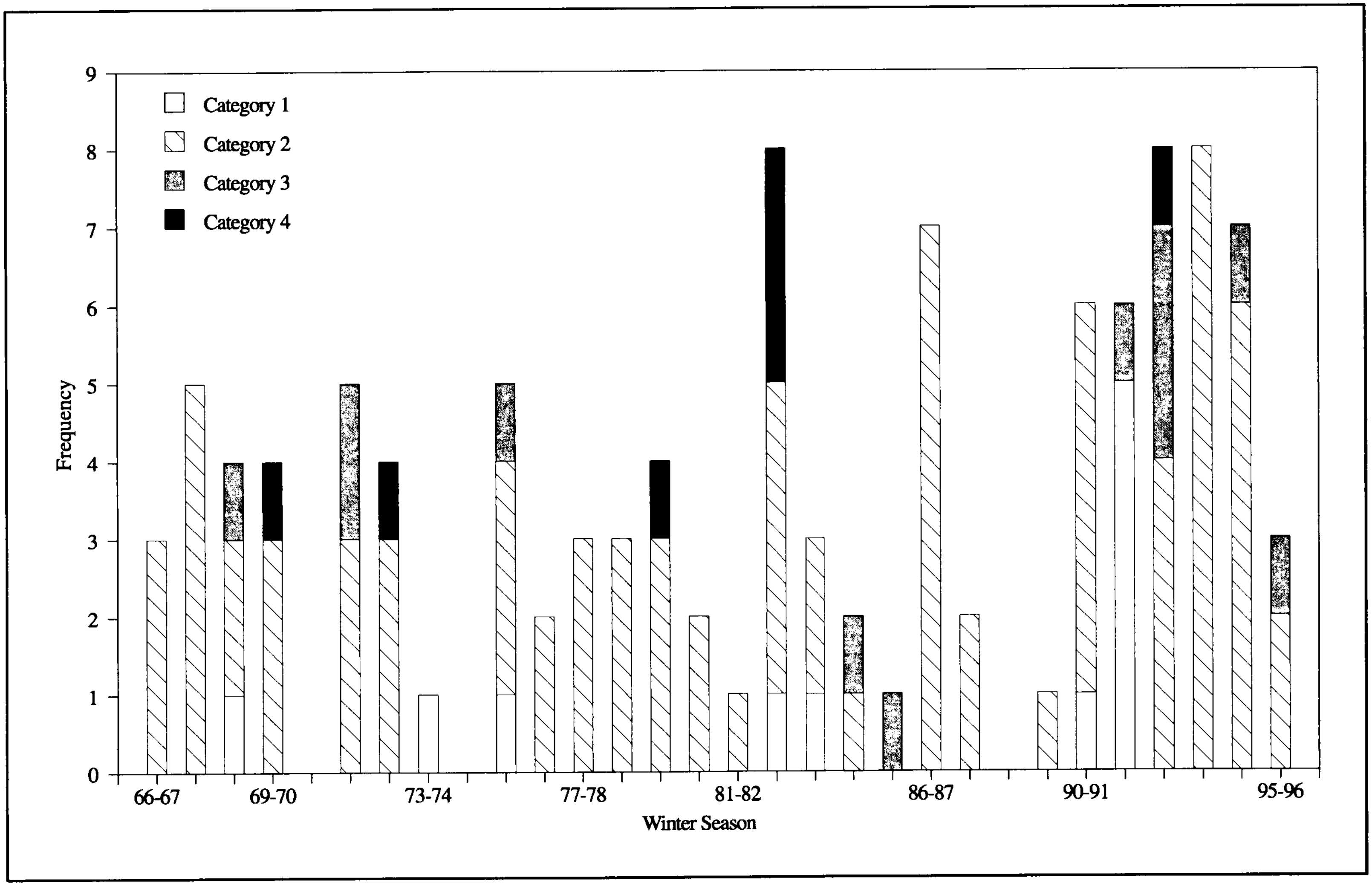

Figure A.2-1. Winter cyclogenesis freqencies and intensities in the northwest Gulf for the winter seasons 1966-1967 to 1995-1996.

APPENDIX B: EXAMPLES OF EFFECTS ON SHELF CIRCULATION BY EPISODIC ATMOSPHERIC FORCING

In this report much attention is directed to the influence on subinertial currents and meso- to large-scale property distributions by regular or long-term forcing agents: seasonal and longer term wind forcing, seasonal and interannual variations in Mississippi-Atchafalaya river discharge, and mesoscale current rings adjacent to the shelf. The mesoscale and even the large scale distributions of currents and water properties are also influenced by an array of episodic forcing functions, including frontal passages, cold air mass outbreaks, cyclogenesis over the shelf, and hurricanes.

During the LATEX observing period, many such events took place. Their study has been of second order priority to the LATEX A science team, in view of the fact that the currents and transports in response to the major regular or long-term forcing are the thrust of the LATEX program. Nevertheless, we have begun to examine the effects of such episodic forcing. In a report of this nature, it is not feasible to present an exhaustive series of investigations or even to detail selected case studies. We have chosen to present in this appendix brief descriptions of the effects of two extreme episodic events: Hurricane Andrew (August 1992) and the "Storm of the Century" (March 1993). We also describe (in Appendix B.3) the episodic nature of coastal upwelling along the Texas coast as non-summer downcoast winds shift to upcoast at the onset of summer conditions.

B.1 Hurricane Andrew (25-27 August 1992)

Hurricane Andrew, the first named tropical storm of 1992 in the Atlantic basin, attained hurricane status winds at approximately 1200 UTC 22 August 1992, 1300 km east of the Bahamas (Grymes and Stone 1995). Forty-eight hours later, Andrew crossed over the southern tip of Florida, weakened slightly, and then moved into the eastern Gulf of Mexico. As the hurricane crossed the Gulf it reintensified to Category 4 status on the Saffir/Simpson scale, with sustained wind speeds in excess of 61 $m \cdot s^{-1}$. The hurricane eye crossed over the Texas-Louisiana shelf edge at approximately 2135 UTC 25 August 1992. A LATEX wave gauge located at mooring 16 was within 30 km of Andrew's eye as the hurricane crossed the eastern edge of the Texas-Louisiana shelf. Hurricane Andrew's path traversed a broad shelf region densely populated with oil and gas structures; more than 145 satellite wells, 38 full platforms, and 450 pipeline segments were damaged or destroyed by the forces Andrew generated (MMS 1994). A number of offshore structures were tilted or toppled as Andrew cut a swath over the shelf.

This section summarizes the measurements made by the LATEX A current meter array during the storm's passage over the Texas-Louisiana shelf. Surface wind waves and the swell environment are summarized; then we present the response to Andrew of currents over the shelf. Appendix G contains a brief discussion of a WAM model-data comparison study during Hurricane Andrew.

Wave environment during Hurricane Andrew

The LATEX program had four bottom-mounted wave gauges deployed along the Texas-Louisiana shelf when Hurricane Andrew crossed the southern tip of Florida and entered the Gulf of Mexico on 24 August (DiMarco et al. 1995a). Figure B.1-1 shows the LATEX wave gauge locations, National Data Buoy Center (NDBC) buoy locations, and the storm track. The wave gauges deployed during the hurricane's passage were three Coastal Leasing, Inc. MiniSpec directional wave gauges, located at moorings 16, 20, and 23, and one SeaData 635-8 non-directional wave gauge at mooring 1. All four gauges were mounted approximately one meter off the bottom and recorded hydrostatic pressure. The MiniSpecs also recorded current velocity and temperature.

Stone et al. (1993) and Grymes and Stone (1995) present a chronological overview of the meteorology, sea state, and storm surge associated with Hurricane Andrew. Breaker et al. (1994) describe its impact on the near-surface marine environment.

The eye of Andrew passed approximately 30 km southwest of mooring 16, which was about 20 km south of Terrebonne Bay, Louisiana. Although a considerable distance from the storm center, the more western moorings 20, 23, and 1 recorded longer period waves. As Andrew traveled westward across the west Florida shelf and into the deeper eastern Gulf of Mexico, the hurricane quickly generated fast-moving long period waves that propagated westward and reached the Texas-Louisiana shelf. Long period waves, i.e., of period 10 seconds and greater, are rare in the Gulf of Mexico for all but the most extreme weather events (NDBC 1990). Such long period waves are of particular interest; because of the larger orbital velocity that is added to the mean flow, these waves can resuspend sediments at much greater depths than under normal circumstances.

Shown in Figure B.1-2 are the significant wave heights at each LATEX mooring during the 48-hour period centered on the time of highest waves at mooring 16. The most striking feature is the peak height of 9.09 meters at that mooring at approximately the time the eye was closest. The maximum wave heights observed at moorings 20, 23, and 1 occurred when long period waves represented a large percentage of spectral energy, i.e. at 0200, 0300, and 0900 UTC 26 August 1992, respectively. In comparison, the second largest significant wave height recorded by LATEX A wave gauges during the field program was during a frontal passage event on 8 April 1993, also at mooring 16; this was 3.5 m with a spectral peak at 8.0 s (DiMarco et al. 1995b).

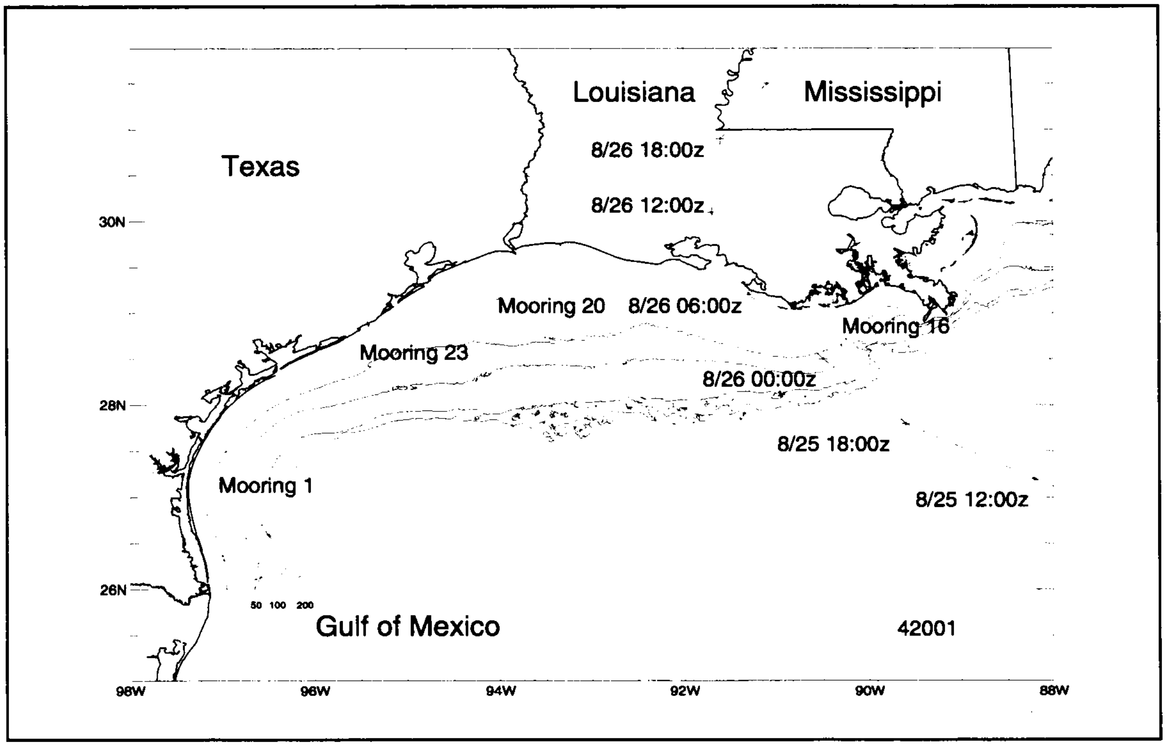

Figure B.1-1. Map of northwestern Gulf of Mexico showing the coastline, the 50-, 100-, and 200-m isobaths, Hurricane Andrew's track, the LATEX A wave gauge locations, and NDBC buoy locations. Moorings 16, 20, and 23 had MiniSpec directional gauges and mooring 1 had a SeaData non-directional wave gauge. All times are UTC. From DiMarco et al. (1995a).

The frequency of the peak spectral value for each wave burst is shown as a function of time in Figure B.1-3. Early in the 24-hour period preceding Andrew, the spectra at moorings 20, 23, and 1 were generally dominated by locally generated high frequency waves. Peak frequency dropped abruptly as the swell generated by Andrew reached each location. The dramatic shift to low frequency was accompanied by a rise in the wave height at each location (Figure B.1-2). After the shift, peak frequency increased gradually with time because of the frequency dependent celerity of the waves. In a few cases, the wave spectra became multi-modal and showed peaks at both high and low frequencies. In constructing the curves of Figure B.1-3 for the case of multi-modal spectra, we chose the peak whose frequency corresponded to swell and had a period greater than eight seconds, thus focusing on energy derived from the distant storm.

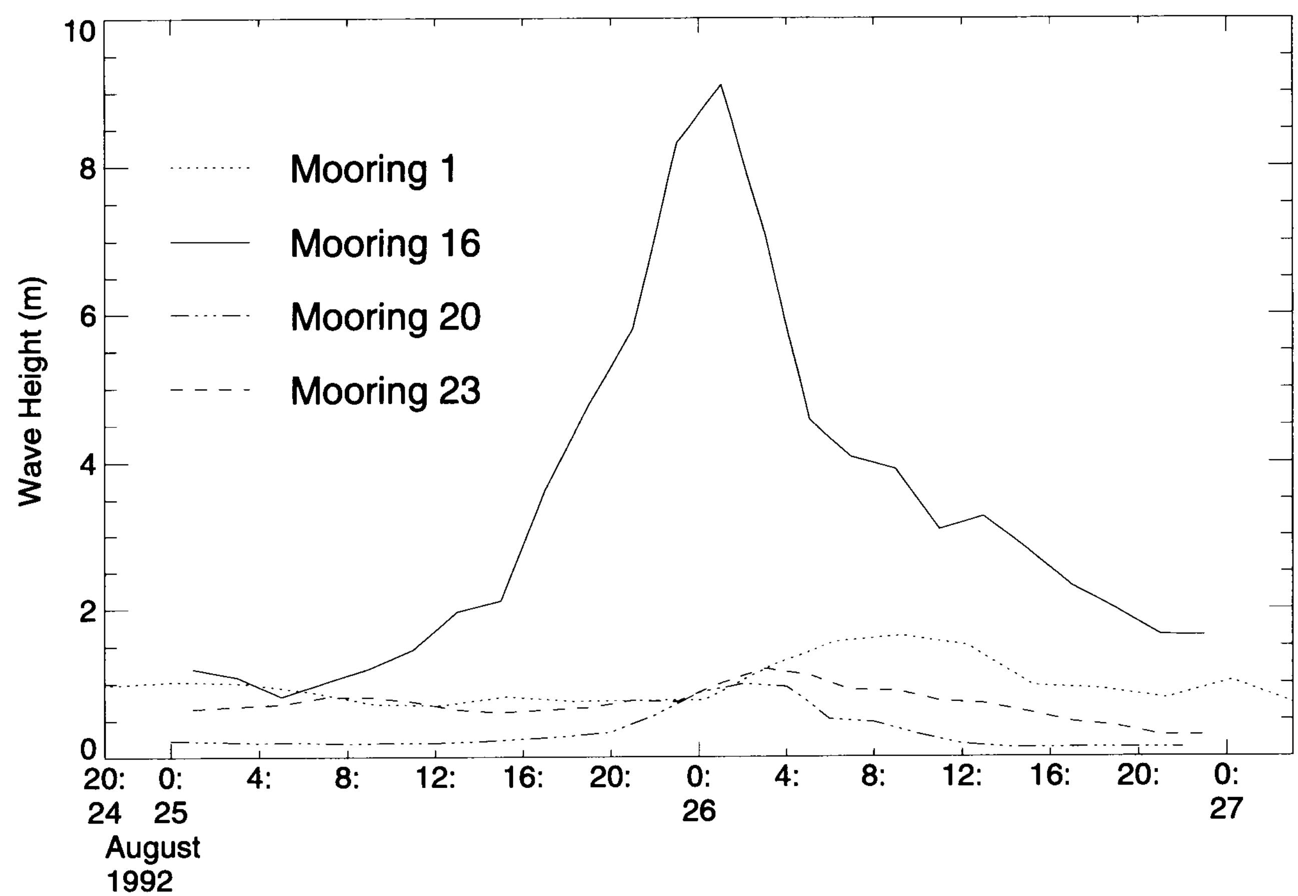

Figure B.1-2. Significant wave heights estimated at moorings 1, 16, 20, and 23 during Hurricane Andrew (from DiMarco et al. 1995a).

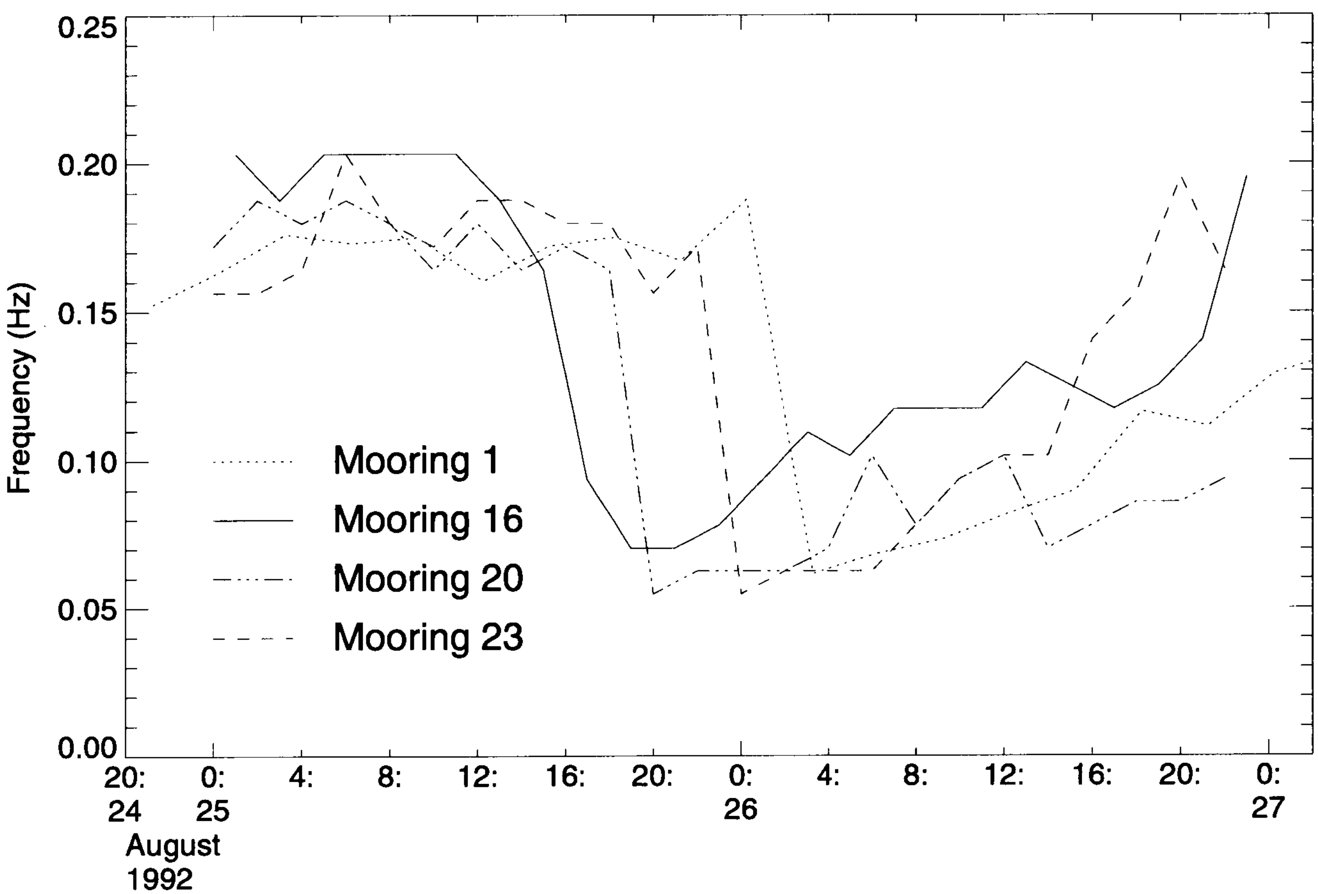

Figure B.1-3. Spectral peak periods estimated at moorings 1, 16, 20, and 23 during Hurricane Andrew (from DiMarco et al. 1995a).

An analysis of the arrival times of the long period swell at each LATEX wave gauge and NDBC wave buoy in the deep eastern Gulf using linear wave propagation theory shows that the swell was generated when the eye of Andrew was located between 83.1° and 85.0°W, or upon entering the deep eastern Gulf of Mexico (DiMarco et al. 1995a). This generation zone was established by extrapolating waves of known period and deep water group velocity from several points along the hurricane track to the observation locations. By comparing the arrival times of the extrapolated waves to the arrival times of the observed waves, boundaries could be set on a region in which the long-period swell was generated and propagated westward across the Gulf. The uncertainty in location of the generation zone is mainly due to the 1-3 hr gaps between observations. Extrapolated waves generated east or west of the generation zone could not have arrived at the LATEX gauges at the observed times.

Directional wave spectra during Hurricane Andrew were estimated using the method of Longuet-Higgins et al. (1963) and utilized the near-bottom pressure and horizontal velocities (DiMarco et al. 1995a). The calculation involves expanding the spectrum as a Fourier series and relating the first five terms in this series to the auto- and cross-spectra of the pressure and horizontal velocity components. Only one (mooring 23) of the three operational LATEX directional wave gauge locations yielded directional wave data throughout the duration of the hurricane. In general, the swell associated with Andrew propagated west-northwestward at mooring 23; the alongshelf isobath direction at this mooring is 245°. The pressure sensor of the wave gauge at mooring 20 failed upon deployment and, therefore, yielded no directional wave spectra. At mooring 16, directional wave spectra were estimated until 2100 UTC 25 August 1992, the time the instrument and frame were toppled. This instrument, however, continued to record bottom pressure throughout the hurricane. The directional wave spectra at mooring 16 prior to the instrument toppling also showed the wave direction of the wave energy associated with Andrew to be aligned with the alongshelf bathymetry. Unfortunately, the instrument was pushed over several hours before the hurricane's eye passed closest to this location, so no directional wave spectra are available for that time.

The combination plot of contoured energy density spectra and significant wave height versus time at mooring 16 (Figure B.1-4) shows the evolution of the correlation between significant wave height and the spectral distribution of wave energy. This figure demonstrates how low frequency energy contributed to the increase of significant wave height at the wave gauge locations far from the storm. At mooring 16, low frequency waves outran the storm center by several hours because deep water, 16-second period waves travel at 45 $km \cdot h^{-1}$ and over the deep eastern Gulf the storm moved at a forward speed of 14 $km \cdot h^{-1}$.

Low frequency waves, however, continued to contribute to the energy spectra after the eye passed mooring 16 (after 0600 UTC 26 August 1992) (Stone et al. 1993; Grymes and Stone 1995). During the eight-hour period when the storm center was closest to mooring 16

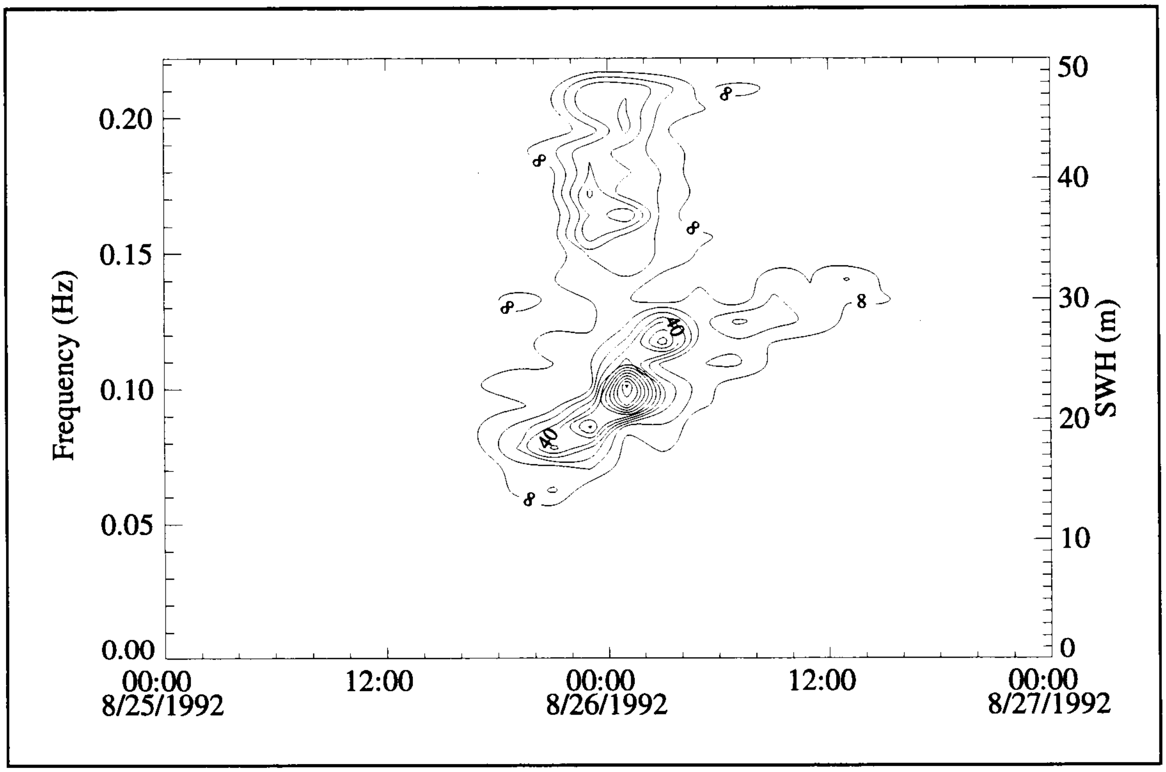

Figure B.1-4. Contour plot of energy density versus time with significant wave height superimposed at mooring 16. Contour interval is 8.0 $m^2 \cdot Hz^{-1}$ (from DiMarco et al. 1995a). All times are UTC.

(2000 UTC 25 August to 0400 UTC 26 August 1992), the spectra had considerable energy in the high frequency range—between 0.15 and 0.22 Hz. For example, at 0100 UTC 26 August 1992, the spectrum consisted of locally generated wind waves and storm generated swell in the deeper Gulf. Similar plots at moorings 1, 23, and 20 show the wave energy due to Andrew present only as swell (DiMarco et al. 1995a).

The multi-modal character of the spectra recorded at mooring 16 at the time of Andrew's closest approach represents a unique data set, in that they are markedly different from other LATEX wave gauge spectra recorded at the time and also differ from historical hurricane wave spectra recorded by deep water buoys (Ochi 1994). We believe the shallow water depth and the gauge's proximity to the storm center are important factors for the bi-modal structure of this spectra. Some of the high frequency energy at mooring 16 may have been locally generated, but a significant portion was probably a result of nonlinear, second-order, sum-frequency effects (Zhang et al. 1992, 1994). Shoaling topography may also have enhanced the nonlinear interaction. The nature of the strongly bi-modal spectra generated by Andrew in shallow water should be pursued for its engineering applications. A study specifically to quantify the nonlinear wave effects in the high frequency range of the Andrew data is currently underway.

Ocean currents and winds during Hurricane Andrew

The effects of Hurricane Andrew were far reaching; evidence of its passing were apparent in every LATEX current meter record. On the eastern shelf the evidence was due to the hurricane's passing directly over 10 mooring locations. On the western shelf, instruments recorded the effects of Andrew that propagated westward from the storm center and across the shelf waters.

The sequence shown in Figures B.1-5 through B.1-9 is of five-minute average current vectors measured at the LATEX current meter locations and wind vectors at selected moorings. The sequence begins at 1100 UTC 25 August, approximately 10 hours prior to Hurricane Andrew's crossing of the Texas-Louisiana shelf and ends two days later at 2300 UTC 27 August. The current vectors are measured from the upper current meters (at approximately 10 m depth) for all locations except moorings 15, 16, and 17; the bottom current vectors are given for those moorings. Mooring 15 has two vectors shown in the first two figures because the surface instrument failed at 2200 UTC 25 August 1992. The wind gauge at mooring 17 recorded direction only, so the magnitude has been prescribed at a constant value for all five figures.

The wind over the Texas-Louisiana shelf was from the northeast and light prior to Andrew's sweep over the shelf. At 1100 UTC 25 August (Figure B.1-5), the eye of Hurricane Andrew was located at approximately 27°N, 88°W. Winds on the eastern shelf had already begun to feel the effect from the northwest quadrant of the hurricane's cloud wall and had increased in magnitude slightly more than the winds to the west. The ocean currents were generally downcoast over the entire shelf region. The influence of an anticyclone-cyclone pair to the west are seen along the 200-m isobath where the shelf bends sharply southward. This feature persisted throughout the hurricane.

As Andrew approached, the winds at the eastern stations increased in magnitude while the directions began to align with the cyclonic winds of the storm. The surface currents on the eastern shelf responded to the increased wind stress and also began to increase in magnitude. At 2330 UTC 25 August (Figure B.1-6), the eye crossed the 50-m isobath near mooring 14. The surface instrument at mooring 15 failed, the bottom-mounted current meter at mooring 16 turned over, and the surface instrument at mooring 16 was swept away. Surface currents at moorings 12-15 exceeded 100 $cm \cdot s^{-1}$. The current speed at mooring 13 (10-m depth) was 163.5 $cm \cdot s^{-1}$ at 2230 UTC 25 August 1992—the largest speed recorded by the LATEX

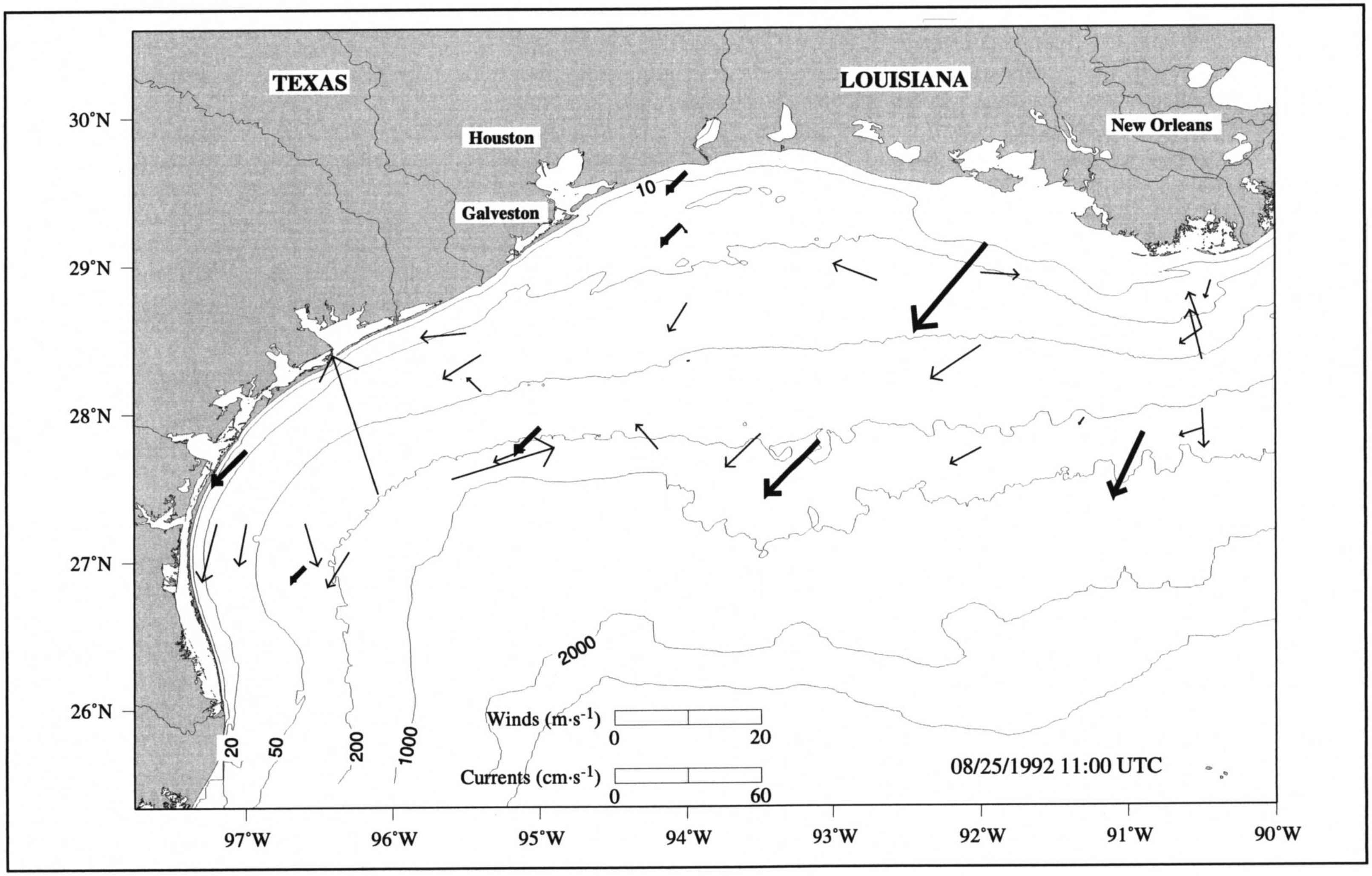

Figure B.1-5. Near surface current and wind vectors (bold) at 1100 UTC 25 August 1992.

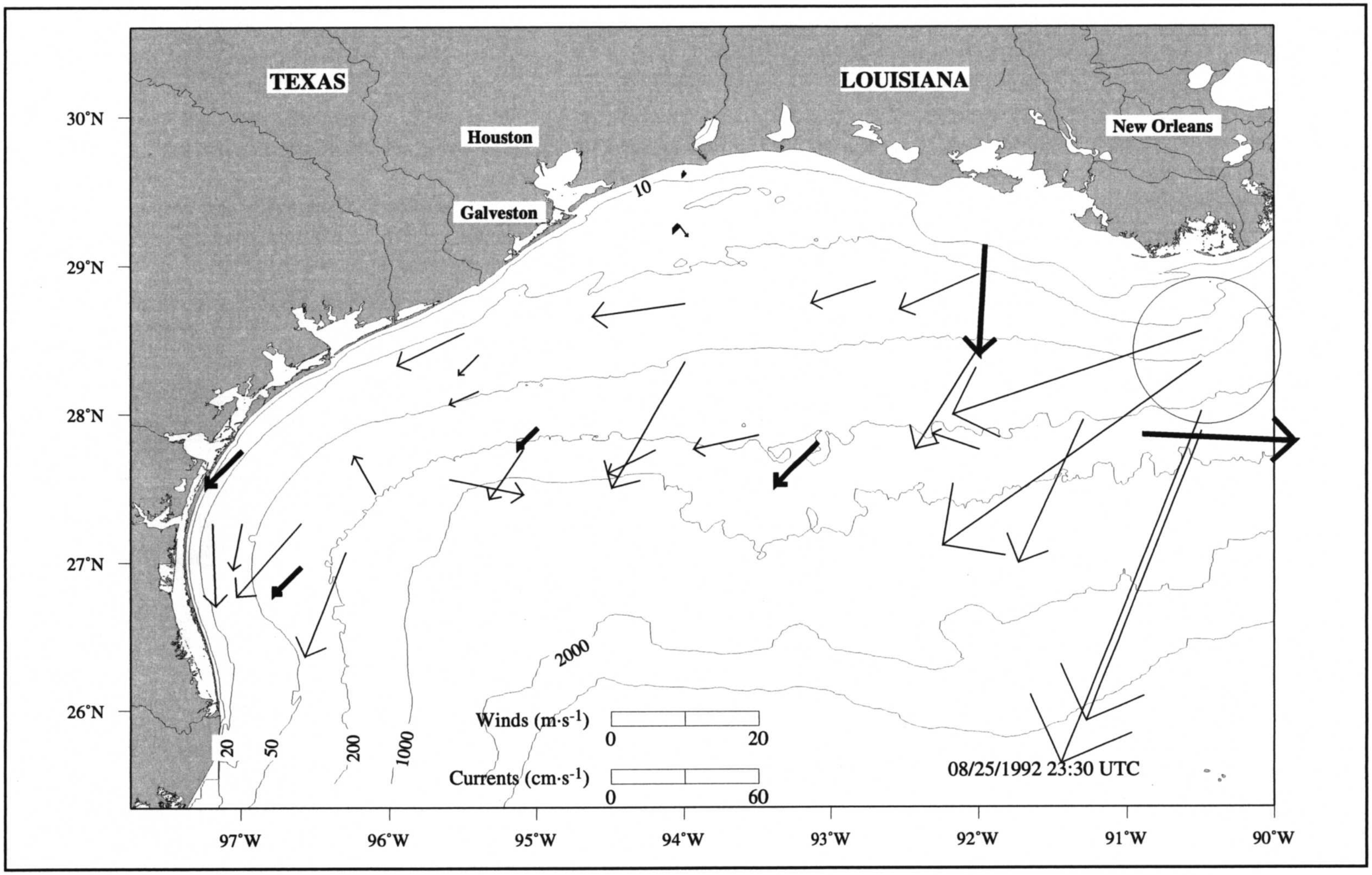

Figure B.1-6. Near surface current and wind vectors (bold) at 2330 UTC 25 August 1992. Circle is approximate radius of hurricane force winds.

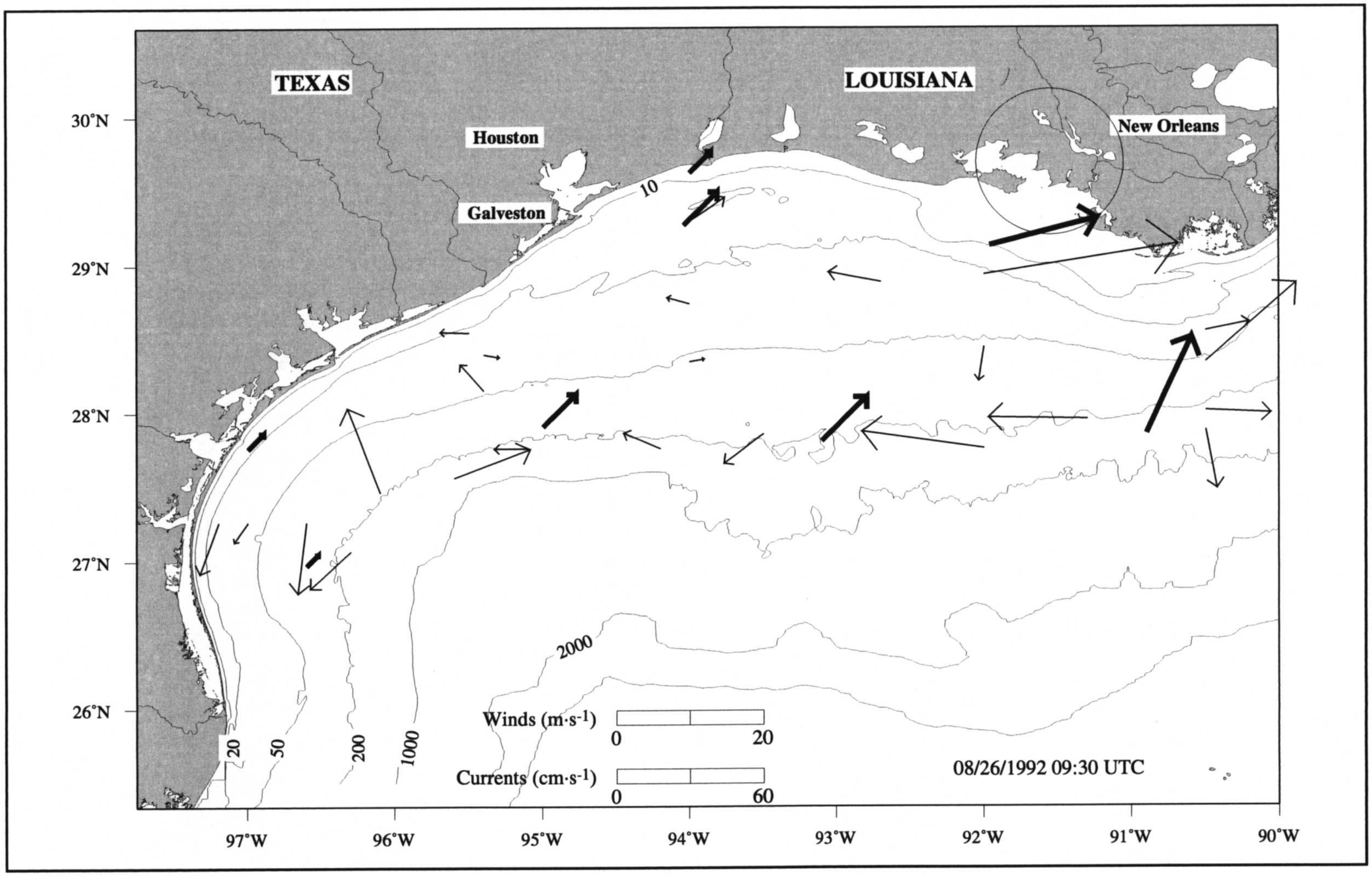

Figure B.1-7. Near surface current and wind vectors (bold) at 0930 UTC 26 August 1992. Circle is approximate radius of hurricane force winds.

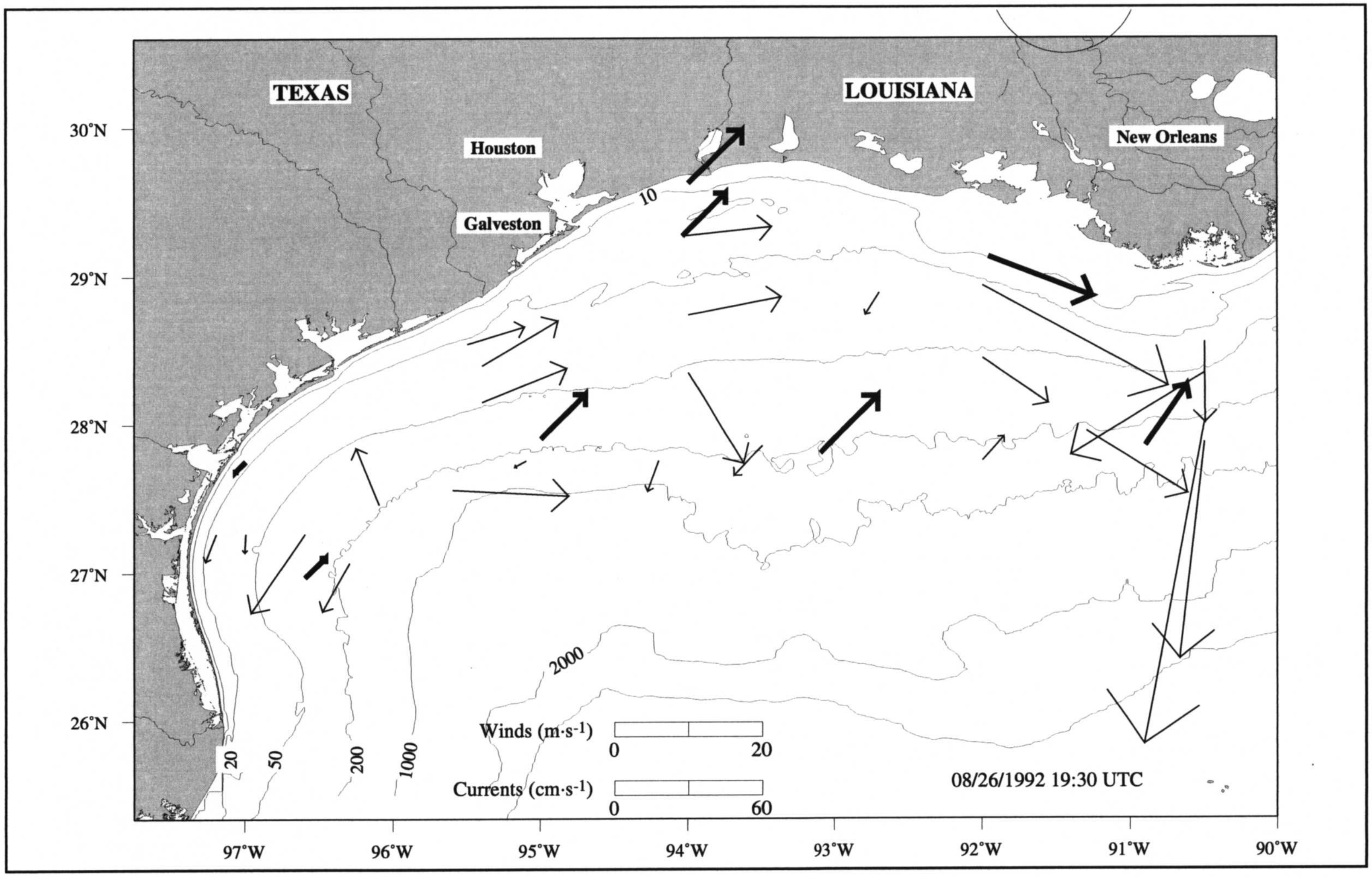

Figure B.1-8. Near surface current and wind vectors (bold) at 1930 UTC 26 August 1992. Circle is approximate radius of tropical storm force winds.

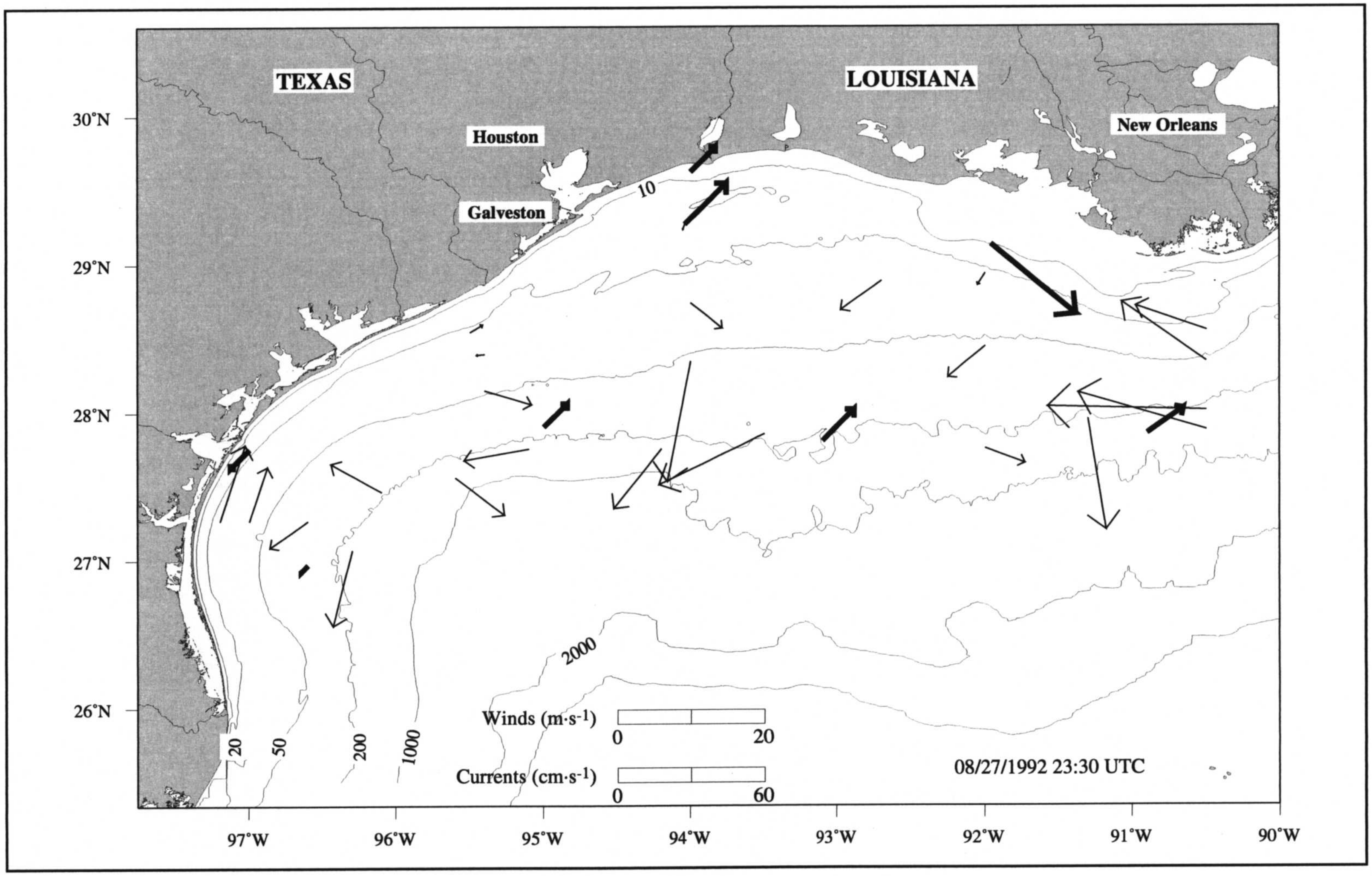

Figure B.1-9. Near surface current and wind vectors (bold) at 2330 UTC 27 August 1992.

array during the field program. The downcoast flow increased at virtually all locations on the shelf, including the stations near South Padre Island, Texas. The ring structures persisted at the coastal bend, although the cross-shelf velocity of the anticyclone was reduced significantly. The winds at the western shelf locations remained northeasterly. In the east, the winds were aligned with the cyclonic rotation of the hurricane winds. The approximate radius of hurricane force winds is depicted in Figure B.1-6 as a circle of 60 km radius. The winds to the south of this circle at BUSL1 (27.9°N, 90.9°W) were perpendicular to the winds measured to the west at mooring 17. The peak sustained winds measured at BUSL1 were 21.3 $m \cdot s^{-1}$ at 2300 UTC 25 August 1992. Peak sustained winds at BURL1 (28.9°N, 89.4°W) were 25 $m \cdot s^{-1}$ at 2200 UTC 25 August 1992 (not shown).

As the storm continued toward the Louisiana coast, the currents at the eastern moorings began to oscillate clockwise as they were turned by Coriolis force. Along the 200-m isobath, the currents remained steadily downcoast, greater than 30 $cm \cdot s^{-1}$. On the inner shelf, the currents also remained downcoast out to the 20-m isobath. At 0200 UTC 26 August 1992, the inner shore current at mooring 20 began to reverse to upcoast and strengthen. The winds in the east continued to track the hurricane as it crossed the shelf and made landfall at approximately 0830 UTC 26 August 1992, near Cypremort Point, Louisiana, with peak sustained wind speeds estimated at 53 $m \cdot s^{-1}$ and peak gusts at 63 $m \cdot s^{-1}$ (Grymes and Stone 1995; Stone et al. 1993).

At 0930 UTC 26 August 1992 (Figure B.1-7), the winds had reversed direction to southwesterly over essentially the entire Texas-Louisiana shelf. Much of the shelf current flow was still downcoast, the notable exceptions being the anticyclonic rotation of the easternmost current vectors, as compared to the previous figure and the strong upcoast coastal currents measured at moorings 17 and 20. Some surface currents responded to the change in direction of the wind stress by decreasing in magnitude (moorings 18 and 21) or changing direction (moorings 19, 22, 24, and 25). We will see below in the time series vector stick plots of the eastern current meters that there are strong inertial oscillations at these stations.

The winds over the Texas-Louisiana shelf continued to increase in magnitude and remained southwesterly as the hurricane proceeded inland. The winds directly associated with the hurricane decreased as the storm progressed inland, and the hurricane was downgraded to a tropical storm at 1800 UTC 26 August 1992 by the National Hurricane Center. By 1930 UTC 26 August 1992 (Figure B.1-8), the currents on the inner shelf (shallower than 100 m) east of 96°W had reversed and were upcoast; the currents along 90.5°W have rotated anticyclonically and indicate southerly flow; and along the 200-m isobath, the currents remained downcoast. Only the wind gauge at mooring 17 continued to show the effects of the winds of the trailing outer wall of the tropical storm. Currents at the cross-shelf line near South Padre Island continued downcoast until approximately 0030 UTC 27 August 1992, when they began to turn upcoast.

At 2300 27 August 1992 (Figure B.1-9), the winds remained southwesterly and much flow over the shelf was upcoast. Exceptions to this trend were the downcoast flow seen in the east and the downcoast flow along the 200-m isobath. Also, the ring structure on the western shelf along the 200-m isobath persisted throughout the hurricane.

Figure B.1-10 shows vector stick plots from the surface instruments along the cross-shelf mooring line along 90.5°W. The southwesterly flow intensified as the hurricane approached the shelf and was first seen at approximately 1800 UTC 25 August 1992. After the hurricane passed and made landfall, the response of the shelf waters was inertial, with anticyclonic rotation of the current vector with periods of slightly greater than 24 hr. This response persisted for more than two days.

In summary, Hurricane Andrew was a dramatic event that drastically affected the general circulation pattern over the entire Texas-Louisiana shelf. Maximum values for significant wave height, peak spectral wave period, current velocity, and wind speed during the LATEX field program were recorded during this hurricane.

B.2 The Storm of the Century (March 1993)

By any criterion, the winter cyclone that crossed the Gulf of Mexico and swept the eastern seaboard of North America 12-14 March 1993 was a major storm. Comparisons between this storm and previous exceptional winter storms ("Great Snow of 1717" and "Blizzard of 1888") prompted some to name the March 1993 event the "Storm of the Century". This storm killed an estimated 100-270 people on land and 48 at sea. Property loss in the U.S. and Cuba is estimated at nearly $3 billion. Tornadoes, high surf, and storm surge threatened thousands of people while millions more were hampered by road and airport closures and by widespread power outages. Over the eastern third of the U.S., the storm produced record low temperatures and atmospheric sea level pressures, and record high snowfalls and wind gusts. Expanded descriptions of the meteorological extrema and accounts of the devastation appear in Lott (1993) and Kocin et al. (1995). The March 1993 storm continues to be a topic of discussion and study in the meteorological community.

Although winter cyclones affecting the northeast are notoriously hard to predict, weather forecasters were able to project many elements of this storm four to six days in advance (Uccellini et al. 1995). This was due to the existence of an extensive weather observing network capable of delivering observational data in near real time to weather centers for assimilation by numerical weather prediction models, a resource weather forecasters of previous "great" storms did not have. Reviews of the performance of the National Center for Environmental Prediction's medium range forecast (MRF) model in relation to this storm appear in Caplan (1995). Data sets, graphics, and satellite imagery of the storm are available via the worldwide web. In the following sections we will examine the storm from

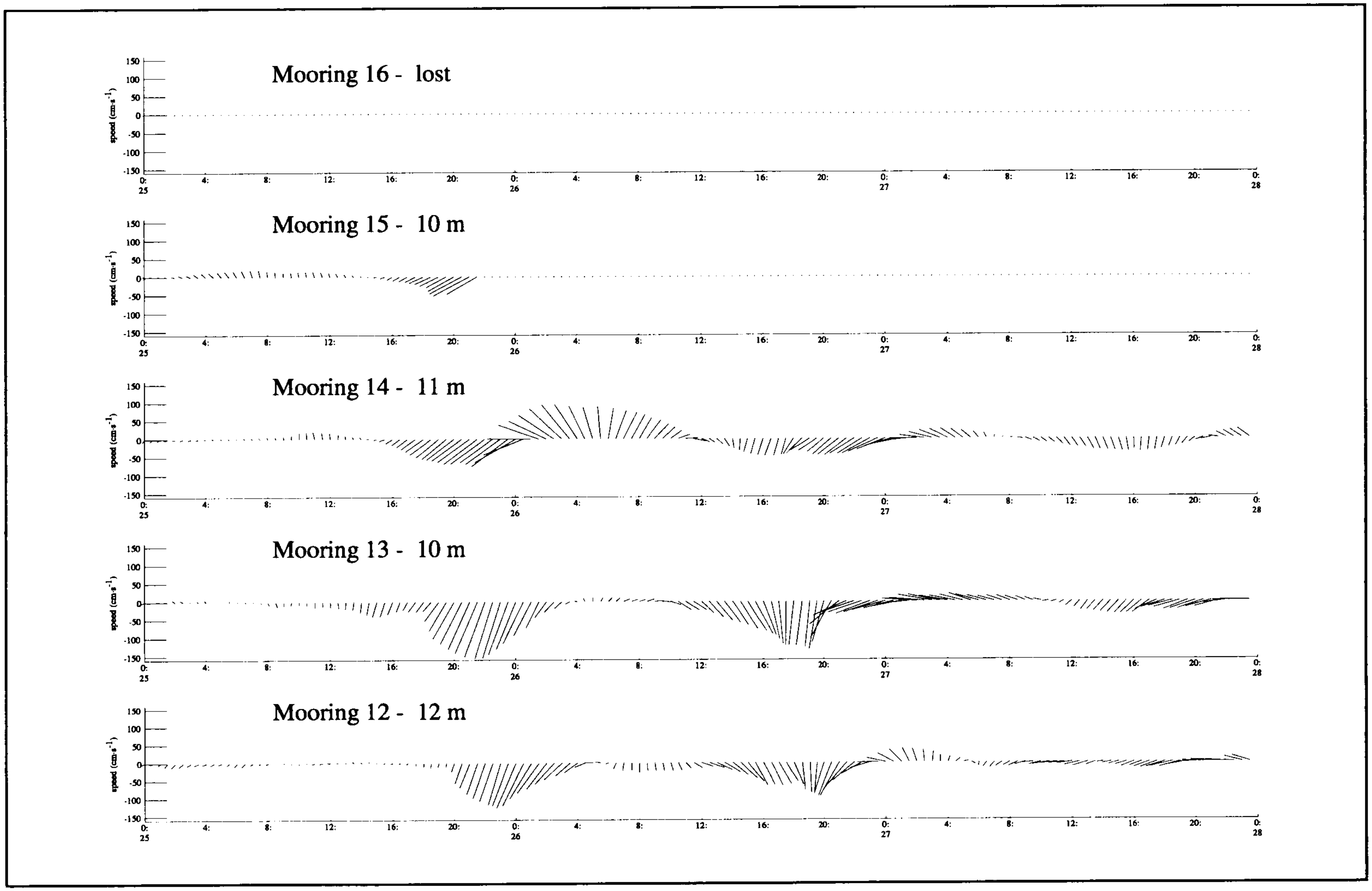

Figure B.1-10. Vector stick plots from the upper instruments of the cross-shelf mooring line along 90.5°W. Instrument depths are indicated on plot, time-step between vectors is 30 minutes.

an oceanographic perspective, particularly its effect on the circulation over the Texas-Louisiana shelf.

Observations of wind and current fields

In the early hours of 12 March 1993, the soon-to-be "Storm of the Century" was a disorganized area of low pressure located over northern Mexico just south of the Texas border. Within 12 hours, this low-pressure feature moved into the coastal waters off south Texas where it consolidated and deepened. Wind speeds at NDBC buoy 42020 (approximately 180 km NE of Brownsville) increased from about 8 to 18 $m \cdot s^{-1}$ as the wind direction changed from east to northwest. Wind speeds at 42020 exceeded 10 $m \cdot s^{-1}$ for the next 36 hours. Over the second 12-hr period, central pressures in the cyclone dropped dramatically as the cyclone moved east-northeast. The rate of pressure decrease, 17 mb in 12 hours, is rarely observed in the Gulf of Mexico (Kocin et al. 1995) and it far exceeded the rate needed to classify the storm as a "bomb" cyclogenic event (see Appendix A.2 for a discussion of bomb cyclogenic events in the Gulf of Mexico). By 0000 UTC 13 March wind speeds at the Bullwinkle oil platform near Southwest Pass, Louisiana (BURL1) had exceeded 25 $m \cdot s^{-1}$, and would continue to do so for the next 12 hours. The storm made landfall near Pensacola, Florida, around 0900 UTC 13 March (see Figure A.1-3 for the storm track) and continued to deepen for the next 15 hours or so, although at a much slower rate, as it continued northward along the eastern seaboard of the U.S.

The near-surface circulation over the Texas-Louisiana shelf was profoundly affected by the passage of the storm. The resulting circulation patterns were caused by the persistent high winds and the sea surface slopes resulting from the convergence and divergence of the waters on the shelf. The response appeared largely barotropic. Tidal forcing was relatively unimportant during the storm passage; even the strong near-surface flow associated with Eddy Vazquez was masked for several days by the storm-driven flow.

Figures B.2-1 through B.2-9 show a time sequence of wind vectors over the northwest Gulf of Mexico on a 0.5° by 0.5° grid paired with near-surface current vectors over the Texas-Louisiana shelf on a 0.25° by 0.25° grid. The sequence shown covers the period from a day preceding the storm's entry into the Gulf to a day after landfall. The winds are described in Section 2.1.1; the currents in Section H.2. The current fields are based on instantaneous current meter observations at the indicated time and were gridded using the adjustable tension continuous curvature surface gridding algorithm found in the GMT package (Smith and Wessel 1990).

Figure B.2-1 shows the winds and currents 24 hours before the storm entered the Gulf. Winds were relatively light from the east or southeast. The current patterns do not appear to be responding to the present wind field. The strongest currents are associated with Eddy Vazquez located in the southwest region of the shelf.

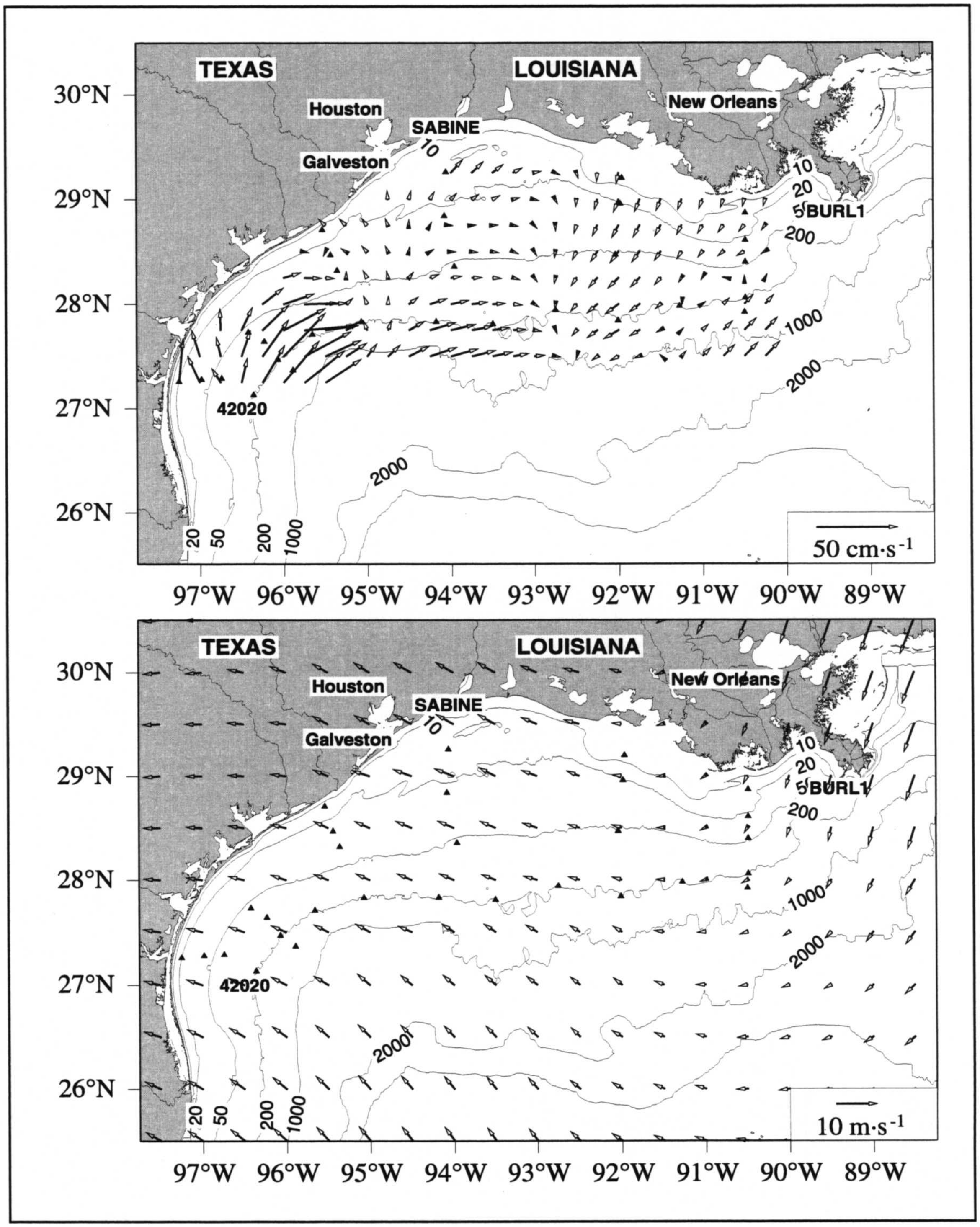

Figure B.2-1. Gridded currents (top) and winds (bottom) for 11 March 1993 1200 UTC showing conditions during the passage of the "Storm of the Century".

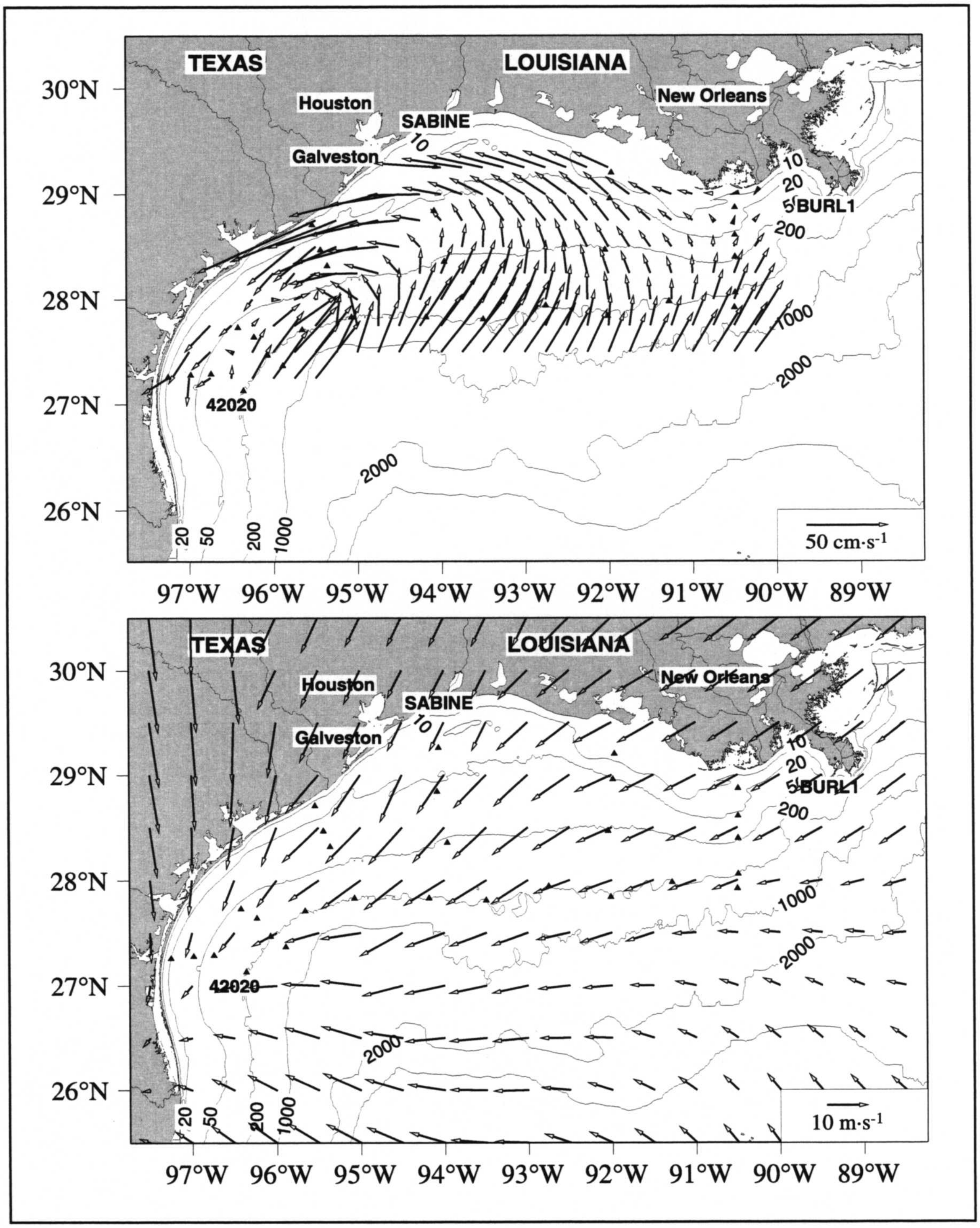

Figure B.2-2. Gridded currents (top) and winds (bottom) for 12 March 1993 1200 UTC showing conditions during the passage of the "Storm of the Century".

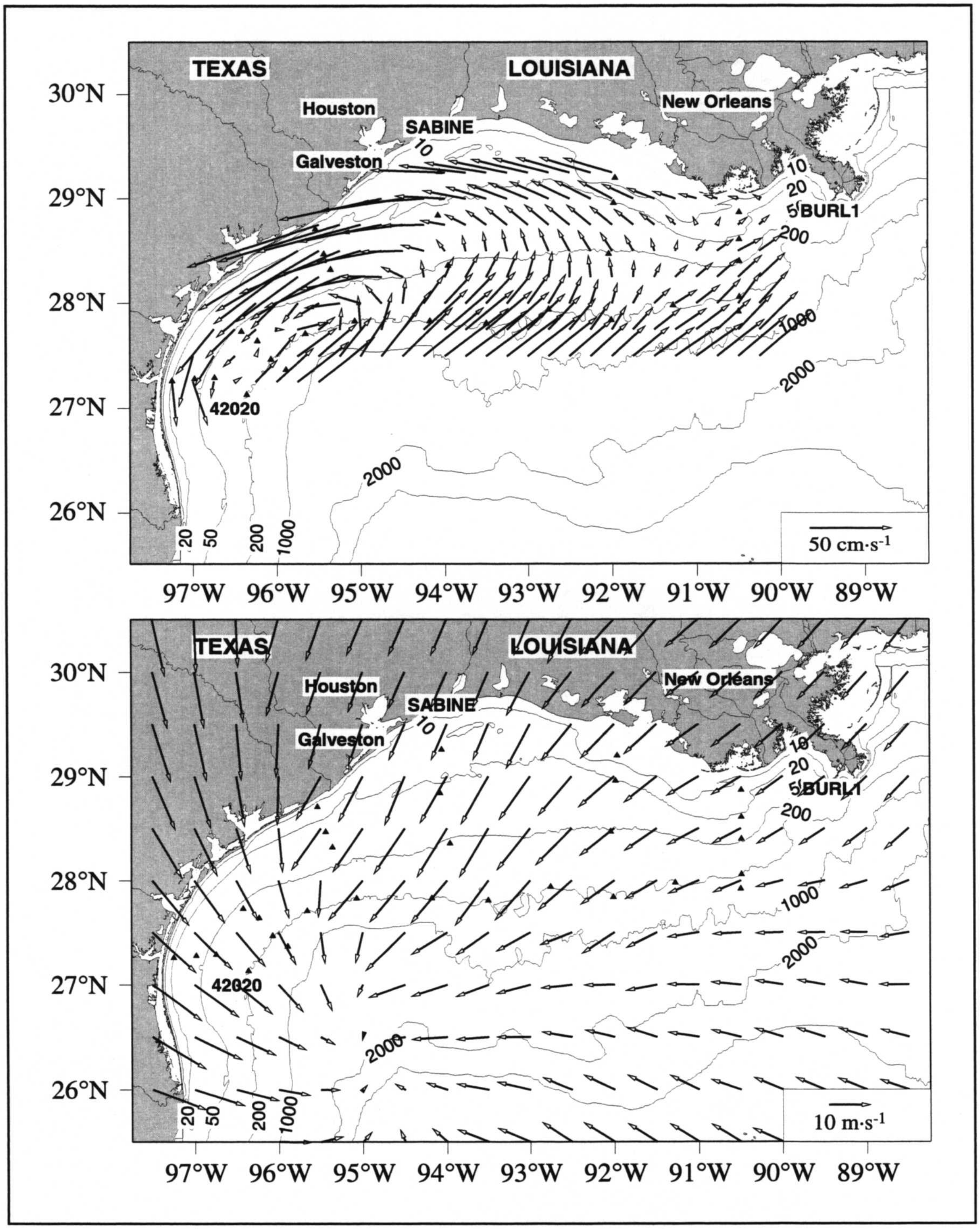

Figure B.2-3. Gridded currents (top) and winds (bottom) for 12 March 1993 1400 UTC showing conditions during the passage of the "Storm of the Century".

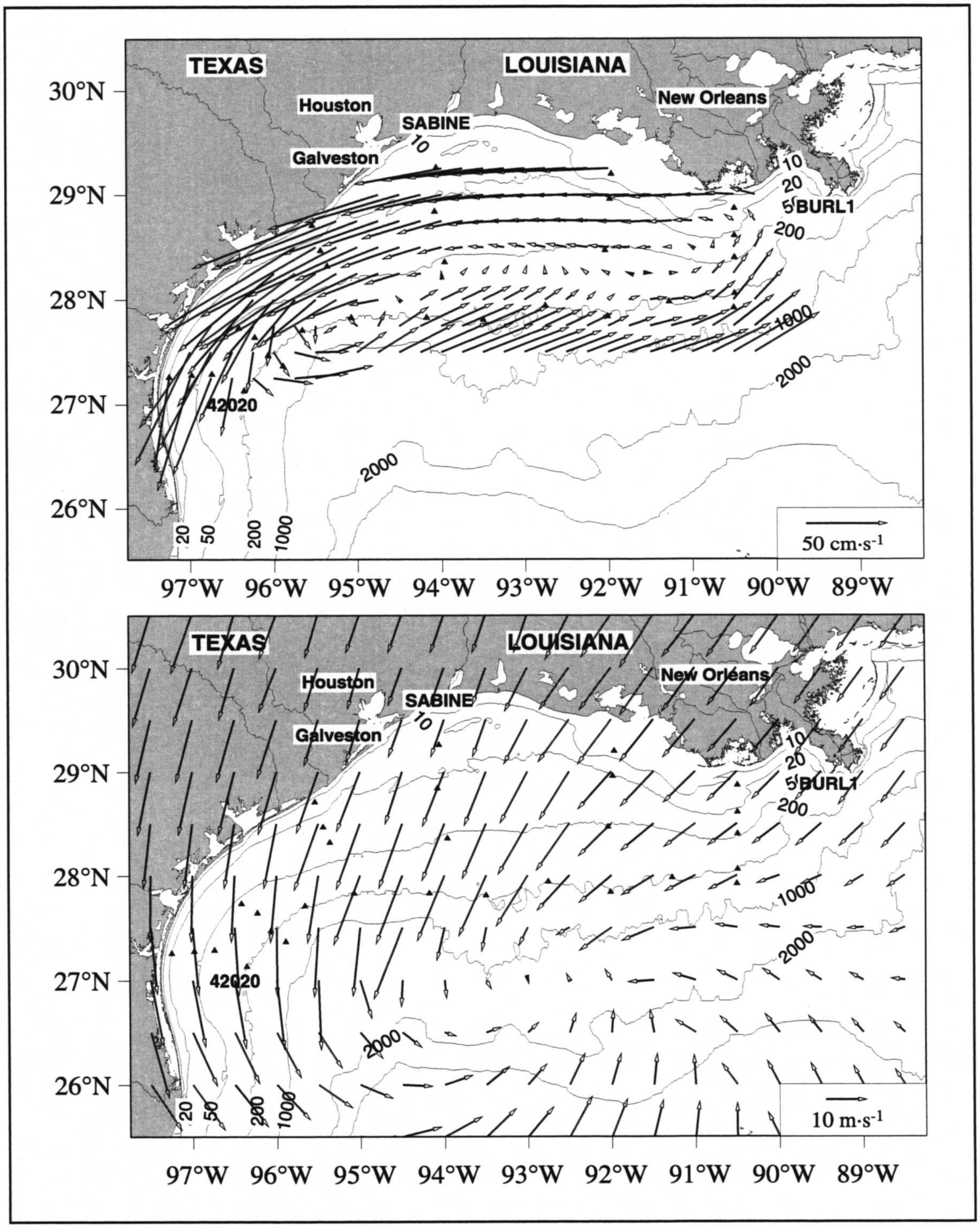

Figure B.2-4. Gridded currents (top) and winds (bottom) for 12 March 1993 1600 UTC showing conditions during the passage of the "Storm of the Century".

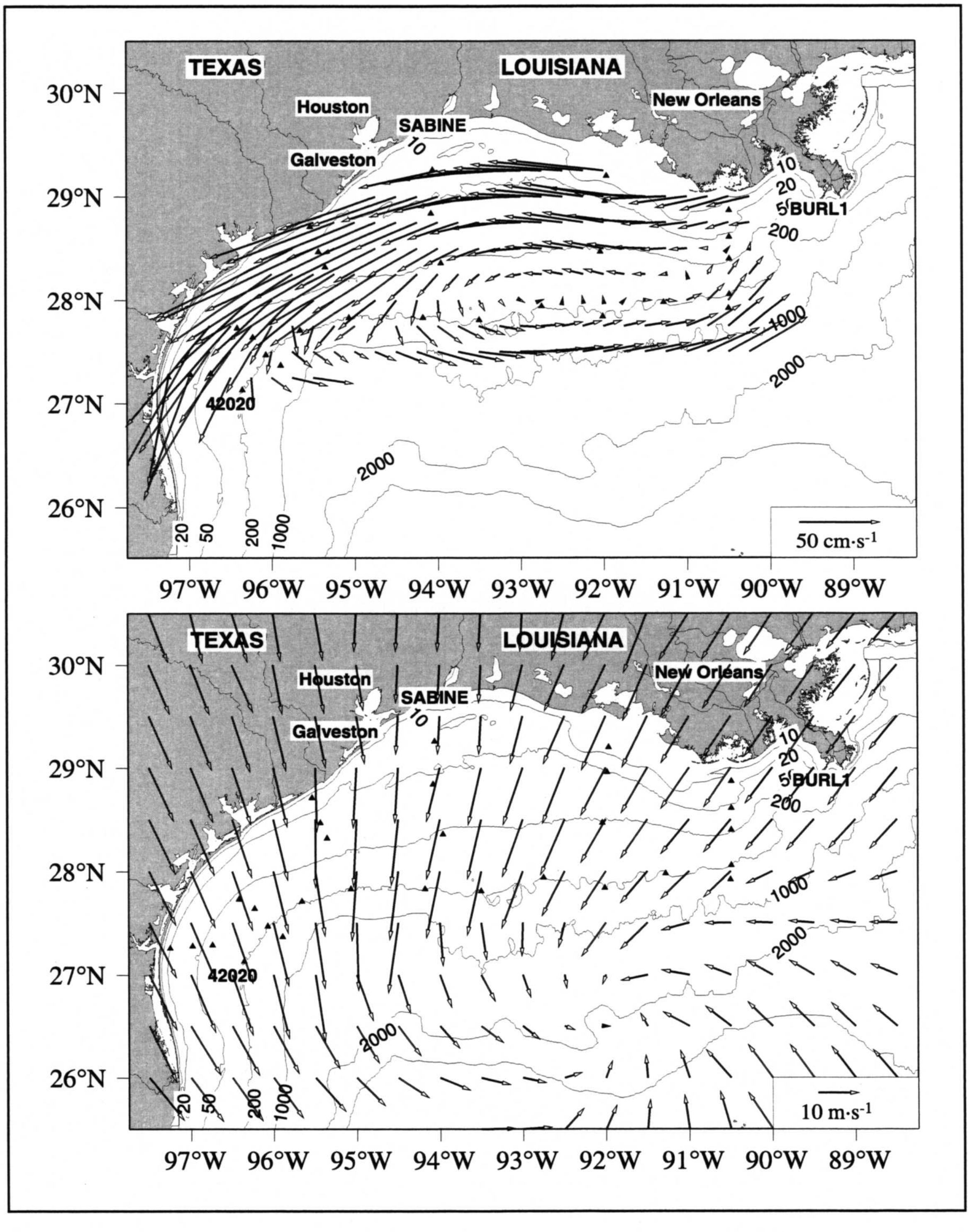

Figure B.2-5. Gridded currents (top) and winds (bottom) for 12 March 1993 1800 UTC showing conditions during the passage of the "Storm of the Century".

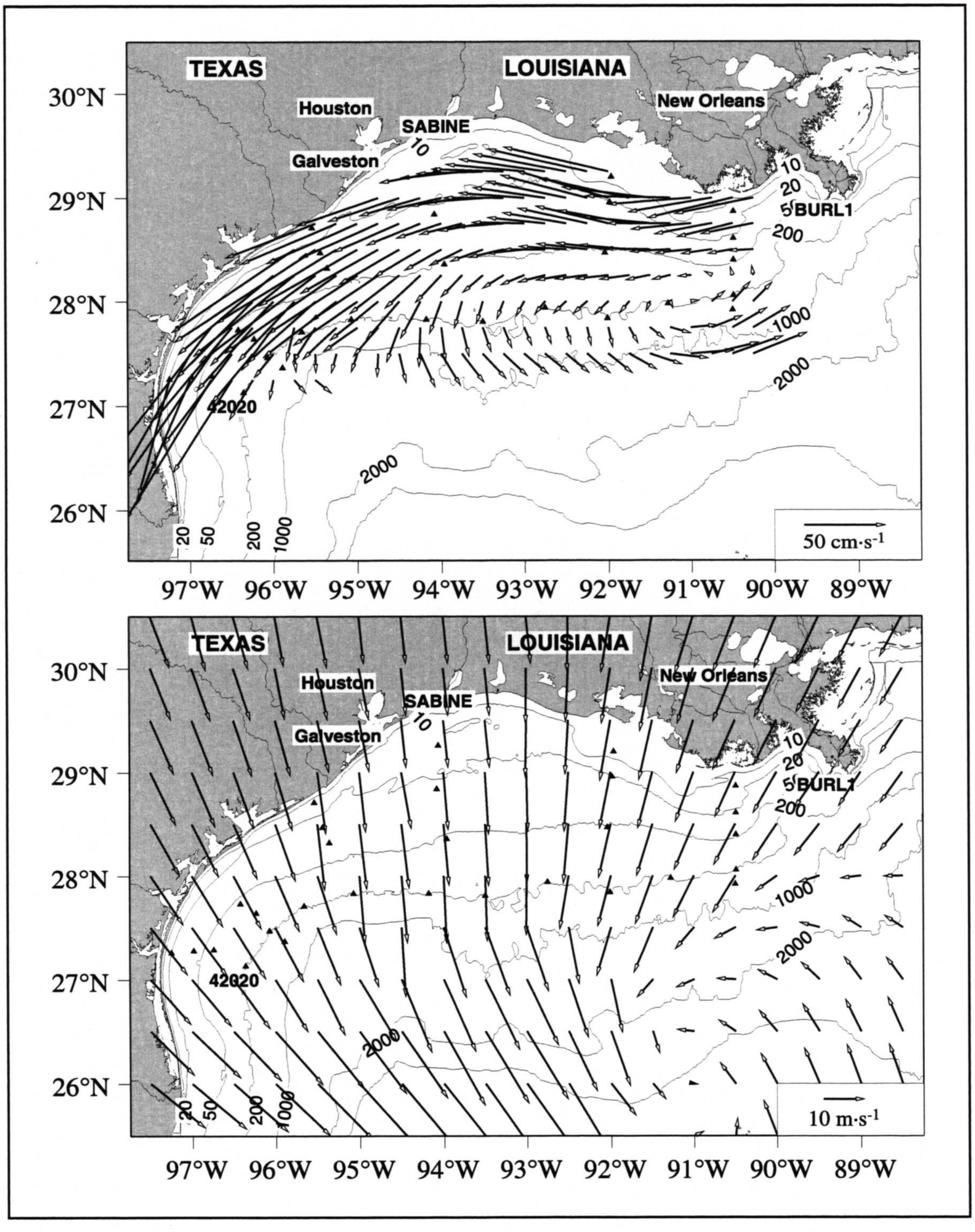

Figure B.2-6. Gridded currents (top) and winds (bottom) for 12 March 1993 2000 UTC showing conditions during the passage of the "Storm of the Century".

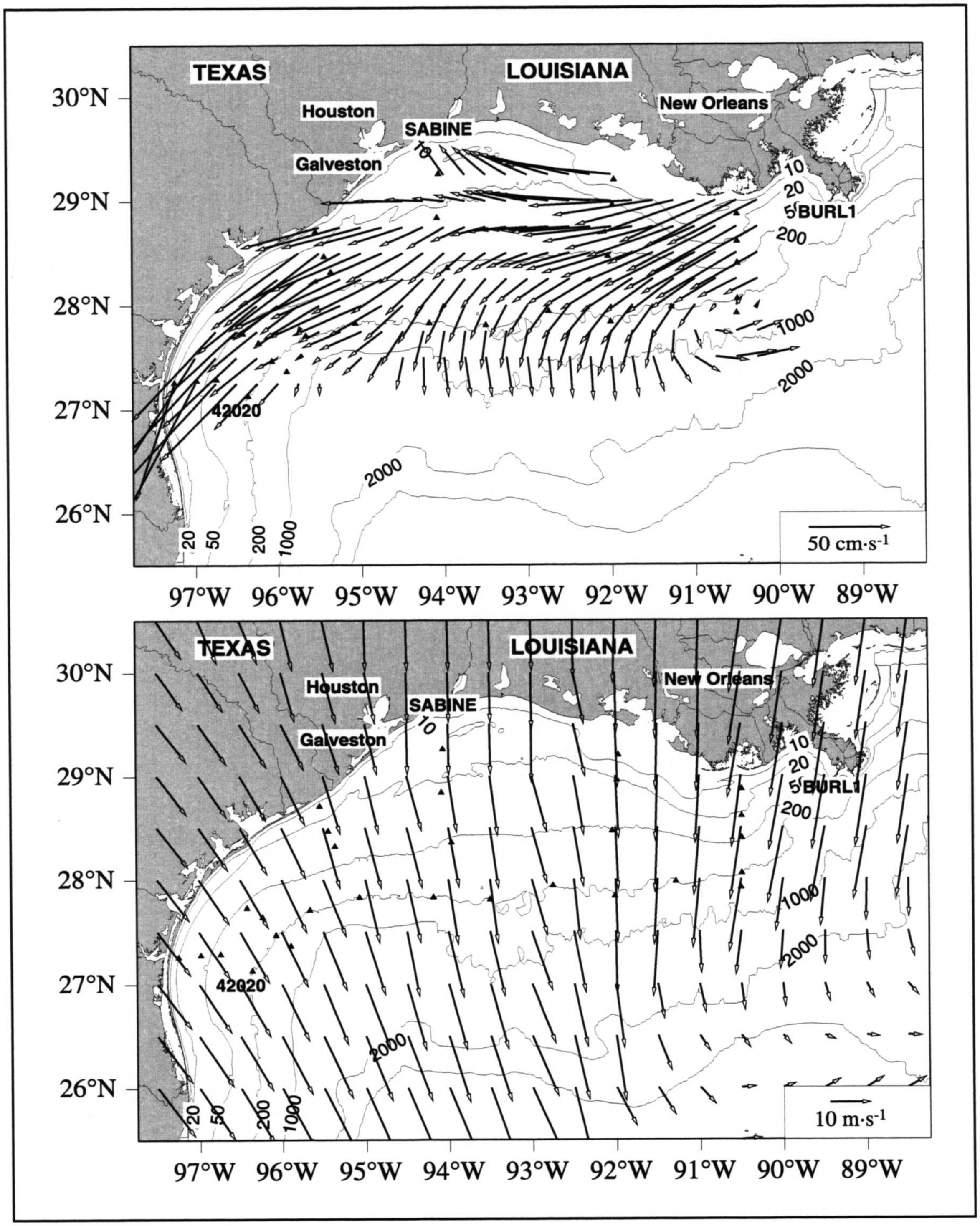

Figure B.2-7. Gridded currents (top) and winds (bottom) for 12 March 1993 2200 UTC showing conditions during the passage of the "Storm of the Century".

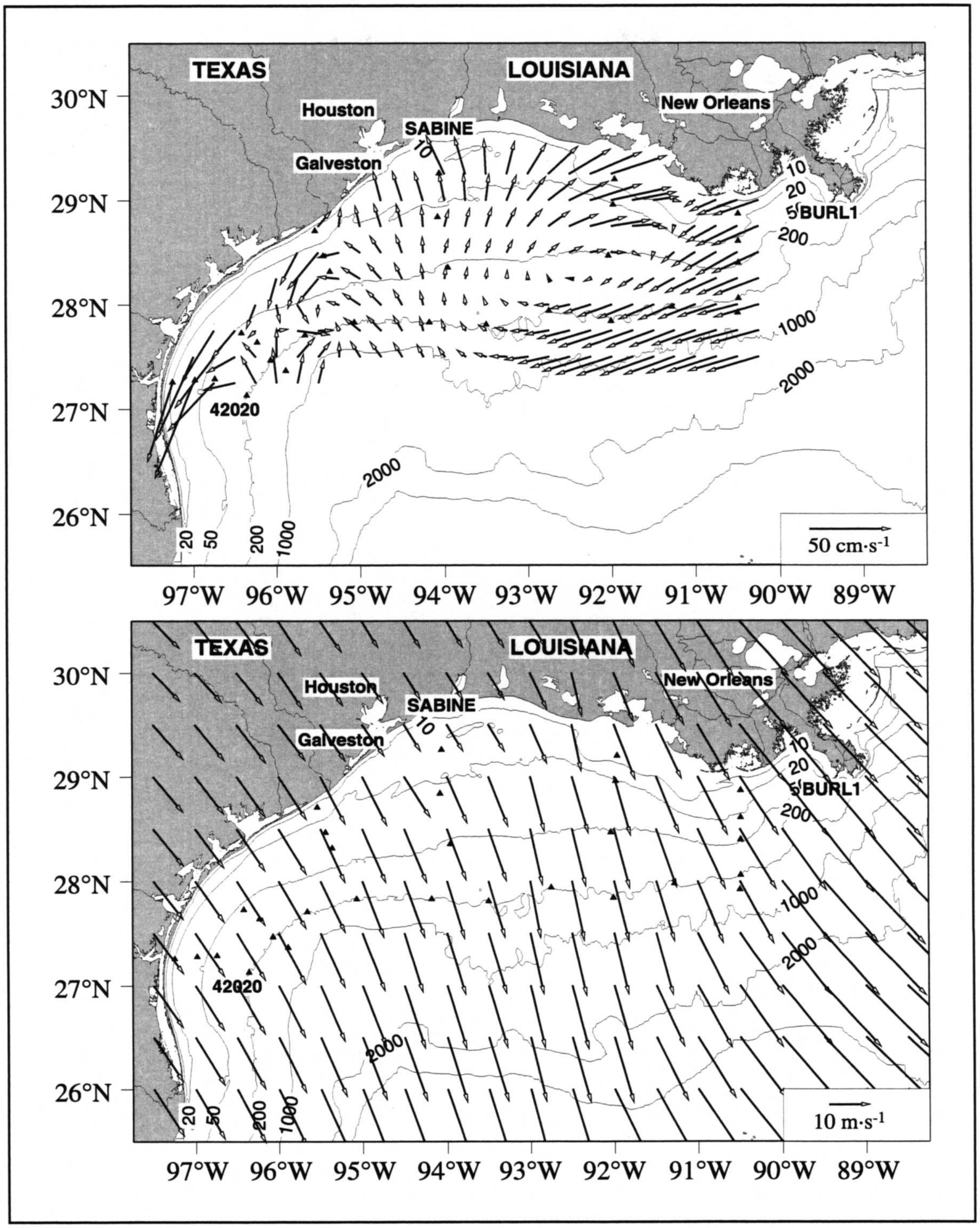

Figure B.2-8. Gridded currents (top) and winds (bottom) for 13 March 1993 1000 UTC showing conditions during the passage of the "Storm of the Century".

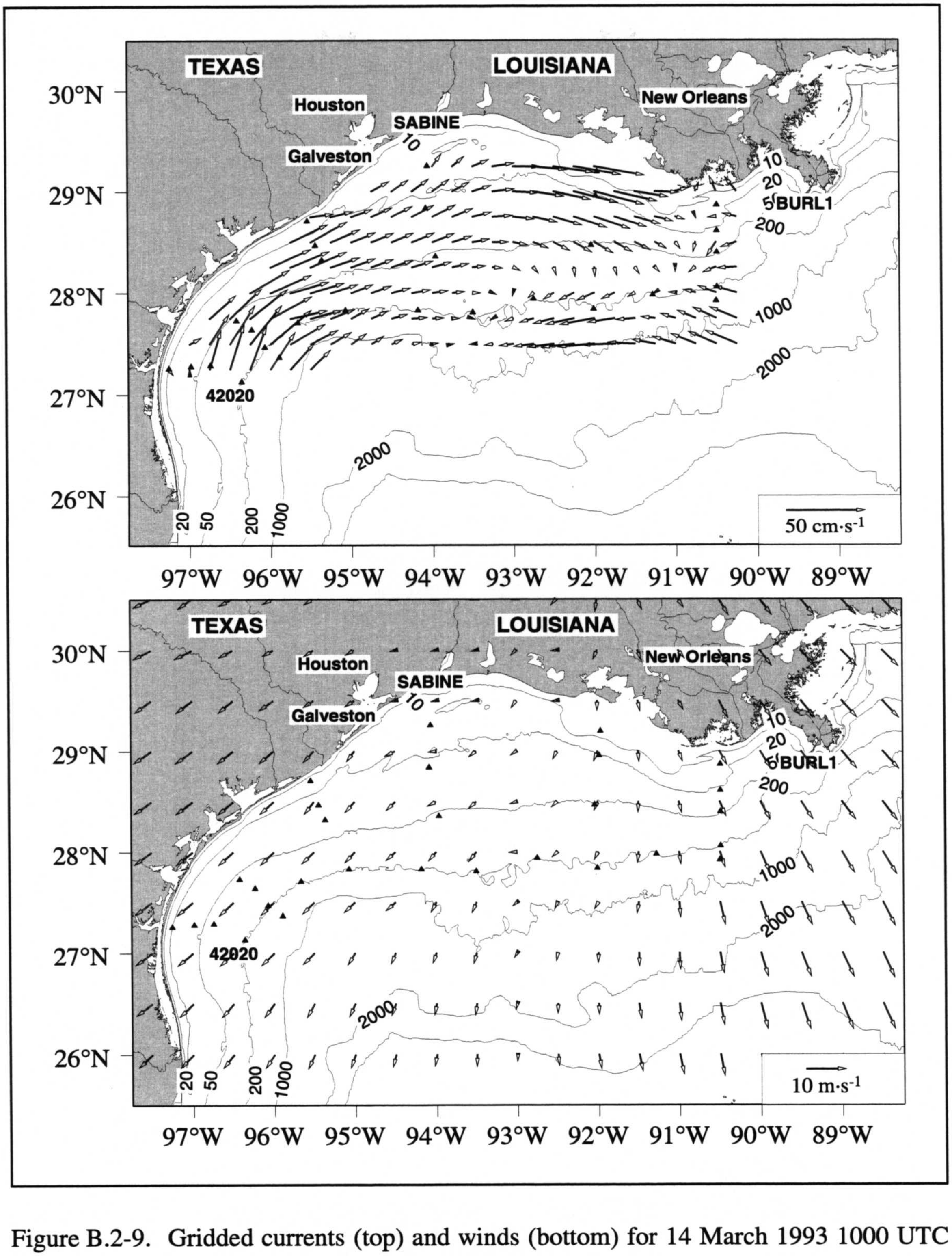

Figure B.2-9. Gridded currents (top) and winds (bottom) for 14 March 1993 1000 UTC showing conditions during the passage of the "Storm of the Century".

Twenty-four hours later (1200 UTC 12 March, Figure B.2-2) wind speeds have increased dramatically. A strong downcoast wind component has developed along the entire coast from south Texas to the Mississippi delta and currents over the inner shelf region have organized and begun to flow west and south along the coast. East of 96°W, easterly winds seaward of the shelf break and northeasterly winds over the shelf combined with the need to replace water transported downcoast in the highly divergent nearshore regime from 96° W to the Mississippi delta have produced strong onshore flow over the eastern half of the Texas-Louisiana shelf. The influence of Eddy Vazquez on the circulation has diminished as the coastal jet begins to overwhelm the northern arm of the eddy. The flow over the shelf is cyclonic with the center of the cyclone occurring near the 50-m isobath in the southwest region of the shelf just north and west of the storm center.

Two hours later (1400 UTC 12 March, Figure B.2-3) the center of the cyclone has moved offshore and winds between it and the coast are from the northwest. An associated cyclone in the water appears with its center between the storm center and the coastline. As will be seen in subsequent frames, the center of the cyclone in the water remains between the 50- and 200-m isobaths and follows the storm as it tracks eastward. Although the coastal flow continues to intensify and transport water south, a strong northward transport continues across a broad region (96°W to 91°W) at the shelf break. This net transport of water onto the shelf must compensate for the downcoast export of water over the inner shelf.

During 1600-2200 UTC 12 March (Figures B.2-4 through B.2-7) central pressures in the cyclone deepened rapidly (approximately 1.5 $mb \cdot h^{-1}$) and wind speeds continued to increase. As the storm center moved east of New Orleans wind directions over the Texas-Louisiana shelf shifted from northeast to northwest. During this time sequence, downcoast currents over the inner shelf intensified in the eastern part of the region. The eastern limit of the strong southward arm of the shelf circulation migrated eastward with the storm and by 2200 UTC surface water was being exported from the shelf everywhere along the shelf break except in a relatively narrow region just west of the Mississippi delta. Currents measured along the south Texas coast reached their peak values of 80-120 $cm \cdot s^{-1}$ between 1600-1730 UTC.

Figure B.2-8 (1000 UTC 13 March) shows conditions an hour after the storm center made landfall. Strong winds persist and are nearly uniformly from the northwest. Downcoast of Galveston, coastal winds had a strong downcoast component and currents there were also directed strongly downcoast. Currents over the inner shelf from 91° to 93°W were upcoast (eastward) in response to the upcoast wind component. East of 91°W the currents remained downcoast, presumably not having yet had time to respond to the wind shift. Between 93° and 95°W flow was inshore perhaps in response to the large scale alongcoast divergence of flow over the inner shelf. In the southwest near the shelf break, Eddy Vazquez appears to have been reasserting its influence on the flow.

Figure B.2-9 (1000 UTC 14 March) shows conditions when the storm was centered near Maine. Wind speeds over the Texas-Louisiana shelf were greatly diminished, with variable direction. Rather than a weak cyclone-anticyclone pair with a zone of shoreward flow between them, the pattern shown is a broad anticyclonic flow similar to the mean summer pattern. This remarkably different flow pattern is consonant with upcoast flow regularly seen in summer in response to upcoast wind components.

Discussion

Immediately following the entry of the "Storm of the Century" into the Gulf, the circulation patterns over the Texas-Louisiana shelf conformed to the expected flow pattern over the inner shelf. As the downcoast flow along the inner shelf of Texas intensified, the flow along the shelf break east of 96°W began to depart significantly from that expected from a consideration of the local wind field alone. It appears that the cyclonic ocean circulation pattern, the eye of which moved eastward with the eye of the atmospheric cyclone, evolved in response to the rapidly moving low pressure region associated with the atmospheric cyclone. Without some measure of the sea surface slopes, either by satellite altimetery or by bottom pressure measurements we are limited to speculation.

Satellite altimetry is not useful because the mean surface is not well known over the shelf and because the repeat cycle is too slow for the rapidly changing elevations we are interested in. Unfortunately, the LATEX A directional wave recorders were not in service during the storm's passage; their low-frequency pressure records would have been useful in determining the spatial patterns of sea surface elevation at least for the inner shelf. We are fortunate, however, to have access to water level records from several locations from the Conrad Blucher Institute at Texas A&M University-Corpus Christi.

Figure B.2-10 shows the water level (mean removed) for stations at Sabine Pass and Galveston Pleasure Pier. These records show an increase in water level which peaked about the time the storm entered the Gulf. The increase appears to be part of the normal tidal cycle except the magnitude appears larger than normal. This enhanced amplitude is probably associated with the increased strength of the coastal current (Figure B.2-2). From 1200 UTC 12 March to about the time of the storm's landfall, water levels at Galveston and Sabine Pass drop to extremely low levels. This descent occurred during the time depicted in Figures B.2-3 through B.2-8. It appears water was moved from the coast. Following landfall, wind speeds in the Gulf began to decrease, and simultaneously, water levels began to rise. Figure B.2-8 represents conditions about an hour after landfall and an hour or so after water levels along the coast began to rise. The same changes as observed in the coastal sea level and inner shelf currents were seen in the circulation model discussed in Appendices K and G (though with amplitudes differing from those observed). The response of the shelf following the passage of the storm is complex and deserves further study.

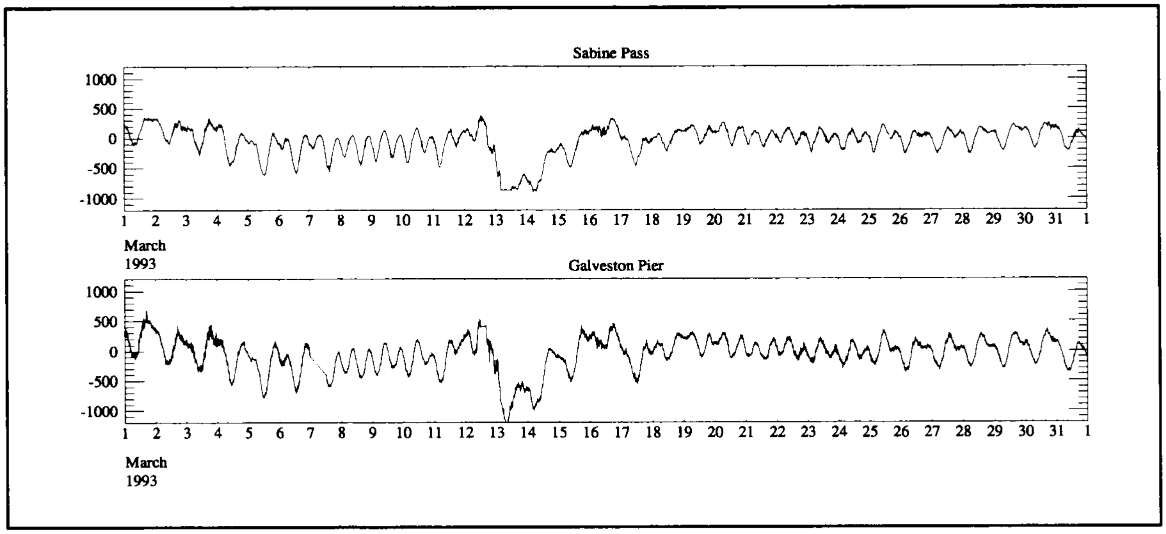

Figure B.2-10. Water level measured during March 1993 at Sabine Pass and Galveston Pleasure Pier.

B.3 Coastal upwelling off south Texas

Wind-driven coastal upwelling likely occurs annually along the south Texas coast. Its occurrence may be a factor contributing to, perhaps even limiting, biological productivity in local waters. To date little has been published on this topic.

Based on averages of meteorological and oceanographic station data and discrete infrared satellite imagery we present evidence of seasonal upwelling along the Texas coast and describe its spatial and temporal extent in broad descriptive terms. The episodic nature of upwelling will be shown through examination of selected time series of winds and currents collected during the LATEX A Program.

Data

The data for this analysis are summarized in Figure B.3-1. Meteorological and hydrographic data collected over several decades have been combined with data from the LATEX A field program. Meteorological data are from the climatology by Hellerman and Rosenstein (1983), from airport weather stations at Brownsville and Corpus Christi, Texas (1951-1960), and from NDBC buoy 42008 off Freeport, Texas (1978-1983). These are fully discussed in Cochrane and Kelly (1986). Data from PTAT2 at Port Aransas, Texas (1992-1994) were obtained from NDBC.

Nearshore temperature and salinity were recorded at the Brazos Santiago tide station near Brownsville, Texas, from 1958 to 1971. In slightly deeper water, temperature and salinity data were collected at two GUS III stations during repeat visits during 1963-1965. Horizontal contours of near surface temperature and salinity were generated from data collected across the entire south Texas shelf during the LATEX hydrography cruises in May and August of 1993 and 1994. Full vertical profiles of CTD data taken along line 7 during the same LATEX cruises were used to produce vertical sections. Currents, temperature, and salinity were measured continuously from April 1992 to December 1994 at moorings 1 and 2 (data from moorings 3 and 4 were not used). Offshore temperature conditions are characterized by bathythermograph data presented by Etter and Cochrane (1975). Infrared imagery from the NOAA/NOS Ocean Products division and from the Coastal Studies Institute at Louisiana State University complete the data set.

One consequence of the planet's rotation is that in the northern hemisphere winds produce a net transport in the upper water column (Ekman layer) that is 90° to the right of the wind direction. If such Ekman transport is offshore, it must be replaced by water upwelled from below. This water is usually cooler, more saline, and often has higher concentrations of nutrients than the water it replaces. Winds that favor upwelling are those that have an upcoast component; i.e., for this discussion, from Brownsville toward New Orleans. As a first step

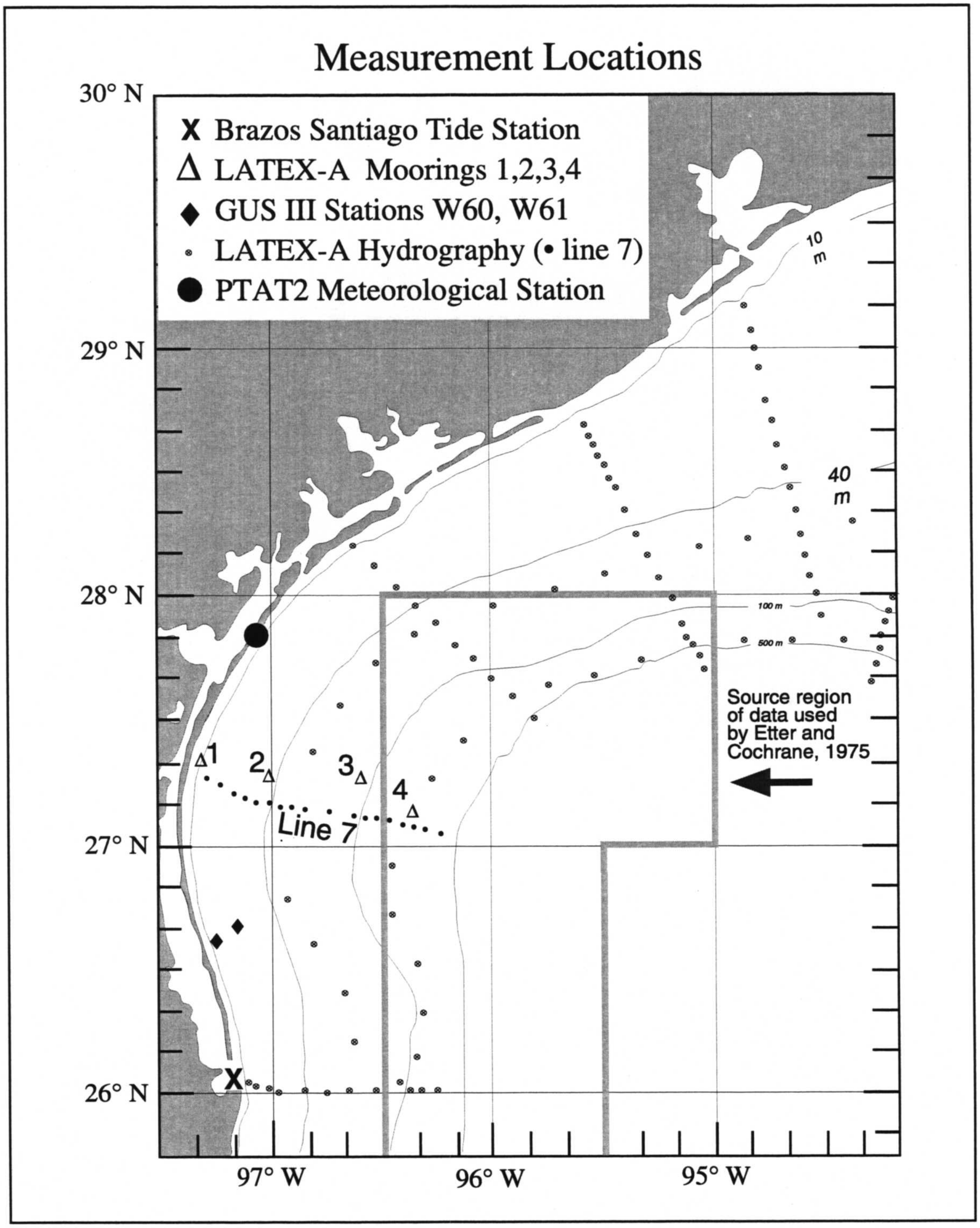

Figure B.3-1. Basemap of the south Texas shelf showing the locations where data discussed were measured.

then, we examine the meteorological record for times when the alongshelf component of the wind is conducive to upwelling.

Monthly mean alongshore wind stress from the climatology prepared by Hellerman and Rosenstein (1983) for 26°, 27°, and 28°N along the Texas coast (Figure B.3-2) shows that alongshelf components are stronger in the south than in the north. This is primarily a consequence of a coastline orientation that is nearly meridional at 26° and 27° and bends toward a more zonal orientation at 28°N. In the south, the alongshore stress becomes upcoast during March or April, reaches maximum strength in late May to early June, and persists until September. In the north, near 28°N, upcoast stress begins mid-May, peaks in July, and is downcoast after August. Examination of the monthly mean alongshore wind stress from station data at Brownsville, Corpus Christi, and off Freeport shows good agreement with the climatology.

Evidence that alongcoast currents over the inner shelf respond to alongshelf wind forcing has been presented throughout this report. Further support for the south Texas inner shelf is given in Table B.3-1. At moorings 1-3 (Figure B.3-1) the 10-m currents were downcoast during April to early May in all three LATEX years. From late May through June they were upcoast two of three years. In July and early August currents were strongly upcoast in each year.

Near-surface mean temperatures for the outer shelf and off shelf are compared to inner shelf stations in Figure B.3-3. Offshelf stations, represented by the bathythermogram compilation of Etter and Cochrane (1975), show an annual cycle with a temperature maximum occurring in August. Nearshore stations follow the offshore warming trend closely until June when the inshore stations begin decreasing to local minima in July. This decrease is attributed to upwelling resulting from upcoast alongshelf wind components. After July, the inner station temperatures gradually increase but do not reach the offshore temperatures until mid-September. Because the current meters were deployed 10 to 14 m below the surface they recorded lower temperatures than those at the surface throughout the year, but they also show a decrease in temperature in July. Although the winds are favorable to upwelling in April and May, cooling in the nearshore waters is not apparent in the monthly averages during these months. This may be due to stratification effects or to upwelling winds being more episodic and weaker in April than in June.

Salinities from the Brazos Santiago tide station and the GUS III cruises (Figure B.3-3 lower panel) increase from May through July or August, and then decrease until October. While increasing salinity is an expected consequence of upwelling, higher salinities can result from the advection of water from the south due to the seasonal reversal in the general circulation at this time of the year. Thus, salinity is not a definitive indicator of upwelling in this region.

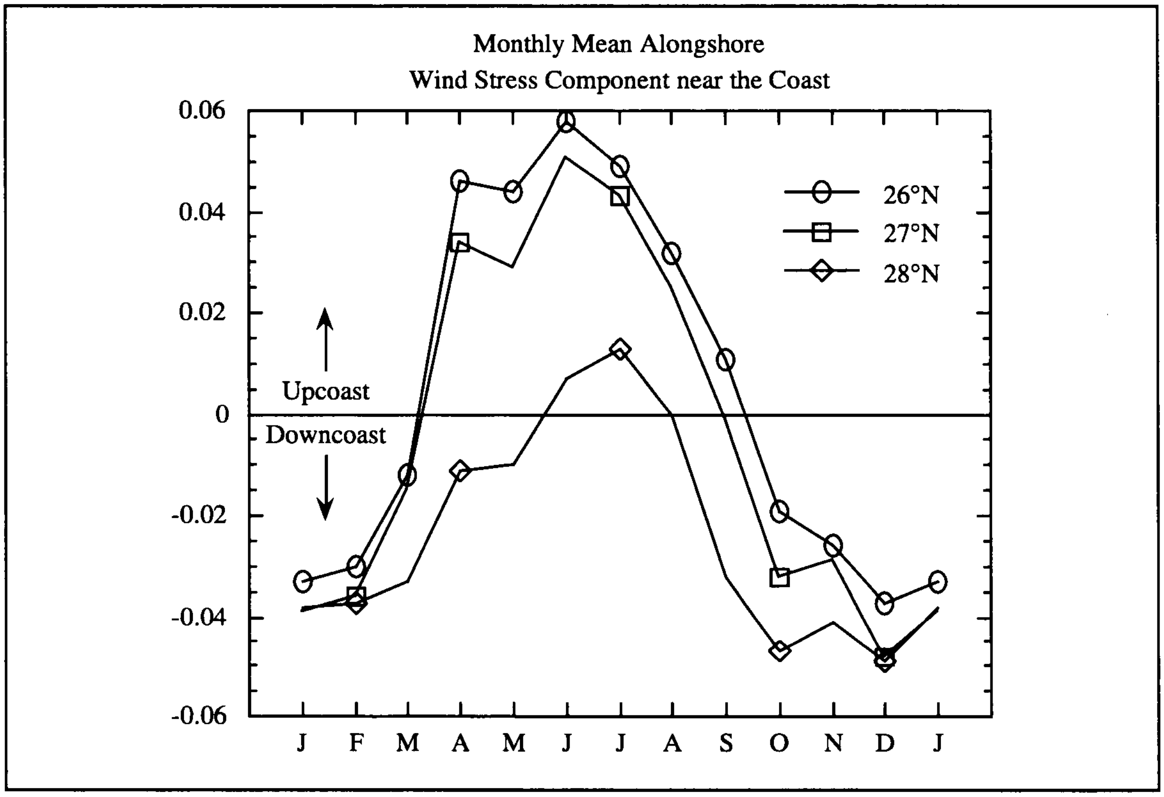

Figure B.3-2. Monthly mean alongshore wind stress component near the coast based on Hellerman and Rosenstein (1983).

Table B.3-1. Six-week means of the alongshore component of currents ($cm \cdot s^{-1}$) at top current meters (10-14 m depth) of moorings 1, 2, and 3 combined. Negative currents are downcoast. All table entries have been given equal weight in computing multi-year means.

	1992	1993	1994	Mean
8 Apr - 19 May	-0.65	-1.08	-8.09	-3.27
20 May - 30 Jun	<5.52>$_3$	-4.44	2.57	1.22
1 Jul - 11 Aug	<4.80>$_3$	<4.76>$_2$	6.72*	5.43
12 Aug - 23 Sep	-5.11	<5.62>$_2$	—	0.26

< > A six-week mean for one of the moorings, identified by subscript, is missing.
* Records ended 27 July.

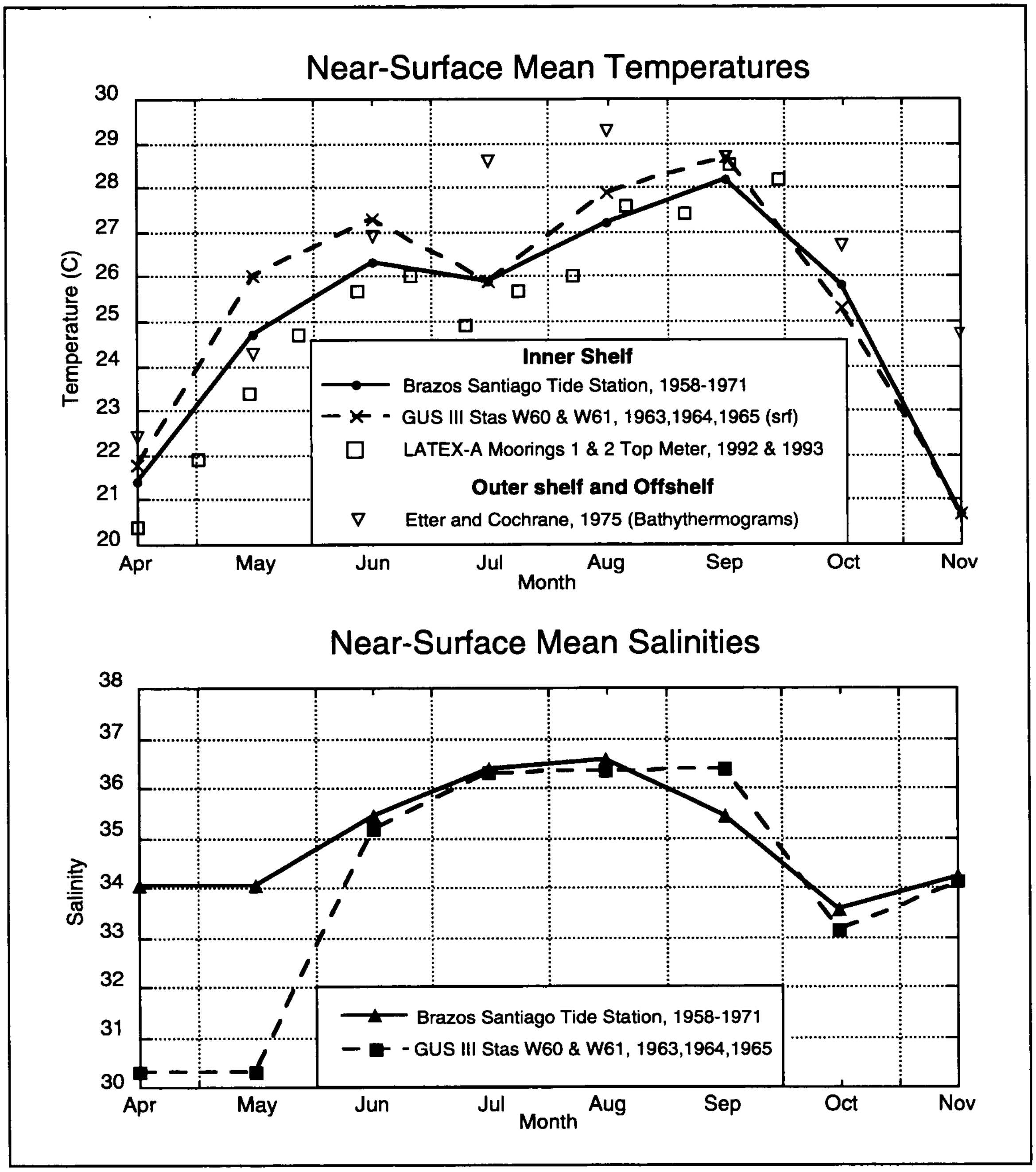

Figure B.3-3. Near-surface mean temperatures and salinities from various locations over the inner shelf and over the outer shelf and offshore.

Compelling evidence of upwelling along the Texas coast is seen in a sequence of AVHRR infrared satellite images taken in 1993 on 7 July, 1 August (shown in Figure B.3-4), and 18 August. They show a coastal cool band of water extending from 24°N to 28°N inshore of the 50-m isobath, coldest in July and waning in early August but still evident in the mid-August image. Table B.3-2 shows the relative frequency of coastal cool bands based on a subjective analysis by John Cochrane (personal communication) of the infrared imagery charts supplied by NOAA/NOS for the months June-September of 1992-1994 (nine charts per month). There is a significant increase in the relative frequency of occurrence of coastal cool bands from June to July, decreasing in August in some years, and definitely less frequent in September. Contour plots of near-surface temperature taken from the LATEX hydrography cruises in early August 1993 and 1994 (Figure B.3-5) confirm that low temperatures exist along the coast and range from 26-27°C in the south to 29-30°C upcoast.

Evidence of upwelling can be seen in the vertical sections of potential density and temperature in Figure B.3-6. In May 1993, isopycnals of potential density anomaly (σ_θ) slope downward toward shore indicating that upwelling is not occurring; in fact, the reverse may be true. In August, the isopycnals and isotherms slope upward toward shore, consistent with upwelling. Shown in Figures B.3-7 and B.3-8 are corresponding fields of near-surface salinity and geopotential anomaly of the surface (3 db) relative to 400 db (calculated as described in Appendix H.1). The fields further describe these before and after upwelling situations.

Figure B.3-9 shows a six-month time series (April-September 1992) of 40-hr low-passed alongshelf wind stress from PTAT2 and alongshelf currents from the top meter on mooring 1, with raw temperature and salinity series from the same current meter. One sees there is fair correlation between major upcoast wind events and episodes of upcoast currents. The most interesting effect is found in the temperature record, which gradually increases until mid-June when a sharp 6-7°C drop occurs and persists for about a month. During the same period salinity increases 4-5 PSU and remains relatively constant for some time. A similar pattern is seen in 1993 although it occurs near the beginning of July. Conductivity data for 1994 were not available, but the temperature record showed an analogous drop in late June.

Discussion

Mean wind stress is favorable for upwelling along much of the western boundary of the Gulf of Mexico between 20°N and 28°N from April through August. Available near surface temperature records, however, indicate that the episodic upwelling that surely occurs in April and May is too infrequent or weak to be discerned in the mean temperature records for those months. Available current measurements suggest a downcoast mean current for April and May, consistent with weak upwelling. Because the mean near surface salinity for June is markedly above the April and May means, and the mean alongshelf current then is weakly

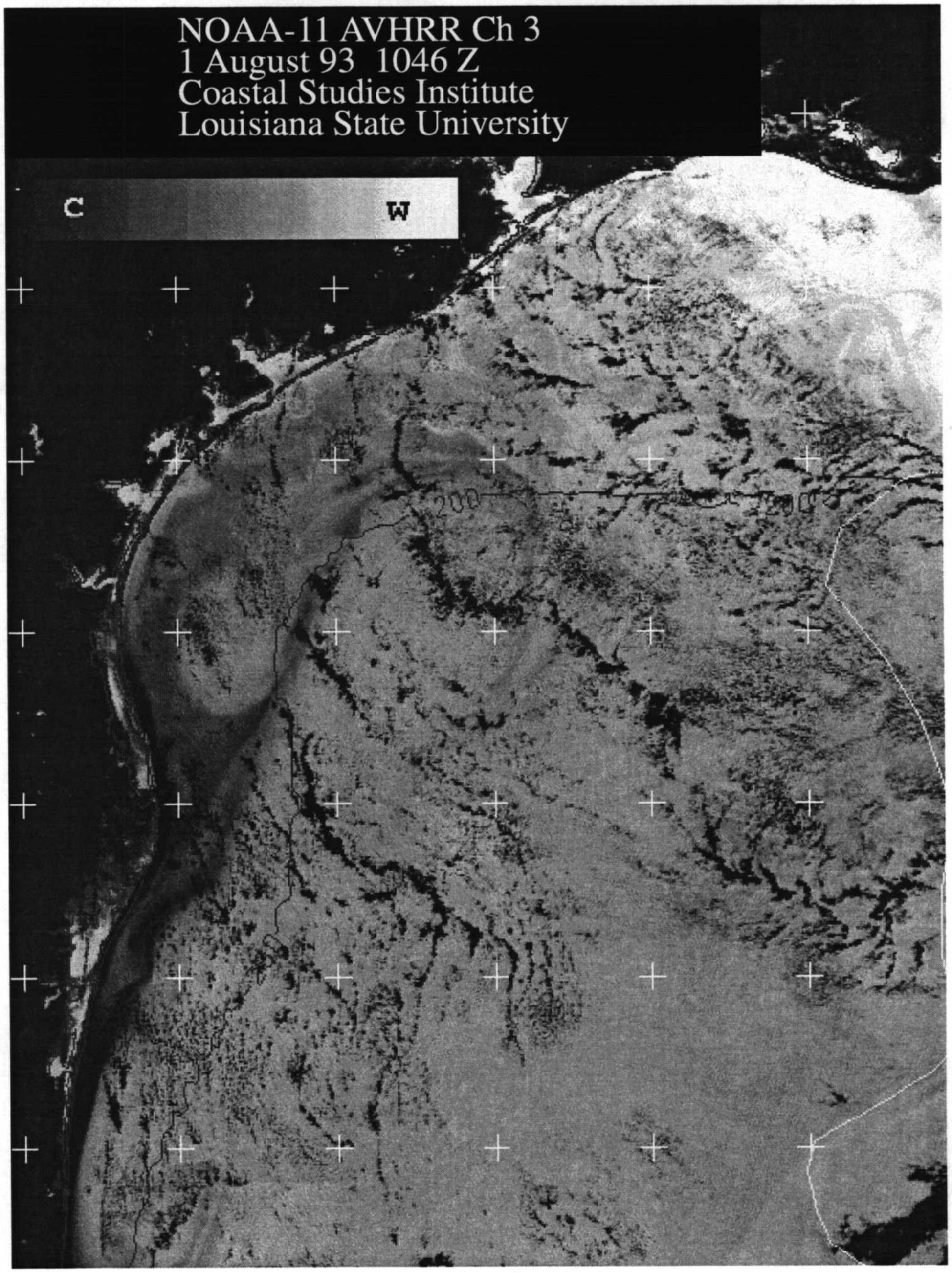

Figure B.3-4. AVHRR image for 1 August 1993 showing a coastal cool band of surface temperatures along the south Texas coast.

Table B.3-2. Relative frequency of occurrence per month of coastal bands that are cooler by 2°C or more than the adjacent open Gulf and extend 4° or more in latitude along the western boundary. An entry of 0.33, e.g., means that cool coastal bands were evident during a third of the month. Based on NOAA/NOS/OPC Oceanographic Features Analyses.

	June	July	August	September
1992	0.33	0.78	0.33	<0.11
1993	<0.11	0.89	0.44	0.22
1994	0.33	0.89	0.89	0.44
Mean	0.22	0.85	0.56	0.22

upcoast, June appears to be a transition month. Marked upwelling and an upcoast current are mean conditions for July and August on the basis of all types of data available.

In the latter half of June or in July of 1992, 1993, and 1994, the inner shelf mooring near 27°N, after a moderate upcoast wind fluctuation, experienced a rapid 4-5°C drop in temperature, which persisted for more than a month in both 1992 and 1993, and with some short interruptions, also in 1994. Further investigation is needed on wind-current interrelation and particularly study of the end of sustained upwelling in late August or early September.

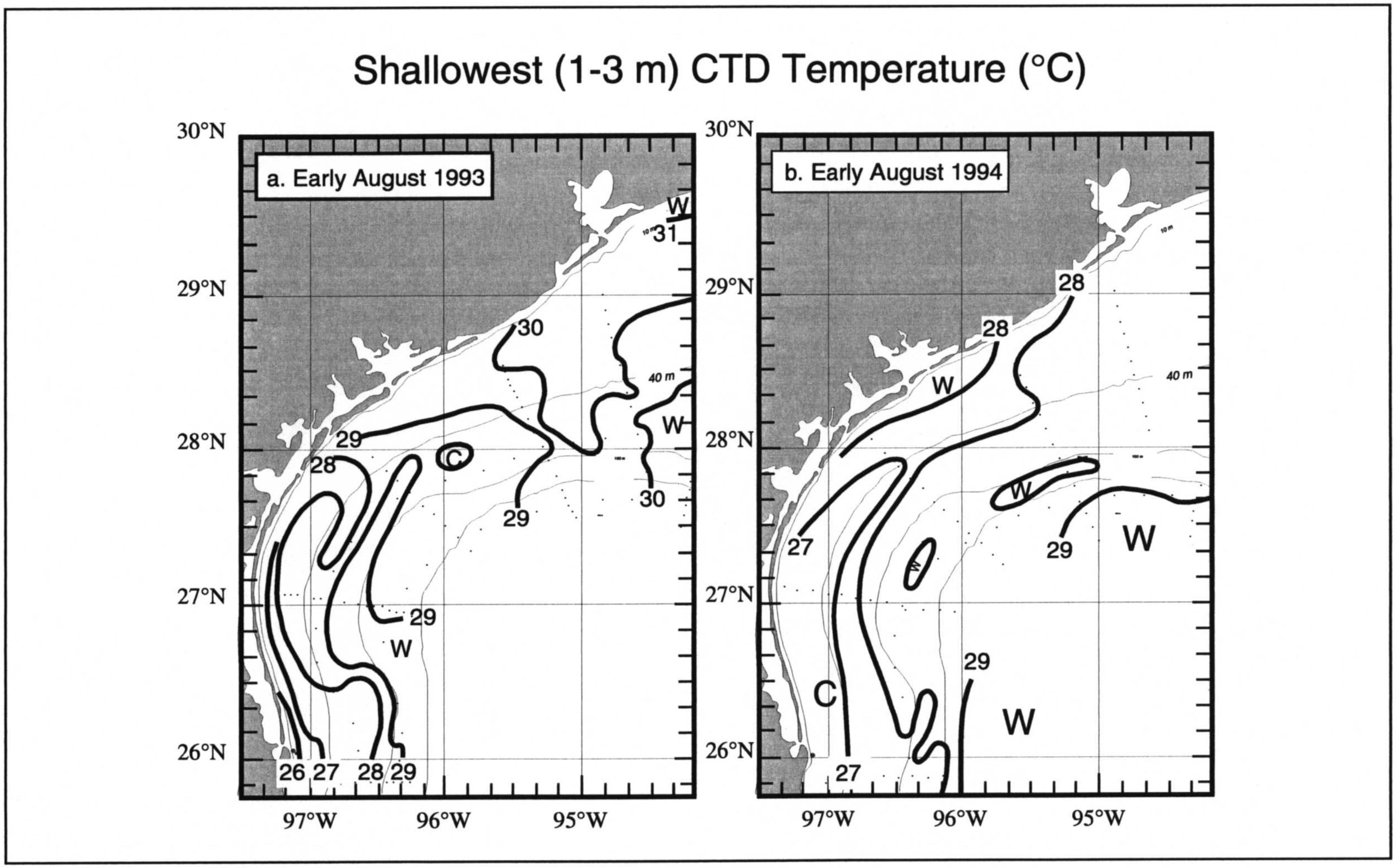

Figure B.3-5. Near-surface (1-3 m) temperature contours from CTD data collected on hydrography cruise (a) H06 in early August 1993 and (b) H09 in early August 1994. Isolated bands of relatively cool water, indicative of upwelling, were found near the surface along the south Texas coast both years.

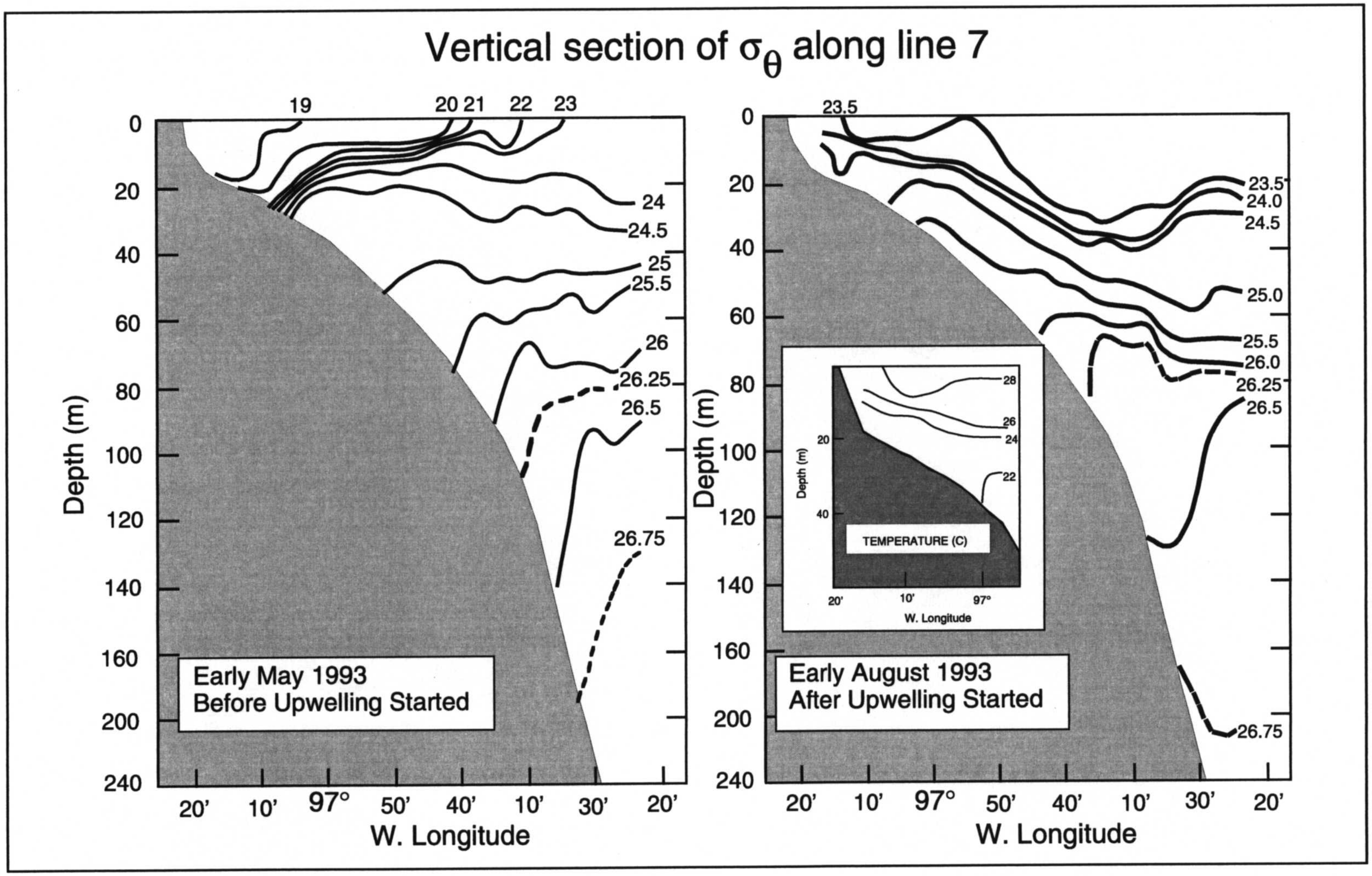

Figure B.3-6. Vertical section of σ_θ along line 7 in early May and early August 1993 and temperature in August 1993.

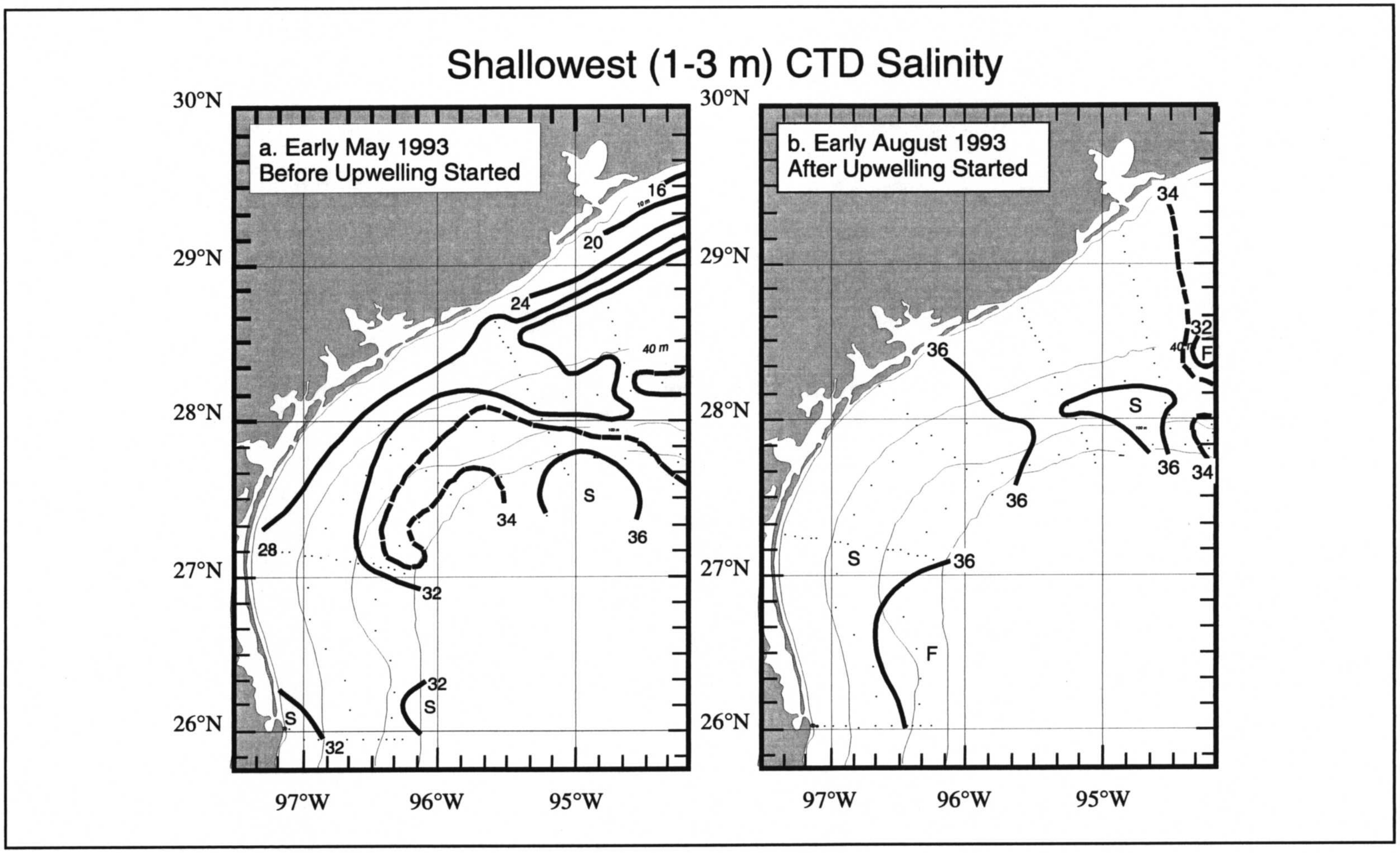

Figure B.3-7. Near-surface (1-3 m) salinity contours from CTD data collected on hydrography cruise (a) H05 in early May 1993 and (b) H06 in early August 1993. High-salinity (> 36) is found throughout the water column as a result of advection of high salinity water from the south.

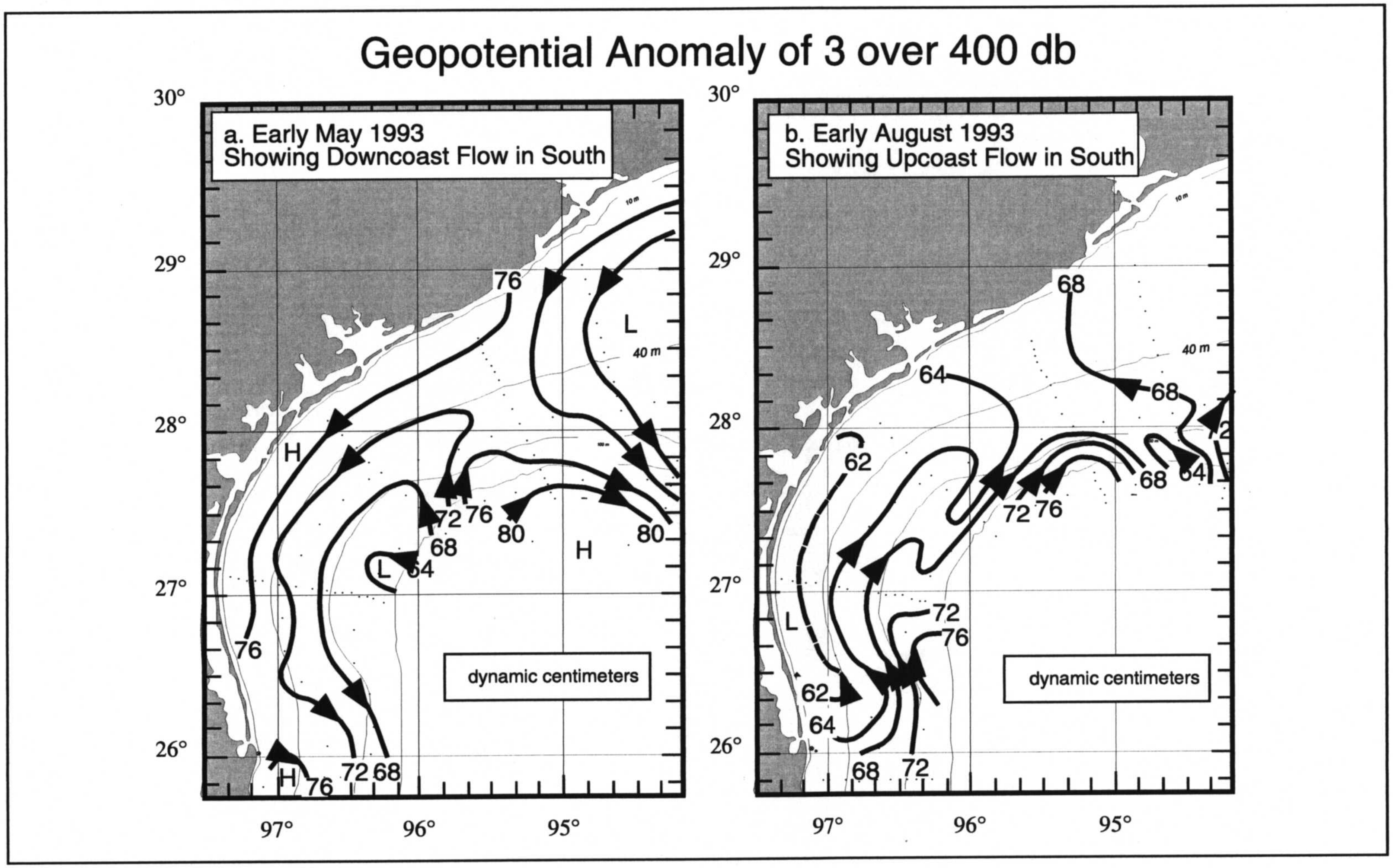

Figure B.3-8. Geopotntial anomaly of the surface relative to 400 db in (a) early May 1993 from CTD data collected on cruise H05 and (b) in early August 1993 from data collected on cruises H051 The flow is downcoast in May and upcoast in August following the change in prevailing winds.

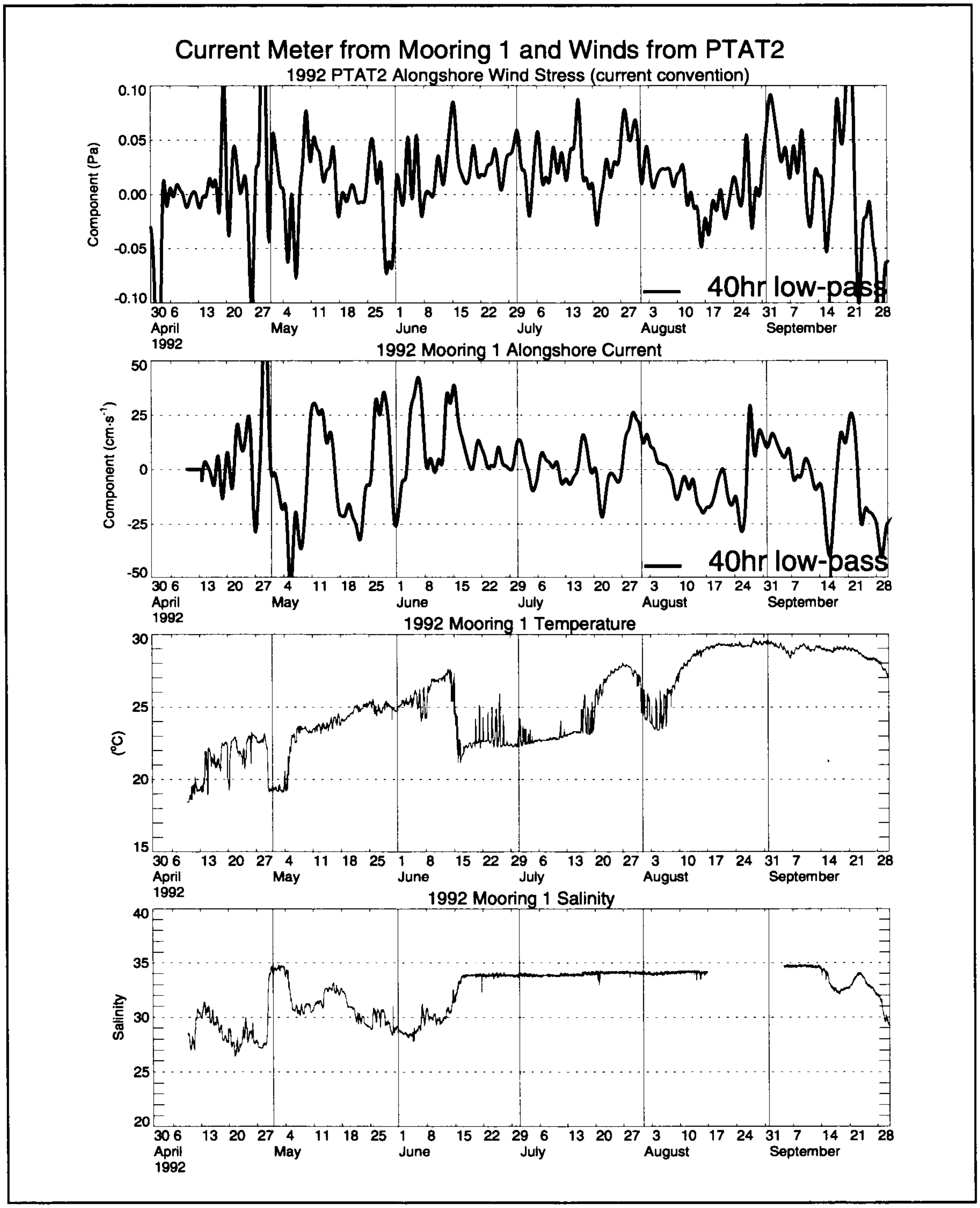

Figure B.3-9. Filtered alongshore wind stress and currents (positive upcoast) with unfiltered temperature and salinity from mooring 1 top and PTAT2 for the period April-September 1992.

Appendix C: Effects of the Texas Flood of October 1994

The Texas flood of October 1994 was the worst recorded in 500 years of local history. Rainfall in southeast Texas for the four-day period 15-19 October ranged from 8 to 28 inches (Liscum and East 1995). A combination of meteorological events—residual atmospheric moisture over southeastern Texas associated with Hurricane Rosa and moisture drawn from the Gulf of Mexico by a low pressure system in the Rockies—spawned vigorous thunderstorms that resulted in severe flooding. The USGS states that historical peak streamflows were exceeded at 23 of 43 stations monitored in the area. The criteria for the 100-year flood were met or exceeded at 19 of the 43 stations, and three streams crested from five to eleven feet above previous maxima. Twenty-three lives were lost, 38 counties were declared disaster areas, and the cost of government assistance came to $112.8 million.

The resulting freshwater input to the shelf was substantial, as seen in the discharge of the Texas rivers for 18-28 October (Figure 2.3-5). Their combined flow on 19 October exceeded that of the Mississippi-Atchafalaya discharge and provided an extremely strong buoyancy signal on the Texas inner shelf. The single largest contribution came from the San Jacinto River, as described in Section 2.3, but the Brazos, Colorado, Lavaca, Neches, and Trinity Rivers contributed significant amounts as well. Of these six rivers, two discharge onto the shelf directly, the Brazos and the Colorado, and four discharge indirectly: the Neches through Sabine Pass, the Trinity and San Jacinto through Galveston Bay, and the Lavaca through Matagorda Bay. Both Galveston and Matagorda Bays lie behind barrier islands and peninsulas.

Consistent with the non-summer circulation pattern, currents along the inner shelf showed a strong and persistent downcoast surface flow during the period (Figure H.2-3 for October 1994). Hence, freshwater input to the inner shelf would have been transported downcoast and represented in the salinities recorded by the moored current meters to the south. Mooring 23 was offshore and slightly downshelf of the Brazos River discharge (Figure 1.2-1). It was the nearest meter to the large freshwater source provided by the San Jacinto. The current meter record shows (Figure C-1) a strong and recognizable decrease in the 10-m salinity beginning around 20 October and continuing through 30 November, at which time it returned to pre-event levels. Associated with the decrease in salinity was a strong diurnal oscillation, which could be attributed to movement of a coastal current front back and forth over the meter. The salinity recorded at the next mooring seaward (24 top) did not show a similar pattern and remained relatively unchanged during this period. Given a mean alongshelf velocity of 20 $cm \cdot s^{-1}$, it should have taken approximately 12 days to travel the 213 km between mooring 23 and the next adjacent southern mooring 2. (No salinity record is available for mooring 1 top for the period in question.) The mooring 2 top current meter, located well to the south of the Brazos River, recorded a rapid decrease in salinity beginning around

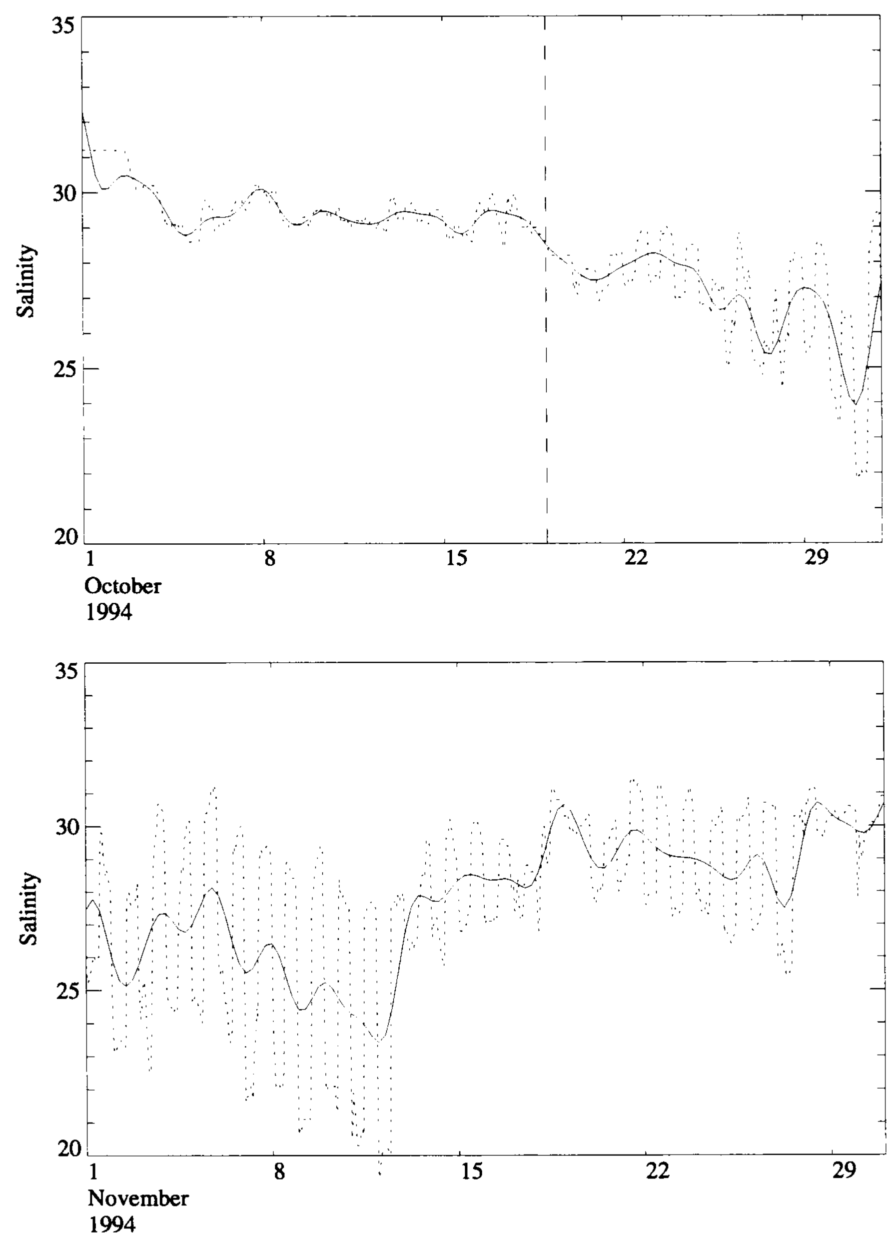

Figure C-1. Raw (dotted) and 40-hr low-pass (solid) salinity for mooring 23 at 10 m for October (top) and November (bottom) 1994. The peak river discharge occurs on 19 October 1994 (dashed).

27 October with diurnal oscillations (Figure C-2). This recording was similar to that of mooring 23 top, except that it did not persist as long.

LATEX hydrographic cruise H10 was conducted two weeks after the flood, from 1-14 November 1994. Horizontal plots of salinity (Figure C-3) at 3 m, 12 m, and the bottom show a significant amount of lower salinity water (≤ 30) remained along the Texas inner shelf and, in particular, off the mouth of the Brazos (line 5). This is in contrast to the November cruise of the previous year, H07, which showed higher salinities (≥ 30). The vertical sections of salinity (Figure C-4) for line 4, located south of Sabine Pass, line 5, located off the Brazos River, and line 6, off Matagorda Bay, show that the lower salinities occurred quite close to shore on line 4 and then spread across the shelf on the downshelf sections. These sections were compared with those from H07, when the Texas river outflow was inconsequential relative to the Atchafalaya input. The comparisons substantiate definite freshening of the nearshore salinity field by the extraordinary river discharge of 1994.

The AVHRR image (obtained from Nan Walker of the Coastal Studies Institute, LSU) for 20 October 1994 shows well defined plumes seaward of Galveston Bay and the Brazos and cold water in the Lavaca Bay. The image for the following day shows that the inner shelf from the Sabine Pass to the Lavaca Bay was colder than the previous day, indicating that cooler river water was flowing onto the shelf. The 6 November 1994 image clearly shows cold water on the inner shelf against the coast from Atchafalaya Bay to the Lavaca.

There were two full shelf LATEX A hydrographic surveys during the peak spring discharge of the Mississippi-Atchafalaya rivers: H05 (25 April-11 May 1993) and H08 (29 April-5 May 1994). Comparison of salinity contours over the inner shelf off Texas on lines 4, 5, and 6 for November 1994 cruise H10 (Figure C-4) with those from the spring cruises H05 and H08 (Figures C-5 and C-6) shows that the 1994 Texas flood led to nearshore salinity distributions similar to those caused by the Mississippi-Atchafalaya spring discharge. The magnitude of the spring Mississippi-Atchafalaya is, of course, much larger than that of the 1994 Texas rivers, but the input occurred some 400 km upcoast.

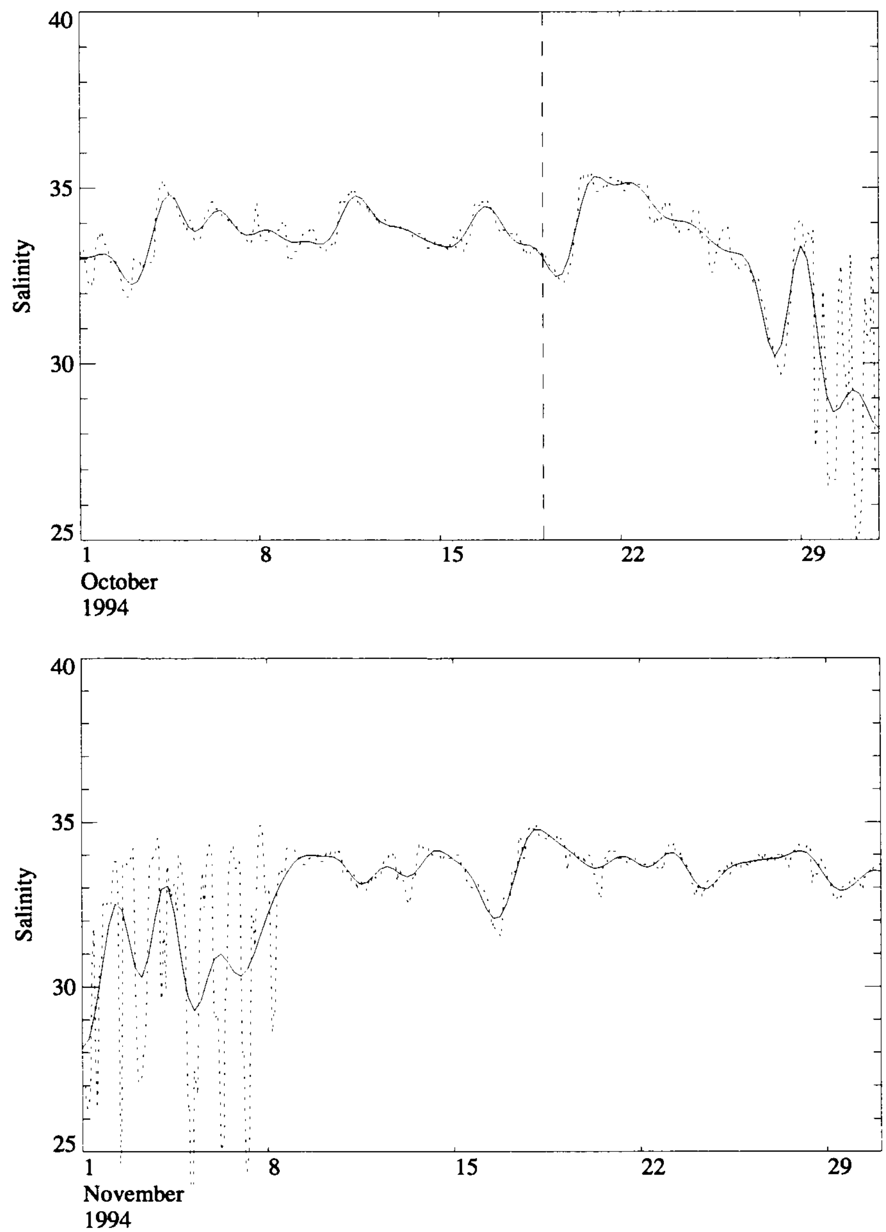

Figure C-2. Raw (dotted) and 40-hr low-pass (solid) salinity for mooring 2 at 10 m for October (top) and November (bottom) 1994. The peak river discharge occurs on 19 October 1994 (dashed).

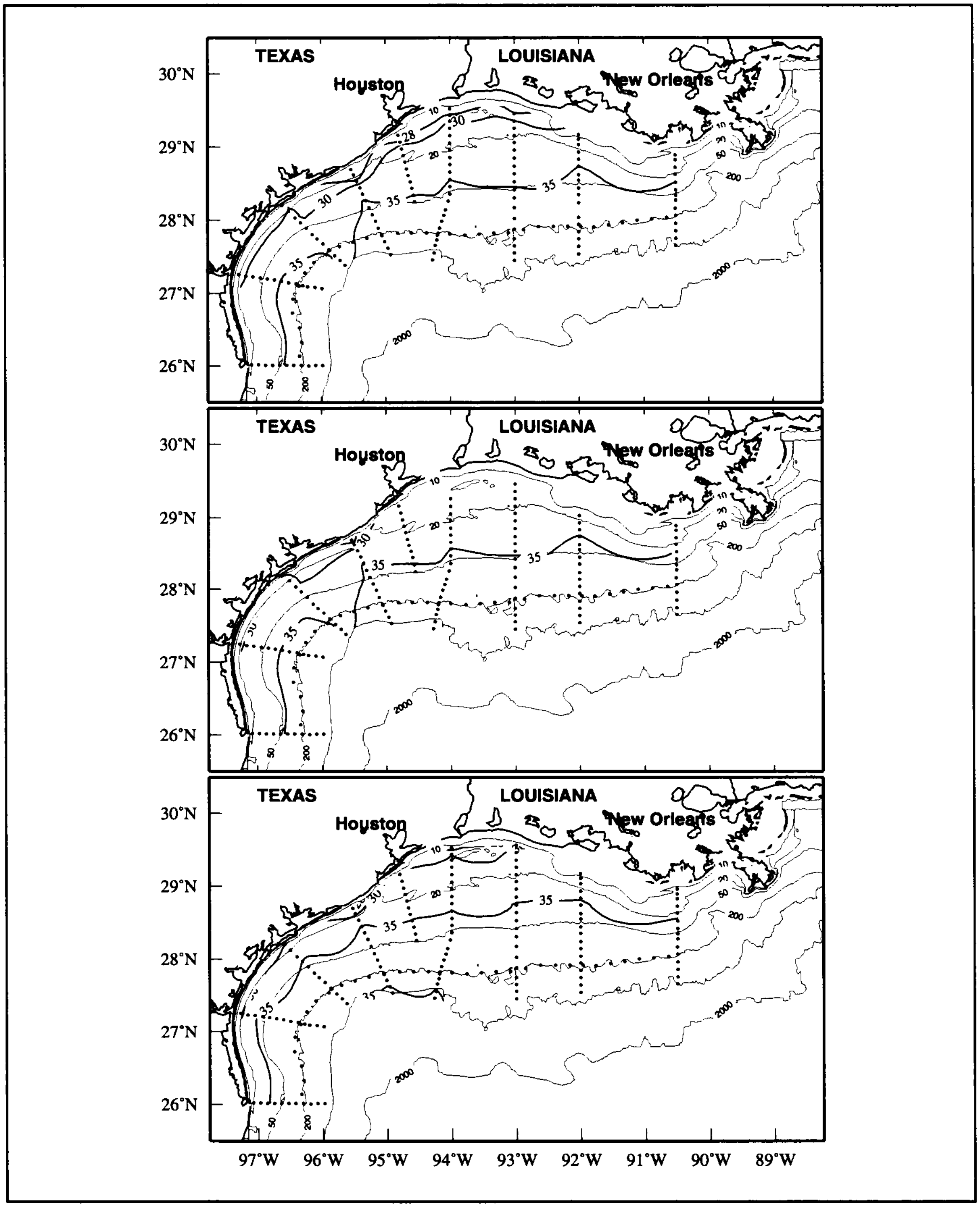

Figure C-3. Surface (3-m) (upper), 12-m (midle), and bottom (lower) salinity for LATEX A cruise H10 in November 1994.

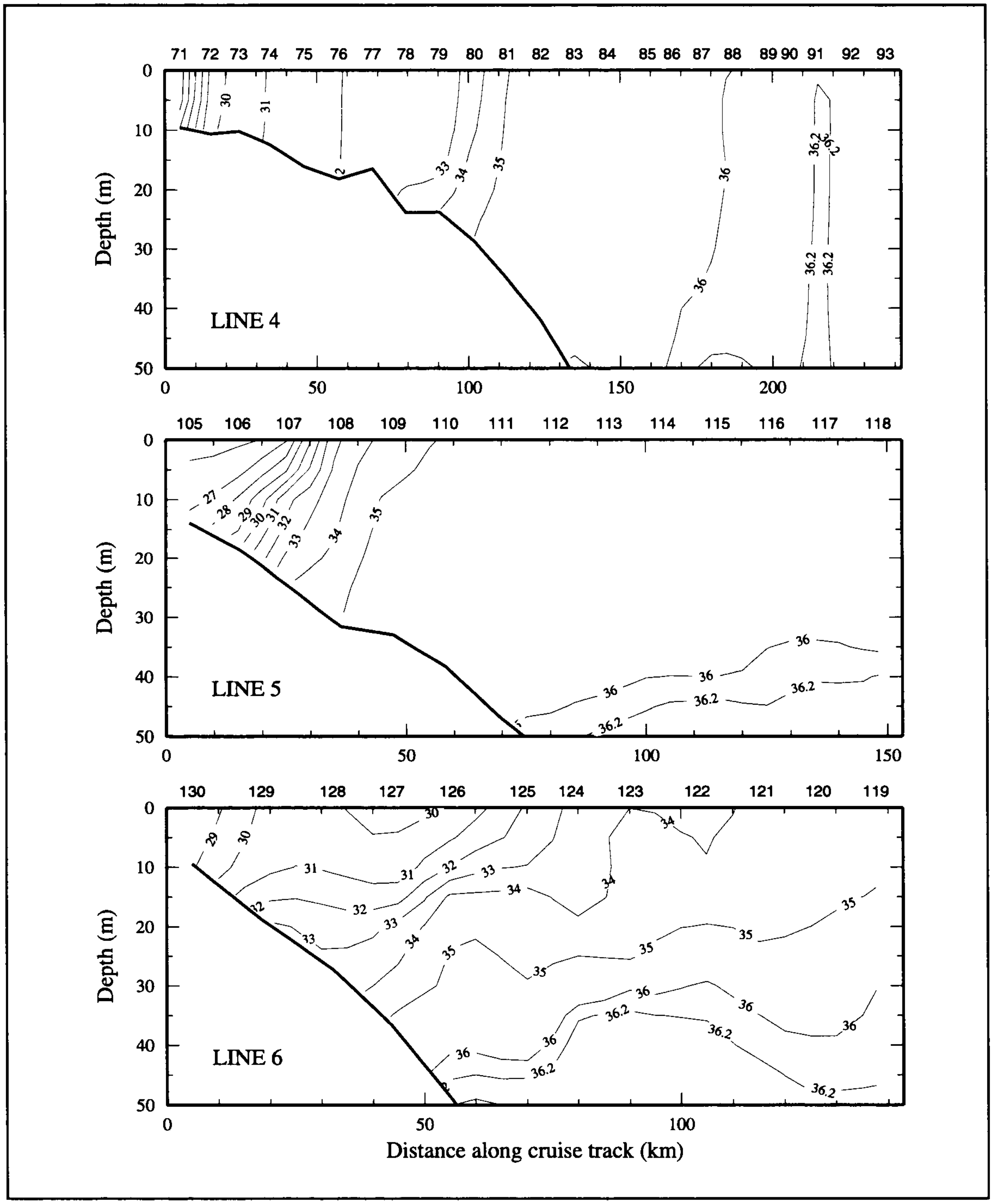

Figure C-4. Contours of salinity in vertical sections for LATEX A cruise H10 (2-3 November 1994). Sections are from onshelf on the left to offshelf on the right.

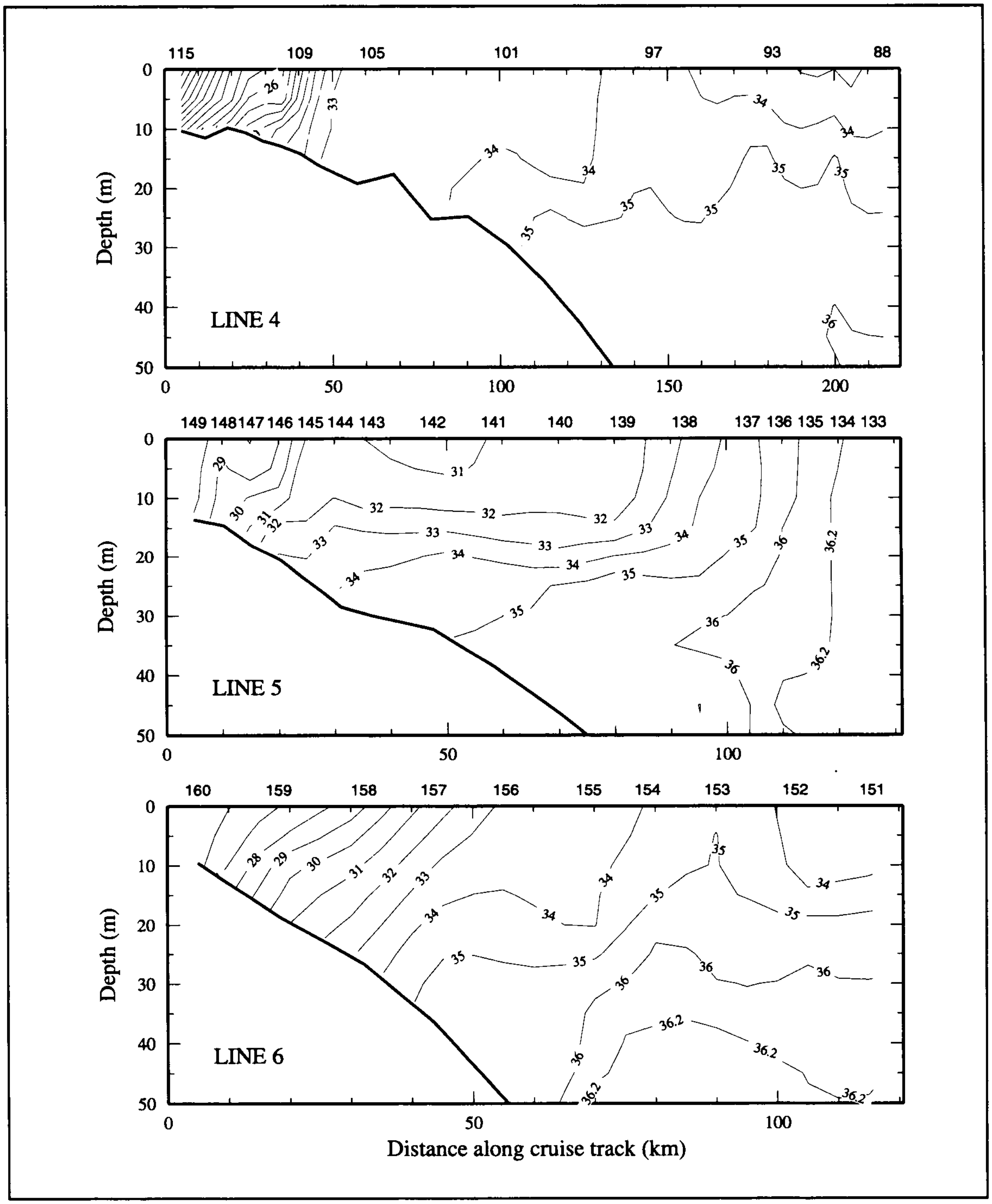

Figure C-5. Contours of salinity in vertical sections for LATEX A cruise H05 (25 April-11 May 1993). Sections are from onshelf on the left to offshelf on the right.

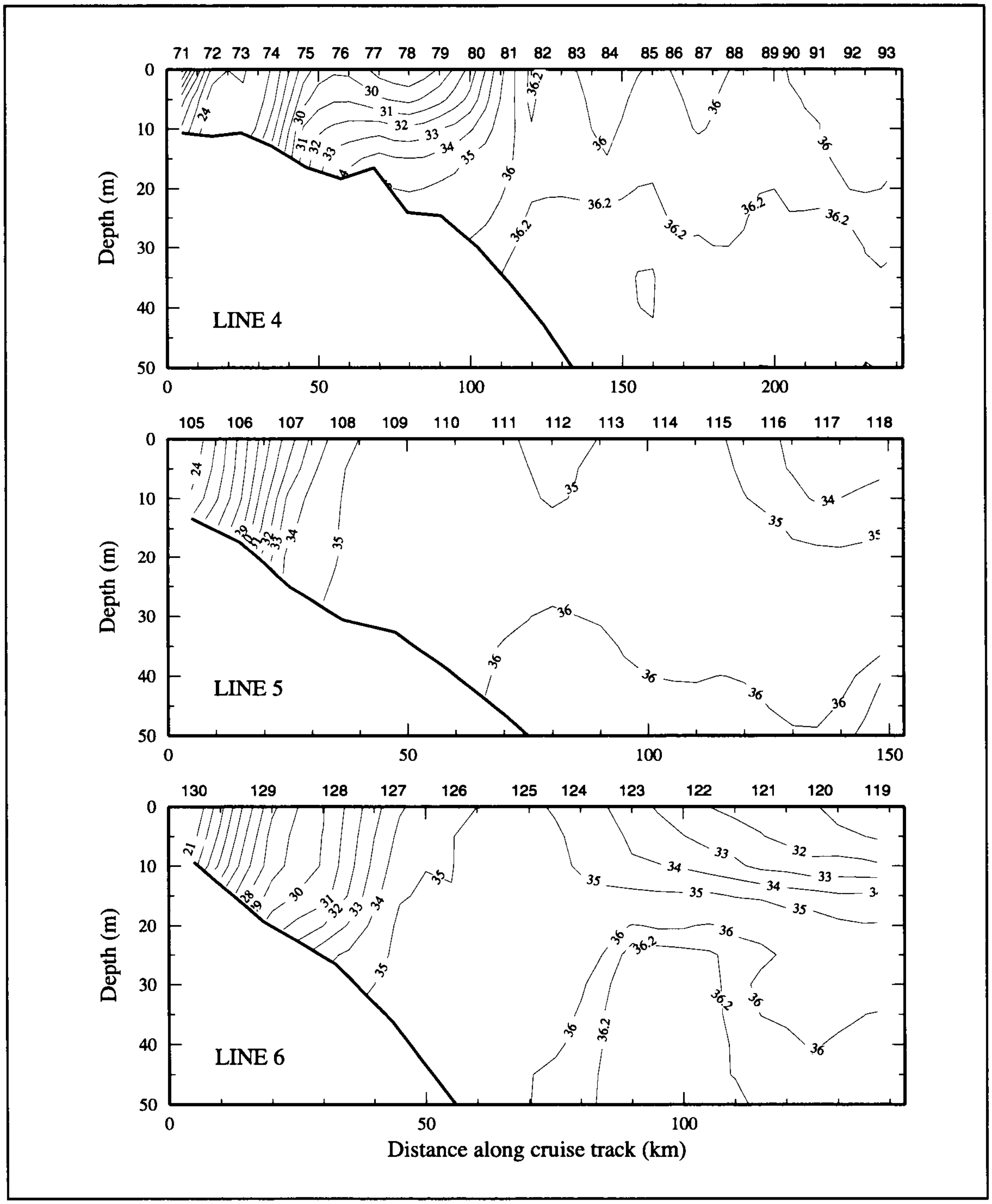

Figure C-6. Contours of salinity in vertical sections for LATEX A cruise H08 (23 April-7 May 1994). Sections are from onshelf on the left to offshelf on the right.

APPENDIX D: CASE STUDY OF EDDY VAZQUEZ

Of the Loop Current eddies noted during the LATEX field program, Eddy Vazquez (V) had the greatest impact on Texas-Louisiana shelf circulation. The evolution of Eddy V in the western Gulf of Mexico was studied using satellite altimeter data provided by CCAR. Hydrographic, current meter, drifter, XBT, and satellite AVHRR data corroborated interpretations based on altimeter data. Eddy V was an identifiable anticyclonic feature for a year, from September 1992 through September 1993. This section presents the evolution of Eddy V and discusses its influence on the Texas shelf circulation. Additional analyses of Eddy V and other eddies observed during the LATEX period are given in Berger et al. (1996).

Evolution of Eddy V. The track of drifter 2447, deployed by LATEX A at the 200-m isobath near 28°N, 92°W on 4 August 1992, traced the movement of Eddy V from September 1992 until the drifter failed in early February 1993 (Figure D-1). On deployment, the drifter was rapidly drawn over the shelf edge by Eddy U. It made one circuit in that eddy before moving into Eddy V in mid-September 1992. In September, Eddy V migrated westward along the 2000-m isobath at the foot of the continental slope. Vukovich and Crissman (1986) consider this pathway to be the least common for Loop Current eddies moving into the western Gulf.

In October, Eddy V turned southward due to topographic steering between 93° and 94.5°W, where the bottom shallows to the west (Figure 2.5.1-4). The shelf edge current velocities show east-west flow with no strong offshelf transport in the region at that time. This is evidence that the southward turning of Eddy V was not the result of veering by entrainment of shelf water, a suggested mechanism for eddy veering at this location (Lewis et al. 1989; but see Glenn and Ebbesmeyer 1993). The southwestward translation of Eddy V slowed briefly in mid-October as the eddy interacted with the remnant anticyclonic Eddy T_n (Figure 2.5.1-1). Eddy T_n then coalesced with Eddy V.

After it passed 94.5°W during November, Eddy V turned to the northwest and moved into the eddy graveyard, the northwest corner of the open Gulf. It remained there from November 1992 through March 1993 (Figures 2.5.1-4 and D-1). The presence of Eddy U to the southeast likely had prevented Eddy V from continuing westward through the deeper part of the Gulf, as had occurred with other eddies after veering southward (Lewis et al. 1989). While Eddy V was to the east of and moving past the shallowing topography, it had blocked the westward movement of Eddy U, which stalled, with its center around 24.5°N, 89.7°W, in October. Eddy V's progress around the topography in November freed Eddy U to move westward. With Eddy V in the northwest corner, Eddy U did not move due west through the deep, central Gulf waters. Instead, Eddy U moved southwest to the Mexican slope. As Eddy U moved northward along the Mexican slope, the two anticyclones met in a series of encounters from November 1992 through March 1993.

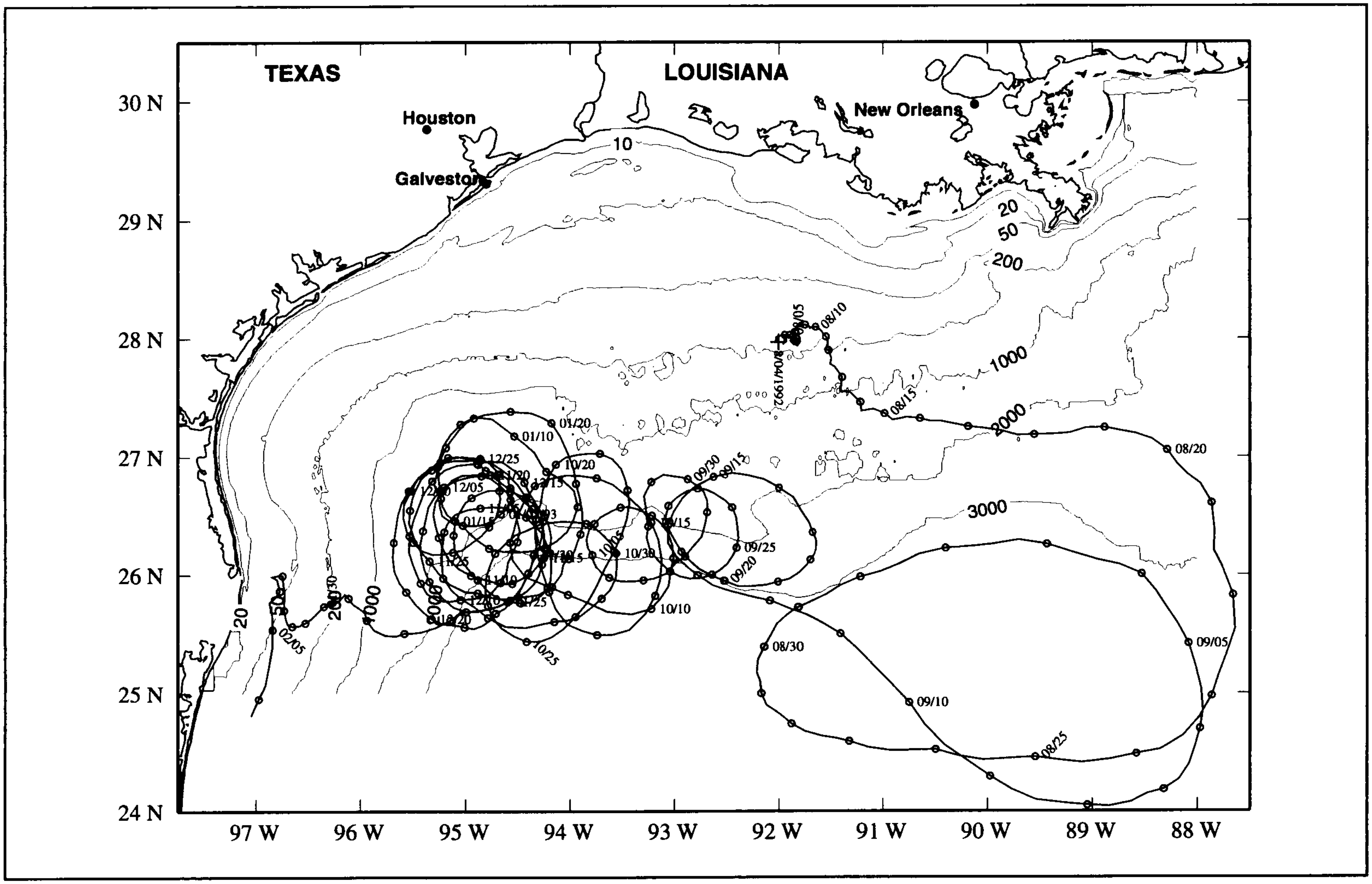

Figure D-1. Track of LATEX A drifter 2447 from its deployment on 4 August 1992 to its failure on 6 February 1993. Circles are the locations at 2200 hrs (UTC) for each day.

In mid-March and April, Eddy V elongated north-south. The SSHA maps (Figures D-2 and D-3) show this elongation was caused by interactions with Eddy U and with cyclones to the east and west. During the exchange with Eddy U, Eddy V gained mass, as indicated by the increasing areal extent and SSHA maximum of Eddy V and decreasing extent of Eddy U. Evidence of this is supported by the LATEX C drifter 2449, which moved out of Eddy U, where it had been since October 1992, into Eddy V (Figure D-2a). As the eastern cyclone elongated north-south, so did Eddy V, developing multiple SSHA maxima in the process (Figures D-2b and D-3a). The bulk of Eddy V and the eastern cyclone moved south, the direction of the strong flow between the two features. During this time, the SSHA maps suggest that Eddy V spun up a cyclone to its west. In May, as the elongation of Eddy V continued, the western cyclone strengthened (Figure D-3a). In regions adjoining Eddy V, the western cyclone moved water northward while the eastern cyclone moved water south. The two cyclones effectively eroded Eddy V, splitting it into north and south eddies, Eddy V_n and Eddy V_s (Figure D-3b). Once Eddy V was split, the east and west cyclones coalesced. The approximate diameters of Eddy V_n and Eddy V_s after the split were 150 km and 220 km, respectively (Figure D-3b; see also Figure H.1-7).

Temperature and salinity data from cruise H05 (25 April-11 May 1993) substantiate that Eddy V_n had the characteristics of a Loop Current eddy, confirming that Eddy V_n was split off Eddy V. Figure D-4 shows the potential temperature and salinity along the 200-m isobath from approximately 94°W to the southern edge of the survey area. By the deepening isotherms that are characteristic of anticyclonic eddies, the potential temperature shows the northern edge of Eddy V_n located approximately between 94.3°W and 95.9°W (from station 212 to between stations 206-207), and the cyclone extended between 27.5°N, 95.9°W and 26.3°N, 96.3°W (from between stations 206-207 to station 202). These locations compare well with those from the SSHA and geopotential anomaly data (Figures D-3 and H.1-7). The core of the salinity maximum associated with Eddy V_n at the shelf edge was greater than 36.6 at temperatures about 20°C, which is indicative of the Subtropical Underwater water mass brought into the Gulf by Loop Current eddies (Elliott 1982).

After the split, Eddy V_s moved to the south where it interacted with the remnant of Eddy U and with cyclones to its north and south. This resulted in its east-west elongation (Figure D-5a), and, in June, its translation eastward across the central Gulf. Eddy V_s coalesced with an unnamed anticyclonic eddy, centered at about 23.5°N, 92°W, that had formed in the course of an interaction between Eddy U and Eddy V in March 1993. During July and August 1993, Eddy V_s coalesced with Eddy W_s (the southern part of Eddy W that also had split into two parts) and ceased to be a separate, identifiable anticyclonic Loop Current eddy (Figure D-5b).

Eddy V_n, which abutted the north continental slope at about 94°W (Figure D-3b), moved west until it adjoined the north and west continental slopes off Texas between 95.5°W and 96.3°W (Figure D-5a). In June and July, Eddy V_n elongated to the northeast-southwest (Figure D-5); it developed into a peanut shape with two SSHA maxima (compare

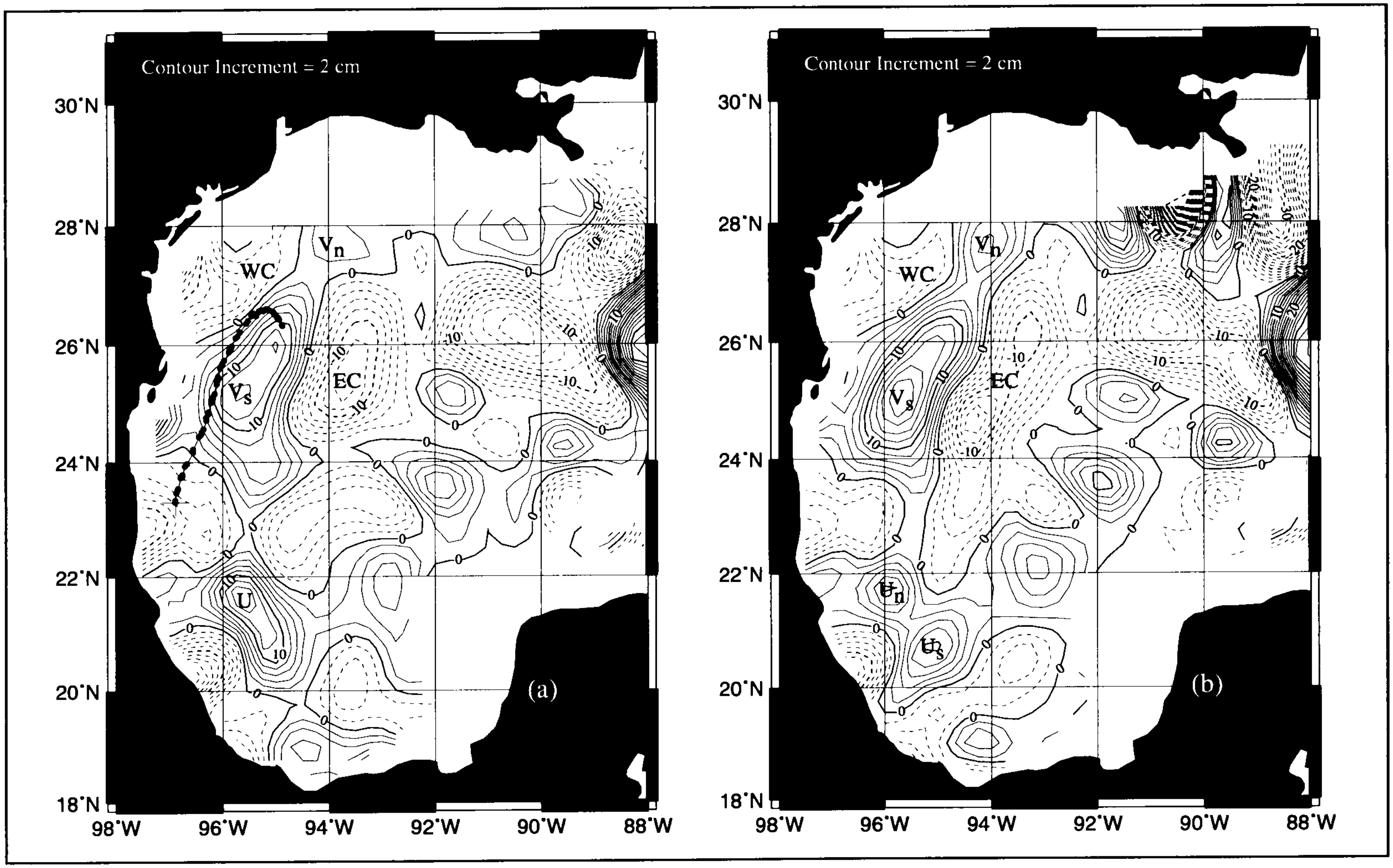

Figure D-2. Sea surface height anomaly with respect to along-track corrected Rapp 95 mean surface, (a) TOPEX cycle 21, 9-19 April 1993 with the track of LATEX C drifter 2449 (line with solid circles) superimposed, and (b) TOPEX cycle 22, 19-29 April 1993. Both cycles include ERS-1 35-day repeat centered on the mid-point of the T/P cycle.

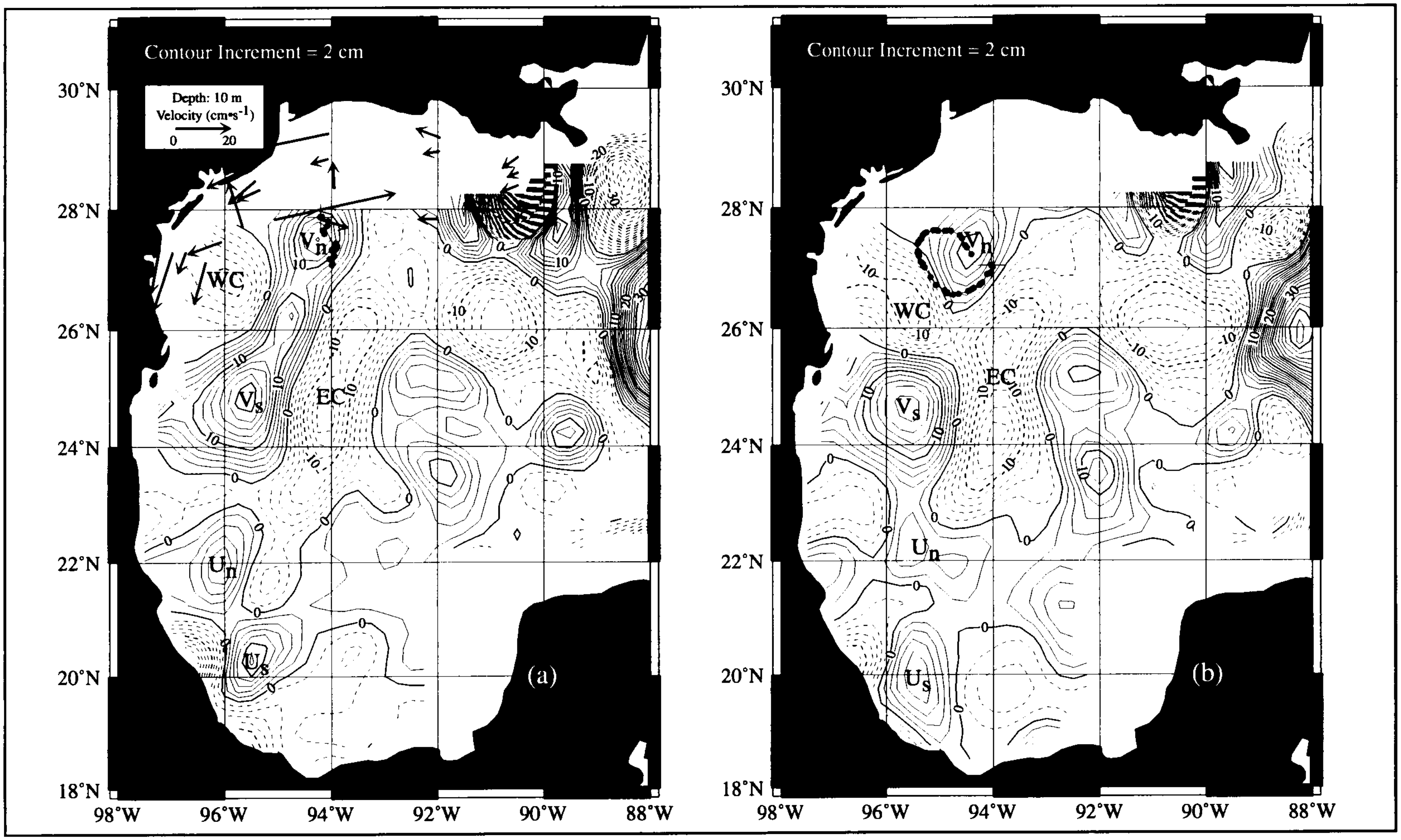

Figure D-3. Sea surface height anomaly with respect to along-track corrected Rapp 95 mean surface, (a) TOPEX cycle 23, 29 April to 9 May 1993, with the 10-day average 10-m currents, and (b) TOPEX cycle 24, 9-19 May 1993. Both cycles include ERS-1 35-day repeat centered on the mid-point of the T/P cycle. The track of LATEX A drifter 6938 (line with solid circles) is shown for the respective time periods of both cycles.

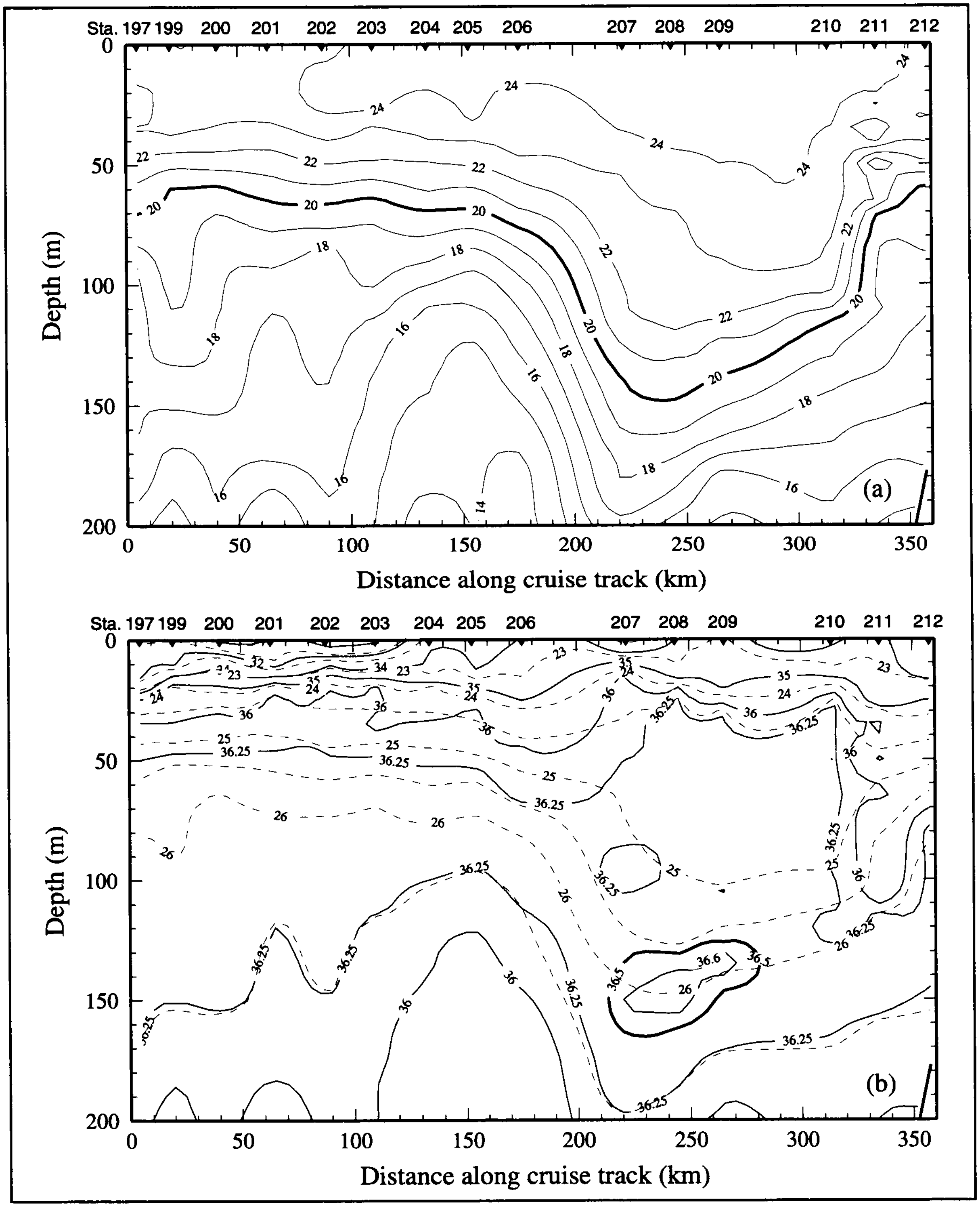

Figure D-4. Vertical section of (a) potential temperature (°C) and (b) salinity (solid lines) and σ_θ (kg·m^{-3}; dashed lines) along the 200-m isobath for the western shelf between 94°W and 96.3°W on cruise H05.

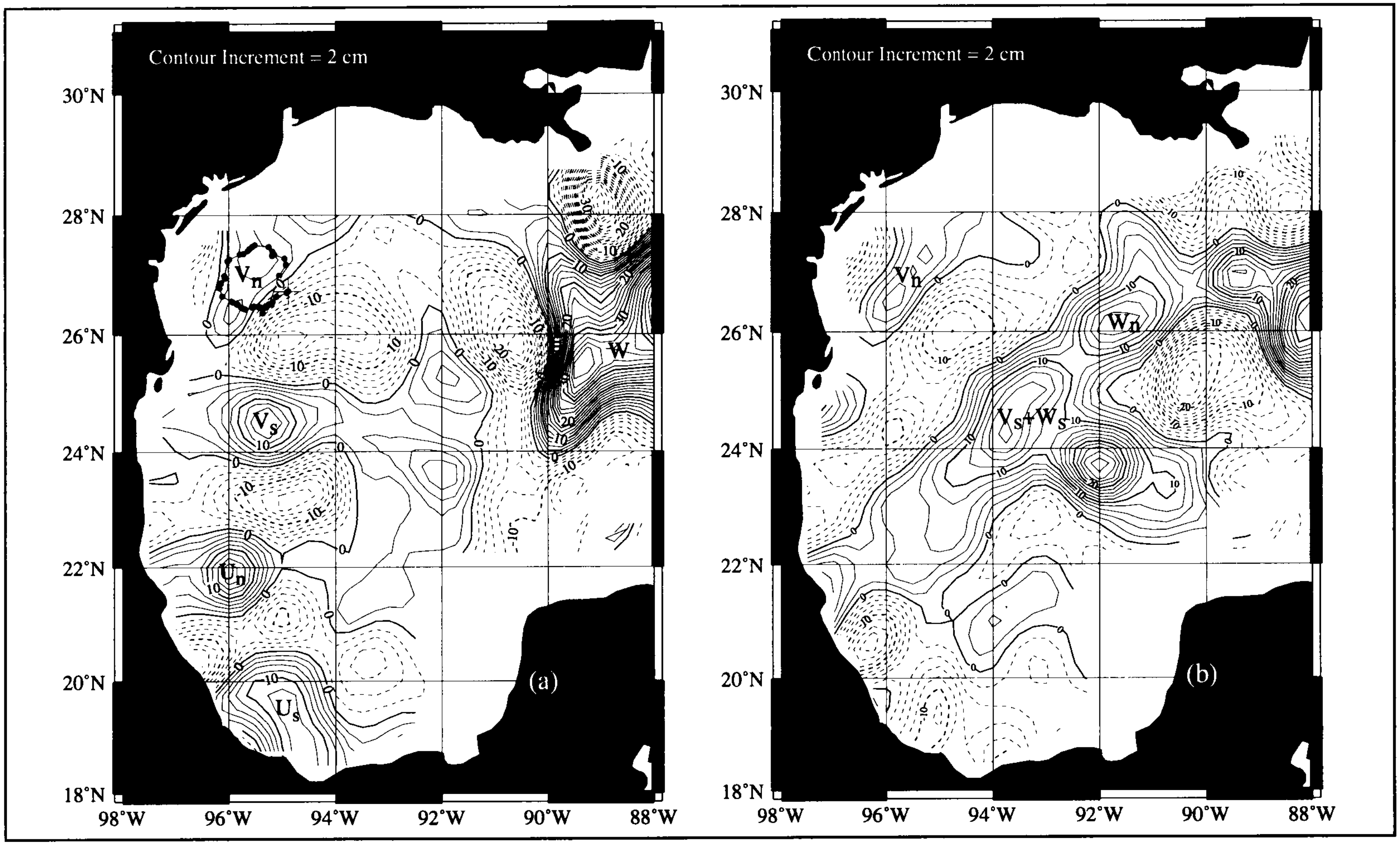

Figure D-5. Sea surface height anomaly with respect to along-track corrected Rapp 95 mean surface, (a) TOPEX cycle 26, 29 May to 7 June 1993, with the track of LATEX A drifter 6938 (solid line with circles) superimposed, and (b) TOPEX cycle 32, 27 July to 6 August 1993. Both cycles include ERS-1 35-day repeat centered on the mid-point of the T/P cycle.

Figures H.1-8 and D-5b). It was surrounded by cyclonic circulation to its northwest and a cyclone to its southeast. At this time, Eddy W_n, moving westward, was located east of Eddy V_n, with a center at about 26.3°N, 91.5°W.

The temperature and salinity data from cruise H06 (26 July-17 August 1993) provide evidence that Eddy V_n still retained its Loop Current eddy character. The SSHA map (Figure D-5b), corroborated by the geopotential anomaly map (Figure H.1-8), shows that Eddy V_n encroached on the 200-m isobath in two regions, at approximately 27.7°N, 95.3°W and 26.5°N, 96.3°W. The vertical section of potential temperature along the 200-m isobath at the shelf edge shows deepening isotherms in both these regions—stations 206 through 209 on the north and stations 197 through 203 on the west in Figure D-6a. The core of the salinity maximum at the shelf edge in both regions contained eroded remnants of high salinity water, including a small number of samples with salinities greater than 36.6 at about 20°C (Figure D-6b).

In August, Eddy V_n contracted northward, becoming more circular, and moved eastward along the north slope. At the end of August and in September (Figure D-7a), Eddy V_n lost most of its mass to Eddy W_n, and its remnant dissipated quickly. By late September 1993, Eddy V_n ceased to be a discernible anticyclonic Loop Current eddy (Figure D-7b).

Characteristics of Eddy V. The characteristics of Eddy V changed throughout its life. Many changes were responses to its interactions with bathymetry, other anticyclones in the area, and cyclones around it. The major events in Eddy V's life, given with TOPEX/POSEIDON (T/P) cycles, are listed in Table D-1. Selected events are letter coded to correspond to the key in Figure D-8a, to relate the events to the graphs of shape, size, SSHA maxima, and strength. Table D-2 shows dates for each T/P cycle.

<u>Shape</u>: The shape of Eddy V changed throughout the course of its life, but was roughly elliptical. The characteristics of the ellipse were used to measure the size and shape of Eddy V through time. Taking the 4-cm SSHA contour as the eddy boundary, the lengths of the major and minor axes of the ellipse were estimated and their ratio determined. The ratio indicates how circular or elongated the eddy was, a value of one being a circle. Figure D-8b presents this ratio by T/P cycle.

Extrema in the ratio reflect elongations and contractions of Eddy V. When Eddy V moved east or west, it generally elongated east-west. This occurred regardless of shallowing topography. For example, when Eddy V moved westward along the north slope in October 1992 and when Eddy V_s moved east across the deep waters of the central Gulf, they both were elongated east-west. These elongations likely were influenced by interaction with other anticyclonic and cyclonic eddies. The elongation of Eddy V in October 1992 occurred as it completed coalescing with Eddy T_n in T/P cycles 5-7. The elongation of Eddy V_s occurred as it interacted with cyclones to its north and south in cycles 26-28 and as it coalesced with the anticyclonic eddy at 23.5°N, 92°W (Figure D-5a). When Eddy V was not translating

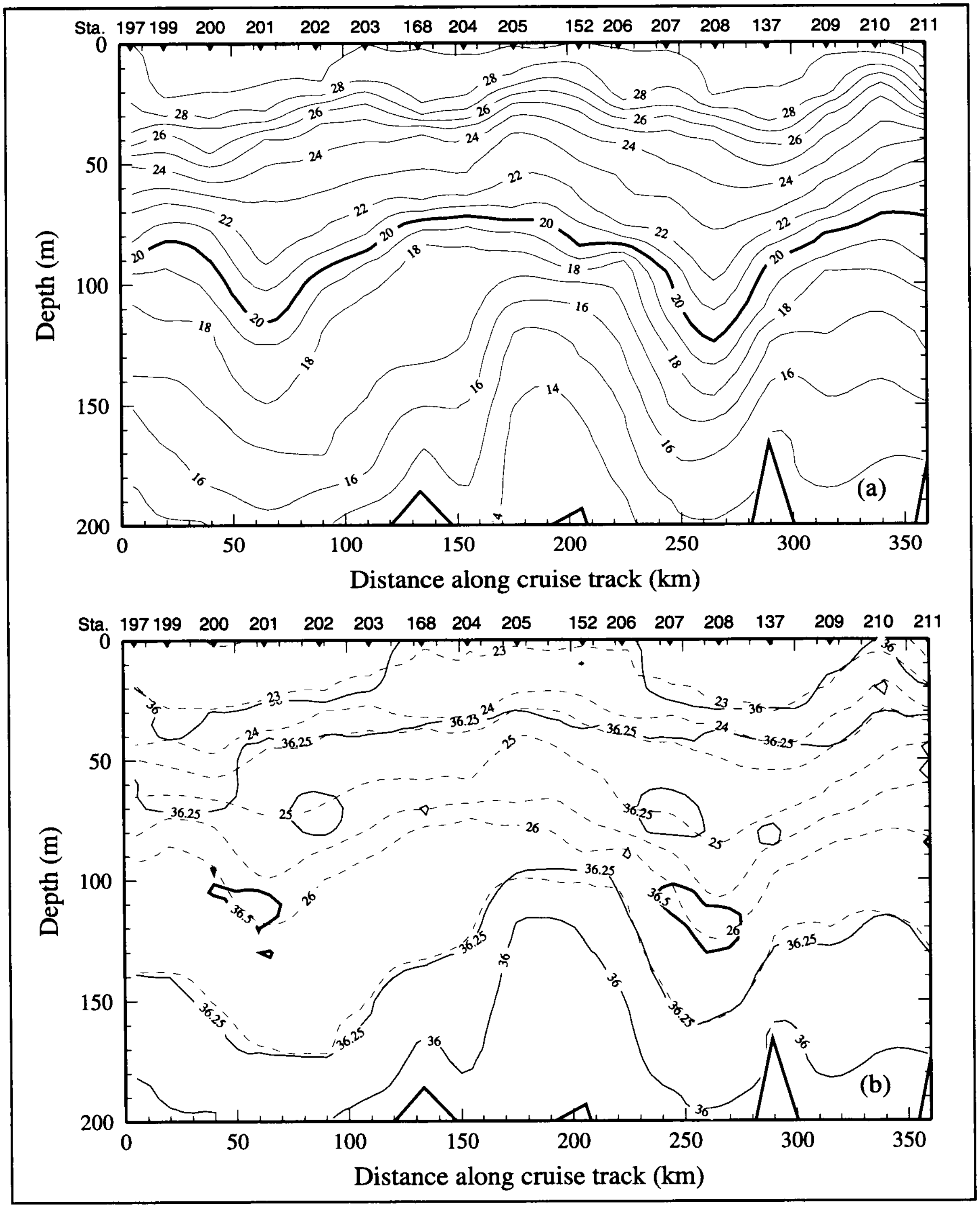

Figure D-6. Vertical section of (a) potential temperature (°C) and (b) salinity (solid lines) and σ_θ (kg·m^{-3}; dashed lines) along the 200-m isobath for the western shelf between 94°W and 96.3°W on cruise H06.

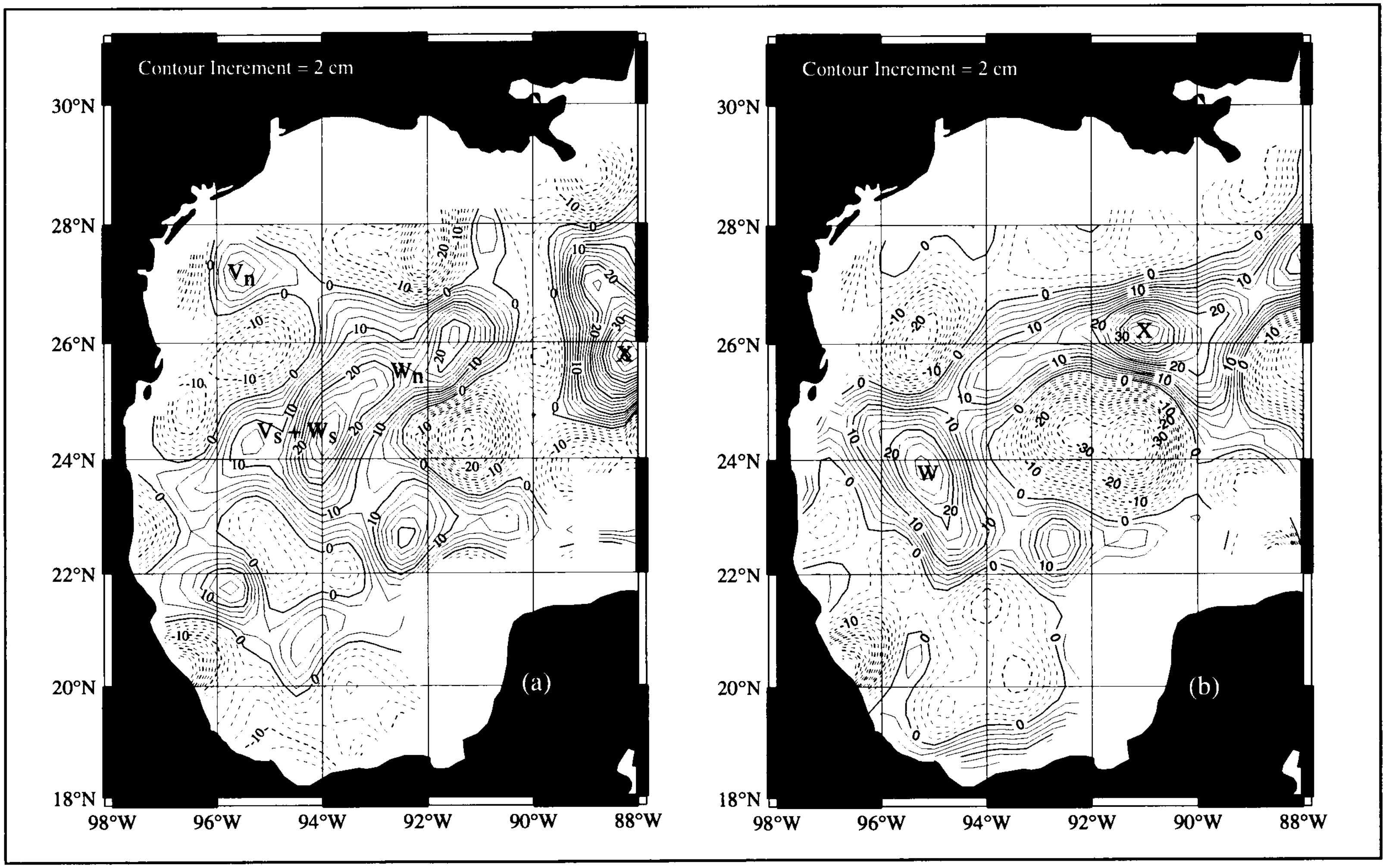

Figure D-7. Sea surface height anomaly with respect to along-track corrected Rapp 95 mean surface, (a) TOPEX cycle 35, 26 August to 5 September 1993, and (b) TOPEX cycle 38, 25 September to 4 October 1993. Both cycles include ERS-1 35-day repeat centered on the mid-point of the T/P cycle.

Table D-1. Major events in the evolution of Eddy V. Code is keyed to Figure D-8a.

	Cycles	Code
Interaction with bottom topography		
V veers southward from 26.5°N to 26°N by topographic steering	2-5	
V affects spin up/spin down of northern cyclonic eddy at 92°-94°W	2-11	
V affects spin up/spin down of western cyclonic eddy	20-24	
Splitting of Eddy V		
Eastern extension develops from V via interaction with topography	5-7	
extension interacts with U and strengthens; V weakens	8-9	B
extension detaches from U & V; moves to 23.5°N, 92°W	10	
part splits off V; part consolidates with V; V strengthens	10-12	C
Southeastern extension develops on V via interaction of V with U	16-17	
extension interacts with U and strengthens; V weakens	16-17	D
extension detaches from U & V; moves to 23.5°N, 92°W	18	
extension coalesces with V_s	26-29	G
Northeast extension develops on V via interaction with U & cyclones	17-23	E
V detaches from U and splits into two parts, V_n and V_s	24	F
Interaction with Eddy Triton		
Eastern remnant of T coalesces with U; possible formation of V	ERS-1*	
T_n slows V westward translation	3	
V coalesces with T_n, V strengthens	2-6	A
Interaction with Eddy Unchained		
V splits off of U	2-3	
V blocks westward translation of U; U stalled	2-5	
East extension of V meets U as U moves southwest; V weakens	8-10	B
V interacts with U to the south; V weakens	14-17	D
V interacts with U to the south; V strengthens	19	
V & U interact; both split into north and south parts; V strengthens	21-24	E
V_s interacts with U and strengthens	24-25	
Interaction with Eddy Whopper		
V_s coalesces with W; V_s ceases existence	30-31	G
V_n coalesces with W; V_n ceases existence	34-37	J
Interaction with cyclonic eddies		
V elongated north-south by cyclonic eddies to the west and east	20-23	
Cyclonic eddies to the east and west enhance split of V	23-24	E
V_n exchanges water with shelf as part of cyclone-anticyclone pair	23-26	
V_s elongated east-west by cyclones to north & south; moved east	26-28	
V_n elongated northeast-southwest by cyclonic eddies to northwest & southeast & by bottom topography; V_n weakens & strengthens	26-32	H
V_n strengthens as cyclone to its east strengthens from W	32-34	I
V_n moves east as cyclone to its south strengthens	32-33	
V_n weakens as it interacts with cyclones and W	35-37	J

* 35-day repeat cycles during April-September 1992

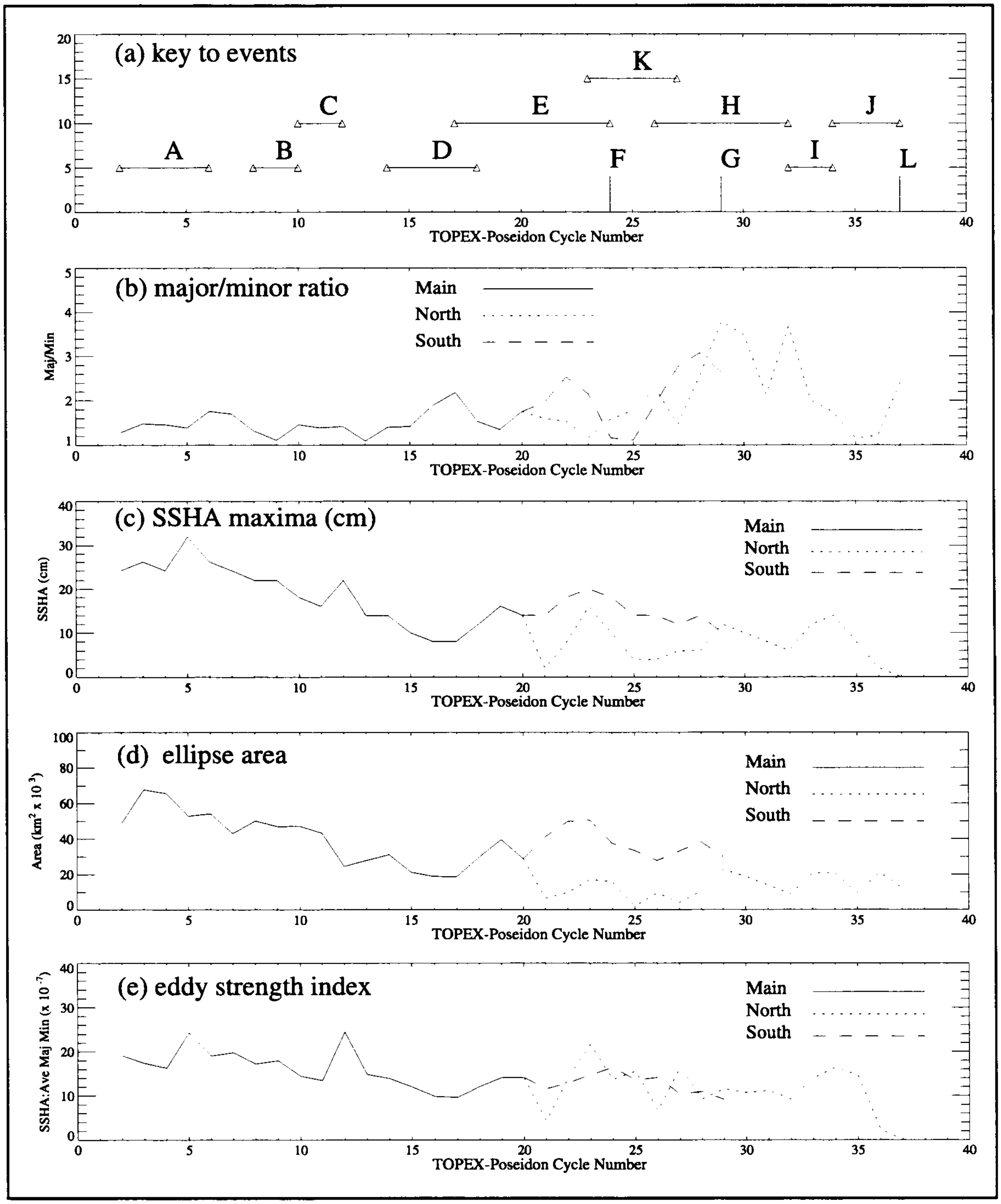

Figure D-8. Properties of Eddy V by T/P cycle: (a) code to events in Table D-1, (b) ratio of major to minor axes, (c) SSHA maxima, (d) area of ellipse formed by major and minor axes, and (e) eddy strength index from SSHA maximum/average axial radius.

Table D-2. Dates of TOPEX/POSEIDON repeat cycles, including mid-point date.

Cycle No.	Dates of Cycle	Mid-point
	1992	
2	3-12 Oct	7 Oct
3	12-22 Oct	17 Oct
4	22 Oct - 1 Nov	27 Oct
5	1-11 Nov	6 Nov
6	11-21 Nov	16 Nov
7	21 Nov - 1 Dec	26 Nov
8	1-11 Dec	6 Dec
9	11-21 Dec	16 Dec
10	21-31 Dec	26 Dec
	1993	
11	31 Dec 1992 - 10 Jan	5 Jan
12	10-20 Jan	15 Jan
13	20-30 Jan	25 Jan
14	30 Jan - 8 Feb	4 Feb
15	8-18 Feb	14 Feb
16	18-28 Feb	24 Feb
17	28 Feb - 10 Mar	5 Mar
18	10-20 Mar	15 Mar
19	20-30 Mar	25 Mar
20	30 Mar - 9 Apr	4 Apr
21	9-19 Apr	14 Apr
22	19-29 Apr	24 Apr
23	29 Apr - 9 May	4 May
24	9-19 May	14 May
25	19-29 May	24 May
26	29 May - 7 Jun	3 Jun
27	7-17 Jun	13 Jun
28	17-27 Jun	23 Jun
29	27 Jun - 7 Jul	2 Jul
30	7-17 Jul	12 Jul
31	17-27 Jul	22 Jul
32	27 Jul - 6 Aug	1 Aug
33	6-16 Aug	11 Aug
34	16-26 Aug	21 Aug
35	26 Aug - 5 Sep	31 Aug
36	5-15 Sep	10 Sep
37	15-25 Sep	20 Sep
38	25 Sep - 4 Oct	30 Sep

significantly or interacting with other eddies, it generally consolidated and became more circular, as when Eddy V consolidated into the northwest corner during cycles 8-9. Other examples are Eddy V_s just after the split of Eddy V into two major parts (cycles 24-25; Figure D-3b) and Eddy V_n in August prior to joining with Eddy W (cycles 32-35; Figure D-7a). North-south elongations occurred generally when Eddy V interacted with Eddy U to the south. For examples, Eddy V elongated southward as it encountered Eddy U during cycles 14-17 and again as it interacted both with cyclones to its west and east and with Eddy U during cycles 19-22 (see Figure D-2). Eddy V_n elongated to the southwest and contracted several times as it interacted with the north and west slope and with cyclones to its northwest and southeast in cycles 26-32 (Figure D-5).

Size: The SSHA maxima and an estimate of the area of the ellipse were analyzed to determine how the size changed through time (Figures D-8c and d). In October, Eddy V's diameter was approximately 290 km (Figure 2.5.1-1). The eddy's size increased generally when it coalesced with remnant anticyclonic eddies, such as with Eddy T_n, or during some exchanges with other cyclonic or anticyclonic features. Eddy V's size decreased during several exchanges with Eddy U and when portions of the eddy were split off (Table D-1), such as occurred between cycles 5 and 17. From the plot of the area after the major split into two parts in cycle 24, Eddy V_s was comparable in size to Eddy V before the split and was much larger than Eddy V_n. After the split, Eddy V_s slowly decreased in size as it interacted with cyclones to its north and south until its coalescence with the southeast anticyclonic eddy and Eddy W (Figure D-5). Eddy V_n also underwent a series of size increases and decreases resulting from its interactions with cyclones and anticyclones in the region, keyed to Table D-1, until its terminal exchange with Eddy W in cycles 35 and 36.

Strength of Eddy V. The strength or intensity of an eddy is related to the horizontal gradient of the SSHA. The ratio of the SSHA maximum to an average axial radius, computed as half the average of the major and minor axes, was used as a qualitative index of eddy strength (Figure D-8e). Extrema in the eddy strength index also can be related to interactions of Eddy V with cyclones and anticyclones or to other events in the eddy's life (Table D-1).

Eddy V generally strengthened when other anticyclonic eddies joined with it, such as with Eddy T_n in cycle 5, and it interacted with surrounding cyclonic eddies. The most significant example occurred during cycles 33-34, when Eddy V_n strengthened as the cyclones to its east and southeast were envigorated by Eddy W as that eddy broke off the Loop Current and moved west. In this case, energy was transferred between anticyclones through cyclones.

A significant cause of weakening in the eddy was the splitting off of parts due to encounters with cyclonic and other anticyclonic eddies. Small parts of Eddy V split off a number of times, resulting in decreases in its strength index (Table D-1 and Figure D-8e). One of many cases occurred during a period of intense interaction of Eddy V with Eddy U and cyclones in cycles 12 through 17. Parts of both Eddy V and Eddy U split off and both were diminished.

The parts then combined and moved to about 24°N 92°W, forming an anticyclonic eddy that persisted until it joined with Eddy V_s (Figure D-5a).

The action of cyclonic eddies about the anticyclonic eddy also can weaken an eddy. This weakening is more gradual than when parts split off. Note, for example, that the strength of Eddy V_s decreased slowly during cycles 24 through 29. During this period, Eddy V_s interacted with cyclones to its north and south and elongated. Finally, the eddy's strength decreased during coalescence with another anticyclonic eddy, as when Eddy V_n interacted directly with Eddy W during cycles 35 and 36. Eddy V_n was weakened substantially, suggesting that most of the mass and energy of Eddy V_n was taken up by Eddy W. The remainder of Eddy V_n then dissipated rapidly and was no longer a discernible anticyclone by cycle 38 in late September 1993 (Figure D-7b).

Influence of Eddy V on the Texas shelf circulation in April-May 1993. SSHA data show Eddy V_n encroached on the Texas shelf in April-May 1993 (Figures D-3b and Figure D-5a). They also show a cyclonic eddy spinning up to the west as Eddy V_n split off Eddy V and encroached on the shelf (Figures D-2 and D-3). As the current vectors on Figure D-3a show, this cyclone-anticyclone pair had a significant influence on the shelf circulation.

LATEX A drifter 6938 was deployed on 2 May 1993, at the 200-m isobath of the Texas-Louisiana shelf just northeast of Eddy V_n. It moved immediately off the shelf at about 94°W into the east flank of Eddy V_n (Figure D-9); this showed that Eddy V_n was drawing water southward, off the shelf. The track of the drifter shows that Eddy V_n translated westward and encroached on the shelf edge throughout May. SSHAs indicate Eddy V_n had an approximate diameter of 140 km during this time. SSHAs show Eddy V_n decreased in size to about 100 km diameter in June and became elongated against the Texas shelf. The drifter left Eddy V_n to circulate in the cyclonic eddy located to the southeast of Eddy V_n (see Figure D-5a).

The influence of the cyclone-anticyclone pair is evident in the sea surface temperature (SST) image for 12 May 1993 (Figure D-10). The SSHA contours for the period 9-19 May 1993 are overlain on the SST image, and the anticyclonic and cyclonic eddies in the northwest corner are labeled for identification. The darker shades on the SST image indicate the warmer water of the anticyclones; the lighter indicate cooler water, such as found on the shelf. The warm waters of Eddy V_n moved onto the shelf at about 95.5°W by the northwestward flowing jet between Eddy V_n and the western cyclone. These warm waters then bifurcated to flow to the east along the northern periphery of Eddy V_n and to the southwest along the outer north and west sectors of the western cyclone. Cooler shelf waters were drawn off the shelf in two locations. One was at about 94°W where the eddy circulation turns southward offshelf. The other was at the southwestern side of the western cyclone, where its circulation turns eastward offshelf at about 26.5°N to 27°N. Eddy V_s, south of the western cyclone, acted with the western cyclone to draw water offshelf at about 26°N to 26.5°N.

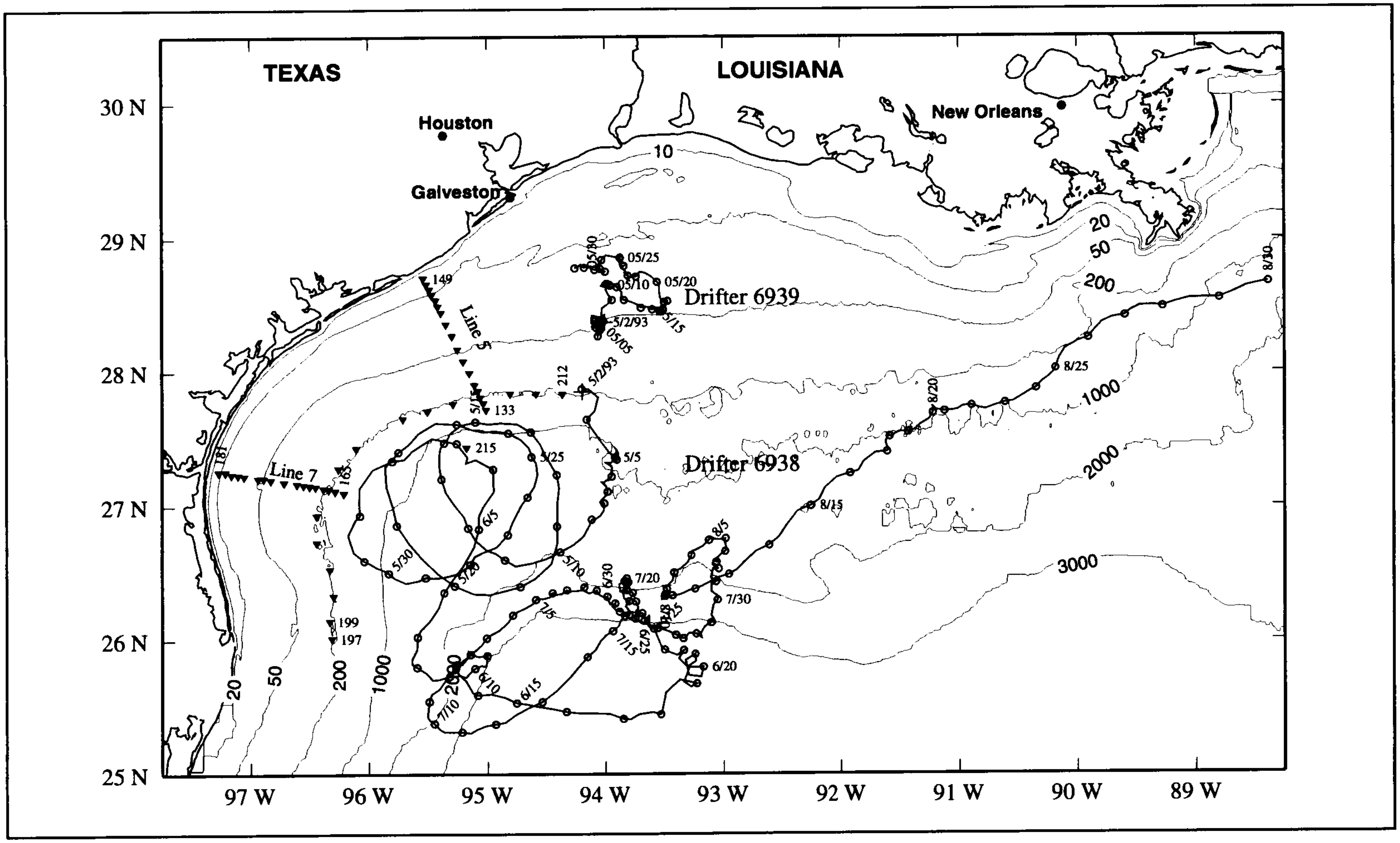

Figure D-9. Track of LATEX A drifter 6938 from its deployment on 2 May 1993, until it left the Texas-Louisiana shelf on 30 August 1993. The track of drifter 6939 for May 1993 also is shown. Circles are locations at 2200 hrs (drifter 6938) and 2300 hrs (6939) in UTC each day. Triangles show locations of hydrographic stations on cruise H05 for the vertical sections given in Figures D-4 and D-12.

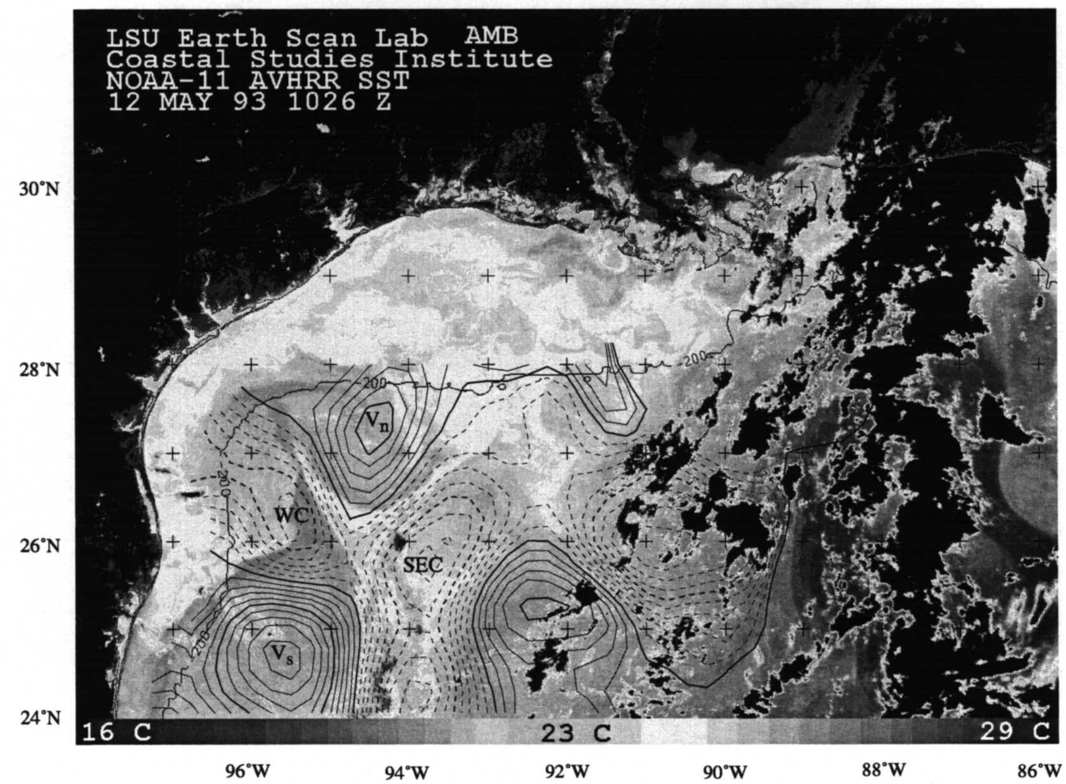

Figure D-10. Satellite AVHRR sea surface temperature for 12 May 1993, with the sea surface height anomaly contours (2 cm). The anticyclonic Eddy V_n and Eddy V_s as well as two cyclones (WC and SEC) are labeled.

The salinity at the 3-m depth indicates that water was being moved onto and off the shelf by the cyclone-anticyclone pair (Figure D-11). The waters of Loop Current Eddy V_n, which were higher in salinity than the surrounding waters, were those with salinity of 36 or more that encroached on the western shelf near 95°W. Salinities greater than 34 extended onto the shelf at about 95.5°W; they wrapped around the cyclone in a counterclockwise direction along the shelf edge and around Eddy V_n in a clockwise direction. This resulted from water being moved onto the shelf by the cyclone-anticyclone pair. The fresher waters of the shelf (< 34) moved offshelf at the eastern side of Eddy V_n (~ 94°W) and at the southwestern side of the western cyclone (26.5°N to 27°N), as in the SST image.

More significantly, the 3-m salinity contours indicate Eddy V_n and its associated cyclone influenced the circulation over much of the western shelf. Eddy V_n drew fresh water across

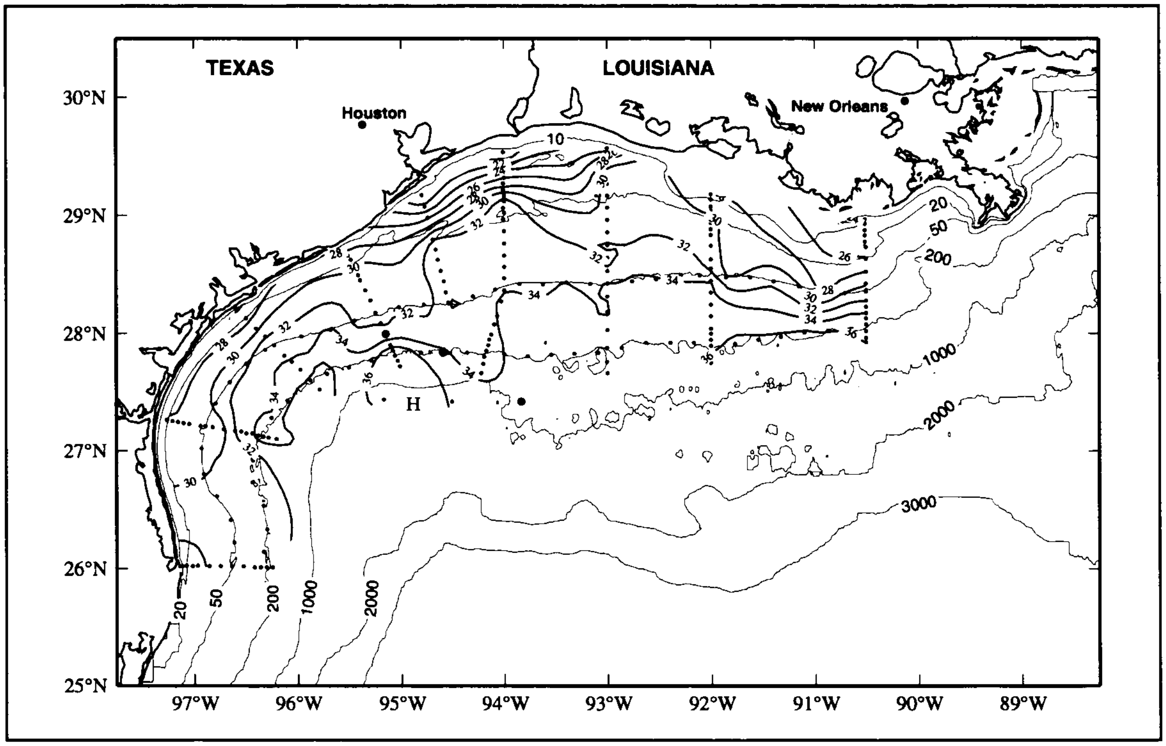

Figure D-11. Salinity at the 3-m depth on cruise H05, 25 April to 11 May 1993. Eddy V_n abuts the shelf edge in the region of high salinity (36) on the western shelf. Large circles are the locations of stations 138, 211, and 213 (west to east).

the shelf in a southeastward squirt from the inner shelf at about 95.5°W. This shelf water moved along the northern periphery of Eddy V_n and then off the shelf at about 94°W on the eastern side of the eddy. The 34 salinity contour in this region denotes the boundary between the squirt and the eddy. The western cyclone also drew fresh water from the inner shelf across and off the shelf at about 27°N. Thus, the near-surface salinity distribution portrays essentially the same picture of water movement as the near-surface temperature distribution.

The geopotential anomaly field and the 10-m current vectors (Figure D-12) confirm the movement of water on and off the shelf that is suggested by the SST and 3-m salinity maps. The geopotential anomaly of 3 db relative to 400 db shows onshelf flow at about 95.5°W and offshelf flow at about 94°W. The squirt is associated with the offshelf flow at about 94°W. The geopotential anomaly map suggests offshelf flow associated with the southwest side of the western cyclone at 26 to 25.5°N. The 10-day average current vectors show strong, alongshelf, eastward flow of up to 50 $cm \cdot s^{-1}$ associated with the northern periphery

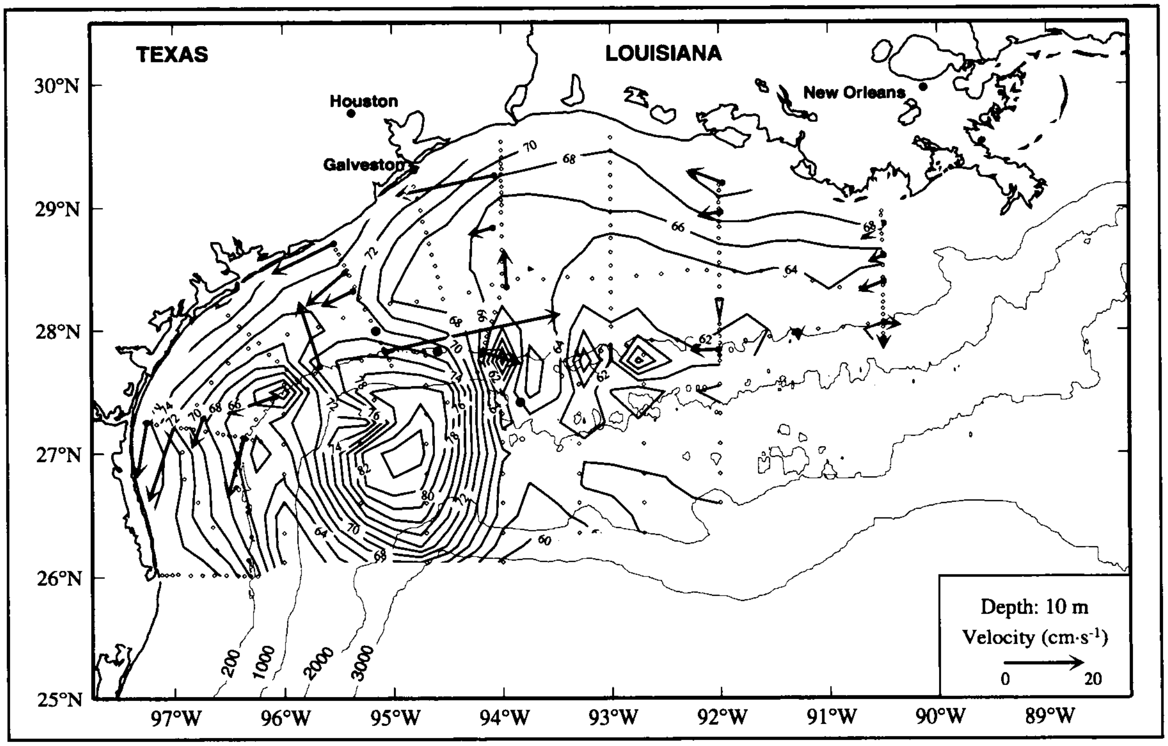

Figure D-12. Geopotential anomaly of 3 db relative to 400 db from a composite of hydrographic data for LATEX A cruise H05 and AXBT data for LATEX C F08 and F09 (26 April to 18 May 1993). Mean current vectors for the ten-day period of T/P cycle 23 (29 April to 9 May 1993) are shown. Solid circles show locations of stations 138, 211, and 213 from cruise H05.

of Eddy V_n and southward alongshelf flow of about 15 $cm{\cdot}s^{-1}$ associated with the western cyclone. The 10-day average current vectors are for the period corresponding to the T/P cycle 23 period (29 April and 9 May 1993). To tie the SSHA map (Figure D-3a) with the in situ data presented here, the cycle 23 SSHA contours are overlain on the SST map (Figure D-10) and the current vectors also are shown on the T/P cycle 23 map (Figure D-3a).

Vertical sections of potential temperature, salinity, and σ_θ extend the picture of the sea-surface features into the water column. Line 9 along the 200-m isobath (Figure D-4) crossed the encroaching portions of both Eddy V_n and its paired western cyclone. The fresh water being drawn off the shelf is evident in the vertical salinity section (Figure D-4b). Stations 197 to 203 are on the southwest flank of the cyclonic eddy (see station locations, shown in Figure D-9). The shallow lens of low salinity (≤ 34) water in the upper 10-20 m was shelf water being moved offshelf in this region. Stations 210 to 212 are located along the northeastern edge of Eddy V_n, in the region where the squirt of cooler, fresher shelf waters (Figure D-11) was drawn off by Eddy V_n. As the saltier water of Eddy V_n circled around its north edge and turned south, it mixed with the fresher waters of the shelf and formed a front that extended to the southeast. The resulting squirt had a salinity between 36 and 35 at stations 210 to 212 (Figure D-4b). This squirt extended to about 100 m depth, as indicated by the dip in the 36 salinity isopleth at these stations.

Line 5 is a cross-shelf transect with offshelf stations in the northern periphery of Eddy V_n (Figure D-13a; see Figure D-9 for the station locations). The isopycnals of the outer shelf region of line 5 slope downward offshelf, indicating the northeastward flow associated with the northern edge of Eddy V_n in that region. The pycnocline becomes vertical in the upper 25 m between stations 134 and 139. This resulted from the meeting of the shelf and Eddy V_n waters. The deepest points of the σ_θ surfaces associated with the eddy tilt towards the shelf (e.g., see σ_θ of 24 through 26). The high salinity core (≥ 36.5) of the Subtropical Underwater, characteristic of anticyclonic Loop Current eddies, was present at the 150-200 m depth in Eddy V_n. The fresh water (≤ 34) drawn across the shelf by Eddy V_n extended from the inner shelf to the boundary region with Eddy V_n where the horizontal gradient of salinity, as well as σ_θ, steepened. The 36 salinity contour shows interleaving of fresher with saltier water centered at the 35-m depth; this is most clear at station 138 (the location of this station is identified relative to the 3-m salinity in Figure D-11 and relative to the geopotential anomaly field in Figure D-12).

Line 7 also is a cross-shelf transect (Figure D-13b; see Figure D-9 for the station locations). Its offshelf stations were located in the western cyclone. The western cyclone is evident in the section by the doming isopycnals, indicating southward flow in this region. Fresh water extended from the inner to the outer shelf in a layer about 10-20 m thick. This water was drawn across the shelf under the influence of the cyclone. Unlike the offshelf freshwater flow from Eddy V_n, however, there was no strong horizontal gradient of salinity between the offshelf and shelf waters.

Stations 138, 211, and 213 lie, from west to east, along the velocity squirt in Figure D-12. The interleaving indicated by the contours of salinity along line 5 (Figure D-13a) is evident in the potential temperature-salinity (θ-S) diagrams for these three stations (Figure D-14). The stations fell along the front between the core of the squirt and Eddy V_n that is indicated by the 34 salinity contour (Figure D-11). The interleaving is evident in the peaks in the θ-S diagrams. All three stations have similar peaks, particularly at σ_θ of 24.25-24.5. As the σ_θ value increases between 24.5 and 25, the potential temperature and salinity both decrease before peaking again. This decrease is less precipitous at station 213, which is offshelf and farther off the front (Figure D-11). Mixing occurs along the front between the high and low salinity waters.

Drifter 6938 (Figure D-9) showed that Eddy V_n moved westward during May. A time series showing the daily average current vectors at the nominal 10-m depth over the western Texas-

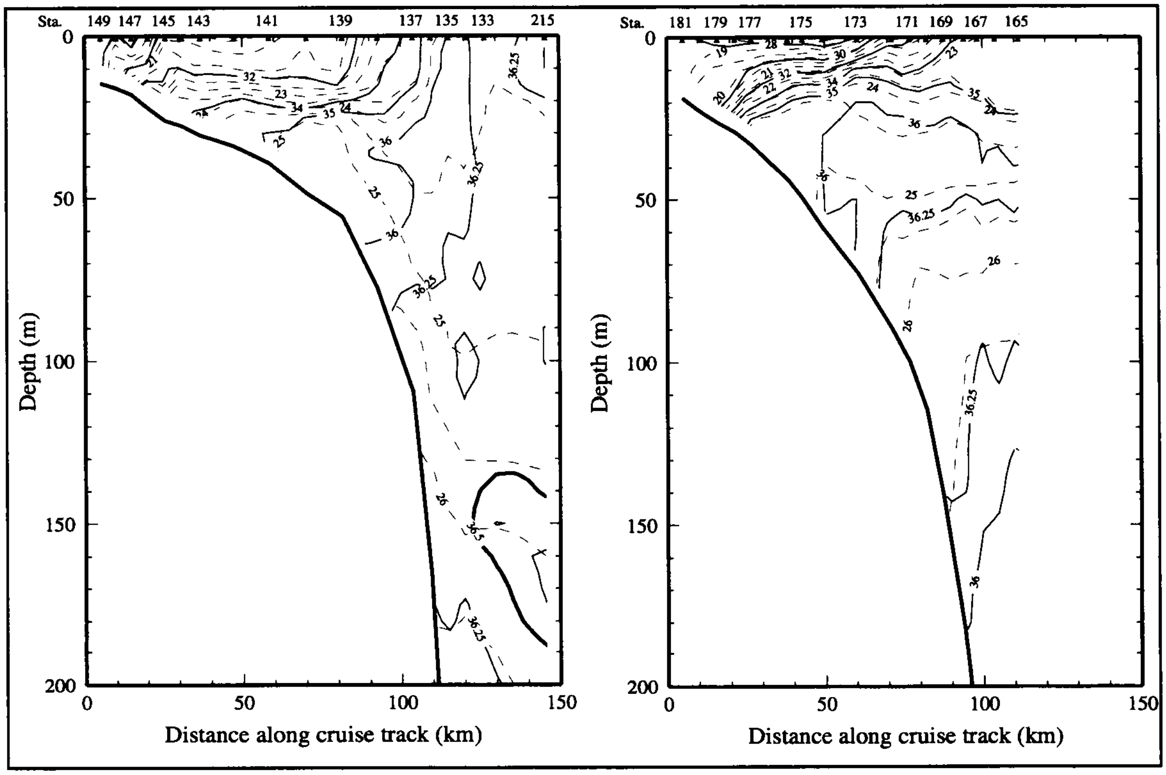

Figure D-13. Vertical section of salinity (solid lines) and σ_θ (kg·m^{-3}; dashed lines) along (a) line 5 and (b) line 7 of cruise H05.

Louisiana shelf every third day shows this westward movement affected the currents at the shelf edge (Figure D-15). In late April, the currents at the shelf edge exhibited the influence of the cyclonic-anticyclonic pair (April 21-30). There was relatively weak onshelf flow at mooring 6 (current jet between an anticyclone and cyclone), weak eastward flow at moorings 7 and 8 (anticyclone), and relatively strong southward flow at mooring 5 and 6 (cyclone). This pattern indicates that the cyclone was located closer to the shelf edge than the anticyclone. As Eddy V_n and its associated western cyclone moved farther onto the continental slope in early May, the currents at the shelf edge increased. Onshelf flow from the current jet between Eddy V_n and the cyclone moved from mooring 6 (May 3-6) to mooring 5 (May 9-18) to mooring 4 (May 21-24), thus tracing Eddy V_n moving west and the western cyclone moving south along the shelf edge.

The time series of temperature and salinity from moorings 4, 5, 6, and 7 at the 100-m depth also show that Eddy V_n moved to the west (Figure D-16). The 20°C isotherm depths show Eddy V_n had warmer water at 100-m depth than surrounding waters (April-May 93 plot in Figure H.1-1). Most of the time, mooring 4 was influenced by the western cyclone. Its temperature consistently was 16-17°C and was cooler than the waters at the other moorings

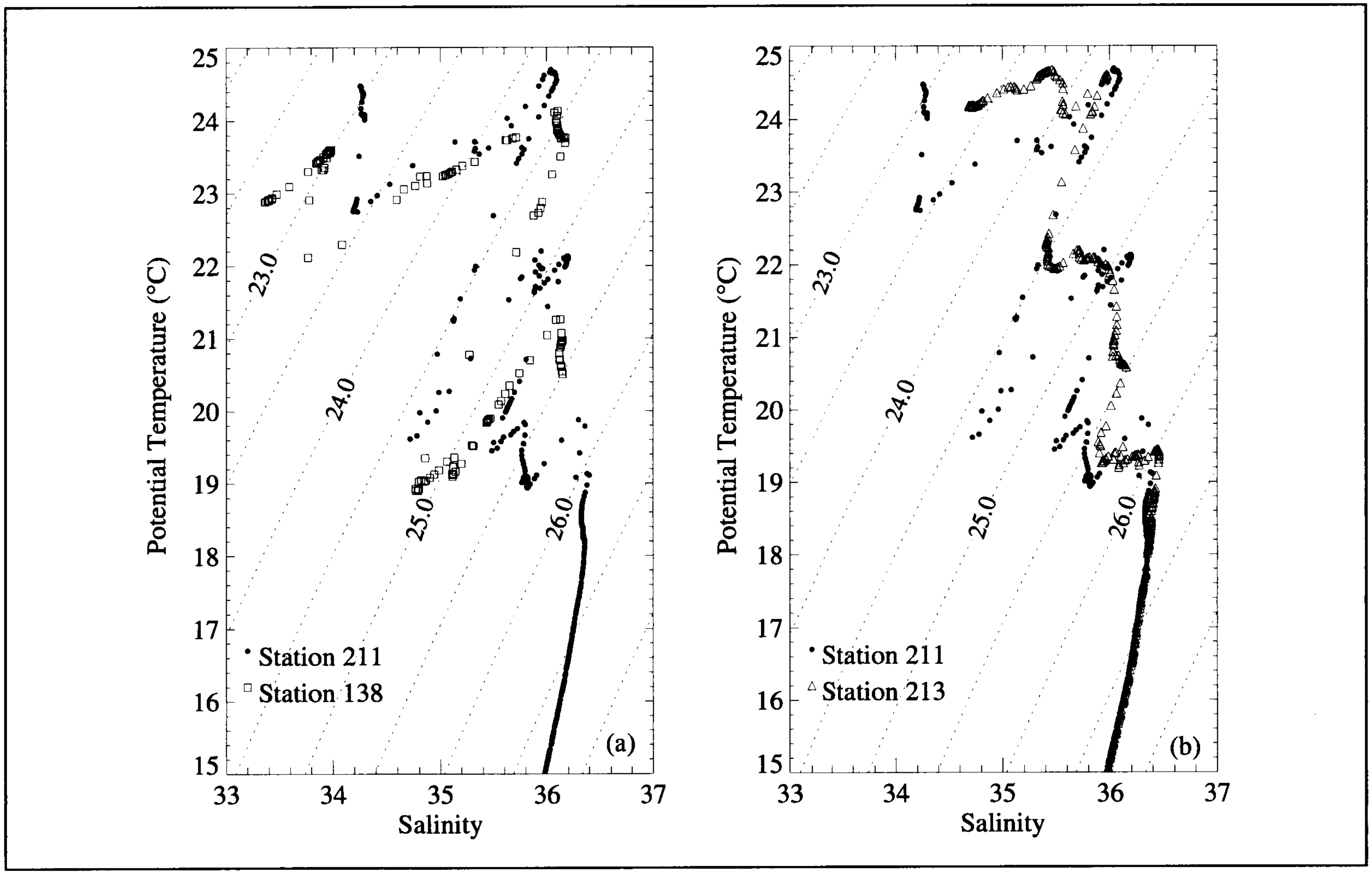

Figure D-14. Potential temperature-salinity diagrams for (a) stations 138 and 211 and (b) stations 211 and 213 from cruise H05. Station locations are shown on Figures D-11 and D-13.

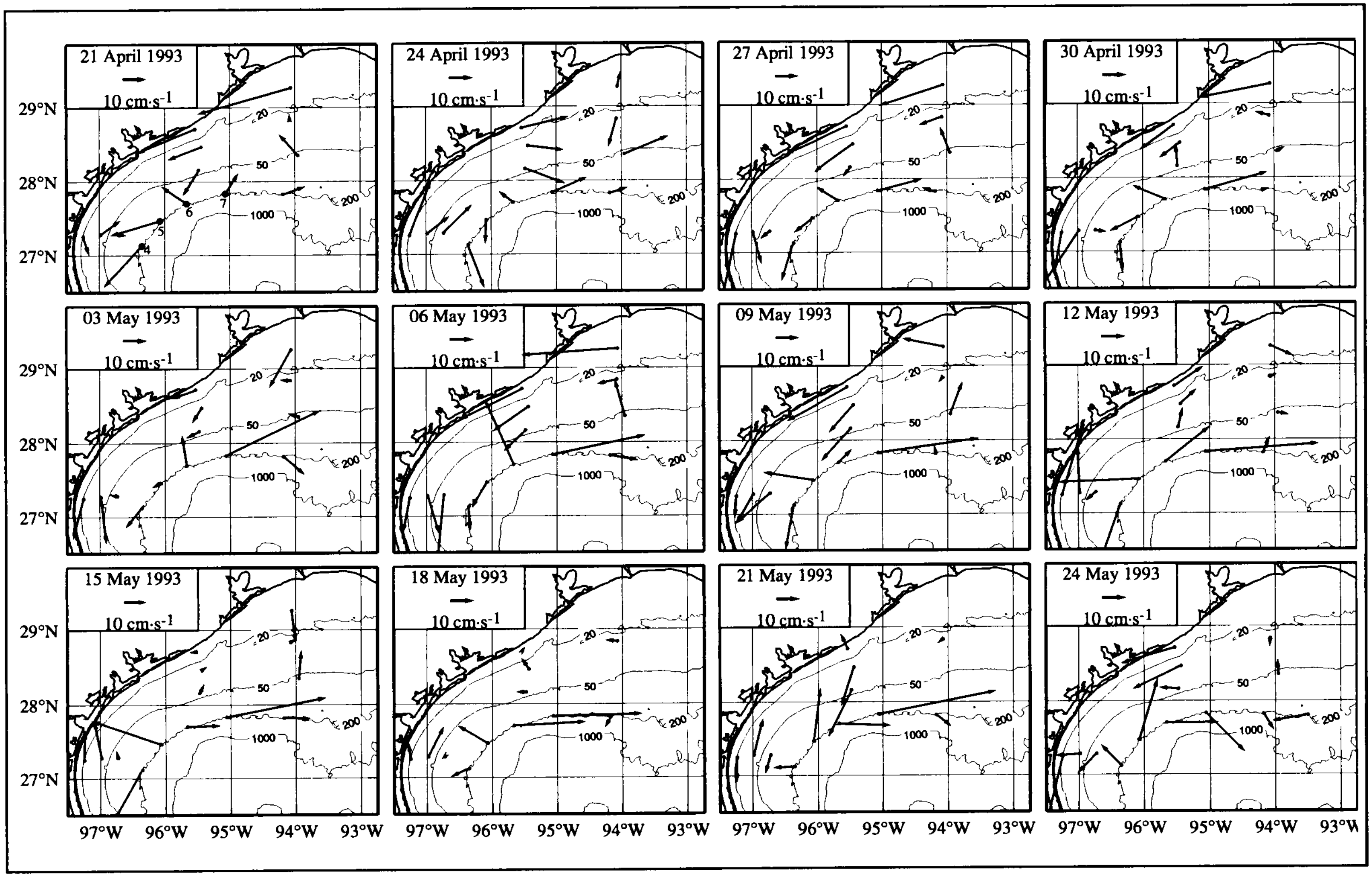

Figure D-15. Daily average current vectors at a nominal 10-m depth over the western shelf for every third day between 21 April and 24 May 1993. The locations of moorings 4, 5, 6, and 7 (west to east) are indicated by the large circles on the plot for 21 April.

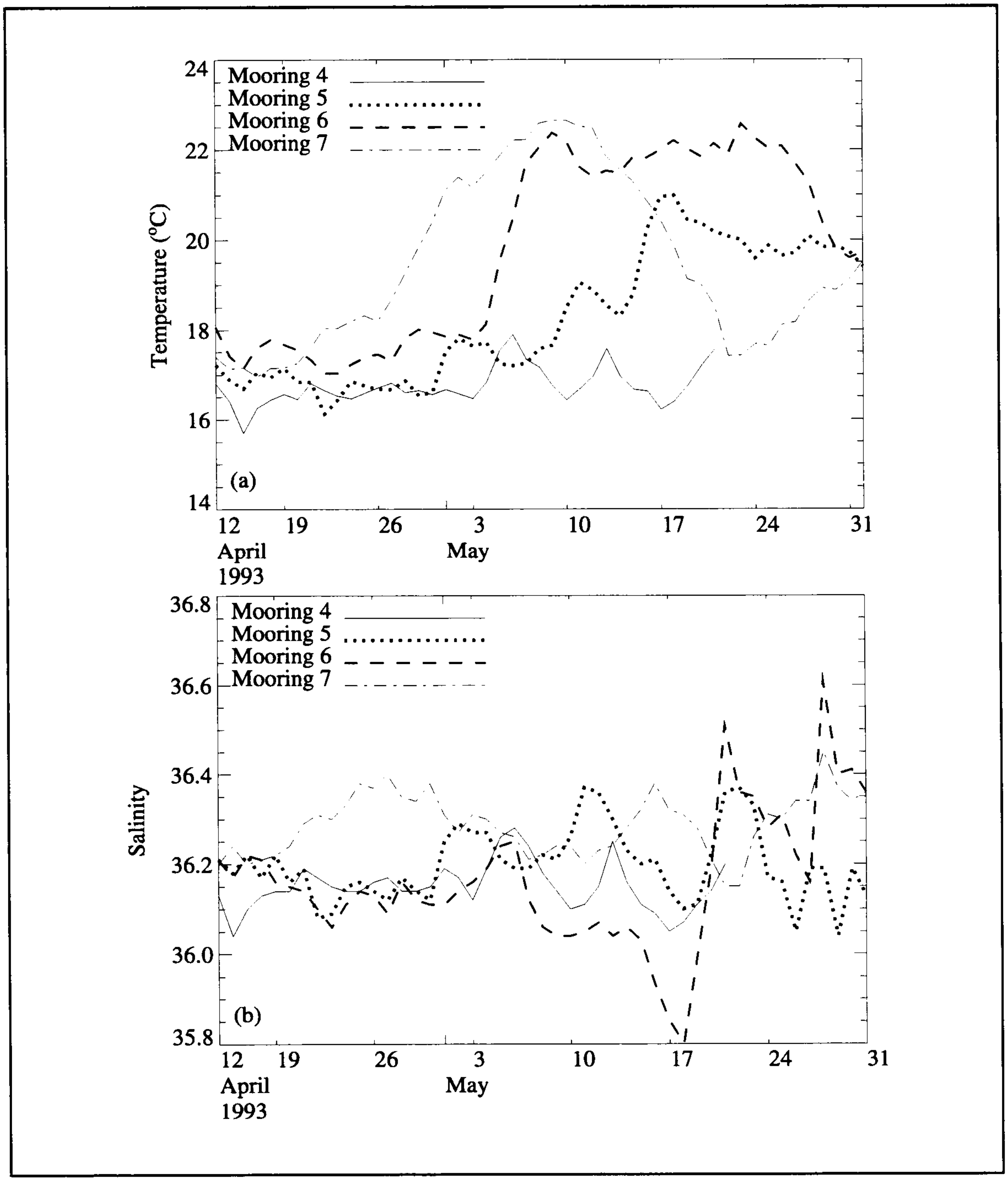

Figure D-16. Time series of (a) temperature (°C) and (b) salinity at 100 m from moorings 4-7 along the 200-m isobath on the western shelf. Figures D-11 and D-13 show mooring locations.

(Figure D-16a). The vector time series in Figure D-15 show that the warmer water of Eddy V_n appeared first in the 100-m temperature time series for mooring 7, where the temperature increased from about 17°C around April 12 to 22°C about 10 May. This warm water appeared at mooring 6 about 6 May and at mooring 5 about 17 May. By the time the warm water appeared at mooring 5, it no longer was detectable at mooring 7. This pattern is consistent with the westward moving eddy.

The salinity time series at 100-m depth (Figure D-16b) is complex but shows the influence of Eddy V_n and the western cyclone. The moorings show oscillating increases and decreases in salinity throughout the time series. Moorings 4, 5, and 6 were influenced by the western cyclone throughout the last half of April, while mooring 7 showed a higher salinity associated with the influence of saltier waters from Eddy V_n. In the first half of May, when Eddy V_n moved westward and farther onto the slope, it brought higher salinity water to moorings 6 and 5. These moorings were in the region where the current jet from the cyclone-anticyclone pair was impinging on the shelf. The complex pattern of salinity at these moorings reflects the changing degree of influence of the fresher water that the cyclone was bringing around and the saltier water that Eddy V_n was moving onto the shelf. The large increase in salinity at moorings 6 and 5 between 17 and 24 May occurred as Eddy V_n moved up against the entire Texas shelf edge at 27°N.

The current vector time series and drifter tracks also show how the flows under various shelf regimes react to wind events. In early May, the winds over the western shelf generally were from the east-southeast. The alongshelf component of this wind was downcoast as far south as 27.2°N, just south of the line 1 moorings. The resulting currents on the inner shelf were generally downcoast (e.g., 3, 6, and 9 May currents in Figure D-15). The currents at the shelf edge, however, responded to the cyclone-anticyclone pair, not the wind regime. About 11 May, there was a frontal passage marked by winds shifting from the north and then, by 12 May, from the south to southeast. The alongshelf component of the winds was upcoast, causing the currents over the inner shelf to flow upcoast (e.g., 12 May in Figure D-15). The currents at the shelf edge, however, continued to be driven by the cyclone-anticyclone pair. The upcoast wind and current regime persisted until another frontal passage on 18-20 May. By 21 May, the alongshelf winds were downcoast along the western shelf to approximately 27.2°N. The currents on the inner shelf returned to downcoast flow while currents at the shelf edge continued to respond to the eddies (compare 18, 21, and 24 May in Figure D-15).

The wind driving of the inner shelf currents and cyclone-anticyclone driving of the outer shelf currents also is seen in the respective tracks of drifters 6938 and 6939 (Figure D-9). Drifter 6939 was deployed about 60 km north of drifter 6938; both were drogued at 9 m. Drifter 6938 was drawn into Eddy V_n whereas drifter 6939 remained on the shelf moving slowly in a northward direction. When the currents reversed due to the wind reversal about 10 May, drifter 6939 moved rapidly eastward or upcoast. Drifter 6938, however, continued to move westward under the influence of the eddy. When the downcoast wind regime was reestablished about 21 May, drifter 6939 turned westward and moved downcoast; drifter 6938 continued to circulate in Eddy V_n. Two other drifters, deployed along 94°W at 12 km and 35 km north of drifter 6938, responded to the wind shift in a manner similar to drifter 6939. This sequence of events is evidence that the upper layer of the western inner shelf circulation is driven primarily by the wind regime and the outer shelf circulation is driven mainly by the anticyclonic eddy systems.

Eddy V_n influenced the suspended particulate matter, nutrient, and oxygen concentrations as well. These are discussed in Sections 5.1, 5.2, and 5.3 respectively.

Appendix E: A Volumetric Temperature-Salinity Census for the Texas-Louisiana Shelf

We developed a volumetric T-S census of the Texas-Louisiana shelf based on the ten hydrographic surveys of the region during the period May 1992 through November 1994. The complete set of T-S figures appears in a technical report by Li et al. (1996). The census includes coarse distributions by intervals of 1°C and 1 in salinity, and finer distributions by intervals of 1°C and 0.2 in salinity, for the entire shelf and for the eastern (east of 94°W) and western half shelves, as allowed by the data distribution.

Montgomery (1958), Cochrane (1958), and Pollak (1958) introduced the volumetric T-S diagram as a quantitative tool for analyzing distributions of temperature and salinity in the world's oceans. The three authors identified water classes by intervals of temperature and salinity values and then calculated the volume of each class. From the plots they produced, the volume contributed to the whole by each class was easily determined, and the classes comprising 50 and 75 percent levels of the total volume were identified.

The data from which the first volumetric censuses were produced were sparse; e.g., Montgomery (1958), who examined the Atlantic, included only one station from the Gulf of Mexico in his calculations. No previous T-S census for the Gulf of Mexico has been published, but two master's theses have presented results of T-S studies of Gulf data. Wilson (1967) based his quantitative estimates of the different T-S classes on data obtained from the *R/V Hidalgo* cruise of February and March 1962, a survey of the entire Gulf of Mexico in 126 stations. A second thesis to examine the T-S distribution of the Gulf of Mexico is that of Ulm (1983). Confining his study to the Texas-Louisiana continental shelf, Ulm based his analysis on historical data from 1958 to the time of his study, plus 1951-1953 cruises of the *M/V Alaska*. His data consisted largely of information obtained during monthly surveys conducted from the *R/V Gus III* between January 1963 and December 1965. Ulm produced monthly volumetric T-S diagrams for the shelf and, separately, bimonthly diagrams for the west and east shelf (divided at 95°W) regions of it. Following Montgomery (1958), Cochrane (1958), and Pollak (1958), he determined 50 and 75 percent contribution levels. Ulm also examined monthly-averaged volumetric distributions of temperature and salinity individually by month for the entire Texas-Louisiana shelf and for the western and eastern regions. He identified and followed modes of high and low volumes with given T-S values through time; he related them to river discharge and seasonal warming and drew seasonal inferences.

After determining volumetric T-S distributions for each of the ten LATEX A cruises for half-shelf and full-shelf regions as feasible, we used the results to prepare temporal distributions of the volume of water within distinct intervals of T and S, called univariate distributions of T and S over time. The unit used for volumetric T-S distributions and for univariate distributions is km^3. Both coarse- and fine-scale volumetric T-S distributions for each cruise are presented in the technical report. Also in that report are T-S distributions averaged over all May, July-August, November, and February cruises; these may be taken as estimates of the four seasonal volumetric distributions for the eastern shelf and as estimates for spring, summer, and fall for the western and entire shelf regions. Finally, univariate distributions in time of T and S for the east, west, and entire shelf also are included in that technical report.

Methods

For the eastern half shelf, data from each cruise were used to calculate volumetric T-S distributions. For the western half and for the whole shelf, data from each of the last six hydrographic cruises (H05-H10) were used to produce volumetric T-S distributions.

Two sets of volumetric T-S distributions were generated. Classes of 1°C by 1 salinity unit were used for the entire range of salinity and temperature. These distributions allow an examination of all fresh water sampled. On a finer scale, classes of 1°C by 0.2 in salinity were used for salinities ranging from 34 to 37. This salinity range encompasses the waters of the off-shelf Gulf of Mexico and shelf waters not directly influenced by river discharge.

For each cruise, a total volume for each T-S class was calculated over the study region. To accomplish this, the area of the study region or sub-region was divided into quadrangles of 15' latitude by 15' longitude (Figure E-1). Total volume for a T-S class is the sum of the volumes for that class under every quadrangle. For quadrangles that included bottom depths greater than 200 m only the upper 200 m of the water column was counted in the census. This decision was made because in the study region the shelf-slope break is near 200 m, and we did not wish to include the large volumes of deeper water seaward of the shelf edge but still within the quadrangles.

Temperature and salinity measured continuously with depth at each hydrographic station were binned in 0.5-m depth increments. For a given T-S class, a measure was found of the vertical thickness over which the T-S class occurred. For most T-S classes, the total thickness was zero. The vertical thicknesses of each T-S class at each station were gridded to regularly distributed points, the four corners of the grid boxes. The gridding scheme used is called a nearest neighbor algorithm (Wessel and Smith, 1993). It assigns an average value to each grid point having one or more observed points within a given search radius around the grid point. The average value was computed as a weighted mean of all the observed points within a search radius of one degree latitude, using the weighting function

$$w(r) = \frac{1.0}{1.0 + \left(\frac{3r}{R}\right)^2},$$

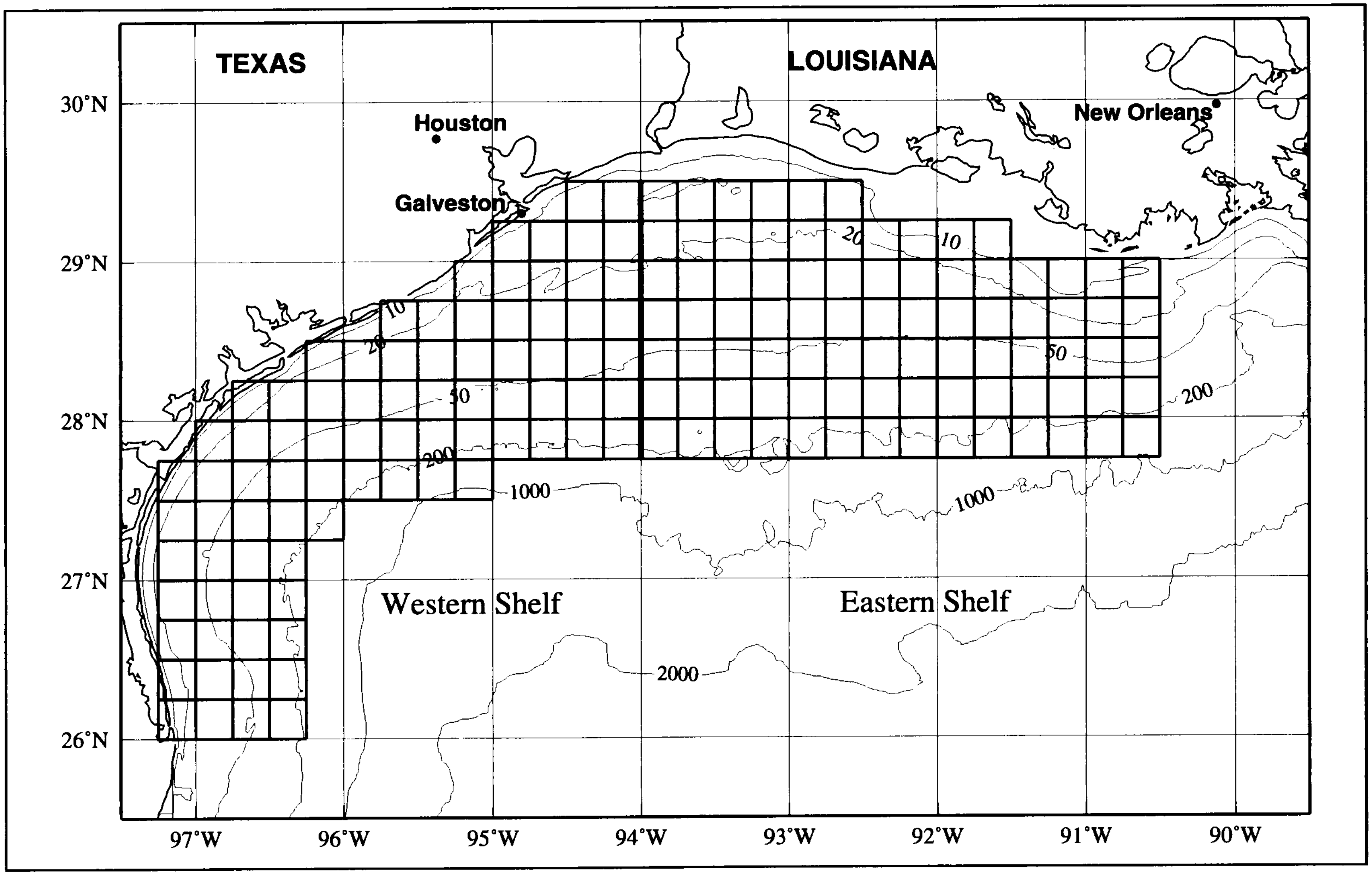

Figure E-1. The grid used for interpolation in the T-S census. Eastern and western shelves are separated at 94°W.

where r is the distance (in degrees) between the grid point and an observation point, and R is 0.2°. The mean vertical thickness for each quadrangle was approximated by averaging the thicknesses at the four corners. Multiplying the mean thickness by the area of the quadrangle yielded the volume for a given T-S class under the quadrangle.

Cruises H08 through H10 did not survey along the 50-m isobath. The method used to estimate volumes of water in each T-S class yielded a difference between the total volume for cruises H01-H07, which did include CTD stations along the 50-m isobath, and for cruises H08-H10, which did not. The total volumes sampled in the census for the eastern shelf were approximately the same for cruises H01-H07 (ranging from 3799.5 to 3821.4 km^3); this also was true for the western shelf portions of cruises H05-H07 (4078.9 to 4108.4 km^3). However, the shape of the bottom in cross-shelf profile is convex, and, without a depth constraint at the 50-m isobath, interpolation between stations produced a larger total volume for cruises H08-H10 without 50-m isobath stations than for cruises H01-H07. To prepare time series of the variation of volumetric distributions of both T and S, we required approximately the same total volumes for each survey of the eastern shelf, and likewise for the western shelf. Different sample volumes for different cruises would affect the time series without physical cause. Therefore, the average volume for the eastern shelf for the first seven cruises was obtained. Then, for each of the last three cruises the volumes for each T-S class in the eastern shelf were multiplied by this average total volume and divided by the total volume for that specific cruise. In this manner, the total volume for each of the last three cruises was prorated to be equal to the average volume over the eastern shelf for the first seven cruises. The same procedure was performed for the western shelf region.

The T-S classes (e.g., 11°-12°C and 35-36) having the largest volumes were summed until 50% of the total volume sampled over the shelf or half-shelf was reached. Those T-S classes are indicated in the volumetric T-S distributions. Likewise, the most voluminous T-S classes were summed to total 75% of the total volume; they, too, are indicated.

Volumetric T-S relationships and their temporal variability

In this section we first describe the "seasonal" volumetric T-S distributions for the eastern shelf. Then we examine the univariate distributions of T and S for the period of observations (May 1992-November 1994) to characterize effects of the seasonal heating cycle, wind-driven circulation, Mississippi-Atchafalaya river discharge, and offshore mesoscale rings on the T and S volumes over the Texas-Louisiana shelf.

For the eastern shelf there were three hydrographic cruises in May, July-August, and November, but only one in February. For each period, the volumetric T-S distributions for the eastern shelf were averaged as estimates of seasonal distributions. The spring, summer, and fall distributions are based only on data from three cruises in different years during the middle of each season (Figures E-2 through E-4). The winter distribution is not likely to be representative because data from only one cruise are available.

Table E-1 shows the salinity and temperature ranges of the T-S classes comprising 50% of the total volume of waters considered for this study. The temperature modes point to the perennial presence of colder, deep water offshore and seasonal heating and mixing of the upper waters. At the 50% volume level, a two- or three-mode pattern for temperature is seen throughout the year except in May. The cold mode, which changes little, represents the deep water at the outer shelf; the warmer modes correspond to volumes higher in the water column, which are subject to seasonal heating, freshwater influx, and mixing.

While results at the 50% volume level present one picture, examination of the coarse-scale plots for each comparison period reflects a different temperature regime over all the salinity classes (Li et al. 1996). When the fresher, inshore T-S classes are included, the peaks in the May temperatures distributions are at temperatures of 21-22°C . In August, inshore water was warmer (28-32°C). November temperatures in our study show evidence of a cooling trend, but are spread over a range (18-24°C).

The May results for the eastern shelf (Figure E-2) show that, at the 50% level, the greatest contribution of volume to the shelf is from open ocean water—temperatures in a continuous range from 17-23°C in the coarse resolution, with salinity of 35.5-36.5. The fine resolution results, omitting river-influenced waters, indicate the largest volumes lie between 15° and 23°C, with salinity slightly more narrowly refined to 35.6 to 36.4.

By August on the eastern shelf (Figure E-3), the 50% level of contribution has split into two modes for temperature and three for salinity in the coarse resolution. In the fine resolution image, both temperature and salinity are more confined, the temperature ranging from 14° to 23°C and salinity from 35.8 to 36.4

In November on the eastern shelf (Figure E-4), bimodal temperature and salinity results are evident in the coarse resolution image. Omitting the river-influenced waters, the 50% level in the fine resolution again illustrates the perennial dominance of the chillier, saltier open ocean.

Effects of wind-driven circulation and river discharge

The univariate distributions of S and T versus time over that part of the shelf east of 94°W are shown in Figure E-5. The contour lines for salinity show larger volumes of fresh waters over the eastern shelf in summer (cruises H02, H06, and H09) than in other seasons. Plotting the total volumes with salinity lower than 34 over the eastern shelf versus time (Figure E-6 upper) shows a peak for each summer cruise. We believe the mechanism responsible for

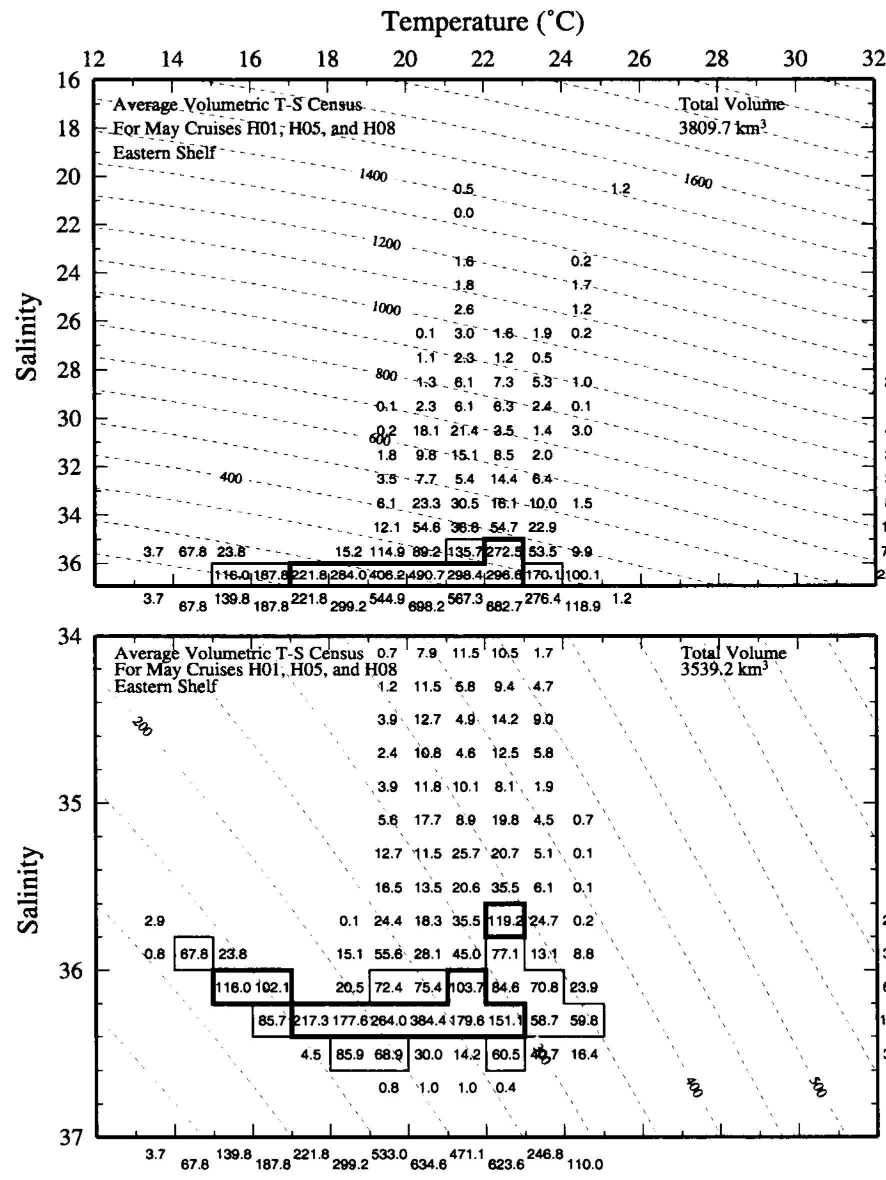

Figure E-2. Average volumetric T-S census for the shelf east of 94°W, based on May cruises (H01, H05, and H08). Resolution is 1°C by 1 (S) (upper panel), and 1°C by 0.2 (S) (lower panel). The heavy (light) line encloses the largest classes whose total volumes just exceed 50% (75%) of the volume of the region. Margin totals are volumes for intervals of T and S. Dashed lines are isopleths of specific volume anomaly in cl·t⁻¹.

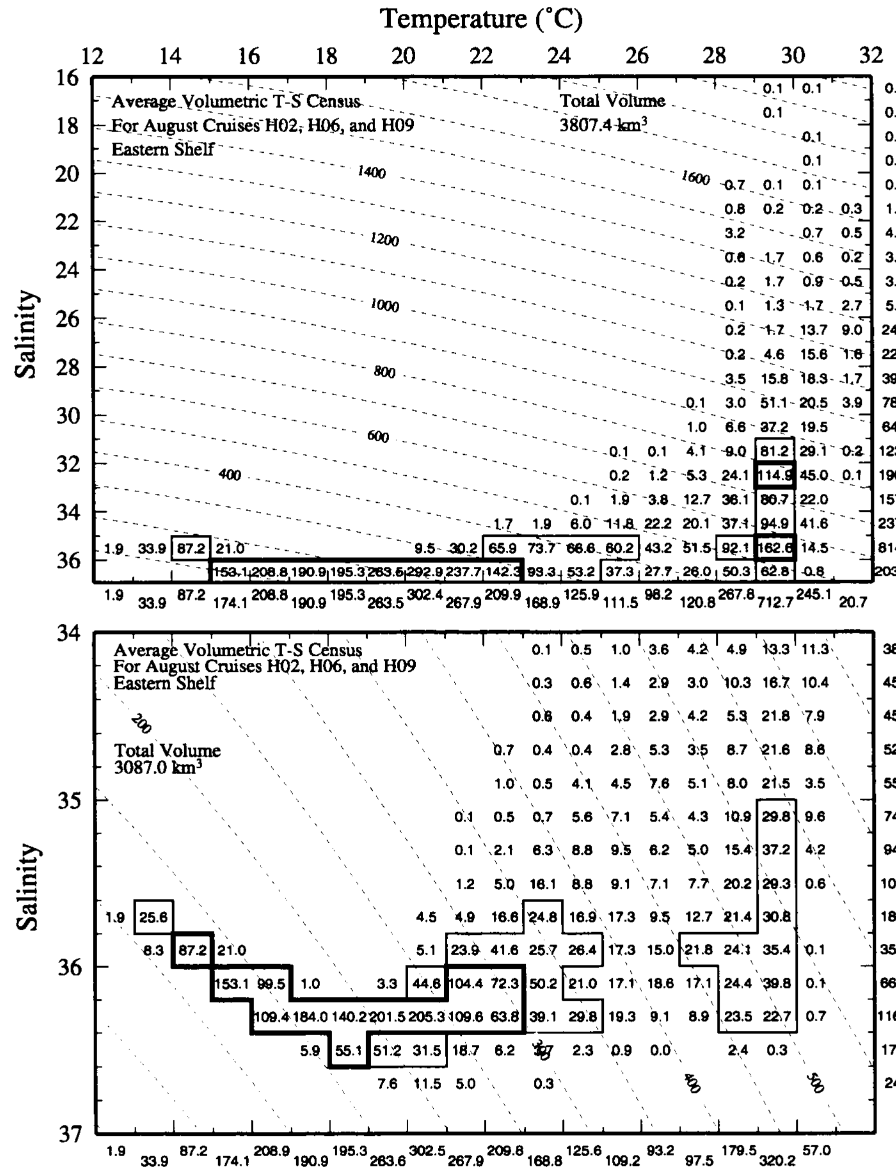

Figure E-3. Average volumetric T-S census for the shelf east of 94°W, based on July-August cruises (H02, H06, and H09). Resolution is 1°C by 1 (S) (upper panel), and 1°C by 0.2 (S) (lower panel). The heavy (light) line encloses the largest classes whose total volumes just exceed 50% (75%) of the volume of the region. Margin totals are volumes for intervals of T and S. Dashed lines are isopleths of specific volume anomaly in cl·t[-1].

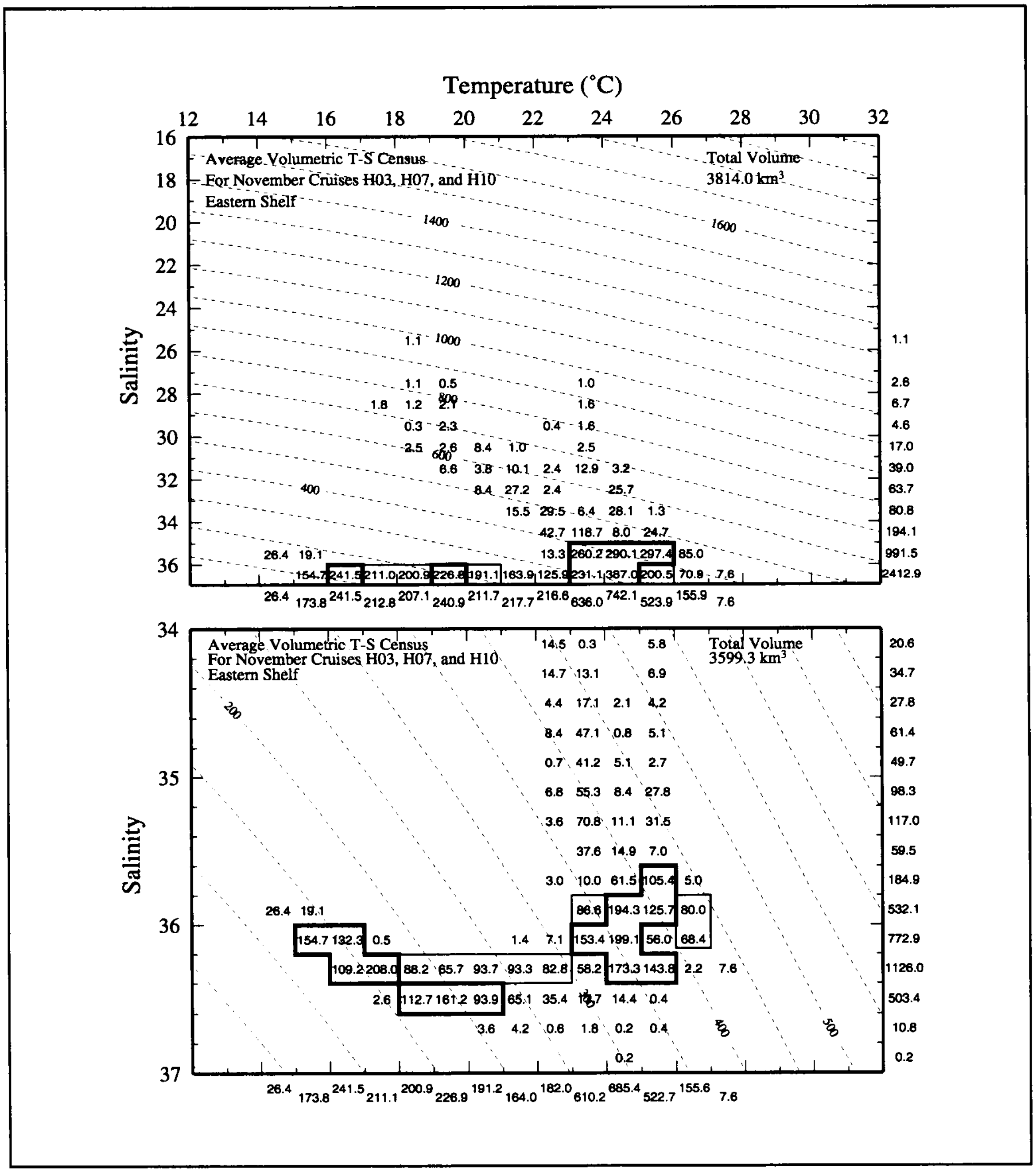

Figure E-4. Average volumetric T-S census for the shelf east of 94°W, based on November cruises (H03, H07, and H10). Resolution is 1°C by 1 (S) (upper panel), and 1°C by 0.2 (S) (lower panel). The heavy (light) line encloses the largest classes whose total volumes just exceed 50% (75%) of the volume of the region. Margin totals are volumes for intervals of T and S. Dashed lines are isopleths of specific volume anomaly in cl·t^{-1}.

Table E-1. Temperature and salinity classes accounting for the most voluminous T-S classes comprising 50% of the volume of the eastern shelf. These are based on average T-S relations.

Month	Temperature	Salinity
May	17-23	35-37
July - August	15-23 29-30	32-37
November	16-17 19-20 23-26	35-37

this pattern of variability is the seasonal circulation regime. The non-summer currents over the inner shelf are driven downcoast by prevailing downcoast components of winds over the shelf; the prevailing winds in summer have upcoast components and force upcoast flow over the inner shelf. The summer currents bring high salinity water upcoast as far as the central or eastern Texas shelf, and fresher water from the Mississippi and Atchafalaya rivers is dammed over the eastern half of the shelf. This results in the largest volumes of fresh water being over the eastern shelf in summer.

The univariate distributions of S and T versus time over the western shelf (west of 94°W) are shown in Figure E-7. There the largest volumes of fresh water were found during the two May cruises (H05 and H08) and the smallest volumes during the two summer cruises (H06 and H09). Figure E-6 (lower) shows total volumes of waters with salinity less than 34 over the western shelf as a function of cruise. The situation is the reverse of that for the eastern shelf (Figure E-6 upper). Again we attribute this pattern to the seasonal circulation over the inner shelf. Generally, April is the month of highest river discharge. During that month, and May as well, the average flow over the inner shelf has a downcoast component. This flow transports the lower salinity waters downcoast, increasing the total volume of fresher waters over the western shelf and decreasing those volumes over the eastern shelf. During summer (see months of July-August in Figure E-6) the upcoast flow transports more saline water from off Mexico, resulting in the largest (smallest) volumes of salty (fresh) water over the western shelf during summer.

Another feature evident in Figure E-5 is the occurrence of relatively fresh waters with salinity less than 24 at the times of cruises H04, H05, H06, H08, and H09. Examining the 1992, 1993, and 1994 daily Mississippi-Atchafayala river discharges relative to the 64-year average (Figure 2.3-1), it is seen that the discharge was higher than average before each of these cruises except H09. Prior to the H09 cruise in August 1994, the discharge had been above average from February through May, though it decreased to below or near average at that time. Thus, as expected, increased river discharge results in low salinity water in the inner region of the eastern shelf. However, increased river discharge does not seem well correlated

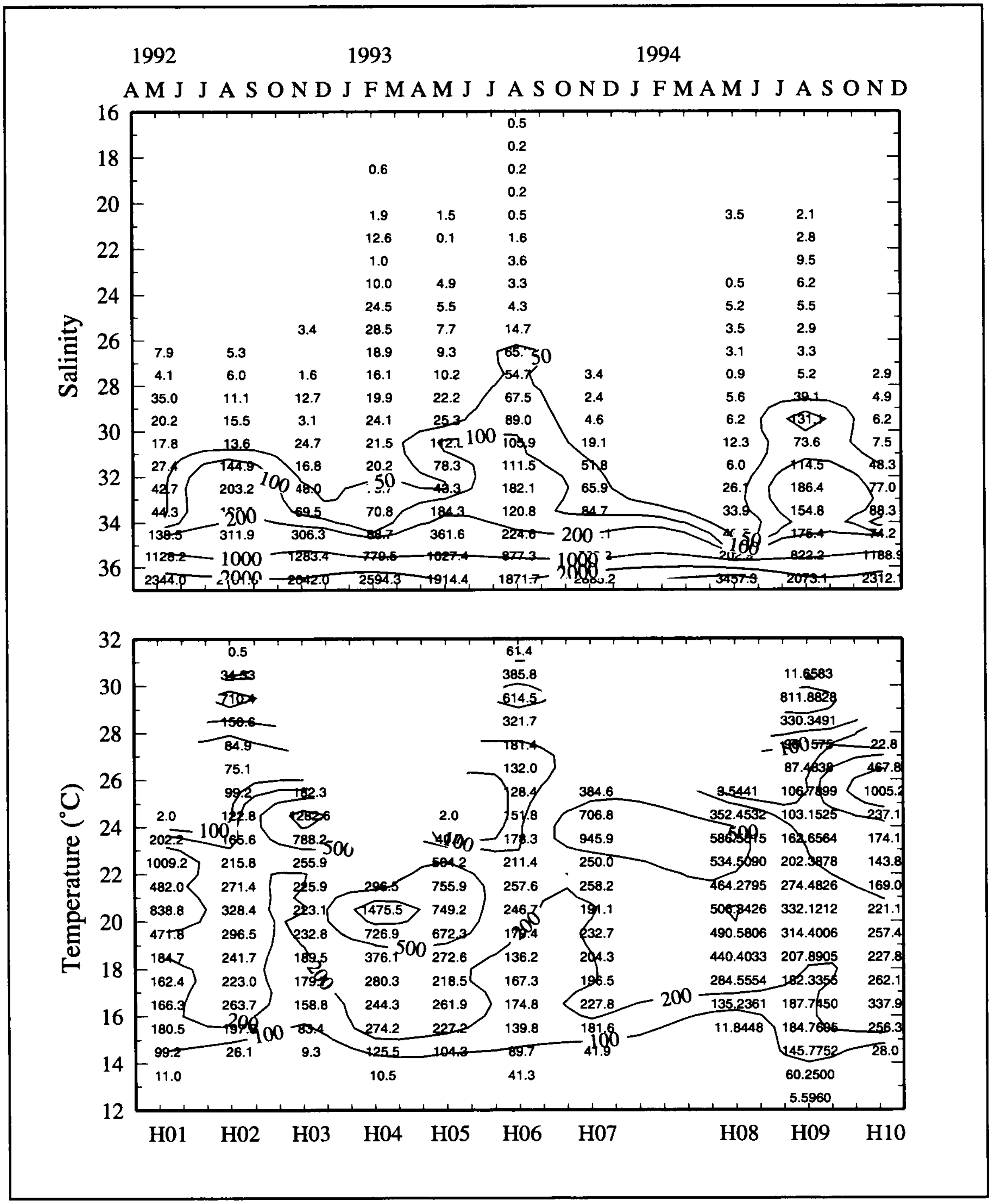

Figure E-5. Volumetric distributions of water within indicated intervals of salinity (upper panel) and temperature (lower panel) versus time (center of cruise period) over the shelf east of 94°W. Contours are in km³.

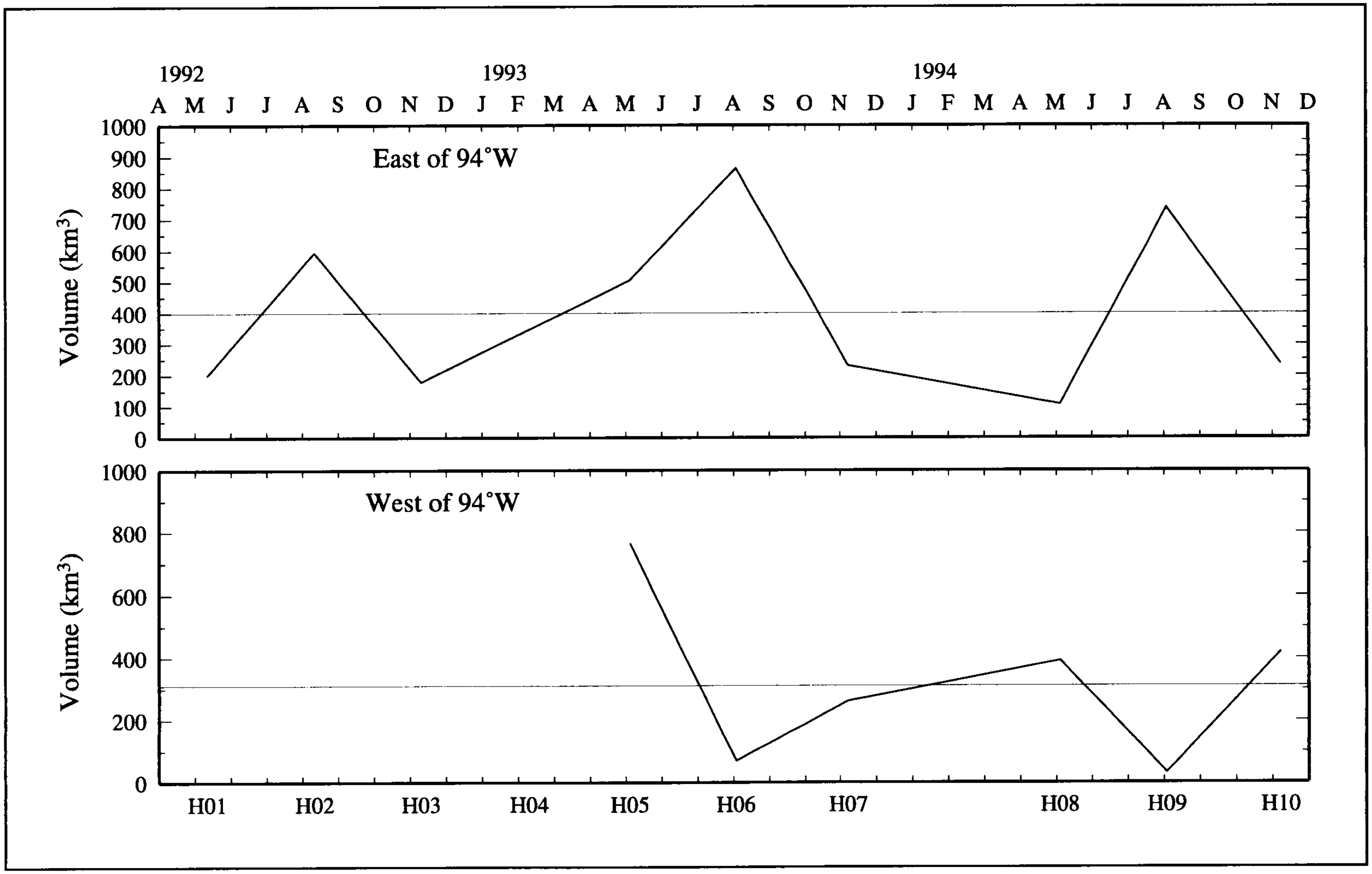

Figure E-6. Volumes of water with salinity < 34 versus time (center of cruise period) over eastern (upper panel) and western (lower panel) shelf.

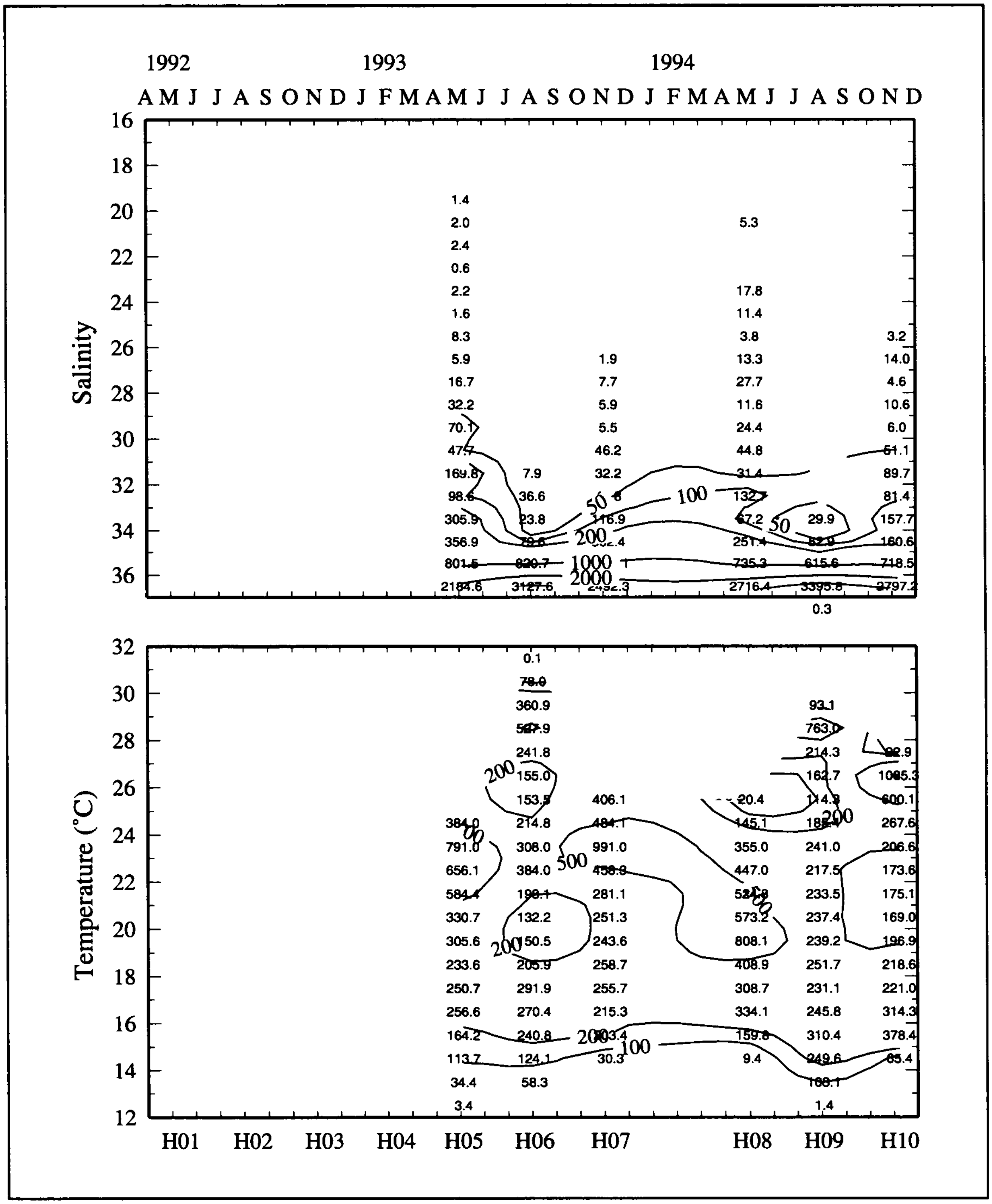

Figure E-7. Volumetric distributions of water within indicated intervals of salinity (upper panel) and temperature (lower panel) versus time over the Texas-Louisiana shelf west of 94°W. Contours are in km³.

with the total volume of fresh water on the eastern shelf, which is mainly controlled by the circulation regime.

Effects of annual heating

As expected because of seasonal heating, the univariate distributions of temperature versus time over the eastern and western shelves (Figures E-5 and E-7 lower) show that waters with highest temperatures were observed on the summer cruises (H02, H06, and H09). We examined the volumetric T-S distributions to determine the most voluminous temperature classes.

In the seasonal volumetric T-S distributions for the eastern shelf (Li et al. 1996), 50% of the volume is encompassed by temperatures in a continuous interval for February and May, but in several intervals of temperature for July-August and November. From the volumetric T-S distributions for each cruise we noted the temperature intervals of the most voluminous T-S classes occupying 50% of the volumes of eastern and western shelves; the results are given in Table E-2. For May cruises there is either only one continuous temperature interval or there are two intervals separated by only 1°; thus, essentially there is only one interval of temperature encompassing the most frequently occurring T-S classes occupying 50% of the shelf volume during May. This also is the case for the one winter cruise. For July-August and November cruises, however, there are two or three distinct temperature intervals, except over the eastern shelf for July-August cruise H09 and November cruise H03. Moreover, the warmest and coldest such intervals on each cruise are separated by relatively large temperature differences (3°-11°).

To understand the reason for this seasonal pattern, we examined vertical sections of T and S constructed from the LATEX CTD measurements along the 200-m isobath (Figures 3.1-4 and 3.1-5). That section is representative of the waters with largest volumes over the shelf because the depths at the shelf edge are so much larger than elsewhere. In winter (February), cooling and surface mixing produce a relatively deep (order of 100 m) surface mixed layer, the most voluminous temperature class. Spring (May) heating of this relatively deep surface mixed layer results in the most vertically uniform temperature gradients of any season; the temperature classes of largest volumes are nearly adjacent. Continued spring and summer heating and light summer winds result in a shallow mixed layer and thermoclines with large gradients. This leads to temperature classes of large volumes separated by differences corresponding to the temperatures of thermoclines. Surface cooling and stronger fall winds cool and deepen the mixed layer, creating large volumes of surface and sub-thermocline waters, both with narrow temperature ranges.

Table E-2. Temperature intervals (in °C) encompassing the most frequently occurring T-S classes occupying 50% of the volumes of the eastern (east of 94°W) and western regions of the LATEX shelf for each hydrographic cruise.

		Eastern shelf	Western shelf
	H01	19-21 22-23	no data
May	H05	16-23	16-25
	H08	18-22 23-24	16-21
	H02	15-22 29-30	no data
July - August	H06	14-25 28-30	16-18 22-24 28-30
	H09	14-23	14-17 18-21 28-29
	H03	23-25	no data
November	H07	16-17 23-26	17-19 23-26
	H10	16-18 19-20 25-27	15-18 25-27
February	H04	19-21	no data

Effects of anticyclonic rings near the shelf edge

Anticyclonic rings detached from the Loop Current, and their associated cyclonic eddies, are often found just offshore of the shelf break (200-m isobath). These Loop Current eddies have high salinity cores; maximum salinity in a vertical profile is associated with the core of the Subtropical Underwater (Wüst 1964). These rings have salinities above 36.7 near 200 m depth on detachment from the Loop Current (Nowlin 1972). Thus, the presence of these anticyclonic rings off the Texas-Louisiana shelf might be expected to affect the salinity of the shelf by transfer of waters between the rings and the shelf.

An example is given in Figure E-8 which shows temperature and salinity in vertical section along the 200-m isobath for cruise H06 (July-August 1993). During that cruise anticyclonic rings called Vazquez and Whopper were present near the shelf edge in the western and eastern shelf regions, respectively. At the time of the cruise, Vazquez was elongated northeast-southwest and impinged on the shelf edge in two regions, centered near 50 km and 225 km, as can be seen by the depression of isotherms in these regions. The large ring Whopper appears to affect the shelf edge waters from about 350 to 600 km judging by the depression of isotherms over that region. Regions affected by Vazquez and Whopper are marked in the salinity section by values greater than 36.4, and in the case of Whopper and one arm of Vazquez by salinities greater than 36.6.

We have found a clear correspondence between the presence of shelf water with salinity greater than 36.6 and the presence of anticyclonic eddies. Shown in Figure E-9 for each cruise are volumes of water over the shelf or sub-region with salinity greater than 36.6. In the western offshore Gulf, water with salinity higher than 36.6 must be contributed by these

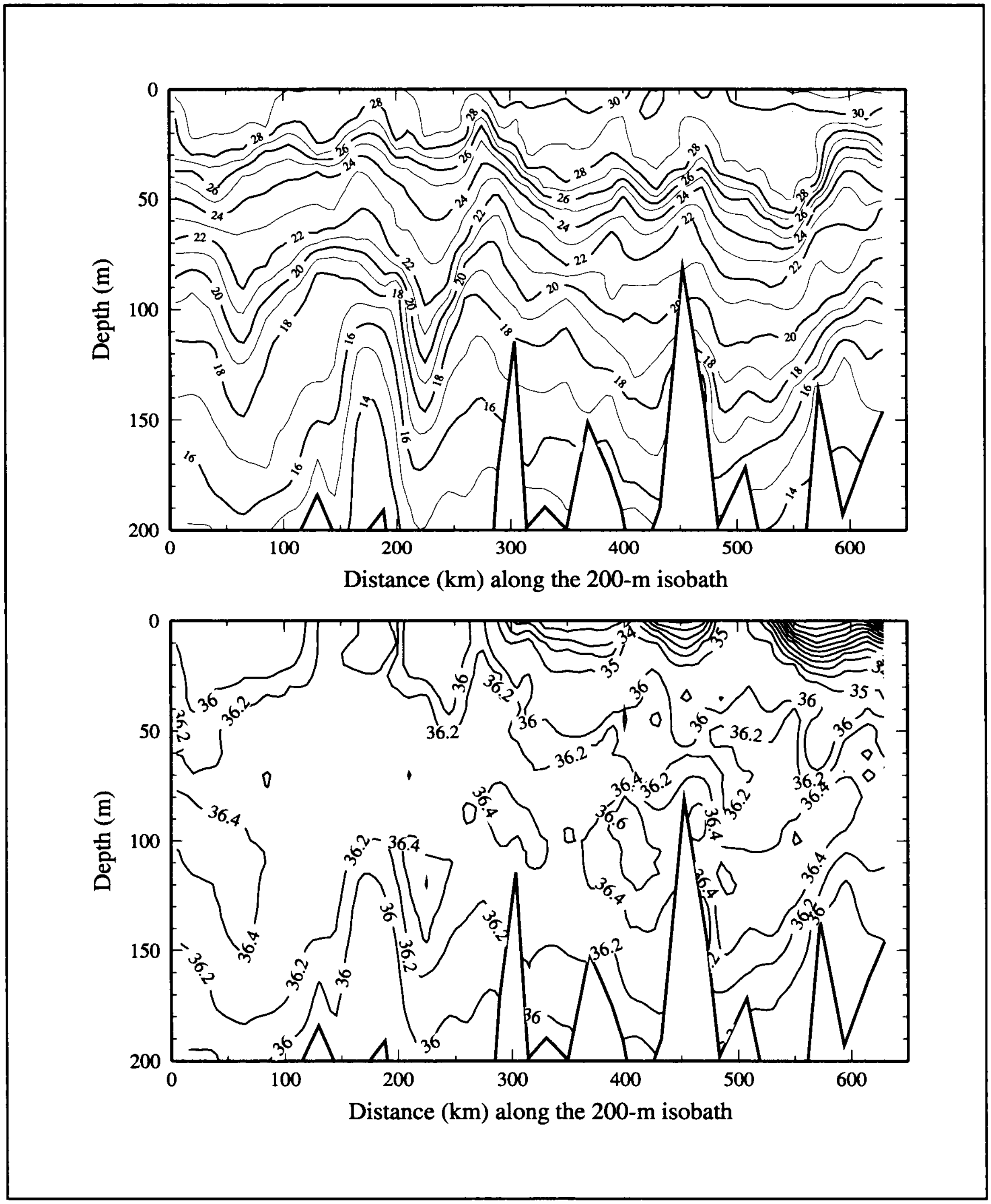

Figure E-8. Temperature (°C; upper panel) and salinity (lower panel) in vertical section along the 200-m isobath for cruise H06, from southwest on the left to east on the right.

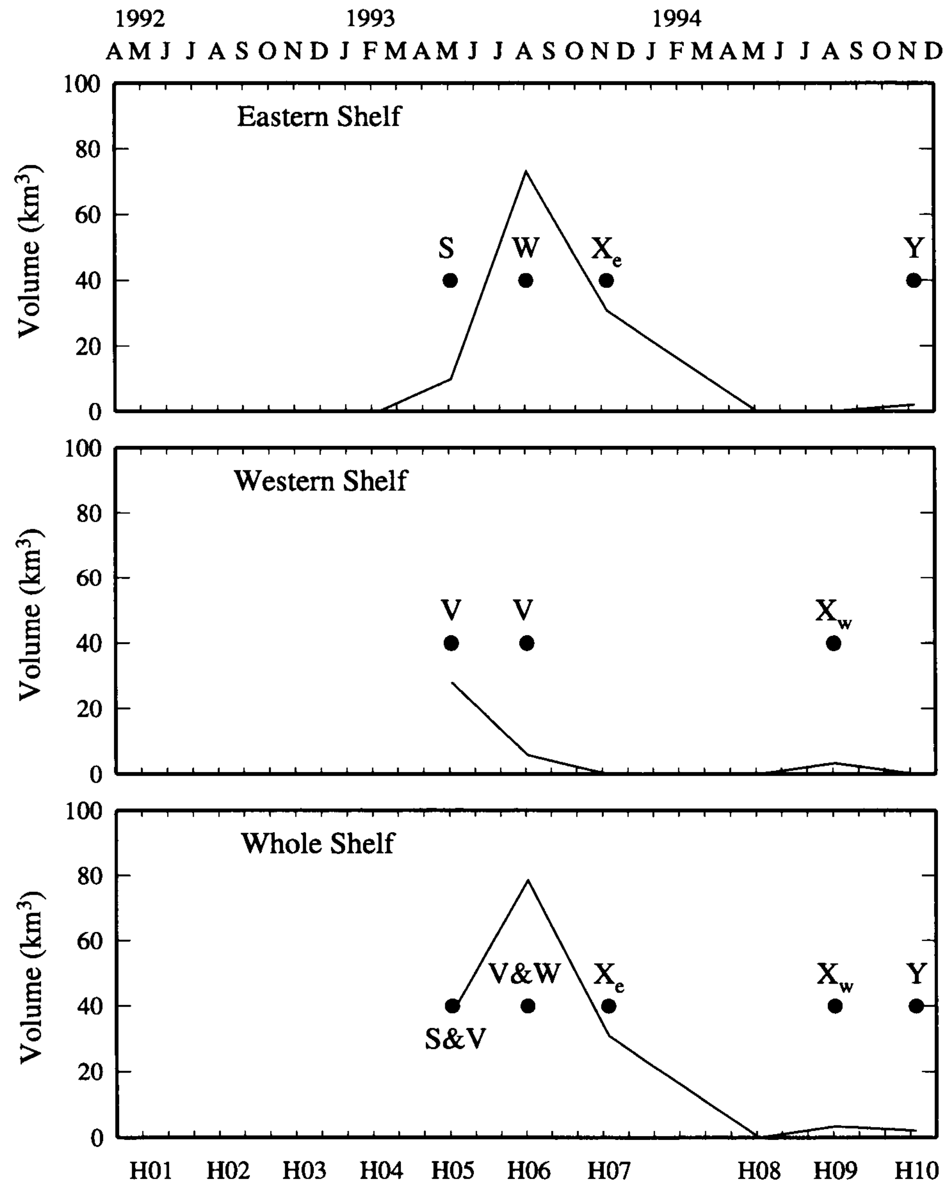

Figure E-9. Volumes of water with salinity > 36.6 over the Texas-Louisiana shelf as a function of time (center of cruise period). The presence at the shelf edge of anticyclonic rings detached from the Loop Current is indicated by the following: S = unnamed eddy south of the Mississippi Delta; V = Eddy Vazquez; W = Eddy Whopper; X_e = eastern ring split from Eddy eXtra; X_w = western ring split from Eddy eXtra; and Y = Eddy Yucatan.

anticyclonic eddies (Nowlin 1972). The dots in Figure E-9 indicate the presence of anticyclonic rings near the shelf edge during the LATEX cruise periods.

Conclusions

The circulation regime over the inner shelf strongly influences the volumetric distribution of salinity over both the eastern and western shelf. The discharge from the Mississippi-Atchafalaya rivers leads to low salinity waters (minimum salinities seen in the census) over the inner regions of both eastern and western shelves in spring. However, this discharge is not correlated with the total volume of fresh water over the eastern shelf. That volume is at a maximum in summer when the wind-driven circulation over the inner shelf is upcoast and maintains a surface layer of fresh water in that region. Over the western shelf, the volume of fresh water is at an annual maximum in spring and a minimum in summer. The spring maximum results from a combination of enhanced river discharge and downcoast flow; the summer minimum results from upcoast transport of salty water from off Mexico by the summer upcoast flow regime. Cochrane and Kelly (1986) discussed the effects of summer versus non-summer current regimes on the surface salinity and arrived at a similar qualitative result.

The annual cycle of heating and cooling and the wind mixing of surface layers principally control the distribution of the temperature versus time over this shelf. This leads to the most voluminous temperature classes exhibiting a continuous temperature range (from 15° to 24°C) in winter and spring, but splitting into several modes, separated by the vertical temperature ranges of the thermoclines, in summer and fall.

The presence of anticyclonic rings near the shelf break seems well correlated with the presence of water saltier than 36.6 on the shelf. Salinities greater than 36.6 associated with the core of Subtropical Underwater are found near 200 m in anticyclonic rings detached from the Loop Current; salinities this great are not generally present at the Subtropical Underwater core outside rings in the western Gulf. Thus, we conclude that the interaction of Loop Current rings with the shelf results in the exchange of waters between the rings and the shelf.

Appendix F: Inertial and Superinertial Motions

F.1 Deterministic tides

This appendix focuses on the description of the principal tidal current and sea surface height (SSH) constituents on the Texas-Louisiana shelf as measured by the LATEX A current meter array (DiMarco and Reid 1998). Eight principal tidal constituents were analyzed. The tidal current ellipses for each constituent were estimated from 81 current velocity time series at the 31 LATEX current meter locations (Section 1.2). Sea surface height tidal constituents were estimated using data recorded from five bottom-mounted pressure gauges. Discussed here are the time series and methods used to estimate the tidal constituents, the principal tidal currents, and the sea surface height tidal constituents.

It should be noted that the tidal estimates presented in this chapter represent the average tidal currents during the period April 1992 through November 1994. If they are to be used for tidal forecasting and prediction, a correction accounting for the nodal variation of the declination of the moon should be applied to these estimates.

Methodology

The principal tidal constituents were determined using the iterated least squares method of cyclic descent (Bloomfield 1976; DiMarco 1998). The phase and amplitude of four diurnal tidal periods (O1, K1, P1, and Q1) and four semi-diurnal tidal periods (S2, M2, K2, and N2) were estimated from a 3 to 40-hr band-passed filtered version of the current meter time series. The names, symbols, and periods of the eight principal tidal constituents analyzed are given in Table F.1-1.

Diurnal stratification of the surface layer during the summer season (June through August) enhances the excitation of strong oscillations of 24-hr period and with amplitudes on the order of 20 $cm \cdot s^{-1}$ at some locations on the Texas-Louisiana shelf (DiMarco et al. 1997). In addition, wind-driven inertial oscillations also contribute to the kinetic energy in the vicinity of the diurnal tidal constituents (Chen et al. 1996). The latitude of the moorings on the shelf defines a range of inertial periods of 24.4 hr at the north and 26.2 hr at the south. This inertial range includes the principal lunar (O1) tide (period = 25.82 hr) and is at slightly longer periods than the lunar-solar diurnal (K1) and principal solar diurnal (P1) tides, of tidal periods 23.93 and 24.07 hr, respectively. Because of the multiple sources for oscillating currents of near-diurnal periods, tidal extraction is not attainable by simply band-pass filtering the raw time series. However, using sufficiently long time series, the deterministic tides can be adequately separated from the randomly phased inertial (wind-driven) events by using a least squares harmonic analysis approach. The large amplitudes of the diurnal oscillations, however, will continue to contaminate the estimates for the diurnal constituents even in a

Table F.1-1. Periods of principal tidal constituents.

Symbol	Name	Period (solar hours)
	Semi-diurnal	
M2	principal lunar	12.42
S2	principal solar	12.00
N2	larger lunar elliptic	12.66
K2	luni-solar semi-diurnal	11.97
	Diurnal	
K1	luni-solar diurnal	23.93
O1	principal lunar diurnal	25.82
P1	principal solar diurnal	24.07
Q1	larger lunar elliptic	26.87

least-squares analysis. For this reason, the time series for June, July, and August are omitted from the analysis presented here. Tidal ellipses were constructed from the phase and amplitudes of the north-south and east-west components of each tidal current constituent (Godin 1972).

Principal tidal currents

The main tidal current constituents were found to be M2, S2, O1, K1, and P1. Together they account for an average of 92 percent of the total tidal variance estimated from the maximum amplitudes of the eight tidal current constituents. Maximum M2, K1, and O1 amplitudes were approximately the same order of magnitude and account for an average of 76 percent of the total near-surface tidal energy at the LATEX moorings. Figure F.1-1 shows contours of the percentage of total tidal energy for the eight analyzed tidal current constituents to total energy variance in the 8-40 hr energy band for the LATEX upper instruments (essentially at 10 m depths). At the shelf edge (along the 200-m isobath), the tidal energy accounts for less than 10 percent of the total variance in the 8-40 hr band of the energy spectrum. The percentage of tidal energy increases closer to shore and in the wider regions of the shelf. The percentage is greatest in the shallow region southwest of Atchafalaya Bay where it exceeds 40 percent. There is also a local maximum in this ratio at the upper meter at mooring 21 in the central shelf southeast of Galveston, which is attributed to low amounts of non-tidal energy in the 8-40 hr energy band.

Semi-diurnal tidal currents

The M2 tide dominated the semi-diurnal energy band (11 to 14 hr) of the energy spectrum at all station locations. A plan view of the M2 tidal current ellipses estimated from the upper current meter at each location is shown in Figure F.1-2. The current ellipses are generally

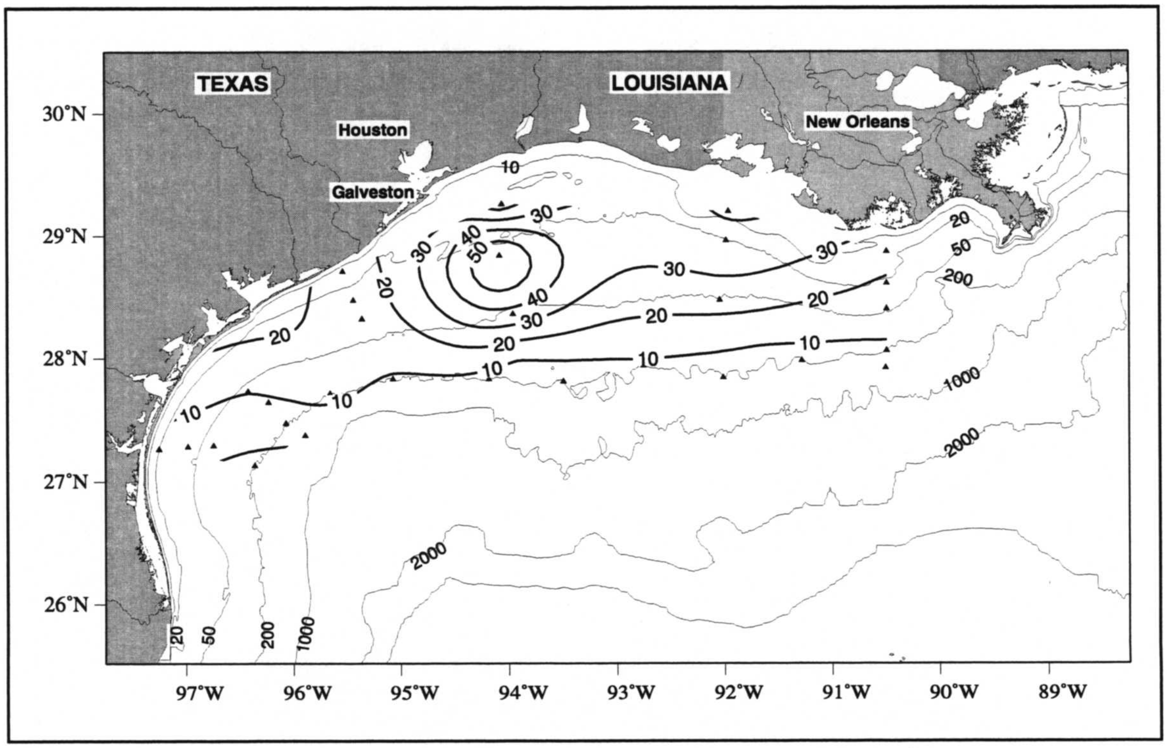

Figure F.1-1. Percentage of energy associated with eight principal tidal current constituents relative to total energy in 8-40 hr energy band for upper instruments. Triangles represent current meter locations. Contour interval is 10% (from DiMarco and Reid 1998).

oriented with major axes across the bathymetry lines at the shelf edge and are rotating anticyclonically. This figure provides qualitative verification of the tidal model of Reid and Whitaker (1981), particularly at the inner shelf and eastern region near Mississippi Canyon where the observed orientations and magnitudes agree with the model results for the same parameters.

Phase information is depicted as a dot on each tidal ellipse to signify the direction of the current vector at an arbitrary time (chosen to be 0000 UTC 7 April 1992). Together these dots essentially represent a synoptic snapshot of the tidal vectors. It has been shown in the model study by Reid and Whitaker (1981) that the sea surface height propagates cyclonically (counterclockwise) around the Gulf of Mexico basin with an amphidromic point north of the Yucatan peninsula. Quantitative interpretation of the phase is difficult because of the error associated with both the amplitude and orientation of the current ellipse. However, the phase of the M2 tidal currents provides qualitative verification of that model, in that there is

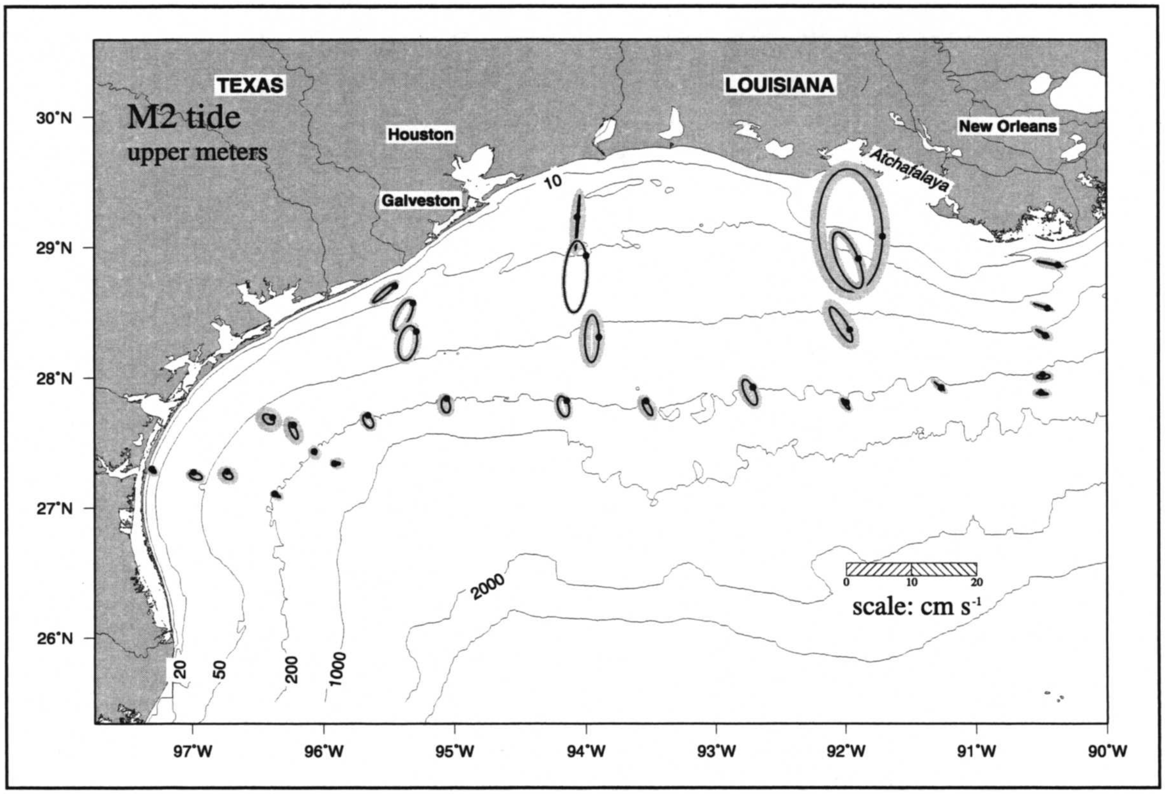

Figure F.1-2. M2 tidal current ellipses of upper current meters showing orientation of tidal current vector at 0000 UTC 7 April 1992 (dot) and least squares error estimates (shaded) (from DiMarco and Reid 1998).

a time lag between the M2 tidal vectors of the western stations relative to those in the east. The phase angle should be considered relative to a local bathymetric (along- and cross-shelf) coordinate system.

Figure F.1-3 shows a vertical section along the 50-m isobath of the M2 tidal current. We see nearly vertical contours (barotropic) and maximum amplitudes at mid-shelf (Clarke and Battisti 1981). There is some evidence of shear at the top current meters of the inner-shelf particularly for the S2 tide. The other semi-diurnal tidal constituents behave similarly along the 50-m isobath.

Along the shelf break, an average of 19.4 percent of the total tidal variance was attributable to the M2 tide. This average percentage increased closer to shore to 24.0 for instruments along the 50-m isobath, to 29.6 at approximately the 20-m isobath, and to 31.2 at the shallowest mooring location of each cross-shelf mooring line. On average over the entire shelf, the M2 tidal current was 21.8 percent of the total tidal variance. The percentage of

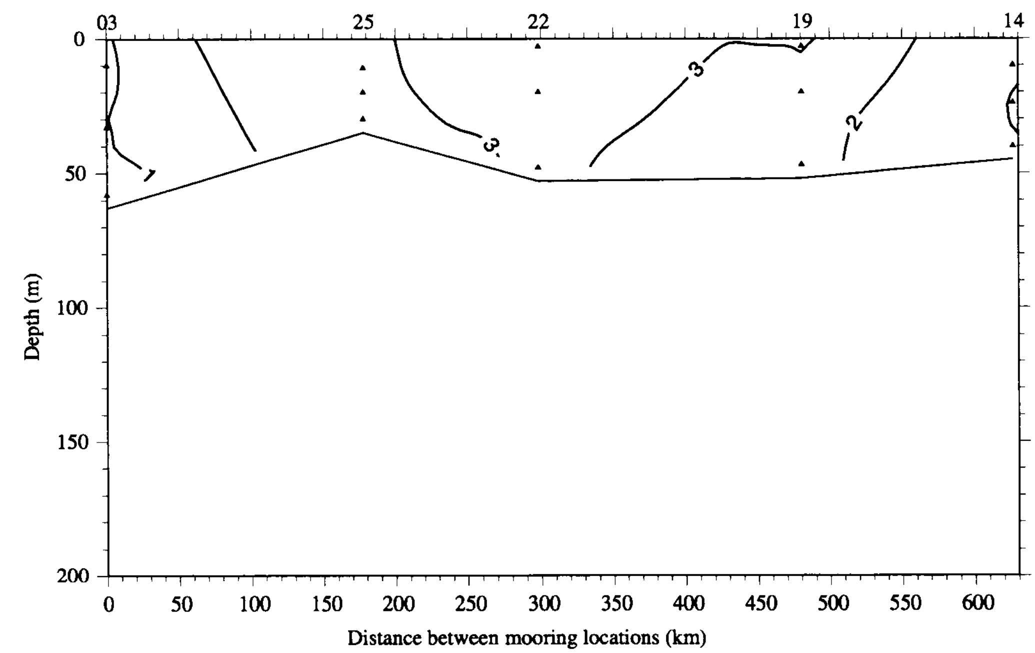

Figure F.1-3. Vertical section of maximum M2 tidal current amplitude along 50-m isobath. Contour interval is 1 cm·s^{-1} (from DiMarco and Reid 1998).

total tidal variance due to the S2, N2, and K2 tides was generally less than 5 percent across the shelf.

Figure F.1-4 shows a cross section of the maximum M2 tidal current amplitudes of the cross-shelf line which follows the 92°W meridional line. The M2 tide shows little evidence of vertical shearing beyond the 50-m isobath. The contours become more inclined in the shallower region near mooring 17 as bottom friction plays a larger role in the shallow water near the coast. This line is representative of the other cross-shelf lines at 92.5°W and 95.5°W. The general pattern is slightly changed for the line along 94°W, where there is a surface maximum at mooring 21.

Diurnal tidal currents

We define the diurnal energy band (22-28 hr) to contain the inertial periods found on the Texas-Louisiana shelf as well as the principal diurnal tidal periods. The two largest diurnal

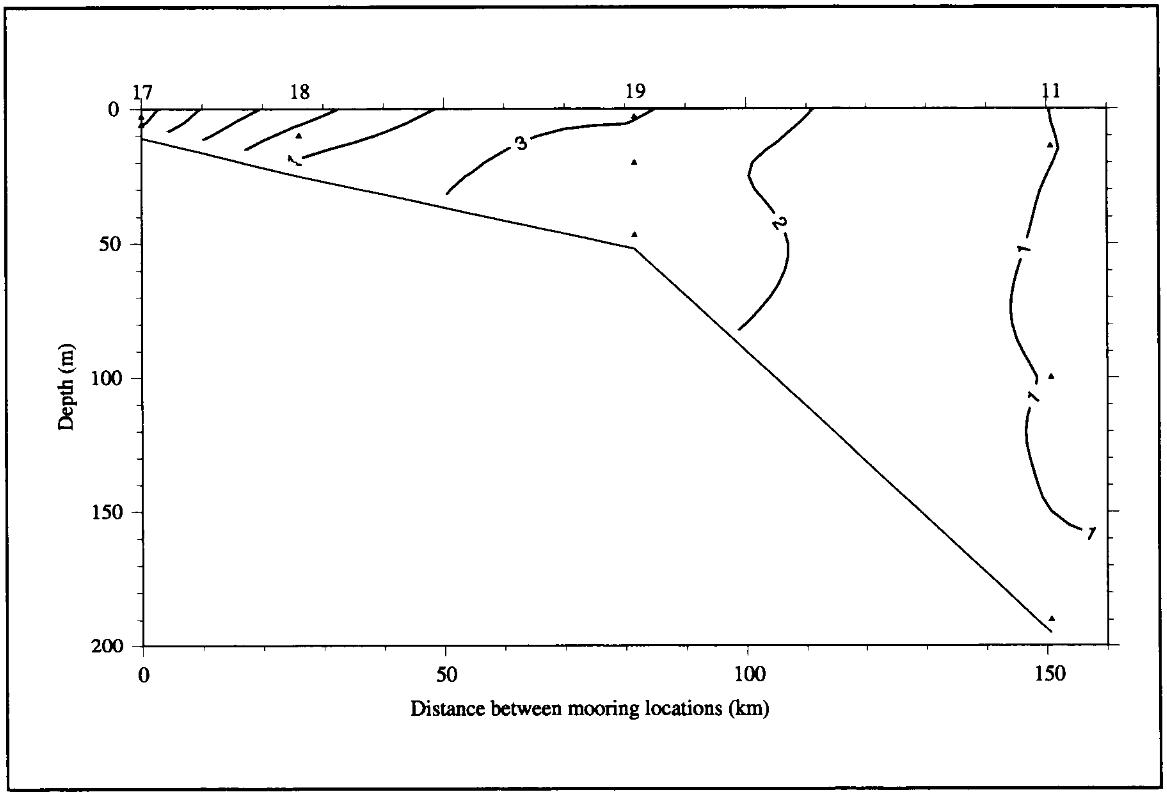

Figure F.1-4. Vertical section of maximum M2 tidal current amplitude along 92°W. Contour interval is 1 cm·s^{-1} (from DiMarco and Reid 1998).

tidal current constituents on the shelf were found to be O1 (period = 25.82 hr) and K1 (period = 23.93 hr).

The O1 tidal component (period = 25.82 hr) ranges from 6 percent to 48 percent (average of 24.8 percent) of the total tidal variance making it on average the second largest tidal current component on the Texas- Louisiana shelf.

The O1 tidal ellipses of the LATEX upper current meters are shown in Figure F.1-5. The upper O1 tidal current ellipses are more circular than those found for the semidiurnal constituents and are clockwise rotating. At the four mooring locations (17, 19, 20, and 22) for which the upper current meter was at a depth of only three meters, maximum amplitudes are larger than for other moorings with the upper instrument at 10 m. This is an indication of the strong vertical shear generally found in the diurnal tidal constituents. The alignment of the tidal ellipses with respect to the bathymetry (when an orientation could be determined) are similar to that found in the semi-diurnal constituents, in that the semi-major axes of the

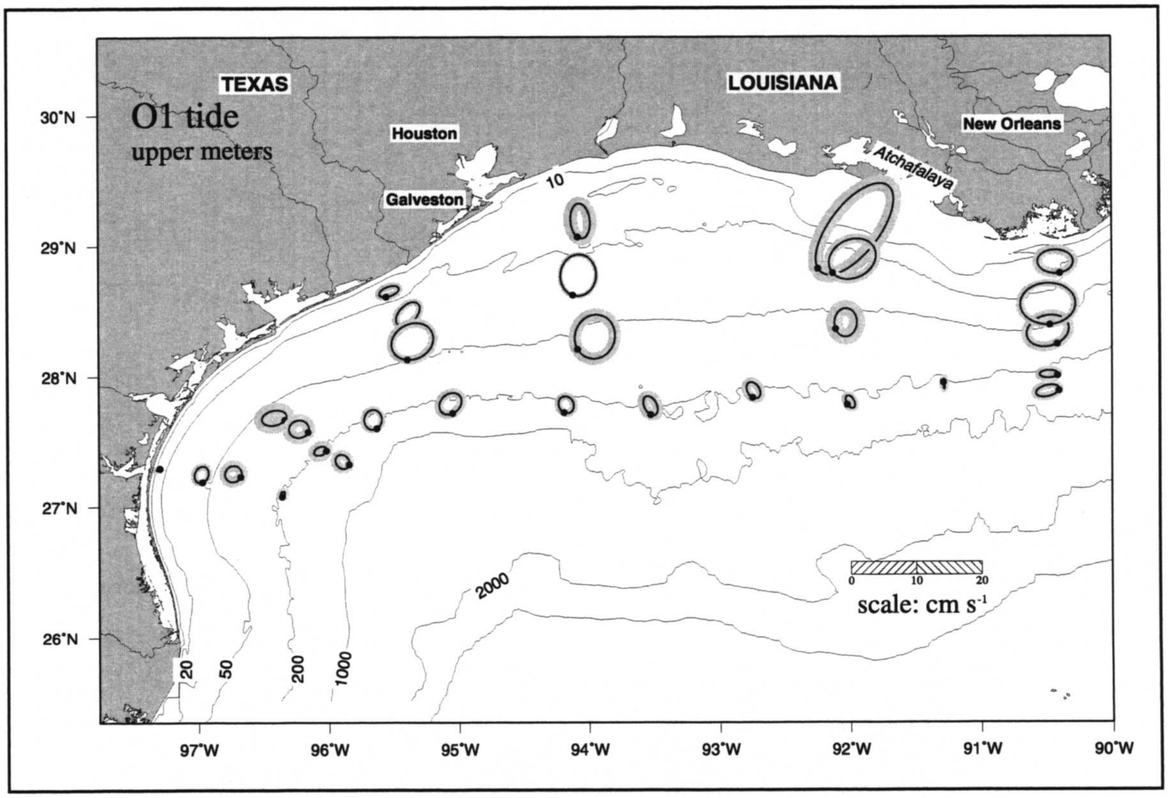

Figure F.1-5. O1 tidal current ellipses of upper current meters showing orientation of tidal current vector at 0000 UTC 7 April 1992 (dot) and least squares estimates (shaded) (from DiMarco and Reid 1998).

ellipses lie across bathymetric lines. Notable exceptions to this are again in the far east along 90.5°W where the ellipses run parallel to the bathymetry and moorings 23 and 24 where the ellipses are essentially parallel to the coast. The latter two moorings are located in a region where the shelf narrows.

The position of the O1 current vector at the time chosen in Figure F.1-2 is also indicated by a dot on the tidal ellipses of Figure F.1-5. The phase angle relative to the local bathymetry is more uniform across the shelf than the phase of the M2 tidal current, particularly along the 200-m isobath. The observed O1 ellipses and uniformity of the phase provide further verification of the Reid and Whitaker model on the shelf, in that there is good qualitative agreement for the O1 current ellipse magnitude, orientation, and phase.

Figure F.1-6 shows the maximum O1 tidal current at moorings along the 50-m isobath. In contrast to the Figure F.1-3 (M2 tidal current), the contours run horizontally (nearly parallel to the bottom) with no indication of amplification by the wide regions of the shelf. There is

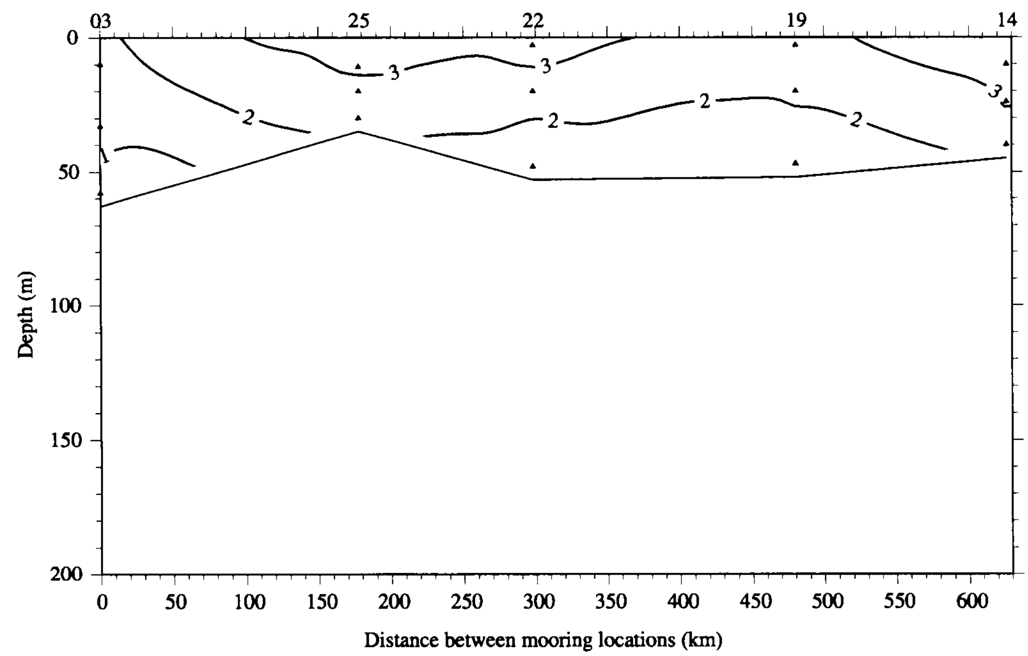

Figure F.1-6. Vertical section of maximum O1 tidal current amplitude along 50-m isobath. Contour interval is 1 cm·s^{-1} (from DiMarco and Reid 1998).

little vertical structure of the O1 tidal current along the 200-m isobath. At moorings east of 93°W, the maximum O1 tidal current amplitudes are more barotropic and uniform with depth.

A vertical cross-section of the maximum O1 tidal current amplitude along the 92°W meridian is shown in Figure F.1-7. Apparent in this figure are the horizontal contours representing significant vertical shear past 100-m depth in the diurnal tidal currents. The shear is greatest near shore, as in the semi-diurnal cross-sections, but extends across the 100-m isobath and close to the shelf edge. For moorings 1-4, located at approximately 27.3°N, the currents are more homogeneous throughout the water column. However, this figure (F.1-7) is representative of all the diurnal tidal current cross-shelf over the inner shelf east of 95.5°W. Presented in Figure F.1-8 are the tidal current ellipses for the K1 tide. The K1 tidal component ranges from 3 percent to 75 percent (average 29 percent) of the total tidal variance and is, therefore, the largest tidal current component on the Texas-Louisiana shelf. At the mid-shelf and eastern shelf regions, the maximum K1 amplitudes are similar to those found for

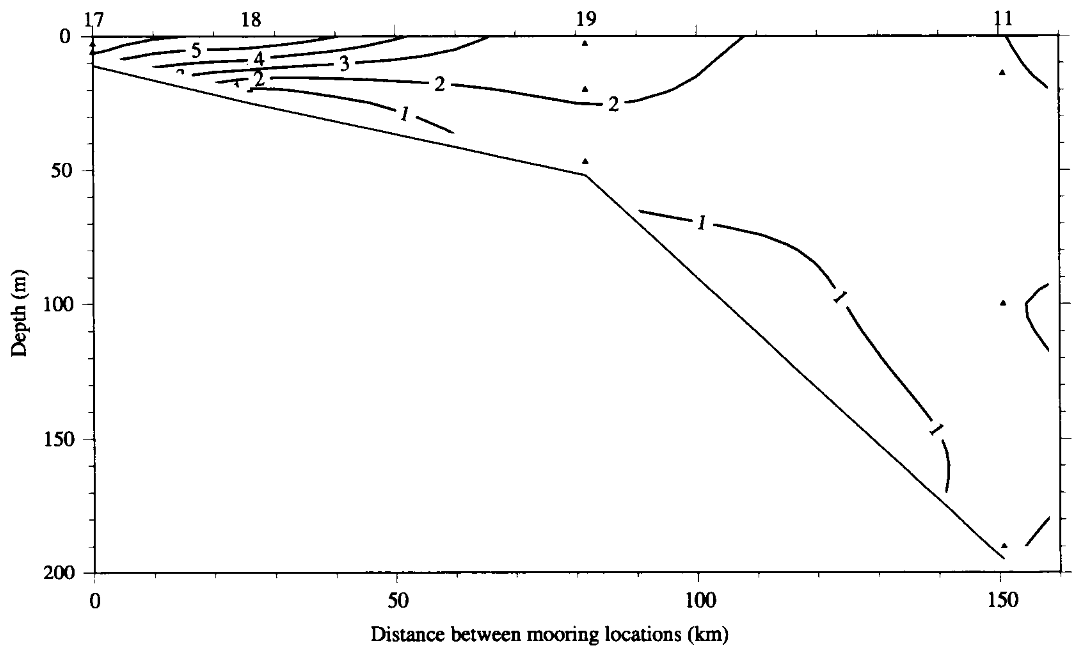

Figure F.1-7. Vertical section of maximum O1 tidal current amplitude along 92°W. Contour interval is 1 cm·s^{-1} (from DiMarco and Reid 1998).

the O1 tidal current. The K1 tide shows similar shear along the 50-m and more shear along 200-m isobaths. As with the O1 tide, the phase of the K1 tide generally is uniform across the shelf.

The root mean square for all eight tidal current constituents of the upper current meters is shown in Figure F.1-9. The figure can be regarded as representing an equivalent amplitude of the average variance attributable to the eight principal tidal constituents. This figure shows that the tidal current amplitudes attributable to the principal tidal constituents are greatest at the wide central shelf regions between 91°W and 95°W. Amplitudes decrease along the narrow shelf region in the west and bending southward. The largest amplitude is found near mooring 17 at the Atchafalaya Bay. The amplitude isopleths run essentially parallel to the bathymetry between the 50- and 200-m isobaths. The variation of these amplitudes is primarily due to the combined effects of the wide shelf amplification processes of the semi-diurnal constituents, stratification, and bottom friction.

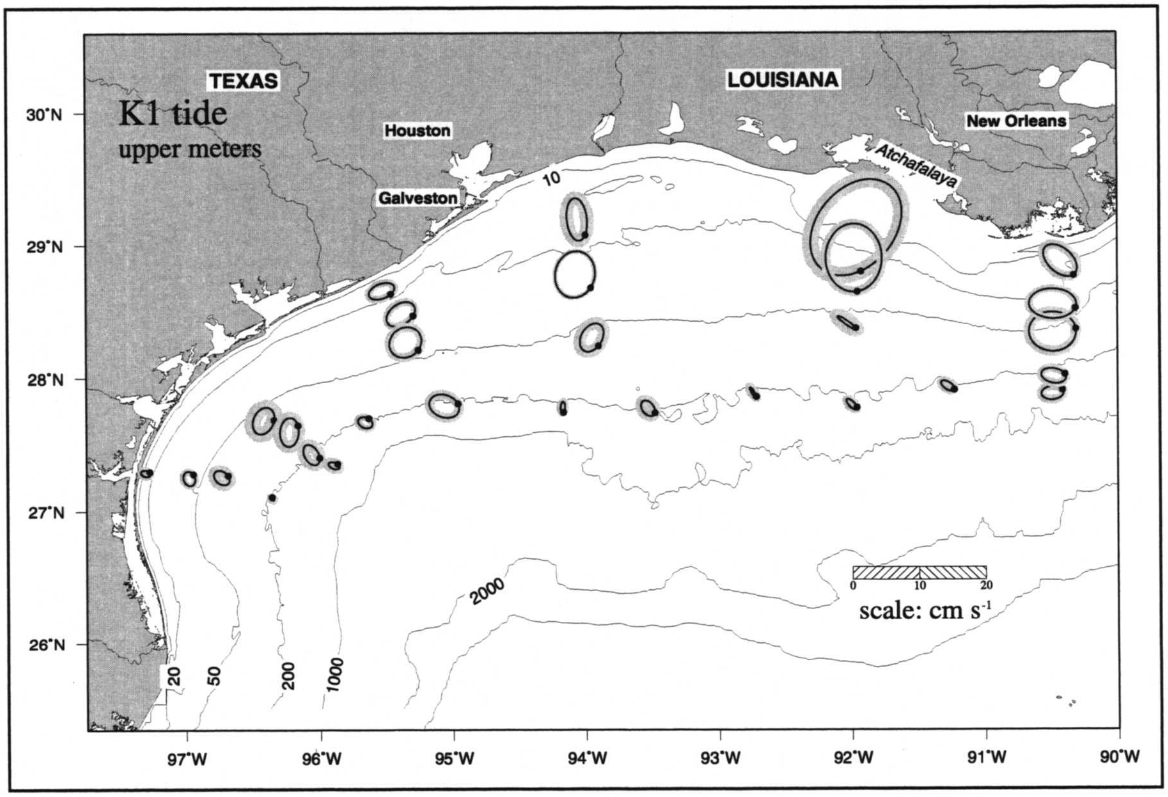

Figure F.1-8. K1 tidal current ellipses of upper current meters showing orientation of tidal current vector at 0000 UTC 7 April 1992 (dot) and least squares error estimat (shaded) (from DiMarco and Reid 1998).

Principal tidal sea surface heights

Sea surface heights were recorded at five mooring locations (moorings 1, 16, 17, 20, and 23 in Figure 1.2-1) using bottom-mounted pressure gauges (MiniSpec directional wave gauges). These gauges were positioned in water depths of 7 to 20 meters. The sea surface height tidal constituents were estimated from the pressure time series using the method of cyclic descent. Table F.1-2 summarizes the magnitude and phase for the five most energetic tidal constituents (M2, S2, K1, O1, and P1). The tidal phases of this table were determined using tables given by Shureman (1976).

From Table F.1-2, we see for the M2 tidal phase a lag between the western stations (1, 23, and 20) relative to stations in the east consistent with the tidal current ellipse and the model study of Reid and Whitaker (1981). This phase lag is also seen in the S2 tide. The phase for each of the diurnal constituents is essentially uniform across the shelf. Also evident is the

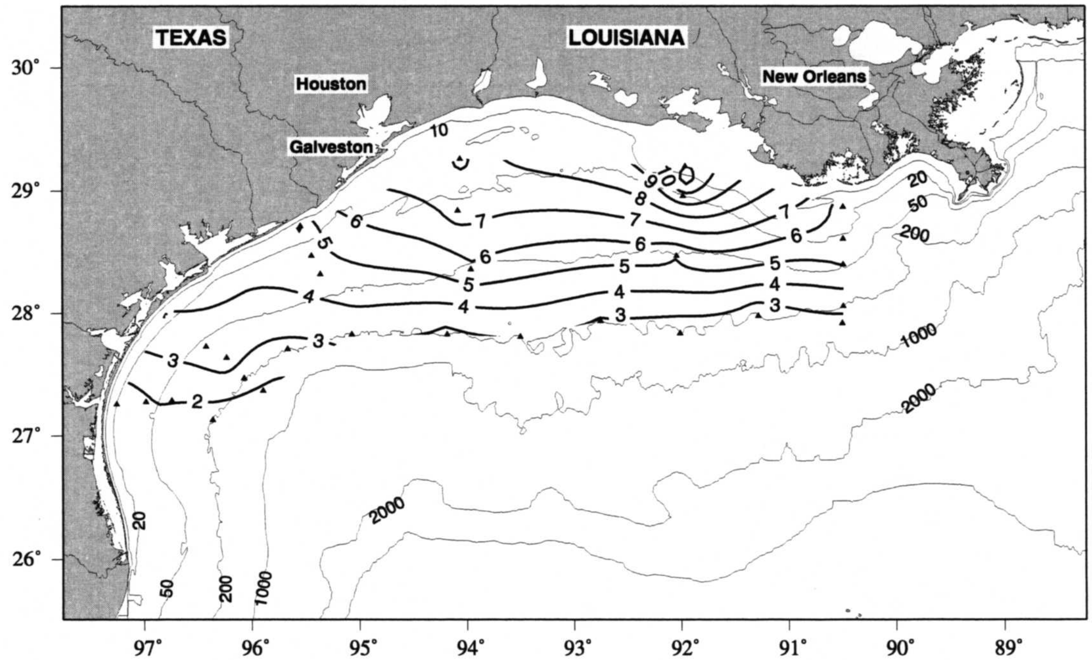

Figure F.1-9. Contour map of root mean square of eight principal tidal current maximum amplitudes for upper current meters. Contour interval is 1 cm·s^{-1} (from DiMarco and Reid 1998).

amplification of the semi-diurnal magnitudes at the mid-shelf locations, particularly at mooring 20.

The tidal amplitudes listed here compare well to historical values recorded at five locations (Capurro and Reid 1972) that were in close proximity to LATEX A mooring locations. For example, the tidal amplitudes for a station at 29.78°N, 93.35°W (near LATEX mooring 20) are 16, 5, 14, and 13 cm, for the M2, S2, K1, and O1 tides, respectively.

Table F.1-2. Magnitude and phase of major sea surface height tidal constituents at LATEX A tide gauge locations. Mooring 16 was easternmost on the Texas-Louisiana shelf; mooring 1 was westernmost.

Mooring	Name	Period (hr)	Magnitude (cm)	Phase (deg)
16	M2	12.42	2.5	172
17	M2	12.42	10.4	239
20	M2	12.42	17.0	265
23	M2	12.42	8.6	268
1	M2	12.42	8.0	260
16	S2	12.00	1.9	129
17	S2	12.00	3.1	218
20	S2	12.00	4.8	252
23	S2	12.00	1.7	245
1	S2	12.00	1.6	233
16	K1	23.93	15.8	15
17	K1	23.93	15.6	21
20	K1	23.93	16.4	28
23	K1	23.93	15.2	25
1	K1	23.93	15.8	25
16	O1	25.82	14.1	10
17	O1	25.82	14.9	14
20	O1	25.82	15.2	17
23	O1	25.82	14.5	16
1	O1	25.82	14.2	16
16	P1	24.07	4.38	35
17	P1	24.07	4.70	31
20	P1	24.07	4.40	27
23	P1	24.07	3.52	37
1	P1	24.07	4.01	46

F.2 Non-deterministic 40-hr high-passed signals

This section addresses the non-tidal signals in the period band 3-40 hrs from the LATEX A current meter data. These signals include near-inertial motions and currents associated with internal gravity waves. (Note: the local inertial period varies from 24.2 to 26.4 hours over the domain of the shelf mooring array.) There also exists a strong thermally induced signal at 24.0-hr period, particularly during the summer months. Unlike the tidal motions that are quite predictable, the non-tidal signals at periods lower than 40 hours are non-deterministic, with the possible exception of motions associated with storm surges, as in the Hurricane Andrew episode of August 1992 (Appendix B.1). The discussion below focuses on the large difference that exists between the near inertial motion in summer and nonsummer and the vastly different sensitivity of these motions to wind forcing on the Texas-Louisiana shelf.

Spectra of currents and winds

Chen et al. (1996) give evidence of inertial-like clockwise rotating motion in a period band of about 22 to 28 hrs based on the LATEX A current meter mooring data for the first 99 days (15 April to 22 July 1992) of the measurement program. Rotary spectra (Gonella 1972) for 10, 100, and 190 m depths at mooring 9 and the 10 m depth at moorings 2, 15 and 21 based on hourly samples of 3-hr low-pass currents showed strong peaks for clockwise relative to counterclockwise rotation centered about 25 hours. Rotary spectra based on wind measurements at five meteorological stations across the shelf near 94°W show similar results for the same time period. One of the conclusions drawn from these preliminary results was that the energetic and ubiquitous occurrence over the Texas-Louisiana shelf of clockwise motion in the 22- to 28-hr band of current and of wind data is largely due to inertial motion in both the atmospheric and oceanic Ekman layers associated with sudden changes of pressure gradient accompanying frontal passages. More complete evidence presented in Section 4.5 and here, based on the 32 months of LATEX A mooring data, shows that the above conclusion was premature because of the small sample that included both spring and summer. However, the 32-month data set does confirm that the rotary motions in the 22- to 28-hr band are predominantly clockwise, even after removing the reliable estimates of tidal signals discussed in section F.1.

Figures 4.5-5a and 4.5-5b show autospectra by seasons of the alongshelf and cross-shelf components of gridded wind near mooring 23 and of the 10-m current at that mooring, respectively, based on all 256-hr non-overlapping segments available for the LATEX A sampling period. In contrast to the spectra presented in Chen et al. (1996) that were based on the spring and summer of 1992, these show striking differences between summer and all other seasons, particulary with respect to the very dominant peak in the summer wind spectra. For all other moorings we have obtained autospectra for gridded wind and top level currents for summer and non-summer months. Figures F.2-1 and F.2-2 show the auto-spectra for

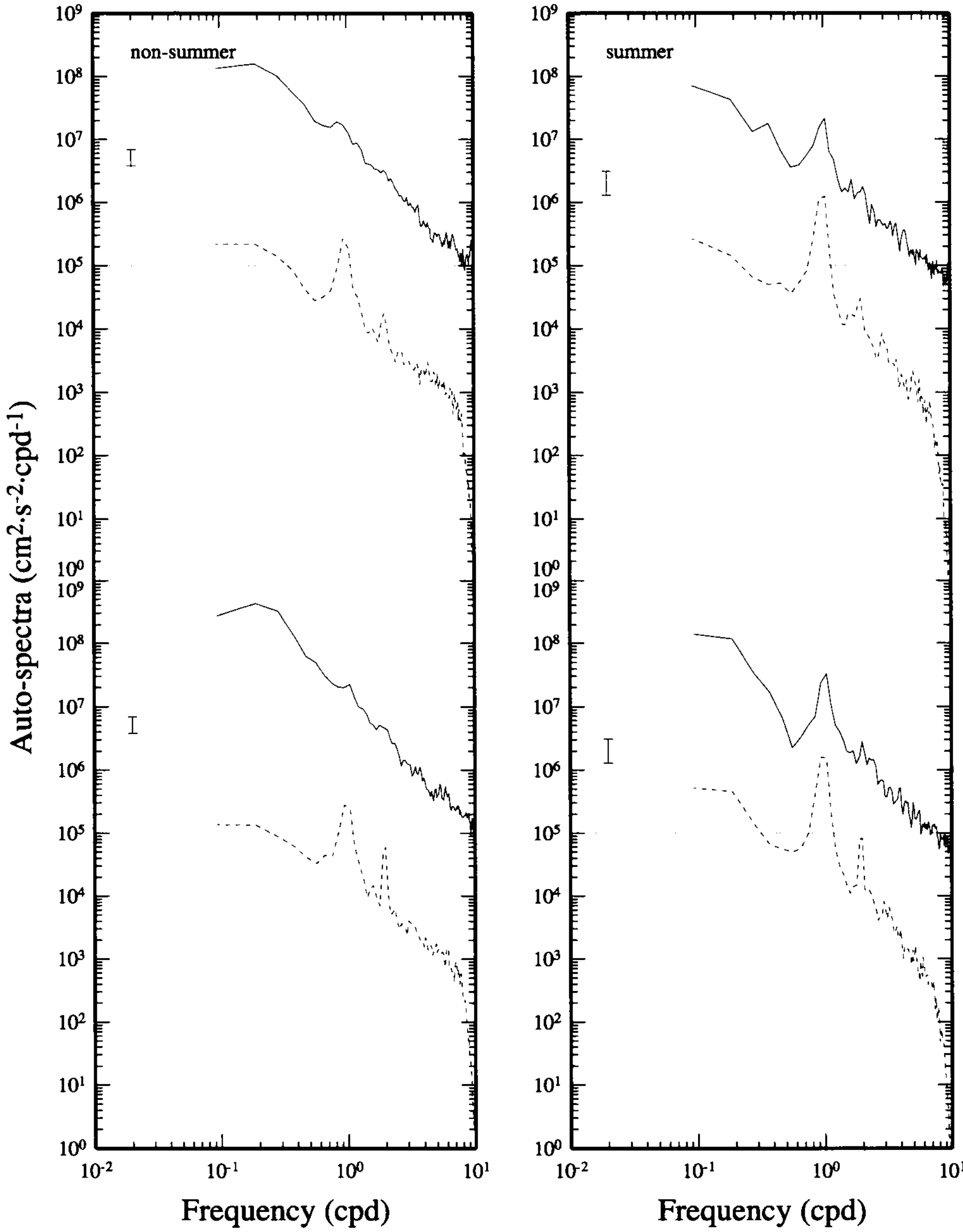

Figure F.2-1. Auto-spectra of alongshelf (upper) and cross-shelf (lower) components of top level current (dashed) and gridded wind (solid) at mooring 22 by season with tide included, based on all 32 months of LATEX A data.

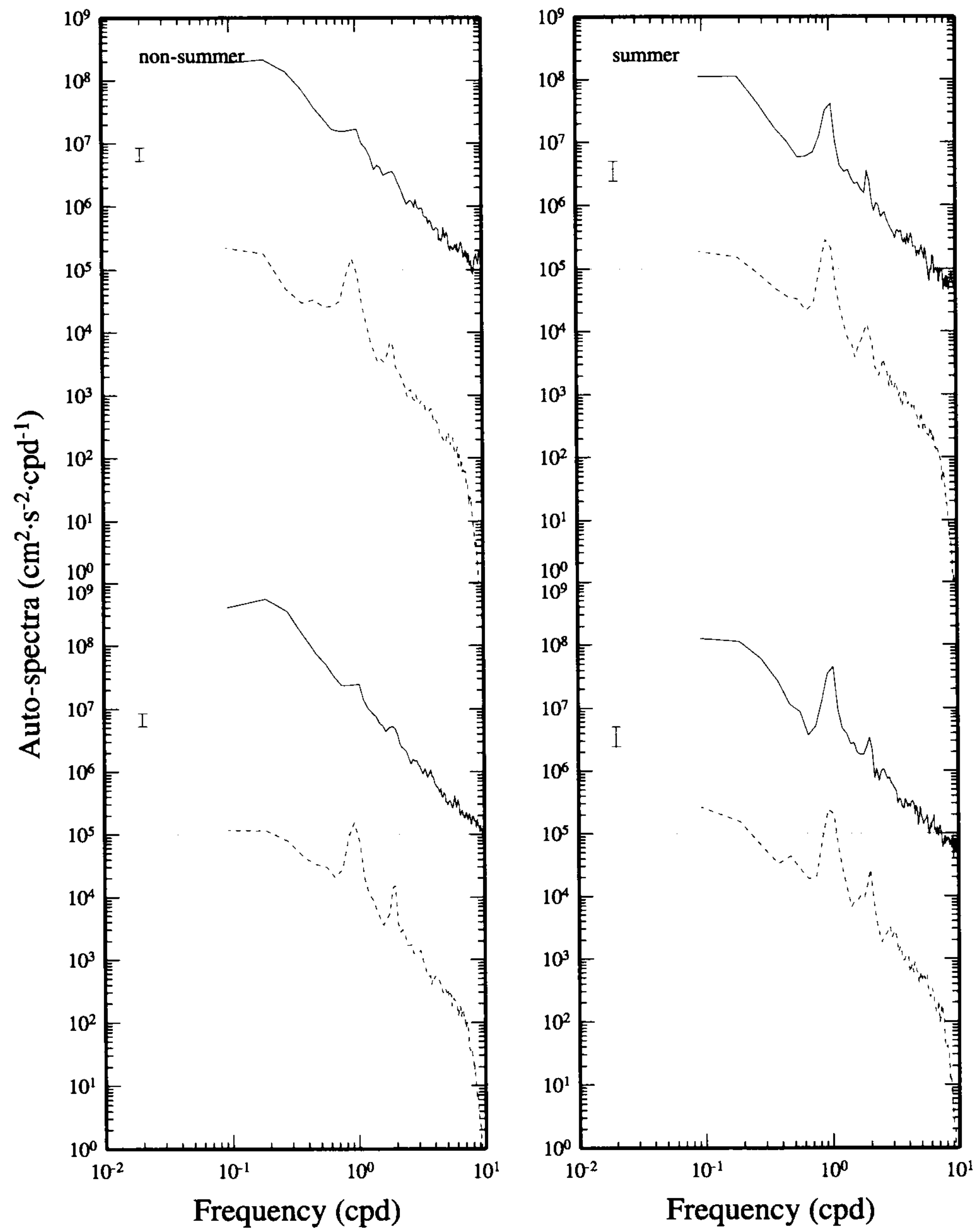

Figure F.2-2. Auto-spectra of alongshelf (upper) and cross-shelf (lower) components of top level current (dashed) and gridded wind (solid) at mooring 8 by season with tide included, based on all 32 months of LATEX A data.

wind and current for these two seasons for moorings 22 and 8. These spectra are typical of all moorings at water depths near 50 and 200 m, respectively, while the spectra in Figure 4.5-5 are typical of all nearshore moorings. We emphasize that the peak in the summer wind spectra near the diurnal period is equally as energetic on the outer shelf as on the inner shelf. Although such a peak in the wind spectrum might be expected nearshore associated with coastal sea breeze (Hsu 1972), it is quite unlikely that a similar peak at shelfbreak locations could be due to the same mechanism.

Time domain analyses

Figure F.2-3 contrasts the 3 to 40-hr band-passed alongshelf current at the top level for mooring 22 during March 1994 with that for June 1994. The periods of largest oscillations (about 20 $cm{\cdot}s^{-1}$) in March follow frontal passages as detected in the wind data at mooring 22. A comparable sequence (not shown) for the band-passed cross-shelf current occurs but leads in phase. The June sequence shows maximum amplitudes of about 60 $cm{\cdot}s^{-1}$ during periods of light winds at mooring 22. The period of greatly diminished amplitude occurs following a frontal passage detected in wind measurements at coastal station SRST2. The mean period of the oscillations for the June 1994 sample is very close to 24.0 hrs and seems to be an illustration of thermally induced cycling (Price et al. 1986), in which large amplitude rotary currents of 24-hr period can in exist in thin mixed layers typical of the summer season. The amplitude of the rotary current during weak wind regimes seems to be governed more by the heat flux than the competing effect of wind stress at the sea surface according to Price et al. (1986). However, during periods of occasional strong winds that deepen the mixed layer without adding much rotary momentum, the rotary current actually decreases.

Motivated by the evidence for a thermally-induced 24.0-hr signal in the June 1994 LATEX data, we carried out complex demodulation analysis (Bloomfield 1976) for the complete mooring 21 current meter data. Basically this allows one to obtain a time sequence of the amplitude for a very narrow band centered on 24.0 hrs. Figure F.2-4 shows the amplitude versus time over the 32 months of LATEX measurements at the top current meter of mooring 21 for the along- and cross-shelf 24-hr current signal. The resulting amplitude sequences for both current components indicate nearly equal maximum values during the three summer months and especially in June of each year. The maximum June amplitude for the top current meter at mooring 21 is seen to be only about 8 $cm{\cdot}s^{-1}$ compared with 60 $cm{\cdot}s^{-1}$ for the top current meter at mooring 22 (Figure F.2-3). This is probably due to the shallower depth (3 m) for mooring 22 compared with 14 m for mooring 21.

The evidence strongly suggests that the summer rotary currents are thermally induced 24.0-hr period oscillations rather than inertial, whose period ranges from 24.2 to 26.4 hrs over the domain of the LATEX A moorings. They are produced in summer during a time when the subinertial winds are small and the water column is highly stratified. Price et al. (1986) provide very complete documentation as to the hourly evolution of thermal structure cycling

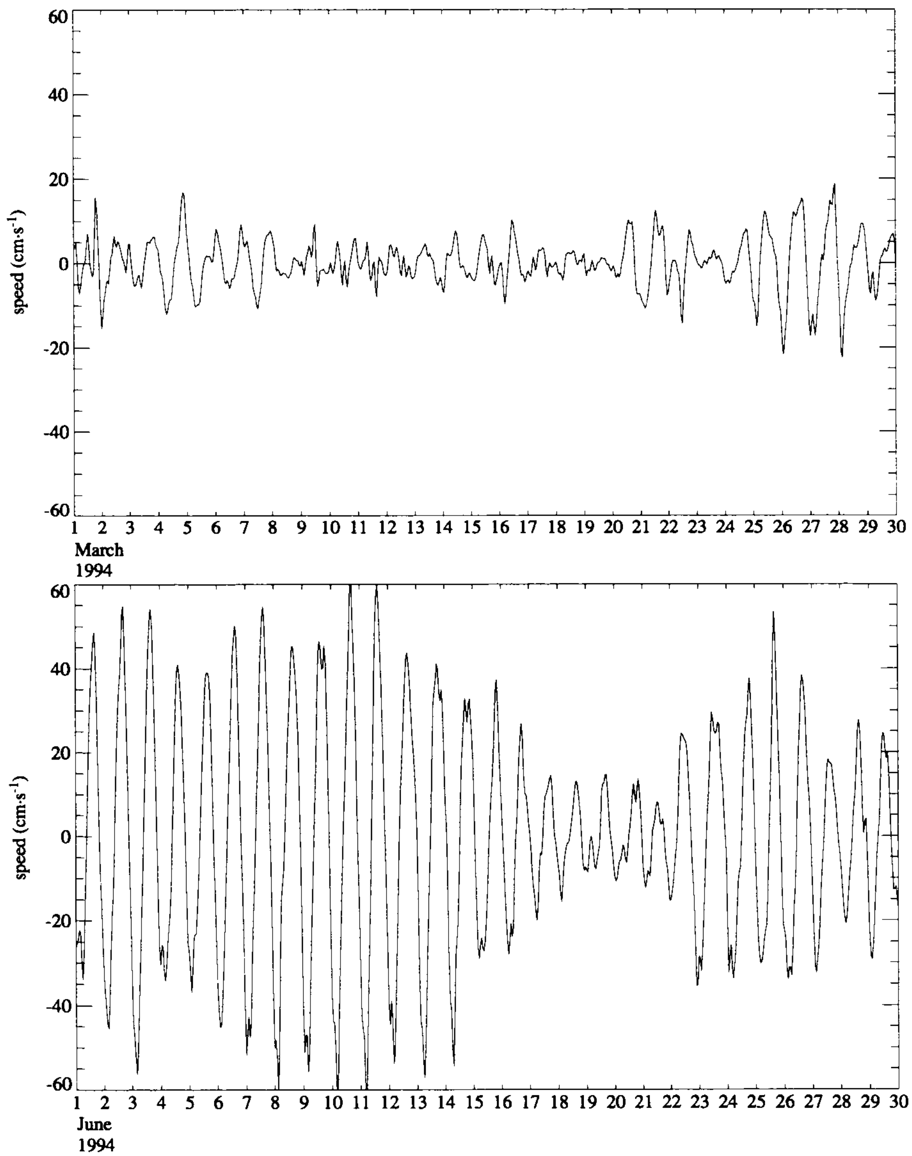

Figure F.2-3. Time sequences in March 1994 (upper) and June 1994 (lower) of 3-40 hr band-passed alongshelf current at top meter (3-m depth) of LATEX A mooring 22.

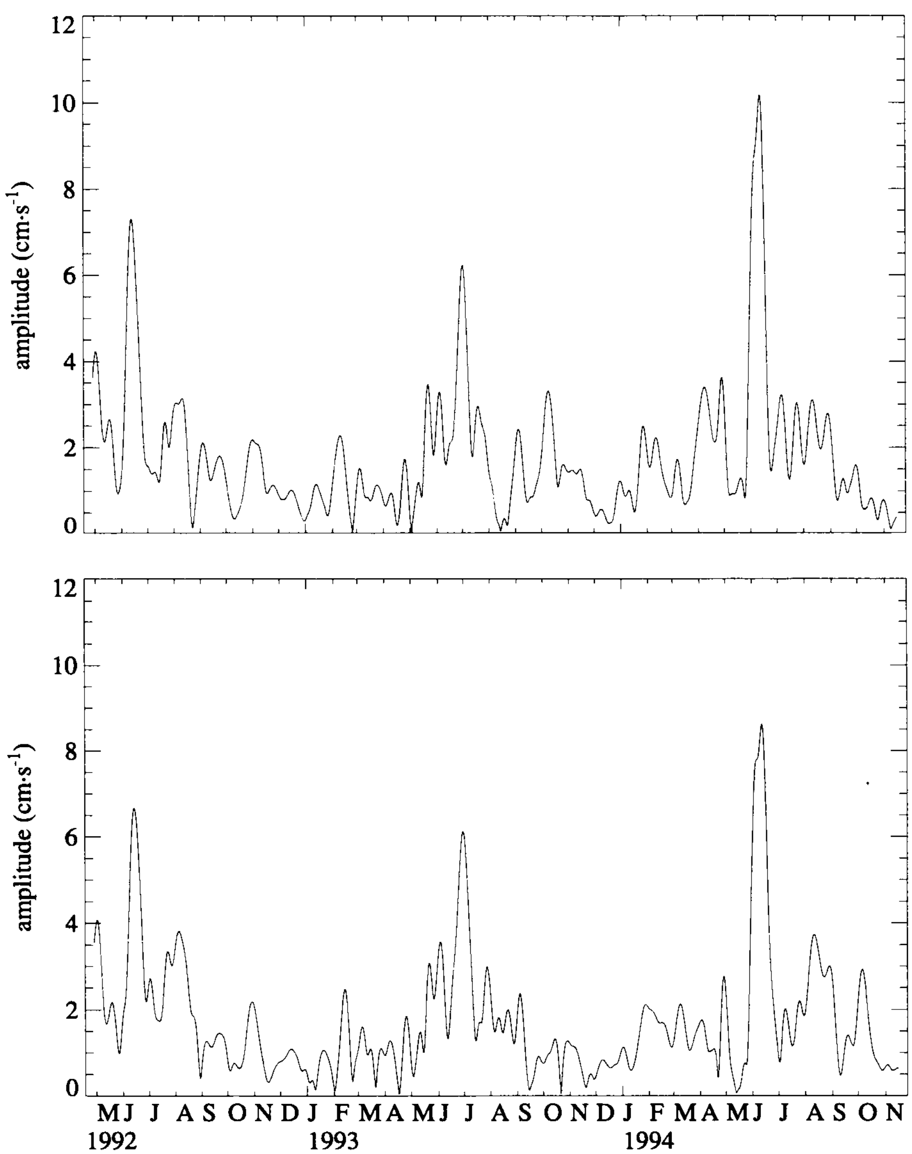

Figure F.2-4. Amplitude of 24-hr signal from complex demodulation of alongshelf (upper) and cross-shelf (lower) current meter at top meter (14-m depth) of mooring 21 for the entire 32 months of the LATEX A field measurements.

in the oceanic layer and a discussion of sensitivity of the rotary motion to heat exchange derived from scaling arguments. However, they offer no insight regarding the associated cycling in the neighboring atmospheric boundary layer. The most definitive model that comes very close to matching the summer LATEX data on 24-hr rotary signals in wind and currents is that of Pandolfo (1969). This important contribution seems not to have recieved the recognition that it deserves in studies of the coupling of atmospheric and oceanic boundary layer dynamics driven by radiative heating and cooling.

Spatial distribution of the 40-hr high-passed variance

Chen et al. (1996) give plots of variance for the 22-28 hr band-passed currents for three cross-shelf vertical sections, based on the April-July 1992 sample of data. These show largest variance in the outer shelf region and in the near surface as should be expected, whether the excitation is thermally induced or wind-induced. Using the full 32 months of data from the top current meters of all moorings, we have constructed horizontal fields of variance (or energy) for different period bands with and without summer but with tidal energy removed. Figure F.2-5 shows the fields of total non-tidal energy for the 8-40 hr band based on the 32 months of data with and without the summers. In the central and eastern Texas-Louisiana shelf the summers account for roughly half of the energy in this band. Figure F.2-6 shows similar plots for the narrower 22-28 hr "inertial" band, each of which contains about half of the energy of the corresponding 8-40 hr band. In the upper panel of both figures, the bull's-eye patterns centered at moorings 22 and 19 are due to the large summer signals that occur at those moorings, whose top current meter is at a depth of only 3 m. This feature is summer related, since it is not evident in the non-summer patterns shown in the lower panels of these figures.

The non-tidal energy of currents in the 22-28 hr band for non-summer probably is associated with wind-induced near-inertial response of the shelf water as discussed by Chen et al. (1996). It increases from about 20 $cm^2 \cdot s^{-2}$ nearshore to about 40 $cm^2 \cdot s^{-2}$ at the shelf break. This may be compared with the tidal energy, which increases from about 10 $cm^2 \cdot s^{-2}$ at the shelf break to well over 60 $cm^2 \cdot s^{-2}$ in the nearshore central region of the Texas-Louisiana shelf (as inferred from Figure F.1-9). The thermally induced non-tidal energy in the 22-28 hr band for summer is at least equal to that for non-summer for all moorings except 19 and 22, where it greatly exceeds that for non-summer.

Thus, in summary, the major contribution to the 40-hr high-pass kinetic energy nearshore is that due to tides, while on the outer shelf the major contribution is non-tidal wind-induced kinetic energy in non-summer but is non-tidal thermally induced kinetic energy in summer. The stated spatial patterns are findings based on the data. The association with causal mechanisms is our interpretation of the data in light of the prior studies of Pandolfo (1969), Price et al. (1986), and Chen et al. (1996).

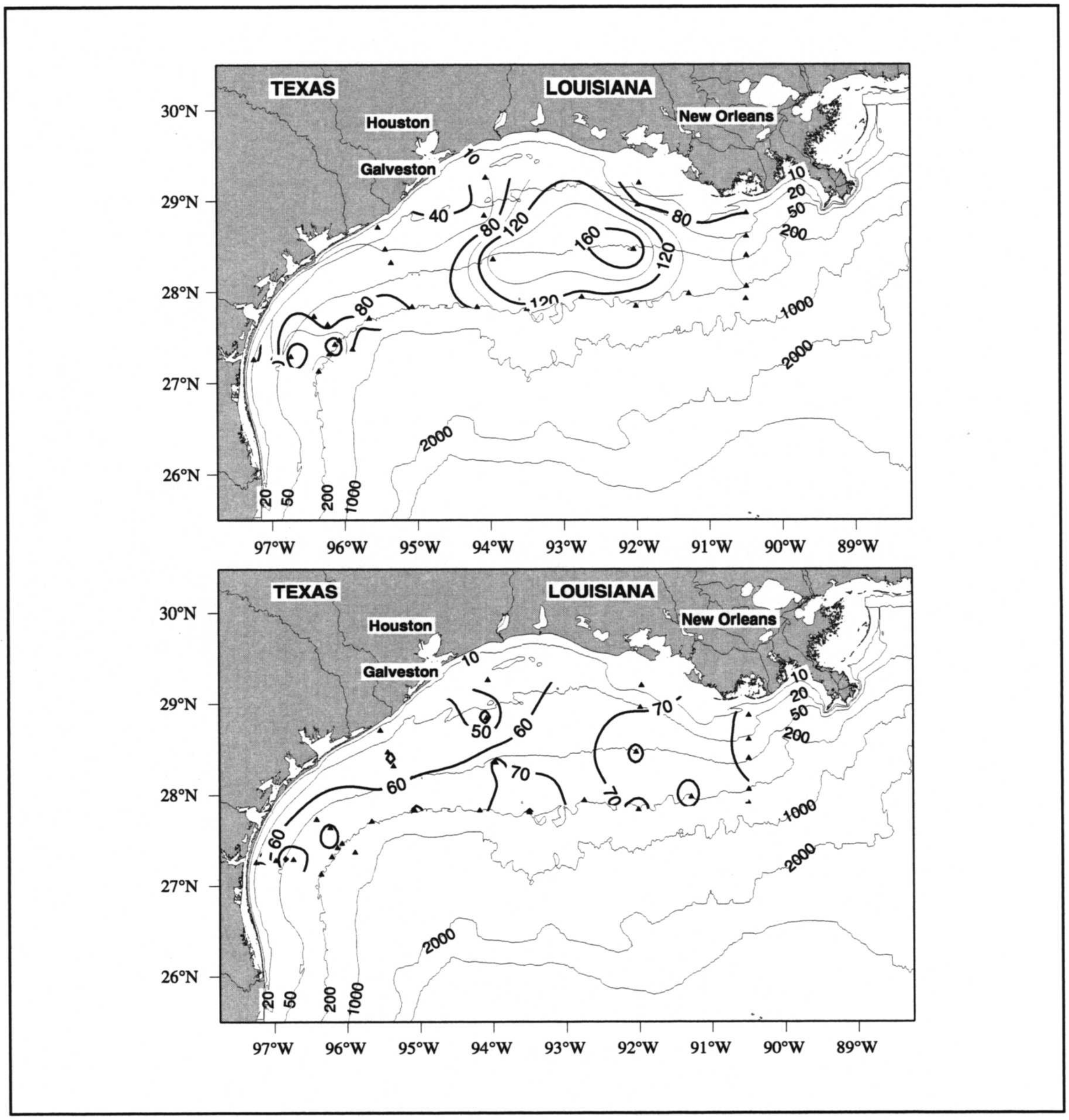

Figure F.2-5. Contours of non-tidal energy ($cm^2 \cdot s^{-2}$) in the 8-40 hr band from top current meter at all moorings based on all 32 months of LATEX A data: (upper) including summer and (lower) excluding summers.

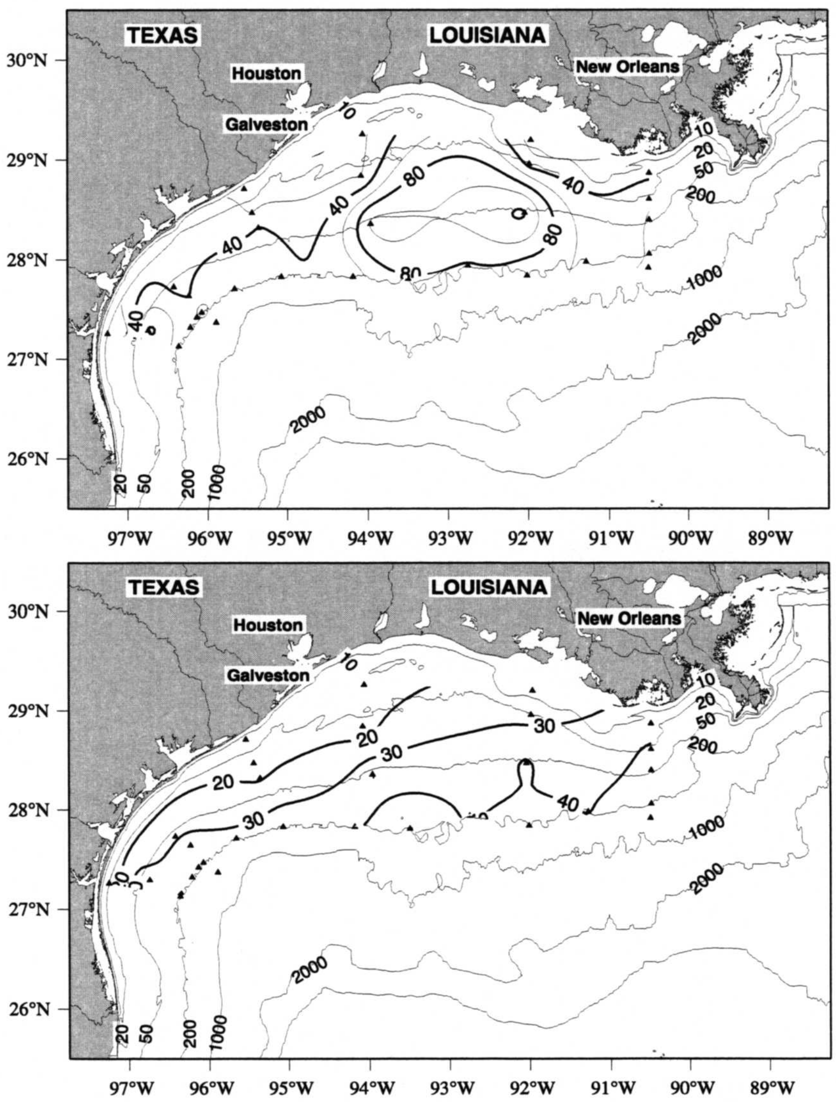

Figure F.2-6. Contours of non-tidal energy (cm^2·s^{-2}) in the 22-28 hr band from top current meter at all moorings based on all 32 months of LATEX A data: (upper) including summer and (lower) excluding summers.

Appendix G: Comparison of Observed and Modeled Surface Gravity Waves

As one comparison of model results with observations, wind fields obtained from the NCEP and those generated by LATEX A (Section 2.1.1) were used in an ocean wave prediction model to determine a hindcast wave field on the Texas-Louisiana shelf. These results were compared to significant heights from three NDBC buoys and five bottom-mounted wave gauges (DiMarco et al. 1995a; DiMarco and Bender 1998). To calculate the wave field, the third generation ocean wave prediction model WAM (WAMDI Group 1988) was used. The WAM model is accepted as state-of-the-art and currently used by over a hundred research and operational sites worldwide.

Model description

The evolution of the energy in a wave field can be modeled by a spectral wave transport equation that balances the propagation of spectral wave energy against the physical processes that cause energy to be gained or lost. These physical processes have been typically described by three terms: wind forcing that adds energy to a wave spectrum; dissipation due to whitecapping and bottom friction that eliminates energy; and nonlinear wave-wave interactions that transfer energy among frequencies within the spectrum. WAM (WAve Model) represents the first concerted attempt to integrate the spectral wave transport equation without assuming an a priori form of the nonlinear wave-wave interaction term. The inclusion of resonant, third order, wave-wave interactions in a wave model represents a significant advance because these interactions determine the shape of the spectrum. Previous, second generation models assumed an a priori form for the spectral shape because computation of the wave-wave interaction required an excessive amount of computer time. The key to the WAM model lies in the Discrete Interaction Approximation, first proposed by Hasselmann et al. (1985); it is an approximation to the nonlinear wave-wave interaction terms that efficiently computes the interaction term. The inclusion of resonant, third order, wave-wave interactions in a wave model is highly desirable because it significantly improves the model's ability to predict wave spectra during rapidly changing winds, conditions that occur frequently on the Texas-Louisiana shelf due in part to numerous frontal passages. For a more detailed description of the physics and numerics in the WAM model, the reader is referred to WAMDI Group (1988).

The wave modeling community has extensively validated the WAM model for different regions and different events (Bender 1996). In December 1991, cycle 4 of the WAM model was released with modified physics that included dynamic coupling between winds and waves (Janssen 1989, 1991); this model was used to determine hindcast wave fields over the Texas -Louisiana shelf for part of the LATEX period.

Model setup

The transport equation was solved on a two-level nested domain to better represent the propagation of remotely generated swell onto the Texas-Louisiana shelf. As such, it required a wave model for the Gulf of Mexico to provide the boundary conditions for a finer grid model of the Texas-Louisiana shelf. The outer level model (the gulf domain) covered the Gulf of Mexico from 18° to 31°N and 98° to 80°W on a grid resolution of one degree. This provided a satisfactory representation of the swell arriving on the Texas-Louisiana shelf. The nested level model (the shelf domain) covered the Texas-Louisiana shelf from 26° to 30°N and from 98° to 89°W on a finer grid resolution of one quarter degree (Figure G-1).

The winds for the gulf domain were obtained from the medium-range weather forecasts disseminated by the National Weather Service. The winds were produced by the NCEP Global Data Assimilation System (GDAS) and Forecast System. The main component of the Forecast System is the NCEP Medium-Range Forecasting (MRF) model. Details of the MRF model appear in a document by the NMC Development Division (1988). The GDAS blends global weather observations at 6-hour intervals with previous MRF model forecasts to produce new initial conditions for the next model run. A detailed description of the GDAS is presented in Kanamitsu (1989) and Kanamitsu et al. (1991). The MRF model predicts winds, temperature, surface pressure, humidity, and precipitation during the integration, and has 18 levels in the vertical. Physical diagnostic parameters include precipitation, cloudiness, surface sensible and latent heat fluxes, surface stress, and others. These fields are known as the high-resolution GDAS data sets, or as the MRF final analysis cycle data set.

The LATEX A program purchased a subset of this data for the period April 1992 through December 1994, including zonal and meridional winds at 10-m height on an 18 x 23 point grid that spans the Gulf of Mexico. These data are for four times daily (0, 6, 12, 18 UTC). As part of the WAM preprocessing, these wind fields were bilinearly interpolated from the spectral grid they were generated on to the WAM-specified uniform 1° grid for the Gulf of Mexico. The wind fields were linearly interpolated in time to every hour by the WAM model.

The winds for the shelf domain were obtained from the LATEX gridded wind fields described in Section 2.1.1. They were hourly zonal and meriodional wind velocities at 10-m height on a half degree grid. These winds were supplied directly to the WAM model. No interpolation in time took place.

The model was run with the standard parameter set supplied with the WAM cycle 4 code. These included 12 angle bins at every 15 degrees and 25 frequency bins from 0.0418 to 0.4114 Hz. The gulf domain was set up on a spherical grid, thereby accounting for the great

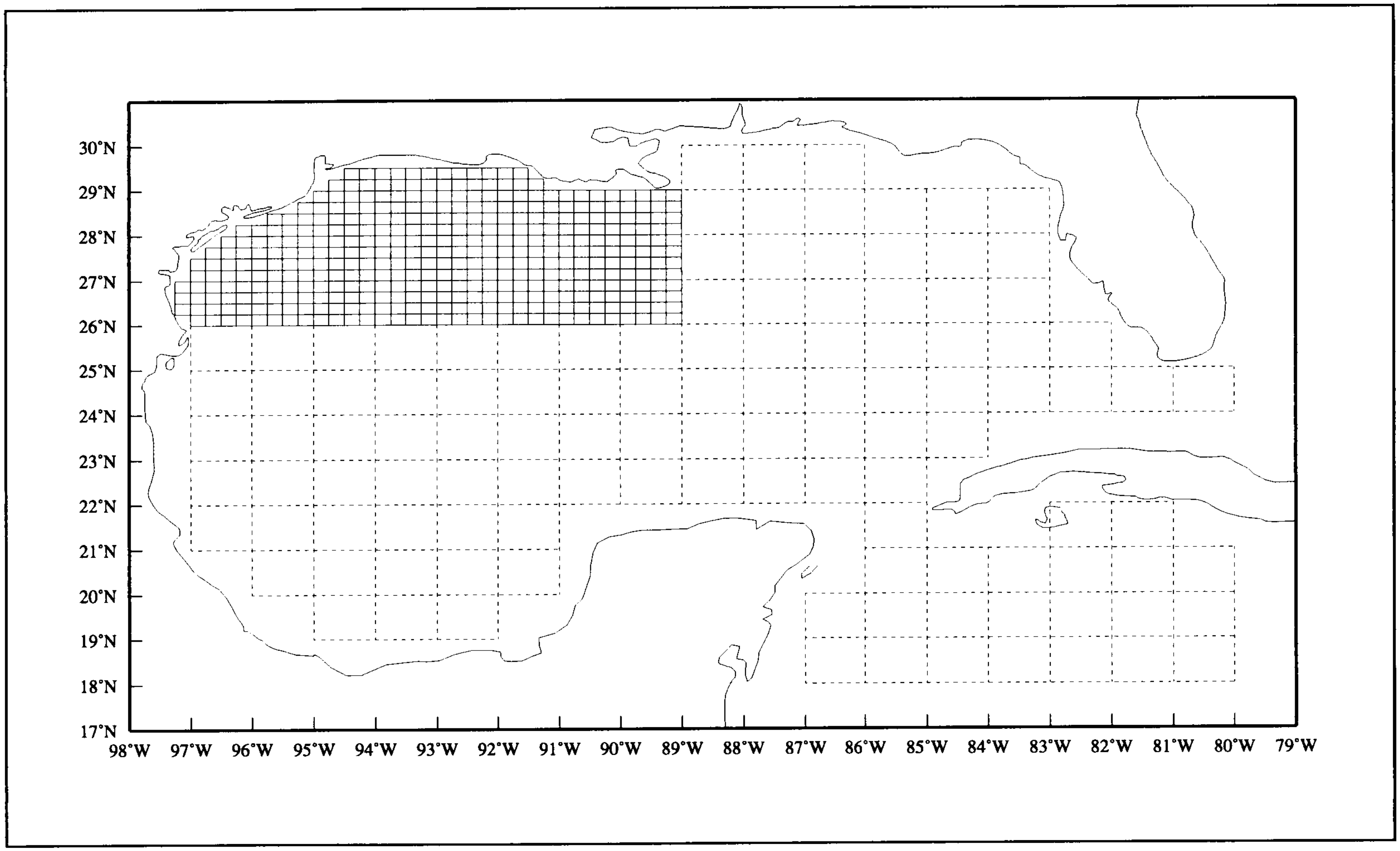

Figure G-1. WAM model domain showing the gulf domain (dotted lines) and the shelf domain (solid lines).

circle propagation of swell, with deep water propagation and no depth or current refraction. The source and propagation terms were integrated every twenty minutes to limit the Courant number to less than 0.3. Significant wave height and direction for the entire gulf and spectra at selected locations were saved after every six hours of integration.

The shelf domain was set up on a Cartesian grid, with shallow water propagation, bottom friction via the standard WAM parameter set, and depth refraction, but no current refraction. The source and propagation terms were integrated every five minutes to limit the Courant number to less than 0.3. Significant wave height and direction for the shelf and spectra at selected locations were saved after every six hours of integration.

Model run

The model was run for the period of 1 April 1992 through 30 September 1992 on the Cray J90 supercomputer at Texas A&M University, only the initial part of the LATEX field program. This period included the passage of Hurricane Andrew, 24-26 August 1992. Model output at specific locations was compared to observations. The data are from locations shown in Figure G-2; the model output was taken from the nearest gridpoints. The observations used in this comparison came from two sources, five bottom-mounted wave gauges maintained by LATEX A and three surface buoy records obtained from NDBC. The five LATEX A wave gauges were deployed along the Texas-Louisiana coast in depths ranging from 7 to 22 m. They consisted of four Coastal Leasing, Inc. MiniSpec directional wave gauges at moorings 16, 17, 20, and 23 and one SeaData 635-8 non-directional wave gauge at mooring 1. The instruments recorded hydrostatic pressure and velocity. Because of inaccuracies in the MiniSpec pressure transducers during this comparison period, the velocity records were used to construct the significant wave heights. The attenuation of wave velocities is significantly affected by the water depth, which means that for meters in deep water the wave signal is lost in the noise. Therefore, each of the wave gauge records was post-processed with a uniform high frequency cutoff of 0.190 Hz (DiMarco et al. 1995a) to eliminate noise in the record. As a result, wave energy with frequencies higher than 0.190 Hz were discarded. In an environment dominated by long period swell, i.e., waves with a frequency less than 0.100 Hz, this would not be a problem, but long period waves are rare for the Gulf of Mexico (NDBC 1990). The three NDBC buoys at 42002, 42019, and 42020 are 3-m discus buoys that ride the surface and record accelerations due to the wave motion. This information is processed into significant wave heights. The NDBC data provide a more reliable estimate of the wave heights than that estimated by the LATEX A wave gauges at the LATEX moorings.

Monthly-averaged significant wave heights for the Texas-Louisiana shelf are shown for for two representative months, May 1992 (Figure G-3) and August 1992 (Figure G-4). Six-hourly values of significant wave heights compared to observations are shown as time series

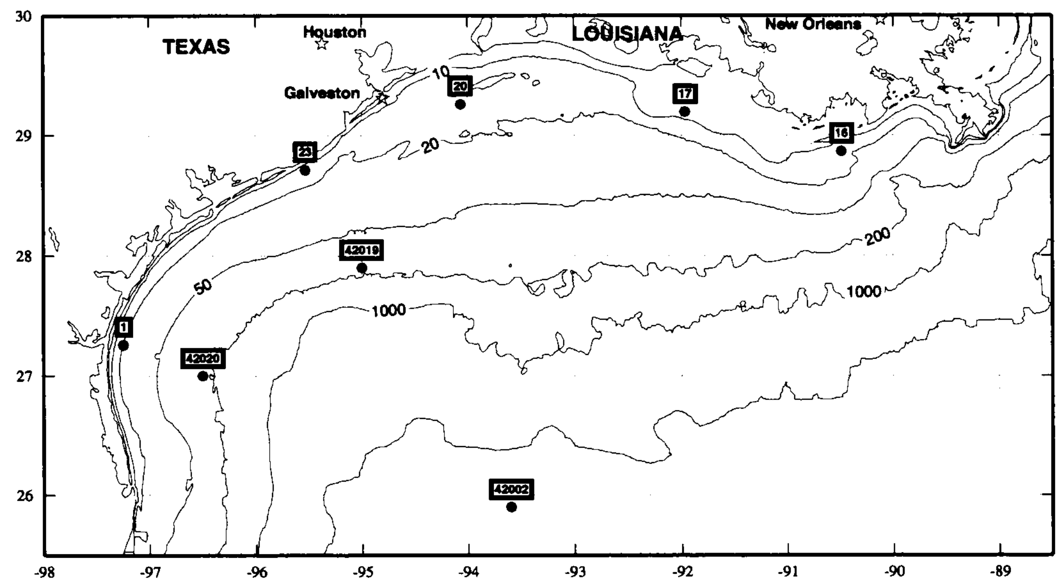

Figure G-2. Locations of LATEX A bottom-mounted wave gauges (moorings 1, 23, 20, 17, and 16) and the NDBC wave buoys (42002, 42019, 42020).

in Figures G-5 through G-12. The average wave heights, the bias, and rms statistics are shown in Table G-1.

Discussion

Of particular interest is the positive bias for the wave gauges located in shallow water (moorings 1, 23, 20, 17, and 16) and the negative bias for the NDBC buoys located in deep water (42020, 42019, and 42002). As noted above, the five bottom-mounted wave gauges did not provide accurate estimates of the wave energy at frequencies higher than 0.190 Hz. Results from the WAM model suggest that a significant amount of energy occurs above 0.190 Hz, which would account for the positive bias. Hence, the wave gauges are, in fact, underreporting the actual wave heights. The NDBC buoys, on the other hand, show a negative bias, which indicates that the WAM model is underpre-dicting wave heights. We believe that, in general, wave heights are consistently underpredicted by WAM. There are a number of steps that could improve the model predictions, such as incorporating better propagation numerics or assimilating wave heights from the NDBC buoys—steps that are ongoing.

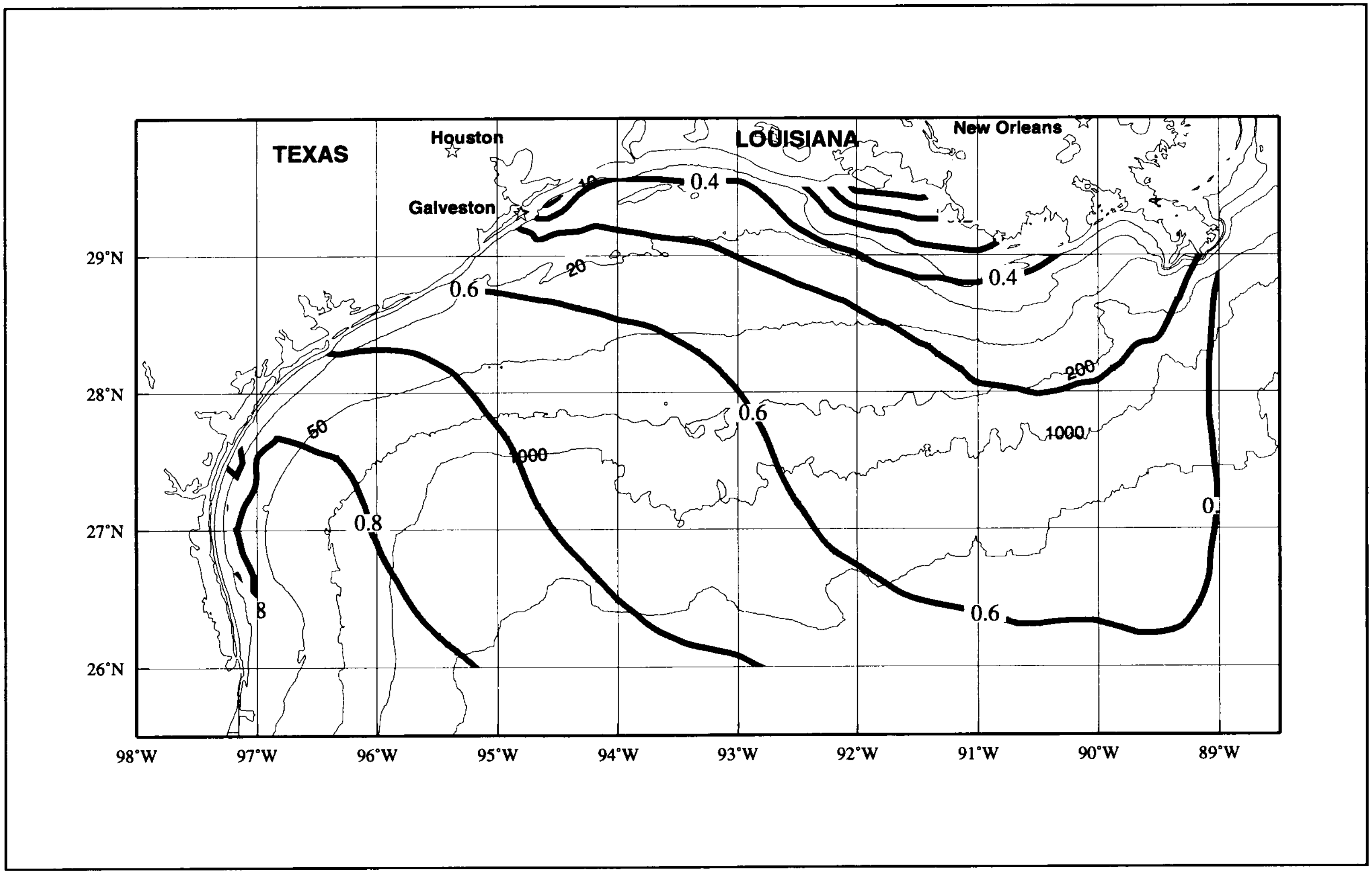

Figure G-3. Monthly averaged significant wave heights (m) for May 1992. Contour interval is 0.1 m.

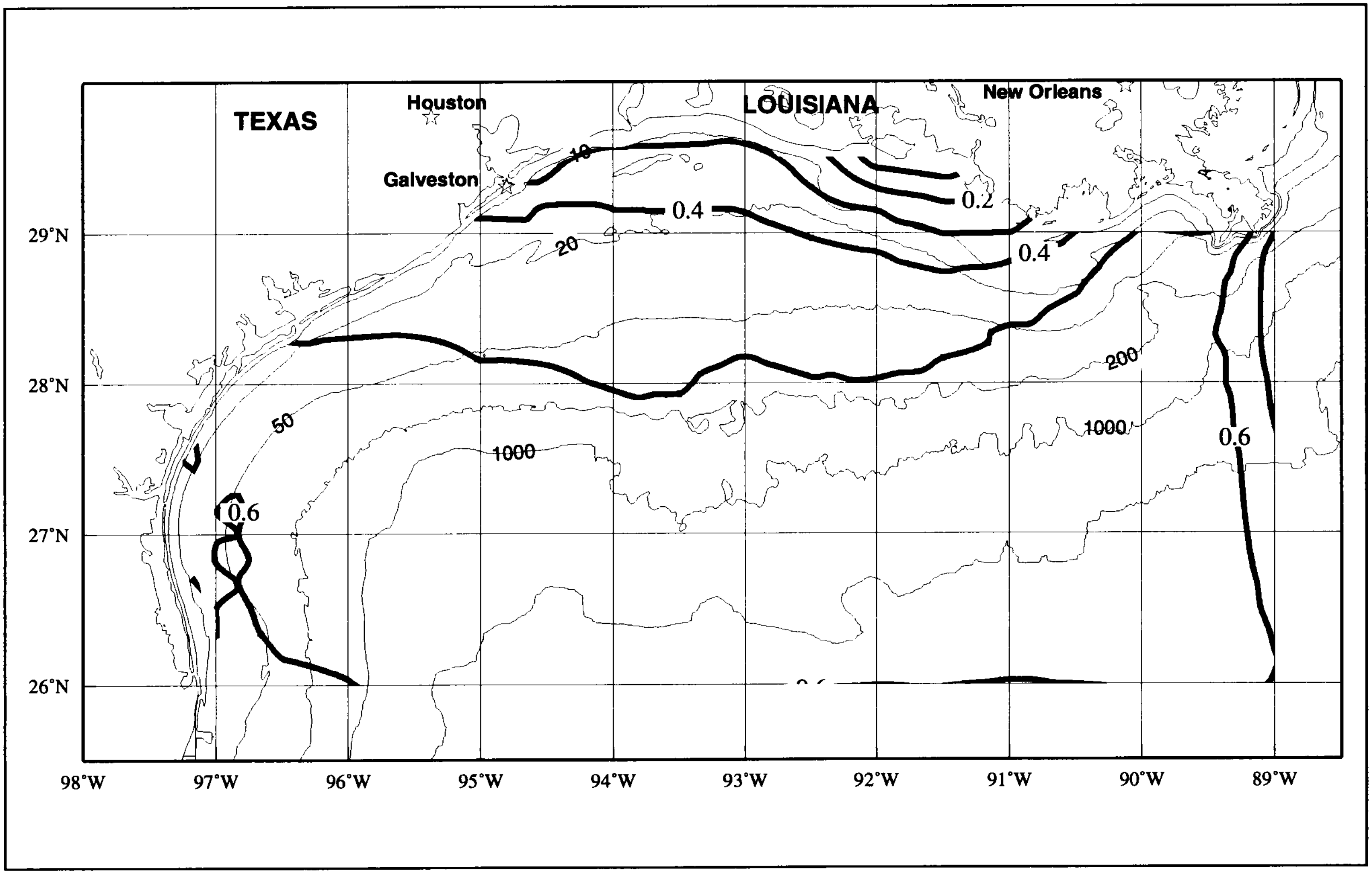

Figure G-4. Monthly averaged significant wave heights (m) for August 1992. Contour interval is 0.1 m.

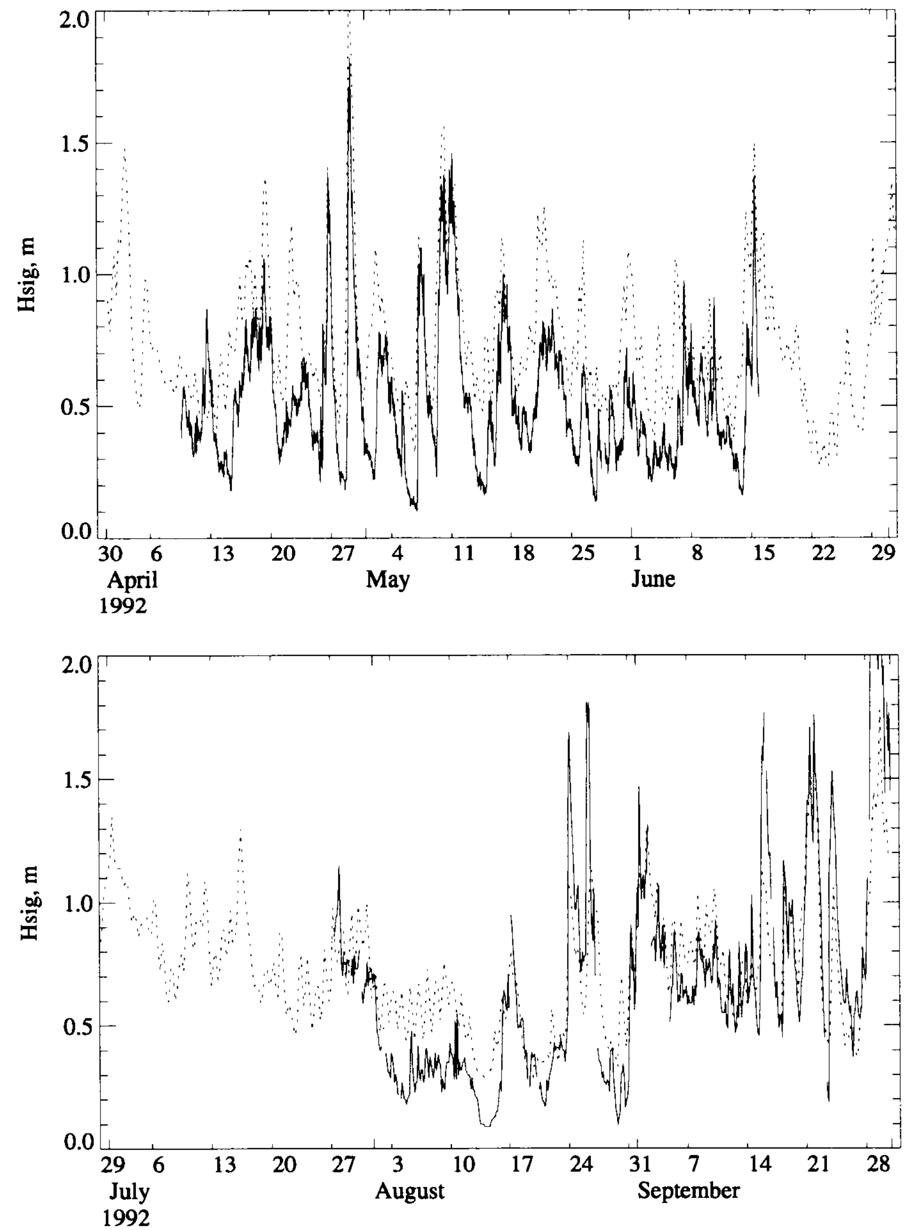

Figure G-5. Significant wave heights for WAM (dotted) vs. mooring 1 (solid).

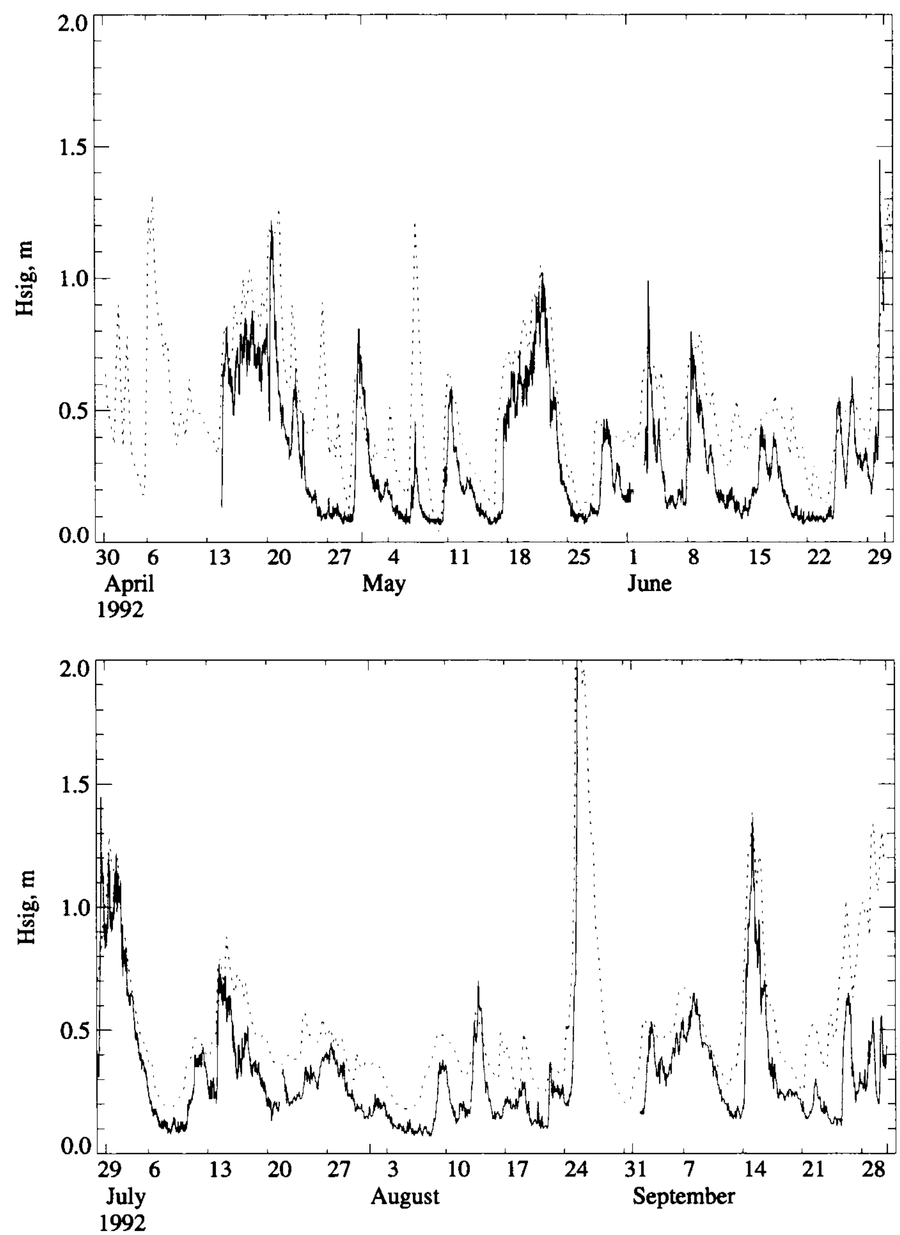

Figure G-6. Significant wave heights for WAM (dotted) vs. mooring 16 (solid).

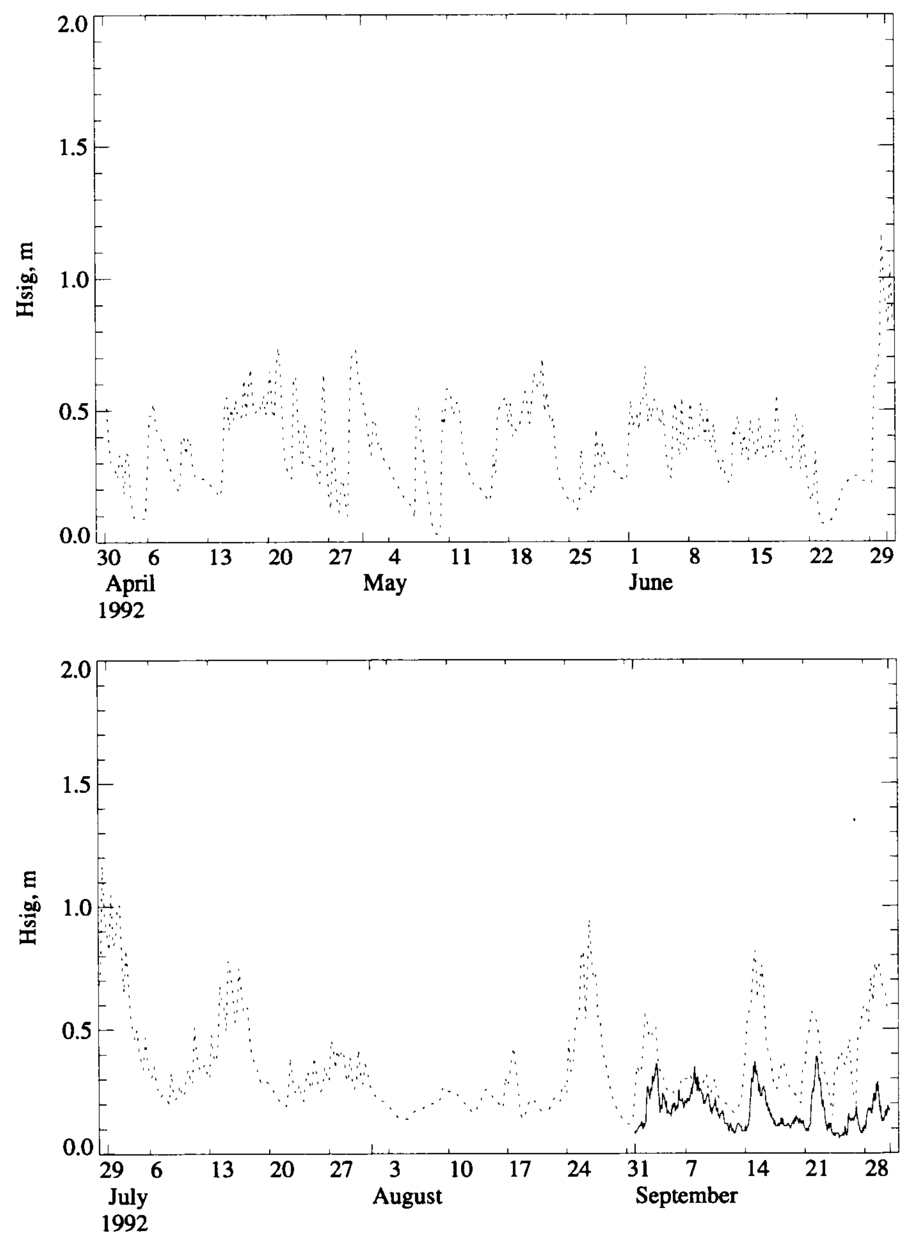

Figure G-7. Significant wave heights for WAM (dotted) vs. mooring 17 (solid).

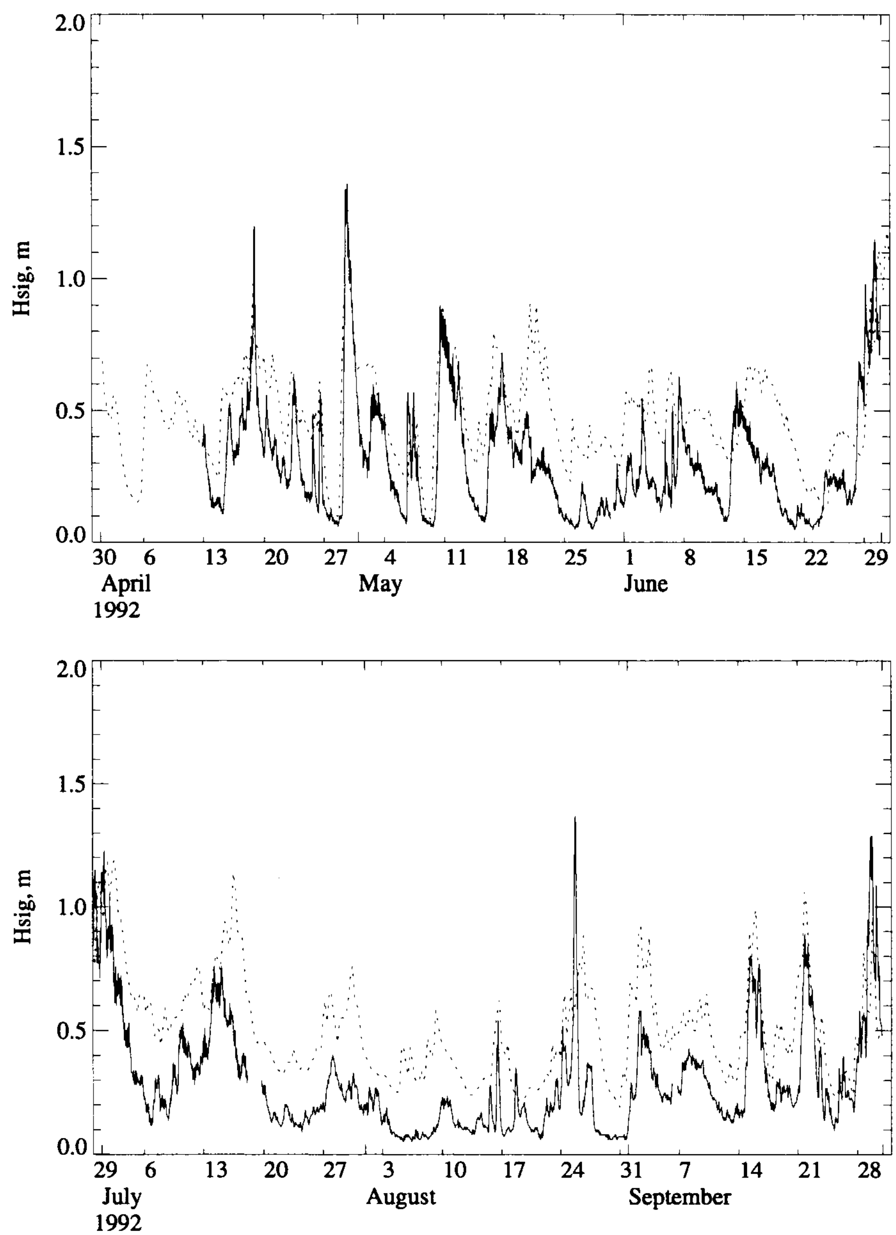

Figure G-8. Significant wave heights for WAM (dotted) vs. mooring 20 (solid).

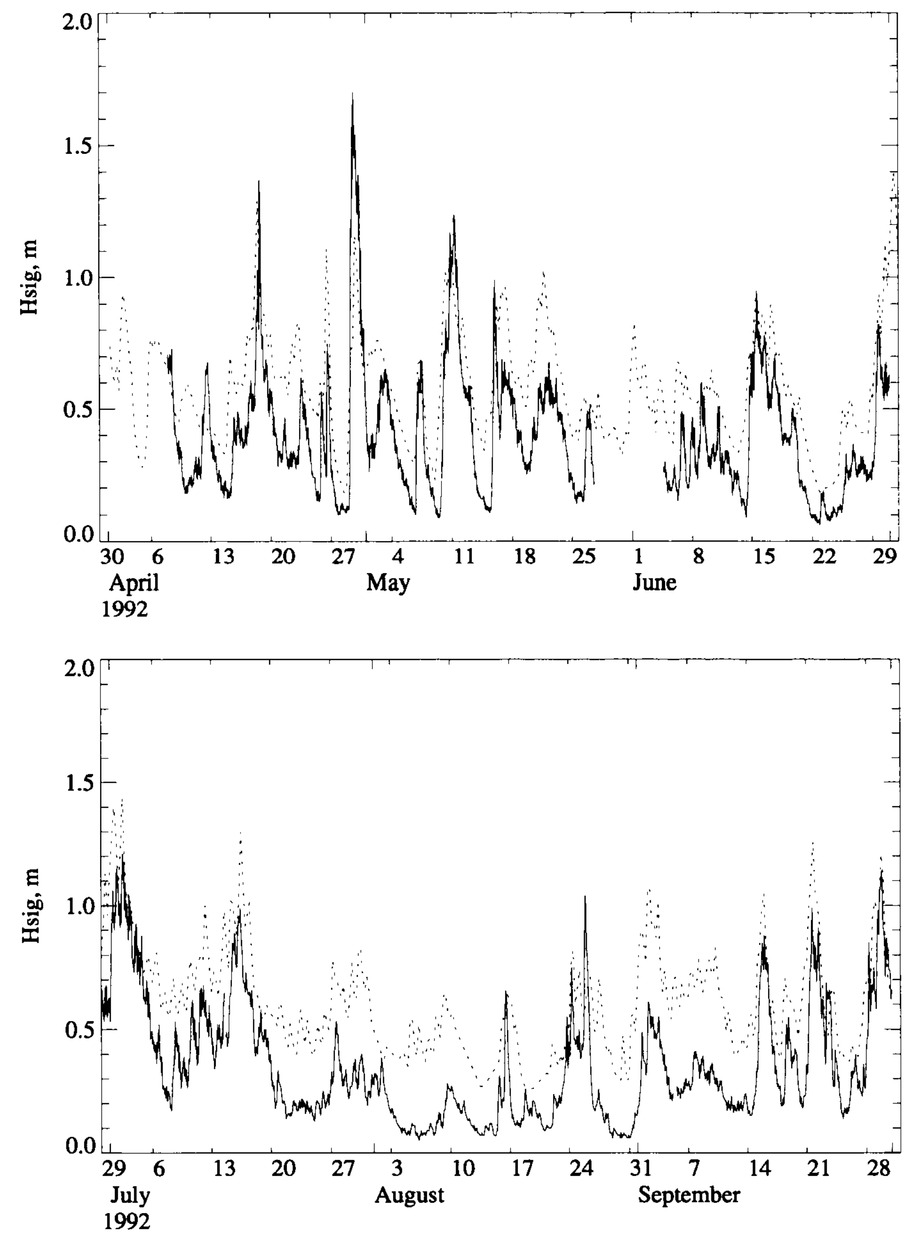

Figure G-9. Significant wave heights for WAM (dotted) vs. mooring 23 (solid).

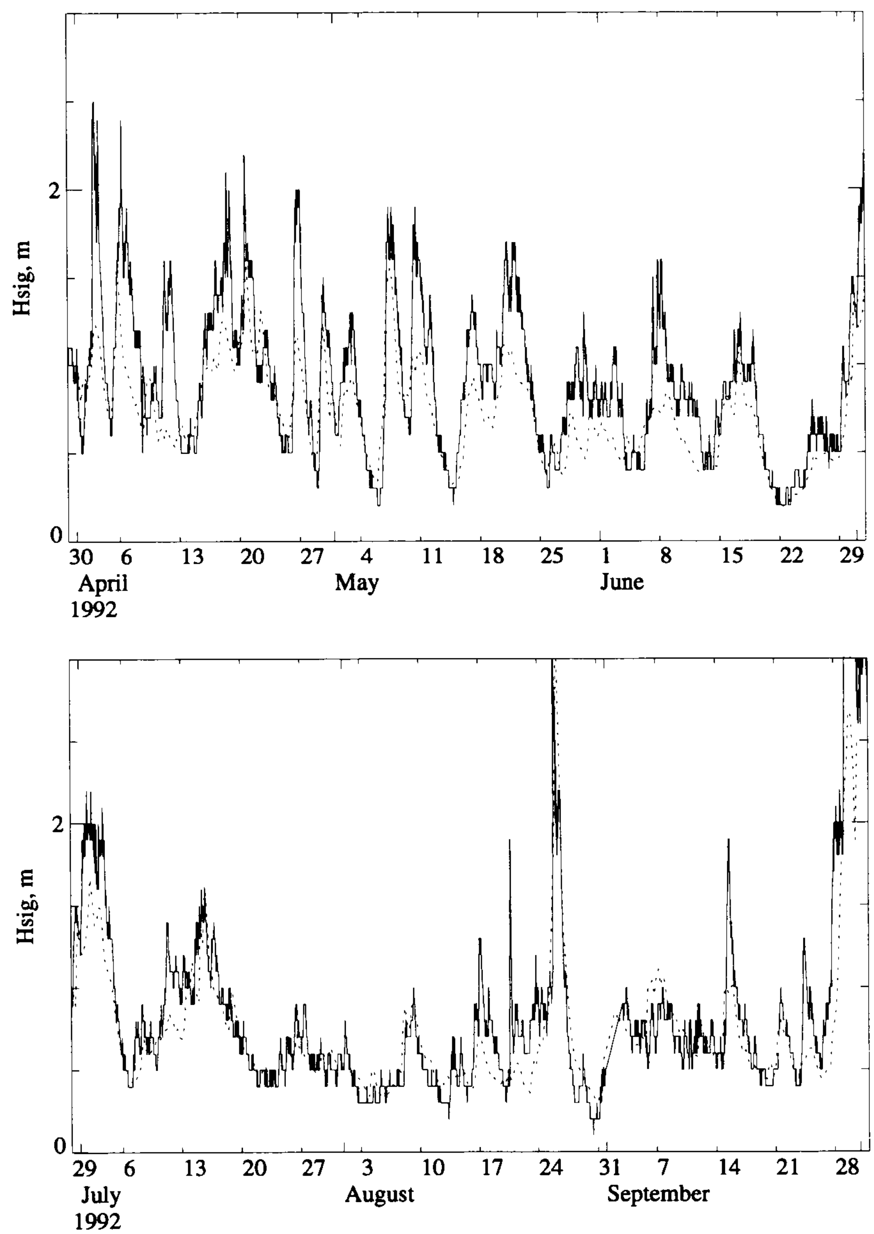

Figure G-10. Significant wave heights for WAM (dotted) vs. NDBC buoy 42002 (solid).

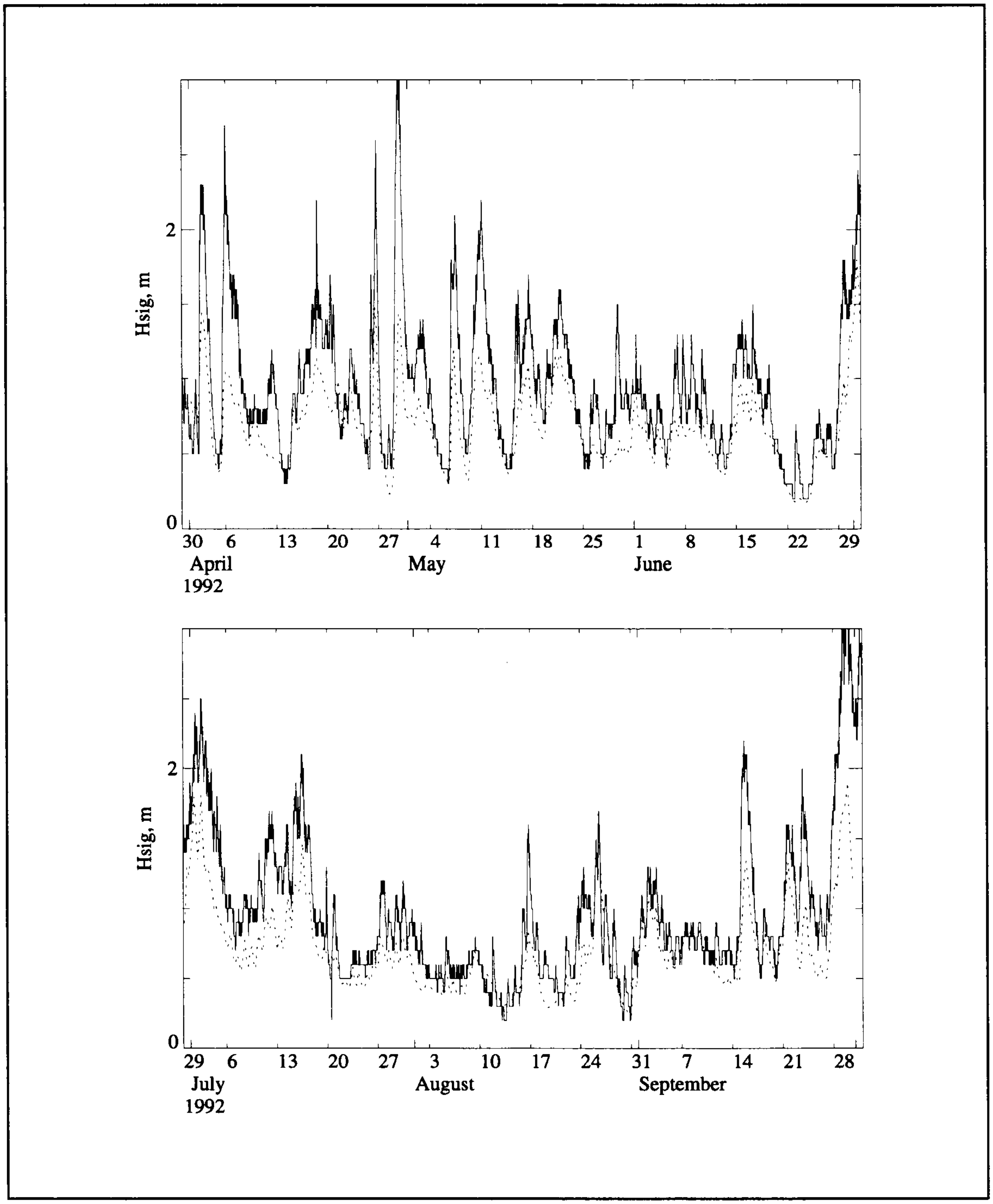

Figure G-11. Significant wave heights for WAM (dotted) vs. NDBC buoy 42019 (solid).

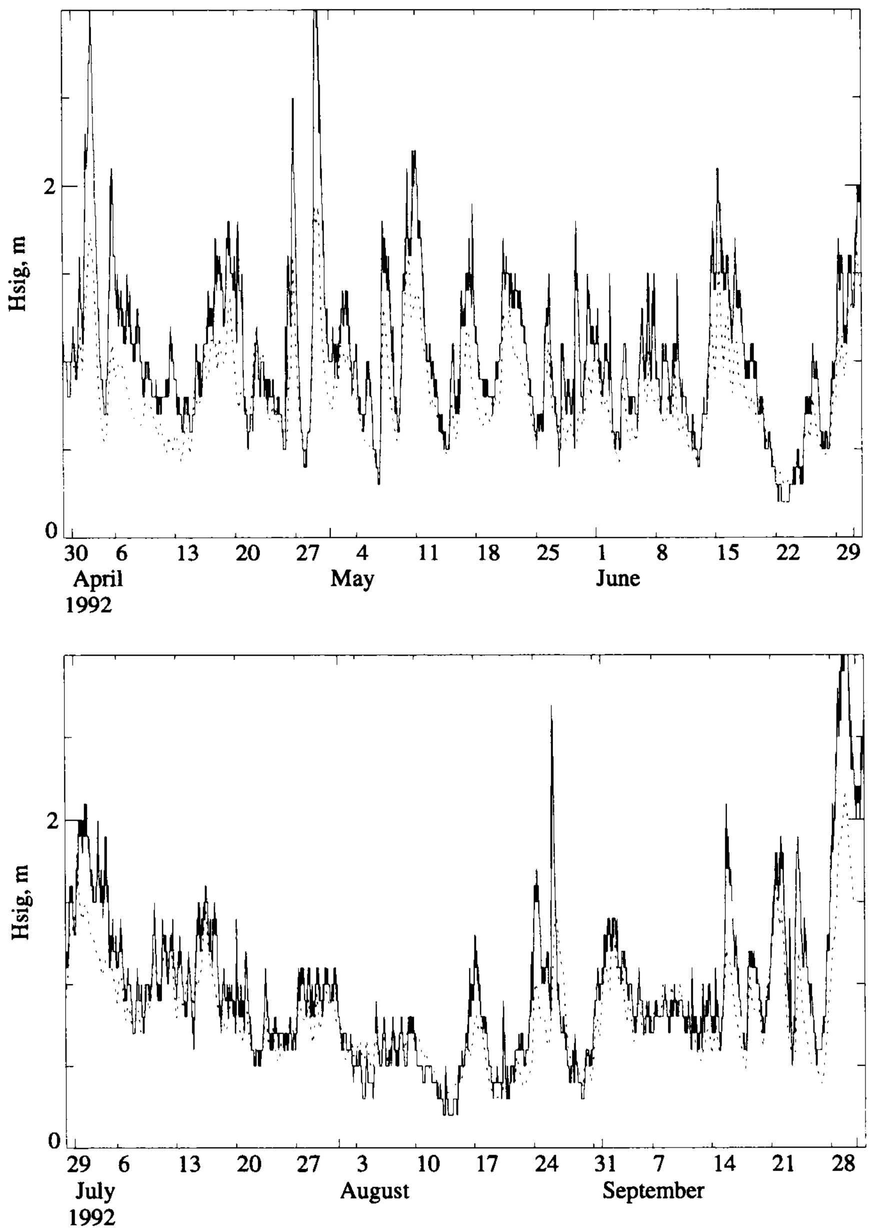

Figure G-12. Significant wave heights for WAM (dotted) vs. NDBC buoy 42020 (solid).

Table G-1. Significant wave heights (cm) showing the average for the model and the data, the bias (defined as model minus data), and the rms of the bias.

Buoy	Model avg	Data avg	Bias	rms
mooring 1	73.6	59.3	+14.3	28.0
mooring 23	59.6	36.8	+22.8	27.4
mooring 20	49.6	29.6	+20.0	25.5
mooring 17	38.2	17.2	+21.0	25.9
mooring 16	51.0	32.7	+18.4	28.4
42020	80.6	99.2	-18.6	30.4
42019	68.6	94.1	-25.4	37.1
42002	72.0	85.2	-13.2	29.2

There is a clear alongshelf pattern seen in the six-month averaged wave heights (Figures G-3, G-4, Table G-1). This is consistently seen in both the model output and the observations, a fact that supports the use of the WAM wave model on the Texas-Louisiana shelf in spite of its prediliction to underpredict. The averaged wave heights along the shelf are largest on the western end of the Texas-Louisiana shelf and decrease toward the eastern end, with the exception of mooring 16 which was significantly affected by the passage of Andrew. A doubling of the wave heights from mooring 17 to mooring 1, as well as the increase from 42019 to 42020, strongly suggests that the average wind speeds must also double; that is, if the waves are generated by local winds and have little if any contribution from swell generated in the Gulf of Mexico. This premise is supported by the observed wind fields (see Section 2.1.2 and Figure 2.1-1) that show for the yearly averaged winds, the strongest (~4 $m{\cdot}s^{-1}$) are in the west and the weakest (~1 $m{\cdot}s^{-1}$) are in the northeast corner. However, there will always be episodic events (e.g., storms in the Gulf) that will contribute remotely generated swell to the shelf, but on the average the waves will be generated by local winds. Consequently, waves on the Texas-Louisiana shelf will rarely exceed a significant wave height of 3 m simply because large waves require a combination of high wind speeds and long open lengths of ocean over which to form. This finding is supported by long term NDBC buoy records that show that long period waves; i.e., swell with a period exceeding ten seconds, are rare for the Gulf of Mexico for all but the most extreme weather events (NDBC 1990).

The obvious exception to this is the passage of a hurricane. As shown in Appendix B.1, at 0100 UTC on 26 August 1992, the eye of Hurricane Andrew passed within 30 km of mooring 16. This MiniSpec recorded a peak significant wave height of 9.1 m before the record terminated. The velocity sensor of the MiniSpec failed to record meaningful data when the bottom-mounted frame holding the instrument was turned on its side by strong bottom currents (DiMarco et al. 1995b). However, because of the large amplitude waves present, it was possible to use the pressure transducer to estimate the significant wave heights. This only occurred for a two-day period. The WAM model results for the nearest gridpoint to mooring 16 are significantly less than that and peak at 2.91 m at 1800 UTC 25 August 1992 (Figure G-6). At 1700 UTC, the MiniSpec record for mooring 16 shows a wave height of 3.62 m, and at 1900 UTC, 4.77 m. Model gridpoints farther to the west of mooring 16 show a model predicted significant wave height of 5.0 m. It is highly probable that the LATEX wind fields do not accurately portray the wind fields of Andrew; smoothing reduces the LATEX winds, especially during times of extreme winds and wind changes (documented in Section 4.5). During extreme weather events it is critical that the wind fields are accurately modeled if the predicted wave fields are to be accurate as well. It would be more appropriate, knowing such storm parameters as the minimum pressure, radius to maximum winds, etc., to construct a synthetic hurricane wind field, though we did not do that.

Acknowledgment

Time on TAMU's Cray J90 supercomputer was at no cost to MMS. We thank the Texas A&M Supercomputer Advisory Committee for their research grant, awarded in November 1995, which allowed this work to be done.

Appendix H: Realizations of Current Fields

The LATEX and collateral data sets offer opportunities for various approaches to estimating the currents and shelfwide circulation over the Texas-Louisiana shelf. These range from approximations of the mean shear flow in the form of geopotential anomaly fields to direct current measurements using moored current meters or shipboard mounted acoustic Doppler current profilers. Presented in this appendix are fields of relative geopotential anomaly constructed from LATEX and collateral data and fields of monthly averaged currents from direct LATEX observations.

H.1 Geopotential anomaly fields

Twelve maps of the depth of the 20°C isotherm and of geopotential anomaly for the sea surface (3-m) were prepared using a combination of data from LATEX A, LATEX C, and GulfCet. Table H.1-1 presents the field operation nomenclature and the periods during which the observations were made. The LATEX A data were CTD temperature and salinity taken during ten hydrographic cruises. LATEX C data were AXBT profiles of temperature versus depth. GulfCet data were a combination of CTD temperature and salinity profiles and XBT temperature profiles. Combining these data sets allowed realizations of geopotential anomaly distributions extending over much of the shelf and past the continental slope into deeper water. Thus, eddies at the shelf edge and their relation to circulation over the shelf can be seen.

Combining temperature data from all sources, fields of isotherm depths for each observing period were obtained by objective analysis. The software used to produce these fields was the GMT (Generic Mapping Tools) software package (Wessel and Smith 1991); the objective analysis method in GMT is based on an extension of the minimum curvature method of gridding described by Smith and Wessel (1990). Gridded values were obtained at 15-minute separations in latitude and longitude and contoured.

Figure H.1-1 shows the depths of the 20°C isotherm for each of the twelve periods. The depths of isothermal surfaces at or near the 20°C isotherm have been shown to be excellent indicators of the presence, configuration, and strength of eddies in the Gulf of Mexico by Leipper (1970) and others. Also shown in Figure H.1-1 are 10-m current vectors averaged over each period of the hydrography and for the two preceding weeks.

In each of the first six periods pictured, an anticyclonic eddy was present offshore of the western shelf. In April-May and November of 1993, there is evidence in these temperature fields and current vectors for a cyclone west of the anticyclone. No data exists offshore of the western shelf for the December 1993 period, but, based on the available data, we can speculate that the situation was much like that in the previous month. Of the three periods in

Table H.1-1. LATEX A, LATEX C, and GulfCet field activities during each of 12 periods with common sampling.

Period	LATEX A Hydrographic cruise	LATEX C Field effort	GulfCet Cruise
15 Apr - 8 May 1992	H01	F01	01
1-11 Aug 1992	H02	F02 and F03	
5-21 Nov 1992	H03		03
4-21 Jan 1993		F06 and F07	
5-24 Feb 1993	H04		04
26 Apr - 18 May 1993	H05	F08 and F09	
26 Jul - 7 Aug 1993	H06	F10 and F11	
28 Oct - 22 Nov 1993	H07	F12	
5-23 Dec 1993		F13 and F14	07
23 Apr - 24 May 1994	H08	F15 and F16	
26 Jul - 14 Aug 1994	H09	F17	
1-16 Nov 1994	H10	F20 and F21	

1994, a distinct anticyclone was situated off the western shelf during the July-August case. For each case of an anticyclone in the west, currents over the shelf edge inshore from the eddy were upcoast — the strength appears to depend on the proximity of the eddy to the shelf edge. Also seen in the current vectors is evidence for onshelf (offshelf) flow across the shelf edge associated with the western (eastern) limb of the eddy.

No one pattern of circulation dominated off the eastern shelf. In August 1992, April-May 1993, August 1993, and November 1994, anticyclones were seen south of the eastern shelf, but they were not close enough to the shelf edge to appreciably affect the average currents during the period. It seems clear from these temperature and current distributions that the currents at the shelf edge are dominated by the offshore eddy field. Seldom are the currents seen to have the same along-shelf direction along the entire shelf edge. More detail regarding the flow near the shelf edge can be inferred from the patterns of geopotential anomaly for the twelve observing periods.

We examined two methods for obtaining geopotential anomaly from XBT/AXBT temperature profiles: use of a regional T-S relationship to estimate salinity from the temperature field and calculate density from temperature and resulting salinity; and use of a regional relationship of temperature to geopotential anomaly. That examination led us to use the T-S relationship. Because the T-S relations within and outside of a Loop Current eddy differ, a T-S relation fit to a combination of both types of data was selected. We estimate that the geopotential anomaly of the sea surface relative to 400 db produced by such an average T-S relation for waters off the Texas-Louisiana shelf can be in error by up to 5 dyn cm at the center of an anticyclone.

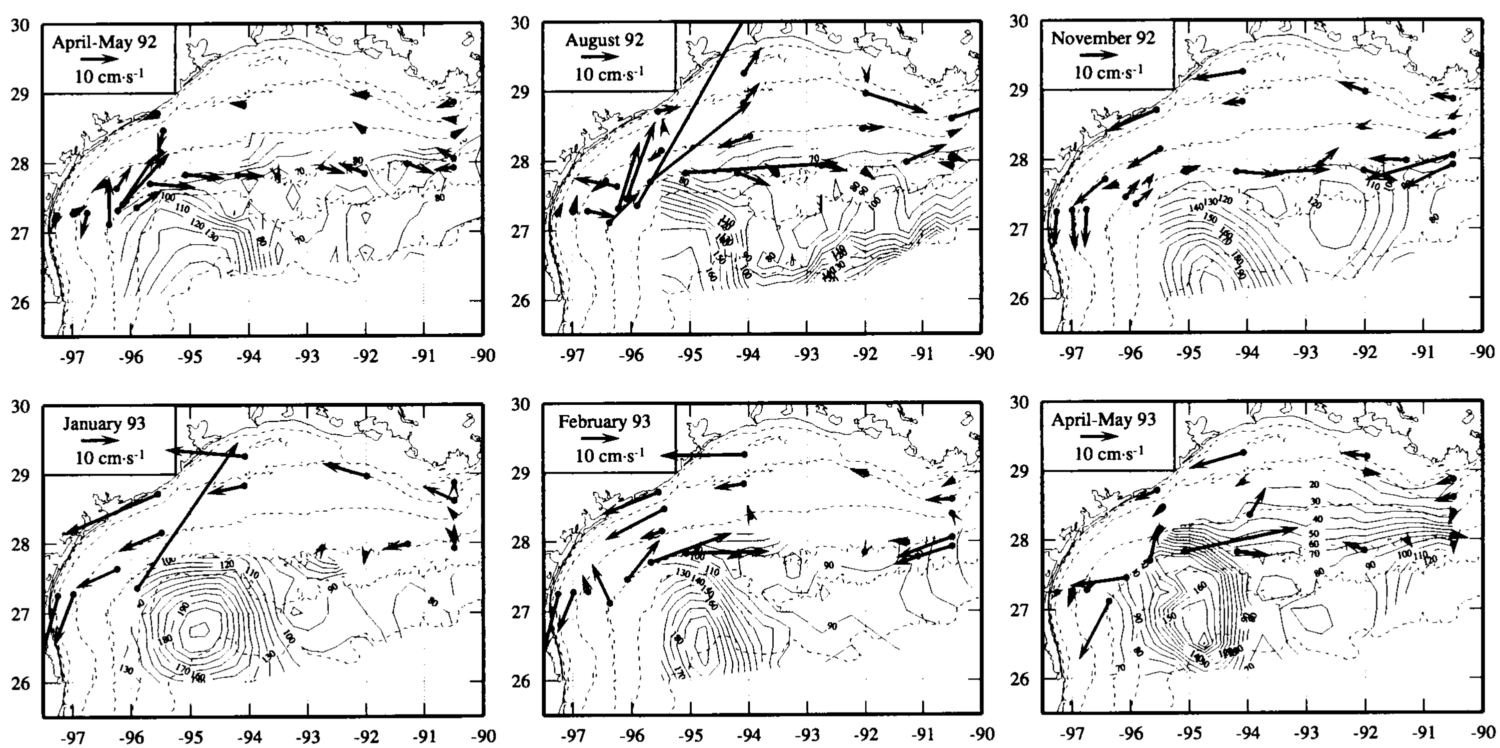

Figure H.1-1. Depth of 20°C isotherm (m) for twelve periods during 1992-1994 based on temperature data from LATEX A, LATEX C, and GulfCet. Specific field activities and dates of sampling are given in Table H.1-1. Vectors represent 10-m current velocities at LATEX A moorings averaged over the sampling periods plus the preceding 14 days.

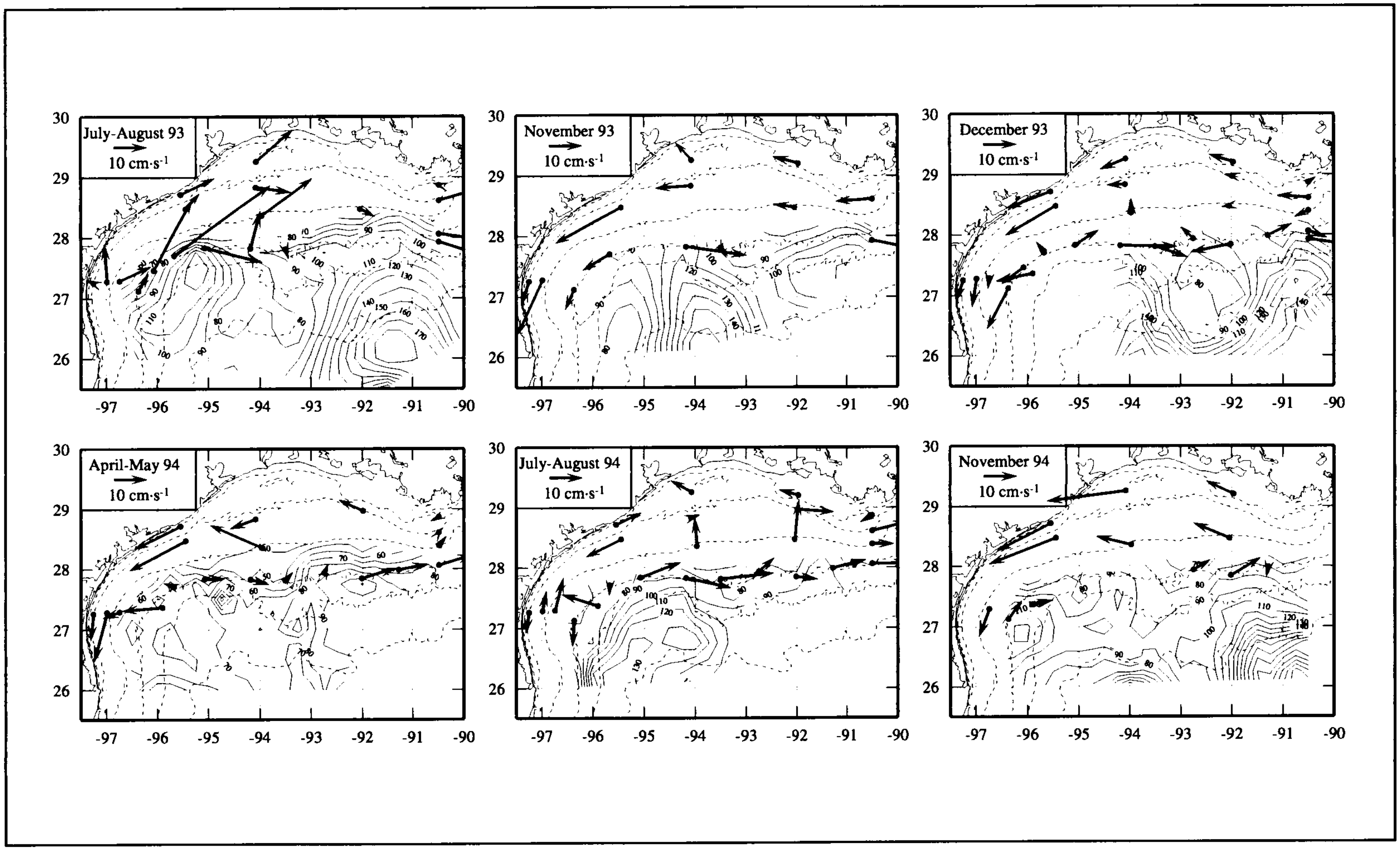

Figure H.1-1. Depth of 20°C isotherm (m) for twelve periods during 1992-1994 based on temperature data from LATEX A, LATEX C, and GulfCet. Specific field activities and dates of sampling are given in Table H.1-1. Vectors represent 10-m current velocities at LATEX A moorings averaged over the sampling periods plus the preceding 14 days. (continued)

Anticyclonic eddies that separate from the Loop Current in the eastern Gulf of Mexico have property and current signals that extend to depths near 1000 m. By the time they reach the northwestern Gulf, their upper waters may have been altered by air-sea exchanges and mixing. Thus, we selected a relatively deep reference level (400 m) for our calculation of surface geopotential anomaly. We do not expect offshore isopycnals to be level at 400 m, but the upper 400 m of the water column contains most of the signal of the Loop Current-derived anticyclones as well as major cyclones present off the shelf

To obtain geopotential anomaly values at stations of less than 400-m depth, specific volume anomaly was interpolated along the bottom along lines of cross-shelf stations. Then geopotential anomalies were estimated by integration along the bottom from the 400-m depth to the next shallowest station and then upward through the water column. The bottom value for that station was then used as a reference for the next shallowest station and the procedure repeated. This methodology, originated by Montgomery (1941), was clarified and used by Csanady (1979, 1981) among others. The condition that bottom potential density be uniform along an isobath ensures the value of geopotential anomaly so determined will be unique, i.e., independent of the path of integration. Density variation along isobaths can give rise to pycnobathic currents, which are not represented by the geopotential anomaly distributions so obtained.

Geopotential anomaly values at each station were objectively interpolated to obtain gridded values and then contoured by the same methods used to produce isotherm depths. The contoured fields for the twelve observing periods are shown in Figures H.1-2 through H.1-13.

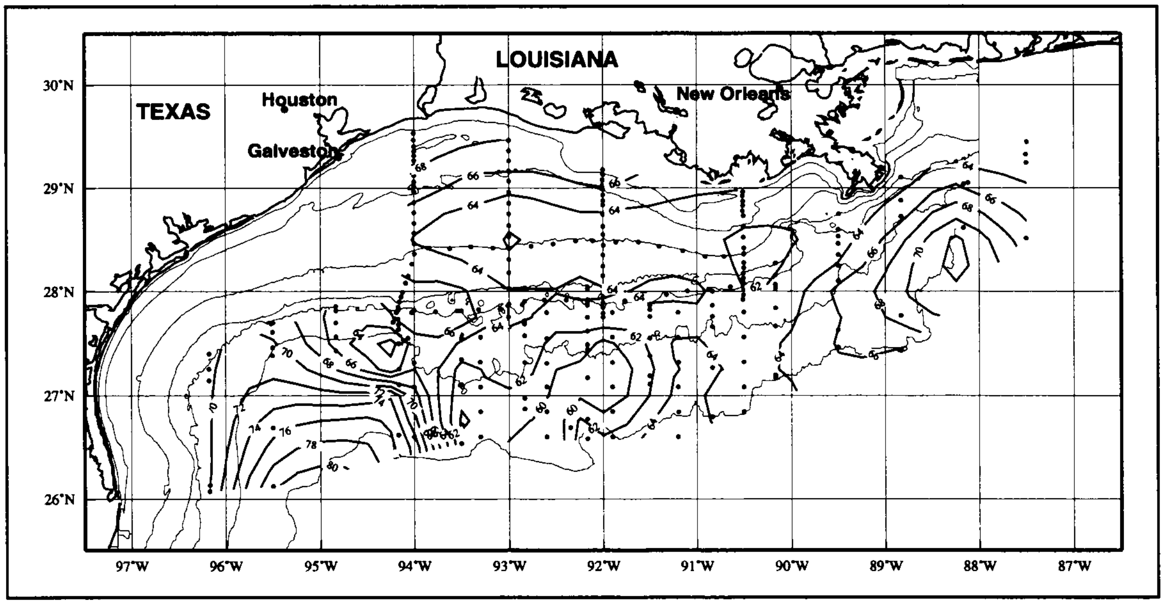

Figure H.1-2. Geopotential anomaly (dyn cm) of sea surface relative to 400 db based on data collected during 15 April-8 May 1992.

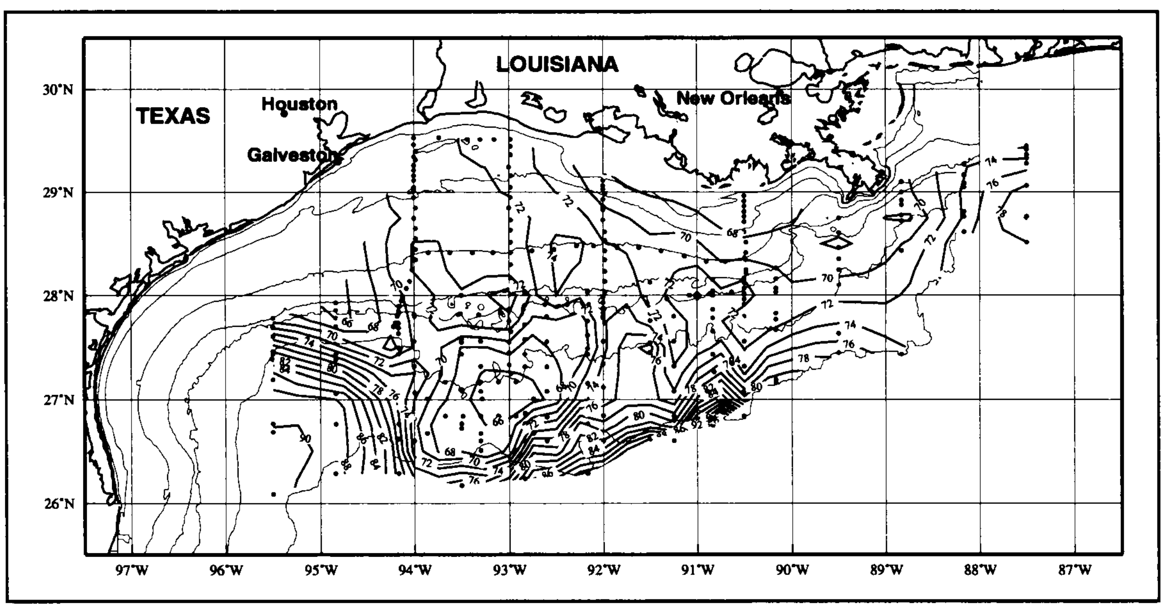

Figure H.1-3. Geopotential anomaly (dyn cm) of sea surface relative to 400 db based on data collected during 1-11 August 1992.

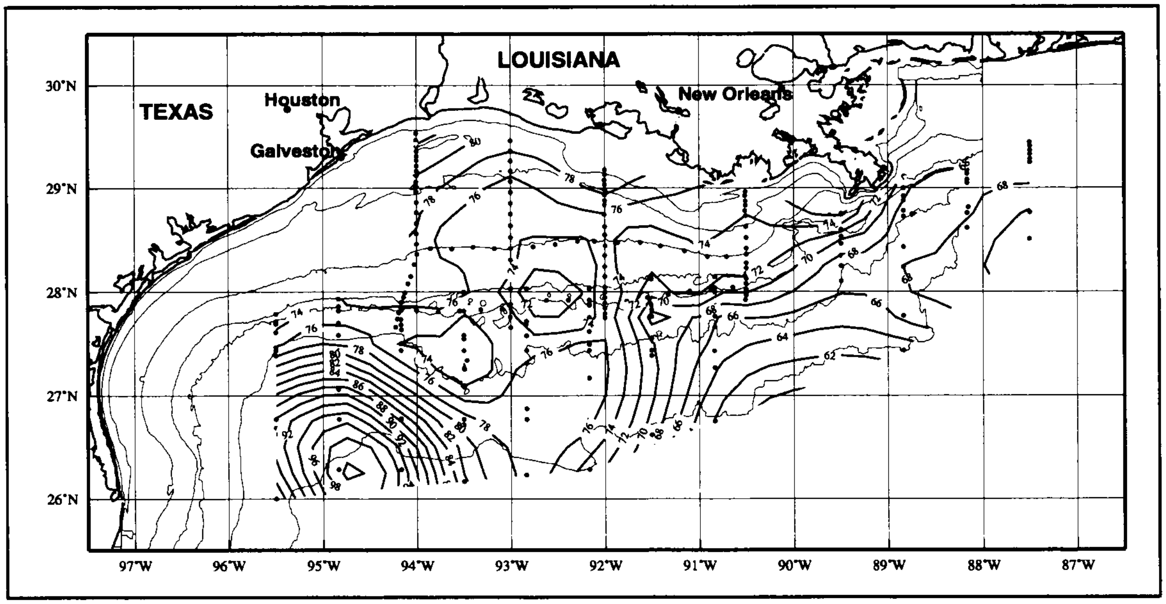

Figure H.1-4. Geopotential anomaly (dyn cm) of sea surface relative to 400 db based on data collected during 5-21 November 1992.

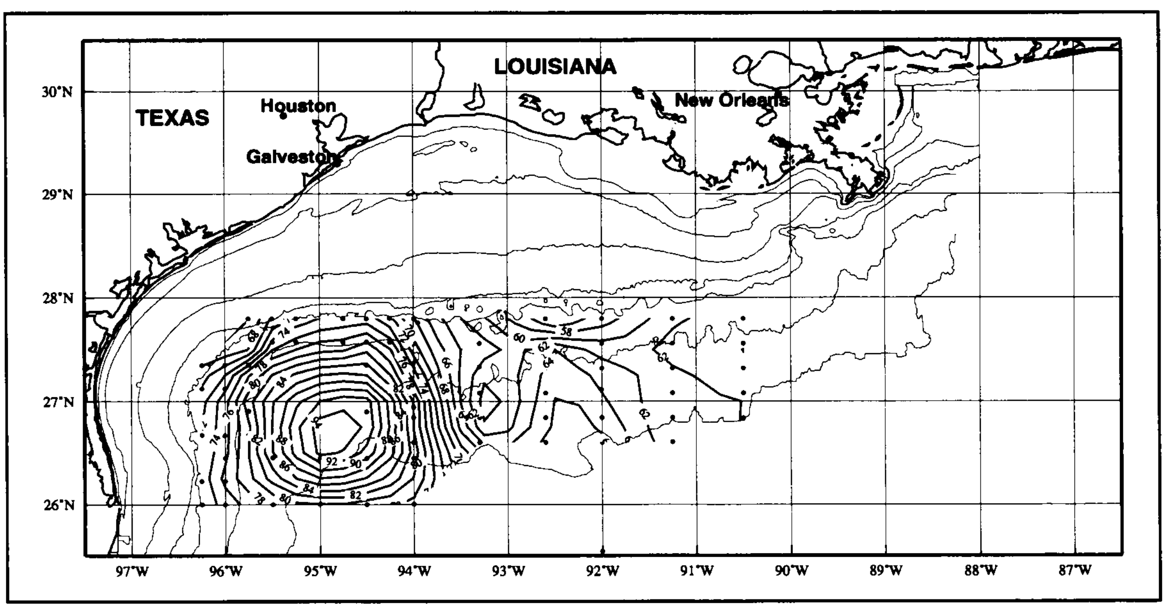

Figure H.1-5. Geopotential anomaly (dyn cm) of sea surface relative to 400 db based on data collected during 4-21 January 1993.

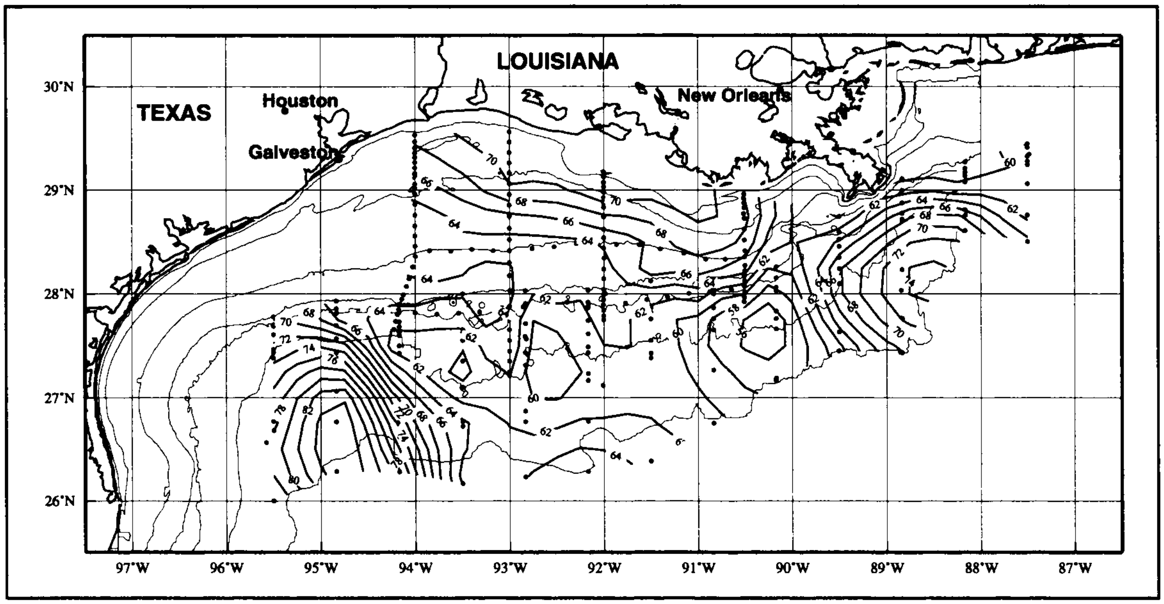

Figure H.1-6. Geopotential anomaly (dyn cm) of sea surface relative to 400 db based on data collected during 5-24 February 1993.

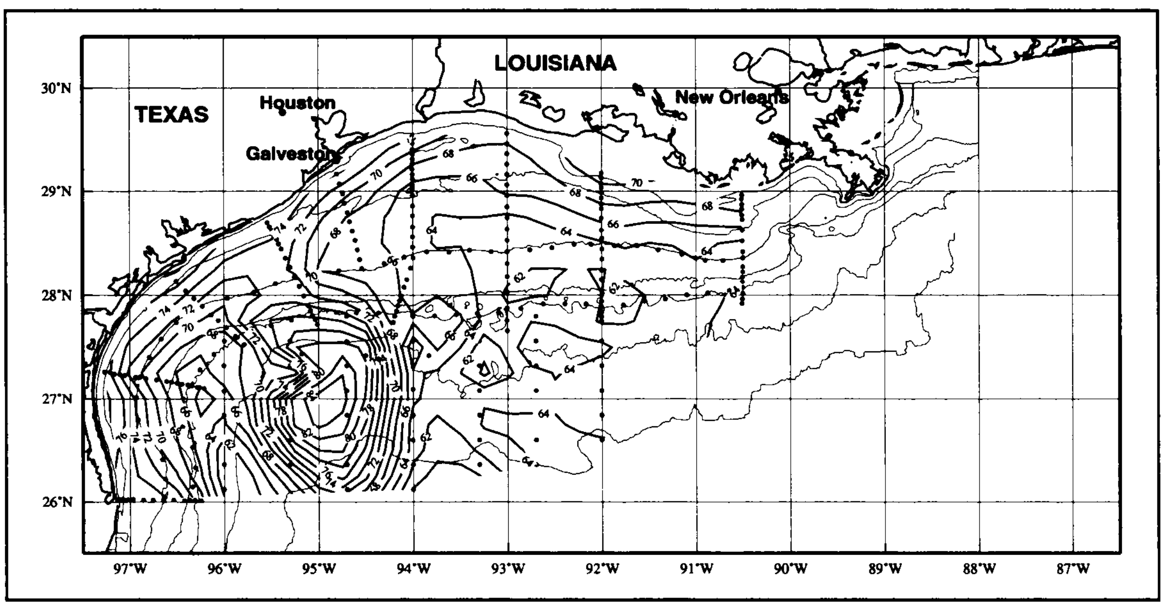

Figure H.1-7. Geopotential anomaly (dyn cm) of sea surface relative to 400 db based on data collected during 26 April-18 May 1993.

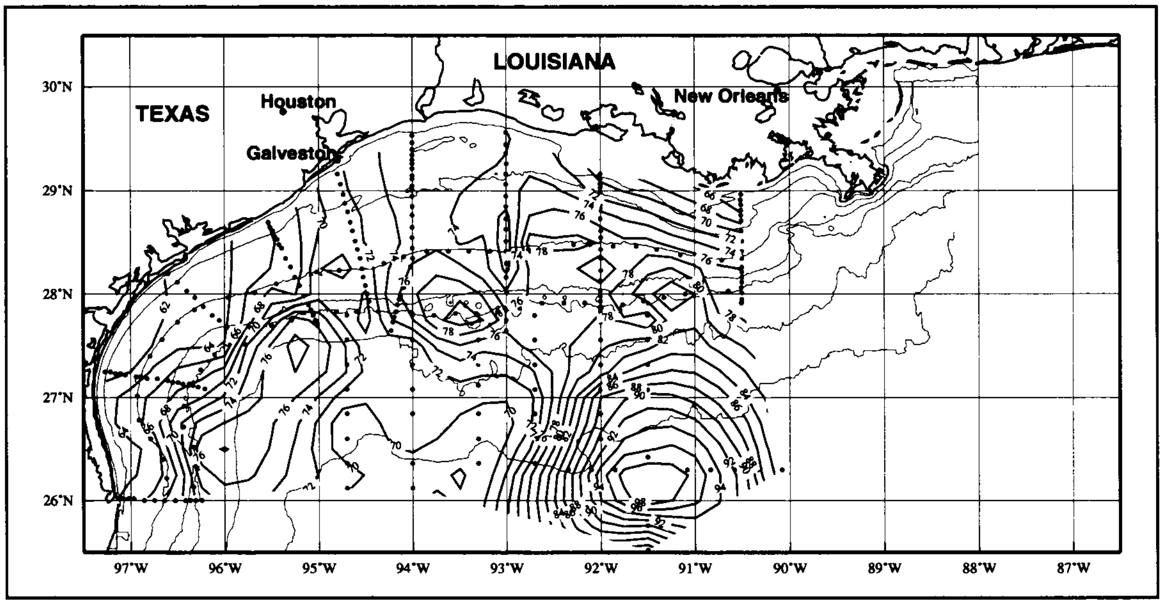

Figure H.1-8. Geopotential anomaly (dyn cm) of sea surface relative to 400 db based on data collected during 26 July-7 August 1993.

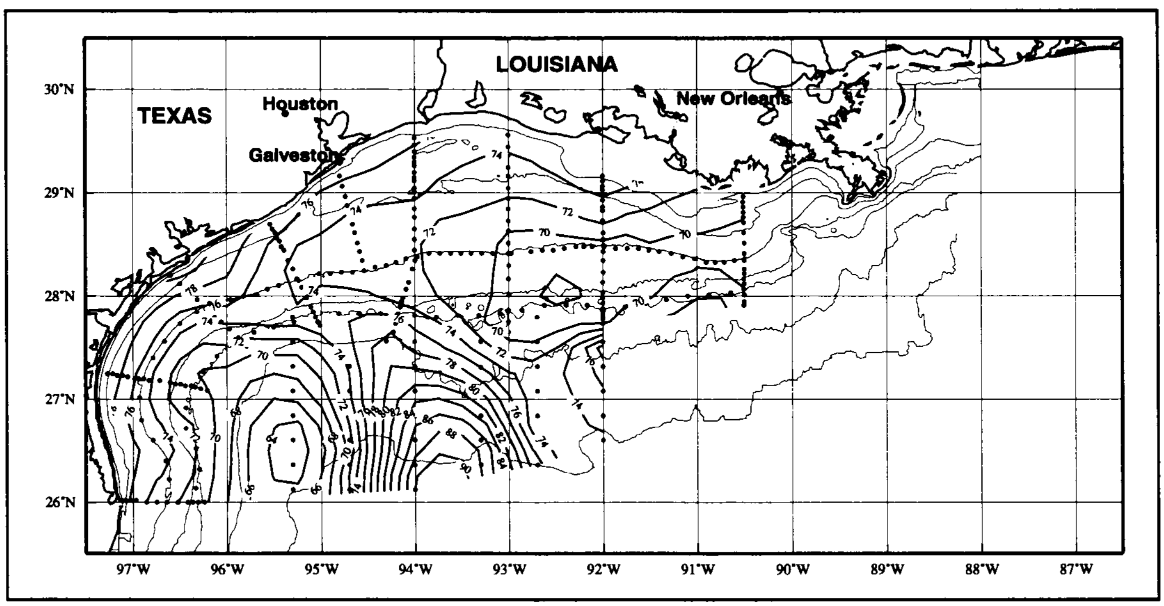

Figure H.1-9. Geopotential anomaly (dyn cm) of sea surface relative to 400 db based on data collected during 28 October-22 November 1993.

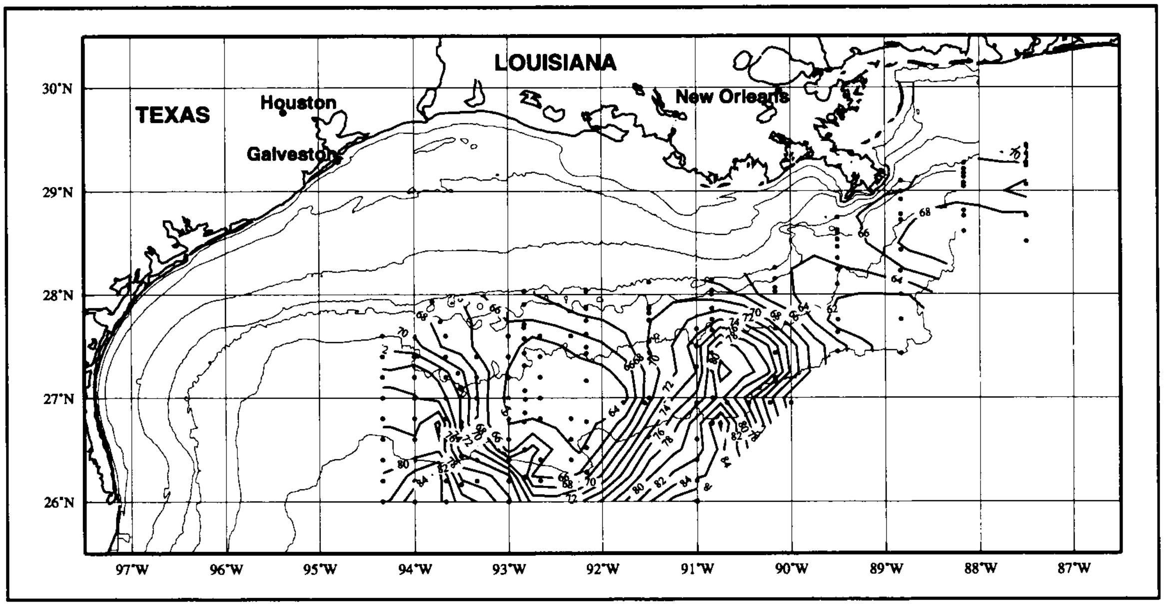

Figure H.1-10. Geopotential anomaly (dyn cm) of sea surface relative to 400 db based on data collected during 15 April-8 May 1992.

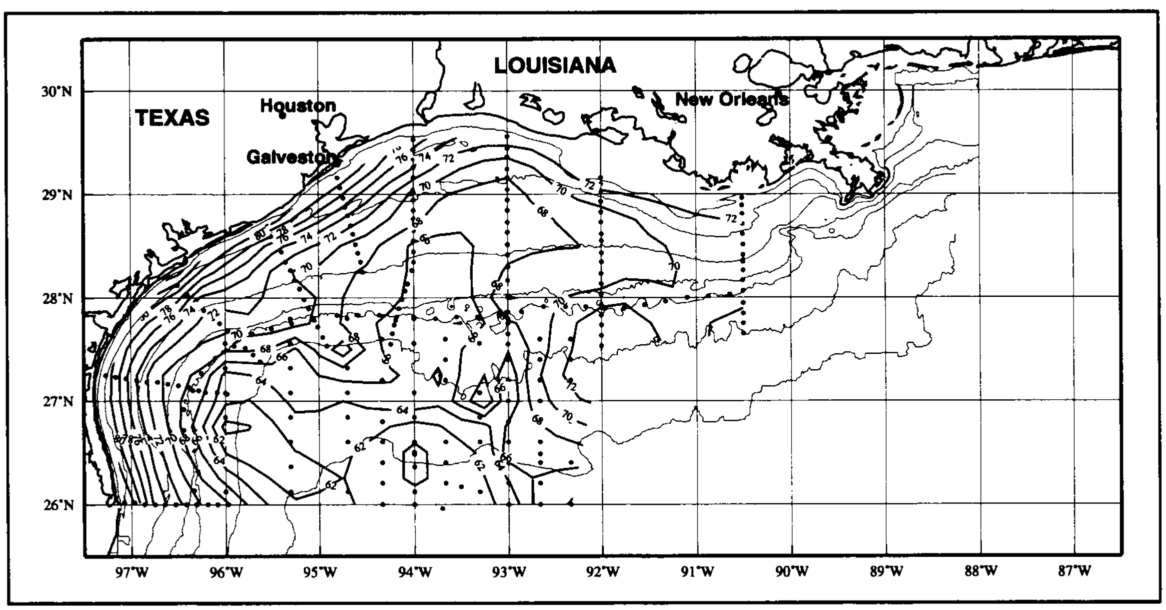

Figure H.1-11. Geopotential anomaly (dyn cm) of sea surface relative to 400 db based on data collected during 1-11 August 1992.

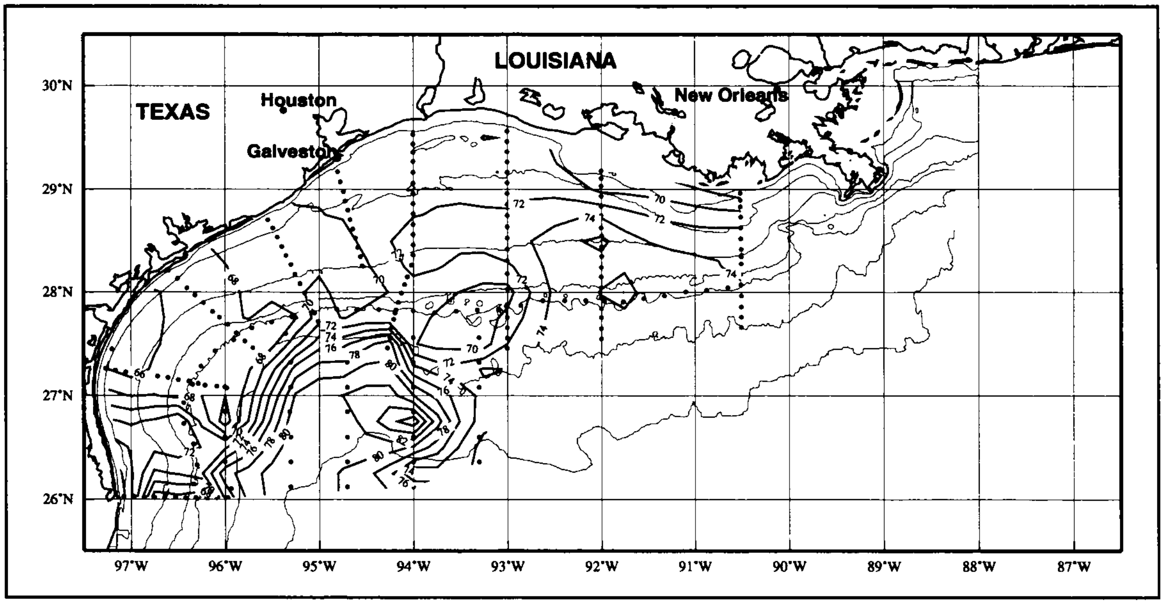

Figure H.1-12. Geopotential anomaly (dyn cm) of sea surface relative to 400 db based on data collected during 5-21 November 1992.

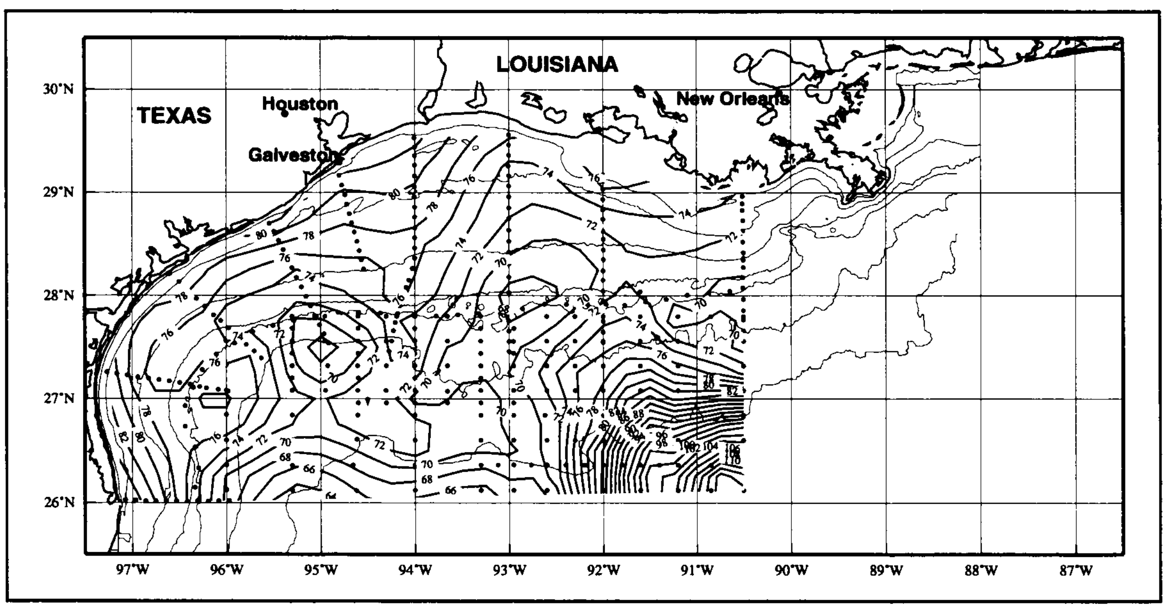

Figure H.1-13. Geopotential anomaly (dyn cm) of sea surface relative to 400 db based on data collected during 4-21 January 1993.

H.2 Monthly average LATEX current fields

Many fields of average current vectors were prepared for study. Here we present for the observation period, April 1992 through November 1994, fields of monthly average current vectors gridded at 0.25° x 0.25° in latitude and longitude, with grid points at whole degrees. Selected as the basic data set were the 40-hr, low-pass time series of currents from the upper instrument at each mooring. Except for four instruments positioned at 3.5 m beneath the sea surface, most of those instruments were located about 10 m below the sea surface (see Table I-2 for average depths and current meter statistics).

A monthly vector average was obtained for each upper instrument having at least 10 days of 40-hr low-pass current records in the month. Based on these averages at all mooring locations, a gridded field of vectors was obtained using the GMT software package. These fields for observed months in the calendar years 1992 through 1994 are shown in Figures H.2-1 through H.2-3, respectively. The patterns are quite consistent with those inferred from patterns of property distributions. They are presented as observed circulation fields and serve as reference material.

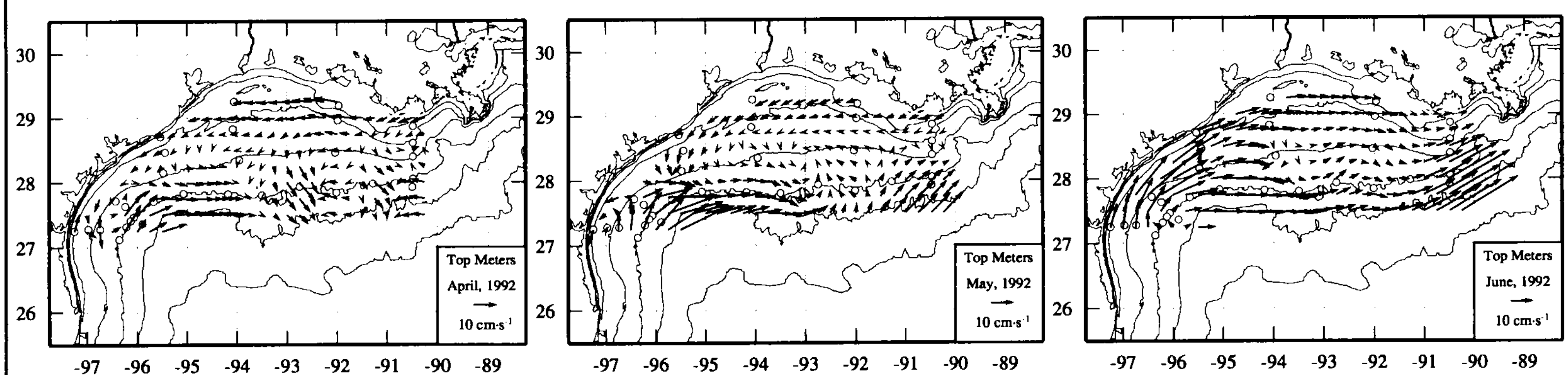

Figure H.2-1. Objectively analyzed 10-m currents from monthly averaged observations for 1992.

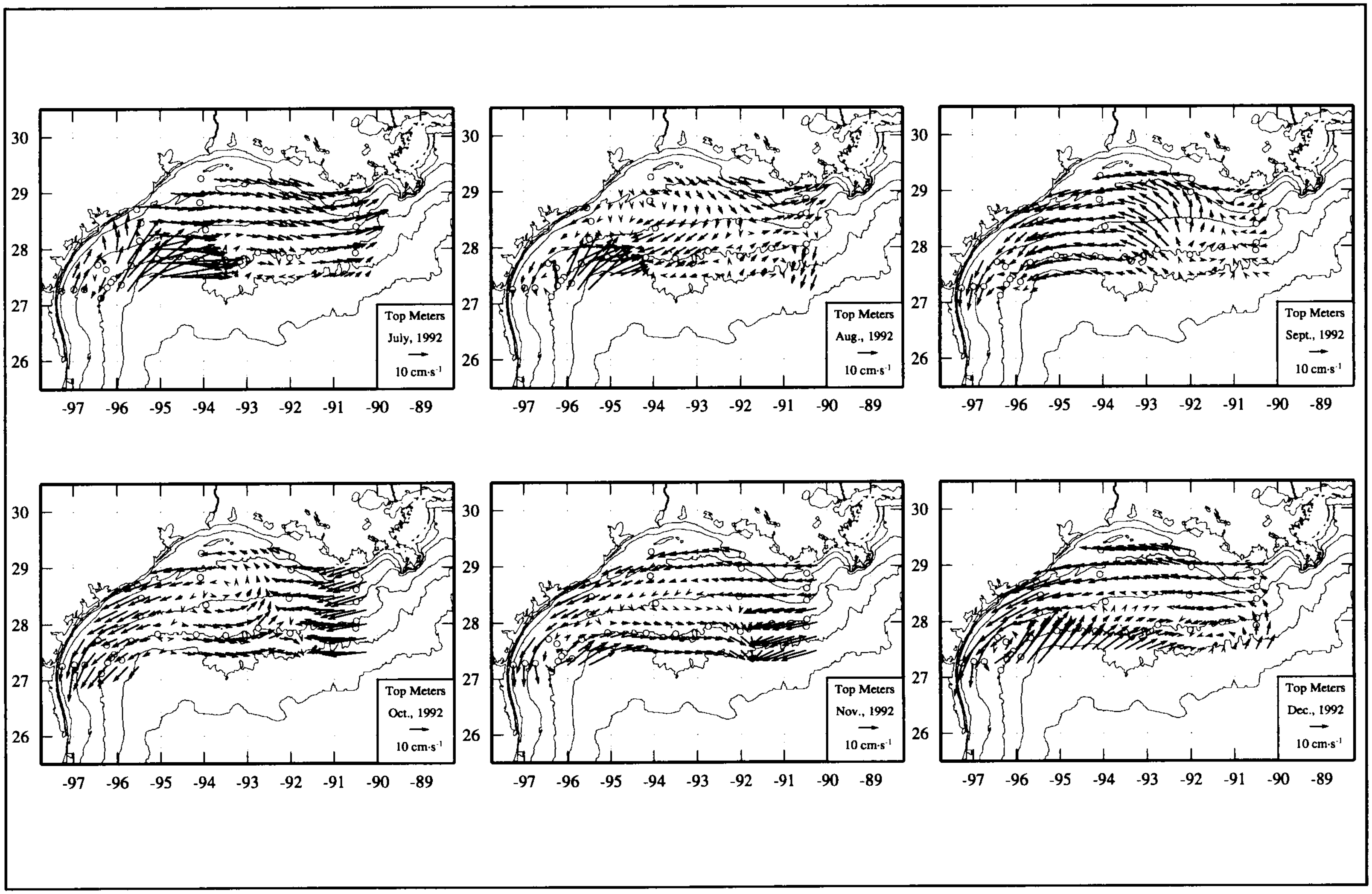

Figure H.2-1. Objectively analyzed 10-m currents from monthly averaged observations for 1992. (continued)

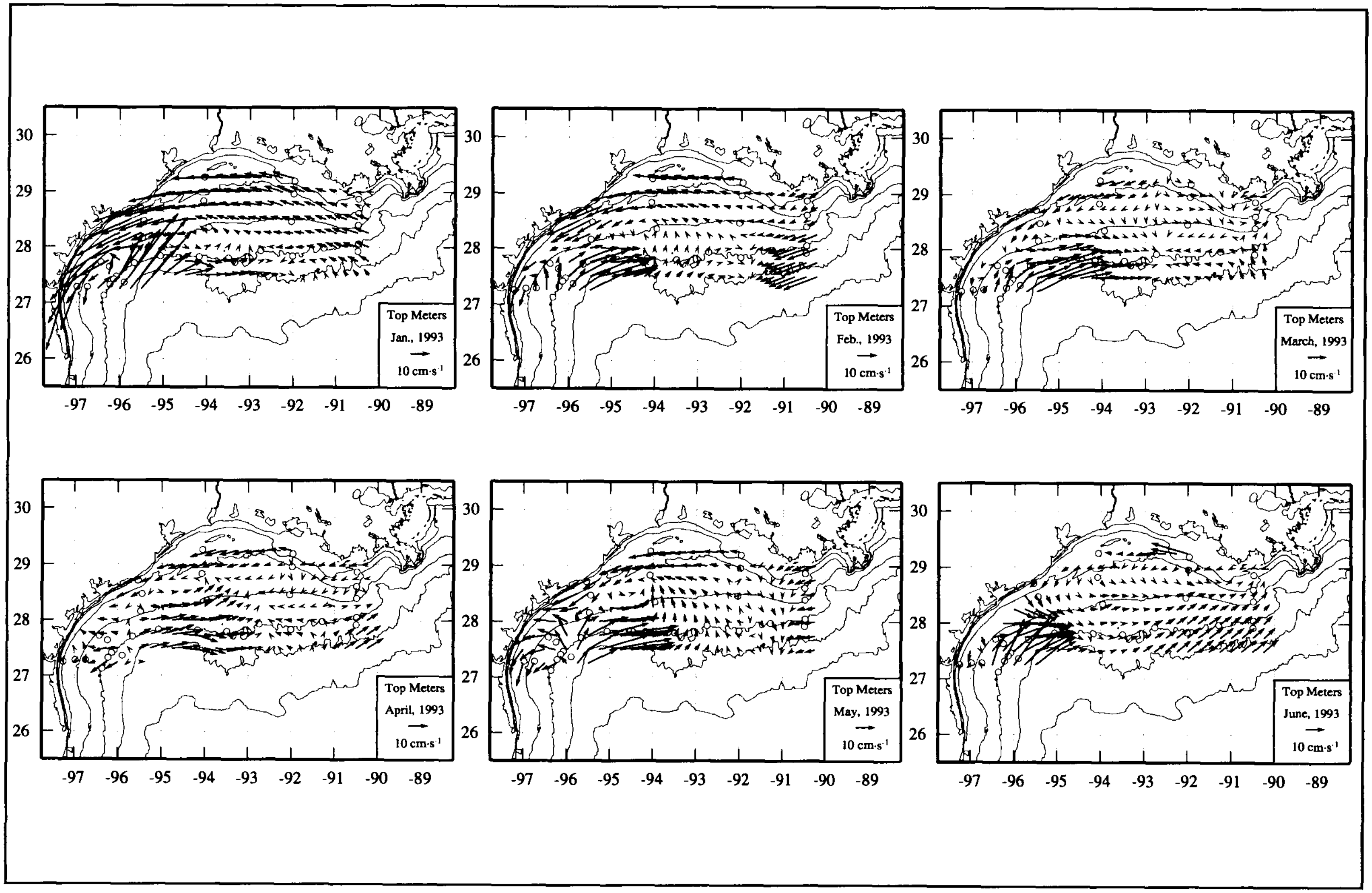

Figure H.2-2. Objectively analyzed 10-m currents from monthly averaged observations for 1993.

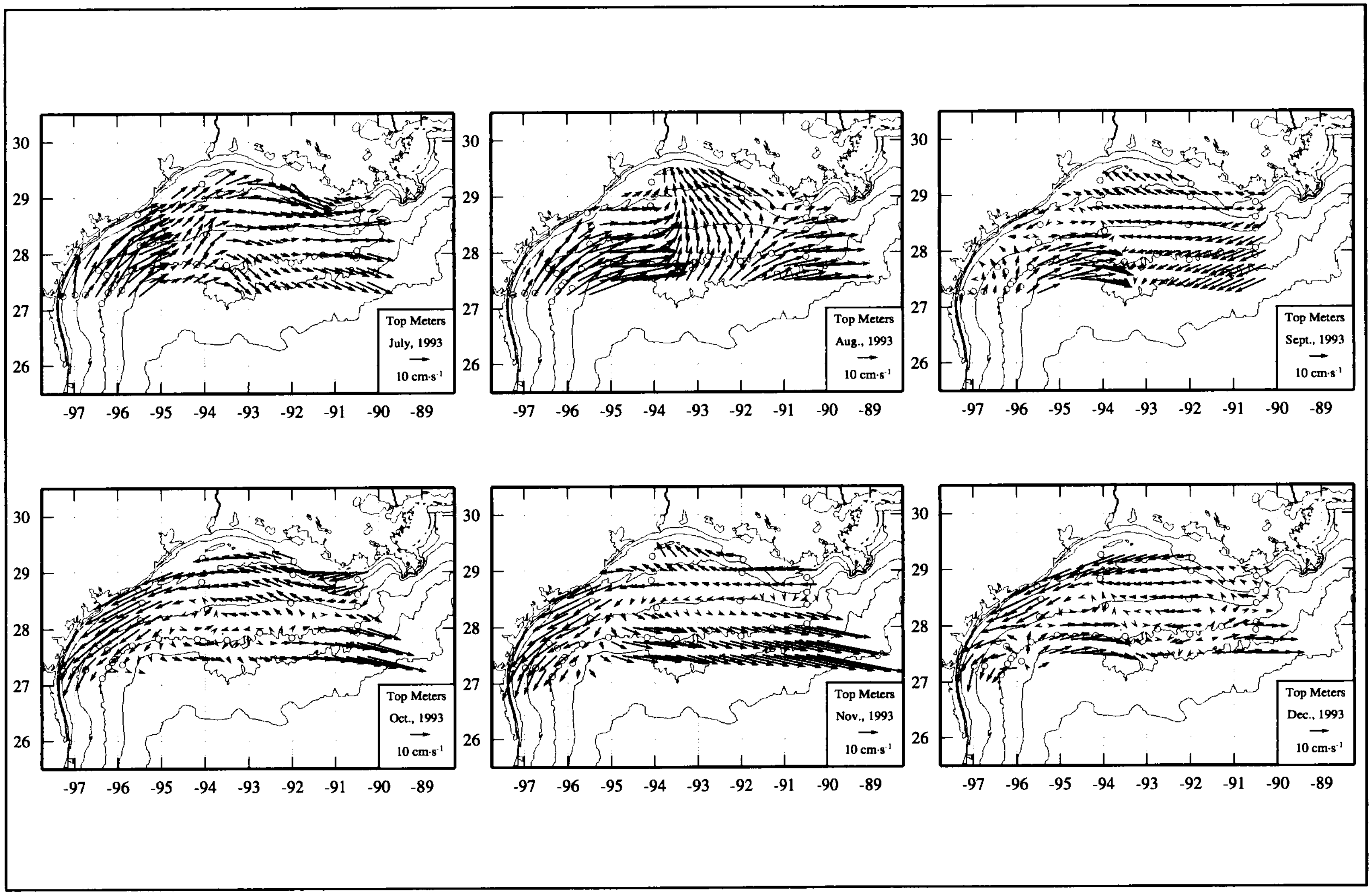

Figure H.2-2. Objectively analyzed 10-m currents from monthly averaged observations for 1993. (continued)

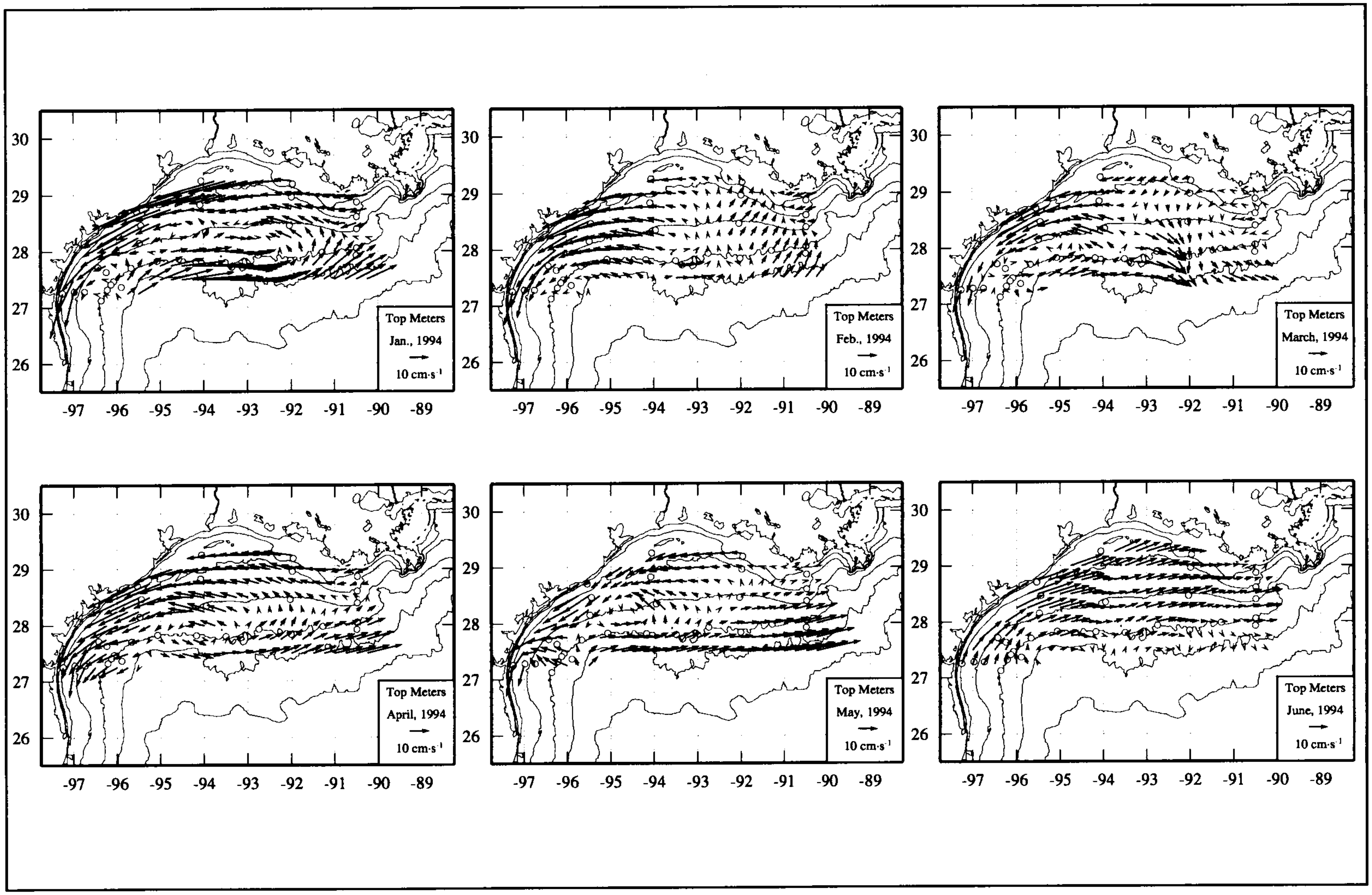

Figure H.2-3. Objectively analyzed 10-m currents from monthly averaged observations for 1994.

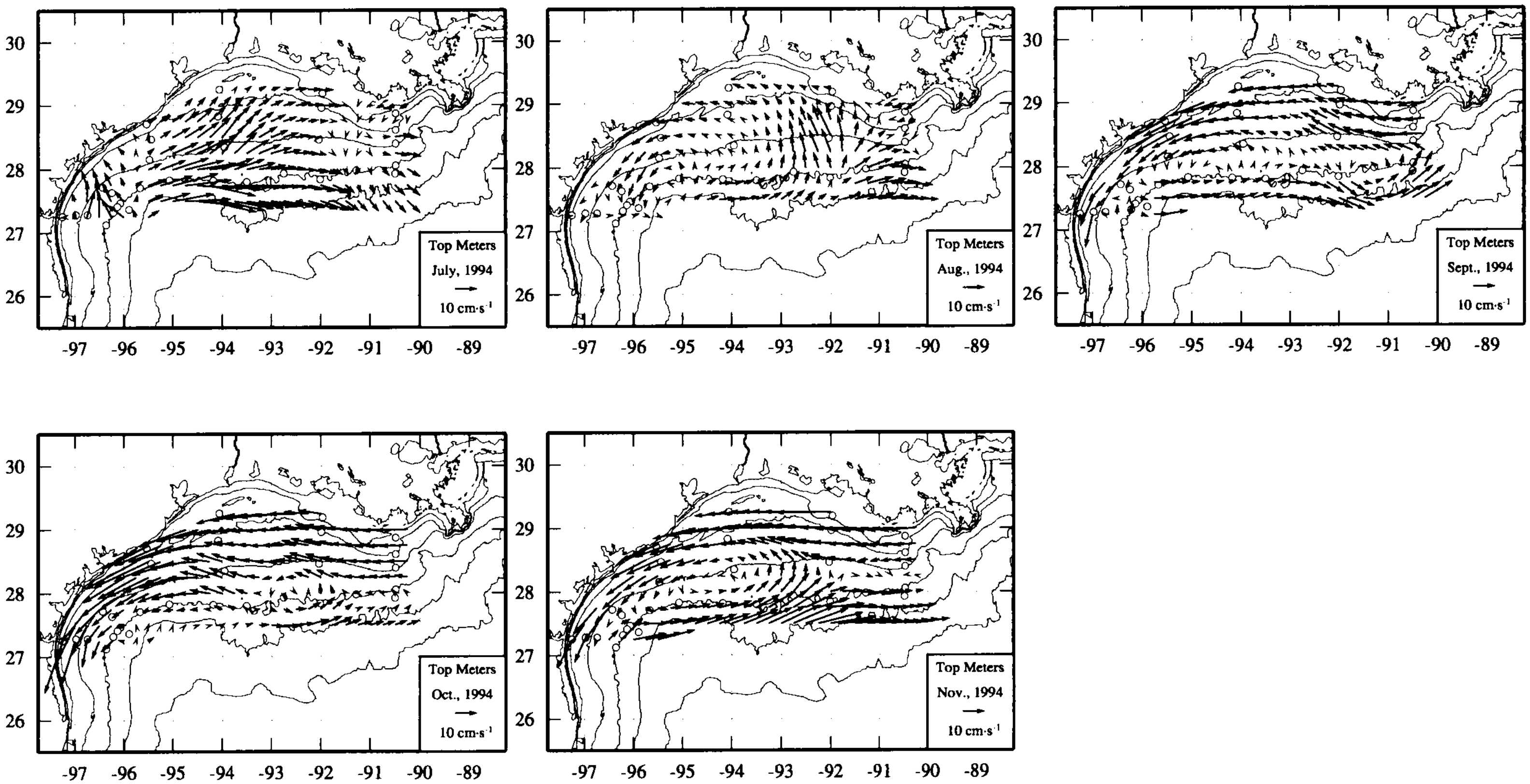

Figure H.2-3. Objectively analyzed 10-m currents from monthly averaged observations for 1994. (continued) There were no LATEX observations for the month of December 1994.

Appendix I: Current, Temperatures, and Salinity Statistics

Included in the LATEX A field program were 37 moorings with current meters, wave gauges, meteorological buoys, and inverted echo sounders. These moorings provided a shelfwide network of current, temperature, and salinity time series. The instrumentation and field maintenance are reviewed in Section 1.2; Figure 1.2-1 shows the locations of the moorings and identifies the mooring numbers; Table 1.2-1 gives the locations, average water depths, and typical mooring configurations for each mooring. The current meter array initially consisted of 83 current meters. Even with spares, attrition reduced the number of meters in the water as the three-year field program ran its course. Details on instrumentation, data returns, and data processing are provided in the LATEX A data report on current meters (DiMarco et al. 1997).

Two cosine-Lanczos filters were used in processing LATEX A time series data: 3-hour low-pass and 40-hour low-pass. The design of the 3-hour kernels depended upon the time interval of the sampling of the instrument. These intervals ranged from 2-min sampling to 3-hr sampling. Table I-1 shows the kernel lengths for selected sampling intervals. The 3-hour low-pass filtering produced hourly data sets from all instrument types. Then, hourly time series of the 3-hour low-passed data were processed through a 40-hour low-pass cosine-Lanczos filter with a kernel of 96+1+96. This filter effectively removed the inertial and superinertial signals, including the diurnal and semidiurnal tides, from the records. The response functions (relative power) for the filters used are given in the data report (DiMarco et al. 1997).

Many standard analyses were carried out on the current records, both in the course of quality control as well as during interpretation. Many of these are included in the data report (DiMarco et al. 1997). For each instrument the data report includes:

- Monthly time series of current vector stick plots, along- and cross-shelf current velocity components, sea temperature, and salinity of 3-hr and 40-hr low pass data.

- Spectral density plots by deployment of velocity components, temperature, salinity, and, for wave gauge sites, bottom pressure.

- Hourly bottom pressure by deployment at each wave gauge location.

- Current rose and joint distributions by deployment.

- Persistence distributions and statistics tables by deployment.

Table I-1. Kernel length for 3-hour low-pass cosine-Lanczos filters applied to time series data.

Sampling interval	Kernel length
1 hour	8+1+8
30 minute	16+1+16
15 minute	32+1+32
10 minute	48+1+48
5 minute	96+1+96
2 minute	240+1+240

- Basic statistics (mean, maximum, and minimum values and standard deviation) tables for all current meter time series by two-week intervals.

Here we present some additional statistics of possible use to engineers, modelers, managers, or others dealing with structures, vessels, or oil spills over the Texas-Louisiana shelf. Two statistical compilations are offered: one based on the hourly data, the other based on the 40-hr low-pass data.

Table I-2 lists current statistics based on the hourly 3-hr low-pass records. The information is organized by year and by month; i.e., the first page of the table gives all statistics for April, May, and June of 1992, the second page for July - September of 1992, etc. The leftmost column on each page lists all of the instruments originally deployed in numerical and depth order—"01t" designates the top instrument on mooring 1; "03m" designates the mid-depth instrument on mooring 3; and "01b" designates the bottom instrument on mooring 1. For each instrument and month the following information is given:

Symbol	Statistic
h	average instrument depth
N	number of hourly samples in monthly record
$\lvert\bar{v}\rvert$	monthly vector average speed
θ	monthly vector average direction
$\overline{\lvert v\rvert}$	monthly scalar average speed
v_M	maximum speed in monthly record

When no data are available for a particular instrument in a particular month, $N = 0$ and all statistical variables are set to -99. It should be noted that moorings 44-47 constituted the wild card array, as mentioned in Section 1.2; these were removed early during the field program and their instruments used as spares. None were maintained after March 1993.

Table I-2. Current meter velocity statistics for 3-hr low-passed filtered data.

		April 1992					May 1992					June 1992				
No.	h	N	$\lvert\bar{v}\rvert$	θ	$\overline{\lvert v\rvert}$	v_M	N	$\lvert\bar{v}\rvert$	θ	$\overline{\lvert v\rvert}$	v_M	N	$\lvert\bar{v}\rvert$	θ	$\overline{\lvert v\rvert}$	v_M
01t	10	501	3	16	20	86	723	5	200	22	65	720	11	16	16	53
01b	12	504	0	116	7	31	719	7	169	10	33	350	1	332	7	23
02t	10	501	4	150	18	57	722	1	179	20	63	720	15	8	24	64
02b	32	501	1	340	11	39	661	1	109	14	42	625	7	15	10	33
03t	10	495	9	192	23	69	540	4	344	14	57	0	-99	-99	-99	-99
03m	33	499	1	295	7	46	44	1	33	1	17	0	-99	-99	-99	-99
03b	58	0	-99	-99	-99	-99	0	-99	-99	-99	-99	0	-99	-99	-99	-99
04t	14	513	10	10	16	52	744	15	3	22	67	720	5	273	18	43
04m	100	513	5	232	9	21	744	7	332	15	34	720	3	263	13	35
04b	190	0	-99	-99	-99	-99	0	-99	-99	-99	-99	0	-99	-99	-99	-99
05t	14	525	12	38	23	80	744	19	46	26	74	720	3	357	19	55
05m	100	525	3	41	7	24	744	13	46	18	36	720	1	359	12	34
05b	190	525	1	286	2	13	744	1	343	4	16	720	2	265	4	13
06t	14	489	10	93	12	35	744	27	90	28	61	720	16	85	26	70
06m	100	489	1	19	8	24	744	1	98	8	37	720	6	66	15	53
06b	190	489	3	303	4	15	744	2	266	6	22	720	2	354	5	26
07t	14	483	11	95	19	54	744	6	97	16	54	720	20	90	26	58
07m	100	483	2	264	7	20	744	4	249	11	27	720	0	357	10	24
07b	190	483	1	104	6	22	744	1	309	4	20	720	1	182	7	22
08t	14	339	5	114	19	70	744	8	78	14	44	720	22	92	25	69
08m	100	339	5	72	12	34	744	3	63	8	21	720	3	66	9	26
08b	190	339	2	331	3	9	744	1	0	2	9	720	1	330	2	8
09t	14	343	4	278	21	43	744	9	123	15	43	720	7	100	15	54
09m	100	344	3	270	13	28	744	3	88	10	23	720	4	292	8	21
09b	190	344	2	284	4	11	744	2	258	2	13	720	2	214	2	12
10t	14	348	8	132	17	48	744	4	4	15	45	720	7	51	15	38
10m	100	348	1	326	9	22	744	3	67	7	18	720	4	73	8	18
10b	190	348	2	280	2	12	744	2	282	2	11	720	1	337	2	8
11t	14	354	7	282	14	44	744	5	292	10	43	720	6	113	13	32
11m	100	378	1	178	4	13	744	3	231	3	15	720	1	218	3	15
11b	190	354	6	270	10	25	744	2	352	6	20	720	5	84	8	20
12t	14	369	4	272	11	38	744	6	33	11	23	720	24	55	24	48
12m	100	369	7	263	11	22	744	3	12	10	25	720	26	57	26	45
12b	490	372	0	234	2	3	744	1	239	2	5	720	1	89	2	3
13t	14	375	7	294	17	51	744	10	57	14	37	720	26	66	27	61
13m	100	375	3	273	14	35	744	10	67	13	28	720	25	66	25	43
13b	190	375	1	313	8	24	744	3	254	8	23	720	2	45	6	22
14t	10	378	5	76	17	37	744	4	119	10	33	698	10	77	13	42
14m	26	378	5	94	15	33	744	3	97	9	24	701	7	93	9	26
14b	40	378	1	178	12	26	744	2	109	7	21	702	1	111	6	18
15t	10	381	2	284	12	33	744	2	221	12	45	702	7	56	14	39
15b	17	381	2	240	6	19	744	1	231	5	19	700	0	355	5	14
16t	10	381	7	252	15	36	744	3	255	12	46	702	2	56	10	33
16b	14	384	4	249	7	18	744	2	263	6	25	699	2	277	5	18
17t	3	0	-99	-99	-99	-99	0	-99	-99	-99	-99	494	6	105	21	54
17b	6	0	-99	-99	-99	-99	0	-99	-99	-99	-99	0	-99	-99	-99	-99
18t	8	399	8	281	22	61	733	1	245	15	50	711	8	95	15	38
18b	19	381	0	324	7	25	673	1	117	7	33	711	1	71	6	18
19t	3	326	4	305	20	77	114	1	353	12	27	499	3	196	21	50
19m	20	419	2	244	8	24	744	1	146	7	21	6	7	298	9	13
19b	45	0	-99	-99	-99	-99	0	-99	-99	-99	-99	669	1	92	4	11
20t	3	0	-99	-99	-99	-99	20	10	241	16	27	500	8	74	19	45
20b	13	426	4	179	11	27	721	4	145	10	27	720	4	7	9	28
21t	14	417	4	264	13	37	725	1	272	13	41	720	11	82	19	46
21b	22	445	1	183	7	22	703	1	88	7	33	720	3	57	7	20
22t	3	93	9	53	21	40	0	-99	-99	-99	-99	510	10	261	29	73
22m	20	464	2	115	9	23	744	2	330	8	39	649	5	310	13	39
22b	48	0	-99	-99	-99	-99	0	-99	-99	-99	-99	649	1	76	6	19
23t	10	543	5	244	21	64	625	0	157	15	55	627	14	66	21	53
23b	13	546	3	220	13	40	629	4	263	12	41	625	2	34	8	31
24t	10	537	5	229	13	43	722	7	177	17	45	720	11	61	18	49
24b	25	481	0	228	8	25	728	1	220	8	22	720	2	16	6	20
25t	11	537	2	195	12	45	709	5	219	14	43	720	3	344	24	54
25m	20	538	1	170	11	34	714	4	216	13	48	720	3	78	21	45
25b	29	0	-99	-99	-99	-99	36	3	92	11	21	720	2	20	12	36
44t	13	526	5	211	16	53	744	3	303	16	47	720	24	51	28	68
44b	55	525	1	184	7	19	744	2	48	9	25	720	5	31	9	26
45t	12	519	16	39	21	72	744	17	46	26	83	720	5	337	19	47
45m	84	513	4	36	7	20	744	12	45	17	44	720	2	293	13	39
46t	14	525	6	30	12	49	744	15	61	22	56	720	21	62	25	64
46m	50	0	-99	-99	-99	-99	0	-99	-99	-99	-99	0	-99	-99	-99	-99
46b	84	525	3	237	6	19	744	3	63	6	24	720	3	45	9	20
47t	12	514	18	36	21	71	744	14	27	23	64	720	5	307	16	38
47m	100	0	-99	-99	-99	-99	0	-99	-99	-99	-99	0	-99	-99	-99	-99
47b	190	0	-99	-99	-99	-99	0	-99	-99	-99	-99	0	-99	-99	-99	-99
48t	14	362	10	118	13	42	744	6	45	11	39	720	6	79	12	31
48m	100	361	5	80	11	31	744	3	68	8	28	720	4	77	7	18
48b	190	0	-99	-99	-99	-99	0	-99	-99	-99	-99	0	-99	-99	-99	-99
49t	14	519	7	57	17	69	744	22	52	26	64	720	6	3	21	73
49m	100	519	1	191	11	25	259	14	42	16	31	0	-99	-99	-99	-99
49b	490	519	3	151	5	15	245	5	146	6	17	0	-99	-99	-99	-99

Table I-2. Current meter velocity statistics for 3-hr low-passed filtered data (continued).

		July 1992					August 1992					September 1992				
No.	h	N	$\lvert\bar{\mathbf{v}}\rvert$	θ	$\overline{\lvert\mathbf{v}\rvert}$	v_M	N	$\lvert\bar{\mathbf{v}}\rvert$	θ	$\overline{\lvert\mathbf{v}\rvert}$	v_M	N	$\lvert\bar{\mathbf{v}}\rvert$	θ	$\overline{\lvert\mathbf{v}\rvert}$	v_M
01t	10	723	2	5	9	30	744	3	176	13	38	697	6	185	16	50
01b	12	0	-99	-99	-99	-99	0	-99	-99	-99	-99	0	-99	-99	-99	-99
02t	10	714	11	19	17	63	744	2	179	13	30	703	8	187	18	75
02b	32	371	4	13	7	23	0	-99	-99	-99	-99	621	7	164	17	61
03t	10	339	6	144	19	42	744	4	160	18	57	720	9	201	19	69
03m	33	0	-99	-99	-99	-99	0	-99	-99	-99	-99	0	-99	-99	-99	-99
03b	58	341	8	189	10	22	744	4	191	9	24	720	5	183	10	45
04t	14	507	12	201	27	61	744	4	221	20	54	720	6	240	19	57
04m	100	507	7	205	13	38	744	7	205	11	43	720	11	200	13	35
04b	190	117	15	184	16	28	744	8	211	19	68	720	13	214	16	45
05t	14	516	8	8	28	73	744	21	16	30	81	720	4	299	19	47
05m	100	515	11	250	18	47	744	5	32	15	35	720	6	248	12	47
05b	190	401	3	258	5	14	658	1	211	7	27	720	6	226	8	20
06t	14	528	33	47	38	90	744	22	70	30	76	720	8	212	18	61
06m	100	406	18	41	25	65	730	4	253	11	29	720	3	263	9	31
06b	190	529	9	270	15	38	744	3	267	7	28	720	1	306	5	20
07t	14	541	43	85	47	87	744	17	84	29	88	720	15	254	18	46
07m	100	410	22	72	26	76	0	-99	-99	-99	-99	0	-99	-99	-99	-99
07b	190	539	3	93	6	28	744	2	257	6	21	720	6	264	8	26
08t	14	744	13	111	20	61	744	3	305	17	54	720	9	292	15	48
08m	100	744	6	267	11	28	719	15	270	17	42	0	-99	-99	-99	-99
08b	190	744	0	285	2	12	715	2	285	2	18	0	-99	-99	-99	-99
09t	14	744	5	332	21	68	719	10	248	17	52	720	6	272	13	34
09m	100	744	3	286	8	20	718	5	265	8	40	720	10	273	14	35
09b	190	744	2	243	2	14	723	1	232	2	14	305	1	286	2	5
10t	14	744	9	103	28	100	704	9	257	16	40	720	14	306	18	36
10m	100	744	5	261	11	32	705	5	285	8	26	720	5	287	10	33
10b	190	744	1	331	2	11	720	1	352	2	11	720	1	129	3	19
11t	14	744	3	239	17	56	705	3	5	15	50	720	2	93	14	38
11m	100	744	2	239	5	21	664	2	226	4	19	720	8	270	12	29
11b	190	744	1	288	8	27	695	2	337	8	22	0	-99	-99	-99	-99
12t	14	744	2	20	17	57	744	6	211	15	134	720	8	256	12	48
12m	100	744	2	16	14	32	744	11	254	14	63	238	25	260	29	55
12b	490	744	1	234	2	4	744	2	231	2	6	720	1	239	2	5
13t	14	720	9	70	27	71	744	10	187	22	162	720	2	14	13	46
13m	100	719	2	22	17	33	744	9	262	13	103	720	12	266	16	43
13b	190	720	3	233	6	25	744	8	231	10	98	720	10	242	13	41
14t	10	725	13	75	24	75	744	4	272	16	129	696	6	69	17	40
14m	26	704	9	102	18	61	50	13	289	20	65	668	6	91	15	40
14b	40	726	3	80	6	23	744	4	255	10	130	34	17	77	17	24
15t	10	727	16	70	20	72	590	13	67	18	50	669	14	246	17	63
15b	17	728	1	62	8	32	744	2	214	9	102	702	3	235	6	39
16t	10	493	5	41	13	34	0	-99	-99	-99	-99	0	-99	-99	-99	-99
16b	14	720	2	298	6	14	592	3	251	6	17	0	-99	-99	-99	-99
17t	3	260	2	229	25	57	249	2	124	24	49	711	9	279	18	42
17b	6	0	-99	-99	-99	-99	0	-99	-99	-99	-99	714	8	336	12	33
18t	8	727	14	105	18	42	731	10	107	17	85	711	8	296	17	64
18b	19	725	2	94	6	28	731	2	54	5	59	716	3	281	9	32
19t	3	166	16	79	38	63	724	5	212	19	53	720	9	11	24	64
19m	20	166	16	79	17	32	725	2	136	15	43	0	-99	-99	-99	-99
19b	45	728	3	99	7	21	725	2	238	6	32	0	-99	-99	-99	-99
20t	3	279	7	33	17	48	238	10	35	17	34	35	7	280	13	22
20b	13	723	5	119	11	39	744	1	320	8	36	700	5	275	11	46
21t	14	725	8	50	17	41	664	4	90	12	49	573	9	249	13	46
21b	22	727	4	51	11	32	728	4	93	9	34	720	4	256	5	37
22t	3	141	4	148	24	48	687	13	238	20	67	0	-99	-99	-99	-99
22m	20	721	7	240	21	55	744	4	253	11	32	702	1	47	9	47
22b	48	722	2	71	6	20	744	0	245	6	17	703	2	219	8	27
23t	10	725	14	81	18	49	744	5	239	14	48	698	10	248	18	73
23b	13	719	8	86	12	32	744	3	276	12	36	100	1	114	7	16
24t	10	726	3	349	16	41	744	4	255	12	43	105	8	227	13	25
24b	25	727	1	250	8	26	744	2	194	8	38	103	3	225	6	17
25t	11	724	3	0	18	58	744	2	216	13	43	698	6	244	15	47
25m	20	725	3	345	13	39	744	1	257	11	50	704	5	252	14	45
25b	29	724	0	202	10	37	744	1	110	14	40	704	5	232	15	45
44t	13	722	9	52	23	61	744	4	224	13	34	720	7	220	16	63
44b	55	723	3	245	9	24	744	1	63	8	29	720	6	214	9	55
45t	12	395	2	102	26	81	0	-99	-99	-99	-99	0	-99	-99	-99	-99
45m	84	395	3	236	10	23	0	-99	-99	-99	-99	0	-99	-99	-99	-99
46t	14	723	2	286	18	44	744	4	299	16	41	720	3	266	15	42
46m	50	376	13	269	15	45	744	5	247	10	35	720	1	202	11	41
46b	84	724	7	230	10	23	708	3	231	8	24	0	-99	-99	-99	-99
47t	12	744	8	354	29	81	744	16	355	27	73	720	6	310	17	38
47m	100	0	-99	-99	-99	-99	0	-99	-99	-99	-99	0	-99	-99	-99	-99
47b	190	0	-99	-99	-99	-99	0	-99	-99	-99	-99	0	-99	-99	-99	-99
48t	14	744	17	86	23	67	721	2	76	19	101	720	1	312	14	39
48m	100	744	3	30	10	25	722	4	281	10	51	720	9	281	12	30
48b	190	0	-99	-99	-99	-99	0	-99	-99	-99	-99	207	1	353	3	16
49t	14	744	54	28	58	99	744	51	34	54	92	720	2	172	15	37
49m	100	0	-99	-99	-99	-99	0	-99	-99	-99	-99	0	-99	-99	-99	-99
49b	490	0	-99	-99	-99	-99	0	-99	-99	-99	-99	0	-99	-99	-99	-99

Table I-2. Current meter velocity statistics for 3-hr low-passed filtered data (continued).

		October 1992					November 1992					December 1992				
No.	h	N	$\lvert\bar{v}\rvert$	θ	$\overline{\lvert v\rvert}$	v_M	N	$\lvert\bar{v}\rvert$	θ	$\overline{\lvert v\rvert}$	v_M	N	$\lvert\bar{v}\rvert$	θ	$\overline{\lvert v\rvert}$	v_M
01t	10	699	7	189	15	55	376	14	180	21	45	333	24	192	25	61
01b	12	386	4	168	15	53	720	9	175	15	46	390	10	179	12	39
02t	10	727	19	185	23	77	720	11	184	21	65	727	15	188	18	71
02b	32	728	8	180	13	52	720	6	169	17	45	394	5	182	13	54
03t	10	715	9	207	17	60	664	9	176	15	54	0	-99	-99	-99	-99
03m	33	373	6	190	11	39	668	8	184	12	41	0	-99	-99	-99	-99
03b	58	720	5	182	11	40	668	4	168	9	39	0	-99	-99	-99	-99
04t	14	349	12	211	15	47	0	-99	-99	-99	-99	0	-99	-99	-99	-99
04m	100	716	3	190	8	42	0	-99	-99	-99	-99	0	-99	-99	-99	-99
04b	190	744	5	210	13	52	268	1	268	4	17	0	-99	-99	-99	-99
05t	14	744	7	233	15	55	720	7	42	14	67	16	6	248	6	8
05m	100	744	4	257	13	51	720	3	32	7	23	10	6	65	8	12
05b	190	744	1	218	9	29	720	5	49	8	22	15	3	33	4	5
06t	14	662	9	246	14	45	720	8	77	11	38	76	12	81	14	32
06m	100	744	3	261	5	23	720	9	65	9	35	62	8	53	12	24
06b	190	744	1	305	4	26	720	5	255	6	25	74	1	358	3	8
07t	14	744	4	288	12	32	720	9	75	16	40	82	31	75	32	63
07m	100	0	-99	-99	-99	-99	0	-99	-99	-99	-99	0	-99	-99	-99	-99
07b	190	744	2	256	6	24	720	3	84	9	22	83	5	76	6	11
08t	14	722	13	91	16	42	720	6	103	13	33	88	6	80	10	23
08m	100	285	4	112	8	24	720	3	117	13	32	88	1	332	7	16
08b	190	285	2	340	2	7	720	1	322	2	10	82	1	176	2	6
09t	14	744	13	99	17	40	720	6	103	13	40	196	6	57	9	21
09m	100	744	1	1	9	26	720	4	101	10	33	744	4	56	8	24
09b	190	0	-99	-99	-99	-99	0	-99	-99	-99	-99	0	-99	-99	-99	-99
10t	14	744	10	46	16	44	720	7	94	10	28	744	6	86	8	27
10m	100	744	1	263	10	37	720	2	98	8	19	744	3	70	8	24
10b	190	744	1	197	2	12	720	1	273	2	13	744	0	216	2	9
11t	14	744	6	126	15	41	720	10	127	20	39	744	3	236	8	29
11m	100	744	3	260	9	30	720	4	94	10	27	744	3	99	8	19
11b	190	0	-99	-99	-99	-99	0	-99	-99	-99	-99	0	-99	-99	-99	-99
12t	14	720	19	249	24	61	720	15	254	18	37	744	6	340	10	29
12m	100	207	20	251	21	38	720	9	263	11	26	744	3	9	9	23
12b	490	723	1	242	2	5	720	1	236	2	6	63	1	61	2	5
13t	14	709	19	254	28	75	720	22	259	24	73	744	5	341	12	49
13m	100	709	20	253	23	80	720	13	261	19	54	744	4	54	14	43
13b	190	710	6	274	14	63	720	3	287	6	28	744	2	37	5	20
14t	10	705	17	257	25	101	720	6	253	15	60	721	2	334	8	36
14m	26	711	11	248	19	71	720	1	210	12	43	300	3	70	6	28
14b	40	0	-99	-99	-99	-99	0	-99	-99	-99	-99	0	-99	-99	-99	-99
15t	10	367	4	270	24	62	720	4	282	13	51	721	8	275	13	56
15b	17	491	5	257	12	62	0	-99	-99	-99	-99	430	2	248	8	21
16t	10	237	4	357	12	40	720	6	263	11	31	721	5	266	15	46
16b	14	242	2	160	8	29	720	6	242	10	29	294	4	187	9	34
17t	3	460	13	270	31	74	0	-99	-99	-99	-99	0	-99	-99	-99	-99
17b	6	727	5	336	12	44	720	4	322	15	79	277	6	323	12	34
18t	8	721	5	281	15	56	720	8	286	13	40	721	11	285	15	51
18b	19	727	2	354	10	34	720	3	319	10	27	728	2	272	9	31
19t	3	723	13	273	25	63	422	6	267	12	32	0	-99	-99	-99	-99
19m	20	255	3	195	13	27	720	2	289	7	27	270	2	303	8	23
19b	45	255	3	224	8	28	720	1	316	7	25	726	1	297	5	19
20t	3	0	-99	-99	-99	-99	568	13	250	18	43	698	18	274	21	44
20b	13	610	5	276	11	35	720	6	309	11	46	247	6	302	10	36
21t	14	724	7	261	11	36	720	6	257	11	32	726	9	257	12	36
21b	22	728	4	258	7	30	720	4	248	9	26	727	6	251	8	34
22t	3	0	-99	-99	-99	-99	0	-99	-99	-99	-99	0	-99	-99	-99	-99
22m	20	726	8	249	13	44	720	3	260	7	20	255	1	199	7	18
22b	48	726	8	234	11	31	720	3	242	7	28	725	4	243	7	20
23t	10	727	15	248	19	95	720	14	251	20	61	724	25	247	27	74
23b	13	410	9	279	16	78	720	10	273	15	57	727	11	263	15	54
24t	10	0	-99	-99	-99	-99	0	-99	-99	-99	-99	0	-99	-99	-99	-99
24b	25	0	-99	-99	-99	-99	0	-99	-99	-99	-99	0	-99	-99	-99	-99
25t	11	721	11	242	14	50	720	10	240	15	49	721	11	246	13	45
25m	20	728	11	243	14	43	720	8	251	14	49	375	9	254	13	45
25b	29	727	9	236	12	38	720	6	249	12	45	727	9	237	11	45
44t	13	722	9	221	12	52	720	9	225	14	56	190	1	211	14	33
44b	55	390	7	215	9	32	0	-99	-99	-99	-99	0	-99	-99	-99	-99
45t	12	0	-99	-99	-99	-99	0	-99	-99	-99	-99	0	-99	-99	-99	-99
45m	84	0	-99	-99	-99	-99	0	-99	-99	-99	-99	0	-99	-99	-99	-99
46t	14	721	7	251	10	45	720	3	65	12	36	744	6	239	13	36
46m	50	724	7	238	10	39	720	2	71	9	36	744	6	223	13	39
46b	84	327	3	225	8	25	720	2	199	7	26	136	1	290	4	14
47t	12	367	10	228	14	58	0	-99	-99	-99	-99	0	-99	-99	-99	-99
47m	100	0	-99	-99	-99	-99	0	-99	-99	-99	-99	0	-99	-99	-99	-99
47b	190	0	-99	-99	-99	-99	0	-99	-99	-99	-99	0	-99	-99	-99	-99
48t	14	744	10	287	20	60	720	15	256	19	46	744	8	254	11	33
48m	100	744	2	254	10	30	720	5	265	11	37	744	3	265	9	26
48b	190	744	1	79	5	17	712	1	4	5	18	0	-99	-99	-99	-99
49t	14	692	15	222	18	47	720	20	44	22	50	744	40	36	42	78
49m	100	321	10	220	12	30	720	17	43	19	45	744	30	36	33	74
49b	490	321	3	138	6	22	720	3	148	5	18	744	4	150	6	21

Table I-2. Current meter velocity statistics for 3-hr low-passed filtered data (continued).

		January 1993					February 1993					March 1993				
No.	h	N	$\lvert\bar{v}\rvert$	θ	$\overline{\lvert v\rvert}$	v_M	N	$\lvert\bar{v}\rvert$	θ	$\overline{\lvert v\rvert}$	v_M	N	$\lvert\bar{v}\rvert$	θ	$\overline{\lvert v\rvert}$	v_M
01t	10	724	30	197	31	82	672	15	191	24	71	727	10	192	22	77
01b	12	0	-99	-99	-99	-99	0	-99	-99	-99	-99	0	-99	-99	-99	-99
02t	10	722	18	202	21	68	672	9	201	16	57	727	10	192	22	91
02b	32	284	12	191	13	39	672	3	173	9	38	420	0	69	17	66
03t	10	278	5	225	12	28	672	8	358	16	47	744	4	35	16	102
03m	33	0	-99	-99	-99	-99	0	-99	-99	-99	-99	0	-99	-99	-99	-99
03b	58	0	-99	-99	-99	-99	0	-99	-99	-99	-99	0	-99	-99	-99	-99
04t	14	272	15	284	19	53	672	12	351	23	81	744	12	3	20	59
04m	100	272	12	253	16	29	672	2	297	13	42	744	13	1	16	55
04b	190	272	8	213	11	24	672	4	21	8	27	744	7	19	12	33
05t	14	229	16	48	19	42	672	10	39	23	72	744	13	47	19	65
05m	100	267	10	62	13	22	672	3	22	17	39	744	14	41	16	41
05b	190	274	1	69	3	6	672	1	45	4	9	744	1	67	3	7
06t	14	300	12	64	16	46	672	27	69	32	91	744	17	84	22	58
06m	100	300	1	4	10	22	672	4	71	16	41	744	12	60	20	56
06b	190	0	-99	-99	-99	-99	0	-99	-99	-99	-99	0	-99	-99	-99	-99
07t	14	318	37	84	40	78	672	24	86	30	74	744	21	72	29	63
07m	100	0	-99	-99	-99	-99	0	-99	-99	-99	-99	0	-99	-99	-99	-99
07b	190	318	1	271	10	24	672	1	262	8	24	744	1	25	9	22
08t	14	369	12	122	17	47	672	4	275	14	39	744	9	104	22	73
08m	100	369	5	100	22	51	672	6	246	20	52	744	3	221	21	68
08b	190	369	1	287	4	12	672	1	6	3	12	744	1	321	4	20
09t	14	0	-99	-99	-99	-99	0	-99	-99	-99	-99	0	-99	-99	-99	-99
09m	100	601	1	335	6	18	672	2	53	7	21	744	4	44	7	21
09b	190	376	2	55	6	15	672	3	278	5	17	744	3	294	6	23
10t	14	237	1	288	4	13	0	-99	-99	-99	-99	0	-99	-99	-99	-99
10m	100	236	2	112	6	16	639	0	123	3	14	744	3	70	6	23
10b	190	722	0	354	2	12	672	0	229	3	11	744	0	23	3	16
11t	14	724	4	234	6	29	672	2	111	8	26	744	5	273	11	46
11m	100	246	4	222	7	15	0	-99	-99	-99	-99	0	-99	-99	-99	-99
11b	190	0	-99	-99	-99	-99	0	-99	-99	-99	-99	0	-99	-99	-99	-99
12t	14	724	7	301	15	68	672	18	252	22	53	602	6	326	15	65
12m	100	723	2	342	10	36	672	18	251	22	58	744	4	291	10	30
12b	490	0	-99	-99	-99	-99	0	-99	-99	-99	-99	0	-99	-99	-99	-99
13t	14	724	9	275	15	56	672	18	250	21	52	744	3	11	15	67
13m	100	384	6	330	19	50	672	13	246	17	51	744	3	22	11	41
13b	190	724	2	261	10	31	672	11	239	13	37	736	3	232	8	35
14t	10	725	4	316	14	52	672	0	174	12	32	723	2	262	17	64
14m	26	447	2	89	6	35	672	1	56	6	28	725	5	92	13	45
14b	40	0	-99	-99	-99	-99	0	-99	-99	-99	-99	0	-99	-99	-99	-99
15t	10	722	13	289	19	62	672	3	238	14	46	726	3	42	16	99
15b	17	294	0	151	6	24	0	-99	-99	-99	-99	280	2	358	6	27
16t	10	722	1	139	15	55	672	5	234	13	41	726	7	254	14	68
16b	14	0	-99	-99	-99	-99	0	-99	-99	-99	-99	284	3	257	7	33
17t	3	0	-99	-99	-99	-99	0	-99	-99	-99	-99	308	7	296	20	49
17b	6	0	-99	-99	-99	-99	0	-99	-99	-99	-99	309	2	302	12	29
18t	8	722	11	291	19	69	672	5	282	21	51	726	1	34	17	64
18b	19	728	1	215	9	56	672	0	49	8	32	727	3	60	10	48
19t	3	0	-99	-99	-99	-99	0	-99	-99	-99	-99	0	-99	-99	-99	-99
19m	20	336	4	296	7	18	672	4	311	9	26	425	1	344	9	39
19b	45	725	2	304	5	16	672	1	290	7	19	730	3	95	6	21
20t	3	727	26	266	30	86	672	20	275	24	68	702	15	260	23	67
20b	13	0	-99	-99	-99	-99	0	-99	-99	-99	-99	335	2	193	10	29
21t	14	721	11	261	13	41	672	7	261	12	43	727	5	260	12	42
21b	22	371	6	256	8	38	0	-99	-99	-99	-99	327	5	253	11	33
22t	3	361	8	323	14	39	672	3	27	12	40	421	11	110	17	43
22m	20	360	5	307	10	26	672	2	60	10	31	725	4	84	11	33
22b	48	369	7	238	9	21	0	-99	-99	-99	-99	0	-99	-99	-99	-99
23t	10	727	26	249	28	67	672	19	248	26	74	726	10	247	20	84
23b	13	419	10	265	14	51	0	-99	-99	-99	-99	217	6	184	10	28
24t	10	309	23	242	25	96	672	19	242	24	71	726	10	234	22	122
24b	25	0	-99	-99	-99	-99	0	-99	-99	-99	-99	212	1	21	12	31
25t	11	722	13	248	14	50	672	7	250	14	51	725	5	250	15	97
25m	20	314	8	244	11	35	672	7	234	14	44	726	3	236	14	65
25b	29	728	11	236	13	34	672	7	227	13	35	519	1	243	15	47
44t	13	0	-99	-99	-99	-99	0	-99	-99	-99	-99	0	-99	-99	-99	-99
44b	55	0	-99	-99	-99	-99	0	-99	-99	-99	-99	0	-99	-99	-99	-99
45t	12	0	-99	-99	-99	-99	0	-99	-99	-99	-99	0	-99	-99	-99	-99
45m	84	0	-99	-99	-99	-99	0	-99	-99	-99	-99	0	-99	-99	-99	-99
46t	14	437	10	257	13	29	0	-99	-99	-99	-99	0	-99	-99	-99	-99
46m	50	439	10	233	12	30	0	-99	-99	-99	-99	0	-99	-99	-99	-99
46b	84	0	-99	-99	-99	-99	0	-99	-99	-99	-99	0	-99	-99	-99	-99
47t	12	0	-99	-99	-99	-99	0	-99	-99	-99	-99	0	-99	-99	-99	-99
47m	100	267	9	44	12	41	672	3	328	16	47	541	16	28	20	53
47b	190	267	6	37	8	23	672	4	33	10	25	542	4	27	9	26
48t	14	720	6	278	11	28	672	6	259	12	37	744	3	258	7	41
48m	100	720	3	268	10	33	672	2	251	8	28	744	3	251	10	30
48b	190	464	1	18	5	21	672	1	62	6	20	688	1	2	6	32
49t	14	429	52	33	53	84	0	-99	-99	-99	-99	0	-99	-99	-99	-99
49m	100	429	46	33	48	87	0	-99	-99	-99	-99	0	-99	-99	-99	-99
49b	490	723	3	158	5	18	672	7	185	9	27	744	3	173	6	21

Table I-2. Current meter velocity statistics for 3-hr low-passed filtered data (continued).

		April 1993					May 1993					June 1993				
No.	h	N	$\lvert\bar{\mathbf{v}}\rvert$	θ	$\overline{\lvert\mathbf{v}\rvert}$	v_M	N	$\lvert\bar{\mathbf{v}}\rvert$	θ	$\overline{\lvert\mathbf{v}\rvert}$	v_M	N	$\lvert\bar{\mathbf{v}}\rvert$	θ	$\overline{\lvert\mathbf{v}\rvert}$	v_M
01t	10	720	1	159	20	72	726	6	189	19	56	720	3	184	23	92
01b	12	0	-99	-99	-99	-99	0	-99	-99	-99	-99	0	-99	-99	-99	-99
02t	10	720	1	243	15	51	723	7	200	24	65	720	3	228	26	95
02b	32	0	-99	-99	-99	-99	241	6	169	12	38	720	2	85	19	82
03t	10	720	5	13	17	57	724	7	214	14	51	720	2	295	19	65
03m	33	0	-99	-99	-99	-99	237	3	212	11	30	720	6	40	13	44
03b	58	0	-99	-99	-99	-99	237	7	190	11	37	720	3	50	11	33
04t	14	720	13	227	20	71	725	9	227	21	44	720	27	13	32	68
04m	100	720	12	201	14	31	725	20	196	21	47	720	19	10	24	71
04b	190	720	7	193	10	22	726	12	201	13	30	720	2	29	10	24
05t	14	720	7	259	17	59	724	16	329	29	57	720	30	46	34	74
05m	100	720	7	224	12	27	724	8	276	22	39	720	27	40	30	91
05b	190	720	2	235	3	6	714	2	238	5	17	720	4	43	9	24
06t	14	720	4	31	14	36	725	19	60	27	72	720	26	85	31	72
06m	100	720	1	293	14	39	664	13	65	27	56	720	20	73	24	68
06b	190	0	-99	-99	-99	-99	0	-99	-99	-99	-99	0	-99	-99	-99	-99
07t	14	720	18	72	21	48	723	36	87	41	78	720	7	85	18	45
07m	100	0	-99	-99	-99	-99	215	15	224	18	39	720	6	268	11	31
07b	190	720	2	77	6	24	514	1	257	14	31	720	2	81	8	23
08t	14	720	13	113	20	52	724	4	109	13	44	720	4	181	13	58
08m	100	720	6	242	15	61	725	6	237	18	69	720	1	253	9	25
08b	190	720	1	303	3	12	699	2	279	3	17	720	1	316	4	11
09t	14	0	-99	-99	-99	-99	202	5	268	14	35	720	1	102	17	43
09m	100	720	4	44	7	29	725	7	268	8	24	720	4	307	7	19
09b	190	720	3	281	7	19	725	0	267	4	15	720	1	294	4	21
10t	14	0	-99	-99	-99	-99	0	-99	-99	-99	-99	0	-99	-99	-99	-99
10m	100	720	2	62	8	28	508	8	267	11	39	720	3	303	17	45
10b	190	720	0	38	2	11	690	1	122	2	15	591	2	103	4	15
11t	14	720	6	282	11	28	724	2	326	12	39	185	1	150	9	18
11m	100	0	-99	-99	-99	-99	0	-99	-99	-99	-99	0	-99	-99	-99	-99
11b	190	0	-99	-99	-99	-99	0	-99	-99	-99	-99	0	-99	-99	-99	-99
12t	14	720	6	41	15	46	744	9	255	12	30	720	5	53	9	27
12m	100	720	2	66	10	26	712	7	253	11	26	0	-99	-99	-99	-99
12b	490	0	-99	-99	-99	-99	0	-99	-99	-99	-99	0	-99	-99	-99	-99
13t	14	720	9	68	15	43	724	6	265	10	30	508	9	58	15	42
13m	100	720	3	67	8	30	603	12	254	13	32	720	4	69	8	22
13b	190	0	-99	-99	-99	-99	0	-99	-99	-99	-99	0	-99	-99	-99	-99
14t	10	720	4	146	17	53	719	6	86	14	54	720	10	65	17	68
14m	26	720	4	80	14	44	666	3	69	10	42	720	5	67	12	34
14b	40	0	-99	-99	-99	-99	116	3	114	9	20	720	2	102	9	22
15t	10	720	4	274	15	49	726	5	260	10	31	720	5	269	14	49
15b	17	720	2	257	8	38	726	2	251	6	22	720	2	242	6	26
16t	10	720	3	268	15	60	658	7	251	15	52	165	9	66	12	25
16b	14	720	1	47	9	37	615	1	292	6	18	0	-99	-99	-99	-99
17t	3	720	7	285	27	97	541	4	227	20	96	720	21	289	38	85
17b	6	720	2	283	18	73	629	3	247	13	56	0	-99	-99	-99	-99
18t	8	720	2	138	22	85	726	1	276	18	53	720	7	150	20	82
18b	19	592	1	57	10	51	171	1	251	5	15	720	1	242	9	61
19t	3	0	-99	-99	-99	-99	165	13	312	26	54	720	5	57	28	70
19m	20	0	-99	-99	-99	-99	164	4	86	9	19	496	3	73	7	20
19b	45	720	1	96	7	30	724	1	259	3	18	720	1	267	4	15
20t	3	720	17	257	24	70	439	18	250	27	83	709	6	290	29	83
20b	13	720	2	197	12	37	640	3	145	10	32	0	-99	-99	-99	-99
21t	14	720	2	239	13	47	727	2	231	11	34	720	4	162	16	67
21b	22	720	0	116	9	31	537	0	241	7	26	0	-99	-99	-99	-99
22t	3	720	12	47	21	46	521	7	345	18	46	369	13	43	35	77
22m	20	720	4	30	15	41	725	3	77	12	30	720	15	64	20	56
22b	48	0	-99	-99	-99	-99	193	1	143	6	17	720	4	86	11	39
23t	10	720	8	250	22	76	727	10	250	18	57	720	2	201	19	86
23b	13	720	6	156	15	84	317	3	138	12	32	0	-99	-99	-99	-99
24t	10	720	5	237	17	55	727	10	227	19	55	720	8	147	23	87
24b	25	720	2	220	13	51	444	2	9	12	40	0	-99	-99	-99	-99
25t	11	720	5	115	16	46	727	6	238	14	40	64	4	42	15	28
25m	20	720	3	98	18	48	446	3	264	16	56	0	-99	-99	-99	-99
25b	29	0	-99	-99	-99	-99	281	6	225	12	42	720	7	92	20	69
44t	13	0	-99	-99	-99	-99	0	-99	-99	-99	-99	0	-99	-99	-99	-99
44b	55	0	-99	-99	-99	-99	0	-99	-99	-99	-99	0	-99	-99	-99	-99
45t	12	0	-99	-99	-99	-99	0	-99	-99	-99	-99	0	-99	-99	-99	-99
45m	84	0	-99	-99	-99	-99	0	-99	-99	-99	-99	0	-99	-99	-99	-99
46t	14	0	-99	-99	-99	-99	0	-99	-99	-99	-99	0	-99	-99	-99	-99
46m	50	0	-99	-99	-99	-99	0	-99	-99	-99	-99	0	-99	-99	-99	-99
46b	84	0	-99	-99	-99	-99	0	-99	-99	-99	-99	0	-99	-99	-99	-99
47t	12	0	-99	-99	-99	-99	0	-99	-99	-99	-99	0	-99	-99	-99	-99
47m	100	0	-99	-99	-99	-99	0	-99	-99	-99	-99	0	-99	-99	-99	-99
47b	190	0	-99	-99	-99	-99	0	-99	-99	-99	-99	0	-99	-99	-99	-99
48t	14	720	1	310	4	22	587	3	157	9	22	0	-99	-99	-99	-99
48m	100	720	3	274	9	25	586	4	283	7	22	0	-99	-99	-99	-99
48b	190	0	-99	-99	-99	-99	0	-99	-99	-99	-99	0	-99	-99	-99	-99
49t	14	0	-99	-99	-99	-99	0	-99	-99	-99	-99	0	-99	-99	-99	-99
49m	100	0	-99	-99	-99	-99	258	46	32	47	61	720	38	51	40	64
49b	490	720	3	181	5	15	724	4	193	5	14	720	5	233	5	15

Table I-2. Current meter velocity statistics for 3-hr low-passed filtered data (continued).

		July 1993					August 1993					September 1993				
No.	h	N	$\lvert\bar{v}\rvert$	θ	$\overline{\lvert v\rvert}$	v_M	N	$\lvert\bar{v}\rvert$	θ	$\overline{\lvert v\rvert}$	v_M	N	$\lvert\bar{v}\rvert$	θ	$\overline{\lvert v\rvert}$	v_M
01t	10	744	3	319	8	35	744	2	266	6	18	696	6	182	10	40
01b	12	0	-99	-99	-99	-99	0	-99	-99	-99	-99	26	11	185	11	15
02t	10	616	20	6	23	68	0	-99	-99	-99	-99	20	10	214	10	13
02b	32	744	6	360	10	38	744	0	61	8	27	441	5	178	9	27
03t	10	744	8	48	19	54	744	20	34	25	63	684	4	12	16	44
03m	33	744	3	332	11	33	744	9	26	13	32	419	4	24	11	32
03b	58	721	1	192	10	26	744	3	60	9	22	325	4	198	6	19
04t	14	744	10	20	21	64	744	14	31	24	79	701	1	305	8	21
04m	100	744	15	203	18	37	744	5	34	10	48	701	1	255	4	14
04b	190	744	7	208	10	24	744	1	17	4	12	700	2	209	5	21
05t	14	744	26	28	31	75	744	22	57	27	70	664	6	351	11	27
05m	100	744	6	308	18	41	744	2	41	12	41	701	1	6	4	12
05b	190	744	7	237	11	25	744	3	54	9	20	667	2	230	5	17
06t	14	744	30	67	33	74	744	31	64	36	87	701	9	63	12	30
06m	100	744	4	55	9	44	744	15	61	25	55	701	5	63	7	29
06b	190	0	-99	-99	-99	-99	0	-99	-99	-99	-99	0	-99	-99	-99	-99
07t	14	744	2	145	19	70	744	45	88	49	92	654	22	72	24	61
07m	100	744	4	268	10	30	744	10	83	20	57	630	6	80	9	35
07b	190	744	1	257	8	18	744	3	270	10	27	545	1	269	7	25
08t	14	744	13	42	20	54	744	7	83	22	65	700	17	105	19	59
08m	100	744	5	83	10	26	690	1	132	16	47	701	5	295	8	21
08b	190	744	2	326	4	14	744	2	300	5	20	512	3	274	4	12
09t	14	744	10	134	18	62	744	10	14	19	53	700	4	176	16	45
09m	100	744	7	60	9	23	650	5	51	7	21	638	5	276	7	20
09b	190	744	3	275	5	16	744	1	333	2	11	700	1	239	3	12
10t	14	0	-99	-99	-99	-99	0	-99	-99	-99	-99	0	-99	-99	-99	-99
10m	100	744	16	67	19	54	693	13	82	18	61	654	4	273	11	37
10b	190	322	2	291	6	15	0	-99	-99	-99	-99	137	1	108	4	14
11t	14	0	-99	-99	-99	-99	0	-99	-99	-99	-99	0	-99	-99	-99	-99
11m	100	305	41	78	42	99	744	4	55	6	22	720	5	266	7	21
11b	190	0	-99	-99	-99	-99	0	-99	-99	-99	-99	0	-99	-99	-99	-99
12t	14	721	14	111	21	73	744	24	84	27	71	720	18	256	22	50
12m	100	0	-99	-99	-99	-99	0	-99	-99	-99	-99	0	-99	-99	-99	-99
12b	490	319	1	209	2	6	744	1	233	3	6	720	5	237	5	10
13t	14	744	14	89	22	60	744	25	88	28	70	584	14	248	17	44
13m	100	744	9	73	11	35	744	6	80	9	30	701	13	259	14	36
13b	190	0	-99	-99	-99	-99	0	-99	-99	-99	-99	101	18	237	18	25
14t	10	393	14	93	19	43	0	-99	-99	-99	-99	0	-99	-99	-99	-99
14m	26	725	15	80	19	51	744	18	82	22	53	316	19	75	22	46
14b	40	725	5	76	11	47	744	3	84	9	36	702	3	101	12	37
15t	10	725	18	77	24	69	744	16	79	21	77	703	4	249	12	31
15b	17	392	1	106	5	15	0	-99	-99	-99	-99	111	4	61	7	29
16t	10	726	2	48	8	24	744	1	13	10	36	701	1	276	15	51
16b	14	0	-99	-99	-99	-99	0	-99	-99	-99	-99	0	-99	-99	-99	-99
17t	3	373	9	138	31	62	0	-99	-99	-99	-99	74	36	286	40	65
17b	6	0	-99	-99	-99	-99	0	-99	-99	-99	-99	75	11	324	16	44
18t	8	370	25	103	28	57	0	-99	-99	-99	-99	89	3	267	15	34
18b	19	370	3	74	5	15	0	-99	-99	-99	-99	87	2	136	6	24
19t	3	724	3	73	34	76	654	9	320	21	61	66	7	83	15	24
19m	20	500	9	93	17	45	375	5	66	11	24	0	-99	-99	-99	-99
19b	45	724	2	93	7	21	744	2	107	8	26	720	3	254	7	23
20t	3	387	16	48	26	63	744	9	20	28	83	700	13	299	42	85
20b	13	0	-99	-99	-99	-99	0	-99	-99	-99	-99	189	5	123	13	35
21t	14	725	11	92	18	44	744	3	97	14	40	702	8	264	13	40
21b	22	381	13	80	15	37	744	4	91	11	34	520	1	220	9	30
22t	3	376	18	45	38	86	744	16	54	21	53	701	4	27	14	41
22m	20	725	11	63	19	45	744	7	51	11	27	512	6	47	9	29
22b	48	351	4	71	7	17	0	-99	-99	-99	-99	168	1	99	7	17
23t	10	461	13	68	15	47	744	7	69	13	42	709	11	246	18	63
23b	13	0	-99	-99	-99	-99	0	-99	-99	-99	-99	0	-99	-99	-99	-99
24t	10	726	14	59	20	62	744	2	59	13	45	707	7	239	13	51
24b	25	407	6	55	12	28	744	2	70	10	39	701	7	213	14	34
25t	11	0	-99	-99	-99	-99	0	-99	-99	-99	-99	0	-99	-99	-99	-99
25m	20	0	-99	-99	-99	-99	0	-99	-99	-99	-99	0	-99	-99	-99	-99
25b	29	691	13	77	18	53	0	-99	-99	-99	-99	0	-99	-99	-99	-99
44t	13	0	-99	-99	-99	-99	0	-99	-99	-99	-99	0	-99	-99	-99	-99
44b	55	0	-99	-99	-99	-99	0	-99	-99	-99	-99	0	-99	-99	-99	-99
45t	12	0	-99	-99	-99	-99	0	-99	-99	-99	-99	0	-99	-99	-99	-99
45m	84	0	-99	-99	-99	-99	0	-99	-99	-99	-99	0	-99	-99	-99	-99
46t	14	0	-99	-99	-99	-99	0	-99	-99	-99	-99	0	-99	-99	-99	-99
46m	50	0	-99	-99	-99	-99	0	-99	-99	-99	-99	0	-99	-99	-99	-99
46b	84	0	-99	-99	-99	-99	0	-99	-99	-99	-99	0	-99	-99	-99	-99
47t	12	0	-99	-99	-99	-99	0	-99	-99	-99	-99	0	-99	-99	-99	-99
47m	100	0	-99	-99	-99	-99	0	-99	-99	-99	-99	0	-99	-99	-99	-99
47b	190	0	-99	-99	-99	-99	0	-99	-99	-99	-99	0	-99	-99	-99	-99
48t	14	0	-99	-99	-99	-99	0	-99	-99	-99	-99	0	-99	-99	-99	-99
48m	100	0	-99	-99	-99	-99	0	-99	-99	-99	-99	0	-99	-99	-99	-99
48b	190	0	-99	-99	-99	-99	0	-99	-99	-99	-99	0	-99	-99	-99	-99
49t	14	0	-99	-99	-99	-99	0	-99	-99	-99	-99	0	-99	-99	-99	-99
49m	100	744	25	30	30	53	744	14	50	16	44	720	2	29	3	15
49b	490	744	5	212	5	18	744	4	217	4	12	720	3	165	5	16

Table I-2. Current meter velocity statistics for 3-hr low-passed filtered data (continued).

		October 1993					November 1993					December 1993				
No.	h	N	$\lvert\bar{\mathbf{v}}\rvert$	θ	$\overline{\lvert\mathbf{v}\rvert}$	v_M	N	$\lvert\bar{\mathbf{v}}\rvert$	θ	$\overline{\lvert\mathbf{v}\rvert}$	v_M	N	$\lvert\bar{\mathbf{v}}\rvert$	θ	$\overline{\lvert\mathbf{v}\rvert}$	v_M
01t	10	744	5	195	10	36	316	10	201	13	32	481	7	203	12	38
01b	12	744	3	203	11	35	720	7	208	11	38	528	6	191	10	41
02t	10	744	14	205	18	82	720	16	200	20	93	727	11	191	17	54
02b	32	744	4	151	12	58	720	4	180	13	68	249	4	179	7	23
03t	10	0	-99	-99	-99	-99	0	-99	-99	-99	-99	473	3	197	14	37
03m	33	744	6	232	14	46	720	6	197	16	45	725	3	206	11	38
03b	58	0	-99	-99	-99	-99	0	-99	-99	-99	-99	474	3	197	11	32
04t	14	744	2	18	12	46	720	12	215	18	49	724	13	198	16	43
04m	100	744	3	9	8	21	720	11	206	16	39	724	9	213	11	28
04b	190	744	2	194	5	16	720	4	205	7	22	726	7	208	10	25
05t	14	0	-99	-99	-99	-99	0	-99	-99	-99	-99	452	7	269	15	33
05m	100	744	1	120	9	28	720	11	238	15	41	725	9	235	11	30
05b	190	0	-99	-99	-99	-99	0	-99	-99	-99	-99	451	5	231	8	19
06t	14	744	7	222	15	39	720	7	249	13	39	695	3	19	15	49
06m	100	744	5	259	8	25	720	8	260	11	36	676	3	247	8	28
06b	190	0	-99	-99	-99	-99	0	-99	-99	-99	-99	445	0	101	4	16
07t	14	0	-99	-99	-99	-99	0	-99	-99	-99	-99	493	10	72	18	40
07m	100	744	9	269	10	30	720	3	294	11	45	231	14	264	16	32
07b	190	744	10	260	12	28	566	6	264	12	46	679	8	260	12	47
08t	14	744	6	95	11	34	720	30	95	32	65	715	16	94	20	61
08m	100	744	6	263	11	38	720	14	95	18	45	715	1	221	7	32
08b	190	0	-99	-99	-99	-99	0	-99	-99	-99	-99	512	1	305	3	16
09t	14	744	5	233	12	30	720	9	113	17	58	724	3	108	15	41
09m	100	142	3	216	4	12	0	-99	-99	-99	-99	527	1	338	7	18
09b	190	744	0	74	5	15	720	1	298	5	16	725	3	277	6	15
10t	14	0	-99	-99	-99	-99	0	-99	-99	-99	-99	545	2	358	12	41
10m	100	744	7	285	11	34	720	6	66	11	30	725	2	315	9	25
10b	190	744	1	103	4	14	720	0	57	4	14	725	1	119	4	12
11t	14	0	-99	-99	-99	-99	0	-99	-99	-99	-99	557	10	261	14	35
11m	100	744	9	319	11	28	618	3	344	8	19	558	6	263	8	22
11b	190	0	-99	-99	-99	-99	0	-99	-99	-99	-99	558	4	246	9	24
12t	14	744	22	106	35	79	720	35	101	38	71	141	25	105	28	59
12m	100	0	-99	-99	-99	-99	0	-99	-99	-99	-99	0	-99	-99	-99	-99
12b	490	744	3	233	4	10	720	1	221	3	7	142	5	232	5	9
13t	14	0	-99	-99	-99	-99	0	-99	-99	-99	-99	587	8	97	14	40
13m	100	744	2	92	12	28	720	4	134	14	31	724	1	34	8	23
13b	190	714	8	230	12	25	674	4	219	9	21	698	4	235	8	25
14t	10	0	-99	-99	-99	-99	0	-99	-99	-99	-99	592	5	273	16	52
14m	26	744	2	257	13	39	720	4	237	10	43	723	2	87	11	38
14b	40	658	2	221	12	42	0	-99	-99	-99	-99	589	4	61	8	25
15t	10	744	9	265	13	53	720	9	267	15	53	727	11	277	21	63
15b	17	744	3	273	7	27	720	2	238	9	31	727	1	34	8	26
16t	10	448	18	256	20	61	0	-99	-99	-99	-99	601	1	28	12	51
16b	14	0	-99	-99	-99	-99	0	-99	-99	-99	-99	602	2	335	9	39
17t	3	744	10	294	22	61	720	7	277	18	51	724	9	279	30	89
17b	6	744	4	352	12	52	720	6	342	12	48	726	3	353	14	57
18t	8	448	13	284	17	51	0	-99	-99	-99	-99	621	4	288	17	61
18b	19	744	1	292	9	42	568	3	261	8	37	278	1	238	9	25
19t	3	744	9	307	19	60	720	2	273	13	63	722	6	269	14	68
19m	20	0	-99	-99	-99	-99	0	-99	-99	-99	-99	612	2	284	8	29
19b	45	744	2	242	11	33	303	3	50	9	23	169	2	56	7	15
20t	3	744	12	255	26	84	720	9	343	20	50	509	16	245	34	77
20b	13	744	4	240	11	41	720	4	235	12	37	510	3	278	14	45
21t	14	744	10	259	17	55	720	12	266	14	42	724	5	263	12	39
21b	22	0	-99	-99	-99	-99	0	-99	-99	-99	-99	0	-99	-99	-99	-99
22t	3	449	6	16	18	45	0	-99	-99	-99	-99	517	5	351	14	37
22m	20	744	3	323	8	23	720	2	326	7	25	725	2	341	7	31
22b	48	744	1	295	9	24	720	2	264	7	31	725	2	269	6	27
23t	10	0	-99	-99	-99	-99	0	-99	-99	-99	-99	502	13	249	23	60
23b	13	597	11	218	15	59	0	-99	-99	-99	-99	503	11	226	20	53
24t	10	734	22	245	25	81	720	21	242	22	91	726	21	240	25	70
24b	25	735	3	247	16	52	720	7	242	13	63	724	5	239	17	49
25t	11	0	-99	-99	-99	-99	0	-99	-99	-99	-99	0	-99	-99	-99	-99
25m	20	742	2	213	17	56	720	7	237	12	53	228	5	233	9	34
25b	29	0	-99	-99	-99	-99	0	-99	-99	-99	-99	0	-99	-99	-99	-99
44t	13	0	-99	-99	-99	-99	0	-99	-99	-99	-99	0	-99	-99	-99	-99
44b	55	0	-99	-99	-99	-99	0	-99	-99	-99	-99	0	-99	-99	-99	-99
45t	12	0	-99	-99	-99	-99	0	-99	-99	-99	-99	0	-99	-99	-99	-99
45m	84	0	-99	-99	-99	-99	0	-99	-99	-99	-99	0	-99	-99	-99	-99
46t	14	0	-99	-99	-99	-99	0	-99	-99	-99	-99	0	-99	-99	-99	-99
46m	50	0	-99	-99	-99	-99	0	-99	-99	-99	-99	0	-99	-99	-99	-99
46b	84	0	-99	-99	-99	-99	0	-99	-99	-99	-99	0	-99	-99	-99	-99
47t	12	0	-99	-99	-99	-99	0	-99	-99	-99	-99	0	-99	-99	-99	-99
47m	100	0	-99	-99	-99	-99	0	-99	-99	-99	-99	0	-99	-99	-99	-99
47b	190	0	-99	-99	-99	-99	0	-99	-99	-99	-99	0	-99	-99	-99	-99
48t	14	0	-99	-99	-99	-99	0	-99	-99	-99	-99	562	9	57	14	42
48m	100	0	-99	-99	-99	-99	0	-99	-99	-99	-99	562	5	254	9	33
48b	190	0	-99	-99	-99	-99	0	-99	-99	-99	-99	573	1	336	4	14
49t	14	0	-99	-99	-99	-99	0	-99	-99	-99	-99	461	11	281	16	48
49m	100	744	2	194	6	19	720	12	236	13	37	722	14	241	15	33
49b	490	744	2	265	4	17	720	4	98	5	18	722	2	130	5	13

Table I-2. Current meter velocity statistics for 3-hr low-passed filtered data (continued).

		January 1994					February 1994					March 1994				
No.	h	N	$\lvert\bar{v}\rvert$	θ	$\overline{\lvert v\rvert}$	v_M	N	$\lvert\bar{v}\rvert$	θ	$\overline{\lvert v\rvert}$	v_M	N	$\lvert\bar{v}\rvert$	θ	$\overline{\lvert v\rvert}$	v_M
01t	10	247	3	210	8	26	0	-99	-99	-99	-99	72	2	137	6	20
01b	12	0	-99	-99	-99	-99	0	-99	-99	-99	-99	73	4	85	8	22
02t	10	744	18	195	24	75	672	14	195	15	54	727	10	193	15	66
02b	32	0	-99	-99	-99	-99	0	-99	-99	-99	-99	0	-99	-99	-99	-99
03t	10	744	3	218	15	53	672	5	215	12	45	724	0	51	12	53
03m	33	744	2	185	14	45	672	8	204	11	41	679	1	161	10	31
03b	58	744	3	176	11	35	672	10	179	11	34	725	2	187	6	19
04t	14	744	2	360	12	41	672	3	327	16	50	683	4	318	13	40
04m	100	744	5	228	10	38	672	6	244	11	31	604	3	315	8	29
04b	190	744	1	219	7	19	672	5	207	9	20	683	2	42	7	18
05t	14	744	4	31	15	56	672	3	213	8	33	634	6	75	12	28
05m	100	744	2	21	9	25	383	4	267	6	19	546	6	88	7	25
05b	190	744	0	303	6	17	672	2	229	8	16	635	2	250	7	19
06t	14	744	6	13	19	49	672	3	273	10	30	724	5	280	10	40
06m	100	744	6	261	15	43	672	7	251	9	23	629	5	256	7	29
06b	190	744	1	275	4	22	672	4	262	6	25	629	0	357	5	25
07t	14	744	10	62	21	70	672	12	275	15	38	724	8	65	13	26
07m	100	0	-99	-99	-99	-99	0	-99	-99	-99	-99	104	7	132	10	27
07b	190	744	1	82	6	18	672	2	274	8	20	725	1	279	9	21
08t	14	744	27	90	30	79	672	10	282	14	35	724	2	61	8	27
08m	100	744	6	92	9	35	375	22	273	23	46	443	2	26	6	18
08b	190	744	0	40	4	13	672	2	291	4	19	724	2	294	3	15
09t	14	744	23	98	31	59	672	6	100	18	45	723	6	50	10	24
09m	100	744	6	83	10	37	672	4	266	8	29	724	1	1	4	28
09b	190	744	1	302	6	20	672	1	277	5	17	666	1	60	3	20
10t	14	744	10	90	18	47	672	2	350	10	32	724	14	117	18	45
10m	100	744	4	73	9	29	672	3	260	7	25	724	6	112	9	25
10b	190	744	1	309	5	15	672	1	71	5	11	722	0	87	4	16
11t	14	744	3	6	14	39	672	4	284	12	42	724	6	174	13	33
11m	100	744	4	310	10	32	615	10	272	13	31	724	4	182	10	35
11b	190	744	2	209	9	24	672	5	245	10	25	724	3	239	8	24
12t	14	0	-99	-99	-99	-99	0	-99	-99	-99	-99	0	-99	-99	-99	-99
12m	100	0	-99	-99	-99	-99	0	-99	-99	-99	-99	0	-99	-99	-99	-99
12b	490	0	-99	-99	-99	-99	0	-99	-99	-99	-99	0	-99	-99	-99	-99
13t	14	744	5	43	16	50	672	5	2	12	28	412	11	48	20	41
13m	100	744	2	55	10	39	672	5	270	11	37	723	2	30	8	26
13b	190	744	2	243	8	25	672	4	248	8	22	724	1	53	7	20
14t	10	744	4	251	15	64	649	0	46	9	33	717	1	34	13	45
14m	26	744	0	352	12	42	650	0	297	8	27	539	1	345	9	28
14b	40	744	0	29	10	35	651	0	265	6	20	718	2	96	9	26
15t	10	744	13	251	20	69	654	10	264	14	56	726	5	282	15	51
15b	17	744	4	268	10	40	655	1	266	7	23	674	1	98	8	25
16t	10	744	10	265	15	43	654	6	250	15	46	727	1	359	13	57
16b	14	744	2	266	7	33	651	1	248	8	37	727	3	280	8	40
17t	3	744	7	281	23	91	295	6	277	19	50	129	30	285	36	75
17b	6	744	3	315	15	60	655	1	300	10	33	536	2	330	12	44
18t	8	744	8	280	18	43	296	5	270	11	27	187	1	226	16	46
18b	19	0	-99	-99	-99	-99	314	5	255	11	30	539	0	31	9	38
19t	3	744	14	285	24	62	344	6	40	13	30	0	-99	-99	-99	-99
19m	20	471	7	291	13	44	0	-99	-99	-99	-99	181	1	231	9	22
19b	45	0	-99	-99	-99	-99	282	2	271	6	16	726	3	95	8	28
20t	3	744	38	253	46	82	269	43	258	48	92	0	-99	-99	-99	-99
20b	13	744	6	271	14	45	554	1	183	10	41	725	2	151	13	33
21t	14	744	11	263	17	47	654	9	269	12	38	732	5	265	12	38
21b	22	0	-99	-99	-99	-99	380	7	248	10	25	721	2	215	10	29
22t	3	744	6	339	16	46	649	17	282	23	50	735	19	283	22	54
22m	20	744	2	292	11	31	650	6	270	9	25	736	2	225	7	26
22b	48	744	4	254	9	24	256	2	234	4	15	0	-99	-99	-99	-99
23t	10	744	25	247	30	70	217	15	241	17	40	19	9	202	21	39
23b	13	744	18	226	22	54	222	6	223	10	30	0	-99	-99	-99	-99
24t	10	744	24	239	29	80	655	22	247	23	65	727	18	240	19	70
24b	25	744	10	241	17	45	655	8	230	11	34	727	3	210	12	45
25t	11	0	-99	-99	-99	-99	0	-99	-99	-99	-99	0	-99	-99	-99	-99
25m	20	0	-99	-99	-99	-99	0	-99	-99	-99	-99	0	-99	-99	-99	-99
25b	29	0	-99	-99	-99	-99	0	-99	-99	-99	-99	0	-99	-99	-99	-99
44t	13	0	-99	-99	-99	-99	0	-99	-99	-99	-99	0	-99	-99	-99	-99
44b	55	0	-99	-99	-99	-99	0	-99	-99	-99	-99	0	-99	-99	-99	-99
45t	12	0	-99	-99	-99	-99	0	-99	-99	-99	-99	0	-99	-99	-99	-99
45m	84	0	-99	-99	-99	-99	0	-99	-99	-99	-99	0	-99	-99	-99	-99
46t	14	0	-99	-99	-99	-99	0	-99	-99	-99	-99	0	-99	-99	-99	-99
46m	50	0	-99	-99	-99	-99	0	-99	-99	-99	-99	0	-99	-99	-99	-99
46b	84	0	-99	-99	-99	-99	0	-99	-99	-99	-99	0	-99	-99	-99	-99
47t	12	0	-99	-99	-99	-99	0	-99	-99	-99	-99	0	-99	-99	-99	-99
47m	100	0	-99	-99	-99	-99	0	-99	-99	-99	-99	0	-99	-99	-99	-99
47b	190	0	-99	-99	-99	-99	0	-99	-99	-99	-99	0	-99	-99	-99	-99
48t	14	744	9	28	17	50	672	7	38	16	48	723	3	133	11	34
48m	100	744	3	201	9	32	672	6	147	11	25	724	3	250	9	22
48b	190	744	1	89	6	18	672	1	341	5	17	724	1	101	6	19
49t	14	744	3	239	13	41	672	5	231	11	38	723	9	185	13	45
49m	100	744	3	251	11	30	672	6	245	12	39	723	10	164	13	28
49b	490	744	3	217	5	18	672	4	187	5	18	688	3	239	4	19

Table I-2. Current meter velocity statistics for 3-hr low-passed filtered data (continued).

		April 1994					May 1994					June 1994				
No.	h	N	$\lvert\bar{v}\rvert$	θ	$\overline{\lvert v\rvert}$	v_M	N	$\lvert\bar{v}\rvert$	θ	$\overline{\lvert v\rvert}$	v_M	N	$\lvert\bar{v}\rvert$	θ	$\overline{\lvert v\rvert}$	v_M
01t	10	711	6	187	10	44	0	-99	-99	-99	-99	0	-99	-99	-99	-99
01b	12	720	5	138	10	50	744	1	135	8	29	720	6	360	8	22
02t	10	720	17	190	20	58	744	11	197	18	65	720	8	23	23	60
02b	32	0	-99	-99	-99	-99	0	-99	-99	-99	-99	0	-99	-99	-99	-99
03t	10	720	10	209	20	60	744	6	332	17	57	720	6	35	22	53
03m	33	0	-99	-99	-99	-99	0	-99	-99	-99	-99	0	-99	-99	-99	-99
03b	58	694	4	205	11	25	17	2	189	5	6	0	-99	-99	-99	-99
04t	14	0	-99	-99	-99	-99	0	-99	-99	-99	-99	0	-99	-99	-99	-99
04m	100	665	4	186	10	36	77	25	208	28	46	0	-99	-99	-99	-99
04b	190	0	-99	-99	-99	-99	0	-99	-99	-99	-99	0	-99	-99	-99	-99
05t	14	0	-99	-99	-99	-99	0	-99	-99	-99	-99	0	-99	-99	-99	-99
05m	100	0	-99	-99	-99	-99	0	-99	-99	-99	-99	0	-99	-99	-99	-99
05b	190	0	-99	-99	-99	-99	0	-99	-99	-99	-99	0	-99	-99	-99	-99
06t	14	720	8	261	15	51	744	5	45	13	45	720	1	30	15	64
06m	100	0	-99	-99	-99	-99	0	-99	-99	-99	-99	0	-99	-99	-99	-99
06b	190	0	-99	-99	-99	-99	0	-99	-99	-99	-99	0	-99	-99	-99	-99
07t	14	720	2	160	14	44	744	12	86	17	42	720	12	73	18	72
07m	100	720	4	263	12	32	744	15	79	17	38	614	8	74	9	30
07b	190	720	1	258	9	21	744	5	78	8	18	720	3	83	5	17
08t	14	720	6	116	14	43	744	8	88	20	59	720	4	132	15	49
08m	100	607	5	245	12	30	744	4	110	13	36	720	0	26	5	22
08b	190	720	2	301	4	21	744	1	328	3	14	112	5	292	6	18
09t	14	720	2	355	13	43	744	7	70	20	57	720	5	46	14	46
09m	100	720	5	264	9	32	744	2	30	10	30	720	3	45	5	15
09b	190	720	2	79	7	20	744	1	121	6	16	720	2	97	3	12
10t	14	720	6	66	16	42	744	3	57	15	42	720	10	78	18	49
10m	100	720	4	271	11	30	744	6	65	10	23	720	5	85	6	27
10b	190	720	0	74	4	15	744	1	64	3	14	720	1	125	2	12
11t	14	720	7	36	17	41	744	13	89	17	41	720	2	127	16	47
11m	100	720	5	285	21	56	744	21	75	23	54	720	5	100	11	40
11b	190	720	6	255	10	31	744	1	107	10	27	720	4	247	7	20
12t	14	0	-99	-99	-99	-99	0	-99	-99	-99	-99	0	-99	-99	-99	-99
12m	100	0	-99	-99	-99	-99	0	-99	-99	-99	-99	0	-99	-99	-99	-99
12b	490	0	-99	-99	-99	-99	0	-99	-99	-99	-99	0	-99	-99	-99	-99
13t	14	720	9	64	17	44	744	16	77	20	41	720	6	84	16	42
13m	100	720	2	274	10	25	744	12	70	14	32	720	1	66	6	18
13b	190	720	5	248	10	27	744	3	258	10	29	720	4	252	10	22
14t	10	720	3	1	13	47	723	5	59	12	38	720	9	78	18	51
14m	26	0	-99	-99	-99	-99	25	9	40	12	25	720	7	64	12	37
14b	40	720	1	246	9	27	701	2	67	8	25	0	-99	-99	-99	-99
15t	10	720	4	283	11	42	726	4	74	11	34	720	16	72	19	56
15b	17	720	1	213	5	18	726	1	84	5	19	720	1	107	5	22
16t	10	720	5	244	13	66	724	1	176	8	31	720	1	281	6	34
16b	14	720	2	229	7	35	727	1	236	5	25	720	1	3	4	28
17t	3	0	-99	-99	-99	-99	44	9	30	19	35	120	19	297	25	55
17b	6	698	6	311	14	48	682	2	340	10	29	0	-99	-99	-99	-99
18t	8	720	11	286	19	59	722	2	314	10	39	720	9	96	14	36
18b	19	0	-99	-99	-99	-99	0	-99	-99	-99	-99	0	-99	-99	-99	-99
19t	3	0	-99	-99	-99	-99	37	8	40	16	32	685	11	78	32	66
19m	20	720	1	46	8	27	720	3	65	7	19	720	4	85	15	37
19b	45	720	1	229	6	22	497	2	104	3	11	0	-99	-99	-99	-99
20t	3	0	-99	-99	-99	-99	0	-99	-99	-99	-99	689	14	49	29	77
20b	13	375	8	257	12	32	727	1	171	10	46	720	7	83	14	37
21t	14	613	11	260	18	51	726	7	247	12	30	720	5	83	18	41
21b	22	715	4	200	13	38	657	3	197	8	29	548	5	65	9	26
22t	3	710	23	285	26	67	724	12	312	23	66	688	10	88	40	78
22m	20	0	-99	-99	-99	-99	60	1	212	6	13	720	4	137	12	46
22b	48	709	3	243	7	24	666	2	69	7	23	0	-99	-99	-99	-99
23t	10	720	27	246	29	77	744	3	242	12	59	701	11	73	19	63
23b	13	0	-99	-99	-99	-99	0	-99	-99	-99	-99	695	4	57	12	40
24t	10	720	16	244	20	71	744	16	232	27	72	701	16	74	23	77
24b	25	720	8	220	13	40	744	2	156	10	36	4	2	131	2	4
25t	11	0	-99	-99	-99	-99	0	-99	-99	-99	-99	0	-99	-99	-99	-99
25m	20	0	-99	-99	-99	-99	0	-99	-99	-99	-99	0	-99	-99	-99	-99
25b	29	0	-99	-99	-99	-99	0	-99	-99	-99	-99	0	-99	-99	-99	-99
44t	13	0	-99	-99	-99	-99	0	-99	-99	-99	-99	0	-99	-99	-99	-99
44b	55	0	-99	-99	-99	-99	0	-99	-99	-99	-99	0	-99	-99	-99	-99
45t	12	0	-99	-99	-99	-99	0	-99	-99	-99	-99	0	-99	-99	-99	-99
45m	84	0	-99	-99	-99	-99	0	-99	-99	-99	-99	0	-99	-99	-99	-99
46t	14	0	-99	-99	-99	-99	0	-99	-99	-99	-99	0	-99	-99	-99	-99
46m	50	0	-99	-99	-99	-99	0	-99	-99	-99	-99	0	-99	-99	-99	-99
46b	84	0	-99	-99	-99	-99	0	-99	-99	-99	-99	0	-99	-99	-99	-99
47t	12	0	-99	-99	-99	-99	0	-99	-99	-99	-99	0	-99	-99	-99	-99
47m	100	0	-99	-99	-99	-99	0	-99	-99	-99	-99	0	-99	-99	-99	-99
47b	190	0	-99	-99	-99	-99	0	-99	-99	-99	-99	0	-99	-99	-99	-99
48t	14	720	5	72	13	49	744	11	79	16	39	720	2	100	11	34
48m	100	720	5	268	11	32	744	6	75	10	27	720	2	73	8	25
48b	190	720	0	77	5	20	744	1	346	5	17	720	0	25	3	14
49t	14	720	13	245	20	50	744	11	280	18	50	720	7	3	20	49
49m	100	720	13	238	15	53	744	7	295	9	26	720	4	269	8	24
49b	490	0	-99	-99	-99	-99	0	-99	-99	-99	-99	0	-99	-99	-99	-99

Table I-2. Current meter velocity statistics for 3-hr low-passed filtered data (continued).

		July 1994					August 1994					September 1994				
No.	h	N	$\lvert\bar{v}\rvert$	θ	$\overline{\lvert v\rvert}$	v_M	N	$\lvert\bar{v}\rvert$	θ	$\overline{\lvert v\rvert}$	v_M	N	$\lvert\bar{v}\rvert$	θ	$\overline{\lvert v\rvert}$	v_M
01t	10	51	11	190	11	18	744	1	123	8	22	569	5	170	9	23
01b	12	676	4	5	7	21	0	-99	-99	-99	-99	0	-99	-99	-99	-99
02t	10	727	5	10	11	34	744	4	208	12	39	720	18	194	22	57
02b	32	48	10	170	11	19	744	5	175	11	33	720	5	161	15	60
03t	10	724	16	20	22	53	744	2	60	13	33	720	3	323	13	39
03m	33	0	-99	-99	-99	-99	0	-99	-99	-99	-99	0	-99	-99	-99	-99
03b	58	41	10	191	13	20	744	3	197	14	25	720	1	354	11	26
04t	14	29	3	150	14	19	744	4	84	22	55	720	10	15	17	47
04m	100	29	4	7	4	9	744	5	22	12	48	720	12	42	17	38
04b	190	29	8	28	8	11	744	1	53	7	17	720	4	43	9	24
05t	14	0	-99	-99	-99	-99	0	-99	-99	-99	-99	0	-99	-99	-99	-99
05m	100	0	-99	-99	-99	-99	0	-99	-99	-99	-99	0	-99	-99	-99	-99
05b	190	0	-99	-99	-99	-99	0	-99	-99	-99	-99	0	-99	-99	-99	-99
06t	14	724	5	82	15	41	744	8	197	16	45	720	9	79	14	53
06m	100	60	18	66	18	27	744	0	195	8	20	720	1	283	10	34
06b	190	0	-99	-99	-99	-99	711	3	261	5	17	448	1	74	5	15
07t	14	725	20	71	23	59	744	5	327	16	47	0	-99	-99	-99	-99
07m	100	725	6	84	9	27	744	2	1	10	27	720	2	71	8	19
07b	190	725	3	80	5	13	744	0	234	7	14	424	1	271	6	13
08t	14	724	22	103	28	65	744	7	88	15	41	720	3	76	10	37
08m	100	725	9	101	15	36	744	3	215	8	29	720	2	56	8	25
08b	190	73	1	146	2	7	744	2	116	3	13	720	1	120	2	13
09t	14	642	16	89	24	63	0	-99	-99	-99	-99	0	-99	-99	-99	-99
09m	100	483	2	292	6	21	744	3	313	7	16	720	6	68	8	23
09b	190	725	0	233	3	12	744	2	263	4	12	720	2	247	3	12
10t	14	724	10	87	19	51	744	7	10	16	34	720	5	103	15	40
10m	100	725	2	64	6	21	744	5	333	9	26	720	3	87	6	22
10b	190	724	0	312	2	11	744	1	95	4	13	720	1	95	4	13
11t	14	707	13	101	21	53	744	3	328	10	34	670	10	123	15	46
11m	100	708	11	87	15	56	744	1	114	6	20	669	1	80	6	17
11b	190	525	1	257	9	20	744	3	252	6	17	670	3	255	8	20
12t	14	0	-99	-99	-99	-99	0	-99	-99	-99	-99	0	-99	-99	-99	-99
12m	100	0	-99	-99	-99	-99	0	-99	-99	-99	-99	0	-99	-99	-99	-99
12b	490	0	-99	-99	-99	-99	0	-99	-99	-99	-99	0	-99	-99	-99	-99
13t	14	724	7	110	19	51	744	5	100	15	58	720	8	26	19	85
13m	100	725	4	82	7	26	744	4	220	12	25	720	3	43	11	26
13b	190	617	1	246	6	22	0	-99	-99	-99	-99	0	-99	-99	-99	-99
14t	10	718	5	95	14	46	744	2	215	17	48	685	14	265	21	82
14m	26	614	1	199	13	34	0	-99	-99	-99	-99	15	11	145	12	22
14b	40	105	5	72	8	22	744	2	248	8	23	685	4	242	10	35
15t	10	715	14	80	20	64	744	1	250	14	45	712	21	268	25	65
15b	17	726	1	231	5	23	744	3	234	10	39	683	8	242	11	45
16t	10	725	4	241	8	31	744	5	249	11	48	680	5	256	12	59
16b	14	604	1	13	5	18	0	-99	-99	-99	-99	0	-99	-99	-99	-99
17t	3	171	4	145	30	68	744	4	287	19	57	653	5	283	18	37
17b	6	0	-99	-99	-99	-99	0	-99	-99	-99	-99	0	-99	-99	-99	-99
18t	8	726	13	96	18	70	744	2	70	12	33	657	5	295	10	37
18b	19	167	3	84	5	20	232	2	252	4	16	0	-99	-99	-99	-99
19t	3	726	4	93	34	83	744	16	333	33	69	702	18	290	36	94
19m	20	563	5	134	17	50	0	-99	-99	-99	-99	0	-99	-99	-99	-99
19b	45	163	2	20	8	22	744	0	199	6	16	703	1	221	10	34
20t	3	705	2	353	16	47	723	8	292	19	49	720	13	254	19	50
20b	13	744	3	100	9	33	11	4	287	5	8	0	-99	-99	-99	-99
21t	14	744	10	56	17	45	724	1	272	10	26	720	12	260	15	40
21b	22	744	4	51	13	39	724	2	229	10	27	720	7	245	12	33
22t	3	697	16	32	33	83	733	3	303	29	80	720	7	299	24	67
22m	20	735	6	39	16	54	732	1	174	9	45	720	1	107	12	34
22b	48	0	-99	-99	-99	-99	0	-99	-99	-99	-99	0	-99	-99	-99	-99
23t	10	726	4	68	12	27	0	-99	-99	-99	-99	0	-99	-99	-99	-99
23b	13	726	6	73	13	30	0	-99	-99	-99	-99	0	-99	-99	-99	-99
24t	10	337	3	278	20	57	743	7	241	14	44	720	13	243	19	77
24b	25	0	-99	-99	-99	-99	0	-99	-99	-99	-99	0	-99	-99	-99	-99
25t	11	0	-99	-99	-99	-99	0	-99	-99	-99	-99	0	-99	-99	-99	-99
25m	20	0	-99	-99	-99	-99	0	-99	-99	-99	-99	0	-99	-99	-99	-99
25b	29	0	-99	-99	-99	-99	0	-99	-99	-99	-99	0	-99	-99	-99	-99
44t	13	0	-99	-99	-99	-99	0	-99	-99	-99	-99	0	-99	-99	-99	-99
44b	55	0	-99	-99	-99	-99	0	-99	-99	-99	-99	0	-99	-99	-99	-99
45t	12	0	-99	-99	-99	-99	0	-99	-99	-99	-99	0	-99	-99	-99	-99
45m	84	0	-99	-99	-99	-99	0	-99	-99	-99	-99	0	-99	-99	-99	-99
46t	14	0	-99	-99	-99	-99	0	-99	-99	-99	-99	0	-99	-99	-99	-99
46m	50	0	-99	-99	-99	-99	0	-99	-99	-99	-99	0	-99	-99	-99	-99
46b	84	0	-99	-99	-99	-99	0	-99	-99	-99	-99	0	-99	-99	-99	-99
47t	12	0	-99	-99	-99	-99	0	-99	-99	-99	-99	0	-99	-99	-99	-99
47m	100	0	-99	-99	-99	-99	0	-99	-99	-99	-99	0	-99	-99	-99	-99
47b	190	0	-99	-99	-99	-99	0	-99	-99	-99	-99	0	-99	-99	-99	-99
48t	14	725	4	135	13	40	744	13	71	19	52	720	3	308	16	39
48m	100	725	2	31	8	37	744	6	290	14	47	720	5	282	14	40
48b	190	480	0	332	2	9	0	-99	-99	-99	-99	0	-99	-99	-99	-99
49t	14	724	11	291	17	43	744	2	52	21	56	720	7	163	22	47
49m	100	724	3	320	7	26	744	3	38	12	33	720	6	103	19	53
49b	490	13	5	59	7	11	296	3	178	6	15	213	5	208	5	16

Table I-2. Current meter velocity statistics for 3-hr low-passed filtered data (continued).

		October 1994					November 1994					December 1994				
No.	h	N	$\lvert\bar{\mathbf{v}}\rvert$	θ	$\overline{\lvert\mathbf{v}\rvert}$	v_M	N	$\lvert\bar{\mathbf{v}}\rvert$	θ	$\overline{\lvert\mathbf{v}\rvert}$	v_M	N	$\lvert\bar{\mathbf{v}}\rvert$	θ	$\overline{\lvert\mathbf{v}\rvert}$	v_M
01t	10	0	-99	-99	-99	-99	0	-99	-99	-99	-99	0	-99	-99	-99	-99
01b	12	0	-99	-99	-99	-99	0	-99	-99	-99	-99	0	-99	-99	-99	-99
02t	10	744	21	198	25	60	720	12	204	17	48	129	14	190	19	54
02b	32	744	10	173	15	61	618	6	178	10	40	0	-99	-99	-99	-99
03t	10	744	11	192	23	64	720	4	210	18	61	132	19	207	23	56
03m	33	0	-99	-99	-99	-99	0	-99	-99	-99	-99	0	-99	-99	-99	-99
03b	58	744	2	149	12	26	720	0	44	13	25	91	3	281	12	25
04t	14	744	9	209	16	49	720	20	30	23	50	136	16	36	17	31
04m	100	744	1	240	6	18	720	10	38	13	32	136	4	44	5	12
04b	190	744	2	211	6	15	720	0	185	4	9	96	1	210	2	5
05t	14	334	11	233	24	51	0	-99	-99	-99	-99	0	-99	-99	-99	-99
05m	100	711	3	48	10	28	720	3	117	9	23	140	3	271	5	10
05b	190	712	2	234	6	17	720	2	220	6	17	141	1	99	5	13
06t	14	744	1	101	16	47	720	6	103	15	53	111	9	266	11	29
06m	100	744	3	66	14	40	720	3	265	5	23	111	7	258	8	23
06b	190	0	-99	-99	-99	-99	0	-99	-99	-99	-99	0	-99	-99	-99	-99
07t	14	0	-99	-99	-99	-99	0	-99	-99	-99	-99	0	-99	-99	-99	-99
07m	100	744	1	271	9	22	720	5	271	8	26	95	8	271	8	13
07b	190	0	-99	-99	-99	-99	0	-99	-99	-99	-99	0	-99	-99	-99	-99
08t	14	744	4	275	11	29	720	7	77	11	35	89	1	186	6	13
08m	100	744	6	270	10	30	720	2	233	7	23	88	11	269	12	24
08b	190	744	2	116	3	15	720	2	114	3	12	88	2	271	3	9
09t	14	0	-99	-99	-99	-99	0	-99	-99	-99	-99	0	-99	-99	-99	-99
09m	100	744	4	315	6	18	720	3	273	5	17	12	7	228	7	15
09b	190	744	1	272	5	15	720	0	342	5	14	12	3	192	3	6
10t	14	744	4	151	13	35	720	11	46	15	34	19	7	94	11	17
10m	100	744	5	293	9	24	720	2	280	5	20	18	4	252	9	14
10b	190	744	1	86	4	12	720	1	81	3	10	18	5	96	6	9
11t	14	744	7	37	15	34	720	14	84	15	42	25	12	74	13	20
11m	100	687	6	259	9	24	720	3	67	6	22	25	3	67	7	15
11b	190	744	3	232	6	21	657	3	178	4	18	0	-99	-99	-99	-99
12t	14	0	-99	-99	-99	-99	0	-99	-99	-99	-99	0	-99	-99	-99	-99
12m	100	0	-99	-99	-99	-99	0	-99	-99	-99	-99	0	-99	-99	-99	-99
12b	490	0	-99	-99	-99	-99	0	-99	-99	-99	-99	0	-99	-99	-99	-99
13t	14	744	3	302	12	33	720	3	86	13	33	62	7	74	8	16
13m	100	744	1	350	9	31	720	4	253	10	27	62	10	253	12	28
13b	190	0	-99	-99	-99	-99	0	-99	-99	-99	-99	0	-99	-99	-99	-99
14t	10	0	-99	-99	-99	-99	0	-99	-99	-99	-99	0	-99	-99	-99	-99
14m	26	719	6	252	15	35	0	-99	-99	-99	-99	0	-99	-99	-99	-99
14b	40	0	-99	-99	-99	-99	0	-99	-99	-99	-99	0	-99	-99	-99	-99
15t	10	744	14	265	19	54	720	9	267	12	48	56	23	265	26	39
15b	17	0	-99	-99	-99	-99	0	-99	-99	-99	-99	0	-99	-99	-99	-99
16t	10	0	-99	-99	-99	-99	0	-99	-99	-99	-99	0	-99	-99	-99	-99
16b	14	0	-99	-99	-99	-99	0	-99	-99	-99	-99	0	-99	-99	-99	-99
17t	3	654	11	284	23	64	254	5	309	19	45	0	-99	-99	-99	-99
17b	6	0	-99	-99	-99	-99	0	-99	-99	-99	-99	0	-99	-99	-99	-99
18t	8	0	-99	-99	-99	-99	0	-99	-99	-99	-99	0	-99	-99	-99	-99
18b	19	0	-99	-99	-99	-99	0	-99	-99	-99	-99	0	-99	-99	-99	-99
19t	3	742	17	280	23	72	720	9	285	12	46	31	23	264	24	37
19m	20	742	15	285	18	53	75	8	291	9	17	0	-99	-99	-99	-99
19b	45	0	-99	-99	-99	-99	0	-99	-99	-99	-99	0	-99	-99	-99	-99
20t	3	727	18	253	25	91	701	25	262	29	63	0	-99	-99	-99	-99
20b	13	665	5	270	12	38	703	4	267	10	28	0	-99	-99	-99	-99
21t	14	726	9	276	12	48	708	7	267	10	27	0	-99	-99	-99	-99
21b	22	727	4	235	10	39	709	4	233	10	27	0	-99	-99	-99	-99
22t	3	723	20	287	26	64	720	2	281	10	53	5	7	262	7	9
22m	20	723	5	321	9	40	720	2	259	4	22	6	5	276	5	8
22b	48	376	2	4	12	40	0	-99	-99	-99	-99	0	-99	-99	-99	-99
23t	10	696	22	244	23	56	720	18	246	21	58	104	32	245	32	50
23b	13	0	-99	-99	-99	-99	0	-99	-99	-99	-99	0	-99	-99	-99	-99
24t	10	725	27	246	29	72	720	16	247	17	59	101	14	245	15	30
24b	25	720	8	234	14	48	631	3	223	11	33	0	-99	-99	-99	-99
25t	11	0	-99	-99	-99	-99	0	-99	-99	-99	-99	0	-99	-99	-99	-99
25m	20	0	-99	-99	-99	-99	0	-99	-99	-99	-99	0	-99	-99	-99	-99
25b	29	0	-99	-99	-99	-99	0	-99	-99	-99	-99	0	-99	-99	-99	-99
44t	13	0	-99	-99	-99	-99	0	-99	-99	-99	-99	0	-99	-99	-99	-99
44b	55	0	-99	-99	-99	-99	0	-99	-99	-99	-99	0	-99	-99	-99	-99
45t	12	0	-99	-99	-99	-99	0	-99	-99	-99	-99	0	-99	-99	-99	-99
45m	84	0	-99	-99	-99	-99	0	-99	-99	-99	-99	0	-99	-99	-99	-99
46t	14	0	-99	-99	-99	-99	0	-99	-99	-99	-99	0	-99	-99	-99	-99
46m	50	0	-99	-99	-99	-99	0	-99	-99	-99	-99	0	-99	-99	-99	-99
46b	84	0	-99	-99	-99	-99	0	-99	-99	-99	-99	0	-99	-99	-99	-99
47t	12	0	-99	-99	-99	-99	0	-99	-99	-99	-99	0	-99	-99	-99	-99
47m	100	0	-99	-99	-99	-99	0	-99	-99	-99	-99	0	-99	-99	-99	-99
47b	190	0	-99	-99	-99	-99	0	-99	-99	-99	-99	0	-99	-99	-99	-99
48t	14	744	2	267	12	36	720	11	95	17	39	69	8	63	11	16
48m	100	744	1	261	16	48	720	3	78	11	44	34	7	272	18	28
48b	190	0	-99	-99	-99	-99	0	-99	-99	-99	-99	0	-99	-99	-99	-99
49t	14	744	5	321	14	37	720	16	107	20	50	113	23	117	24	35
49m	100	744	3	270	7	21	720	3	114	4	22	113	2	164	3	7
49b	490	416	3	160	6	17	549	2	177	6	16	41	3	11	5	11

Of particular note in Table I-2 is that monthly maximum speeds in excess of 100 cm·s^{-1} were recorded only ten times during the LATEX field period. Of these, seven were associated with the passage of Hurricane Andrew in August 1992 (see Appendix B.1), and two were associated with the Storm of the Century in March 1993 (see Appendix B.2). The remaining occurrence is associated with cyclogenesis in October 1992. The number of monthly maximum speeds greater than 90 cm·s^{-1} more than triples to 33 occurrences. The largest monthly maximum speed recorded during LATEX was 162 cm·s^{-1} at 10-m depth on mooring 13 during Hurricane Andrew.

For each month and instrument, Table I-3 gives monthly averages of recorded temperatures and salinities, together with the number of samples used to perform each average. N_T (N_S) and $\overline{T}$ ($\overline{S}$) denote the number of samples of temperature (salinity) in a given month and the monthly mean temperature (salinity). As before, -99 means that statistics are not available because samples were lacking in that month. For Table I-3, the maximum (minimum) values of monthly averaged temperature and salinity are 30.8°C (7.5°C) and 36.7 (16.9), respectively.

Listed in Table I-4 for each instrument and month are maximum observed speeds (V_M), the direction associated with the maximum (θ), and the day of the month on which the maximum occurred. These are based on the 40-hr low-pass records. Note that there were eleven occurrences of maximum speeds in excess of 80 cm·s^{-1} after 40-hr low-pass filtering. Of those, six are from locations associated with the eddy graveyard (see Section 2.5.1) near the vicinity of mooring 5 (Figure 1.2-1).

Table I-3. Current meter temperature and salinity statistics for 3-hr low-passed filtered data.

		April 1992				May 1992				June 1992				July 1992			
No.	h	N_T	$\bar{T}$	N_S	$\bar{S}$	N_T	$\bar{T}$	N_S	$\bar{S}$	N_T	$\bar{T}$	N_S	$\bar{S}$	N_T	$\bar{T}$	N_S	$\bar{S}$
01t	10	501	21.3	501	28.9	723	23.5	723	31.3	720	24.2	720	31.8	723	24.7	723	34.0
01b	12	504	19.5	0	-99.0	59	19.0	0	-99.0	0	-99.0	0	-99.0	0	-99.0	0	-99.0
02t	10	501	20.5	501	30.1	722	24.0	722	32.3	720	26.4	720	32.3	714	26.4	714	34.4
02b	32	501	19.1	501	35.2	722	19.9	661	36.8	720	21.5	0	-99.0	726	22.8	355	35.9
03t	10	495	20.6	495	29.7	744	24.1	744	31.4	720	27.2	720	32.8	713	28.5	713	34.7
03m	33	499	19.8	0	-99.0	44	21.9	0	-99.0	0	-99.0	0	-99.0	0	-99.0	0	-99.0
03b	58	0	-99.0	0	-99.0	0	-99.0	0	-99.0	0	-99.0	0	-99.0	341	22.0	0	-99.0
04t	14	513	22.8	513	33.3	744	25.0	744	33.5	720	27.4	720	34.2	507	27.0	389	34.4
04m	100	513	19.2	513	36.5	744	19.5	744	36.4	720	19.1	720	36.4	507	16.5	507	36.2
04b	190	0	-99.0	0	-99.0	0	-99.0	0	-99.0	0	-99.0	0	-99.0	117	16.7	117	36.3
05t	14	525	22.7	525	32.7	744	24.8	744	33.5	720	27.9	720	34.7	516	28.3	516	35.1
05m	100	525	19.3	525	36.2	744	20.4	744	36.3	720	20.9	720	36.3	515	18.2	515	36.2
05b	190	525	15.9	525	36.1	744	15.3	744	36.0	720	14.7	720	35.9	401	14.0	401	35.8
06t	14	489	22.6	489	33.6	744	23.3	744	33.4	720	27.6	720	33.4	528	28.4	528	34.3
06m	100	489	18.7	489	36.2	744	18.3	744	36.3	720	21.2	720	36.3	406	24.1	406	36.3
06b	190	489	15.4	489	36.0	744	14.3	744	35.9	720	15.6	720	36.0	529	16.5	529	36.1
07t	14	483	23.1	483	34.4	744	23.3	744	33.3	720	27.1	720	34.4	541	28.3	541	35.3
07m	100	483	18.9	483	36.2	744	18.4	744	36.4	720	18.7	720	36.4	410	19.4	410	36.4
07b	190	483	15.6	483	36.1	744	14.7	744	36.0	720	14.7	720	36.0	539	14.9	539	36.0
08t	14	339	22.1	339	33.7	744	23.9	744	33.0	720	26.8	720	33.5	744	28.8	744	34.1
08m	100	339	19.0	339	36.3	744	18.8	744	36.4	720	18.8	720	36.4	744	18.5	744	36.3
08b	190	339	15.3	339	36.0	744	14.5	744	35.9	720	14.6	720	35.9	744	14.8	744	35.9
09t	14	343	22.3	343	33.9	744	23.9	744	33.0	720	26.7	720	33.1	744	29.3	744	33.4
09m	100	344	19.2	344	36.4	744	18.9	744	36.4	720	18.3	720	36.5	744	18.7	744	36.6
09b	190	344	15.4	344	35.7	744	14.4	744	35.9	720	14.8	720	35.9	744	15.0	744	35.9
10t	14	348	22.5	348	34.3	744	23.7	744	33.8	720	26.6	720	33.5	744	29.2	744	33.1
10m	100	348	19.3	348	36.4	744	19.0	744	36.4	720	19.0	720	36.4	744	18.8	744	36.3
10b	190	348	15.5	348	36.1	744	14.6	744	35.9	720	14.9	720	36.0	744	15.0	744	36.0
11t	14	354	22.2	354	34.6	744	23.1	744	34.4	720	25.1	720	34.0	744	27.2	744	34.0
11m	100	378	15.3	378	36.0	744	15.1	744	36.0	720	16.2	720	36.1	744	17.1	744	36.2
11b	190	354	18.7	354	36.4	744	17.8	744	36.3	720	17.5	720	36.2	744	16.9	744	36.2
12t	14	369	22.6	369	35.5	744	22.9	744	35.3	720	24.5	720	35.4	744	26.3	744	34.9
12m	100	0	-99.0	0	-99.0	0	-99.0	0	-99.0	0	-99.0	0	-99.0	0	-99.0	0	-99.0
12b	490	372	7.5	372	35.2	744	7.9	744	35.3	720	7.6	720	35.2	744	7.6	744	35.2
13t	14	375	22.9	0	-99.0	744	23.9	0	-99.0	720	26.6	0	-99.0	720	29.4	207	33.5
13m	100	375	19.3	375	36.5	744	19.3	744	36.4	720	19.9	720	36.3	719	18.9	719	36.4
13b	190	375	15.1	375	36.0	744	14.5	744	35.9	720	15.0	720	35.8	720	15.0	720	35.7
14t	10	378	22.1	378	35.6	744	23.3	744	35.0	698	26.9	20	34.4	725	29.6	217	30.8
14m	26	0	-99.0	0	-99.0	0	-99.0	0	-99.0	681	23.3	681	34.2	724	23.1	724	34.2
14b	40	378	20.1	0	-99.0	744	20.3	0	-99.0	702	20.6	682	35.9	726	20.8	726	36.3
15t	10	381	21.6	381	35.2	744	23.0	744	34.6	702	26.9	702	31.5	727	29.2	727	29.4
15b	17	381	20.6	381	34.8	744	21.8	744	33.8	700	22.3	700	34.6	728	22.2	728	34.3
16t	10	381	21.4	381	33.4	744	22.9	744	33.5	702	24.7	702	32.7	493	26.5	493	31.0
16b	14	384	20.3	0	-99.0	744	21.6	0	-99.0	699	22.6	0	-99.0	720	23.7	0	-99.0
17t	3	0	-99.0	0	-99.0	0	-99.0	0	-99.0	494	28.1	197	28.7	260	29.9	132	26.8
17b	6	403	17.9	0	-99.0	730	19.6	0	-99.0	607	20.6	0	-99.0	0	-99.0	0	-99.0
18t	8	399	21.6	399	32.0	733	23.1	733	33.0	711	25.5	679	34.0	727	28.8	256	29.4
18b	19	381	21.0	381	33.2	673	22.6	673	33.1	711	22.8	711	33.7	725	23.7	725	32.7
19t	3	326	22.5	326	35.3	114	22.7	114	35.2	499	27.7	499	30.6	166	29.9	166	30.7
19m	20	419	21.0	0	-99.0	744	22.5	0	-99.0	6	23.1	0	-99.0	166	26.3	166	35.2
19b	45	0	-99.0	0	-99.0	0	-99.0	0	-99.0	669	21.3	669	34.5	728	21.3	728	34.7
20t	3	0	-99.0	0	-99.0	20	25.4	20	23.7	500	27.2	500	23.7	279	29.6	279	31.9
20b	13	426	21.3	0	-99.0	721	23.5	0	-99.0	720	24.1	0	-99.0	723	28.2	0	-99.0
21t	14	417	21.5	417	35.2	725	22.9	725	33.8	720	26.1	720	30.3	725	29.2	725	32.1
21b	22	445	21.1	445	33.4	703	22.0	703	34.4	720	22.6	720	34.3	727	26.7	727	33.1
22t	3	93	21.7	93	35.4	0	-99.0	0	-99.0	510	28.0	510	30.6	141	29.7	141	32.4
22m	20	464	20.4	464	35.0	744	21.9	744	34.2	649	23.3	649	33.6	721	26.4	721	33.1
22b	48	0	-99.0	0	-99.0	0	-99.0	0	-99.0	649	19.9	649	35.1	722	20.1	722	36.1
23t	10	543	20.4	543	30.1	625	23.4	625	30.0	627	25.1	627	30.5	725	28.2	725	33.8
23b	13	546	20.6	0	-99.0	629	22.9	0	-99.0	625	22.6	0	-99.0	719	27.0	0	-99.0
24t	10	537	20.6	537	33.0	722	24.0	722	28.6	720	26.9	720	30.3	726	28.8	726	34.5
24b	25	481	19.6	0	-99.0	728	20.8	0	-99.0	720	20.5	0	-99.0	727	24.5	400	34.4
25t	11	537	20.4	537	34.8	709	23.0	709	32.2	720	26.6	720	32.6	724	28.4	724	35.2
25m	20	538	19.7	538	33.6	714	21.2	677	33.2	720	24.3	0	-99.0	418	27.3	0	-99.0
25b	29	0	-99.0	0	-99.0	36	19.6	0	-99.0	720	20.4	0	-99.0	724	22.2	0	-99.0
44t	13	526	20.1	526	30.7	744	23.8	744	29.4	720	27.2	720	32.3	722	27.4	722	33.6
44b	55	525	19.4	525	36.2	744	19.7	744	36.1	720	21.0	720	36.3	723	21.9	723	36.6
45t	12	519	22.6	519	33.5	744	24.9	744	34.0	720	27.7	720	34.9	395	28.4	395	35.3
45m	84	513	19.6	513	36.1	744	21.0	744	36.3	720	21.7	720	36.3	395	20.6	395	35.8
46t	14	525	20.9	525	32.5	744	24.1	744	32.6	720	27.6	720	34.3	723	27.7	723	35.1
46m	50	0	-99.0	0	-99.0	0	-99.0	0	-99.0	0	-99.0	0	-99.0	376	22.4	376	36.4
46b	84	525	19.0	525	36.1	744	19.2	744	36.1	720	20.6	720	36.2	724	19.4	724	36.3
47t	12	514	22.9	514	34.1	744	24.8	744	34.3	720	27.4	720	34.7	744	27.5	744	34.9
47m	100	82	18.8	82	36.2	744	19.7	744	36.3	720	19.4	720	36.3	744	17.1	744	36.2
47b	190	231	15.7	231	35.9	744	15.2	744	35.9	720	14.2	720	35.7	744	13.8	744	35.6
48t	14	362	22.0	362	34.2	744	23.1	744	34.5	720	24.6	720	34.6	744	27.3	744	34.4
48m	100	361	19.4	361	36.3	744	18.9	744	36.3	720	18.8	720	36.3	744	18.6	744	36.2
48b	190	359	15.1	359	35.6	744	14.4	744	35.5	720	14.7	720	35.6	744	14.8	744	35.7
49t	14	519	23.3	519	33.8	744	24.8	744	33.7	720	27.2	720	34.1	744	26.9	744	34.4
49m	100	519	19.7	519	36.5	259	19.3	259	36.4	0	-99.0	0	-99.0	0	-99.0	0	-99.0
49b	490	519	8.3	519	35.0	245	8.0	245	34.9	0	-99.0	0	-99.0	0	-99.0	0	-99.0

Table I-3. Current meter temperature and salinity statistics for 3-hr low-passed filtered data (continued).

		August 1992				September 1992				October 1992				November 1992			
No.	h	N_T	$\bar{T}$	N_S	$\bar{S}$	N_T	$\bar{T}$	N_S	$\bar{S}$	N_T	$\bar{T}$	N_S	$\bar{S}$	N_T	$\bar{T}$	N_S	$\bar{S}$
01t	10	744	27.9	376	34.1	697	28.8	621	33.3	699	25.5	699	30.7	720	21.8	720	32.1
01b	12	0	-99.0	0	-99.0	0	-99.0	0	-99.0	386	25.7	0	-99.0	720	22.2	0	-99.0
02t	10	744	27.9	744	34.5	703	28.9	703	33.3	727	26.1	727	31.5	720	22.8	720	30.6
02b	32	744	24.9	744	34.5	703	27.9	703	35.5	728	26.6	728	35.8	720	23.6	720	35.7
03t	10	744	28.3	744	34.8	720	28.8	720	33.8	715	26.5	715	33.9	664	23.9	664	33.0
03m	33	0	-99.0	0	-99.0	0	-99.0	0	-99.0	0	-99.0	0	-99.0	0	-99.0	0	-99.0
03b	58	744	21.6	0	-99.0	720	22.8	0	-99.0	720	26.9	373	31.1	668	24.4	668	31.0
04t	14	744	25.7	0	-99.0	720	28.2	0	-99.0	349	27.5	0	-99.0	0	-99.0	0	-99.0
04m	100	744	14.5	744	36.0	720	15.7	720	36.2	716	16.1	716	36.0	0	-99.0	0	-99.0
04b	190	744	17.8	744	36.4	720	19.0	720	36.4	744	20.0	744	36.4	268	20.4	268	36.3
05t	14	744	28.7	744	34.2	720	28.7	720	34.3	744	26.8	744	34.4	720	24.7	720	33.8
05m	100	744	19.0	744	36.4	720	20.0	720	36.3	744	20.7	744	36.3	720	21.3	720	36.1
05b	190	658	15.6	658	36.0	720	16.3	720	36.1	744	16.5	744	36.1	720	16.3	720	36.1
06t	14	744	27.5	744	35.3	720	28.5	720	35.1	744	26.8	744	35.2	720	24.6	720	35.0
06m	100	730	18.6	730	36.3	720	19.0	720	36.1	744	20.1	744	36.1	720	20.2	720	36.1
06b	190	744	15.1	744	35.9	720	16.2	720	36.0	744	16.0	744	35.8	720	15.3	720	35.7
07t	14	744	27.9	744	35.5	720	28.8	720	35.2	744	27.0	744	35.6	720	24.6	720	35.2
07m	100	0	-99.0	0	-99.0	0	-99.0	0	-99.0	0	-99.0	0	-99.0	0	-99.0	0	-99.0
07b	190	744	15.2	744	36.1	720	16.1	720	36.2	744	16.1	744	36.1	720	15.5	720	36.0
08t	14	744	29.0	744	34.1	720	28.9	720	34.1	722	27.1	722	34.1	720	24.8	720	34.2
08m	100	719	18.3	719	36.2	0	-99.0	0	-99.0	285	20.6	285	36.4	720	20.7	673	36.3
08b	190	715	15.1	715	35.8	0	-99.0	0	-99.0	285	15.9	285	36.2	720	15.3	720	36.1
09t	14	719	29.7	719	34.1	720	28.8	720	34.7	744	26.8	744	34.9	720	24.7	720	34.9
09m	100	718	18.3	718	36.5	720	18.7	720	36.4	744	20.2	744	36.4	720	20.5	720	36.4
09b	190	723	15.3	685	35.8	720	16.2	0	-99.0	744	16.1	0	-99.0	720	15.4	0	-99.0
10t	14	704	29.6	704	34.1	720	28.8	720	35.0	744	26.7	744	35.2	720	24.4	720	35.3
10m	100	705	18.7	705	36.2	720	19.1	720	36.4	744	19.9	744	36.3	720	20.2	720	36.3
10b	190	720	15.3	720	35.9	720	16.3	720	36.2	744	16.6	744	36.2	720	15.7	720	36.0
11t	14	705	28.8	705	34.6	720	28.3	720	35.2	744	26.6	744	35.4	720	24.3	720	35.7
11m	100	664	17.9	664	36.2	720	18.9	720	36.4	744	19.6	744	36.3	720	20.0	720	36.3
11b	190	695	16.1	695	36.1	711	15.9	711	36.1	744	16.1	744	36.1	720	15.2	720	36.0
12t	14	744	26.6	744	35.0	720	27.7	720	34.8	720	25.7	720	34.8	720	24.0	720	35.3
12m	100	0	-99.0	0	-99.0	0	-99.0	0	-99.0	207	18.3	207	36.5	720	18.2	720	36.5
12b	490	744	7.9	744	35.3	720	8.8	720	35.5	723	8.5	723	35.4	720	8.1	720	35.4
13t	14	744	28.7	744	33.1	720	28.1	720	33.4	709	25.5	709	33.5	720	23.7	720	34.3
13m	100	744	18.4	744	36.4	720	18.8	720	36.4	709	19.6	709	36.5	720	19.8	720	36.5
13b	190	744	15.1	744	36.0	720	16.3	720	36.2	710	16.1	710	36.2	720	15.5	720	36.2
14t	10	744	28.8	744	31.7	696	27.2	696	32.5	705	25.2	705	32.3	720	23.2	720	32.8
14m	26	744	23.4	744	33.5	701	24.7	701	33.2	711	25.9	711	33.1	720	23.5	720	33.9
14b	40	744	20.7	744	35.2	702	22.3	702	34.5	493	24.7	493	34.3	0	-99.0	0	-99.0
15t	10	744	28.7	744	30.8	697	27.1	697	32.1	721	25.2	721	31.2	720	22.6	720	32.7
15b	17	744	22.6	744	34.2	702	24.9	30	33.8	321	25.3	0	-99.0	0	-99.0	0	-99.0
16t	10	0	-99.0	0	-99.0	0	-99.0	0	-99.0	237	24.4	237	31.9	720	21.7	720	32.3
16b	14	744	23.6	0	-99.0	8	25.2	0	-99.0	0	-99.0	0	-99.0	0	-99.0	0	-99.0
17t	3	249	30.3	0	-99.0	711	28.1	198	27.1	460	23.6	0	-99.0	0	-99.0	0	-99.0
17b	6	0	-99.0	0	-99.0	0	-99.0	0	-99.0	265	23.0	0	-99.0	720	19.0	0	-99.0
18t	8	731	28.7	731	29.0	711	28.0	711	30.9	721	24.6	721	30.1	720	21.2	720	32.0
18b	19	731	24.0	731	33.7	716	26.5	716	33.0	727	25.4	466	31.5	720	21.5	0	-99.0
19t	3	724	29.3	724	32.3	720	28.6	720	32.1	723	26.0	723	34.2	422	24.2	422	35.1
19m	20	725	26.2	725	34.7	0	-99.0	0	-99.0	255	25.2	255	33.7	720	23.5	720	33.9
19b	45	725	21.2	725	34.8	0	-99.0	0	-99.0	255	24.8	255	35.6	720	23.5	720	35.5
20t	3	238	30.1	238	32.8	35	28.8	35	32.0	0	-99.0	0	-99.0	568	19.0	568	32.1
20b	13	744	29.2	0	-99.0	700	28.5	0	-99.0	610	24.5	0	-99.0	720	20.1	0	-99.0
21t	14	664	29.4	664	34.2	573	28.5	573	34.0	724	25.5	724	33.9	720	21.8	720	34.0
21b	22	728	27.4	665	34.1	720	27.4	0	-99.0	728	25.5	192	33.9	720	21.8	720	33.4
22t	3	687	29.3	687	34.3	0	-99.0	0	-99.0	0	-99.0	0	-99.0	0	-99.0	0	-99.0
22m	20	744	28.6	744	35.0	702	28.5	54	34.6	726	25.8	281	36.6	720	23.3	720	37.0
22b	48	744	20.1	744	36.4	703	21.6	703	36.6	726	25.4	726	35.9	720	23.6	720	35.7
23t	10	744	29.3	744	31.2	698	28.6	101	23.6	727	24.4	410	32.1	720	20.1	720	30.6
23b	13	744	29.0	0	-99.0	54	28.8	0	-99.0	410	24.2	0	-99.0	720	20.2	0	-99.0
24t	10	744	29.2	744	34.4	105	28.8	105	33.2	0	-99.0	0	-99.0	0	-99.0	0	-99.0
24b	25	744	26.5	744	34.4	103	26.0	103	34.7	0	-99.0	0	-99.0	0	-99.0	0	-99.0
25t	11	744	29.0	744	34.9	698	28.7	698	34.3	721	26.0	721	34.3	720	22.8	720	34.4
25m	20	0	-99.0	0	-99.0	596	28.9	596	30.3	328	26.6	328	30.6	0	-99.0	0	-99.0
25b	29	744	25.9	0	-99.0	704	26.4	596	36.5	727	25.7	727	36.3	720	22.8	720	35.6
44t	13	744	28.6	744	33.7	720	28.8	720	33.1	722	26.4	722	33.5	720	23.9	720	33.1
44b	55	744	22.2	744	37.2	720	23.2	720	36.3	390	26.9	390	33.8	0	-99.0	0	-99.0
45t	12	0	-99.0	0	-99.0	0	-99.0	0	-99.0	0	-99.0	0	-99.0	0	-99.0	0	-99.0
45m	84	0	-99.0	0	-99.0	0	-99.0	0	-99.0	0	-99.0	0	-99.0	0	-99.0	0	-99.0
46t	14	744	28.3	744	35.2	720	28.7	720	35.0	721	26.7	721	34.9	720	24.2	720	34.4
46m	50	744	22.3	744	36.3	720	23.3	720	36.1	724	26.5	395	35.6	720	24.4	0	-99.0
46b	84	744	19.5	744	36.3	720	20.9	720	36.0	721	21.7	721	36.1	720	22.7	720	36.0
47t	12	744	28.4	744	34.8	720	28.6	720	34.8	367	27.3	367	34.7	0	-99.0	0	-99.0
47m	100	744	18.6	744	36.4	183	19.6	183	36.4	0	-99.0	0	-99.0	0	-99.0	0	-99.0
47b	190	544	15.1	544	35.8	0	-99.0	0	-99.0	0	-99.0	0	-99.0	0	-99.0	0	-99.0
48t	14	721	27.6	721	35.1	720	27.9	720	33.9	744	25.7	744	34.2	720	23.7	720	34.9
48m	100	722	18.4	722	36.2	720	18.3	720	36.4	744	19.8	744	36.5	720	19.9	720	36.7
48b	190	712	15.1	712	36.1	207	16.5	207	36.2	744	16.3	744	36.2	720	15.4	720	36.1
49t	14	744	28.1	744	34.4	720	28.9	720	34.4	692	26.9	692	34.3	720	25.0	720	33.8
49m	100	0	-99.0	0	-99.0	0	-99.0	0	-99.0	321	19.9	321	36.4	720	20.4	720	36.3
49b	490	0	-99.0	0	-99.0	0	-99.0	0	-99.0	321	9.1	321	34.9	720	8.7	720	34.9

Table I-3. Current meter temperature and salinity statistics for 3-hr low-passed filtered data (continued).

		December 1992				January 1993				February 1993				March 1993			
No.	h	N_T	$\bar{T}$	N_S	$\bar{S}$	N_T	$\bar{T}$	N_S	$\bar{S}$	N_T	$\bar{T}$	N_S	$\bar{S}$	N_T	$\bar{T}$	N_S	$\bar{S}$
01t	10	721	16.8	721	29.8	724	16.4	724	29.3	672	16.5	672	29.2	727	17.6	727	30.7
01b	12	390	17.5	0	-99.0	0	-99.0	0	-99.0	0	-99.0	0	-99.0	0	-99.0	0	-99.0
02t	10	727	19.3	727	31.3	722	19.9	722	33.3	672	18.7	672	32.8	727	18.1	727	31.0
02b	32	394	20.6	394	35.3	284	19.4	284	32.8	672	20.5	161	33.3	420	21.0	0	-99.0
03t	10	0	-99.0	0	-99.0	278	20.9	278	35.7	672	20.8	672	35.8	744	20.3	744	35.0
03m	33	0	-99.0	0	-99.0	0	-99.0	0	-99.0	0	-99.0	0	-99.0	0	-99.0	0	-99.0
03b	58	0	-99.0	0	-99.0	0	-99.0	0	-99.0	0	-99.0	0	-99.0	0	-99.0	0	-99.0
04t	14	0	-99.0	0	-99.0	272	21.6	272	34.6	672	22.4	672	34.8	744	22.2	744	34.6
04m	100	0	-99.0	0	-99.0	272	20.2	272	36.3	672	20.3	672	36.3	744	19.8	744	36.4
04b	190	0	-99.0	0	-99.0	272	14.2	272	35.9	672	15.0	672	36.1	744	14.4	744	36.0
05t	14	16	23.5	16	33.6	267	21.8	267	35.7	672	22.3	672	35.8	744	22.2	744	35.8
05m	100	10	21.3	10	36.1	267	20.5	267	36.3	672	20.8	672	36.2	744	20.4	744	36.4
05b	190	15	16.0	15	36.1	274	15.0	0	-99.0	672	15.3	0	-99.0	744	14.4	0	-99.0
06t	14	76	23.4	76	35.0	300	22.5	300	35.9	672	22.0	672	35.9	744	21.5	744	35.4
06m	100	62	19.9	62	36.0	300	20.7	300	36.2	672	20.1	672	36.1	744	19.6	744	36.2
06b	190	74	15.2	74	35.7	300	14.9	300	35.9	672	14.6	672	35.9	744	14.0	744	35.8
07t	14	82	23.2	82	35.1	318	22.2	318	35.1	672	21.5	672	35.0	744	21.9	744	34.7
07m	100	0	-99.0	0	-99.0	318	20.6	318	36.0	672	19.7	672	36.1	744	18.9	744	36.2
07b	190	83	15.0	83	35.9	318	14.6	318	35.9	672	14.5	672	35.8	744	14.0	744	35.8
08t	14	88	23.1	88	34.0	369	22.4	369	36.0	672	21.3	672	35.7	744	21.6	744	35.2
08m	100	88	20.0	0	-99.0	369	20.7	369	36.2	672	19.5	672	36.2	744	18.0	744	36.2
08b	190	82	14.9	82	36.0	369	14.7	369	36.0	672	14.4	672	36.0	744	13.8	744	35.9
09t	14	196	23.3	196	34.9	0	-99.0	0	-99.0	0	-99.0	0	-99.0	0	-99.0	0	-99.0
09m	100	744	20.0	744	36.3	601	19.9	601	36.4	672	20.1	672	36.4	744	19.3	744	36.4
09b	190	744	14.8	0	-99.0	600	14.8	376	36.1	672	14.4	672	36.0	744	13.9	744	35.9
10t	14	744	22.8	744	35.3	237	22.5	237	35.3	0	-99.0	0	-99.0	0	-99.0	0	-99.0
10m	100	744	20.0	744	36.3	236	20.8	236	36.2	639	19.6	639	36.4	744	18.4	744	36.3
10b	190	744	14.9	744	35.6	722	14.9	722	35.9	672	14.4	672	35.9	744	14.1	744	35.9
11t	14	744	22.3	744	36.0	724	21.9	724	36.1	672	21.0	672	36.0	744	20.2	744	36.1
11m	100	744	19.4	744	36.3	525	19.9	525	36.4	672	19.7	672	36.4	744	18.6	744	36.2
11b	190	744	14.8	744	35.9	723	14.8	723	36.1	672	14.4	672	36.0	744	14.2	744	36.0
12t	14	744	22.4	744	35.8	724	21.9	724	35.9	672	21.5	672	36.2	744	21.7	744	36.4
12m	100	744	18.6	744	36.5	723	19.2	723	36.4	672	17.9	672	36.3	744	18.1	744	36.5
12b	490	63	8.3	63	35.4	456	8.1	456	35.0	672	8.2	672	35.1	744	8.1	744	35.1
13t	14	744	22.3	744	35.3	724	21.7	724	35.7	672	21.8	672	36.1	744	21.6	744	36.2
13m	100	744	19.8	744	36.5	384	19.8	384	36.4	672	17.7	672	36.4	744	18.2	744	36.5
13b	190	744	15.4	744	36.2	724	14.7	724	36.0	672	14.3	672	35.8	744	14.0	744	35.5
14t	10	721	21.4	721	33.6	725	20.9	278	33.7	672	20.1	0	-99.0	723	19.6	258	34.7
14m	26	300	21.9	300	35.4	447	21.1	447	35.4	672	20.9	672	35.7	725	20.2	466	35.6
14b	40	0	-99.0	0	-99.0	0	-99.0	0	-99.0	0	-99.0	0	-99.0	0	-99.0	0	-99.0
15t	10	721	20.8	721	34.0	722	21.2	722	34.4	672	20.3	672	35.4	726	19.2	718	34.5
15b	17	430	21.0	430	33.9	294	21.3	294	34.0	0	-99.0	0	-99.0	280	19.3	0	-99.0
16t	10	721	19.6	721	31.7	722	18.9	722	30.7	672	18.7	672	31.7	726	18.4	726	32.3
16b	14	0	-99.0	0	-99.0	0	-99.0	0	-99.0	0	-99.0	0	-99.0	284	18.7	0	-99.0
17t	3	0	-99.0	0	-99.0	0	-99.0	0	-99.0	0	-99.0	0	-99.0	308	16.9	308	31.2
17b	6	277	16.4	0	-99.0	0	-99.0	0	-99.0	0	-99.0	0	-99.0	309	16.6	0	-99.0
18t	8	721	18.2	721	31.7	722	18.6	722	33.5	672	17.9	672	34.2	726	18.1	726	32.6
18b	19	728	19.3	453	30.3	728	19.9	728	31.9	672	19.0	672	31.7	727	18.3	421	32.2
19t	3	0	-99.0	0	-99.0	0	-99.0	0	-99.0	0	-99.0	0	-99.0	0	-99.0	0	-99.0
19m	20	270	22.1	270	34.3	336	20.5	0	-99.0	672	19.8	0	-99.0	425	19.5	0	-99.0
19b	45	726	21.6	726	35.7	725	21.0	650	35.4	672	20.0	672	34.5	730	19.6	579	34.6
20t	3	698	17.2	698	32.7	727	17.1	727	29.4	672	16.0	672	28.7	702	16.5	702	25.2
20b	13	247	16.8	0	-99.0	0	-99.0	0	-99.0	0	-99.0	0	-99.0	335	16.9	0	-99.0
21t	14	726	19.1	726	35.2	721	18.8	721	35.0	672	17.8	672	35.3	727	18.1	727	34.1
21b	22	727	19.0	250	33.6	371	19.1	0	-99.0	0	-99.0	0	-99.0	327	18.1	327	33.5
22t	3	0	-99.0	0	-99.0	361	21.0	0	-99.0	672	19.6	0	-99.0	421	19.7	232	35.2
22m	20	255	21.4	255	37.4	360	21.1	360	33.7	672	19.8	672	34.1	493	19.7	493	34.2
22b	48	725	21.5	255	35.6	369	21.4	0	-99.0	0	-99.0	0	-99.0	232	18.4	232	36.5
23t	10	724	15.6	724	27.9	727	16.0	727	26.9	672	15.6	672	27.4	726	16.6	512	26.2
23b	13	367	15.7	0	-99.0	0	-99.0	0	-99.0	0	-99.0	0	-99.0	217	17.0	0	-99.0
24t	10	0	-99.0	0	-99.0	309	17.5	309	31.1	672	17.2	672	31.8	726	17.3	726	30.6
24b	25	0	-99.0	0	-99.0	0	-99.0	0	-99.0	0	-99.0	0	-99.0	212	18.1	212	34.9
25t	11	721	19.6	721	35.0	722	19.8	722	35.0	672	19.0	672	35.0	725	18.4	725	34.2
25m	20	0	-99.0	0	-99.0	314	19.3	314	35.8	672	18.5	672	35.9	726	17.9	726	35.0
25b	29	727	19.8	727	35.4	728	19.7	728	35.7	672	18.4	672	35.7	519	18.4	519	35.5
44t	13	190	21.8	190	32.9	0	-99.0	0	-99.0	0	-99.0	0	-99.0	0	-99.0	0	-99.0
44b	55	0	-99.0	0	-99.0	0	-99.0	0	-99.0	0	-99.0	0	-99.0	0	-99.0	0	-99.0
45t	12	0	-99.0	0	-99.0	0	-99.0	0	-99.0	0	-99.0	0	-99.0	0	-99.0	0	-99.0
45m	84	0	-99.0	0	-99.0	0	-99.0	0	-99.0	0	-99.0	0	-99.0	0	-99.0	0	-99.0
46t	14	744	22.5	744	34.4	437	22.3	437	34.3	0	-99.0	0	-99.0	0	-99.0	0	-99.0
46m	50	744	22.3	0	-99.0	439	22.1	0	-99.0	0	-99.0	0	-99.0	0	-99.0	0	-99.0
46b	84	136	22.2	136	35.8	0	-99.0	0	-99.0	0	-99.0	0	-99.0	0	-99.0	0	-99.0
47t	12	0	-99.0	0	-99.0	0	-99.0	0	-99.0	0	-99.0	0	-99.0	0	-99.0	0	-99.0
47m	100	0	-99.0	0	-99.0	267	20.2	267	36.2	672	20.7	672	36.2	541	20.4	541	36.3
47b	190	0	-99.0	0	-99.0	267	15.6	267	35.9	672	15.4	672	35.8	542	14.6	542	35.7
48t	14	744	22.2	744	35.7	720	21.9	720	35.9	672	20.7	672	35.6	744	20.6	744	36.1
48m	100	744	19.7	744	36.7	720	20.0	720	36.5	672	19.1	672	36.5	744	18.1	744	36.4
48b	190	744	15.3	744	35.9	917	14.9	917	35.9	672	14.6	672	35.9	744	14.2	744	35.7
49t	14	744	23.4	744	33.9	429	23.6	429	34.1	0	-99.0	0	-99.0	0	-99.0	0	-99.0
49m	100	744	19.6	744	36.4	429	20.3	429	36.3	0	-99.0	0	-99.0	0	-99.0	0	-99.0
49b	490	744	8.7	744	34.9	723	8.6	723	35.0	672	8.3	672	35.1	744	8.6	744	35.1

Table I-3. Current meter temperature and salinity statistics for 3-hr low-passed filtered data (continued).

No.	h	April 1993 N_T	$\bar{T}$	N_S	$\bar{S}$	May 1993 N_T	$\bar{T}$	N_S	$\bar{S}$	June 1993 N_T	$\bar{T}$	N_S	$\bar{S}$	July 1993 N_T	$\bar{T}$	N_S	$\bar{S}$
01t	10	720	20.6	720	32.2	726	23.3	726	31.9	720	26.2	720	32.8	744	23.6	744	36.6
01b	12	0	-99.0	0	-99.0	0	-99.0	0	-99.0	0	-99.0	0	-99.0	0	-99.0	0	-99.0
02t	10	720	21.6	720	32.7	723	23.9	723	32.0	720	26.5	720	32.7	744	26.7	744	35.4
02b	32	0	-99.0	0	-99.0	241	22.7	241	34.9	720	24.3	544	35.0	744	22.8	0	-99.0
03t	10	720	21.9	720	34.1	724	24.0	724	33.9	720	26.6	720	34.1	744	27.7	744	35.6
03m	33	0	-99.0	0	-99.0	237	24.3	237	36.0	720	25.0	720	35.6	744	24.8	744	36.0
03b	58	0	-99.0	0	-99.0	237	22.2	99	35.8	720	22.4	580	35.5	744	21.1	744	35.8
04t	14	720	22.5	720	33.5	725	24.6	725	33.7	720	26.8	720	34.9	744	27.8	744	34.8
04m	100	720	16.8	720	36.2	495	16.9	495	36.2	0	-99.0	0	-99.0	0	-99.0	0	-99.0
04b	190	720	13.6	720	35.8	726	14.0	495	35.9	720	14.3	0	-99.0	744	13.2	0	-99.0
05t	14	720	22.8	720	34.9	724	24.6	724	34.9	720	26.6	720	34.6	744	27.2	744	35.2
05m	100	720	17.5	720	36.3	724	19.0	724	36.2	720	20.5	720	36.3	744	17.2	744	36.2
05b	190	720	13.8	0	-99.0	714	14.6	251	36.2	720	14.5	692	36.1	744	13.2	744	36.0
06t	14	720	22.8	720	34.9	725	24.6	725	35.2	720	26.6	720	33.9	744	27.2	424	34.0
06m	100	720	17.7	720	36.2	664	21.0	664	36.2	720	19.9	720	36.2	744	18.1	744	36.3
06b	190	720	14.2	720	35.8	724	15.4	724	35.9	720	14.8	720	35.8	744	14.6	744	35.7
07t	14	720	22.6	720	34.2	723	24.6	723	34.3	720	26.6	720	34.2	744	28.2	744	34.7
07m	100	720	18.2	720	36.3	724	20.4	724	36.3	720	18.6	720	36.6	744	18.1	744	36.2
07b	190	720	14.3	720	35.8	514	15.2	514	36.0	720	14.7	720	36.0	744	14.3	744	35.9
08t	14	720	22.9	720	34.4	724	24.8	724	33.9	720	26.9	720	33.6	744	29.4	744	34.4
08m	100	720	17.6	720	36.3	725	18.6	725	36.3	720	18.8	720	36.3	744	19.0	744	36.4
08b	190	720	14.1	720	35.9	699	14.8	699	35.9	720	14.5	720	35.8	744	14.3	744	35.7
09t	14	0	-99.0	0	-99.0	202	24.4	202	35.0	720	26.2	720	34.5	744	28.7	744	34.2
09m	100	720	18.2	720	36.5	725	18.4	725	36.3	720	18.6	720	36.3	744	19.1	744	36.4
09b	190	720	13.9	720	35.9	725	15.1	725	36.0	720	14.8	720	35.9	744	14.3	744	35.7
10t	14	0	-99.0	0	-99.0	0	-99.0	0	-99.0	0	-99.0	0	-99.0	0	-99.0	0	-99.0
10m	100	720	17.7	720	36.1	508	18.6	508	36.2	720	19.3	720	36.5	744	19.3	744	36.4
10b	190	720	14.0	720	35.7	715	15.1	715	35.9	720	14.7	720	36.0	744	14.8	744	36.0
11t	14	720	21.4	720	36.1	724	24.0	724	36.1	185	26.2	185	34.9	0	-99.0	0	-99.0
11m	100	720	18.0	720	36.2	400	19.1	400	36.3	0	-99.0	0	-99.0	305	21.5	305	36.5
11b	190	720	14.1	720	35.9	580	15.2	580	36.1	0	-99.0	0	-99.0	310	17.1	310	36.5
12t	14	720	22.3	720	36.3	744	24.3	744	36.2	720	27.0	720	36.1	721	28.6	721	34.6
12m	100	720	19.1	720	36.5	744	18.8	744	36.5	720	19.2	720	36.5	721	18.9	721	36.3
12b	490	720	8.1	720	35.0	744	8.3	744	35.1	720	7.9	720	35.0	720	8.2	401	35.1
13t	14	720	22.2	720	36.1	724	24.0	724	36.1	720	26.9	720	36.1	744	28.5	744	34.2
13m	100	720	18.8	720	36.6	603	19.1	603	36.5	720	19.3	720	36.5	744	18.7	744	36.4
13b	190	720	14.3	720	35.2	594	15.0	594	35.0	0	-99.0	0	-99.0	0	-99.0	0	-99.0
14t	10	720	19.9	720	32.9	719	22.8	719	34.9	720	25.9	720	34.8	393	28.0	393	32.4
14m	26	720	19.5	0	-99.0	666	21.1	0	-99.0	720	23.5	0	-99.0	725	26.0	0	-99.0
14b	40	0	-99.0	0	-99.0	116	21.0	0	-99.0	720	21.4	0	-99.0	725	21.7	0	-99.0
15t	10	720	20.1	0	-99.0	726	22.5	113	34.9	720	25.4	720	34.9	725	28.7	725	31.8
15b	17	720	20.0	0	-99.0	726	21.9	0	-99.0	720	23.4	0	-99.0	726	23.8	334	35.8
16t	10	720	19.9	720	30.6	658	22.7	658	31.5	165	27.4	165	35.0	726	27.5	726	34.8
16b	14	720	19.7	0	-99.0	615	21.7	0	-99.0	0	-99.0	0	-99.0	0	-99.0	0	-99.0
17t	3	720	19.3	720	26.1	442	23.9	442	27.0	0	-99.0	0	-99.0	0	-99.0	0	-99.0
17b	6	720	19.4	0	-99.0	629	23.8	0	-99.0	0	-99.0	0	-99.0	0	-99.0	0	-99.0
18t	8	720	19.4	720	30.7	726	23.0	726	28.7	720	27.1	720	28.7	370	28.0	370	27.2
18b	19	592	18.9	0	-99.0	171	21.2	171	34.0	720	23.5	720	33.8	726	22.9	726	34.5
19t	3	0	-99.0	0	-99.0	165	25.2	0	-99.0	720	27.4	0	-99.0	724	30.0	361	27.6
19m	20	0	-99.0	0	-99.0	164	20.9	164	35.8	720	22.3	720	35.2	725	25.2	725	32.5
19b	45	720	19.4	720	34.2	560	19.6	560	33.9	0	-99.0	0	-99.0	360	20.5	0	-99.0
20t	3	720	19.4	720	26.4	439	22.9	439	29.2	709	27.9	375	25.4	387	30.0	0	-99.0
20b	13	720	19.2	0	-99.0	640	22.5	0	-99.0	0	-99.0	0	-99.0	0	-99.0	0	-99.0
21t	14	720	19.6	720	33.7	727	22.8	727	32.8	720	26.5	720	31.5	725	28.8	725	30.6
21b	22	720	19.4	720	34.5	727	22.2	727	34.0	720	25.2	720	33.4	723	25.1	723	33.9
22t	3	720	20.7	720	34.2	521	23.6	330	34.4	369	26.3	0	-99.0	376	30.4	376	30.9
22m	20	0	-99.0	0	-99.0	193	24.2	193	33.9	720	26.1	720	33.6	725	28.2	350	32.5
22b	48	720	19.7	720	36.6	725	20.5	265	36.4	720	22.3	0	-99.0	351	21.7	0	-99.0
23t	10	720	19.2	0	-99.0	727	23.0	0	-99.0	720	27.1	0	-99.0	725	28.5	409	34.5
23b	13	720	19.2	0	-99.0	441	21.8	0	-99.0	0	-99.0	0	-99.0	0	-99.0	0	-99.0
24t	10	720	19.3	720	31.2	727	23.0	727	29.3	720	26.9	720	27.7	726	28.4	726	33.0
24b	25	720	18.9	720	35.2	444	21.4	444	34.7	0	-99.0	0	-99.0	407	26.3	0	-99.0
25t	11	720	19.5	720	33.2	727	23.3	727	30.6	720	26.8	720	29.9	324	28.4	324	31.1
25m	20	720	18.6	720	34.6	446	21.6	446	33.8	0	-99.0	0	-99.0	0	-99.0	0	-99.0
25b	29	0	-99.0	0	-99.0	281	22.0	281	34.2	720	23.3	720	34.1	691	25.0	324	35.2
44t	13	0	-99.0	0	-99.0	0	-99.0	0	-99.0	0	-99.0	0	-99.0	0	-99.0	0	-99.0
44b	55	0	-99.0	0	-99.0	0	-99.0	0	-99.0	0	-99.0	0	-99.0	0	-99.0	0	-99.0
45t	12	0	-99.0	0	-99.0	0	-99.0	0	-99.0	0	-99.0	0	-99.0	0	-99.0	0	-99.0
45m	84	0	-99.0	0	-99.0	0	-99.0	0	-99.0	0	-99.0	0	-99.0	0	-99.0	0	-99.0
46t	14	0	-99.0	0	-99.0	0	-99.0	0	-99.0	0	-99.0	0	-99.0	0	-99.0	0	-99.0
46m	50	0	-99.0	0	-99.0	0	-99.0	0	-99.0	0	-99.0	0	-99.0	0	-99.0	0	-99.0
46b	84	0	-99.0	0	-99.0	0	-99.0	0	-99.0	0	-99.0	0	-99.0	0	-99.0	0	-99.0
47t	12	0	-99.0	0	-99.0	0	-99.0	0	-99.0	0	-99.0	0	-99.0	0	-99.0	0	-99.0
47m	100	0	-99.0	0	-99.0	0	-99.0	0	-99.0	0	-99.0	0	-99.0	0	-99.0	0	-99.0
47b	190	0	-99.0	0	-99.0	0	-99.0	0	-99.0	0	-99.0	0	-99.0	0	-99.0	0	-99.0
48t	14	720	21.8	720	36.1	587	22.3	587	35.5	0	-99.0	0	-99.0	0	-99.0	0	-99.0
48m	100	720	18.3	720	36.5	586	19.0	586	36.4	0	-99.0	0	-99.0	0	-99.0	0	-99.0
48b	190	720	14.2	720	35.7	256	15.8	256	36.0	0	-99.0	0	-99.0	0	-99.0	0	-99.0
49t	14	0	-99.0	0	-99.0	258	24.9	258	32.9	720	26.2	720	32.7	744	27.2	744	32.5
49m	100	0	-99.0	0	-99.0	258	21.7	258	36.7	720	21.2	720	36.6	744	19.0	744	36.6
49b	490	720	8.6	720	35.1	724	8.7	724	35.1	720	7.6	720	35.5	494	7.9	494	35.4

Table I-3. Current meter temperature and salinity statistics for 3-hr low-passed filtered data (continued).

No.	h	August 1993 N_T	$\bar{T}$	N_S	$\bar{S}$	September 1993 N_T	$\bar{T}$	N_S	$\bar{S}$	October 1993 N_T	$\bar{T}$	N_S	$\bar{S}$	November 1993 N_T	$\bar{T}$	N_S	$\bar{S}$
01t	10	744	24.3	744	36.1	696	27.1	696	35.2	744	26.4	744	31.7	720	19.6	720	30.4
01b	12	0	-99.0	0	-99.0	26	27.7	0	-99.0	744	26.5	0	-99.0	720	19.7	0	-99.0
02t	10	744	27.8	744	35.8	701	28.1	701	35.8	744	27.1	744	34.7	720	21.9	720	34.2
02b	32	744	22.5	0	-99.0	441	24.5	21	35.7	744	27.6	744	34.9	720	23.3	720	34.8
03t	10	744	27.9	744	35.2	684	28.4	684	36.2	0	-99.0	0	-99.0	0	-99.0	0	-99.0
03m	33	744	24.0	744	35.8	419	26.9	419	35.7	744	27.6	744	35.9	720	23.8	720	35.7
03b	58	744	21.2	744	36.0	406	22.4	406	36.0	0	-99.0	0	-99.0	0	-99.0	0	-99.0
04t	14	744	29.2	744	35.3	701	29.2	701	35.6	744	27.5	744	35.8	720	24.4	720	35.9
04m	100	0	-99.0	0	-99.0	13	19.8	13	36.5	744	20.0	744	36.5	720	19.4	720	36.4
04b	190	744	14.6	0	-99.0	700	14.4	13	36.0	744	15.2	489	36.1	720	15.7	379	36.2
05t	14	744	28.8	744	35.5	664	29.3	664	35.8	0	-99.0	0	-99.0	0	-99.0	0	-99.0
05m	100	744	18.6	744	36.2	701	19.4	701	36.3	744	19.3	744	36.5	720	19.4	720	36.5
05b	190	744	14.0	692	36.5	667	13.8	325	36.6	0	-99.0	0	-99.0	0	-99.0	0	-99.0
06t	14	744	28.7	0	-99.0	701	29.1	41	35.2	744	27.6	744	35.0	720	21.5	720	35.1
06m	100	744	19.2	744	36.2	701	19.2	701	36.3	744	18.9	744	36.5	720	19.3	720	36.5
06b	190	744	14.4	744	35.7	653	14.8	653	35.8	744	15.2	744	36.0	720	15.3	720	36.0
07t	14	744	29.0	744	35.9	654	29.4	654	35.8	0	-99.0	0	-99.0	0	-99.0	0	-99.0
07m	100	744	19.0	744	35.4	701	19.5	701	36.0	744	18.9	744	36.4	720	20.2	720	36.4
07b	190	744	14.1	744	35.7	653	14.7	653	35.6	744	15.0	744	36.0	720	15.1	720	36.0
08t	14	744	30.0	744	35.4	700	29.4	700	35.9	744	27.4	744	36.1	720	25.0	720	36.2
08m	100	744	18.9	744	36.2	701	19.4	701	36.2	744	18.9	744	36.5	720	20.5	720	36.6
08b	190	744	14.3	744	35.8	673	14.7	673	36.0	744	15.1	744	36.1	720	14.9	720	36.1
09t	14	744	29.9	744	35.4	700	29.1	700	36.0	744	27.5	744	35.8	720	24.5	720	35.9
09m	100	744	19.0	744	36.3	702	18.3	702	36.3	142	18.7	142	36.4	0	-99.0	0	-99.0
09b	190	744	14.2	744	35.6	700	14.7	700	35.8	744	15.2	744	36.3	720	15.1	720	36.2
10t	14	0	-99.0	0	-99.0	0	-99.0	0	-99.0	0	-99.0	0	-99.0	0	-99.0	0	-99.0
10m	100	744	19.4	744	36.4	702	18.3	702	36.3	744	18.5	744	36.5	720	19.0	720	36.6
10b	190	744	14.0	744	35.9	711	14.3	711	35.9	744	15.3	744	36.1	720	15.3	720	36.1
11t	14	0	-99.0	0	-99.0	0	-99.0	0	-99.0	0	-99.0	0	-99.0	0	-99.0	0	-99.0
11m	100	744	19.4	744	36.5	720	18.1	720	36.4	744	19.3	744	36.4	618	19.1	618	36.4
11b	190	744	14.8	744	36.2	720	14.3	720	36.1	744	15.1	744	36.2	720	15.5	720	36.1
12t	14	744	30.1	744	35.3	720	29.4	720	35.8	744	28.0	744	35.8	720	25.4	720	36.0
12m	100	744	19.6	744	36.3	720	18.1	720	36.3	744	20.3	744	36.1	720	19.9	720	36.0
12b	490	744	8.1	0	-99.0	720	8.7	0	-99.0	744	9.0	0	-99.0	696	8.8	0	-99.0
13t	14	744	30.0	744	35.1	584	29.7	584	35.6	0	-99.0	0	-99.0	0	-99.0	0	-99.0
13m	100	744	18.7	744	36.3	701	18.1	701	36.3	744	19.4	744	36.5	720	18.3	720	36.4
13b	190	0	-99.0	0	-99.0	117	14.0	117	35.8	744	14.9	744	35.9	720	15.0	720	35.9
14t	10	0	-99.0	0	-99.0	0	-99.0	0	-99.0	0	-99.0	0	-99.0	0	-99.0	0	-99.0
14m	26	744	26.8	0	-99.0	702	27.9	113	35.8	744	27.5	744	35.6	720	24.3	720	35.0
14b	40	744	21.1	0	-99.0	702	22.8	0	-99.0	744	25.7	0	-99.0	720	24.3	0	-99.0
15t	10	744	29.8	744	32.9	703	29.4	703	34.1	744	27.1	400	35.1	720	23.3	0	-99.0
15b	17	744	22.9	744	35.6	699	25.7	588	35.5	744	27.1	0	-99.0	720	23.7	0	-99.0
16t	10	744	28.1	744	33.1	701	29.5	701	31.9	744	26.5	448	28.8	720	21.8	0	-99.0
16b	14	0	-99.0	0	-99.0	0	-99.0	0	-99.0	0	-99.0	0	-99.0	0	-99.0	0	-99.0
17t	3	0	-99.0	0	-99.0	74	26.7	0	-99.0	744	25.0	0	-99.0	720	18.5	0	-99.0
17b	6	0	-99.0	0	-99.0	75	27.6	0	-99.0	744	25.6	0	-99.0	720	19.7	0	-99.0
18t	8	0	-99.0	0	-99.0	89	28.7	89	31.7	744	26.7	448	30.2	720	21.4	0	-99.0
18b	19	744	23.9	744	34.3	702	27.6	702	34.7	744	27.6	744	34.2	720	22.1	720	32.6
19t	3	654	30.8	111	28.2	66	28.8	66	35.0	744	27.6	744	35.5	720	23.9	720	35.7
19m	20	375	24.1	375	31.5	0	-99.0	0	-99.0	0	-99.0	0	-99.0	0	-99.0	0	-99.0
19b	45	744	21.2	0	-99.0	720	21.7	0	-99.0	744	24.6	0	-99.0	303	24.3	0	-99.0
20t	3	744	30.7	0	-99.0	700	29.3	0	-99.0	744	25.1	0	-99.0	720	18.0	0	-99.0
20b	13	0	-99.0	0	-99.0	189	29.1	0	-99.0	744	25.8	0	-99.0	720	18.9	0	-99.0
21t	14	744	30.0	744	34.6	702	29.4	702	34.5	744	26.9	744	33.6	720	22.0	720	34.8
21b	22	744	28.9	744	35.1	520	28.8	520	35.4	0	-99.0	0	-99.0	0	-99.0	0	-99.0
22t	3	744	30.3	744	34.8	701	29.3	701	35.8	449	27.8	449	36.1	0	-99.0	0	-99.0
22m	20	744	29.1	0	-99.0	512	28.8	167	36.0	744	27.4	744	36.0	720	23.9	720	36.0
22b	48	0	-99.0	0	-99.0	168	23.4	168	36.2	744	25.0	645	36.2	720	23.6	720	36.2
23t	10	744	29.7	744	35.9	709	29.0	709	34.1	0	-99.0	0	-99.0	0	-99.0	0	-99.0
23b	13	0	-99.0	0	-99.0	0	-99.0	0	-99.0	725	26.4	0	-99.0	720	19.3	0	-99.0
24t	10	744	29.6	744	35.9	707	29.3	707	35.8	734	26.5	734	32.5	720	20.9	720	33.2
24b	25	744	27.9	0	-99.0	701	29.3	0	-99.0	735	27.4	0	-99.0	720	21.7	0	-99.0
25t	11	0	-99.0	0	-99.0	0	-99.0	0	-99.0	0	-99.0	0	-99.0	0	-99.0	0	-99.0
25m	20	0	-99.0	0	-99.0	0	-99.0	0	-99.0	742	27.4	0	-99.0	720	22.2	0	-99.0
25b	29	0	-99.0	0	-99.0	0	-99.0	0	-99.0	744	27.3	744	35.6	720	22.3	720	34.6
44t	13	0	-99.0	0	-99.0	0	-99.0	0	-99.0	0	-99.0	0	-99.0	0	-99.0	0	-99.0
44b	55	0	-99.0	0	-99.0	0	-99.0	0	-99.0	0	-99.0	0	-99.0	0	-99.0	0	-99.0
45t	12	0	-99.0	0	-99.0	0	-99.0	0	-99.0	0	-99.0	0	-99.0	0	-99.0	0	-99.0
45m	84	0	-99.0	0	-99.0	0	-99.0	0	-99.0	0	-99.0	0	-99.0	0	-99.0	0	-99.0
46t	14	0	-99.0	0	-99.0	0	-99.0	0	-99.0	0	-99.0	0	-99.0	0	-99.0	0	-99.0
46m	50	0	-99.0	0	-99.0	0	-99.0	0	-99.0	0	-99.0	0	-99.0	0	-99.0	0	-99.0
46b	84	0	-99.0	0	-99.0	0	-99.0	0	-99.0	0	-99.0	0	-99.0	0	-99.0	0	-99.0
47t	12	0	-99.0	0	-99.0	0	-99.0	0	-99.0	0	-99.0	0	-99.0	0	-99.0	0	-99.0
47m	100	0	-99.0	0	-99.0	0	-99.0	0	-99.0	0	-99.0	0	-99.0	0	-99.0	0	-99.0
47b	190	0	-99.0	0	-99.0	0	-99.0	0	-99.0	0	-99.0	0	-99.0	0	-99.0	0	-99.0
48t	14	0	-99.0	0	-99.0	0	-99.0	0	-99.0	0	-99.0	0	-99.0	0	-99.0	0	-99.0
48m	100	0	-99.0	0	-99.0	0	-99.0	0	-99.0	0	-99.0	0	-99.0	0	-99.0	0	-99.0
48b	190	0	-99.0	0	-99.0	0	-99.0	0	-99.0	0	-99.0	0	-99.0	0	-99.0	0	-99.0
49t	14	744	29.0	744	32.5	720	29.3	720	32.6	744	27.5	744	32.9	720	24.6	720	33.0
49m	100	744	19.2	744	36.5	720	19.5	720	36.7	744	19.4	744	36.7	720	19.2	720	36.7
49b	490	744	7.6	744	35.4	720	8.4	720	35.2	688	9.1	688	35.0	720	8.2	471	35.2

Table I-3. Current meter temperature and salinity statistics for 3-hr low-passed filtered data (continued).

No.	h	December 1993 N_T	$\bar{T}$	N_S	$\bar{S}$	January 1994 N_T	$\bar{T}$	N_S	$\bar{S}$	February 1994 N_T	$\bar{T}$	N_S	$\bar{S}$	March 1994 N_T	$\bar{T}$	N_S	$\bar{S}$
01t	10	727	17.2	246	30.2	744	14.5	0	-99.0	672	13.7	0	-99.0	725	17.1	72	28.7
01b	12	727	17.4	0	-99.0	744	14.7	0	-99.0	672	13.9	0	-99.0	726	17.3	0	-99.0
02t	10	727	19.5	727	34.5	744	16.6	744	34.1	672	16.5	672	35.5	727	17.7	727	34.3
02b	32	249	21.6	249	35.2	0	-99.0	0	-99.0	0	-99.0	0	-99.0	51	17.8	0	-99.0
03t	10	473	21.3	473	35.6	744	19.7	744	35.2	672	17.8	672	35.1	724	18.8	724	34.6
03m	33	725	22.0	725	35.8	744	20.0	744	35.9	672	17.7	432	35.9	679	18.8	486	35.9
03b	58	474	21.7	0	-99.0	744	20.1	0	-99.0	672	17.2	0	-99.0	725	18.3	46	36.2
04t	14	724	22.8	255	36.3	744	21.4	0	-99.0	672	20.7	0	-99.0	683	20.5	0	-99.0
04m	100	724	19.0	724	36.4	744	19.4	744	36.5	672	19.4	672	36.2	724	18.8	664	36.0
04b	190	726	15.0	707	36.0	744	14.6	641	35.9	672	14.8	538	35.9	683	15.1	546	36.0
05t	14	452	22.5	0	-99.0	744	21.4	0	-99.0	672	19.7	0	-99.0	634	20.0	0	-99.0
05m	100	725	18.8	725	36.4	744	19.5	744	36.3	672	18.8	672	36.0	635	18.8	635	36.0
05b	190	451	14.7	451	35.9	744	14.2	744	36.1	672	14.5	672	36.3	635	13.8	635	36.7
06t	14	724	21.5	279	35.3	744	21.2	0	-99.0	672	20.1	0	-99.0	724	20.3	95	36.1
06m	100	676	19.0	676	36.5	744	18.8	744	36.3	672	18.7	672	36.0	724	18.8	724	35.8
06b	190	724	15.3	724	36.0	744	14.9	744	35.8	672	15.5	672	35.9	724	15.3	724	35.9
07t	14	493	22.8	0	-99.0	744	21.4	0	-99.0	672	20.3	0	-99.0	724	20.4	104	36.1
07m	100	724	19.4	724	36.2	744	19.3	744	35.9	672	18.9	672	35.6	724	19.6	724	35.5
07b	190	724	15.1	724	36.0	744	14.7	744	35.9	672	15.2	672	36.0	725	15.3	725	36.0
08t	14	715	23.0	203	36.1	744	21.3	0	-99.0	672	21.0	0	-99.0	724	20.6	112	36.0
08m	100	715	19.0	715	36.6	744	19.3	744	36.4	672	19.1	672	36.3	724	19.1	724	36.1
08b	190	716	15.1	716	36.1	744	14.5	744	36.1	672	15.0	672	36.2	724	14.9	724	36.2
09t	14	724	22.6	724	36.2	744	21.0	744	36.1	672	21.4	672	36.1	723	21.0	723	36.1
09m	100	527	19.1	527	36.6	744	18.8	744	36.5	672	19.2	672	36.4	724	19.1	724	36.4
09b	190	725	15.1	725	36.2	744	14.2	744	36.1	672	15.0	647	36.3	666	14.9	614	36.3
10t	14	545	22.6	545	36.4	744	20.5	744	36.3	672	20.4	672	36.4	724	20.2	724	36.3
10m	100	725	19.0	725	36.7	744	18.9	744	36.5	672	19.3	672	36.4	724	18.9	724	36.4
10b	190	725	15.2	725	36.3	744	14.6	682	36.5	672	15.2	568	36.6	722	15.3	128	36.2
11t	14	557	22.9	557	36.4	744	21.0	744	36.4	672	20.6	672	36.4	724	20.9	724	36.4
11m	100	558	19.2	558	36.6	663	19.8	663	36.5	672	19.8	672	36.5	724	19.5	724	36.5
11b	190	769	15.2	769	36.1	744	14.6	744	36.0	672	15.1	672	36.1	724	15.0	724	36.1
12t	14	141	24.7	141	36.4	0	-99.0	0	-99.0	0	-99.0	0	-99.0	0	-99.0	0	-99.0
12m	100	142	19.8	142	36.1	0	-99.0	0	-99.0	0	-99.0	0	-99.0	0	-99.0	0	-99.0
12b	490	142	9.2	0	-99.0	0	-99.0	0	-99.0	0	-99.0	0	-99.0	0	-99.0	0	-99.0
13t	14	587	22.5	587	35.9	744	21.0	744	36.1	672	20.9	672	36.3	723	21.8	723	36.4
13m	100	724	18.7	724	36.5	744	18.7	744	36.5	672	19.2	672	36.4	723	19.3	670	36.3
13b	190	726	14.6	726	35.9	744	13.5	744	35.8	672	14.4	672	36.1	724	14.7	724	36.2
14t	10	592	20.8	592	34.5	744	19.1	744	35.2	649	19.7	649	36.2	717	20.1	717	35.8
14m	26	723	21.8	130	35.2	744	19.6	0	-99.0	650	19.5	0	-99.0	566	19.8	0	-99.0
14b	40	720	22.3	0	-99.0	744	20.1	0	-99.0	651	19.3	0	-99.0	718	19.7	0	-99.0
15t	10	727	19.8	599	31.9	744	18.3	744	34.3	654	19.1	654	35.9	726	19.7	726	33.8
15b	17	727	22.3	599	35.3	744	19.5	744	35.4	655	19.1	327	36.1	727	19.6	0	-99.0
16t	10	727	19.1	601	30.3	744	16.2	744	31.4	654	17.1	654	30.8	727	18.6	727	31.7
16b	14	602	20.6	0	-99.0	744	16.9	0	-99.0	651	17.8	0	-99.0	727	18.9	0	-99.0
17t	3	724	15.9	623	25.1	744	13.3	744	27.3	654	14.6	654	24.8	665	17.3	665	21.4
17b	6	726	17.7	0	-99.0	744	14.2	0	-99.0	655	15.6	0	-99.0	536	17.5	0	-99.0
18t	8	726	18.3	621	31.5	744	15.7	744	30.8	296	15.6	296	31.1	0	-99.0	0	-99.0
18b	19	278	20.9	106	32.0	0	-99.0	0	-99.0	314	17.7	0	-99.0	727	18.4	0	-99.0
19t	3	722	21.8	722	35.4	744	19.2	744	35.3	344	19.6	344	36.6	182	20.1	182	34.2
19m	20	612	21.7	0	-99.0	271	19.5	0	-99.0	0	-99.0	0	-99.0	181	19.6	181	36.0
19b	45	169	22.7	0	-99.0	0	-99.0	0	-99.0	306	19.3	0	-99.0	726	19.4	0	-99.0
20t	3	509	14.7	0	-99.0	744	12.7	0	-99.0	551	13.5	0	-99.0	723	16.8	0	-99.0
20b	13	510	15.7	0	-99.0	744	13.3	0	-99.0	554	14.2	0	-99.0	727	16.6	0	-99.0
21t	14	724	19.1	724	34.7	744	16.4	744	34.5	654	16.2	654	34.6	732	17.4	732	34.0
21b	22	0	-99.0	0	-99.0	0	-99.0	0	-99.0	380	16.5	380	34.5	732	17.5	732	34.6
22t	3	517	21.2	517	35.2	744	19.3	744	34.9	649	19.1	649	35.0	735	19.2	349	35.0
22m	20	725	21.7	725	36.3	744	19.4	744	36.4	650	18.8	650	36.0	736	18.6	736	36.0
22b	48	725	21.6	208	36.4	744	19.1	0	-99.0	256	18.4	0	-99.0	0	-99.0	0	-99.0
23t	10	502	16.1	0	-99.0	744	13.6	0	-99.0	217	12.4	0	-99.0	19	18.2	0	-99.0
23b	13	726	17.0	0	-99.0	744	13.9	0	-99.0	222	13.1	0	-99.0	0	-99.0	0	-99.0
24t	10	726	18.2	726	33.9	744	15.2	744	33.8	655	15.7	655	34.2	727	17.1	727	33.6
24b	25	644	19.2	502	34.8	744	16.2	744	34.6	655	16.2	655	35.0	727	17.4	701	35.0
25t	11	0	-99.0	0	-99.0	0	-99.0	0	-99.0	0	-99.0	0	-99.0	0	-99.0	0	-99.0
25m	20	228	20.6	0	-99.0	0	-99.0	0	-99.0	0	-99.0	0	-99.0	0	-99.0	0	-99.0
25b	29	228	20.5	228	35.8	0	-99.0	0	-99.0	0	-99.0	0	-99.0	0	-99.0	0	-99.0
44t	13	0	-99.0	0	-99.0	0	-99.0	0	-99.0	0	-99.0	0	-99.0	0	-99.0	0	-99.0
44b	55	0	-99.0	0	-99.0	0	-99.0	0	-99.0	0	-99.0	0	-99.0	0	-99.0	0	-99.0
45t	12	0	-99.0	0	-99.0	0	-99.0	0	-99.0	0	-99.0	0	-99.0	0	-99.0	0	-99.0
45m	84	0	-99.0	0	-99.0	0	-99.0	0	-99.0	0	-99.0	0	-99.0	0	-99.0	0	-99.0
46t	14	0	-99.0	0	-99.0	0	-99.0	0	-99.0	0	-99.0	0	-99.0	0	-99.0	0	-99.0
46m	50	0	-99.0	0	-99.0	0	-99.0	0	-99.0	0	-99.0	0	-99.0	0	-99.0	0	-99.0
46b	84	0	-99.0	0	-99.0	0	-99.0	0	-99.0	0	-99.0	0	-99.0	0	-99.0	0	-99.0
47t	12	0	-99.0	0	-99.0	0	-99.0	0	-99.0	0	-99.0	0	-99.0	0	-99.0	0	-99.0
47m	100	0	-99.0	0	-99.0	0	-99.0	0	-99.0	0	-99.0	0	-99.0	0	-99.0	0	-99.0
47b	190	0	-99.0	0	-99.0	0	-99.0	0	-99.0	0	-99.0	0	-99.0	0	-99.0	0	-99.0
48t	14	562	23.2	562	36.3	744	21.3	744	36.4	672	21.0	672	36.4	723	21.0	723	36.4
48m	100	562	19.6	562	36.5	744	19.1	744	36.6	672	19.5	672	36.6	724	18.9	724	36.4
48b	190	0	-99.0	0	-99.0	0	-99.0	0	-99.0	0	-99.0	0	-99.0	142	15.5	142	36.2
49t	14	723	23.2	262	33.1	744	21.5	0	-99.0	672	20.1	0	-99.0	723	20.3	35	36.3
49m	100	722	18.8	722	36.4	744	19.8	744	36.4	672	19.1	672	36.2	723	19.0	723	36.2
49b	490	722	8.4	722	35.1	744	8.1	744	35.0	672	8.0	672	35.0	688	8.4	688	35.1

Table I-3. Current meter temperature and salinity statistics for 3-hr low-passed filtered data (continued).

		April 1994				May 1994				June 1994				July 1994			
No.	h	N_T	$\bar{T}$	N_S	$\bar{S}$	N_T	$\bar{T}$	N_S	$\bar{S}$	N_T	$\bar{T}$	N_S	$\bar{S}$	N_T	$\bar{T}$	N_S	$\bar{S}$
01t	10	711	20.5	711	27.9	0	-99.0	0	-99.0	0	-99.0	0	-99.0	51	25.5	0	-99.0
01b	12	720	20.5	0	-99.0	744	24.0	0	-99.0	720	25.9	0	-99.0	676	24.0	0	-99.0
02t	10	720	19.5	720	33.5	744	23.7	329	32.3	720	26.7	0	-99.0	727	26.0	48	36.5
02b	32	720	18.9	0	-99.0	744	19.9	0	-99.0	720	20.3	0	-99.0	603	20.9	48	31.7
03t	10	720	20.3	720	34.6	744	24.8	744	32.8	720	28.0	720	32.1	724	28.1	724	36.3
03m	33	0	-99.0	0	-99.0	0	-99.0	0	-99.0	0	-99.0	0	-99.0	0	-99.0	0	-99.0
03b	58	694	19.4	694	36.0	684	19.6	329	35.9	666	19.7	125	36.7	670	20.4	168	36.6
04t	14	0	-99.0	0	-99.0	0	-99.0	0	-99.0	0	-99.0	0	-99.0	29	28.9	29	36.3
04m	100	720	18.8	720	36.3	77	19.3	77	36.4	0	-99.0	0	-99.0	29	18.8	29	36.4
04b	190	0	-99.0	0	-99.0	0	-99.0	0	-99.0	0	-99.0	0	-99.0	29	14.1	29	35.8
05t	14	0	-99.0	0	-99.0	0	-99.0	0	-99.0	0	-99.0	0	-99.0	0	-99.0	0	-99.0
05m	100	0	-99.0	0	-99.0	0	-99.0	0	-99.0	0	-99.0	0	-99.0	0	-99.0	0	-99.0
05b	190	0	-99.0	0	-99.0	0	-99.0	0	-99.0	0	-99.0	0	-99.0	0	-99.0	0	-99.0
06t	14	720	21.7	720	35.9	744	23.7	744	35.5	720	26.3	720	34.7	724	28.7	724	36.0
06m	100	720	19.1	720	36.3	744	19.0	638	36.4	720	18.6	0	-99.0	725	19.3	712	36.5
06b	190	720	15.5	720	36.0	744	15.3	744	35.9	720	14.8	720	35.7	665	14.4	665	35.7
07t	14	720	21.7	720	36.0	744	24.0	744	35.1	720	26.6	720	34.8	725	29.0	725	35.8
07m	100	720	19.1	720	36.2	744	19.4	744	36.2	720	19.1	720	36.4	725	19.2	725	36.5
07b	190	720	15.8	720	36.1	744	15.5	359	36.2	720	15.3	0	-99.0	725	14.8	66	35.9
08t	14	720	21.6	720	36.0	744	24.9	744	34.7	720	27.5	720	33.0	724	29.2	724	35.1
08m	100	720	19.1	720	36.3	744	19.3	744	36.3	720	18.9	720	36.4	725	19.3	725	36.4
08b	190	720	15.6	720	36.3	744	15.1	744	36.1	720	14.8	720	35.8	725	14.2	725	35.6
09t	14	720	21.6	720	36.0	744	25.1	744	35.2	720	27.0	720	34.1	642	29.1	642	34.1
09m	100	720	18.7	720	36.4	744	19.4	744	36.5	720	19.1	720	36.4	725	18.9	725	36.3
09b	190	720	15.6	720	36.1	744	15.1	744	35.9	720	14.7	720	35.7	725	14.2	333	35.7
10t	14	720	22.2	720	36.2	744	25.0	744	35.8	720	26.1	720	34.7	724	28.9	213	34.8
10m	100	464	18.8	464	36.6	0	-99.0	0	-99.0	0	-99.0	0	-99.0	90	19.3	90	36.4
10b	190	720	15.7	720	36.2	744	15.2	744	36.1	720	14.6	720	36.0	724	14.4	724	35.8
11t	14	720	22.8	720	36.3	744	25.6	744	35.8	720	26.5	720	35.0	707	29.0	707	34.0
11m	100	720	19.4	720	36.5	744	19.8	744	36.3	720	19.2	720	36.3	708	19.3	708	36.3
11b	190	720	15.7	720	36.3	744	14.9	744	36.1	720	14.5	720	36.0	525	14.4	525	35.8
12t	14	0	-99.0	0	-99.0	0	-99.0	0	-99.0	0	-99.0	0	-99.0	0	-99.0	0	-99.0
12m	100	0	-99.0	0	-99.0	0	-99.0	0	-99.0	0	-99.0	0	-99.0	0	-99.0	0	-99.0
12b	490	0	-99.0	0	-99.0	0	-99.0	0	-99.0	0	-99.0	0	-99.0	0	-99.0	0	-99.0
13t	14	720	23.3	720	36.1	744	25.7	744	35.9	720	27.3	364	35.4	724	29.3	108	33.6
13m	100	720	19.3	720	36.5	744	19.6	744	36.3	720	18.8	720	36.3	725	18.9	725	36.3
13b	190	720	16.0	528	36.3	744	14.5	744	36.0	720	14.4	720	36.0	725	14.2	725	35.9
14t	10	720	22.2	720	35.7	723	25.5	723	35.6	720	27.4	720	34.1	718	29.0	718	31.0
14m	26	0	-99.0	0	-99.0	25	24.9	25	36.1	720	24.7	720	36.0	614	25.3	614	35.8
14b	40	720	20.2	0	-99.0	701	21.1	0	-99.0	0	-99.0	0	-99.0	105	21.7	0	-99.0
15t	10	720	21.8	720	35.3	726	25.1	726	35.4	720	27.4	720	33.5	608	28.8	608	27.1
15b	17	720	20.6	0	-99.0	726	22.6	0	-99.0	720	22.3	0	-99.0	726	24.0	0	-99.0
16t	10	720	21.1	720	32.4	724	24.3	724	33.9	720	24.7	720	35.7	425	26.2	425	34.9
16b	14	720	21.2	0	-99.0	727	24.3	0	-99.0	720	24.5	0	-99.0	604	26.3	0	-99.0
17t	3	0	-99.0	0	-99.0	44	26.9	44	17.9	120	26.7	120	16.9	171	29.1	171	30.9
17b	6	698	21.7	0	-99.0	682	25.9	0	-99.0	0	-99.0	0	-99.0	0	-99.0	0	-99.0
18t	8	0	-99.0	0	-99.0	41	26.2	41	33.9	720	26.7	720	34.0	726	28.2	726	30.6
18b	19	720	19.7	0	-99.0	723	23.6	0	-99.0	720	24.3	0	-99.0	726	24.9	167	35.7
19t	3	720	21.4	720	36.0	726	25.2	92	35.8	685	27.7	685	32.9	726	29.6	726	26.8
19m	20	720	20.9	720	36.1	679	23.2	679	36.1	0	-99.0	0	-99.0	162	29.1	162	34.3
19b	45	720	20.0	0	-99.0	689	20.3	0	-99.0	0	-99.0	0	-99.0	163	21.6	0	-99.0
20t	3	720	20.7	720	22.7	727	26.0	668	20.4	689	28.4	528	21.4	705	29.4	0	-99.0
20b	13	720	20.4	0	-99.0	727	24.8	0	-99.0	720	27.2	0	-99.0	744	28.7	0	-99.0
21t	14	714	20.0	714	33.7	726	23.8	726	34.9	720	26.7	720	32.5	744	28.9	744	31.9
21b	22	715	19.7	715	34.7	657	22.6	657	35.5	0	-99.0	0	-99.0	0	-99.0	0	-99.0
22t	3	710	20.6	221	35.9	724	25.0	60	31.6	688	28.2	688	29.9	697	29.4	697	32.0
22m	20	709	19.9	0	-99.0	721	22.8	60	35.6	720	24.3	720	34.2	735	28.0	735	33.7
22b	48	709	19.2	709	35.7	666	20.0	666	35.3	0	-99.0	0	-99.0	0	-99.0	0	-99.0
23t	10	720	20.1	0	-99.0	744	24.4	0	-99.0	701	27.0	0	-99.0	727	27.8	0	-99.0
23b	13	0	-99.0	0	-99.0	0	-99.0	0	-99.0	695	25.9	0	-99.0	726	27.1	0	-99.0
24t	10	720	20.2	720	32.6	744	24.6	744	30.1	701	27.9	701	30.1	724	28.5	724	35.2
24b	25	720	19.6	0	-99.0	744	21.4	0	-99.0	4	22.0	0	-99.0	0	-99.0	0	-99.0
25t	11	0	-99.0	0	-99.0	0	-99.0	0	-99.0	0	-99.0	0	-99.0	0	-99.0	0	-99.0
25m	20	0	-99.0	0	-99.0	0	-99.0	0	-99.0	0	-99.0	0	-99.0	0	-99.0	0	-99.0
25b	29	0	-99.0	0	-99.0	0	-99.0	0	-99.0	0	-99.0	0	-99.0	0	-99.0	0	-99.0
44t	13	0	-99.0	0	-99.0	0	-99.0	0	-99.0	0	-99.0	0	-99.0	0	-99.0	0	-99.0
44b	55	0	-99.0	0	-99.0	0	-99.0	0	-99.0	0	-99.0	0	-99.0	0	-99.0	0	-99.0
45t	12	0	-99.0	0	-99.0	0	-99.0	0	-99.0	0	-99.0	0	-99.0	0	-99.0	0	-99.0
45m	84	0	-99.0	0	-99.0	0	-99.0	0	-99.0	0	-99.0	0	-99.0	0	-99.0	0	-99.0
46t	14	0	-99.0	0	-99.0	0	-99.0	0	-99.0	0	-99.0	0	-99.0	0	-99.0	0	-99.0
46m	50	0	-99.0	0	-99.0	0	-99.0	0	-99.0	0	-99.0	0	-99.0	0	-99.0	0	-99.0
46b	84	0	-99.0	0	-99.0	0	-99.0	0	-99.0	0	-99.0	0	-99.0	0	-99.0	0	-99.0
47t	12	0	-99.0	0	-99.0	0	-99.0	0	-99.0	0	-99.0	0	-99.0	0	-99.0	0	-99.0
47m	100	0	-99.0	0	-99.0	0	-99.0	0	-99.0	0	-99.0	0	-99.0	0	-99.0	0	-99.0
47b	190	0	-99.0	0	-99.0	0	-99.0	0	-99.0	0	-99.0	0	-99.0	0	-99.0	0	-99.0
48t	14	720	22.8	720	36.3	744	25.7	744	35.8	720	27.1	720	35.0	725	28.7	725	33.5
48m	100	720	18.8	720	36.5	744	19.4	744	36.4	720	18.9	720	36.4	665	18.7	665	36.3
48b	190	720	15.9	720	36.2	744	14.3	744	36.0	720	14.4	720	35.9	566	14.1	433	35.7
49t	14	720	21.8	720	36.0	744	23.9	744	35.2	720	26.6	720	34.4	724	28.4	724	36.3
49m	100	720	18.7	720	36.4	744	18.4	744	36.5	720	18.3	720	36.4	724	18.9	724	36.4
49b	490	0	-99.0	0	-99.0	0	-99.0	0	-99.0	0	-99.0	0	-99.0	23	8.1	23	35.1

Table I-3. Current meter temperature and salinity statistics for 3-hr low-passed filtered data (continued).

		August 1994				September 1994				October 1994				November 1994			
No.	h	N_T	$\bar{T}$	N_S	$\bar{S}$	N_T	$\bar{T}$	N_S	$\bar{S}$	N_T	$\bar{T}$	N_S	$\bar{S}$	N_T	$\bar{T}$	N_S	$\bar{S}$
01t	10	744	28.9	0	-99.0	720	29.1	0	-99.0	744	26.0	0	-99.0	720	23.6	0	-99.0
01b	12	0	-99.0	0	-99.0	0	-99.0	0	-99.0	0	-99.0	0	-99.0	0	-99.0	0	-99.0
02t	10	744	28.1	744	36.4	720	28.9	720	34.8	744	26.8	744	33.3	720	25.0	720	33.0
02b	32	744	26.0	744	32.5	720	28.8	720	32.8	744	27.3	744	32.0	618	26.1	618	32.5
03t	10	744	28.7	744	36.3	720	29.0	720	36.3	744	27.3	744	34.1	720	25.5	720	34.0
03m	33	0	-99.0	0	-99.0	0	-99.0	0	-99.0	0	-99.0	0	-99.0	0	-99.0	0	-99.0
03b	58	744	22.3	744	36.6	720	23.6	720	36.6	744	25.6	744	36.7	720	24.2	720	36.9
04t	14	744	28.7	744	36.4	720	29.0	720	36.5	744	27.4	744	36.2	720	26.2	720	36.2
04m	100	744	19.1	744	36.4	720	20.8	720	36.4	744	19.5	744	36.4	720	20.9	720	36.3
04b	190	744	14.4	744	35.7	720	14.8	720	34.8	744	14.7	744	33.5	720	15.1	720	33.2
05t	14	0	-99.0	0	-99.0	0	-99.0	0	-99.0	334	27.6	334	36.8	0	-99.0	0	-99.0
05m	100	0	-99.0	0	-99.0	0	-99.0	0	-99.0	711	20.0	0	-99.0	720	19.4	0	-99.0
05b	190	0	-99.0	0	-99.0	0	-99.0	0	-99.0	712	14.9	712	36.2	720	15.0	720	36.2
06t	14	744	28.9	744	36.3	720	28.7	720	36.2	744	27.2	744	35.5	720	25.4	720	35.1
06m	100	744	19.2	744	36.5	720	18.9	720	36.5	744	19.4	744	36.3	720	19.1	720	36.3
06b	190	711	14.6	0	-99.0	720	14.6	0	-99.0	744	15.1	0	-99.0	720	15.3	0	-99.0
07t	14	744	28.9	744	36.5	720	29.0	720	35.8	744	27.2	744	35.5	720	25.7	720	35.7
07m	100	744	18.9	744	36.6	720	18.9	720	36.6	744	19.0	744	36.5	720	18.7	720	36.5
07b	190	744	14.5	343	36.0	720	14.6	0	-99.0	744	15.0	0	-99.0	720	15.2	0	-99.0
08t	14	744	28.9	744	36.3	720	29.0	720	36.1	744	27.2	744	36.0	720	26.1	720	36.0
08m	100	744	18.7	744	36.6	720	18.8	720	36.6	744	18.8	744	36.3	720	19.4	720	36.3
08b	190	744	14.5	744	36.0	720	14.6	720	36.0	744	15.1	744	35.8	720	15.5	720	35.6
09t	14	0	-99.0	0	-99.0	0	-99.0	0	-99.0	0	-99.0	0	-99.0	0	-99.0	0	-99.0
09m	100	744	18.9	744	36.5	720	19.0	720	36.5	744	18.9	744	36.5	720	18.3	720	36.4
09b	190	744	14.4	744	36.1	720	14.4	720	36.1	744	15.1	744	36.1	720	15.3	720	36.1
10t	14	744	29.2	744	35.5	720	29.1	720	35.6	744	26.8	744	35.0	720	25.6	720	35.5
10m	100	744	19.0	744	36.4	720	19.0	720	36.4	744	18.1	744	36.4	720	18.9	720	36.3
10b	190	744	14.5	744	35.9	720	14.8	720	36.0	744	15.1	744	36.0	720	15.4	720	35.9
11t	14	744	29.4	744	34.1	670	29.0	665	34.3	744	27.2	0	-99.0	720	26.9	0	-99.0
11m	100	744	18.9	744	36.5	669	18.0	669	36.5	744	18.1	744	36.7	720	19.5	720	36.7
11b	190	744	14.4	744	35.9	670	14.6	670	36.0	744	15.0	744	36.1	657	15.6	657	36.2
12t	14	0	-99.0	0	-99.0	0	-99.0	0	-99.0	0	-99.0	0	-99.0	0	-99.0	0	-99.0
12m	100	0	-99.0	0	-99.0	0	-99.0	0	-99.0	0	-99.0	0	-99.0	0	-99.0	0	-99.0
12b	490	0	-99.0	0	-99.0	0	-99.0	0	-99.0	0	-99.0	0	-99.0	0	-99.0	0	-99.0
13t	14	744	28.6	744	34.5	720	28.5	720	35.9	744	27.4	744	35.9	720	25.8	720	35.9
13m	100	744	18.2	744	36.5	720	18.4	720	36.6	744	18.8	744	36.6	720	18.0	720	36.4
13b	190	744	14.3	744	35.9	720	14.9	720	36.0	744	14.7	744	36.0	720	15.2	720	36.1
14t	10	744	28.8	744	32.4	700	28.7	685	34.7	744	27.5	0	-99.0	720	25.5	0	-99.0
14m	26	0	-99.0	0	-99.0	0	-99.0	0	-99.0	0	-99.0	0	-99.0	0	-99.0	0	-99.0
14b	40	744	22.0	0	-99.0	700	24.0	0	-99.0	744	26.5	0	-99.0	720	25.2	0	-99.0
15t	10	0	-99.0	0	-99.0	19	27.9	19	32.2	744	26.5	744	34.1	720	24.5	720	35.1
15b	17	744	25.3	0	-99.0	683	27.9	0	-99.0	0	-99.0	0	-99.0	0	-99.0	0	-99.0
16t	10	744	28.3	744	30.8	680	28.7	680	30.1	0	-99.0	0	-99.0	0	-99.0	0	-99.0
16b	14	0	-99.0	0	-99.0	0	-99.0	0	-99.0	0	-99.0	0	-99.0	0	-99.0	0	-99.0
17t	3	744	29.2	182	32.0	653	28.8	0	-99.0	654	24.2	246	34.3	254	22.9	0	-99.0
17b	6	0	-99.0	0	-99.0	0	-99.0	0	-99.0	0	-99.0	0	-99.0	0	-99.0	0	-99.0
18t	8	744	29.0	744	30.3	657	29.0	657	29.5	0	-99.0	0	-99.0	0	-99.0	0	-99.0
18b	19	232	25.4	232	35.6	0	-99.0	0	-99.0	0	-99.0	0	-99.0	0	-99.0	0	-99.0
19t	3	744	28.9	135	29.5	702	28.6	0	-99.0	742	27.0	742	35.3	720	25.5	150	36.0
19m	20	744	28.0	744	36.5	703	28.9	703	35.9	742	26.9	0	-99.0	75	26.0	0	-99.0
19b	45	744	21.7	0	-99.0	703	23.1	0	-99.0	0	-99.0	0	-99.0	0	-99.0	0	-99.0
20t	3	723	29.4	297	32.5	720	28.5	0	-99.0	727	24.5	348	28.7	701	21.7	0	-99.0
20b	13	11	29.2	0	-99.0	0	-99.0	0	-99.0	665	24.6	0	-99.0	703	22.2	0	-99.0
21t	14	724	29.1	724	34.4	720	28.9	720	32.3	726	26.4	726	32.9	708	24.0	708	33.5
21b	22	720	28.4	720	35.4	720	29.3	720	34.5	727	26.6	727	34.3	709	24.3	709	35.2
22t	3	733	29.0	733	33.2	720	28.8	720	34.1	723	26.9	167	33.8	720	25.2	720	35.3
22m	20	0	-99.0	0	-99.0	0	-99.0	0	-99.0	683	27.3	0	-99.0	720	25.6	0	-99.0
22b	48	0	-99.0	0	-99.0	0	-99.0	0	-99.0	376	26.4	0	-99.0	0	-99.0	0	-99.0
23t	10	744	29.0	744	34.0	720	28.9	720	28.0	726	25.0	726	28.4	720	22.3	720	27.7
23b	13	0	-99.0	0	-99.0	0	-99.0	0	-99.0	696	25.1	0	-99.0	720	22.7	0	-99.0
24t	10	743	29.0	743	34.9	720	28.9	720	33.1	725	26.0	725	32.3	720	23.7	720	33.4
24b	25	743	28.7	0	-99.0	720	29.0	0	-99.0	727	26.4	0	-99.0	631	24.4	0	-99.0
25t	11	0	-99.0	0	-99.0	0	-99.0	0	-99.0	0	-99.0	0	-99.0	0	-99.0	0	-99.0
25m	20	0	-99.0	0	-99.0	0	-99.0	0	-99.0	0	-99.0	0	-99.0	0	-99.0	0	-99.0
25b	29	0	-99.0	0	-99.0	0	-99.0	0	-99.0	0	-99.0	0	-99.0	0	-99.0	0	-99.0
44t	13	0	-99.0	0	-99.0	0	-99.0	0	-99.0	0	-99.0	0	-99.0	0	-99.0	0	-99.0
44b	55	0	-99.0	0	-99.0	0	-99.0	0	-99.0	0	-99.0	0	-99.0	0	-99.0	0	-99.0
45t	12	0	-99.0	0	-99.0	0	-99.0	0	-99.0	0	-99.0	0	-99.0	0	-99.0	0	-99.0
45m	84	0	-99.0	0	-99.0	0	-99.0	0	-99.0	0	-99.0	0	-99.0	0	-99.0	0	-99.0
46t	14	0	-99.0	0	-99.0	0	-99.0	0	-99.0	0	-99.0	0	-99.0	0	-99.0	0	-99.0
46m	50	0	-99.0	0	-99.0	0	-99.0	0	-99.0	0	-99.0	0	-99.0	0	-99.0	0	-99.0
46b	84	0	-99.0	0	-99.0	0	-99.0	0	-99.0	0	-99.0	0	-99.0	0	-99.0	0	-99.0
47t	12	0	-99.0	0	-99.0	0	-99.0	0	-99.0	0	-99.0	0	-99.0	0	-99.0	0	-99.0
47m	100	0	-99.0	0	-99.0	0	-99.0	0	-99.0	0	-99.0	0	-99.0	0	-99.0	0	-99.0
47b	190	0	-99.0	0	-99.0	0	-99.0	0	-99.0	0	-99.0	0	-99.0	0	-99.0	0	-99.0
48t	14	744	29.1	744	32.3	720	26.7	720	33.5	744	27.2	744	34.3	720	26.0	720	35.5
48m	100	744	18.0	744	36.4	720	17.4	720	36.4	744	18.2	744	36.4	720	18.5	720	36.4
48b	190	744	14.3	0	-99.0	720	14.6	0	-99.0	744	14.6	0	-99.0	383	15.4	0	-99.0
49t	14	744	28.9	744	36.1	720	29.1	720	36.0	744	27.7	744	36.0	720	26.1	720	35.5
49m	100	744	19.0	744	36.4	720	20.1	720	36.4	744	20.3	744	36.4	720	19.7	720	36.3
49b	490	744	8.7	744	35.3	720	8.9	720	35.3	744	8.7	744	35.3	720	8.9	720	35.3

Table I-3. Current meter temperature and salinity statistics for 3-hr low-passed filtered data (continued).

No.	h	December 1994 N_T	$\bar{T}$	N_S	$\bar{S}$
01t	10	126	20.6	0	-99.0
01b	12	0	-99.0	0	-99.0
02t	10	129	22.6	129	32.8
02b	32	0	-99.0	0	-99.0
03t	10	132	23.9	132	34.8
03m	33	0	-99.0	0	-99.0
03b	58	91	24.5	91	36.2
04t	14	136	25.3	136	36.1
04m	100	136	19.9	136	36.3
04b	190	96	15.3	96	33.0
05t	14	0	-99.0	0	-99.0
05m	100	140	19.1	0	-99.0
05b	190	141	15.7	141	36.3
06t	14	111	24.5	111	36.1
06m	100	111	19.2	111	36.2
06b	190	26	15.7	0	-99.0
07t	14	95	24.8	95	35.9
07m	100	95	19.3	95	36.5
07b	190	95	15.9	0	-99.0
08t	14	89	24.4	89	36.0
08m	100	88	18.5	88	36.3
08b	190	88	15.9	88	35.6
09t	14	0	-99.0	0	-99.0
09m	100	12	19.0	12	36.4
09b	190	12	15.0	12	35.9
10t	14	19	24.4	19	34.2
10m	100	18	19.8	18	36.3
10b	190	18	15.2	18	35.8
11t	14	25	26.2	0	-99.0
11m	100	25	20.1	25	36.7
11b	190	0	-99.0	0	-99.0
12t	14	0	-99.0	0	-99.0
12m	100	0	-99.0	0	-99.0
12b	490	0	-99.0	0	-99.0
13t	14	62	24.8	62	36.2
13m	100	62	18.5	62	36.5
13b	190	62	15.8	62	36.1
14t	10	59	24.2	0	-99.0
14m	26	0	-99.0	0	-99.0
14b	40	60	24.0	0	-99.0
15t	10	56	22.7	56	34.5
15b	17	0	-99.0	0	-99.0
16t	10	0	-99.0	0	-99.0
16b	14	0	-99.0	0	-99.0
17t	3	0	-99.0	0	-99.0
17b	6	0	-99.0	0	-99.0
18t	8	0	-99.0	0	-99.0
18b	19	0	-99.0	0	-99.0
19t	3	31	23.7	0	-99.0
19m	20	0	-99.0	0	-99.0
19b	45	0	-99.0	0	-99.0
20t	3	0	-99.0	0	-99.0
20b	13	0	-99.0	0	-99.0
21t	14	0	-99.0	0	-99.0
21b	22	0	-99.0	0	-99.0
22t	3	5	23.8	5	35.6
22m	20	6	24.2	0	-99.0
22b	48	0	-99.0	0	-99.0
23t	10	104	19.1	104	29.6
23b	13	104	19.4	0	-99.0
24t	10	101	21.4	101	34.4
24b	25	0	-99.0	0	-99.0
25t	11	0	-99.0	0	-99.0
25m	20	0	-99.0	0	-99.0
25b	29	0	-99.0	0	-99.0
44t	13	0	-99.0	0	-99.0
44b	55	0	-99.0	0	-99.0
45t	12	0	-99.0	0	-99.0
45m	84	0	-99.0	0	-99.0
46t	14	0	-99.0	0	-99.0
46m	50	0	-99.0	0	-99.0
46b	84	0	-99.0	0	-99.0
47t	12	0	-99.0	0	-99.0
47m	100	0	-99.0	0	-99.0
47b	190	0	-99.0	0	-99.0
48t	14	69	25.2	69	36.3
48m	100	34	19.3	34	36.4
48b	190	0	-99.0	0	-99.0
49t	14	113	24.9	113	35.2
49m	100	113	19.3	113	36.4
49b	490	108	8.4	108	35.2

Table I-4. Current meter statistics: maximum speed and direction for 40-hr low-passed filtered data.

		April 1992			May 1992			June 1992			July 1992			August 1992			September 1992		
No.	h	day	v_M	θ_M	day	v_M	θ_M	day	v_M	θ_M	day	v_M	θ_M	day	v_M	θ_M	day	v_M	θ_M
01t	10	29	78	19	5	57	197	6	43	10	29	27	23	27	29	13	29	41	194
01b	12	29	24	350	8	26	164	4	9	336	-99	-99	-99	-99	-99	-99	-99	-99	-99
02t	10	29	36	34	22	61	189	16	49	12	6	44	20	16	24	197	30	64	198
02b	32	29	28	342	7	28	185	16	27	16	7	19	6	-99	-99	-99	29	45	186
03t	10	14	34	241	14	44	12	-99	-99	-99	22	21	106	26	36	204	29	51	218
03m	33	28	16	19	-99	-99	-99	-99	-99	-99	-99	-99	-99	-99	-99	-99	-99	-99	-99
03b	58	-99	-99	-99	-99	-99	-99	-99	-99	-99	21	10	177	30	15	194	30	36	191
04t	14	25	29	28	16	59	41	17	28	222	5	52	202	5	47	24	1	43	218
04m	100	28	16	68	18	27	24	16	21	217	6	36	212	28	38	197	3	31	205
04b	190	-99	-99	-99	-99	-99	-99	-99	-99	-99	31	14	182	28	57	196	3	42	212
05t	14	29	41	84	20	47	58	21	32	235	12	41	166	22	65	31	30	34	234
05m	100	28	13	49	22	31	51	20	20	230	31	26	261	7	32	60	30	42	237
05b	190	30	6	46	29	12	53	20	10	258	8	9	258	29	23	231	30	18	233
06t	14	30	27	84	27	55	88	28	46	90	10	75	43	4	55	47	29	50	256
06m	100	23	18	261	6	27	240	18	45	79	10	53	45	23	24	74	29	24	258
06b	190	15	10	278	29	19	263	27	18	58	2	32	267	25	21	257	21	12	264
07t	14	26	25	67	14	34	103	21	41	83	11	72	86	4	74	86	29	44	280
07m	100	22	15	240	24	23	249	28	19	253	11	63	72	-99	-99	-99	-99	-99	-99
07b	190	26	11	83	27	12	96	14	18	252	1	20	89	28	18	265	29	16	265
08t	14	30	34	100	1	35	100	18	53	113	15	44	124	31	29	245	1	27	263
08m	100	20	18	74	27	11	75	22	15	279	17	19	262	16	34	266	-99	-99	-99
08b	190	25	5	68	2	4	300	14	3	307	3	3	276	26	7	296	-99	-99	-99
09t	14	30	22	87	23	28	152	19	28	120	17	25	306	24	23	230	7	21	282
09m	100	22	19	258	1	18	66	23	14	305	28	13	226	25	14	279	20	25	277
09b	190	28	4	219	6	6	278	16	5	186	26	5	267	24	5	240	9	3	297
10t	14	27	24	148	31	21	357	27	19	50	19	34	176	24	35	267	9	27	237
10m	100	30	17	72	1	17	72	16	10	79	26	17	265	24	20	267	19	27	276
10b	190	20	3	285	2	5	285	20	3	303	25	4	303	5	2	311	23	11	111
11t	14	21	27	250	8	25	275	15	13	86	25	21	233	26	28	278	17	30	118
11m	100	20	8	229	6	8	242	17	5	162	25	12	257	24	12	240	28	23	267
11b	190	22	17	269	8	11	266	27	11	85	27	12	255	25	14	269	-99	-99	-99
12t	14	21	25	296	15	18	35	15	39	60	19	23	254	28	49	268	1	37	256
12m	100	22	18	269	6	18	308	20	38	65	28	25	245	31	49	245	1	49	246
12b	490	23	2	245	5	3	237	12	2	78	16	3	241	31	4	214	3	4	236
13t	14	19	29	244	12	25	53	14	41	66	15	42	146	27	61	260	28	22	287
13m	100	19	29	250	15	25	69	23	36	63	27	26	271	27	49	258	1	30	267
13b	190	20	14	247	5	18	244	12	14	49	27	11	247	30	25	202	23	24	53
14t	10	19	24	266	21	17	118	11	22	82	16	33	43	25	43	276	30	28	285
14m	26	25	21	86	9	15	87	11	18	103	7	20	111	-99	-99	-99	9	28	83
14b	40	19	19	244	9	18	72	11	10	85	29	13	73	26	40	284	-99	-99	-99
15t	10	19	12	72	7	19	266	30	21	57	1	37	77	3	47	75	30	41	252
15b	17	22	7	248	17	10	250	25	7	266	7	6	68	25	27	266	29	22	253
16t	10	22	13	224	23	20	248	20	12	65	1	17	70	-99	-99	-99	-99	-99	-99
16b	14	21	9	286	22	12	227	22	9	206	30	8	238	20	9	241	-99	-99	-99
17t	3	-99	-99	-99	-99	-99	-99	5	22	107	29	28	121	3	21	128	15	25	260
17b	6	-99	-99	-99	-99	-99	-99	-99	-99	-99	-99	-99	-99	-99	-99	-99	15	22	305
18t	8	18	37	298	21	32	292	11	22	80	3	30	117	26	61	108	15	47	293
18b	19	23	10	72	17	16	263	5	9	79	2	8	105	26	42	42	29	24	315
19t	3	28	24	273	1	6	9	19	17	264	31	18	152	25	34	220	30	49	286
19m	20	19	8	277	12	10	108	-99	-99	-99	30	21	76	27	14	211	-99	-99	-99
19b	45	-99	-99	-99	-99	-99	-99	28	4	273	30	7	97	27	17	208	-99	-99	-99
20t	3	-99	-99	-99	-99	-99	-99	16	26	38	27	30	62	4	18	326	-99	-99	-99
20b	13	30	15	176	17	15	181	30	16	12	3	25	122	26	24	58	29	32	265
21t	14	25	20	7	22	20	206	11	27	72	25	25	350	12	17	100	28	29	267
21b	22	17	11	199	20	19	196	21	12	60	12	14	54	24	14	176	29	24	264
22t	3	-99	-99	-99	-99	-99	-99	11	23	229	30	19	84	14	46	227	-99	-99	-99
22m	20	26	11	95	10	12	55	13	10	21	13	22	271	10	15	242	29	29	271
22b	48	-99	-99	-99	-99	-99	-99	30	5	253	31	10	41	27	12	237	28	17	231
23t	10	18	43	257	9	34	81	21	45	66	1	44	76	20	34	244	16	63	249
23b	13	29	19	55	10	23	79	21	20	60	3	22	85	27	29	64	1	5	250
24t	10	23	26	245	7	35	247	22	45	80	19	27	269	27	36	66	1	13	227
24b	25	25	15	49	25	13	18	4	13	15	28	19	39	27	30	33	1	5	220
25t	11	29	22	99	18	30	231	29	37	350	4	35	304	27	37	73	16	36	248
25m	20	23	17	262	7	25	224	23	36	190	3	21	304	27	31	61	16	39	246
25b	29	-99	-99	-99	-99	-99	-99	29	17	325	31	13	65	27	30	37	16	36	221
44t	13	15	31	238	21	34	281	22	48	55	10	42	65	26	30	231	29	53	235
44b	55	28	17	14	7	18	180	3	20	13	21	18	224	27	24	24	30	44	228
45t	12	28	39	26	19	46	61	28	29	323	12	42	161	-99	-99	-99	-99	-99	-99
45m	84	28	14	28	21	36	53	19	24	229	12	16	199	-99	-99	-99	-99	-99	-99
46t	14	28	20	359	27	45	61	14	55	57	20	27	287	3	29	239	30	36	264
46m	50	-99	-99	-99	-99	-99	-99	-99	-99	-99	30	30	264	2	28	242	30	32	231
46b	84	23	12	218	25	15	46	14	14	48	31	20	230	1	20	235	-99	-99	-99
47t	12	30	43	63	18	45	65	27	35	312	16	63	6	21	65	11	1	27	295
47m	100	-99	-99	-99	-99	-99	-99	-99	-99	-99	-99	-99	-99	-99	-99	-99	-99	-99	-99
47b	190	-99	-99	-99	-99	-99	-99	-99	-99	-99	-99	-99	-99	-99	-99	-99	-99	-99	-99
48t	14	29	29	108	1	24	79	25	22	77	16	37	79	26	29	225	26	23	328
48m	100	30	23	79	1	23	79	22	12	78	25	15	296	1	15	127	28	21	280
48b	190	-99	-99	-99	-99	-99	-99	-99	-99	-99	-99	-99	-99	-99	-99	-99	29	8	118
49t	14	13	21	26	18	49	72	30	68	30	3	87	53	5	81	53	11	26	162
49m	100	23	14	211	2	21	95	-99	-99	-99	-99	-99	-99	-99	-99	-99	-99	-99	-99
49b	490	20	10	156	4	7	146	-99	-99	-99	-99	-99	-99	-99	-99	-99	-99	-99	-99

Table I-4. Current meter statistics: maximum speed and direction for 40-hr low-passed filtered data (continued).

		October 1992			November 1992			December 1992			January 1993			February 1993			March 1993		
No.	h	day	v_M	θ_M	day	v_M	θ_M	day	v_M	θ_M	day	v_M	θ_M	day	v_M	θ_M	day	v_M	θ_M
01t	10	23	40	187	5	38	195	25	44	195	30	60	196	28	48	194	13	64	198
01b	12	23	39	174	4	38	189	6	30	190	-99	-99	-99	-99	-99	-99	-99	-99	-99
02t	10	1	63	196	14	44	185	6	45	197	26	50	207	5	43	204	13	81	205
02b	32	23	42	182	7	29	160	6	32	189	25	30	194	1	32	192	8	46	182
03t	10	3	52	204	4	34	221	-99	-99	-99	30	23	221	22	43	28	13	69	222
03m	33	23	30	183	9	30	177	-99	-99	-99	-99	-99	-99	-99	-99	-99	-99	-99	-99
03b	58	2	27	184	4	19	116	-99	-99	-99	-99	-99	-99	-99	-99	-99	-99	-99	-99
04t	14	5	38	228	-99	-99	-99	-99	-99	-99	24	29	254	13	77	358	6	45	33
04m	100	2	27	197	-99	-99	-99	-99	-99	-99	27	26	266	13	36	347	14	44	4
04b	190	2	41	210	3	6	5	-99	-99	-99	28	22	207	26	23	16	14	29	8
05t	14	3	49	257	1	35	72	-99	-99	-99	29	28	52	15	61	35	8	56	46
05m	100	1	41	238	20	18	56	-99	-99	-99	31	20	56	11	32	96	14	34	56
05b	190	9	26	54	20	17	46	-99	-99	-99	31	5	48	15	8	49	14	7	181
06t	14	1	39	267	30	31	90	-99	-99	-99	31	26	72	15	83	94	11	47	95
06m	100	1	19	260	13	29	65	-99	-99	-99	25	17	242	16	34	66	14	50	58
06b	190	1	9	261	24	21	257	-99	-99	-99	-99	-99	-99	-99	-99	-99	-99	-99	-99
07t	14	3	28	261	18	31	74	-99	-99	-99	23	68	76	25	65	83	2	57	84
07m	100	-99	-99	-99	-99	-99	-99	-99	-99	-99	-99	-99	-99	-99	-99	-99	-99	-99	-99
07b	190	5	18	266	11	15	83	-99	-99	-99	23	24	252	5	19	247	19	17	66
08t	14	30	31	109	9	25	70	-99	-99	-99	20	31	110	5	29	285	10	61	144
08m	100	29	8	170	4	22	91	-99	-99	-99	21	28	86	4	37	234	28	53	264
08b	190	29	2	3	15	4	83	-99	-99	-99	20	5	279	11	6	84	31	8	293
09t	14	10	28	100	3	32	67	4	16	117	-99	-99	-99	-99	-99	-99	-99	-99	-99
09m	100	11	20	72	13	23	67	10	13	61	31	15	72	1	14	74	7	15	60
09b	190	-99	-99	-99	-99	-99	-99	-99	-99	-99	24	6	10	4	11	280	27	10	268
10t	14	14	39	50	4	21	102	1	22	111	2	9	338	-99	-99	-99	-99	-99	-99
10m	100	4	24	263	10	12	72	2	12	74	1	10	78	16	4	38	14	14	46
10b	190	3	5	276	6	6	104	15	3	113	26	4	323	22	9	94	14	6	94
11t	14	12	29	69	10	32	92	8	27	265	25	19	280	22	20	101	13	29	239
11m	100	5	24	261	8	21	81	2	13	77	6	9	205	-99	-99	-99	-99	-99	-99
11b	190	-99	-99	-99	-99	-99	-99	-99	-99	-99	-99	-99	-99	-99	-99	-99	-99	-99	-99
12t	14	16	53	307	27	26	261	3	20	294	25	40	307	17	44	244	15	47	19
12m	100	28	33	246	20	21	259	31	15	52	28	24	269	17	46	225	1	18	271
12b	490	4	4	228	20	5	234	-99	-99	-99	-99	-99	-99	-99	-99	-99	-99	-99	-99
13t	14	28	54	247	5	51	267	5	36	264	26	33	227	17	36	257	16	50	36
13m	100	28	71	250	1	39	248	14	26	59	7	27	271	18	44	246	17	24	75
13b	190	11	50	49	19	23	257	16	15	232	31	24	227	18	28	243	18	17	215
14t	10	3	76	262	15	27	236	31	18	338	29	27	102	28	27	277	13	34	229
14m	26	3	56	262	4	25	108	1	7	98	29	23	92	19	17	56	13	23	228
14b	40	-99	-99	-99	-99	-99	-99	-99	-99	-99	-99	-99	-99	-99	-99	-99	-99	-99	-99
15t	10	2	46	266	24	25	47	31	25	320	27	44	271	27	28	259	13	52	246
15b	17	2	52	271	-99	-99	-99	18	14	261	4	12	281	-99	-99	-99	24	10	17
16t	10	26	14	0	18	20	257	6	36	249	30	43	259	12	23	45	13	40	250
16b	14	27	6	136	11	19	253	6	15	287	-99	-99	-99	-99	-99	-99	24	9	299
17t	3	7	50	296	-99	-99	-99	-99	-99	-99	-99	-99	-99	-99	-99	-99	30	25	315
17b	6	2	23	313	5	27	61	6	23	302	-99	-99	-99	-99	-99	-99	31	16	22
18t	8	3	41	285	8	27	294	28	33	290	30	39	292	24	40	277	13	57	106
18b	19	2	22	300	9	19	295	6	18	285	30	19	234	25	18	263	14	43	79
19t	3	2	55	267	13	19	239	-99	-99	-99	-99	-99	-99	-99	-99	-99	-99	-99	-99
19m	20	31	17	158	1	16	169	6	14	271	27	14	295	18	18	316	13	18	276
19b	45	30	10	149	30	12	94	6	14	274	25	11	275	12	12	240	13	12	305
20t	3	-99	-99	-99	27	28	201	17	33	261	24	60	239	5	45	269	12	53	266
20b	13	1	25	267	10	21	275	6	29	275	-99	-99	-99	-99	-99	-99	29	14	81
21t	14	3	30	259	18	20	269	6	28	262	30	30	259	5	26	258	12	26	254
21b	22	3	23	262	24	16	257	6	26	263	10	21	259	-99	-99	-99	23	15	227
22t	3	-99	-99	-99	-99	-99	-99	-99	-99	-99	23	26	14	9	33	35	31	24	103
22m	20	3	38	259	2	11	344	6	9	282	30	23	273	10	23	53	12	15	300
22b	48	3	25	258	19	12	238	6	12	245	4	14	241	-99	-99	-99	-99	-99	-99
23t	10	23	71	247	11	47	249	6	61	252	30	56	253	25	55	248	12	74	248
23b	13	23	56	273	11	41	271	6	48	273	3	27	264	-99	-99	-99	31	11	39
24t	10	-99	-99	-99	-99	-99	-99	-99	-99	-99	30	65	248	5	51	243	12	88	238
24b	25	-99	-99	-99	-99	-99	-99	-99	-99	-99	-99	-99	-99	-99	-99	-99	31	17	67
25t	11	3	38	242	11	32	239	6	39	235	30	32	243	5	29	248	12	71	242
25m	20	23	38	246	11	30	242	6	39	241	30	32	242	5	33	239	12	56	241
25b	29	23	35	241	11	26	239	6	40	236	30	28	248	5	29	231	14	38	43
44t	13	23	36	223	4	41	226	2	18	86	-99	-99	-99	-99	-99	-99	-99	-99	-99
44b	55	2	25	234	-99	-99	-99	-99	-99	-99	-99	-99	-99	-99	-99	-99	-99	-99	-99
45t	12	-99	-99	-99	-99	-99	-99	-99	-99	-99	-99	-99	-99	-99	-99	-99	-99	-99	-99
45m	84	-99	-99	-99	-99	-99	-99	-99	-99	-99	-99	-99	-99	-99	-99	-99	-99	-99	-99
46t	14	2	38	256	12	22	337	26	24	246	10	22	239	-99	-99	-99	-99	-99	-99
46m	50	3	33	235	11	20	201	25	32	222	8	24	218	-99	-99	-99	-99	-99	-99
46b	84	23	15	211	24	17	214	2	5	14	-99	-99	-99	-99	-99	-99	-99	-99	-99
47t	12	4	42	250	-99	-99	-99	-99	-99	-99	-99	-99	-99	-99	-99	-99	-99	-99	-99
47m	100	-99	-99	-99	-99	-99	-99	-99	-99	-99	29	17	29	13	35	43	14	41	38
47b	190	-99	-99	-99	-99	-99	-99	-99	-99	-99	26	16	37	6	19	34	13	20	19
48t	14	22	51	13	16	41	283	10	22	297	25	18	275	28	28	259	13	23	231
48m	100	3	23	265	25	29	275	20	13	297	29	15	99	28	23	258	1	22	254
48b	190	28	13	293	21	11	108	-99	-99	-99	30	14	100	11	12	108	22	14	107
49t	14	3	44	260	13	40	48	26	62	48	7	79	33	-99	-99	-99	-99	-99	-99
49m	100	22	16	219	27	38	53	19	70	12	7	81	37	-99	-99	-99	-99	-99	-99
49b	490	31	8	140	3	11	153	26	16	156	1	14	151	24	21	191	25	9	160

Table I-4. Current meter statistics: maximum speed and direction for 40-hr low-passed filtered data (continued).

		April 1993			May 1993			June 1993			July 1993			August 1993			September 1993		
No.	h	day	v_M	θ_M	day	v_M	θ_M	day	v_M	θ_M	day	v_M	θ_M	day	v_M	θ_M	day	v_M	θ_M
01t	10	8	45	198	12	43	23	20	86	196	2	19	357	24	14	344	14	25	349
01b	12	-99	-99	-99	-99	-99	-99	-99	-99	-99	-99	-99	-99	-99	-99	-99	-99	-99	-99
02t	10	28	38	196	29	57	172	20	71	199	4	49	23	-99	-99	-99	-99	-99	-99
02b	32	-99	-99	-99	27	20	157	20	69	189	5	27	18	27	18	175	13	7	258
03t	10	24	26	41	6	39	186	5	30	108	5	32	28	16	38	23	1	34	38
03m	33	-99	-99	-99	26	8	21	4	29	21	14	16	230	16	25	20	8	17	346
03b	58	-99	-99	-99	27	9	167	19	22	176	9	13	27	27	19	178	4	6	182
04t	14	15	36	232	13	38	213	13	58	12	10	59	7	8	63	44	1	14	318
04m	100	17	28	190	13	41	197	13	54	26	29	32	192	11	45	35	6	4	196
04b	190	11	19	183	12	26	196	19	21	36	1	19	220	1	10	356	25	8	208
05t	14	21	27	243	31	48	29	13	56	40	16	61	33	12	64	63	13	18	46
05m	100	29	22	223	8	34	218	12	86	39	13	35	35	14	37	55	11	6	42
05b	190	10	5	212	31	8	47	10	17	39	29	21	234	1	17	235	1	11	50
06t	14	10	22	68	7	41	7	12	54	93	31	74	48	1	77	45	1	27	52
06m	100	6	34	63	25	51	72	14	61	71	5	34	75	24	46	69	1	25	64
06b	190	-99	-99	-99	-99	-99	-99	-99	-99	-99	-99	-99	-99	-99	-99	-99	-99	-99	-99
07t	14	30	41	74	12	57	88	20	31	82	31	64	102	4	83	99	7	49	70
07m	100	-99	-99	-99	28	20	235	2	23	55	24	24	258	27	54	81	12	16	91
07b	190	30	22	76	5	27	68	5	18	80	30	13	84	31	23	88	1	19	90
08t	14	7	36	97	4	28	136	4	19	193	26	47	343	31	57	127	1	56	128
08m	100	17	45	262	8	56	255	24	14	262	10	22	79	15	39	107	17	13	279
08b	190	17	7	284	2	10	287	18	7	283	10	9	312	20	10	294	17	8	294
09t	14	-99	-99	-99	28	14	299	19	18	35	9	40	139	26	41	11	14	27	92
09m	100	5	23	63	11	16	267	10	12	302	8	13	75	23	12	40	3	18	264
09b	190	15	10	299	5	6	219	10	8	276	18	10	282	4	5	281	30	4	181
10t	14	-99	-99	-99	-99	-99	-99	-99	-99	-99	-99	-99	-99	-99	-99	-99	-99	-99	-99
10m	100	6	14	96	29	19	285	22	19	272	13	40	77	8	34	93	16	17	252
10b	190	11	4	298	20	3	121	13	6	101	-99	-99	-99	-99	-99	-99	29	3	313
11t	14	15	22	252	4	17	239	3	7	191	-99	-99	-99	-99	-99	-99	-99	-99	-99
11m	100	-99	-99	-99	-99	-99	-99	-99	-99	-99	23	57	83	10	18	74	27	13	253
11b	190	-99	-99	-99	-99	-99	-99	-99	-99	-99	-99	-99	-99	-99	-99	-99	-99	-99	-99
12t	14	19	27	70	28	21	266	30	23	73	31	50	122	10	56	68	21	31	263
12m	100	30	20	106	17	18	267	-99	-99	-99	-99	-99	-99	-99	-99	-99	-99	-99	-99
12b	490	-99	-99	-99	-99	-99	-99	-99	-99	-99	31	3	244	1	4	242	27	8	234
13t	14	8	30	36	19	16	269	13	15	62	18	46	94	17	54	87	21	25	272
13m	100	24	16	78	8	25	258	30	19	71	12	23	84	24	23	72	19	27	252
13b	190	-99	-99	-99	-99	-99	-99	-99	-99	-99	-99	-99	-99	-99	-99	-99	-99	-99	-99
14t	10	27	22	238	20	23	88	11	34	38	6	25	52	-99	-99	-99	-99	-99	-99
14m	26	1	21	83	19	20	81	10	18	61	22	37	94	20	38	71	5	38	82
14b	40	-99	-99	-99	31	6	98	19	17	248	22	18	79	17	16	81	3	11	71
15t	10	25	24	252	15	16	256	18	18	269	29	51	64	7	59	80	14	21	261
15b	17	9	16	291	15	10	232	19	17	257	6	4	112	-99	-99	-99	30	5	299
16t	10	8	33	266	2	30	216	28	17	67	1	9	55	29	19	318	22	34	43
16b	14	30	16	122	13	11	3	-99	-99	-99	-99	-99	-99	-99	-99	-99	-99	-99	-99
17t	3	9	55	107	13	31	126	20	62	303	3	22	115	-99	-99	-99	-99	-99	-99
17b	6	9	38	30	13	20	24	-99	-99	-99	-99	-99	-99	-99	-99	-99	-99	-99	-99
18t	8	8	69	271	30	30	273	18	52	269	10	44	106	-99	-99	-99	-99	-99	-99
18b	19	16	20	63	28	6	256	20	40	279	1	12	79	-99	-99	-99	-99	-99	-99
19t	3	-99	-99	-99	31	29	141	17	28	335	26	49	65	11	52	309	-99	-99	-99
19m	20	-99	-99	-99	31	14	107	1	14	106	25	28	126	2	8	77	-99	-99	-99
19b	45	1	10	94	18	4	255	20	6	241	24	8	113	18	12	124	2	8	273
20t	3	4	49	267	6	48	262	19	49	277	22	30	22	26	71	262	13	73	12
20b	13	15	22	342	9	13	190	-99	-99	-99	-99	-99	-99	-99	-99	-99	28	17	153
21t	14	1	21	74	14	18	76	19	46	264	9	35	72	25	25	115	30	31	260
21b	22	2	17	66	14	13	40	-99	-99	-99	20	29	82	27	22	218	17	15	96
22t	3	19	33	61	31	19	269	3	36	113	20	58	21	8	43	77	14	21	52
22m	20	5	26	33	9	17	10	4	29	114	23	29	88	1	23	81	6	17	75
22b	48	-99	-99	-99	28	4	154	20	21	240	10	7	79	-99	-99	-99	30	4	212
23t	10	4	57	254	9	39	240	19	72	246	22	32	64	27	35	248	21	53	238
23b	13	4	40	213	6	23	163	-99	-99	-99	-99	-99	-99	-99	-99	-99	-99	-99	-99
24t	10	28	42	236	28	48	236	20	68	240	9	47	52	27	29	238	21	24	250
24b	25	4	27	213	13	25	40	-99	-99	-99	21	20	61	27	30	222	21	25	225
25t	11	2	36	87	9	23	222	-99	-99	-99	-99	-99	-99	-99	-99	-99	-99	-99	-99
25m	20	2	37	73	14	23	49	-99	-99	-99	-99	-99	-99	-99	-99	-99	-99	-99	-99
25b	29	-99	-99	-99	24	21	229	20	46	229	5	34	70	-99	-99	-99	-99	-99	-99
44t	13	-99	-99	-99	-99	-99	-99	-99	-99	-99	-99	-99	-99	-99	-99	-99	-99	-99	-99
44b	55	-99	-99	-99	-99	-99	-99	-99	-99	-99	-99	-99	-99	-99	-99	-99	-99	-99	-99
45t	12	-99	-99	-99	-99	-99	-99	-99	-99	-99	-99	-99	-99	-99	-99	-99	-99	-99	-99
45m	84	-99	-99	-99	-99	-99	-99	-99	-99	-99	-99	-99	-99	-99	-99	-99	-99	-99	-99
46t	14	-99	-99	-99	-99	-99	-99	-99	-99	-99	-99	-99	-99	-99	-99	-99	-99	-99	-99
46m	50	-99	-99	-99	-99	-99	-99	-99	-99	-99	-99	-99	-99	-99	-99	-99	-99	-99	-99
46b	84	-99	-99	-99	-99	-99	-99	-99	-99	-99	-99	-99	-99	-99	-99	-99	-99	-99	-99
47t	12	-99	-99	-99	-99	-99	-99	-99	-99	-99	-99	-99	-99	-99	-99	-99	-99	-99	-99
47m	100	-99	-99	-99	-99	-99	-99	-99	-99	-99	-99	-99	-99	-99	-99	-99	-99	-99	-99
47b	190	-99	-99	-99	-99	-99	-99	-99	-99	-99	-99	-99	-99	-99	-99	-99	-99	-99	-99
48t	14	16	11	248	15	18	139	-99	-99	-99	-99	-99	-99	-99	-99	-99	-99	-99	-99
48m	100	17	15	271	6	12	270	-99	-99	-99	-99	-99	-99	-99	-99	-99	-99	-99	-99
48b	190	-99	-99	-99	-99	-99	-99	-99	-99	-99	-99	-99	-99	-99	-99	-99	-99	-99	-99
49t	14	-99	-99	-99	-99	-99	-99	-99	-99	-99	-99	-99	-99	-99	-99	-99	-99	-99	-99
49m	100	-99	-99	-99	25	52	27	5	54	68	4	48	25	9	39	80	30	12	56
49b	490	29	11	189	12	10	179	8	8	222	26	10	190	27	8	201	4	9	202

Table I-4. Current meter statistics: maximum speed and direction for 40-hr low-passed filtered data (continued).

		October 1993			November 1993			December 1993			January 1994			February 1994			March 1994		
No.	h	day	v_M	θ_M	day	v_M	θ_M	day	v_M	θ_M	day	v_M	θ_M	day	v_M	θ_M	day	v_M	θ_M
01t	10	22	28	195	6	26	198	19	26	197	7	13	353	-99	-99	-99	-99	-99	-99
01b	12	21	29	203	15	29	203	19	27	197	-99	-99	-99	-99	-99	-99	-99	-99	-99
02t	10	23	68	203	10	81	204	31	38	192	19	62	189	10	46	203	13	34	192
02b	32	31	35	9	10	51	193	2	18	183	-99	-99	-99	-99	-99	-99	-99	-99	-99
03t	10	-99	-99	-99	-99	-99	-99	19	23	233	4	43	28	13	32	228	3	28	22
03m	33	26	32	195	17	35	205	19	22	210	4	40	34	13	25	220	3	27	31
03b	58	-99	-99	-99	-99	-99	-99	19	20	191	4	27	21	10	20	160	13	16	187
04t	14	30	23	250	9	40	194	6	32	190	4	24	32	25	34	166	2	29	216
04m	100	4	18	15	21	25	203	6	20	202	19	21	228	22	26	256	15	24	16
04b	190	26	10	202	21	14	209	6	20	197	6	14	204	27	15	200	4	14	202
05t	14	-99	-99	-99	-99	-99	-99	19	27	320	6	53	75	24	20	256	15	24	88
05m	100	4	20	58	20	33	235	6	22	232	13	16	60	26	16	221	11	17	77
05b	190	-99	-99	-99	-99	-99	-99	18	17	225	20	12	228	20	13	228	13	14	240
06t	14	25	26	263	19	29	257	21	34	50	2	39	94	16	19	297	12	19	287
06m	100	26	23	258	18	27	262	17	24	253	20	37	258	14	20	253	12	23	254
06b	190	-99	-99	-99	-99	-99	-99	17	10	84	10	19	257	7	17	258	14	14	78
07t	14	-99	-99	-99	-99	-99	-99	29	32	159	4	56	65	15	30	267	14	22	80
07m	100	26	24	267	16	26	266	5	27	264	-99	-99	-99	-99	-99	-99	31	4	219
07b	190	7	22	259	16	24	262	18	12	263	6	11	75	14	16	258	21	16	268
08t	14	29	20	118	25	59	103	28	43	108	15	60	94	21	30	340	2	19	189
08m	100	26	26	267	25	40	88	4	15	249	14	25	100	15	38	270	22	6	320
08b	190	-99	-99	-99	-99	-99	-99	16	11	293	27	5	296	25	15	289	17	9	294
09t	14	8	17	275	28	48	122	1	36	80	6	51	94	1	39	121	1	18	305
09m	100	1	6	201	-99	-99	-99	20	8	51	6	20	76	28	21	275	1	21	277
09b	190	15	9	76	29	7	254	16	10	284	17	11	30	1	8	260	31	8	74
10t	14	-99	-99	-99	-99	-99	-99	28	23	61	23	35	120	4	22	49	8	39	87
10m	100	24	24	264	22	20	79	4	17	290	8	19	99	12	18	278	6	21	116
10b	190	7	8	300	9	8	115	19	5	116	20	8	299	16	6	290	20	9	120
11t	14	-99	-99	-99	-99	-99	-99	16	28	237	16	32	28	24	29	288	21	23	74
11m	100	27	21	11	1	16	324	31	11	256	15	19	293	12	22	301	1	21	245
11b	190	-99	-99	-99	-99	-99	-99	13	15	247	7	14	98	12	17	241	15	15	245
12t	14	27	68	103	4	67	95	1	33	101	-99	-99	-99	-99	-99	-99	-99	-99	-99
12m	100	-99	-99	-99	-99	-99	-99	-99	-99	-99	-99	-99	-99	-99	-99	-99	-99	-99	-99
12b	490	29	9	230	1	7	227	2	7	226	-99	-99	-99	-99	-99	-99	-99	-99	-99
13t	14	-99	-99	-99	-99	-99	-99	28	32	64	7	33	89	3	19	40	6	33	54
13m	100	14	22	69	27	22	74	22	13	77	6	21	69	23	24	241	12	13	257
13b	190	16	20	217	5	18	223	1	15	223	19	17	247	3	12	59	8	16	237
14t	10	-99	-99	-99	-99	-99	-99	29	29	308	8	42	262	9	22	122	11	26	276
14m	26	19	27	222	9	24	222	28	25	78	7	26	82	10	14	143	5	21	85
14b	40	10	26	81	-99	-99	-99	27	19	49	11	22	82	22	10	261	5	21	75
15t	10	26	33	264	10	36	267	24	40	287	21	51	251	20	33	273	11	32	274
15b	17	25	18	251	4	18	256	25	17	45	18	24	268	21	15	49	7	16	246
16t	10	8	52	267	-99	-99	-99	31	26	259	21	38	265	1	32	264	4	33	37
16b	14	-99	-99	-99	-99	-99	-99	14	31	330	4	21	355	20	14	130	2	21	329
17t	3	23	33	287	8	40	294	25	54	100	4	45	85	4	36	277	-99	-99	-99
17b	6	31	29	84	2	23	285	14	40	110	3	34	96	25	13	227	10	28	30
18t	8	8	36	295	-99	-99	-99	15	39	110	11	33	276	1	22	285	28	15	75
18b	19	31	37	54	9	18	293	1	10	249	-99	-99	-99	20	17	220	3	30	63
19t	3	21	37	274	7	29	262	30	53	275	13	45	299	5	19	67	-99	-99	-99
19m	20	-99	-99	-99	-99	-99	-99	25	20	283	8	26	284	-99	-99	-99	29	9	253
19b	45	18	15	260	2	12	71	-99	-99	-99	-99	-99	-99	22	10	285	2	16	70
20t	3	15	57	233	22	43	304	24	60	252	16	71	262	1	62	251	-99	-99	-99
20b	13	21	27	275	2	35	272	20	26	269	16	44	268	4	18	238	12	24	158
21t	14	8	39	245	9	31	264	14	30	83	19	31	261	19	18	258	12	26	265
21b	22	-99	-99	-99	-99	-99	-99	-99	-99	-99	-99	-99	-99	19	14	212	2	24	28
22t	3	15	23	66	-99	-99	-99	28	21	51	6	41	78	21	39	293	25	34	299
22m	20	25	21	268	10	17	277	14	15	86	6	27	76	24	15	276	1	13	168
22b	48	25	18	268	16	20	233	14	13	81	19	18	242	7	4	252	-99	-99	-99
23t	10	-99	-99	-99	-99	-99	-99	15	54	65	21	60	247	1	31	252	-99	-99	-99
23b	13	21	40	217	-99	-99	-99	19	39	225	19	49	230	1	17	225	-99	-99	-99
24t	10	22	71	242	9	83	240	23	51	240	10	60	240	27	51	248	13	57	237
24b	25	30	38	28	9	43	245	15	44	49	4	36	47	18	22	207	3	27	41
25t	11	-99	-99	-99	-99	-99	-99	-99	-99	-99	-99	-99	-99	-99	-99	-99	-99	-99	-99
25m	20	23	40	251	9	43	242	1	22	230	-99	-99	-99	-99	-99	-99	-99	-99	-99
25b	29	-99	-99	-99	-99	-99	-99	-99	-99	-99	-99	-99	-99	-99	-99	-99	-99	-99	-99
44t	13	-99	-99	-99	-99	-99	-99	-99	-99	-99	-99	-99	-99	-99	-99	-99	-99	-99	-99
44b	55	-99	-99	-99	-99	-99	-99	-99	-99	-99	-99	-99	-99	-99	-99	-99	-99	-99	-99
45t	12	-99	-99	-99	-99	-99	-99	-99	-99	-99	-99	-99	-99	-99	-99	-99	-99	-99	-99
45m	84	-99	-99	-99	-99	-99	-99	-99	-99	-99	-99	-99	-99	-99	-99	-99	-99	-99	-99
46t	14	-99	-99	-99	-99	-99	-99	-99	-99	-99	-99	-99	-99	-99	-99	-99	-99	-99	-99
46m	50	-99	-99	-99	-99	-99	-99	-99	-99	-99	-99	-99	-99	-99	-99	-99	-99	-99	-99
46b	84	-99	-99	-99	-99	-99	-99	-99	-99	-99	-99	-99	-99	-99	-99	-99	-99	-99	-99
47t	12	-99	-99	-99	-99	-99	-99	-99	-99	-99	-99	-99	-99	-99	-99	-99	-99	-99	-99
47m	100	-99	-99	-99	-99	-99	-99	-99	-99	-99	-99	-99	-99	-99	-99	-99	-99	-99	-99
47b	190	-99	-99	-99	-99	-99	-99	-99	-99	-99	-99	-99	-99	-99	-99	-99	-99	-99	-99
48t	14	-99	-99	-99	-99	-99	-99	31	34	54	7	42	85	8	40	76	9	20	138
48m	100	-99	-99	-99	-99	-99	-99	18	11	274	4	13	205	7	24	243	30	15	269
48b	190	-99	-99	-99	-99	-99	-99	13	8	308	20	9	289	23	6	301	9	11	118
49t	14	-99	-99	-99	-99	-99	-99	29	26	320	11	27	260	10	26	275	2	29	240
49m	100	1	13	62	21	29	232	7	24	241	10	18	295	28	33	243	1	26	251
49b	490	17	8	284	21	7	128	16	10	153	6	11	202	7	9	202	11	10	196

Table I-4. Current meter statistics: maximum speed and direction for 40-hr low-passed filtered data (continued).

		April 1994			May 1994			June 1994			July 1994			August 1994			September 1994		
No.	h	day	v_M	θ_M	day	v_M	θ_M	day	v_M	θ_M	day	v_M	θ_M	day	v_M	θ_M	day	v_M	θ_M
01t	10	12	28	195	-99	-99	-99	-99	-99	-99	-99	-99	-99	20	19	14	16	20	171
01b	12	12	23	174	1	22	181	24	15	330	12	15	16	-99	-99	-99	-99	-99	-99
02t	10	11	38	196	1	52	203	27	53	16	1	22	24	10	35	203	16	47	204
02b	32	-99	-99	-99	-99	-99	-99	-99	-99	-99	-99	-99	-99	11	27	183	16	38	186
03t	10	28	41	207	1	25	287	30	44	23	1	45	19	17	19	148	25	25	259
03m	33	-99	-99	-99	-99	-99	-99	-99	-99	-99	-99	-99	-99	-99	-99	-99	-99	-99	-99
03b	58	8	15	194	-99	-99	-99	-99	-99	-99	-99	-99	-99	11	19	197	4	19	32
04t	14	-99	-99	-99	-99	-99	-99	-99	-99	-99	-99	-99	-99	30	48	34	1	38	30
04m	100	16	17	199	-99	-99	-99	-99	-99	-99	-99	-99	-99	30	37	28	9	30	19
04b	190	-99	-99	-99	-99	-99	-99	-99	-99	-99	-99	-99	-99	25	12	38	7	16	32
05t	14	-99	-99	-99	-99	-99	-99	-99	-99	-99	-99	-99	-99	-99	-99	-99	-99	-99	-99
05m	100	-99	-99	-99	-99	-99	-99	-99	-99	-99	-99	-99	-99	-99	-99	-99	-99	-99	-99
05b	190	-99	-99	-99	-99	-99	-99	-99	-99	-99	-99	-99	-99	-99	-99	-99	-99	-99	-99
06t	14	30	28	247	2	23	254	13	26	87	15	29	57	17	26	217	28	38	124
06m	100	-99	-99	-99	-99	-99	-99	-99	-99	-99	-99	-99	-99	23	14	65	12	27	254
06b	190	-99	-99	-99	-99	-99	-99	-99	-99	-99	-99	-99	-99	29	13	256	11	9	267
07t	14	12	28	261	8	29	115	30	57	60	1	57	61	24	27	265	-99	-99	-99
07m	100	11	23	263	18	36	80	14	20	80	22	20	77	2	19	81	29	14	84
07b	190	22	14	86	9	14	75	16	11	83	21	8	77	5	11	82	5	9	69
08t	14	3	25	108	23	32	124	25	25	76	4	57	113	3	31	87	30	17	202
08m	100	26	21	272	25	28	102	30	7	109	4	32	93	1	15	97	29	18	68
08b	190	29	10	292	2	7	298	1	5	281	-99	-99	-99	15	6	99	30	5	114
09t	14	11	20	88	24	27	92	19	18	57	13	46	108	-99	-99	-99	-99	-99	-99
09m	100	29	27	268	1	26	256	27	10	63	11	13	279	9	14	299	25	19	76
09b	190	28	8	63	31	10	81	1	10	87	11	3	49	7	8	263	30	10	237
10t	14	2	30	90	3	17	259	26	31	79	21	29	83	15	27	312	24	26	124
10m	100	27	23	268	19	20	89	27	18	73	1	13	86	2	13	290	26	10	99
10b	190	16	7	108	4	12	103	26	6	104	17	5	300	24	5	103	26	7	105
11t	14	7	22	289	6	22	77	25	21	101	30	27	134	1	28	103	23	30	137
11m	100	10	31	267	18	39	68	26	20	109	3	34	81	15	11	257	6	8	89
11b	190	28	20	252	9	18	119	5	14	254	5	12	264	15	13	247	3	13	247
12t	14	-99	-99	-99	-99	-99	-99	-99	-99	-99	-99	-99	-99	-99	-99	-99	-99	-99	-99
12m	100	-99	-99	-99	-99	-99	-99	-99	-99	-99	-99	-99	-99	-99	-99	-99	-99	-99	-99
12b	490	-99	-99	-99	-99	-99	-99	-99	-99	-99	-99	-99	-99	-99	-99	-99	-99	-99	-99
13t	14	3	30	62	23	28	86	24	16	96	19	24	93	3	27	63	20	72	58
13m	100	18	17	242	22	24	78	28	10	72	22	11	69	25	20	255	24	20	60
13b	190	9	18	244	29	20	249	5	18	249	7	11	60	-99	-99	-99	-99	-99	-99
14t	10	13	23	351	15	19	98	9	30	78	9	20	164	28	31	186	15	42	273
14m	26	-99	-99	-99	-99	-99	-99	25	19	92	4	16	259	-99	-99	-99	-99	-99	-99
14b	40	17	19	234	14	10	81	-99	-99	-99	31	7	74	14	13	253	16	20	235
15t	10	16	25	267	18	18	81	30	41	89	1	37	69	30	31	265	15	51	275
15b	17	8	10	245	3	9	213	16	7	123	7	10	264	17	14	256	15	28	256
16t	10	30	26	276	8	10	25	25	10	277	6	27	263	13	36	257	15	46	258
16b	14	21	12	243	3	7	239	25	7	282	6	7	227	-99	-99	-99	-99	-99	-99
17t	3	-99	-99	-99	-99	-99	-99	-99	-99	-99	29	36	283	9	31	292	22	22	291
17b	6	6	18	23	6	14	297	-99	-99	-99	-99	-99	-99	-99	-99	-99	-99	-99	-99
18t	8	17	37	301	6	16	291	24	22	86	30	34	91	1	26	79	14	25	286
18b	19	-99	-99	-99	-99	-99	-99	-99	-99	-99	29	5	117	2	9	240	-99	-99	-99
19t	3	-99	-99	-99	-99	-99	-99	23	39	98	20	29	88	7	54	295	25	63	279
19m	20	3	13	123	23	8	103	3	13	151	17	21	190	-99	-99	-99	-99	-99	-99
19b	45	17	8	246	17	5	103	-99	-99	-99	31	4	81	15	10	262	15	17	250
20t	3	-99	-99	-99	-99	-99	-99	24	71	92	23	34	63	13	32	284	23	35	256
20b	13	28	23	259	2	18	262	25	30	60	27	26	84	-99	-99	-99	-99	-99	-99
21t	14	17	33	252	1	18	109	30	38	94	6	31	48	13	16	215	23	29	285
21b	22	17	24	236	1	16	91	30	17	80	28	25	64	31	16	259	14	24	220
22t	3	17	34	283	1	33	294	2	25	73	13	39	10	15	54	214	15	52	271
22m	20	-99	-99	-99	-99	-99	-99	15	22	185	20	30	42	24	13	107	4	15	69
22b	48	17	12	239	3	8	76	-99	-99	-99	-99	-99	-99	-99	-99	-99	-99	-99	-99
23t	10	17	58	243	2	57	244	24	44	63	23	21	61	-99	-99	-99	-99	-99	-99
23b	13	-99	-99	-99	-99	-99	-99	24	23	34	23	26	61	-99	-99	-99	-99	-99	-99
24t	10	30	49	237	20	51	254	28	68	81	2	45	95	10	29	249	15	66	246
24b	25	17	32	222	3	18	98	-99	-99	-99	-99	-99	-99	-99	-99	-99	-99	-99	-99
25t	11	-99	-99	-99	-99	-99	-99	-99	-99	-99	-99	-99	-99	-99	-99	-99	-99	-99	-99
25m	20	-99	-99	-99	-99	-99	-99	-99	-99	-99	-99	-99	-99	-99	-99	-99	-99	-99	-99
25b	29	-99	-99	-99	-99	-99	-99	-99	-99	-99	-99	-99	-99	-99	-99	-99	-99	-99	-99
44t	13	-99	-99	-99	-99	-99	-99	-99	-99	-99	-99	-99	-99	-99	-99	-99	-99	-99	-99
44b	55	-99	-99	-99	-99	-99	-99	-99	-99	-99	-99	-99	-99	-99	-99	-99	-99	-99	-99
45t	12	-99	-99	-99	-99	-99	-99	-99	-99	-99	-99	-99	-99	-99	-99	-99	-99	-99	-99
45m	84	-99	-99	-99	-99	-99	-99	-99	-99	-99	-99	-99	-99	-99	-99	-99	-99	-99	-99
46t	14	-99	-99	-99	-99	-99	-99	-99	-99	-99	-99	-99	-99	-99	-99	-99	-99	-99	-99
46m	50	-99	-99	-99	-99	-99	-99	-99	-99	-99	-99	-99	-99	-99	-99	-99	-99	-99	-99
46b	84	-99	-99	-99	-99	-99	-99	-99	-99	-99	-99	-99	-99	-99	-99	-99	-99	-99	-99
47t	12	-99	-99	-99	-99	-99	-99	-99	-99	-99	-99	-99	-99	-99	-99	-99	-99	-99	-99
47m	100	-99	-99	-99	-99	-99	-99	-99	-99	-99	-99	-99	-99	-99	-99	-99	-99	-99	-99
47b	190	-99	-99	-99	-99	-99	-99	-99	-99	-99	-99	-99	-99	-99	-99	-99	-99	-99	-99
48t	14	11	27	69	27	21	73	11	13	91	20	13	23	8	40	85	30	24	24
48m	100	27	26	281	23	16	86	12	8	95	31	14	309	2	20	298	10	26	271
48b	190	29	9	126	4	15	110	24	9	115	16	5	302	-99	-99	-99	-99	-99	-99
49t	14	20	32	254	1	28	254	27	39	67	17	29	290	27	45	63	3	37	91
49m	100	21	31	235	1	20	258	10	12	303	16	8	307	31	27	88	14	43	105
49b	490	-99	-99	-99	-99	-99	-99	-99	-99	-99	-99	-99	-99	-99	-99	-99	-99	-99	-99

Table I-4. Current meter statistics: maximum speed and direction for 40-hr low-passed filtered data (continued).

		October 1994			November 1994			December 1994		
No.	h	day	v_M	θ_M	day	v_M	θ_M	day	v_M	θ_M
01t	10	-99	-99	-99	-99	-99	-99	-99	-99	-99
01b	12	-99	-99	-99	-99	-99	-99	-99	-99	-99
02t	10	2	56	210	29	40	206	1	43	205
02b	32	2	55	173	13	15	192	-99	-99	-99
03t	10	2	44	220	30	30	235	2	37	203
03m	33	-99	-99	-99	-99	-99	-99	-99	-99	-99
03b	58	17	19	199	26	21	351	-99	-99	-99
04t	14	1	36	248	20	34	44	2	25	39
04m	100	31	10	18	17	22	49	1	4	28
04b	190	2	11	25	19	7	20	-99	-99	-99
05t	14	6	43	242	-99	-99	-99	-99	-99	-99
05m	100	27	16	65	4	18	85	2	7	237
05b	190	6	11	234	28	9	228	1	5	150
06t	14	8	30	260	3	34	122	1	19	236
06m	100	20	36	79	23	16	251	1	1	86
06b	190	-99	-99	-99	-99	-99	-99	-99	-99	-99
07t	14	-99	-99	-99	-99	-99	-99	-99	-99	-99
07m	100	26	18	258	8	20	264	-99	-99	-99
07b	190	-99	-99	-99	-99	-99	-99	-99	-99	-99
08t	14	3	23	144	5	26	62	-99	-99	-99
08m	100	5	25	268	26	16	255	-99	-99	-99
08b	190	4	11	113	8	7	109	-99	-99	-99
09t	14	-99	-99	-99	-99	-99	-99	-99	-99	-99
09m	100	4	12	289	22	11	265	-99	-99	-99
09b	190	1	11	242	1	9	50	-99	-99	-99
10t	14	1	25	318	14	25	45	-99	-99	-99
10m	100	6	18	281	7	8	287	-99	-99	-99
10b	190	13	7	100	12	7	98	-99	-99	-99
11t	14	25	27	10	20	22	88	-99	-99	-99
11m	100	21	18	271	18	12	73	-99	-99	-99
11b	190	22	15	244	7	11	227	-99	-99	-99
12t	14	-99	-99	-99	-99	-99	-99	-99	-99	-99
12m	100	-99	-99	-99	-99	-99	-99	-99	-99	-99
12b	490	-99	-99	-99	-99	-99	-99	-99	-99	-99
13t	14	1	17	22	27	27	106	-99	-99	-99
13m	100	23	22	247	6	20	257	-99	-99	-99
13b	190	-99	-99	-99	-99	-99	-99	-99	-99	-99
14t	10	-99	-99	-99	-99	-99	-99	-99	-99	-99
14m	26	4	25	255	-99	-99	-99	-99	-99	-99
14b	40	-99	-99	-99	-99	-99	-99	-99	-99	-99
15t	10	29	38	268	4	21	257	-99	-99	-99
15b	17	-99	-99	-99	-99	-99	-99	-99	-99	-99
16t	10	-99	-99	-99	-99	-99	-99	-99	-99	-99
16b	14	-99	-99	-99	-99	-99	-99	-99	-99	-99
17t	3	15	46	306	7	11	324	-99	-99	-99
17b	6	-99	-99	-99	-99	-99	-99	-99	-99	-99
18t	8	-99	-99	-99	-99	-99	-99	-99	-99	-99
18b	19	-99	-99	-99	-99	-99	-99	-99	-99	-99
19t	3	10	41	262	15	24	285	-99	-99	-99
19m	20	5	35	261	-99	-99	-99	-99	-99	-99
19b	45	-99	-99	-99	-99	-99	-99	-99	-99	-99
20t	3	26	50	252	17	49	279	-99	-99	-99
20b	13	16	31	270	23	15	283	-99	-99	-99
21t	14	29	19	268	10	19	266	-99	-99	-99
21b	22	17	18	223	23	15	260	-99	-99	-99
22t	3	14	46	267	1	27	232	-99	-99	-99
22m	20	9	21	353	1	11	277	-99	-99	-99
22b	48	9	20	33	-99	-99	-99	-99	-99	-99
23t	10	17	50	244	29	52	245	1	46	247
23b	13	-99	-99	-99	-99	-99	-99	-99	-99	-99
24t	10	9	55	237	24	40	254	1	24	244
24b	25	16	25	247	9	25	56	-99	-99	-99
25t	11	-99	-99	-99	-99	-99	-99	-99	-99	-99
25m	20	-99	-99	-99	-99	-99	-99	-99	-99	-99
25b	29	-99	-99	-99	-99	-99	-99	-99	-99	-99
44t	13	-99	-99	-99	-99	-99	-99	-99	-99	-99
44b	55	-99	-99	-99	-99	-99	-99	-99	-99	-99
45t	12	-99	-99	-99	-99	-99	-99	-99	-99	-99
45m	84	-99	-99	-99	-99	-99	-99	-99	-99	-99
46t	14	-99	-99	-99	-99	-99	-99	-99	-99	-99
46m	50	-99	-99	-99	-99	-99	-99	-99	-99	-99
46b	84	-99	-99	-99	-99	-99	-99	-99	-99	-99
47t	12	-99	-99	-99	-99	-99	-99	-99	-99	-99
47m	100	-99	-99	-99	-99	-99	-99	-99	-99	-99
47b	190	-99	-99	-99	-99	-99	-99	-99	-99	-99
48t	14	1	25	20	27	33	88	-99	-99	-99
48m	100	3	33	280	23	23	94	-99	-99	-99
48b	190	-99	-99	-99	-99	-99	-99	-99	-99	-99
49t	14	1	33	226	27	33	117	1	22	119
49m	100	31	13	120	1	13	122	1	3	157
49b	490	-99	-99	-99	27	5	200	-99	-99	-99

Appendix J: Comparisons of Currents Derived From ADCP, Current Meter, and Hydrographic Observations

J.1 Comparison of vertical shear from ADCP and hydrography

Oceanographers still rely heavily on traditional geostrophic current shear estimation based on observed density fields, even in coastal circulation regimes. Direct measurements of currents from survey vessels, particularly acoustic Doppler current profiler (ADCP) data, provide a means to verify the oceanographers' faith in geostrophic vertical shear. This issue is addressed here for the Texas-Louisiana shelf.

Using ADCP and CTD measurements made on LATEX A cruises H06 and H07 (July/August and November of 1993) at stations having a water depth greater than 120 m, Chen (1995) compared the vertical shear computed from ADCP data and the geostrophic shear obtained from CTD data to establish a common reference. Cruises H06 and H07 were selected as representative of summer and non-summer, respectively, and on the basis of good coverage with high quality ADCP data.

Here we first discuss the analysis methodology, then present some of Chen's (1995) results and an extension thereof. In contrast to other comparisons of ADCP and CTD-based shear, such as that of Kosro and Huyer (1986) for the California coastal region, the present analysis addresses the statistical distribution of correlation and of rms difference based on a sample ensemble of profile pairs of vertical shear in the upper 100 m. We follow with an analysis of the EOF decomposition of the ADCP and CTD-based vertical shear to gain some insight as to differences between these for the Texas-Louisiana shelf, and conclude with a summary of the important findings. Throughout this appendix we use the term "current shear" as synonymous with the phrase "profile of relative current" from which the vertical average in the case of ADCP, or reference in the case of CTD-derived profile, has been removed.

Data analysis and sample comparisons

For the 150-kHz ADCP system used during the LATEX A cruises, vertical resolution is 4 m, with the uppermost measurement typically centered at 10 m depth. The comparison of ADCP and CTD-inferred shear was restricted to the depth range 10-98 m, or 23 levels at ADCP data resolution. The spacing of CTD stations along the 200-m isobath for cruises H06 and H07 was about 20 km, allowing at most about eight ADCP vertical profiles between stations. For cross-shelf transects on the outer shelf (near 200 m water depth) the station spacing was only 5 km, allowing only one or two ADCP profiles between stations. The component of geostrophic current relative to 98 m normal to the line between adjacent CTD stations was computed from the thermal wind equation, based on density profiles at the adjacent stations and subsampled at levels common to the ADCP data. Components of ADCP velocity normal to the line between adjacent CTD stations at a given level were averaged for all ADCP profiles available between those stations. The average ADCP profile thus obtained for the 23 levels was then demeaned, as was the associated normal component of the geostrophic velocity calculated from the CTD data at the adjacent stations.

In this way shear profiles based separately on ADCP and on CTD data, with zero mean over the 23 levels, were obtained for each CTD station pair having at least one usable ADCP profile in between. Shear profiles characterizing the cross-shelf flow were obtained from stations along the 200-m isobath; profiles characterizing the alongshelf flow were obtained from the cross-shelf transects near 200 m. Figure J.1-1 shows the CTD stations from LATEX A cruises H06 and H07 used in this analysis. In the comparisons discussed below, it should be borne in mind that the cross-shelf shear profiles are based on averages over about 20 km, while alongshelf shear profiles are based on averages over only 5 km.

Figures J.1-2 and J.1-3 show sample comparisons of alongshelf and cross-shelf shear profiles for cruises H06 and H07, respectively. These were deliberately selected as the best three profiles for both directions on each cruise; each profile pair looks qualitatively good regardless of direction or season. It will be shown below that despite the wide range in correlation for individual profile pairs, the good sample pairs illustrated in Figures J.1-2 and J.1-3 in fact represent the most probable (or typical) pairs.

Correlation and rms difference distributions

As a quantitative measure of the agreement of the profile pairs, the correlation coefficient (r) and root mean square difference (rms) were computed for each profile pair (Tables J.1-1 and J.1-2). From these tables it may be noted that the twelve sample profile pairs in Figures J.1-2 and J.1-3 have r values ranging from 0.88 to 0.99 and rms differences in the range 1.4 to 4.0 $cm{\cdot}s^{-1}$. Notice, however, that for other profile pairs, r ranges from large negative to large positive values, and the maximum rms difference is over 11 $cm{\cdot}s^{-1}$. The values of rms difference and of correlation coefficient based on sample profiles in Tables J.1-1 and J.1-2 were sorted in ascending order, regardless of direction or cruise, to produce the cumulative distributions shown in Figures J.1-4 and J.1-5.

The cumulative distribution of rms difference in ADCP and CTD-inferred shear (Figure J.1-4) represents an estimate of the probability that the rms difference has a value between zero and a given value on the abscissa. The difference of this distribution from unity is the probability of an rms greater than a given value on the abscissa; this is nearly a one-sided Gaussian distribution with standard deviation relative to zero rms of about 3.2 $cm{\cdot}s^{-1}$ as computed from the sample data. The derivative of this cumulative distribution, the probability density function (pdf), is thus nearly a Rayleigh distribution (Longuet-Higgins, 1952) with a mode near 3.2, while the median and mean based on the sample data are about 3.7 and 4.1, respectively.

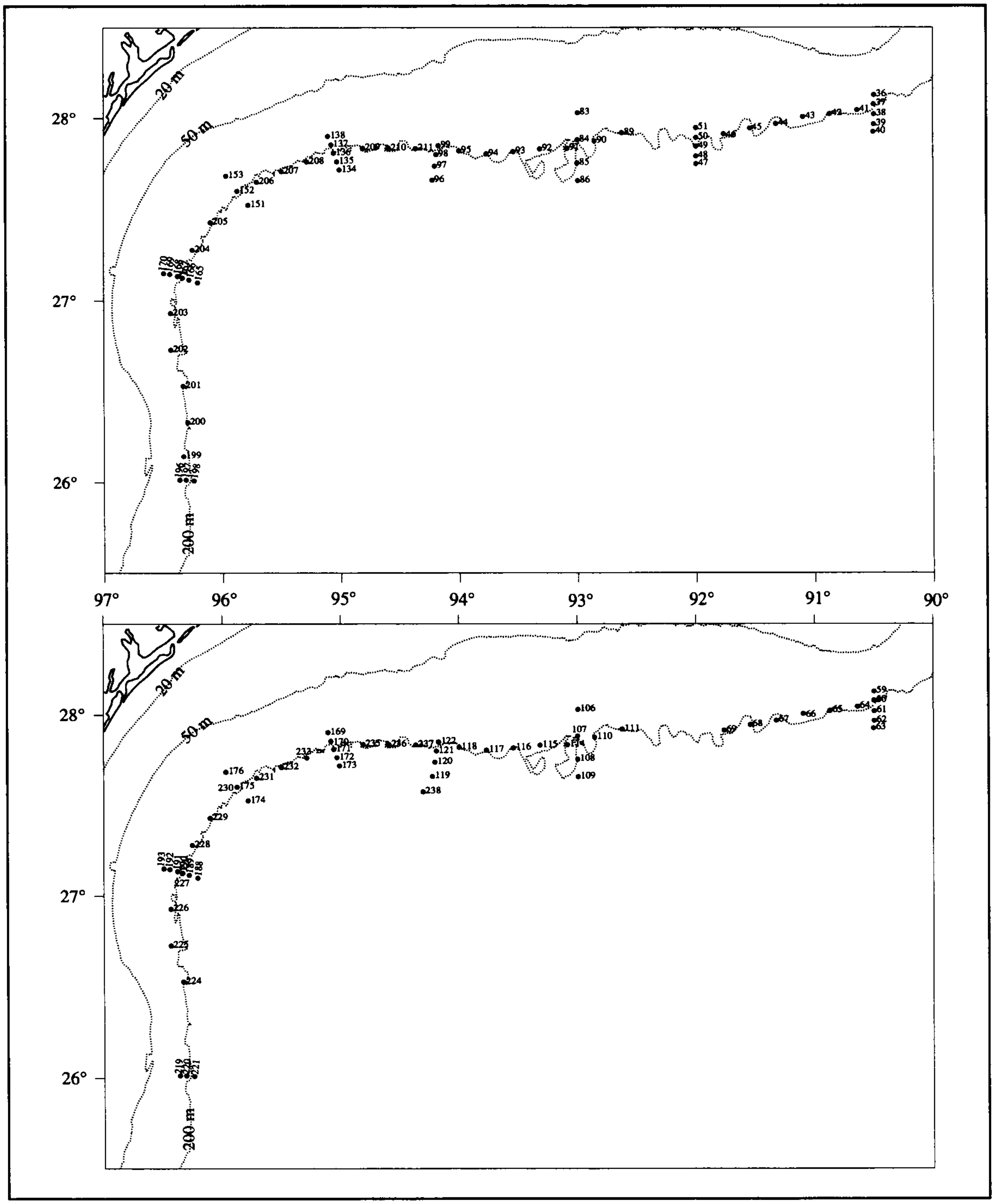

Figure J.1-1. CTD stations used in geostrophic computations from LATEX A hydrographic cruises: (upper) H06, 26 July-7 August 1993, and (lower) cruise H07, 7-21 November 1993.

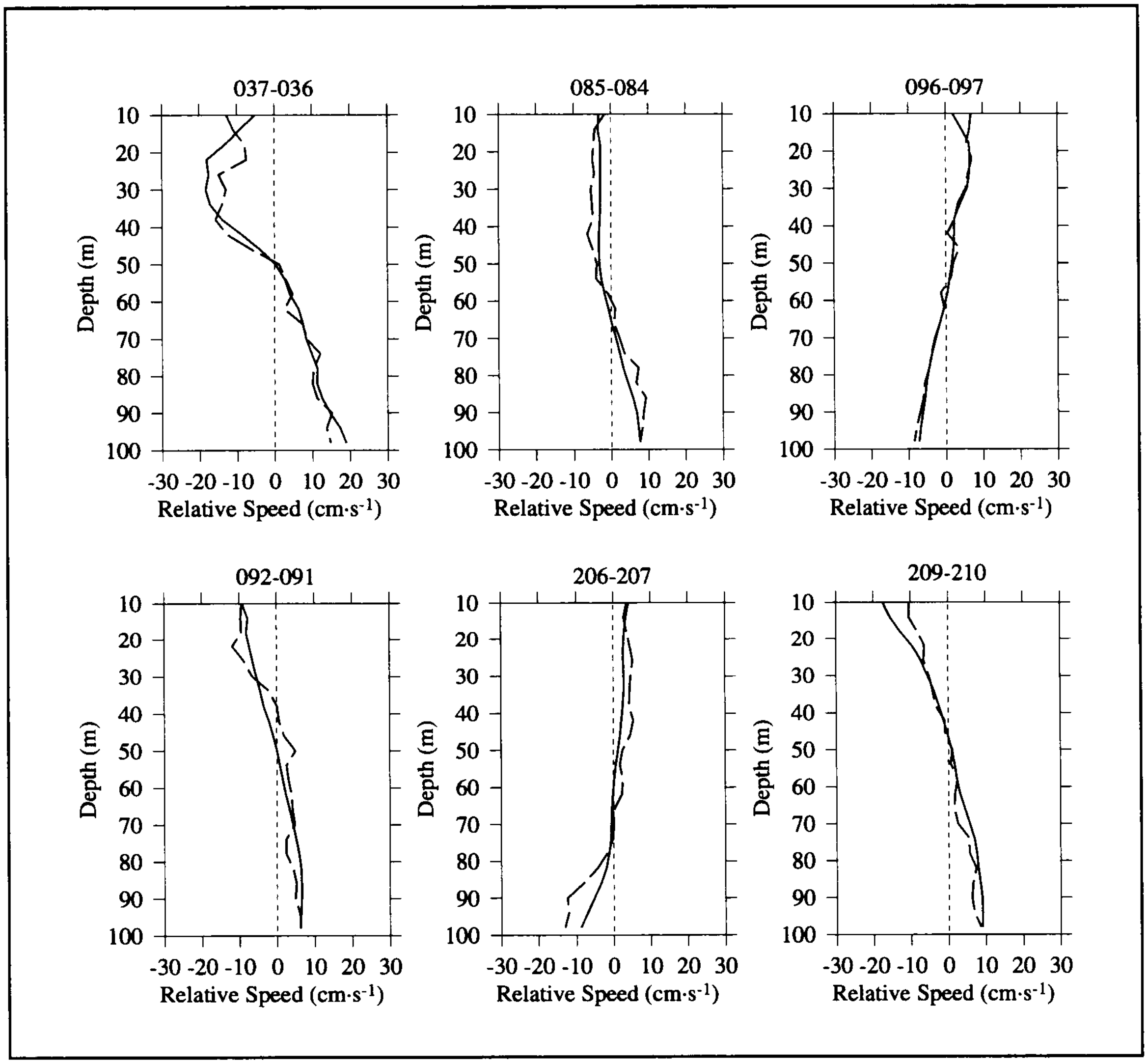

Figure J.1-2. Comparisons of demeaned ADCP current shears (dashed) with CTD-inferred geostrophic shears (solid) for the summer cruise (H06). The upper row shows three profile pairs for the alongshelf component of these two shears. The lower row shows three profile pairs for the cross-shelf components. CTD station pairs are indicated for each profile pair.

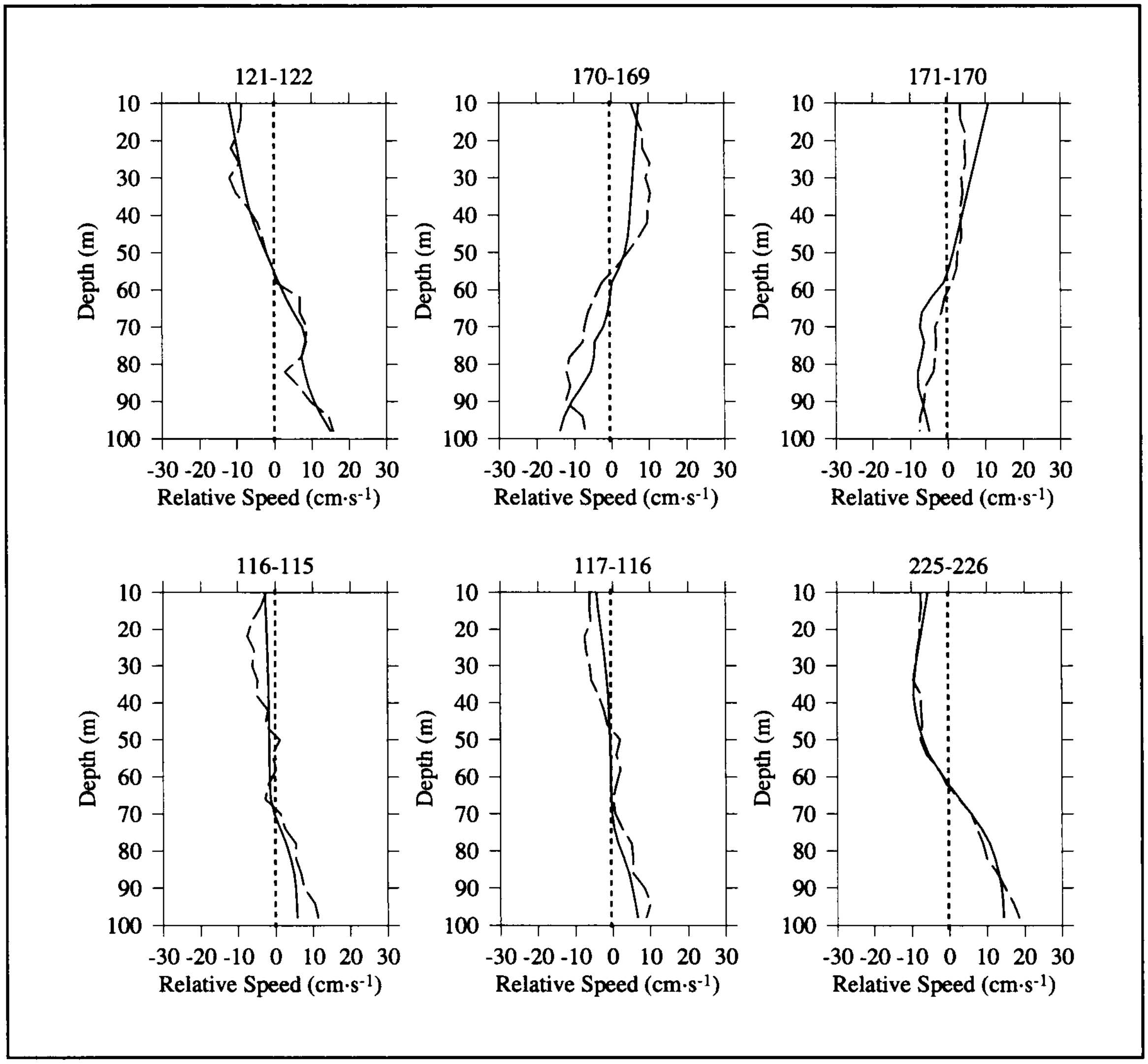

Figure J.1-3. Comparisons of demeaned ADCP current shears (dashed) with CTD-inferred geostrophic shears (solid) for the fall cruise (H07). The upper row shows three profile pairs for the alongshelf component of these two shears. The lower row shows three profile pairs for the cross-shelf components. CTD station pairs are indicated for each profile pair.

Table J.1-1. List of rms differences ($cm \cdot s^{-1}$) and correlation coefficients (r) between ADCP and CTD-inferred geostrophic shears for each station pair during the summer cruise (H06).

Alongshelf component			Cross-shelf component		
stations	rms	r	stations	rms	r
37-36	3.8	0.95	41-37	5.1	-0.06
39-38	7.6	0.91	42-41	5.0	0.77
40-39	5.3	0.93	43-42	4.1	0.93
47-48	3.3	0.22	44-43	4.7	0.81
48-49	3.9	0.32	45-44	3.5	0.22
50-51	3.8	0.65	46-45	5.2	0.14
84-83	4.3	0.86	50-46	1.7	0.86
85-84	2.0	0.96	90-89	4.8	0.83
86-85	1.8	0.94	91-90	2.7	0.61
96-97	1.4	0.96	92-91	2.3	0.92
97-98	3.1	0.79	93-92	1.8	0.72
98-99	4.8	0.80	94-93	3.8	0.96
134-135	5.9	0.65	95-94	3.3	0.94
135-136	4.0	0.87	197-199	5.0	-0.03
137-138	6.2	0.96	199-200	3.6	0.92
151-152	4.6	0.99	200-201	6.2	-0.26
152-153	3.2	0.94	201-202	4.6	-0.58
165-166	7.2	-0.62	202-203	2.4	0.87
166-167	5.8	0.90	203-204	2.0	0.48
167-168	4.7	0.85	204-205	3.9	0.71
168-169	9.2	0.34	205-206	3.8	0.34
169-170	5.2	-0.55	206-207	2.8	0.96
197-196	7.0	0.94	207-208	5.4	-0.31
198-197	7.5	0.96	208-209	5.4	0.92
			209-210	2.6	0.98
			210-211	2.0	0.78

Table J.1-2. List of rms differences ($cm \cdot s^{-1}$) and correlation coefficients (r) between ADCP and CTD-inferred geostrophic shears for each station pair during the fall cruise (H07).

Alongshelf component			Cross-shelf component		
stations	rms	r	stations	rms	r
60-59	11.1	0.82	65-64	7.0	-0.76
63-62	3.6	0.44	66-65	5.7	0.99
107-106	2.3	0.58	67-66	7.5	0.97
108-107	1.5	0.84	68-67	3.7	0.71
109-108	2.9	0.53	69-68	2.7	-0.51
119-120	3.0	0.86	110-111	1.4	0.39
120-121	3.4	0.86	114-110	2.5	0.74
121-122	2.0	0.97	115-114	1.4	0.88
170-169	4.0	0.88	116-115	2.8	0.94
171-170	3.4	0.88	117-116	2.8	0.93
172-171	3.2	0.80	118-117	2.5	0.35
173-172	6.5	-0.07	224-225	3.9	0.39
174-175	2.1	0.44	225-226	1.5	0.99
175-176	5.0	-0.47	228-229	3.2	0.76
188-189	3.3	0.79	229-230	3.5	0.65
191-192	7.6	0.89	230-231	4.3	0.42
192-193	2.6	0.78	231-232	4.4	0.11
221-220	4.5	-0.23	232-233	3.0	0.50
238-119	2.9	0.04	233-234	3.7	0.71
			235-236	3.2	0.22
			236-237	3.8	-0.52

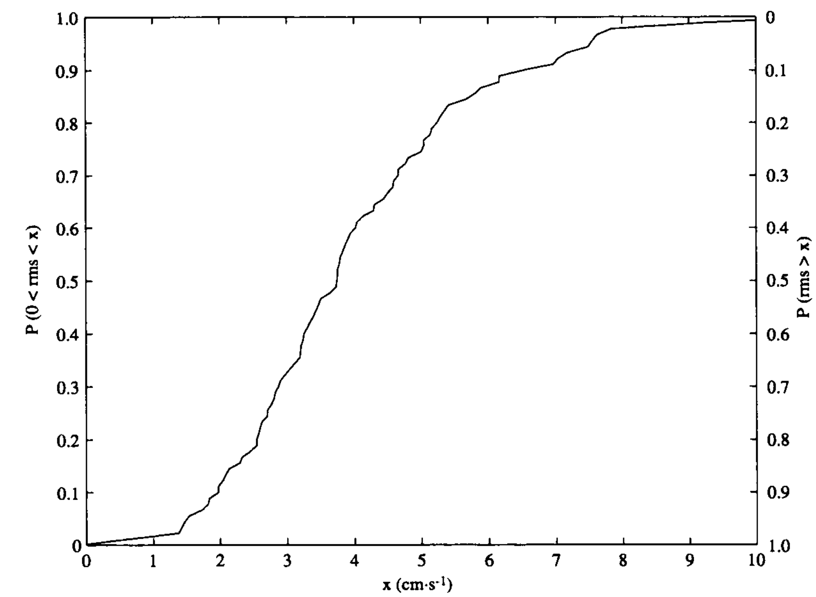

Figure J.1-4. Cumulative distribution of rms difference between the demeaned ADCP and CTD-inferred vertical shears (cm·s^{-1}) based on cruises H06 and H07. The left vertical scale is the probability P that the rms difference is less than given value x, while the right vertical scale give the probability that the rms is greater than x.

The cumulative distribution of correlation coefficient for the profile pairs (Figure J.1-5) represents an estimate of the probability that r has a value between -1 and given value on the abscissa. For positive r values, this cumulative distribution is very nearly exponential and hence, its derivative (the pdf) is also nearly exponential. Thus, the most probable (mode) value of r is nearly 1.0, while the median and mean based on the sample data are 0.78 and 0.57, respectively. For an exponential pdf with mode of unity, the departure of the mean from unity (0.43 in the present case) is the e-folding scale for the distribution.

Of the many comparisons of ADCP and CTD-based vertical shear profiles in the literature, none give sufficient information to assess the distribution of r values for an ensemble of profile pairs as given here. In the analysis by Kosro and Huyer (1986) of survey data in coastal waters off northern California, the focus is primarily on horizontal current patterns at 30 m and 100 m based on ADCP data together with (CTD-based) geostrophic current relative to 500 m. They provide correlations of like components of velocity at 30 m relative to that at 100 m from the ADCP and CTD data. A correlation of 0.70 based on 67 sample pairs was found for survey data taken in 1981, and one of 0.87 based on 44 pairs from 1982

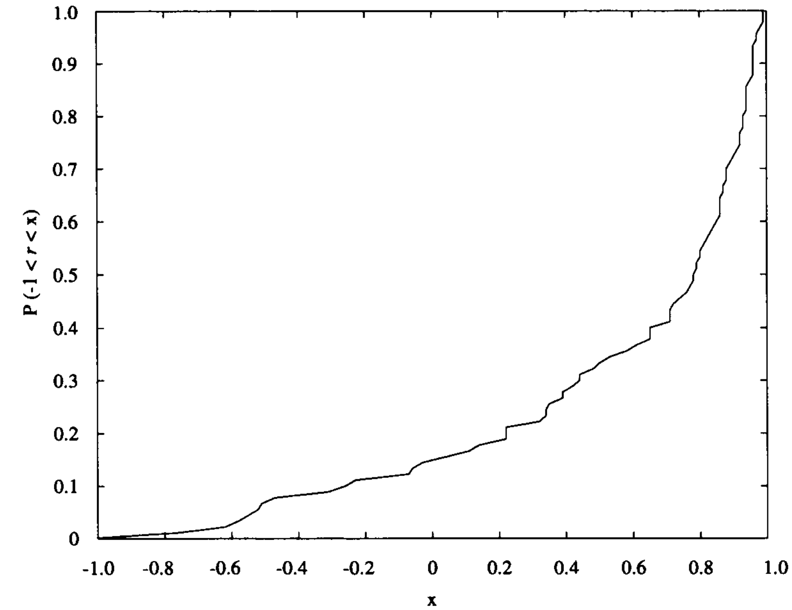

Figure J.1-5. Cumulative distribution of correlation (r) between the demeaned ADCP and CTD-inferred vertical shears based on cruises H06 and H07. The vertical scale is the probability P that the correlation r is less than given value x.

survey data. These correlations (averaging 0.77) are significantly higher than the mean of 0.57 computed from the ensemble of r values from the LATEX A data.

One conclusion that may be drawn from this contrast to the Kosro and Huyer values of r is that the correlation is quite sensitive to the method of analysis. As confirmation of this conclusion, sample estimates of correlation for 10-m pairs based on LATEX A data show significantly larger values (order 0.8) than the mean (0.57) of the ensemble of profile r values shown in Figure J.1-5. Another conclusion is that the high r values based on the gross shear, like 30 m relative to 100 m, must be related to the findings of Figure J.1-5, which indicate a nearly exponential distribution of r, with a median value significantly higher that the mean and a mode near unity.

EOF analyses of shear profiles

To gain additional insight regarding the differences that exist between the ADCP and CTD-based vertical shear, an EOF analysis was applied to the LATEX A profile pairs. We first carried out EOF analyses for ADCP current shear and CTD-based geostrophic shear individually and found that the results were very similar, including the structures of the eigenfunctions and the percentages of total variance contained in the first three modes. Therefore, we combined the covariance matrices for both cruises into a single covariance matrix for each component of shear and then performed the EOF analysis based on the composite matrices, each of size 23 by 23. Figure J.1-6 shows the first three eigenfunctions for the along- and cross-shelf components. The first EOF modes for both components account for about 77 percent of the total variance and have one zero crossing near the middle of the depth range. The first three modes account for about 95 percent of the total variance for each component. The EOF modal profiles of relative current components are based on a sample size of 180, and the first three eigenvalues differ from one another by at least a factor of two. Using the North et al. (1982) sample variability relations, it can be shown that both the EOF eigenvalues and the associated modal profiles are reasonably stable estimates.

Using the common EOF modes for the given component of shear, we analyzed the amplitudes for the first three modes associated with each profile pair (ADCP and CTD-based shear). Here we discuss only the cross-shelf results of this analysis, they being typical of both. Figure J.1-7 shows plots of the amplitudes of the first three modes based on cross-shelf ADCP shear and for CTD-based shear versus distance along the 200-m isobath, based on the summer cruise H06. Similar plots based on the fall cruise H07 are shown in Figure J.1-8. The correlation between the amplitudes for the first mode based on ADCP and CTD for both cruises is nearly 0.80, while the second and third modes are characterized by correlations of order 0.4 and 0.2, respectively, the latter being not significantly different from zero. The high correlation for the first EOF mode is comparable to what one gets using the method of correlation of the gross shear (upper level relative to lower level), as in the analysis of Kosro and Huyer (1986). In retrospect, this is what one should expect, since the dominant EOF modal shape is nearly a linear trend profile, as tacitly implied in the method of Kosro and Huyer.

Of course, the physical reason for the difference between ADCP and CTD-inferred vertical shear profiles lies in the ageostrophic effects contained in the ADCP direct measurements, plus any measurement error in either ADCP or CTD data. Of the ageostrophic effects included in the ADCP, frictionally-induced shear associated with the wind-induced upper Ekman layer could play a significant role. Another possible source of ageostrophic shear included in the ADCP data could be that associated with frequencies near and higher than the inertial frequency, namely inertial motion, baroclinic tidal motion, and internal waves. The near inertial motion is fairly energetic on the Texas-Louisiana shelf (Chen et al., 1996). Because of their smaller vertical scale, it is speculated that these ageostrophic effects show up more strongly in the second and higher EOF modes, and probably account for the very low correlations found for these modes.

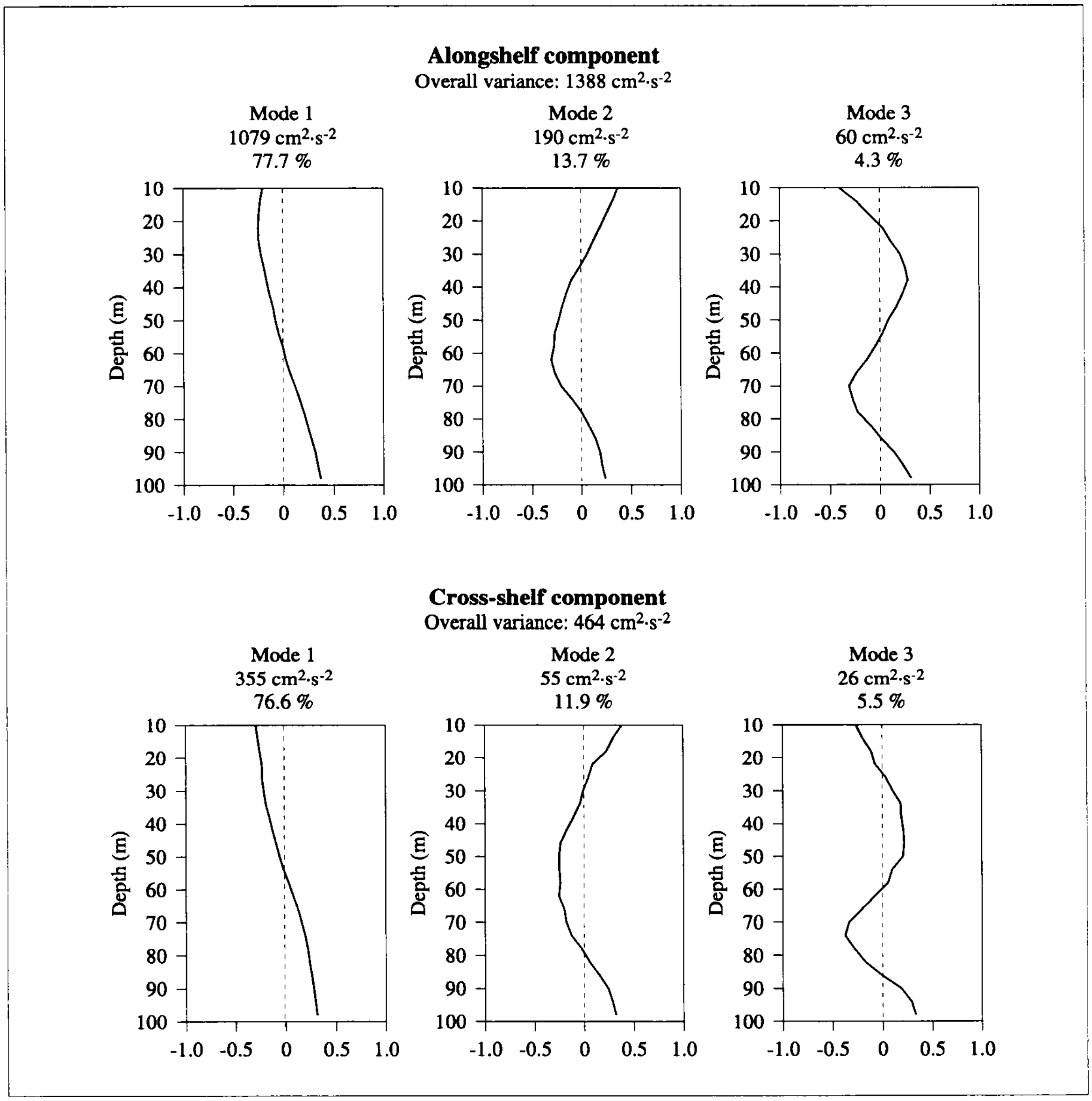

Figure J.1-6. The first three EOF profiles of alongshelf (upper) and cross-shelf (lower) components derived from the composite covariance matrix based on ADCP and CTD-inferred shears based on cruises H06 and H07. The variance and the percentage of the total variance explained by each EOF mode is shown.

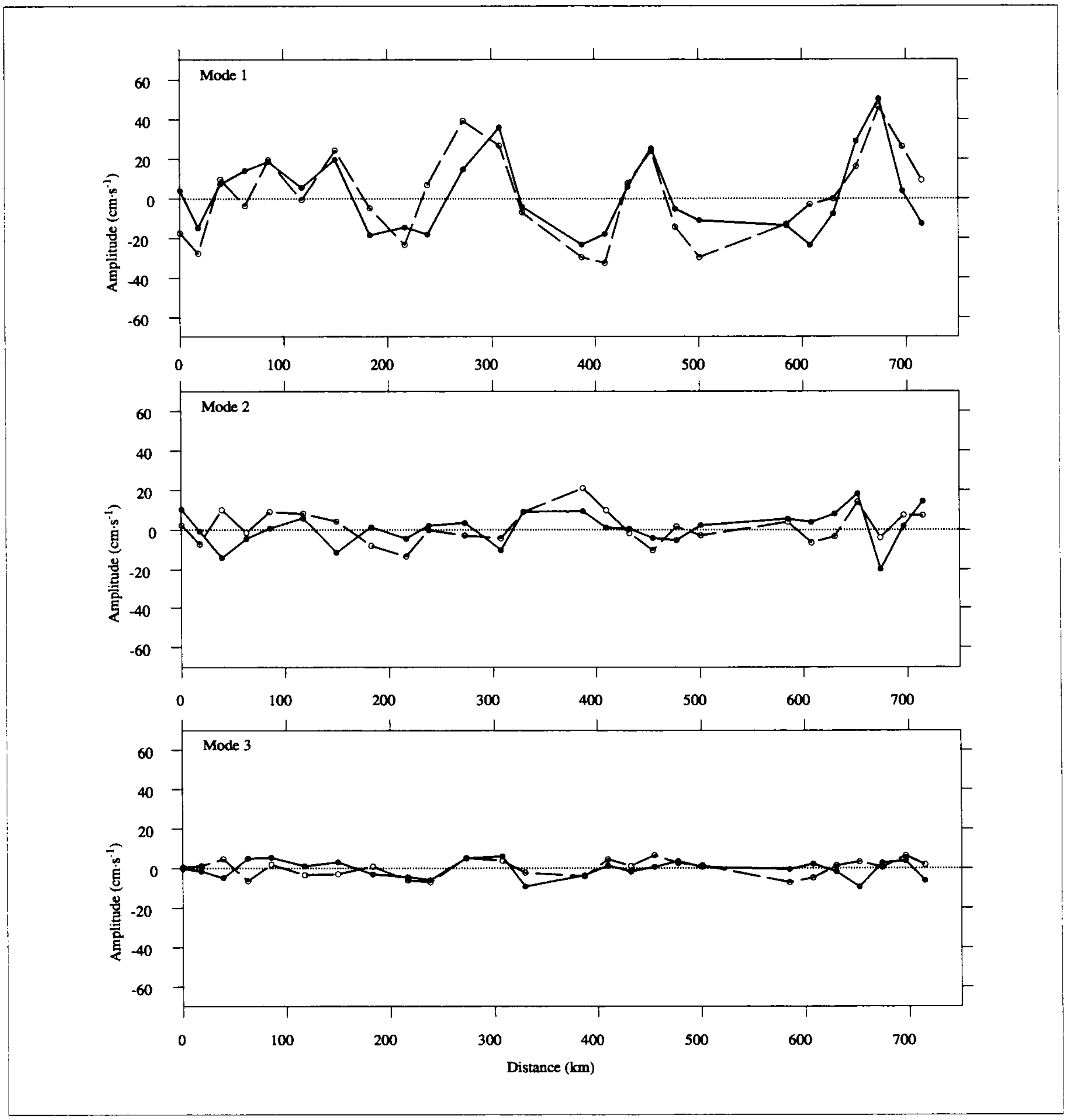

Figure J.1-7. The first three EOF modal amplitudes of the cross-shelf components of ADCP (dashed) and geostrophic (solid) shears as a function of arc distance along the 200-m isobath from station 197 for the summer cruise (H06).

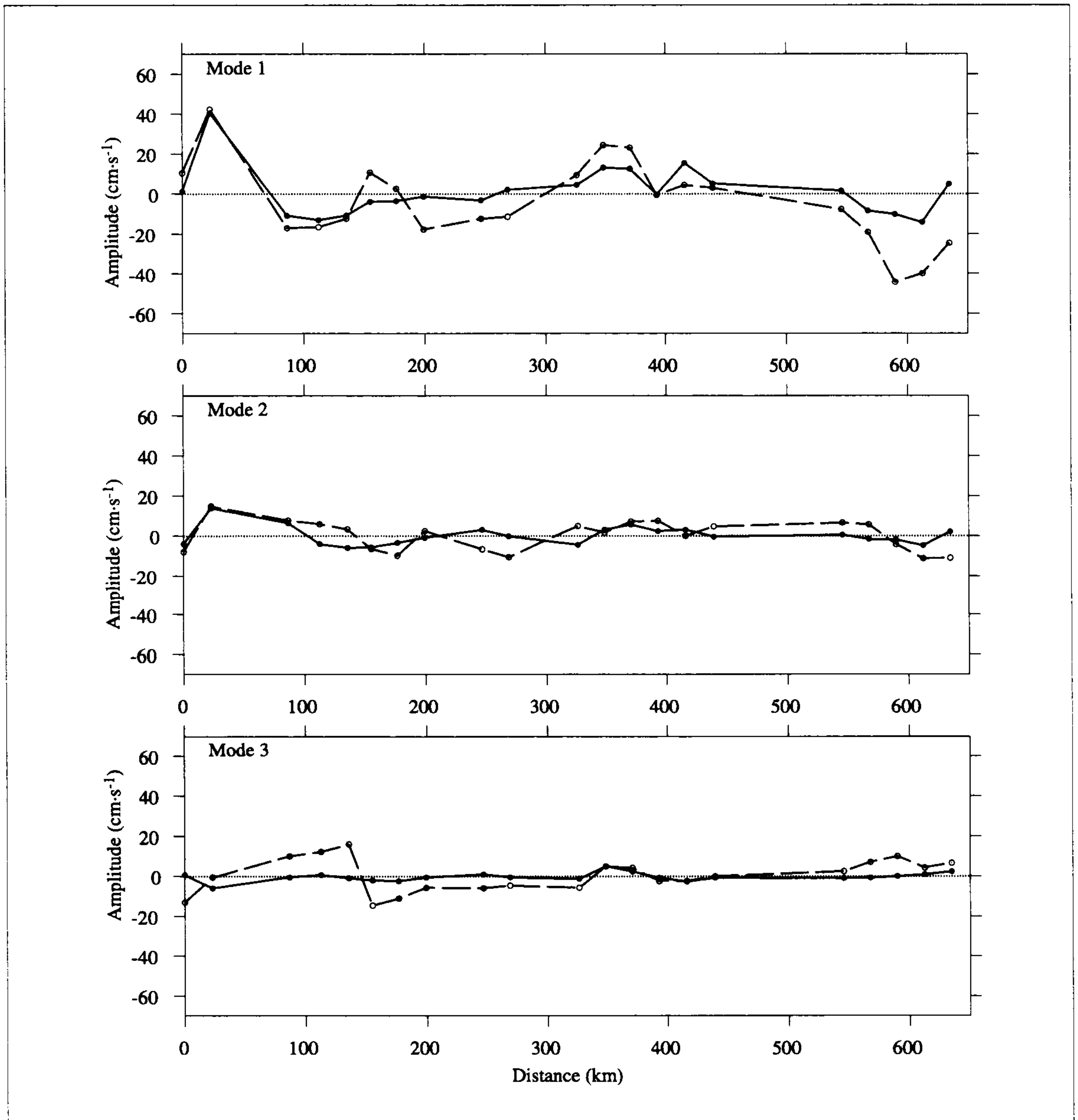

Figure J.1-8. The first three EOF modal amplitudes of the cross-shelf components of ADCP (dashed) and geostrophic (solid) shears as a function of arc distance along the 200-m isobath from station 224 for the fall cruise (H07).

Summary

The ensemble of correlation coefficients *r*, computed for individual demeaned profile pairs based on ADCP shear and CTD-inferred geostrophic shear over the depth range 10-98 m at 4-m resolution, have a nearly exponential cumulative distribution with mode, median and mean of about 1.0, 0.78, and 0.57, respectively, for the Texas-Louisiana shelf near the 200-m isobath. This exponential character of the distribution implies that a profile pair picked at random from the ensemble typically has high correlation. The difference between mode and mean (0.43) is essentially a measure of the e-folding scale of the exponential distribution. The median, which is close to 0.8, seems to characterize the correlation from pairs of 10-m ADCP and geostrophic current relative to that at about 100 m. This is consistent with the correlation between the amplitudes of the first EOF mode derived from the ADCP and geostrophic shears. The differences that occur between the ADCP and geostrophic shear are probably due to the ageostrophic wind-induced Ekman shear and baroclinic near-inertial motion that is present in the ADCP data. These effects seem to be confined largely to the second and higher EOF modes of the shear profiles, since the correlations between the amplitudes for like modes derived from ADCP and geostrophic shear profiles are very small (order 0.4 or less). No attempt has been made to estimate the contribution to differences between ADCP and CTD-inferred shear based on measurement error. However, the statistics of rms difference, having nearly a Rayleigh distribution, could be useful in follow-on studies of this and other issues within the topic of geostrophic comparison.

J.2 Comparison of current meter and ADCP velocities

A complete discussion of LATEX A ADCP data is contained in a data report by Bender and Kelly (1998). Using measurements obtained during nine LATEX A cruises (H03, M03, H04, H05, H06, H07, H08, H09, and H10), we compared ADCP-determined velocity to the velocity from the nearest current meter mooring. To make that comparison, we established three screening criteria: (1) the distance of closest approach between the ship as it recorded the profile and the location of the mooring had to be less than 10 km; (2) the difference between the two sample times had to be less than or equal to 30 minutes; (3) the depth of the instrument had to be within a 4-m depth bin of the Doppler current profile; and (4) the current meters had to be recording usable data when the ship steamed by the mooring.

Given these criteria, we found 2551 matches between current meters and associated ADCP velocity: 160 from cruise H03, 294 from M03, 238 from H04, 139 from H05, 416 from H06, 393 from H07, 349 from H08, 184 from H09, and 378 from H10. It should be noted that multiple matches could occur at each mooring location if there was more than one current meter in the vertical.

Figures J.2-1 and J.2-2 show examples of the comparisons for H06, where u is the zonal velocity and v is the meridional velocity. These comparisons present some of the best agreement between current meter and ADCP velocities of all nine cruises. As a quantitative measure of the agreement, we employed two separate statistical measures: the rms error based on the speed and a complex regression analysis to determine the average angle between the two velocities.

The rms difference between current meter speed and ADCP speed is given by

$$\mathrm{rms} = \sqrt{\left\langle (\bar{u}_2 - \bar{u}_1)^2 \right\rangle},$$

where $\bar{u}_1$ is the current meter speed, $\bar{u}_2$ is the ADCP speed, and < > denotes the average over n matches. The rms difference does not provide any information about the difference in the angles between the ADCP and the current meter velocities. Complex linear regression analysis, on the other hand, yields the average angle between two sets of vectors as well as a measure of the regression modulus and coherence. The method presented here is further described in Vastano and Barron (1994) and Kundu (1976).

If u_j and v_j are the zonal and meridional velocity components, where j = 1 denotes the current meter velocities and j = 2 the ADCP velocities, then it can be shown that the average angle between two sets of vectors is given by

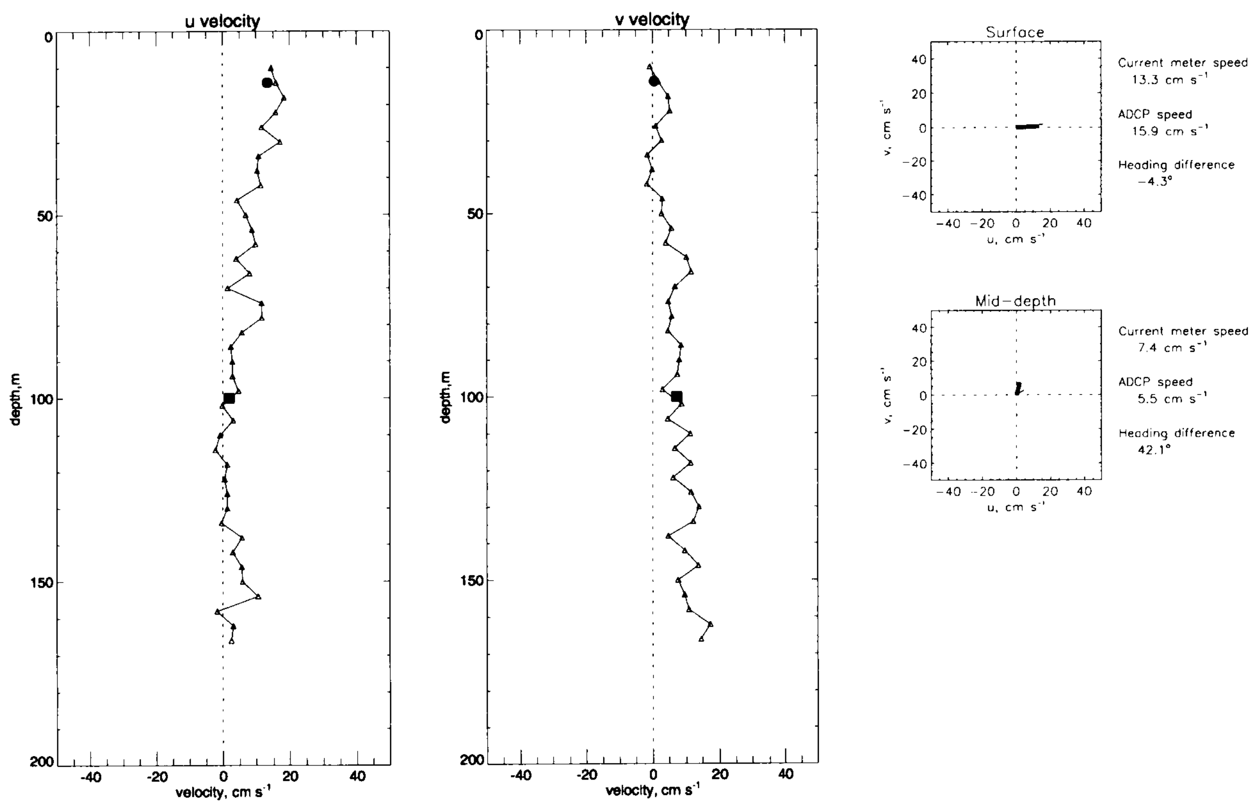

Figure J.2-1. ADCP profile taken on 4 August 1993 at 1342 UTC (cruise H06) while passing mooring 4 at a distance of 1.2 km. Velocities for the surface meter (14 m) are marked with a circle and were recorded at 1330 UTC. Velocities for the middle meter (100 m) are marked with a square and were recorded at 1330 UTC. The right panels show the velocity vectors for the current meter (thick line) and the corresponding ADCP bin (thin line).

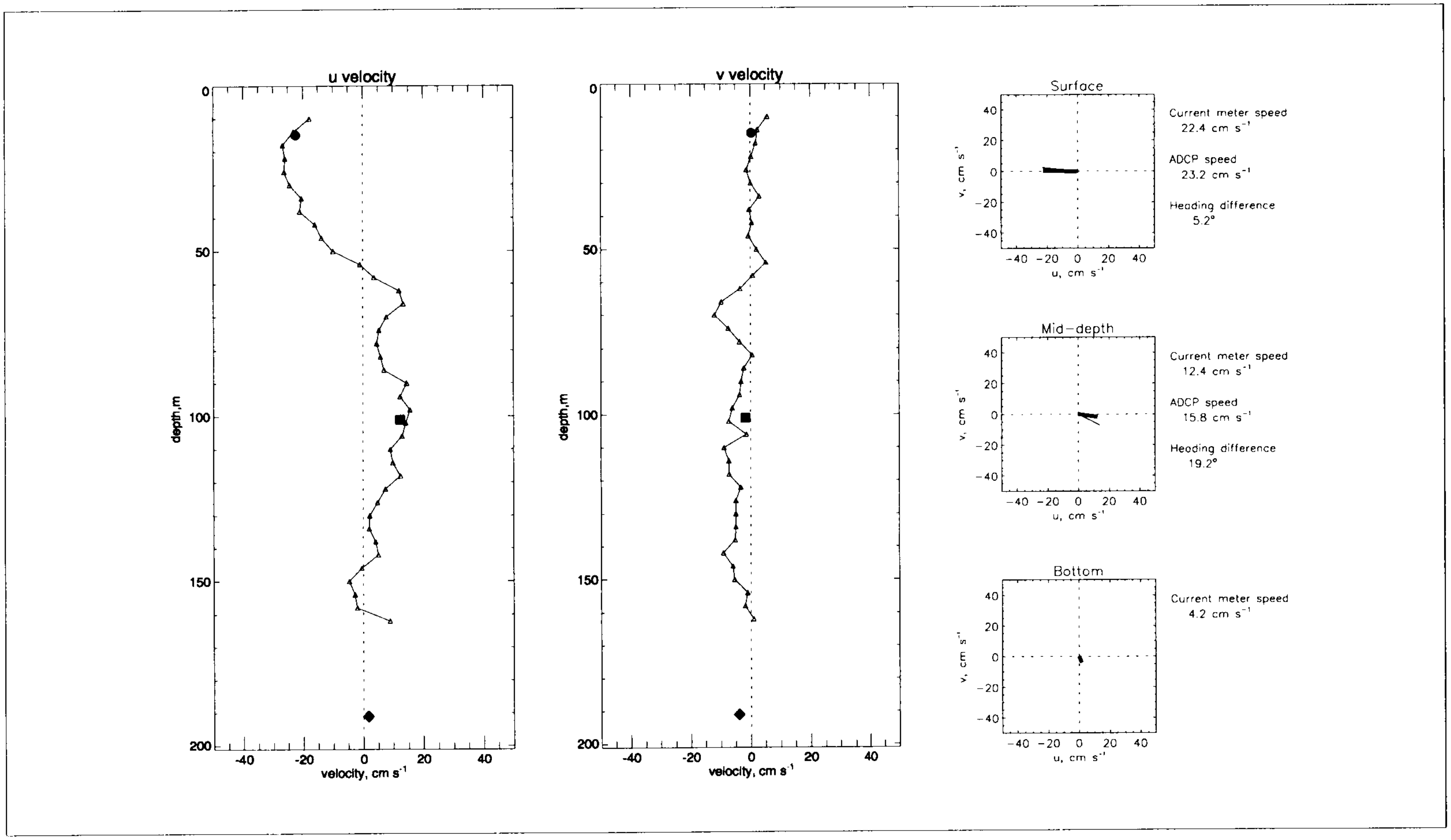

Figure J.2-2. ADCP profile taken on 31 July 1993 at 1854 UTC (cruise H06) while passing mooring 9 at a distance of 0.8 km. Velocities for the surface meter (15 m) are marked with a circle and were recorded at 1900 UTC. Velocities for the middle meter (101 m) are marked with a square and were recorded at 1900 UTC. Velocities for the bottom meter (191 m) are marked with a diamond and were recorded at 1900 UTC. The right panels show the velocity vectors for the current meter (thick line) and the corresponding ADCP bin (thin line).

$$\alpha = \arctan\left(\frac{\langle u_1 v_2 - u_2 v_1 \rangle}{\langle u_1 u_2 + v_1 v_2 \rangle}\right).$$

The parameter α is the counterclockwise regression angle of the $j = 2$ vectors relative to the $j = 1$ vectors. It is effectively the phase of the ensemble of the vector pairs; e.g., if the angle of the current meter velocity vector was 30° and that of the ADCP velocity vector was 45°, then α would be -15°.

The regression modulus b_m is found by

$$b_m = \frac{\langle u_1 u_2 + v_1 v_2 \rangle}{\langle u_1^2 + v_1^2 \rangle} \sec\alpha .$$

It provides a measure of the gain or bias between the two vector sets; e.g., if the current meter velocity were 10 cm·s^{-1} and the ADCP velocity were 20 cm·s^{-1}, then b_m would be 2.0.

The fraction of the variance of the $j = 2$ vector set explained by linear relation with the $j = 1$ vector set is given by ρ, and can be determined from

$$\rho^2 = b_m^2 \frac{\langle u_1^2 + v_1^2 \rangle}{\langle u_2^2 + v_2^2 \rangle}.$$

The parameter ρ^2 is effectively the square of the coherence; i.e., if all of the variance in the ADCP vectors were described by the current meter vectors, then ρ^2 would be 1.0. However, any value above 0.5 is considered good. The ideal agreement between current meter velocities and ADCP velocities would yield $\alpha = 0$, $b_m = 1.0$, and $\rho^2 = 1.0$. As will be seen, this is rarely even approached.

Figure J.2-3 shows the statistics, on a cruise by cruise basis, for every match between current meter and ADCP measurements that meets the requirements of distance, time, vertical position, and an operational current meter. Table J.2-1 shows the actual data. The ADCP speeds are clearly biased higher than the current meter speeds. The rms difference in speed averaged for all nine cruises is 12.30 cm·s^{-1} (shown with a dotted line on Figure J.2-3), the regression angle α averaged for all nine cruises is -1.56°, the cruise-averaged regression modulus b_m is 0.835, and the cruise-averaged variance fraction ρ is 0.483 (all shown with a dotted line). The variance fraction can be interpreted as a sensitive indicator of the goodness of the comparison. Using the average variance as the standard, there are three cruises (H05, H06, and H10) that are distinctly better than average, three cruises (H07, H08, and H09)

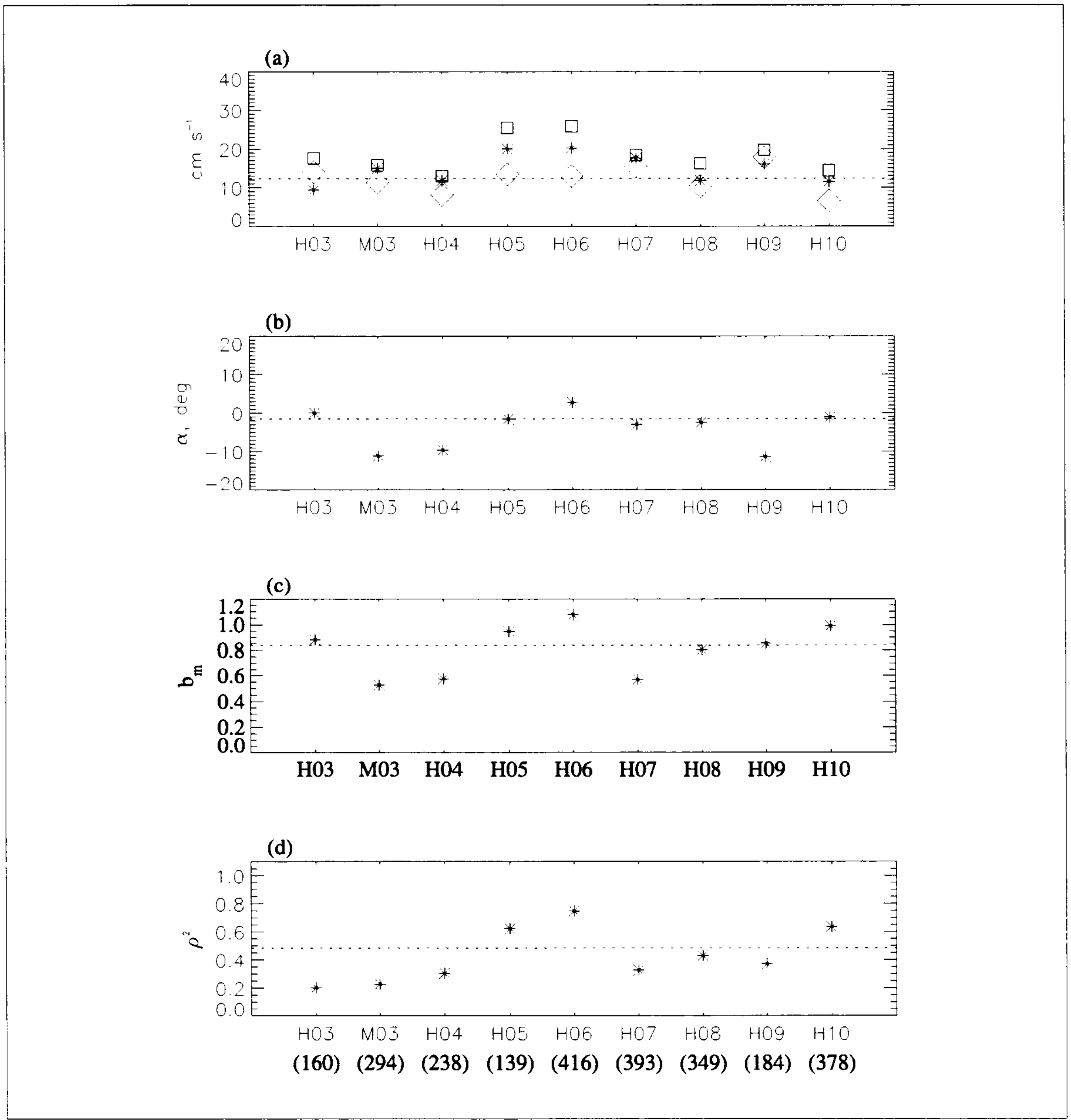

Figure J.2-3. Comparison statistics for all pairs that met the primary requirements. Panel (a) shows for each individual cruise the rms error (diamond), average current meter speed (asterisk), and average ADCP speed (square), as well as the cruise averaged rms error (dotted line). Panel (b) shows the counterclockwise regression angle, panel (c) the regression coefficient, b_m, and panel (d) the variance fraction or coherence squared. The sample size is in parenthesis.

Table J.2-1. ADCP-current meter comparison statistics ≤ 10-km separation distance.

LATEX ID	Sample Size	Mean Speed CM, cm·s^{-1}	Mean Speed ADCP, cm·s^{-1}	rms cm·s^{-1}	Alignment Angle, α	Regression Modulus, b_m	Variance Fraction, ρ
H03	160	9.38	17.61	14.03	0.02	0.880	0.202
M03	294	14.96	15.81	11.36	-11.17	0.529	0.227
H04	238	11.80	12.96	8.14	-9.58	0.575	0.304
H05	139	20.05	25.40	13.42	-1.57	0.949	0.624
H06	416	20.22	25.79	12.95	2.75	1.075	0.747
H07	393	17.61	18.39	15.45	-2.95	0.569	0.326
H08	349	11.77	16.20	10.30	-2.50	0.803	0.430
H09	184	16.04	19.72	17.62	-11.38	0.853	0.370
H10	378	11.48	14.34	6.62	-1.10	0.993	0.635
All	2551	14.98	18.32	12.30	-1.56	0.835	0.482

that are slightly worse than average, and three cruises (H03, M03, and H04) that are distinctly worse than average. There appears to be no correlation between the sample size, shown in parentheses, and the statistical measures. The best comparison resulted for cruise H06. The rms speed difference is 12.95 cm·s^{-1}, the regression angle α is 2.75°, the variance fraction ρ is 0.747, and the regression modulus b_m is 1.075.

The closer the distance between the current meter and the ADCP profile, the better the agreement becomes. Figure J.2-4 shows the comparison statistics for all pairs (no distinction is made for individual cruises) within the specified distance range between the ADCP and current meter. Reducing the distance between the ADCP profile and the current meter improves the agreement. The bias between current meter speed and ADCP speed is reduced; the rms difference in speed is greatly reduced; the cruise-averaged regression angle α is not greatly affected; and the cruise-averaged regression modulus b_m is slightly improved. The most dramatic improvement is seen in the cruise-averaged variance fraction ρ. It can be inferred that, over a long enough period of time, an ADCP and a current meter placed in the same location would produce the same values.

We show in Table J.2-2 the statistics on a cruise by cruise basis for each pair of current meter and ADCP measurements that met the requirements of time, vertical position, and an operational current meter, but were within 2 km rather than 10 km. Comparing with Table J.2-1, we see overall improvement for all cruises except M03 and H03.

As a result of this analysis, we can state with a high degree of confidence that except for M03, H03, and possible H04, the ADCP and the current meter are measuring the same thing. The fact that the statistics presented in Table J.2-1 for a 10-km separation distance criteria are worse for some cruises (e.g., H04) than for other cruises (e.g., H10) should not

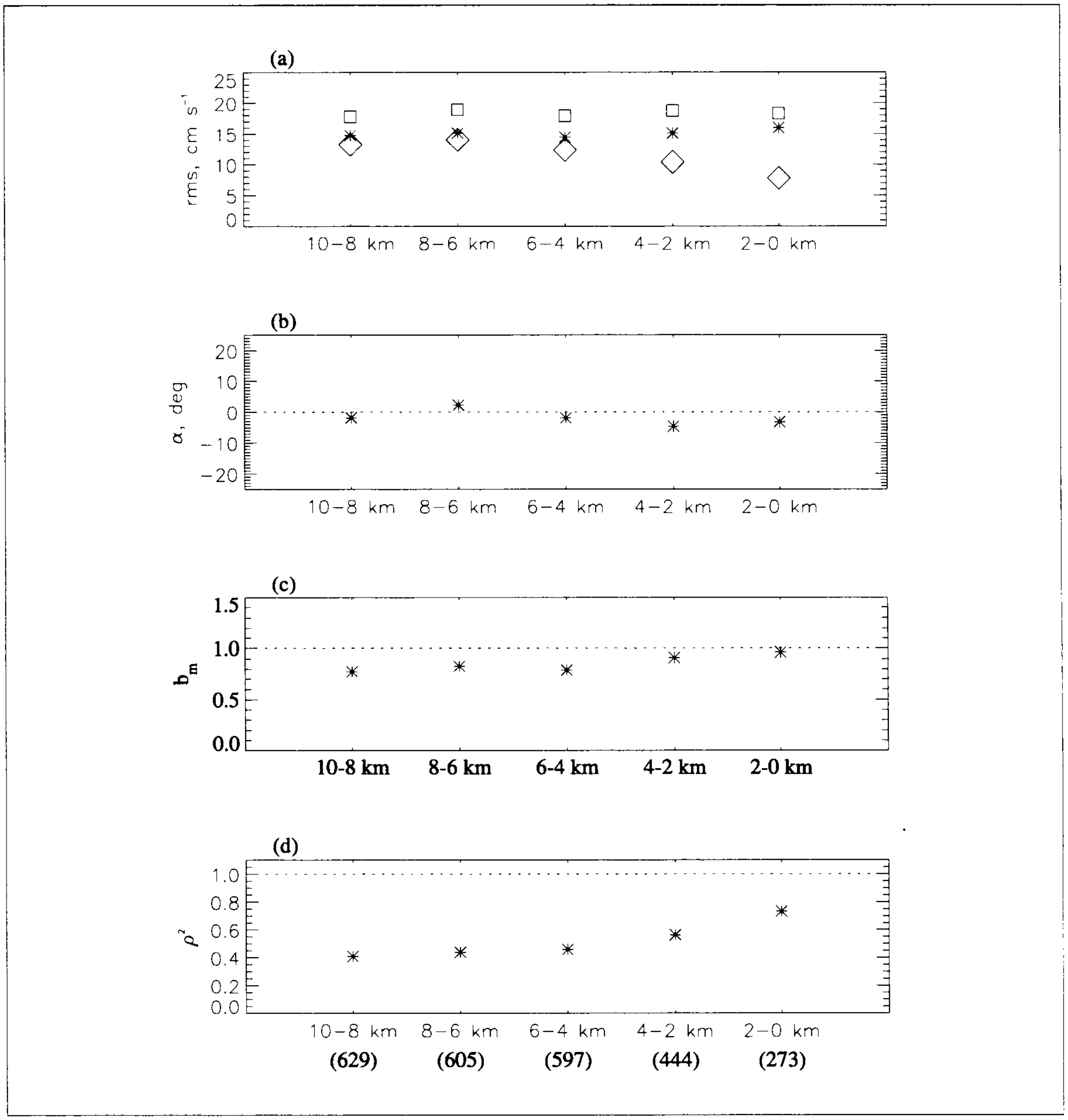

Figure J.2-4. Comparison statistics for all pairs within the specified distance range between ADCP and bottom current meters. Panel (a) shows for each distance the rms error (diamond), average current meter speed (asterisk), and average ADCP speed (square). Panel (b) shows the counterclockwise regression angle, panel (c) the regression coefficient, b_m, and panel (d) the variance fraction or coherence squared.

Table J.2-2. ADCP-current meter comparison statistics ≤ 2-km separation distance.

LATEX ID	Sample Size	Mean Speed CM, $cm \cdot s^{-1}$	Mean Speed ADCP, $cm \cdot s^{-1}$	rms $cm \cdot s^{-1}$	Alignment Angle, α	Regression Modulus, b_m	Variance Fraction, ρ
H03	19	9.50	14.80	8.95	19.48	0.869	0.326
M03	44	14.76	13.78	7.68	-11.85	0.607	0.358
H04	26	16.08	15.14	9.68	-2.21	0.719	0.589
H05	17	24.28	26.77	6.97	-6.94	1.010	0.840
H06	37	18.17	21.43	6.92	-1.38	1.103	0.919
H07	22	19.80	23.12	9.05	2.74	1.029	0.834
H08	43	12.88	17.02	8.83	2.99	0.939	0.638
H09	24	21.03	22.61	6.03	-12.80	1.061	0.929
H10	44	12.95	16.45	5.95	0.24	1.128	0.826
All	276	15.93	18.25	7.79	-3.21	0.961	0.731

necessarily be interpreted as the result of poor quality ADCP data. The differences could also be attributed to the presence of significant horizontal variations (with scales 10 km and less) in the velocity field. Those variations could be more pronounced during some cruises and would result in a poorer agreement when all the pairs within 10 km of a current meter are considered. However, as shown in Figure J.2-4 and Table J.2-2, decreasing the separation distance eliminates the effect of horizontal variations and shows a better agreement.

Appendix K: Wave Propagation Along the Shelf and Slope

This section addresses evidence for the existence of coastal trapped wave phenomena in the LATEX and collateral data on the Texas-Louisiana continental shelf or along the much steeper continental slope. We analyzed current, temperature, and salinity data from the LATEX A mooring array along the 200-m isobath. Time domain plots show evidence of both downcoast and upcoast propagation of coherent features in alongshelf and cross-shelf currents and in temperature and/or salinity records, from one mooring to neighboring moorings. Considerable effort was made using spectral domain analysis of the current meter data along the 200-m mooring array after the method of Hayashi (1979) in attempts to resolve transient signals into propagating and standing waves. An understanding of the results of such spectral domain analyses in terms of linear free wave theory is hampered either by the presence of forcing or by nonlinear current-wave interaction (Church et al. 1986a; Narayanan and Webster 1987, 1988). We, therefore, restrict the discussion of evidence for free wave propagation to only three, but very definitive, examples in the space-time domain. The first two are illustrations of free shelf wave propagation using moored current meter and water level data on the inner shelf. The third is an illustration of what we believe to be an example of solitonlike eddy propagation (Nakamoto 1989) seen in the 200-m mooring array data along the Texas-Louisiana shelf and supported by the analyses discussed in Section 2.5. Eddies over the slope are essentially free (unforced) disturbances that are seen often. Free shelf waves are much more elusive, at least on the Texas-Louisiana shelf. This in no way implies, however, that locally wind-induced shelf waves are not present. Rather, it is the presence of the latter that masks the evidence of the free waves on the inner shelf.

Evidence of free shelf wave propagation

Initially, coherence and phase calculations were made between water level records (adjusted for local air pressure) at neighboring NOAA/NOS tide gauges along the Texas-Louisiana coast for the entire 32-month period of the LATEX field program. The resulting phase differences showed upcoast propagation, i.e., opposite to that of free shelf wave propagation. We interpret this as resulting from the dominance of intermittent wind forcing over the inner shelf, associated with frontal outbreaks that affect the western region of the shelf first, thus causing a forced signal of response propagating upcoast. This prompted us to look for episodes in the time domain where local forcing was virtually absent in the downcoast region, but with wind forcing present in the eastern region of the shelf, thus producing shelf wave energy that subsequently propagated down coast. Current (1996) identified two clear illustrations of such episodes in the current meter data, supplemented by the collateral water level and sea surface air pressure data.

The first episode was that of a storm, produced by cyclogenesis centered near 27°N, 96°W on 11 March 1993, that rapidly intensified and moved to the east and then northeast, eventually becoming the "Storm of the Century" on the east coast. The effect of this storm on the Texas-Louisiana shelf was to produce very strong downcoast flow on the inner shelf of about 36 hours duration followed by medium strength upcoast flow (see Appendix B.2 for a more complete description of this event). By 14 March, the alongshelf component of the winds were negligible in the region downcoast of the cross-shelf array of moorings 23, 24, and 25 and remained weak for several days. East of this array, an upcoast component of the wind persisted. Figure K-1 shows the alongshelf component of the currents at moorings 25 and 3 for the period during which the local forcing was minimal. Recall from Figure 1.2-1 that mooring 3 is downcoast of 25. The model-simulated alongshelf flow (Current 1996) indicates that the model and data time lags (about 12 hrs) of identifiable features at mooring 3 relative to those at mooring 25 are comparable. The lag of 12 hrs is consistent with a propagation speed of about 420 $km \cdot d^{-1}$ (or 5 $m \cdot s^{-1}$) for the first and dominant nondispersive shelf mode of the model. Since the observed data shows about the same time lag, and since there was little local wind forcing during the period 14-16 March, the observed response at mooring 3 is regarded as primarily due to downcoast free wave propagation of the signal from mooring 25. Similar evidence exists for mooring pairs 1, 23 and 2, 24 (not shown).

Hurricane Andrew in August 1992 provides further evidence for free shelf wave propagation on the inner Texas-Louisiana shelf. The eye of this hurricane made landfall near the eastern array of LATEX moorings on 26 August (see Appendix B.1 for a discussion of winds, currents, and waves associated with this event). Much of the water level response (storm surge) was confined to a spatial scale comparable to that of the hurricane and governed primarily by gravitational restoring forces. The surprising thing is that the hurricane generated a significant topographic shelf wave response as well. This must have been produced by downcoast winds well in advance (24-36 hrs) of Andrew's landfall. The disturbance propagated downcoast on the inner shelf far from any direct forcing and showed up very clearly in the 40-hr low pass water level at Port Isabel as a rise and fall feature of about three-day time scale, with an amplitude of about 20 cm. It also appeared as a similar geostrophically consistent signal in the alongshelf currents (downcoast followed by upcoast) at moorings 24 and 2 (Figure K-2). As in Figure K-1, the shelf model simulation is also compared with the 40-hr low pass current records at the two moorings. Based on the observed data, the time lag at mooring 2 relative to mooring 24 is somewhat larger than for the 14 March 1993 event, however the distance between mooring pair 24, 2 is greater than for pair 25, 3. The model (Current 1996) is constrained to be nondispersive (i.e., restricted to very long waves), and the simulated signal cannot give as good a match for the observed as in Figure K-1 because of the relatively small spatial scale of the free wave produced by the hurricane. Thus, while simulation of observations in the downcoast region leaves room for improvement, the qualitative agreement in configurations leaves little doubt that we have captured another elusive free shelf wave in the observed data.

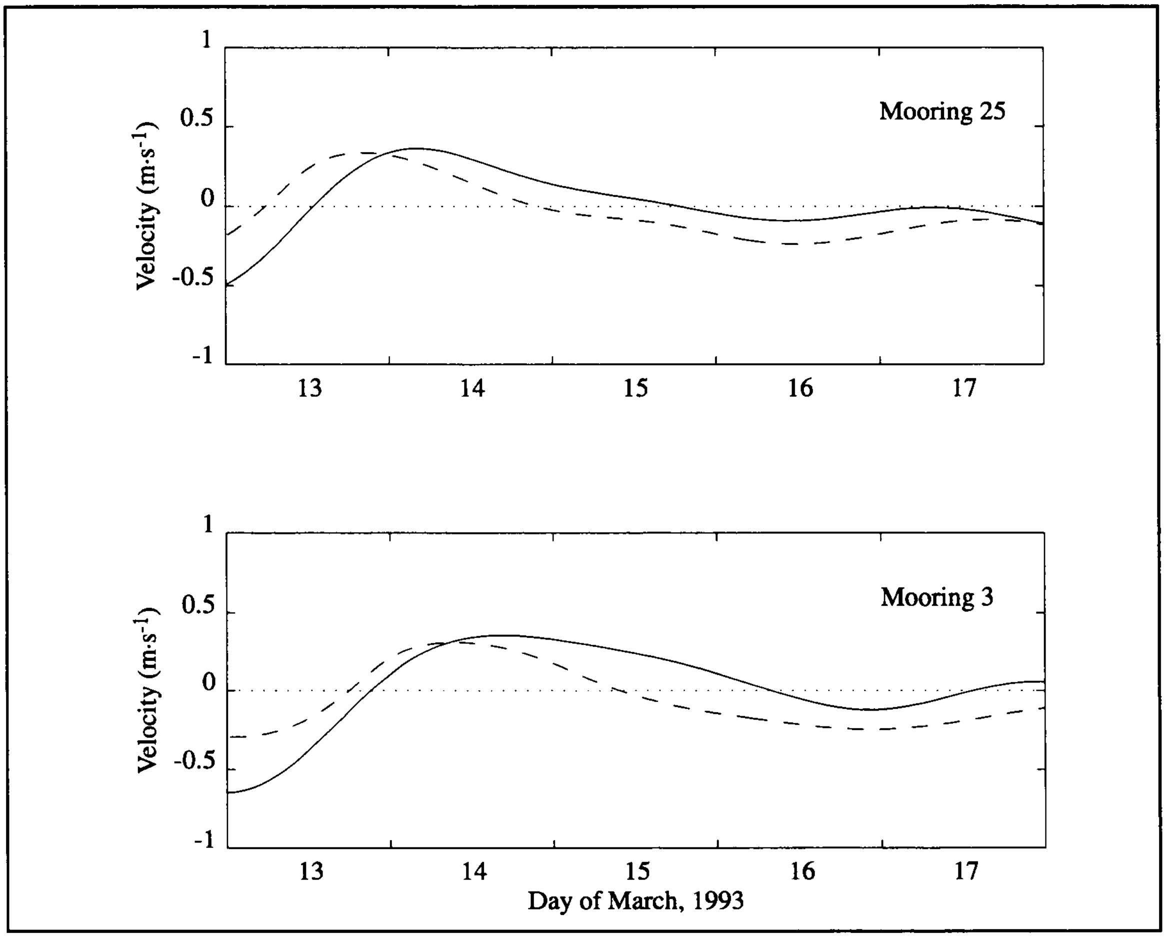

Figure K-1. Five-day time series in March 1993 of 40-hr, low-pass, observed (solid) alongshelf current for the middle level at mooring 25 (upper) and at the top level of mooring 3 (lower). The shelf model simulation of current for each mooring is also shown (dashed). Positive is upcoast.

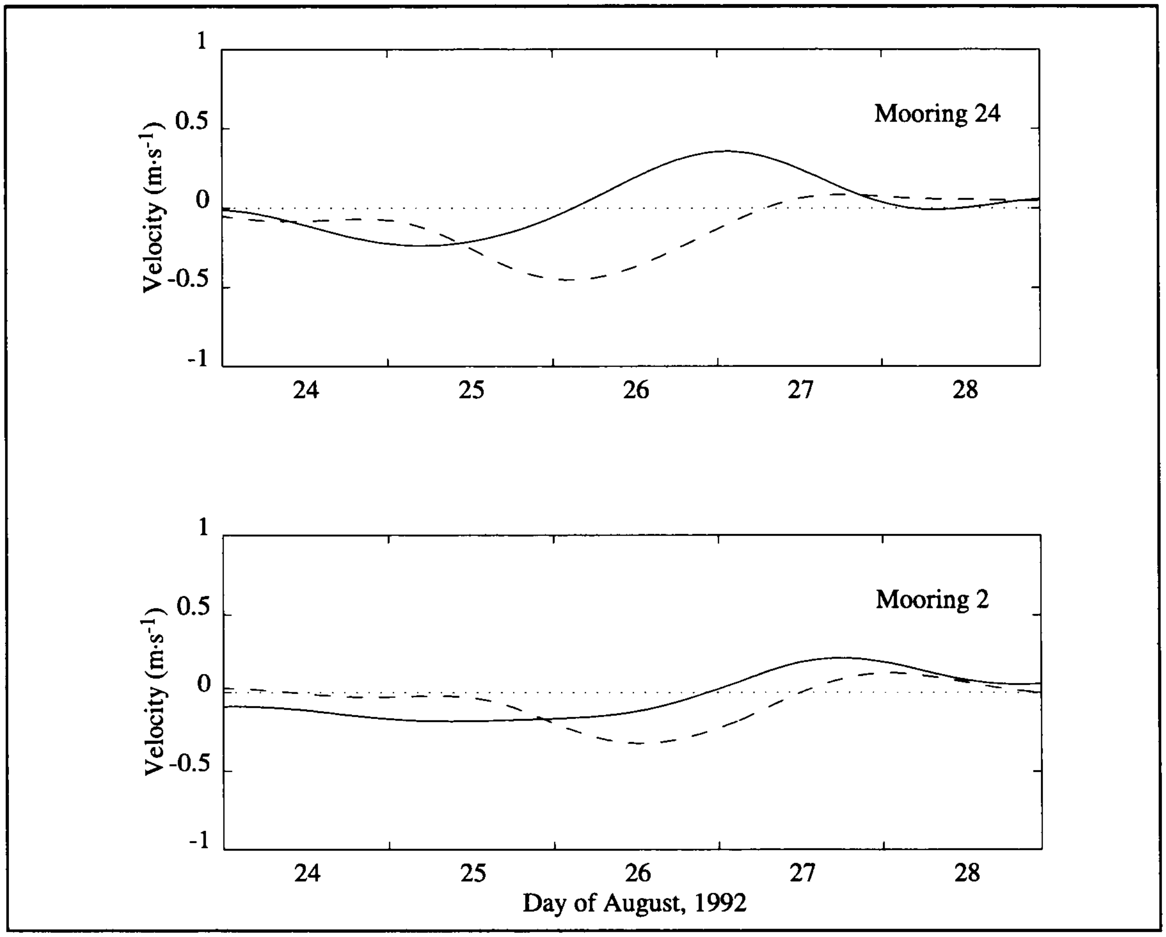

Figure K-2. Five-day time series in August 1992 of 40-hr, low-pass, observed (solid) alongshelf current for the top level at mooring 24 (upper) and mooring 2 (lower). The shelf model simulation of current for each mooring is also shown (dashed). Positive is upcoast.

Evidence of solitonlike eddy propagation

The free waves discussed above are nearshore topographic coastal trapped waves (or shelf waves) whose dynamics are governed to first order by linear theory based on the vorticity equation. For sufficiently large alongshelf wave lengths, their energy as well as their phase propagates such that the land is to the right of the propagation vector in the northern hemisphere. We can detect these, when they occur, on the inner Texas-Louisiana shelf more readily than on the outer shelf, where energetic anticyclonic eddies are frequently present and mask the presence of the weaker seaward extension of the coastal trapped waves. In this section we address the propagation of closed energetic eddies along the continental slope. Their dynamics are strikingly different from the nondispersive long shelf waves in terms of sense of propagation.

It is well established that the energetic anticyclonic eddies in the western Gulf of Mexico are shed from the Loop Current and frequently drift along a southwestward path until they intercept the continental slope off Mexico, where the path then turns northwards (Vukovich and Crissman 1986). The dynamics governing the southwestward drift (in the northern hemisphere) of an energetic anticyclonic eddy was first addressed by Flierl (1979) and includes nonlinear self-advection as well as the westward drift associated with linear Rossby waves. When the Loop Current eddy reaches the Mexican continental slope, the planetary Rossby beta effect is replaced by the much greater topographic beta effect, which governs the propagation of linear coastal trapped waves. Along the Mexican continental slope the latter propagation tendency would be southwards. However, for sufficiently energetic eddies self-advection can dominate over the topographic beta effect and cause the path of propagation to turn northwards, trapping the eddy in the continental slope wave guide but going in the opposite direction to that of weak circulational features. A simple qualitative explanation for the northward tendency by self-advection is that the western side of the anticyclonic eddy gets compressed, thus strengthening the northward flow over the slope relative to the southward flow over the seaward side. The average net fluid velocity is then northwards. The quantitative treatment of the dynamics of an eddy trapped in a topographic wave guide is addressed by Nakamoto (1989), and a demonstration of the Vukovich and Crissman preferred path for a detached Loop Current eddy (from mid-Gulf to the Texas Bight slope region via the slope wave guide off Mexico) is given by Arango and Reid (1991) using an equivalent-barotropic, nonlinear, quasigeostrophic numerical model applied to the Gulf of Mexico.

The Texas Bight slope region is the distinct bend region of the 200- to 1000-m isobaths centered near 27°N, 96°W. It seems to be a preferred terminal region (the "eddy graveyard") for detached Loop Current eddies, as discussed in Section 2.5. The more recently spawned anticyclonic eddies can approach this region from the south as discussed above, or they can approach from the east or east-southeast, with centers in the very deep water. In the later spin down stage of life when an eddy's diameter and kinetic energy diminish, the evidence gathered during the LATEX field program suggests that smaller eddies can be influenced in their propagation characteristics by the continental slope east of the Texas Bight. In particular, during the final stages of the life of Eddy Vazquez in late summer of 1993, this feature propagated to the east as seen in satellite altimeter data. Here we make use of the time series data from LATEX A moorings 6 to 9 along the 200-m isobath as verification and quantification of the propagational speed of this eddy.

Figure K-3 presents the time series of cross-shelf current from mid-July to mid-September 1993, at the top, middle, and bottom meters (where the data exist) for moorings 6, 7, 8, and 9, whose relative locations are respectively about 0, 60, 150, and 220 km east of mooring 6. Reversals and near reversals are marked by circles for a nearly coherent feature seen in the top level for each mooring. The signal at the middle level almost mimics that of the top level for given mooring. Figure K-4 shows similar plots for the alongshelf current, but with circles denoting those times of maximum eastward flow at the top meter for each mooring. The times of maximum eastward flow tend to occur near the time of reversal (from offshelf to onshelf) of the cross-shelf flow at each mooring, as would be expected of an eastward propagating anticyclonic eddy whose center lies to the south of the line of moorings. This deduction is supported by the fact that the temperature time series (not presented) at the middle levels of each mooring show maximum temperature at about the time of reversal of the cross-shelf flow, as one would expect for a warm core ring. The average speed of eastward propagation of this eddy, as estimated from the two figures is about 12 $km{\cdot}d^{-1}$ (or 14 $cm{\cdot}s^{-1}$). The feature seen in the time series data is assumed to be Eddy Vazquez in its final stages. The direction and speed of propagation are consistent with the theoretical deductions of Nakamoto (1989), suggesting that during the several weeks of its eastward propagation along the continental slope it had the characteristics of solitonlike eddy.

Closing interpretive comments

The examples discussed herein deal with disturbances in a topographic wave guide. The disturbances, whether wave-like or eddy-like, are basically governed by common physics: namely, approximate conservation of potential vorticity. One might argue, then, that the striking difference in the propagational characteristics of the near coastal shelf waves and eddies over the continental slope must be due to the latter being phenomena of high energy while the former are of low energy. But such an argument by itself offers no real physical insight. So, what is the real distinction between shelf waves, which prefer to propagate downcoast on the inner shelf, and anticyclonic eddies, which prefer to propagate upcoast in the outer continental slope wave guide?

We believe that the really important distinction is that the downcoast propagating shelf or coastal trapped waves have very little potential energy relative to kinetic energy. The baroclinic eddies on the other hand have very nearly equal partitioning of potential and

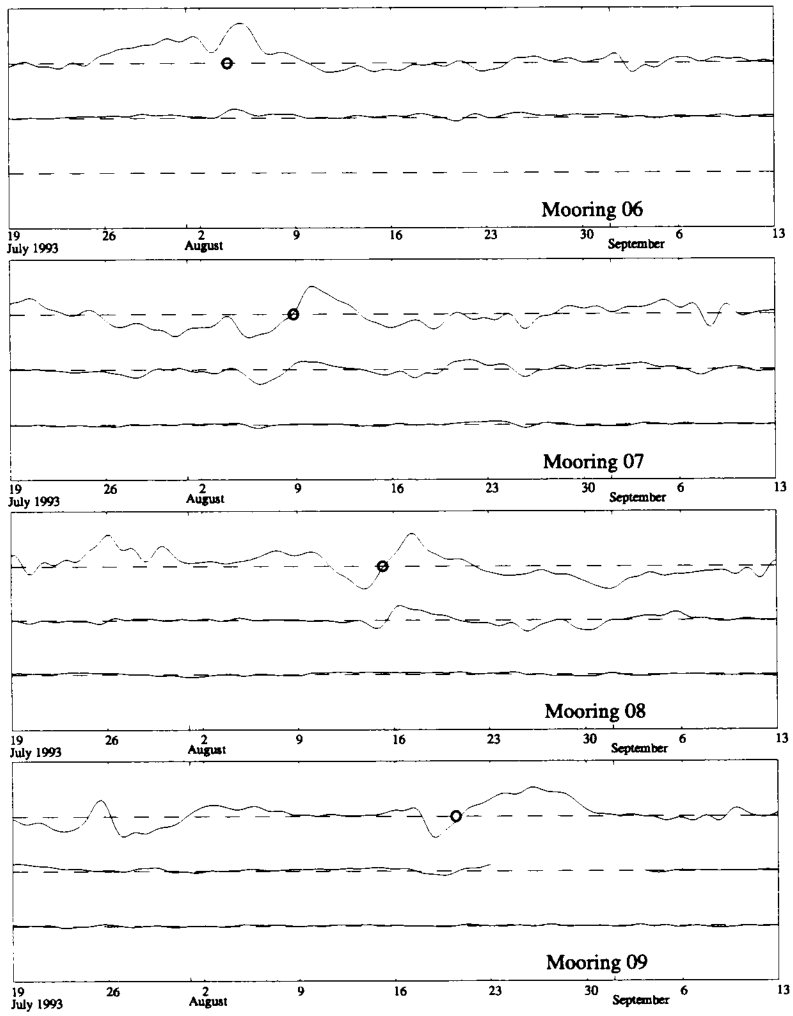

Figure K-3. Two-month time series in 1993 of 40-hr, low-pass, cross-shelf currents from moorings 6, 7, 8, and 9 along the 200-m isobath. Each panel displays current data (solid) relative to zero (dashed) at the top, middle, and bottom current meter. The vertical interval between dashed lines is 75 $cm \cdot s^{-1}$ and onshelf flow is upwards relative to zero.

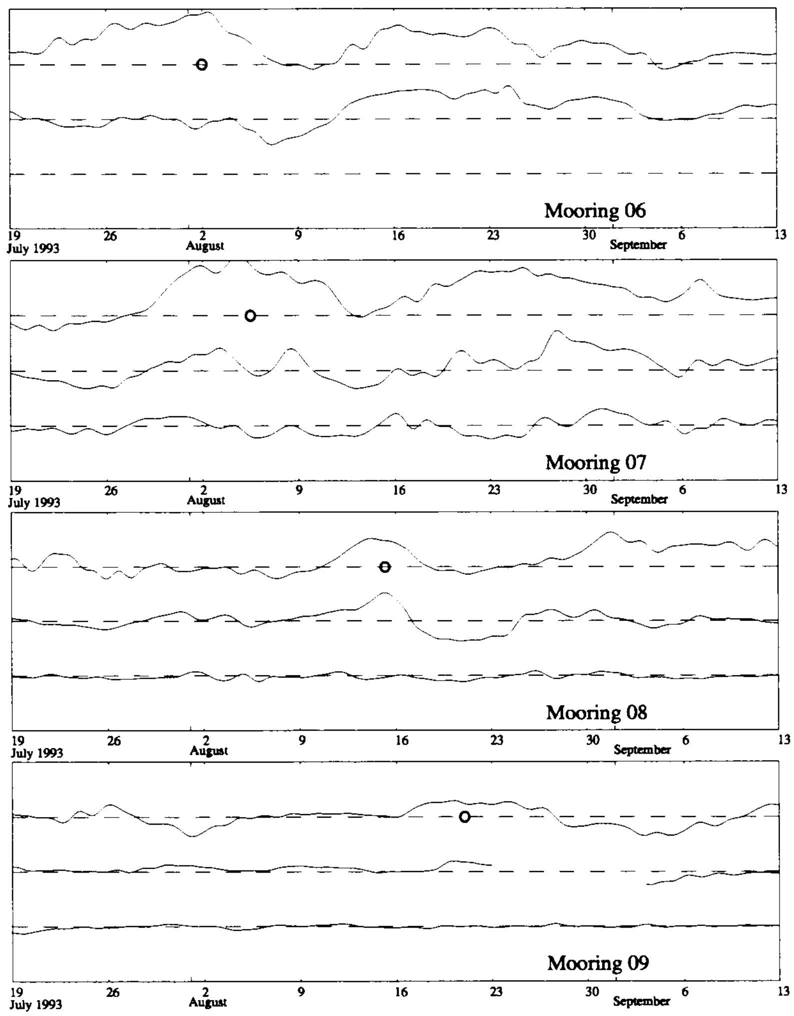

Figure K-4. Two-month time series in 1993 of 40-hr, low-pass, alongshelf currents from moorings 6, 7, 8, and 9 along the 200-m isobath. Each panel displays current data (solid) relative to zero (dashed) at the top, middle, and bottom current meter. The vertical interval between dashed lines is 75 $cm{\cdot}s^{-1}$ and onshelf flow is upwards relative to zero.

kinetic energy. This latter characteristic is consistent with the preferred scale of a ring, namely a scale governed by the (deep water) first baroclinic radius of deformation. Nonlinear dynamics are responsible for providing the mechanism for locking into this preferred eddy scale. The closed configuration of the eddy, on the other hand, is responsible for allowing self-advection to be an effective mechanism for opposing the tendency for downcoast propagation. This interpretation is no doubt an over simplification of the physics but may be regarded as a first cut conceptual model.

The final interpretive comment addresses the question of why we do not see more evidence of free shelf waves propagating downcoast on the inner or outer shelf. Cross-spectral calculations of like current components between moorings show evidence of phase propagation upcoast as well as downcoast. In the presence of wind stress forcing at a shelfwide scale, the resulting time evolving circulation represents forced shelf wave phenomena. The phasing of these wind-driven disturbances at adjacent moorings is strongly dependent on the propagation of the forcing field, whose alongshelf component is often upcoast rather than downcoast as free waves. Also, the spatial scale of typical wind fields is such that forcing occurs essentially over the whole shelf. The ideal scenario where one should expect to see free shelf waves propagating downcoast is when the wind stress forcing is confined to a portion of the eastern shelf, which then allows energy to propagate out of that region toward the west. Hurricane Andrew is an example of such a scenario.

Appendix L: Model and Observations of Wind-Driven Circulation Over the Inner Shelf

In this appendix we compare the results of a subinertial wind-driven shelf model (Current 1996) with measured alongshelf currents and coastal water level data from LATEX A moorings and NOAA/NOS coastal tide gauges. We start with a narrative description of the wind-driven model as applied to the Texas-Louisiana shelf. While the domain of the model extends outwards to 250 m depth, it is the inner shelf (depths of ≤ 50 m) where wind-forcing dominates, a region comprising well over half the total area of the model domain. Model development, tuning, and verification relied heavily on LATEX observations and collateral data including bathymetry, currents, coastal water level, and winds. Comparisons of model response to subinertial (40-hr low-pass) observations are made: (a) in the time domain, where quantification of model skill is assessed in terms of squared correlation and gain factor for a broad band of subinertial frequencies; and (b) in the frequency domain, where squared coherence, phase, and transfer function are employed as measures of skill. The frequency domain model-data comparison of currents is the counterpart of the purely empirical current-wind comparisons given in Section 4.5. We close the model-data comparisons with presentations of seasonal signals for alongshelf current and coastal water level. It is in the seasonal cycle that we see the most obvious effects of thermal and river discharge variations on the observed currents and water level, relative to the purely wind-driven model response.

The shelf mode model

The wind-driven shelf model we worked with is based essentially on the same physics as embodied in that of Mitchum and Clarke (1986), but incorporating boundary fitted coordinates, realistic bathymetry, and nonlinear bottom friction (Section 2.4). The physics governing free (unforced) coastally-trapped shelf waves is basically conservation of potential vorticity, in which planetary rotation and bottom slope play central roles as the basic restoring "force" in the presence of cross-shelf component of flow. As explained at the end of Appendix K, the physics that produce free or coastally trapped waves should be valid on the Texas-Louisiana shelf, even though the forcing is such as to make evidence of free shelf waves rare. Coastally trapped waves are forced by the torque (curl) associated with τ/h (wind stress divided by water depth), which for large scale wind systems can be approximated by the alongshelf component of τ/h^2 multiplied by bottom slope as in Mitchum and Clarke (1986). The present model, however, employs a more exact torque forcing. The boundary fitted orthogonal grid shown in Figure L-1 defines the computational domain of the model, the seaward limit being along a smoothed version of the 250-m isobath, and the open eastern boundary being at 90.5°W, where LATEX current meter moorings 13, 14, 15, and 16 were located. The grid was developed by Current (1996) using the power conformal transformation of Ives and Zacharias (1987). Grid separation distances range from 1.5 km to 8.4 km, with

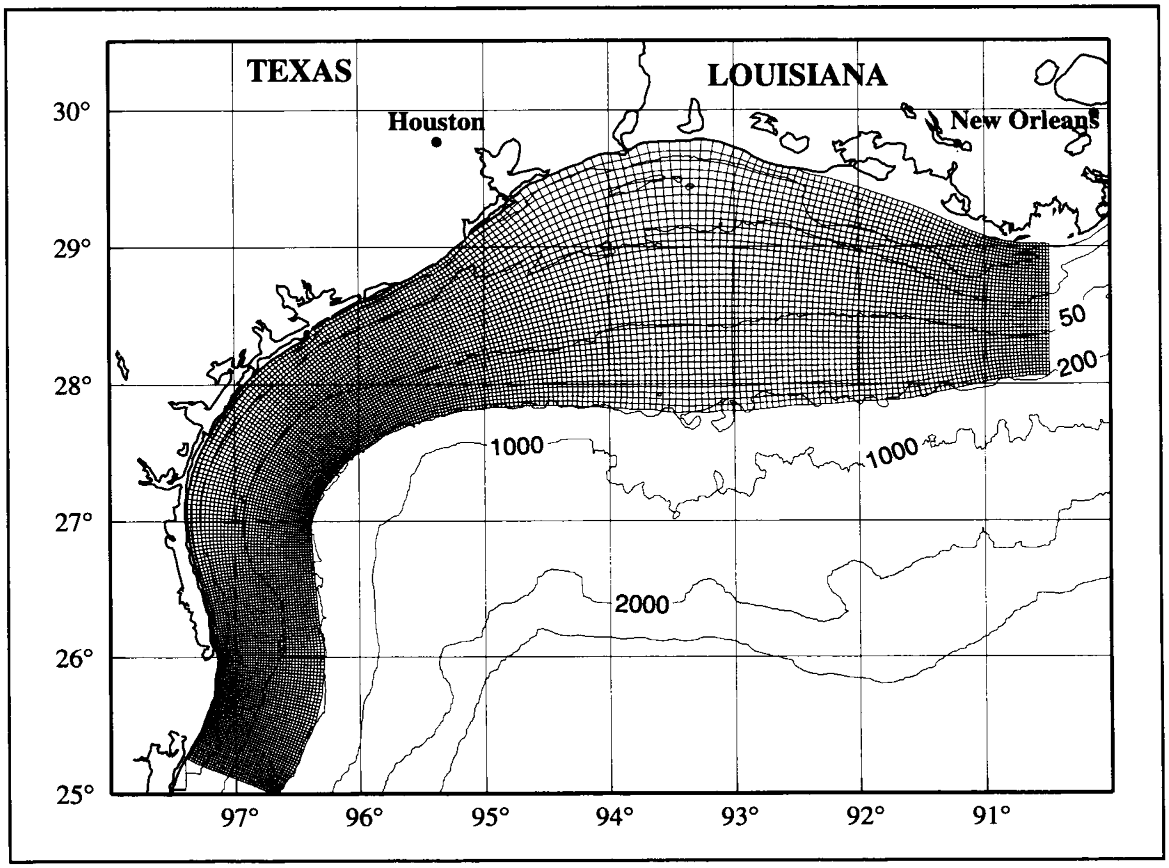

Figure L-1. Boundary fitted, orthogonal, curvilinear grid designed for the Texas-Louisiana continental shelf. Grid dimensions are 297 x 40. Mean grid separation distance is 2.8 km.

a mean of 2.8 km. The numerical model is implemented within the curvilinear coordinate grid, in which ξ and η (of uniform spacing) denote the alongshelf and cross-shelf coordinates, respectively.

The dependent variables defining the circulation field at any time (t) are the alongshelf (u) and the cross-shelf (v) components of current and the pressure anomaly (p) for given position on the shelf and elevation in the water column. Although the model employs a rigid lid, the equivalent water level anomaly can be obtained from the surface value of p. For given ξ,t the cross-shelf structure of each of the dependent variables is represented in terms of a linear combination of η, z -dependent (nearly) orthogonal modes as in Middleton and Wright (1990), but with an outer boundary condition of zero alongshelf flow.

Stability profiles and bathymetry are required for computation of coastally trapped wave modes. Mean stability profiles were computed by season from corresponding density profiles and used in approximating coastally trapped wave modes. Bathymetry was smoothed by application of a binomial filter, followed by a two dimensional polynomial fit to the filtered seafloor depth field. This fit was of sufficiently high order to preserve much of the variability in the seafloor depth field. Because h depends strongly on η but only weakly on ξ, the structure functions for u, v, p, and their associated eigencelerity c for given mode n are slowly varying alongshelf. This, in turn, implies minimal scattering of the transient coastal trapped waves.

The modal representation of the dependent variables share a common vector set of ξ,t -dependent amplitudes A_n whose governing equation has the following form:

$$\frac{\partial A_n}{\partial t} + c_n \frac{\partial A_n}{\partial \xi} = F_n - \sum_{n=1}^{N} A_m R_{mn}, \qquad \text{(L-1)}$$

where F_n and R_{mn} are respectively the wind stress dependent forcing and the bottom stress dependent mode coupling matrix, while c_n is the free wave celerity for mode n. Because a nonlinear rendition of bottom stress (Section 2.4) is employed, R_{mn} is a function of the entire vector set of A_n. The nonlinear coupling is treated in a semi-implicit manner in the numerical rendition of (L-1). East and north wind stress components over the shelf for a given time are represented versus ξ,η by a simple bilinear approximation, using available data from 15 meteorological moorings. Alongshelf and cross-shelf components of the wind stress (needed in evaluating F_n) force the model, and are found by rotation of coordinates at individual shelf locations.

Remote forcing effects enter the model domain at the upstream boundary (90.5°W), where the conditions are entirely data driven. Hourly alongshelf components of flow at moorings 14, 15, and 16 were used to produce time varying upstream boundary conditions over the entire 32-month LATEX observational period. The total number of modes N was taken as three in all comparisons presented below, which is consistent with the maximum number that can be computed at the upstream open boundary. Further details regarding the model, its sensitivity to N, and other parameters are available in Current (1996).

Time domain tuning and verification

Alongshelf currents at 12 moorings (those shown in Figure L-2 except 14, 15, and 16) were used in model tuning and verification. Adjusted water levels at six tide gauges (Little Bayou Cocodrie, LA, and Sabine Pass North, Galveston Pleasure Pier, Freeport, Rockport, and Port Isabel, TX; Figure L-2) were employed for model verification. The only parameter tuning carried out involved finding the optimal (shelfwide) value of the bottom drag

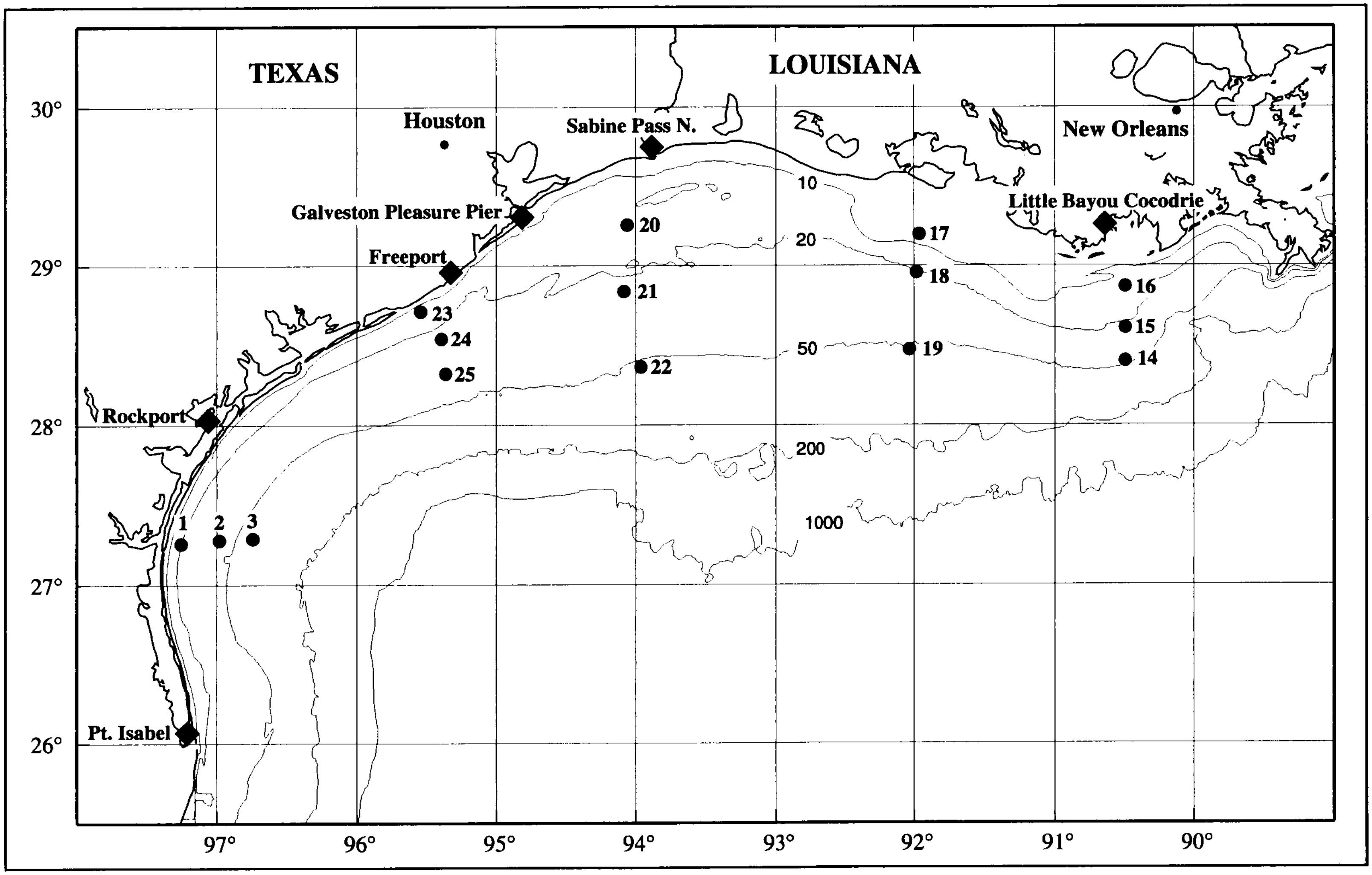

Figure L-2. Locations of 15 LATEX A moorings (circles) and 6 NOAA/NOS tide gauges (diamonds) used for model verification and dynamically driven upstream boundary conditions.

coefficient c_b (Section 2.4). The adopted wind stress drag coefficient parameterization is that of Hsu (1994), used here and elsewhere in this report (e.g., Section 2.1.2).

Model tuning employed five episodes of one-month length that were characterized by weatherband meteorological activity. These episodes were November 1992; March, June, and November 1993; and January 1994. Quantitative criteria for the tuning procedure included the squared correlation coefficient (r^2), a gain factor (m), and the bias (b). The gain and bias were obtained from a linear regression of data onto model (as in Mitchum and Clarke 1986),

$$u_0 = mu_m + b, \tag{L-2}$$

for which optimal parameters m and b were found by standard methods. Here, u_m is model alongshelf velocity and u_0 is observed alongshelf velocity. Simulated alongshelf velocity averaged through the water column was selected as the representative model velocity (u_m) for tuning and verification at each of 12 inner shelf moorings. The predominantly barotropic nature of the circulation on the inner shelf suggested this simplification, although model velocities were available at the depths of individual current meters. Observed alongshelf currents (u_0) used in tuning and model verification were generally taken from the top current meter, which was deployed near the middle of the water column for coastal moorings in very shallow water. The middle current meter was used only for the outermost mooring on each cross-shelf line (Figure L-2); the bottom current meter was never used in tuning and verification. In summary, choice of current meter at a given mooring was intended to provide values of u_0 that roughly corresponded to vertically averaged velocity.

The optimal value of c_b was found to be 0.00065, based on maximum average r^2 for the five selected tuning episodes. The associated optimum value of m was very close to unity.

For verification, the tuned model was run nonstop for the entire 32-month LATEX field observation period to predict current velocity and water level throughout the model domain. Comparison of these simulation results with observations was the primary means of model verification, and examples of these comparisons are presented in Figures L-3 and L-4. These figures span a time period that includes the March 1993 "Storm of the Century" (Appendices A.1 and B.2) as well as Tropical Storm Arlene, an event of somewhat larger time scale during June 1993. Quantitative verification of model performance was based on evaluation of the squared correlation coefficient (r^2), gain (m), and bias (b). Recall that r^2 is the squared correlation coefficient, and consequently, represents a measure of the fraction of the total variance in the data that is explained by the model. Gain and bias are obtained from the linear regression of data onto model results, as in Equation (L-2).

The entire 32-month model run produced squared correlation coefficients for model results versus observations at individual moorings and tide stations as plotted in Figure L-5.

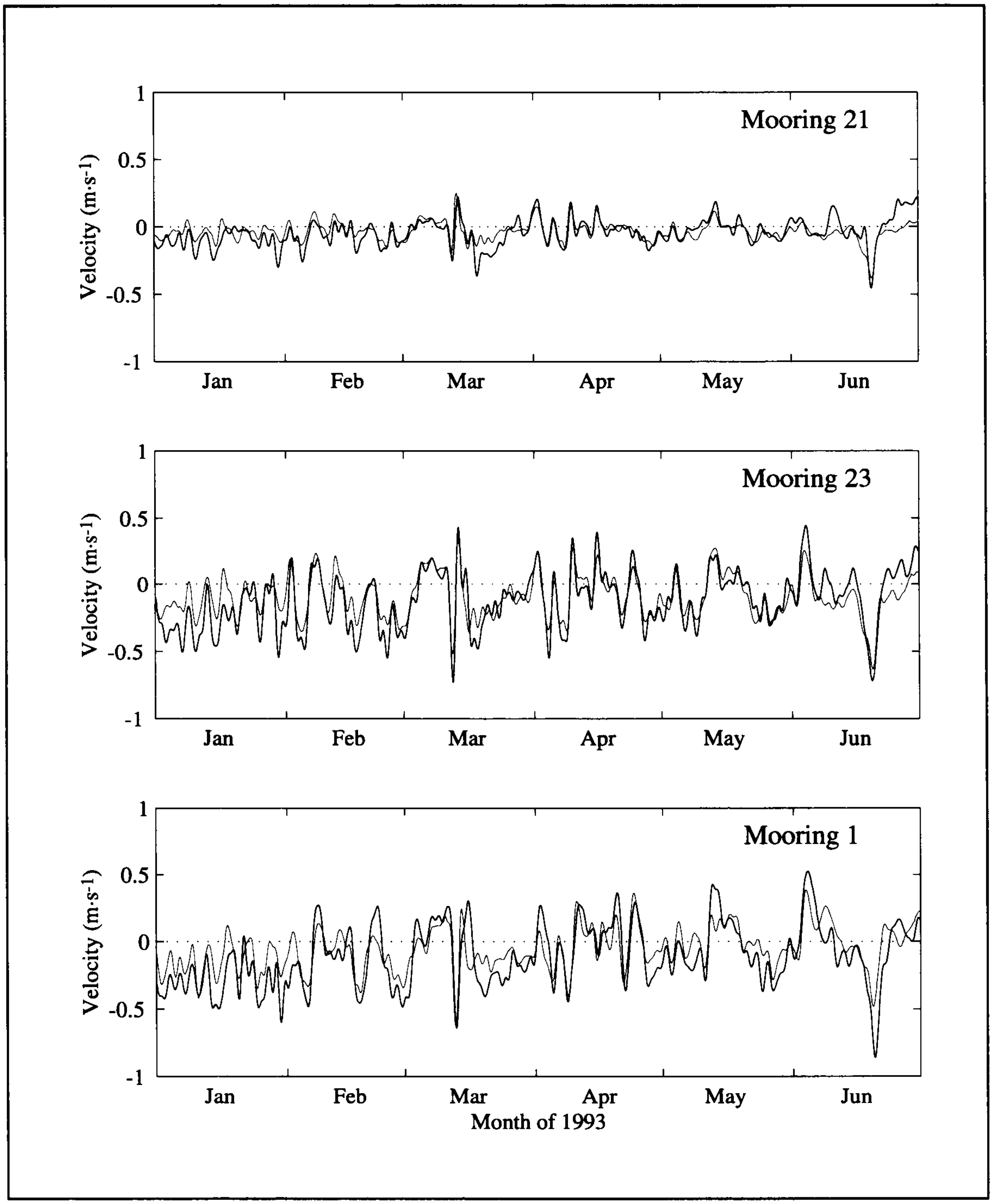

Figure L-3. Direct comparison of simulated (thin) and observed (heavy) LATEX A January-June 1993 time sequences of alongshelf currents provide qualitiative model verification at inner shelf current meters at representative moorings.

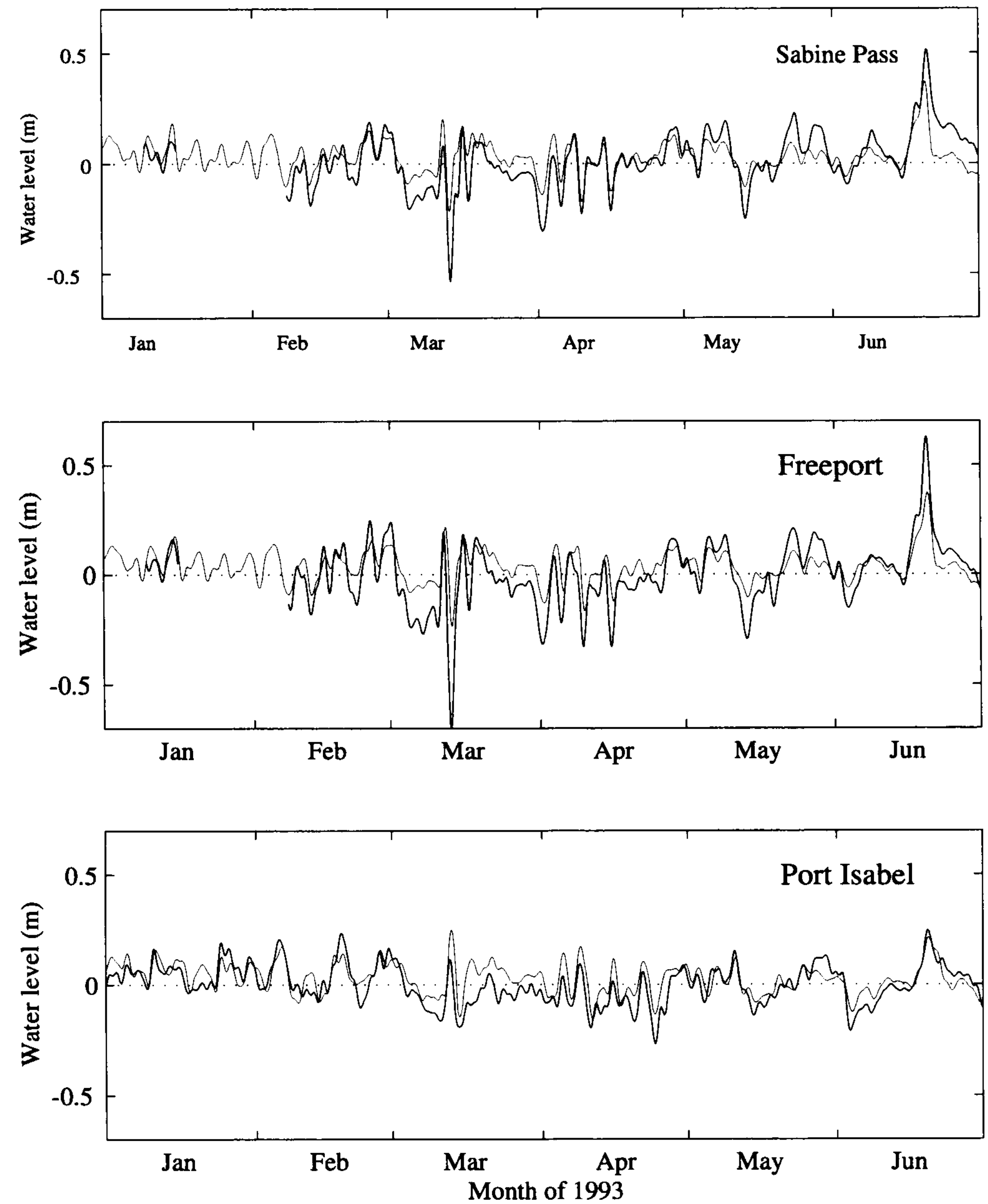

Figure L-4. Direct comparison of simulated (thin) and observed (heavy) NOAA/NOS January-June 1993 time sequences of adjusted water level provide qualitiative model verification at inner shelf current meters at representative moorings.

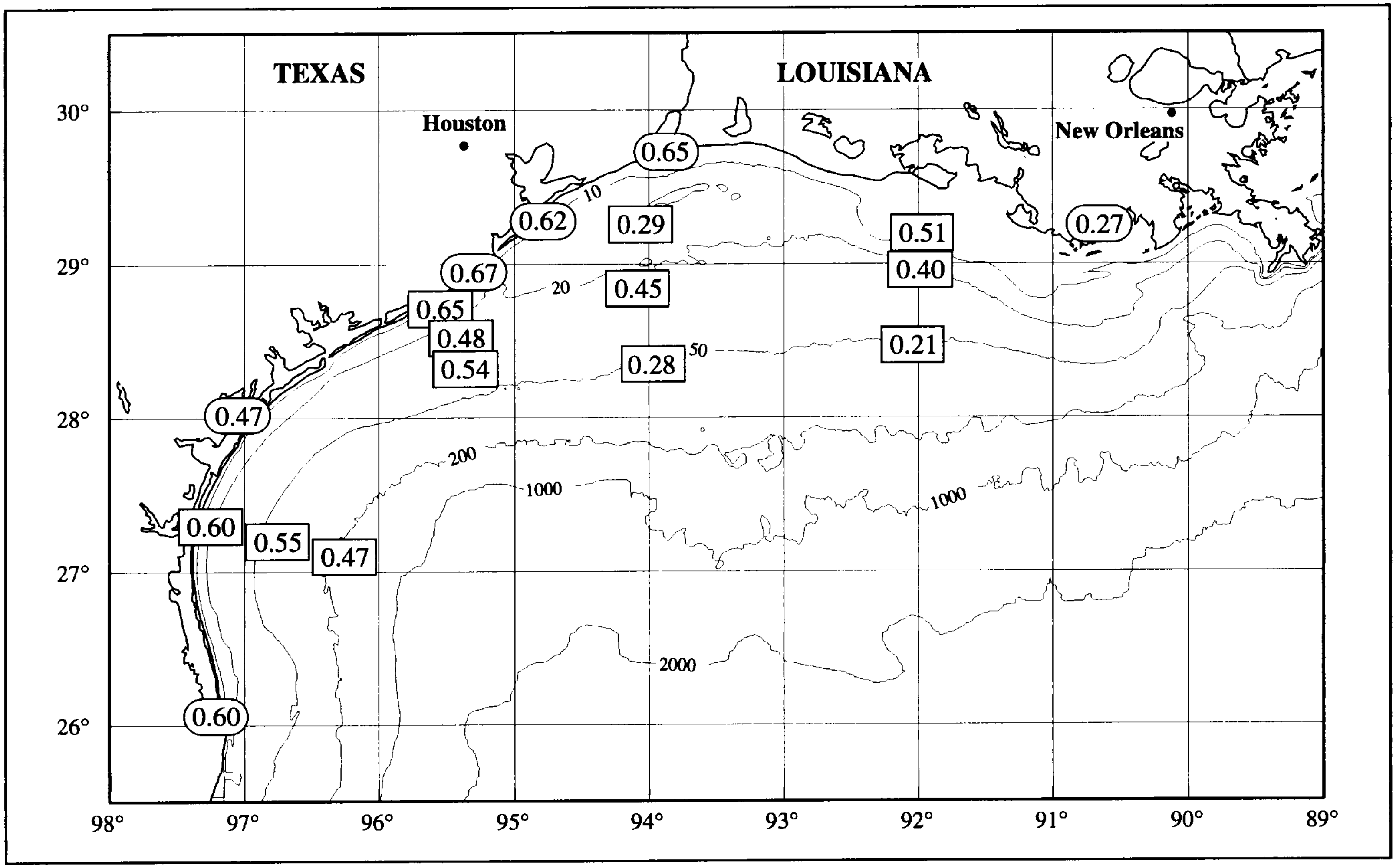

Figure L-5. Spatial distribution of squared correlation between the 32-month simulated and observed alongshelf currents and water levels on the Texas-Louisiana shelf. Ellipses indicate NOAA/NOS tide gauges used for verification; boxes are LATEX moorings used for verification of currents.

Simulation for the wide eastern shelf proved to be more difficult than in downcoast regions where the shelf is narrower. A probable cause for the difficulties is that the bottom stress coefficient (c_b) may be generally different in upcoast than in downcoast regions, as suggested by results of a simpler pilot model application not reported here. In addition, mooring 20 is located very near to the downstream end of Sabine Shoals, a major topographic feature on the Texas-Louisiana shelf. The squared correlation of 0.29 at mooring 20 may be associated with nonlinear flow and scattering from Sabine Shoals that were not simulated by the model. We remind the reader that influences of the freshwater plume are not included in the model physics. Squared correlation coefficients for water level generally exceed those for alongshelf currents, although water level was not well predicted at Little Bayou Cocodrie, Louisiana. The model was designed to simulate inner shelf circulation well, and generally model skill is best at current meters near the coast. However, the model also simulates alongshelf currents reasonably well over the outer shelf. For example, a squared correlation of 0.47 and gain of 0.78 were produced for mooring 3, located in 66 meters of water.

Squared correlation coefficients (r^2), gain (m), and bias (b), were also produced for each month from the 32-month comparison of simulated and observed hourly alongshelf current velocities over all moorings. These statistics are presented in Table L-1. Table L-2 lists similar results for water level. Correlations for currents appear to be weakest in July and August, when winds are generally low and baroclinic effects are strong. Gain is high during July and August, indicating that the model also underestimates current observations. Correlation of simulated and observed current is highest and gain is near unity in December and January, when winter storms enhance the wind-driven, barotropic component of response. Correlation of modeled and observed coastal adjusted water level is low in July and August, consistent with the low correlation of simulated and measured currents during these months, discussed above.

Frequency domain verification

Bivariate spectral analyses, including squared coherence, phase, and transfer function, were computed for model results versus observations. These analyses were done separately at each of the 12 current meters and six tide gauges used for model verification, as illustrated in Figure L-6 for mooring 23. As a shelfwide measure of skill, 32-month coherence, phase, and transfer function were obtained from the combined set of alongshelf current observations at all 12 verification moorings (Figure L-7), as well as for the combined set of adjusted water level time series at all six verification tide gauges (Figure L-8). The full shelf analyses employed all hourly observations (of segment length sufficient to allow estimates at periods of 42 days or less) within the 32-month field observation period and corresponding hourly simulation. The results of these analyses demonstrate encouraging performance of the model as a prognostic tool.

Table L-1. A 32-month comparison of simulated versus observed hourly alongshelf currents at 12 moorings on the Texas-Louisiana shelf produced these monthly squared correlation coefficients (r^2), gains (m), and biases (b).

	J	F	M	A	M	J	J	A	S	O	N	D	Mean
r^2	0.55	0.46	0.49	0.52	0.42	0.41	0.29	0.37	0.49	0.52	0.48	0.59	0.46
m	1.05	1.03	0.97	1.02	1.05	1.11	1.13	1.10	0.97	0.92	0.87	1.03	1.01
b	0.00	0.01	0.01	0.02	0.02	0.02	-0.04	-0.01	0.03	0.02	0.06	0.04	0.01

Table L-2. A 32-month comparison of simulated versus observed hourly water level time series at 6 tide gauges on the Texas-Louisiana coast produced these monthly squared correlation coefficients (r^2), gains (m), and biases (b).

	J	F	M	A	M	J	J	A	S	O	N	D	Mean
r^2	0.56	0.56	0.58	0.49	0.65	0.67	0.49	0.46	0.55	0.47	0.59	0.61	0.55
m	1.22	1.45	1.34	1.21	2.09	1.63	1.60	1.18	1.52	1.21	1.40	1.49	1.44
b	0.08	0.04	0.05	0.04	0.01	0.00	-0.01	0.00	0.02	0.00	0.03	0.04	0.02

Because wind stress, currents, and water level were filtered using a 40-hr low-pass Lanczos filter, useful information from the bivariate analysis is restricted to frequencies below the filter cutoff frequency. Model results were significantly coherent with observations throughout the weatherband and lower frequencies at nearly all individual locations. Phase shift is nearly zero and the model slightly underestimates the data at mooring 23 in low frequencies. In the weatherband, phase shift is small but mixed in sign. Coherence was restricted primarily to the lower frequencies at moorings 20 and 22, and the Little Bayou Cocodrie tide gauge. Mooring 19 predictions alone were not generally coherent with observations. Simulation in these wide shelf regions may be more difficult than elsewhere, due to the simplicity of the wind parameterization scheme and the sensitivity of the model results to wind forcing.

Combined squared coherence for simulated and observed alongshelf currents for the set of all 12 verification moorings during the 32-month run is provided in Figure L-7. Coherence exceeds the 95% significance level for all periods greater than 40 hours. Squared coherence in frequencies lower than the weatherband is fairly stable and ranges from 0.54-0.60. This range of values exceeds the squared correlation (the time domain analog of squared coherence) of 0.45 over all 12 moorings for the three-year period (Table L-1). Weatherband squared coherence ranges from 0.37-0.57, increasing with increasing period, and this range is consistent with the squared correlation. The coherence plots demonstrate that model

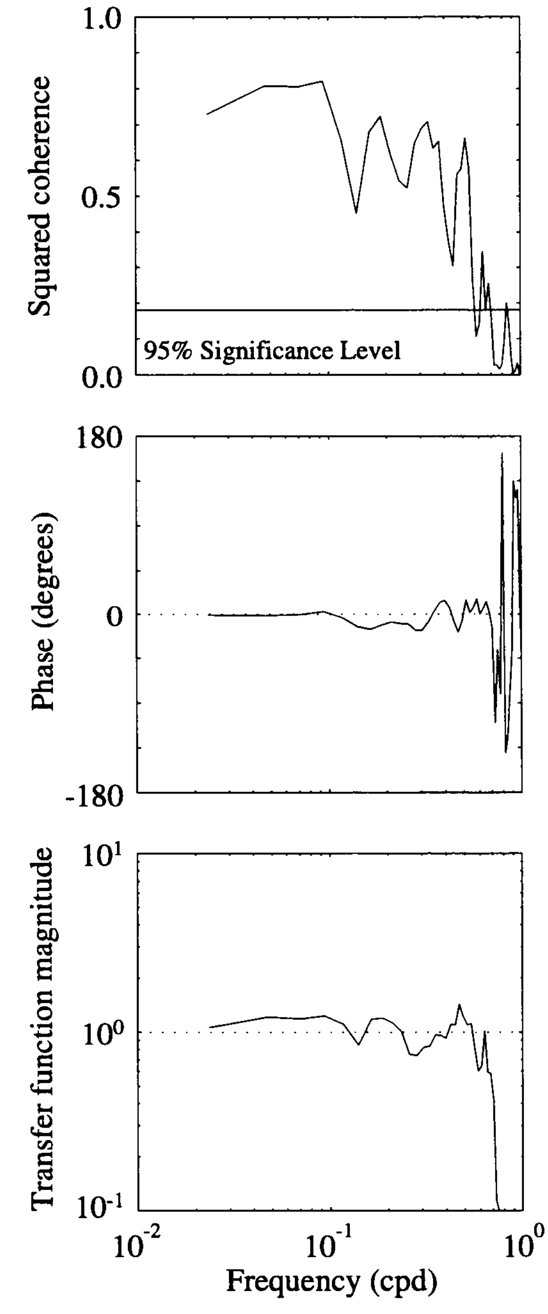

Figure L-6. Squared coherence, phase, and transfer function of simulated and observed alongshelf currents for mooring 23 during the 32-month LATEX field observation period. Positive phase indicates that the data lead the model, and transfer function exceeding unity indicates that the model underestimates the data.

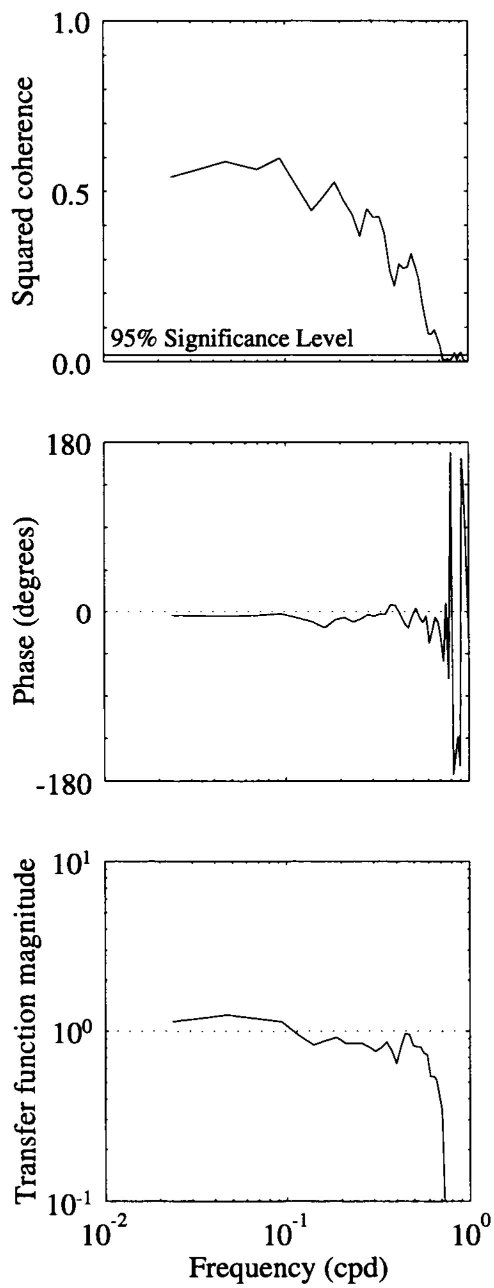

Figure L-7. Squared coherence, phase, and transfer function of simulated and observed alongshelf currents for the combined set of 12 verification moorings during the 32-month LATEX field observation period. Positive phase indicates that the data lead the model, and transfer function exceeding unity indicates that the model underestimates the data.

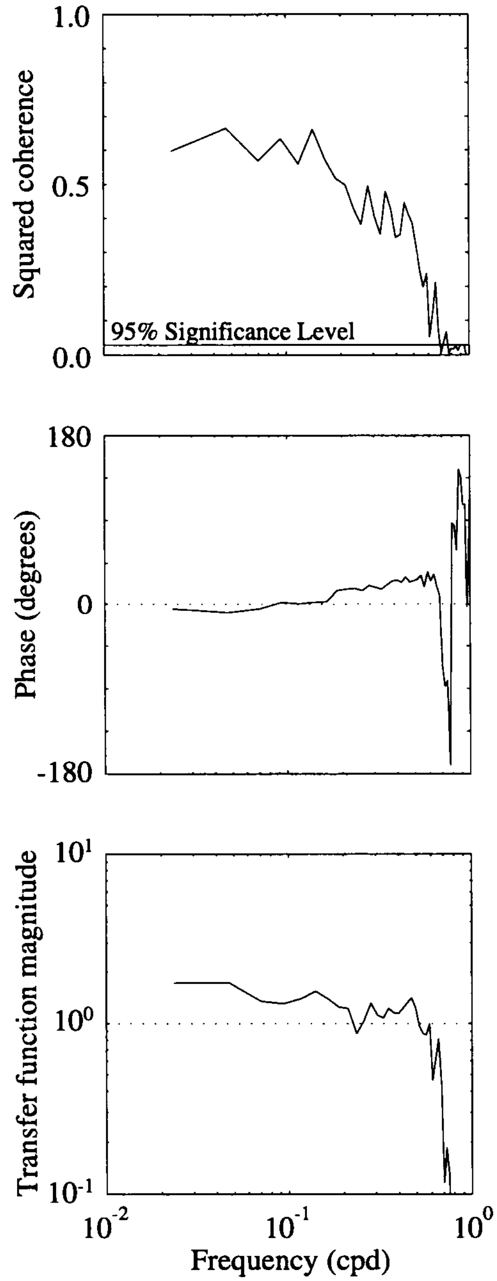

Figure L-8. Squared coherence, phase, and transfer function of simulated and observed alongshelf currents for the combined set of six verification tide gauges during the 32-month LATEX field observation period. Positive phase indicates that the data lead the model, and transfer function exceeding unity indicates that the model underestimates the data.

performance is best at low frequencies and low weatherband frequencies, and coherence falls off fairly regularly with increasing frequency in the weatherband. Transfer function magnitudes are generally slightly greater than one at low frequencies, indicating that the model underestimates the data. The model slightly overestimates the data in the weatherband. Phase shift is nearly zero in the low frequencies, and is small but mixed in sign in the weatherband, validating the tuning of the friction coefficients. If the friction is too great, the phase could be expected to lag noticeably as in Church et al. (1986b). Transfer function magnitude and phase of model response with respect to alongshelf current observations appear to be good throughout weatherband and lower frequencies.

Figure L-8 shows the combined squared coherence for simulated and observed water level for the set of all six verification tide gauges during the 32-month run. Coherence exceeds the 95% significance level for all periods greater than 40 hours. Squared coherence in frequencies lower than the weatherband is fairly stable and ranges from 0.57-0.67. This range of values exceeds the squared correlation of 0.55 over all six tide gauges for the three-year period, listed in Table L-2. Weatherband squared coherence ranges from 0.37-0.67, increasing with increasing period, and this range is consistent with the squared correlation. The squared coherence plots for simulation of water level confirm that model performance is best at low frequencies and low weatherband frequencies, and squared coherence decreases with increasing frequency in the weatherband. The transfer function is such that the model underestimates the data at low frequencies and at most weatherband frequencies. Phase shift is nearly zero in the low frequencies, and the model lags by 30° or less in the weatherband. The phase shift envelope is expected to narrow to zero as frequencies decrease, and in fact this is the case overall. Transfer function magnitude and phase of model response with respect to water level observations appear to be satisfactory throughout weatherband and lower frequencies. The transfer function magnitude for the combined set of tide gauges is greater than that for the combined set of current meters at all periods in excess of 40 hours.

Seasonal patterns

The present study supplements existing evidence confirming the existence of annual current and water level cycles described by Cochrane and Kelly (1986) and by Whitaker (1971), and, more importantly, provides a dynamical basis for the assertion that the annual cycle on the inner shelf is wind forced.

Figure L-9 shows the annual signal of coastal water level for the Texas-Louisiana shelf (adjusted for atmospheric pressure), based on Fourier fits of monthly averages for the 32 months of observed and model simulated values for the LATEX measurement period. Since observed water level has an arbitrary reference, here it is adjusted so as to have a yearly average equal to that derived from the model. The model-simulated water level has a

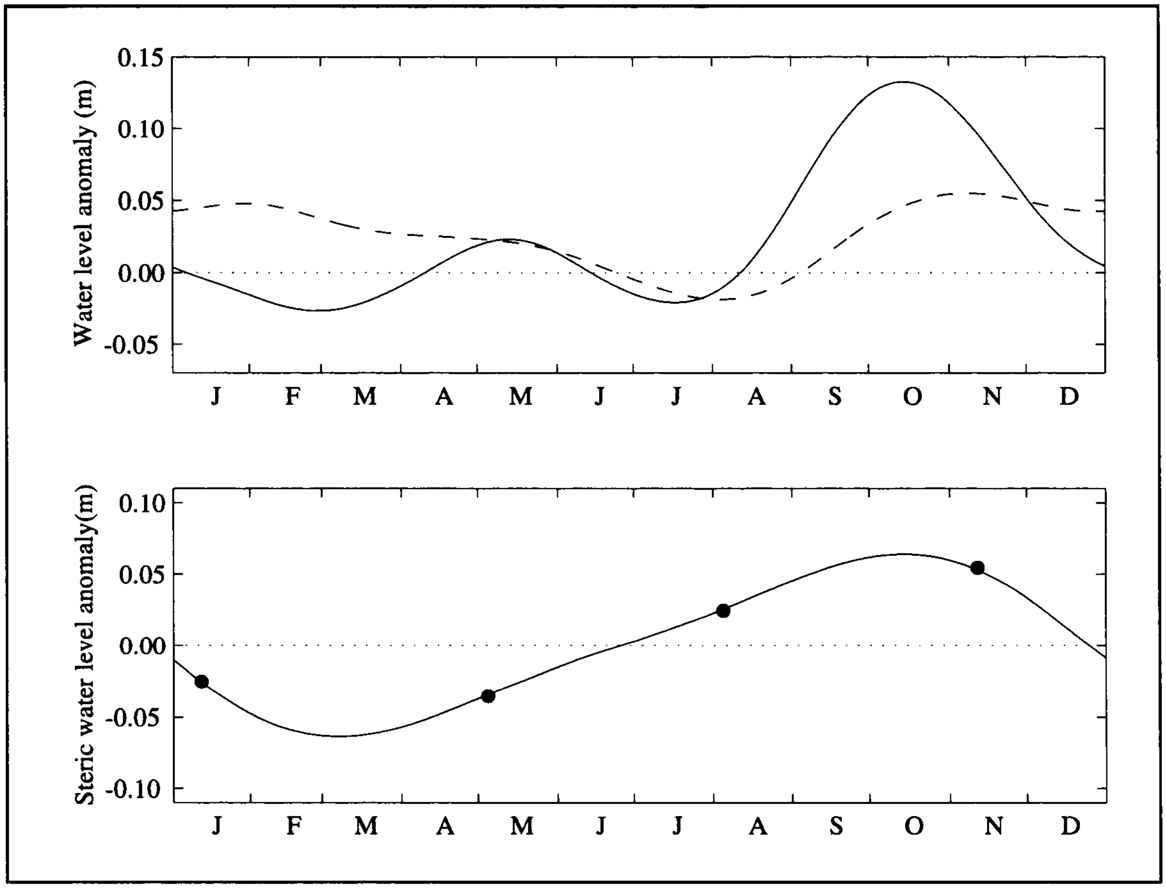

Figure L-9. Adjusted water level and its seasonal steric component. (Upper) Fourier fit of monthly means for simulated (dashed) and observed (solid) adjusted water level for the combined set of six tide gauges based on the 32-month LATEX field observation period. The observed signal is referenced so that the yearly average is equal to that simulated. (Lower) Two-component Fourier fit of four season steric water level determined from LATEX A and C cruise data at about 94°W near the 200-m isobath. The fit has a standard error of 0.12 cm to the four points derived from averaging the times and the steric levels from three surveys for each of the four seasons. The annual mean has been removed from the steric levels.

shape very similar to that of the model-simulated alongshelf currents, as it should since that component of the flow is nearly geostrophic. However, the observed annual signal of water level differs significantly in shape from the model simulation.

The large contrast of the wind-driven model signal with that observed is certainly not unexpected, since it is known from the study of Whitaker (1971) that there is a very large thermally-induced range (order 13 cm) in water level even off the Texas shelf break. In fact, Whitaker found an essentially common annual signal of steric water level throughout the northern and western part of the Gulf of Mexico; in particular, near the shelf break off Cedar Keys, Pensacola, Eugene Island, Galveston, and Tampico. This signal was characterized by a single minimum close in time to the vernal equinox, and a single maximum near the autumnal equinox. The annual signal in coastal water level deduced from long-term tidal records (61 years) at Galveston is in striking contrast to that along the shelf break. In addition to the fall peak of 13.5 cm in coastal water level, there is a secondary peak of 5.2 cm in late spring coinciding with the time of the maximum freshwater discharge from the Mississippi and Atchafalaya Rivers. The primary minimum of -10.5 cm normally occurs in January with a secondary minimum of -4.4 cm in July. These were adjusted for atmospheric pressure and the reference is taken as the 61-year mean (Whitaker 1971). This characteristic signal, typical of the coastal tidal records along the Texas-Louisiana shelf, is perceived here to be due to the combination of thermally induced, wind-induced, and river-induced annual signals. The July minimum in coastal water level is regarded as due to (a) the combination of the geostrophic depression of coastal water level associated with the upcoast wind driven flow, and (b) the upcoast advection of salty and dense water from the southwestern region of the shelf.

During the period of the LATEX field measurements, the associated average annual signal of the coastal water level displayed the characteristic double maximum and double minimum features, but the amplitude of the semiannual part of the signal was smaller than normal (Figure L-9), presumably because of atypical river discharge during that period. To obtain a water level signal more suitable for comparison with that simulated by the wind-driven model, which has a minimal pressure anomaly signal offshore, the demeaned shelf break steric water level signal should be subtracted. This also implies that the resulting residual level at the coast is an index of the average cross-shelf slope, as it is in the model. The estimated thermal signal for the LATEX measurement period was deduced from the sea surface geopotential anomaly evaluated from seasonal hydrographic cruises at the shelf break for line 4 near 94°W. Specifically, estimates of the mean steric level for winter, spring, summer, and fall were obtained from the data provided by a combination of 12 LATEX A and C surveys, three per season. A Fourier fit using the annual and semi-annual periods gives a representation of the annual thermal signal very similar to that of Whitaker (1971) but with a slightly smaller range (Figure L-9).

The resulting residual signal of observed coastal water level (after removal of the offshore signal) is plotted along with the wind forced model simulation signal in Figure L-10. Having suppressed the major annual thermal signal, the remaining difference between observational and simulated results may reflect that associated with the river-induced signal. More precisely, and with the caveat that the subtracted thermal signal is correct, this final residual could represent the freshwater discharge effect in the presence of advection.

Monthly means of currents from the 32 months of current data and model simulation thereof for the 12 verification moorings were employed to construct the model/data comparison for the annual signal presented in Figure L-10. This confirms the Cochrane and Kelly (1986) bimodal pattern of downcoast flow from September through May interrupted by upcoast flow in the summer on the inner Texas-Louisiana shelf. The wind-induced model simulation tracks the observed flow well, but underestimates the range (consistent with the results of the spectral transfer function at low frequencies, Figures L-7 and L-8). The effect of the annual thermal changes as discussed by Reid and Mantyla (1976) or of seasonal variations in river discharge (Oey 1995) may account for the larger range of the observed current signal compared with that predicted by wind forcing alone.

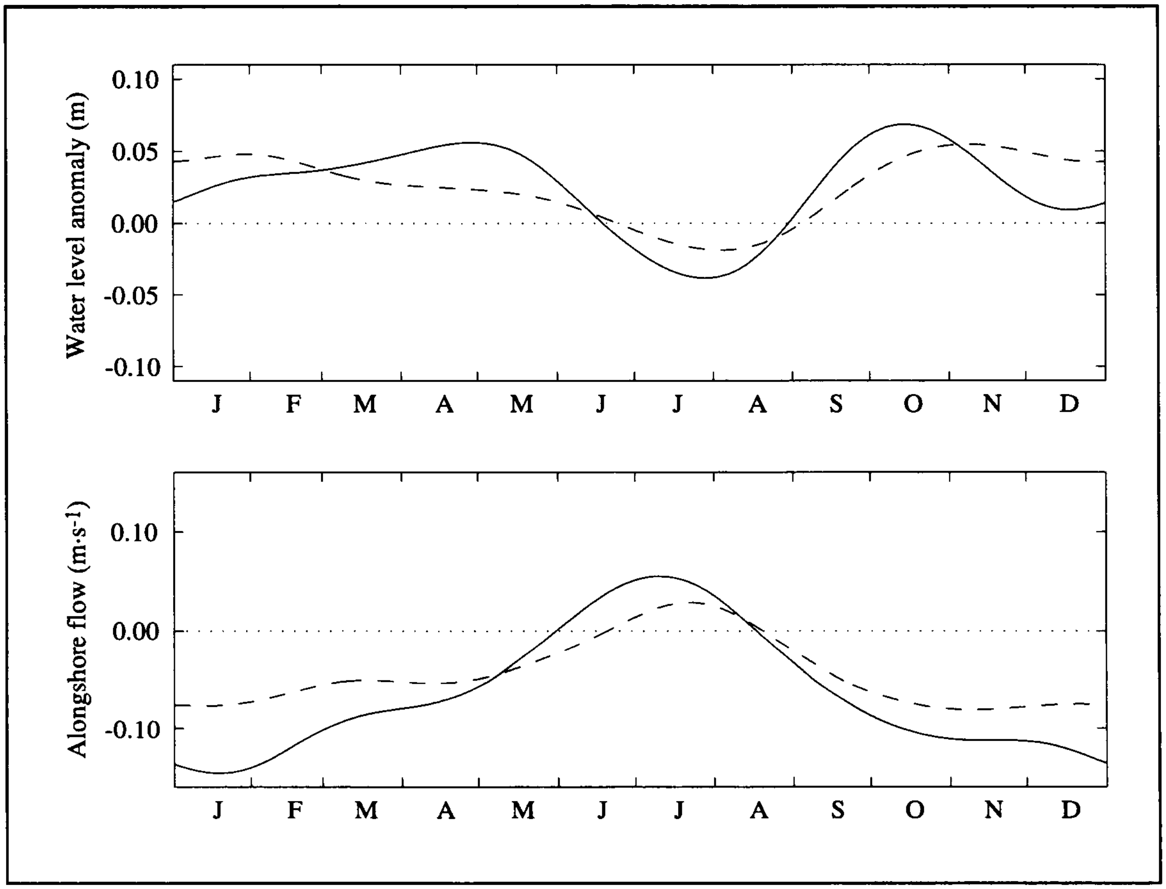

Figure L-10. Model/data comparison at seasonal periods for water level and alongshelf currents. (Upper) Comparison of the annual signal of the water level from the wind-forced model simulation (dashed) and the residual observed signal (solid) after subtracting the offshore steric water level signal. (Lower) Comparison of the annual signal of alongshelf current velocity from the model (dashed line) and from LATEX A data (solid line).

Appendix M: Estimates of Property Exchanges Between Shelf Subregimes Using Box Models

The LATEX A Technical Proposal offered a quantitative "box-type" model for the circulation, replacement and removal of water masses to provide "zero-order" estimates of alongshelf and cross-shelf exchanges into and out of specified volumes.

Introduction

The design of a box model is typically based on either hydrographic data or moored current meter data, but usually not both. Hydrographic data typically consist of temperature, salinity, nutrient, and oxygen measurements that are temporally limited to the times of the cruises. The spatial coverage in the vertical is extensive, usually every half meter, and the horizontal coverage is defined by the spacing between CTD stations, usually on the order of tens of kilometers. Geostrophic fluxes can be calculated from the thermal wind equations using data from adjacent CTD stations. Moored current meter data consists of horizontal velocity and often temperature and salinity. The vertical and horizontal coverage of the current meters, as compared to that of CTD stations, is much coarser; typically, vertical separation is at least ten meters and horizontal separation is on the order of hundreds of kilometers, but the temporal coverage is nearly continuous. However, the method of converting sparse, point-specific time series data into a flux across a face is error prone. The methods range from simply averaging the individual current meter velocities and multiplying by the area of the face to using some objective analysis routine to interpolate spatially.

Our box model is based primarily on data from the current meter moorings (velocity, temperature, and salinity), but it heavily utilizes hydrographic and ADCP data as well. As shown in Figure M-1, the current meter moorings coincide well with cruise tracks represented by a typical set of hydrographic stations from which we obtained concurrent hydrographic and ADCP data. This provided us with the opportunity to create a box model—four boxes for the inner shelf and four boxes for the outer shelf—that aligned with the cruise tracks and had current meters at all the box corners and along some box sides (Figure M-2). With this choice we were able to incorporate the spatially extensive temperature and salinity fields provided by the hydrographic data and the extensive spatial coverage of the horizontal velocity fields of the ADCP data into the box model.

The method used to convert temporally extensive but spatially limited current meter velocity data into flux estimates assumed that the dominant velocity pattern for a box side could be estimated independently using the ADCP data. We used EOFs (see Section 4.4.1 for a general description) to describe the inherent structure in the ADCP velocity fields. This approach takes advantage of the spatial extent of the ADCP velocity data, which is collected for bins typically 4-m deep by not more than 1.5-km long, to literally fill in the blanks between

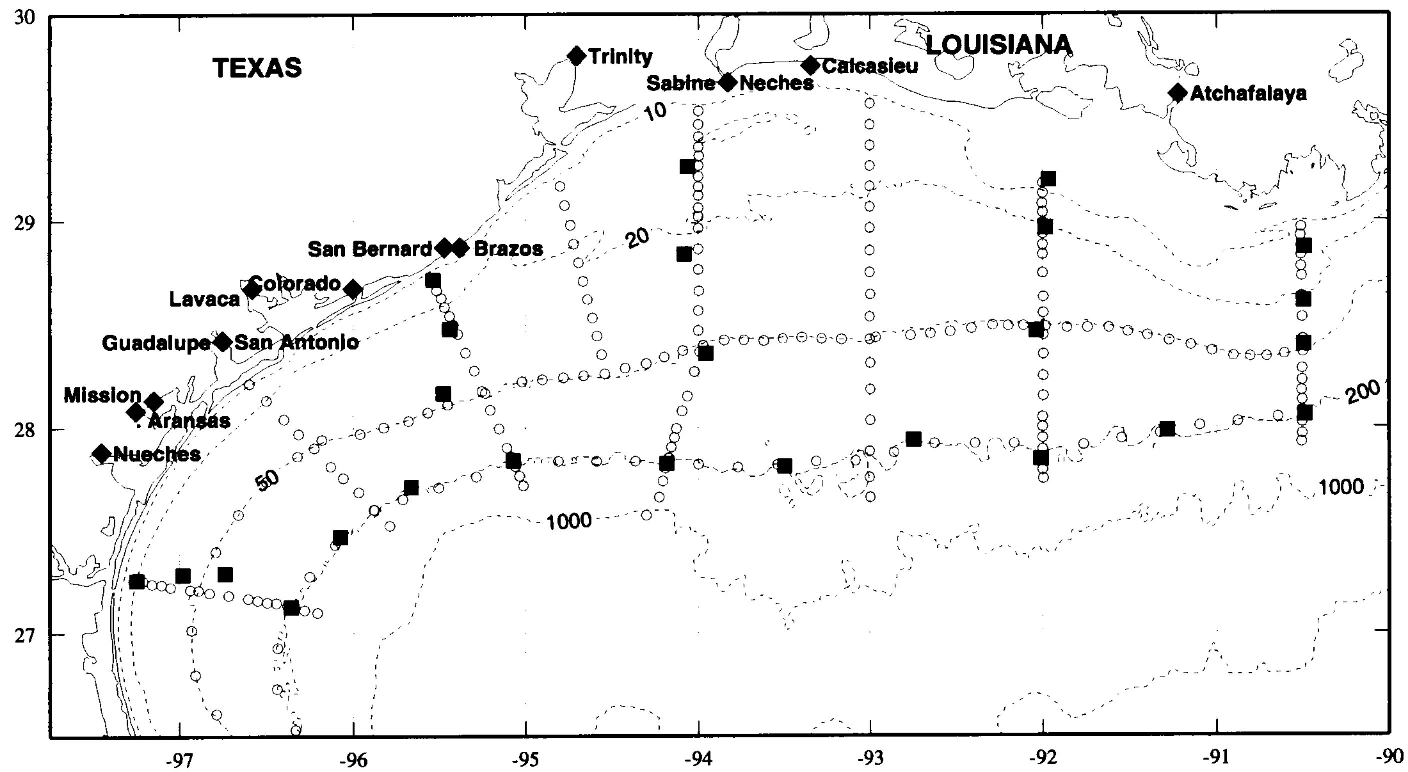

Figure M-1. Locations of LATEX A current meter moorings (solid squares) over the Texas-Louisiana shelf. Typical locations of hydrographic stations (open circles) and river discharges (solid diamonds) are also shown.

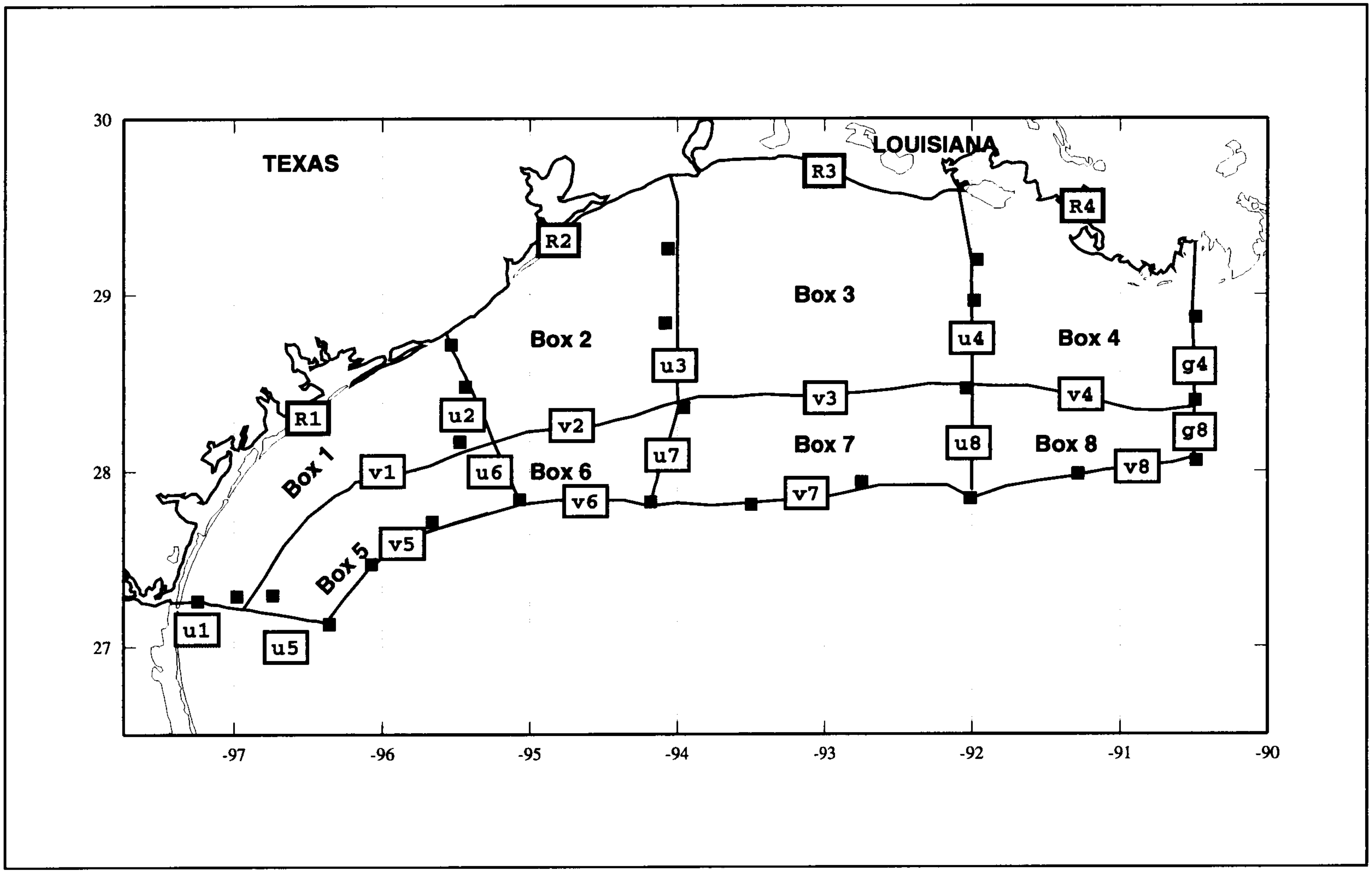

Figure M-2. Designations of boxes and fluxes. The box sides follow cruise tracks of hydrographic stations as shown in Figure M-1.

sparse, point-specific current meter velocity data. (The actual bin length depended on the ship's speed as 5-minute ensembles were collected; 1.5 km represents the largest expected distance based on a maximum possible ship speed of 5 $m \cdot s^{-1}$.) We used objective analysis to smooth the ADCP velocity data into a set of 4-m deep by 10-km long bins, averaged each available ADCP cruise, and then computed the individual velocity EOFs for the eighteen box sides. The shoreward sides of boxes 1-4 were taken as closed except for river discharge. We constructed the covariance matrix with a mean velocity of zero, rather than with a mean based on the ADCP data, because we anticipated using the current meter velocities to determine the amplitudes. Figure M-3 shows an example of the dominant mode EOF for the box sides g4 and g8.

The velocity for each bin was then estimated using

$$\tilde{v}(x,z) = \sum_{n=1}^{N} E_n^v \text{Ø}_n^v (x, z) , \qquad \text{(M-1)}$$

where E_n^v are the amplitudes, Ø_n^v are the two-dimensional eigenvectors, $\tilde{v}$ is the estimated velocity, and N is taken to be 4. The amplitudes were obtained by minimizing the error associated with fitting the EOF-estimated velocity to the current meter velocity data. Rather than fit each of the box sides independently, we imposed the additional constraint that the monthly averaged volume flux within a box be balanced, i.e., a net horizontal divergence of zero, so that the total error was given by

$$E = \left\langle (\tilde{v} - v)^2 \right\rangle + \lambda_i \left\langle \Delta q \right\rangle_i , \qquad \text{(M-2)}$$

where < > represents a sum over all possible realizations, v is the known velocity from current meters, Δq is the flux divergence for each box i, and λ_i is the Lagrangian multiplier. The first term on the righthand side represents the velocity fit, and the second the mass constraint. Once the amplitudes were obtained, it was a simple matter to use (M-1), integrate across a box side, and obtain the monthly averaged flux.

Estimations of the heat and freshwater fluxes then followed. We made the usual assumption that temperature and salinity were passive tracers transported by the volume flux, where the volume flux was estimated in the previous step. As we noted above, some, but not all, of the current meter moorings recorded temperature and salinity. This presented the same problem faced with sparse, point-specific velocity data. We assumed that the dominant pattern in the variability of the temperature and salinity for a box side could be estimated a priori from the hydrographic data. As in the case of the velocity field, we used EOFs to describe the dominant variance in the temperature and salinity fields. Similar to the volume flux, this approach takes advantage of the spatial extent of the hydrographic data to literally fill in the blanks

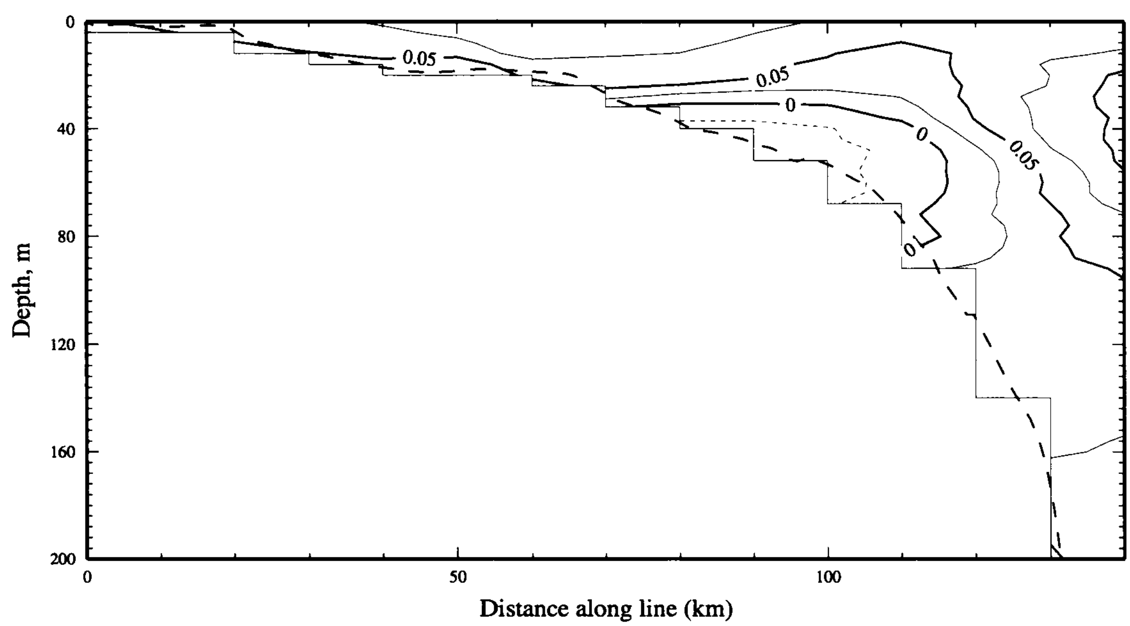

Figure M-3. ADCP normal velocity: EOF mode 1 for sides g4 and g8. The dotted line shows the actual bottom.

between sparse, point-specific mooring data. We used objective analysis to smooth the temperature and salinity data into a series of 4-m deep by 10-km long bins for each hydrographic cruise, averaged each hydrographic cruise, and then computed the individual temperature and salinity EOFs for the 18 box sides. We constructed the covariance matrix with a shelfwide mean temperature of 21.60°C and a mean salinity of 35.48. Figure M-4 shows an example of the dominant mode temperature EOF for the box side corresponding to g4 and g8, and Figure M-5 shows the corresponding dominant mode salinity EOF.

The temperature for each bin was then estimated using

$$\tilde{T}(x,z) = \sum_{n=1}^{N} E_n^T \varnothing_n^T (x,z) + \overline{T}, \tag{M-3}$$

where E_n^T are the amplitudes, $\varnothing_n^T$ are the two-dimensional eigenvectors, $\overline{T}$ is the shelfwide mean temperature, and N is taken to be 4. The salinity is estimated with

$$\widetilde{S}(x,z) = \sum_{n=1}^{N} E_n^S \varnothing_n^S (x, z) + \overline{S}, \tag{M-4}$$

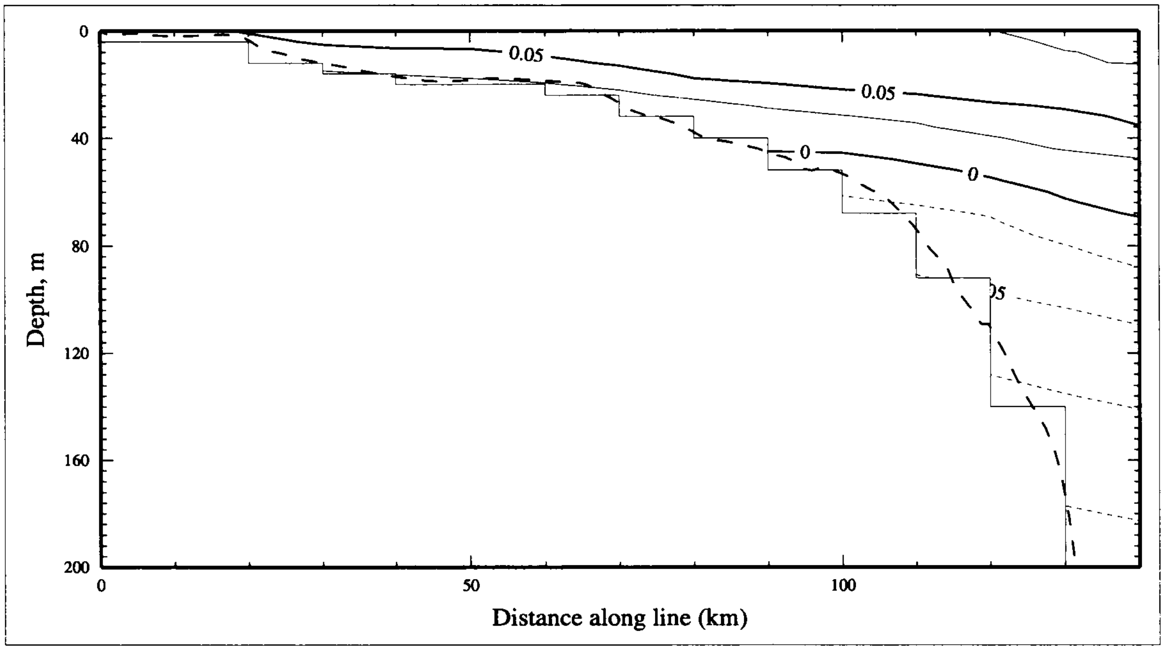

Figure M-4. Temperature variance: EOF mode 1 for sides g4 and g8. The dotted line shows the actual bottom.

where E_n^S are the amplitudes, $\emptyset_n^S$ are the eigenvectors, $\overline{S}$ is the shelfwide mean salinity, and N is taken to be 4. Each of the amplitudes was obtained by minimizing the error associated with fitting the EOF estimated temperature and salinity, (M-3) and (M-4), to the available mooring temperature and salinity data. The errors are defined as

$$E^T = \left\langle (\tilde{T} - T)^2 \right\rangle, \tag{M-5}$$

$$E^S = \left\langle (\tilde{S} - S)^2 \right\rangle, \tag{M-6}$$

where T and S are the known temperature and salinity from the the current meter sensors.

The flux of freshwater was defined to be the salinity fraction transported by the volume flux,

$$q_f = A \cdot \frac{\overline{S} - \tilde{S}}{\overline{S}} \cdot q, \tag{M-7}$$

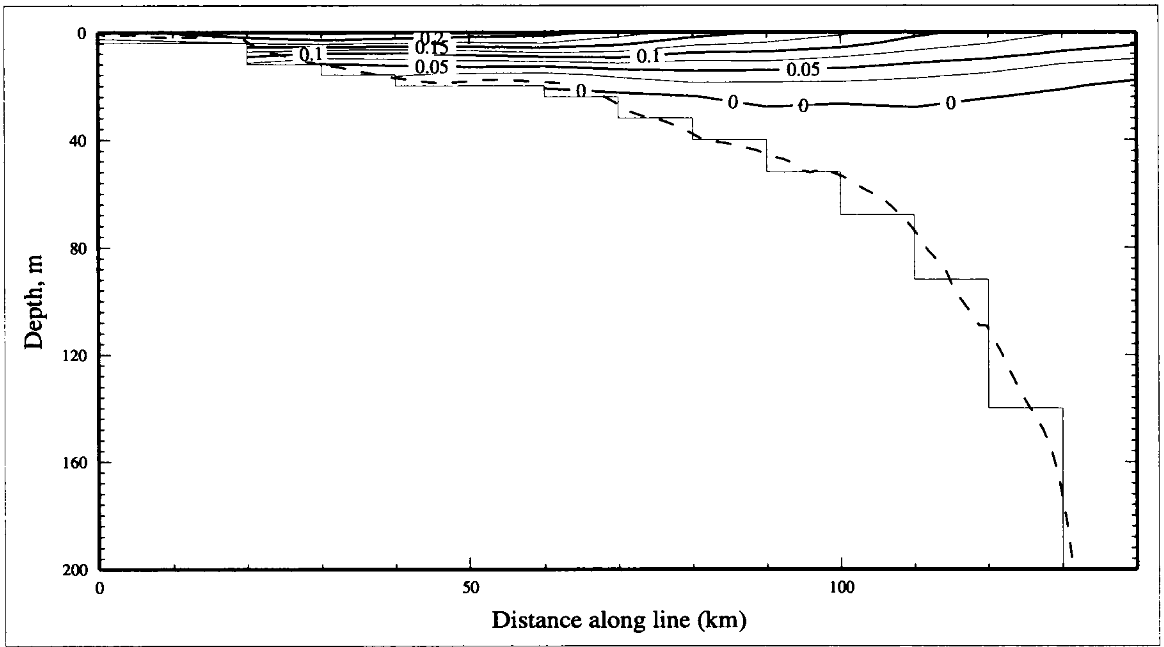

Figure M-5. Salinity variance: EOF mode 1 for sides g4 and g8. The dotted line shows the actual bottom.

where A is the area of a bin (40,000 m^2), q is the volume flux in $m^3 \cdot s^{-1}$, $\tilde{S}$ is the salinity as determined from the EOF fit, and $\overline{S}$ is the shelfwide mean salinity of 35.48. Because of this definition, the freshwater flux can be in the opposite direction of the volume flux if the observed salinity is greater than the mean. Because we assumed that salt was a passive tracer, it is physically unrealistic to expect a freshwater to flow against the volume flux. Hence, the freshwater flux should be interpreted in one of two ways. The first interpretation is the amount of freshwater needed to dilute a model ocean with a mean salinity of $\overline{S}$ down to the observed salinity $\tilde{S}$; thus, when the real ocean is fresher than the mean, the salinity fraction is positive and the freshwater flux is in the same direction as the volume flux. The second interpretation is the amount of freshwater that would have to be removed to increase $\overline{S}$ up to the observed salinity; when the real ocean is saltier than the mean, the salinity fraction is negative and the freshwater flux is against the volume flux. The first interpretation is more likely to occur on the inner shelf due to freshwater input from river discharge, and the second on the outer shelf when Loop Current rings with high salinities are adjacent to the shelf and cause freshwater to be drawn off.

The flux of heat was defined to be

$$q_h = A \cdot \rho C_p \cdot (\tilde{T} - \overline{T}) \cdot q \, , \qquad \text{(M-8)}$$

where A is the area of a bin, q is the volume flux in $m^3 \cdot s^{-1}$, $\tilde{T}$ is the temperature as determined from the EOF fit, $\overline{T}$ is the shelfwide mean temperature of 21.60°C, and ρC_p, the heat capacity, is taken to be 4.04×10^6 $J \cdot m^3$. Because we are using the shelfwide mean temperature as the reference temperature, it is possible to have heat flux opposite in direction to volume flux. An advective flux of heat against the volume flux indicates that the observed temperatures are less than the shelfwide mean, $\overline{T}$, and heat would have to be transported to the box side to raise its temperature. If the observed temperature is greater than $\overline{T}$, then heat would have to be transported with the volume flux to remove heat from the box side and cool the observed temperature down to the mean. For both freshwater and heat flux estimates, the reader should bear in mind that the results are simply a measure of the perturbation flux needed to adjust the real ocean to the mean conditions.

Model runs

The box model volume fluxes were determined for the 31 months from May 1992 through November 1994. They represent the monthly averaged flux, in cubic meters per second, determined by a fit of the EOF amplitudes to the monthly averaged, bridged 40-hr low passed current meter records. The river discharges for 12 major Texas rivers, and the Calcasieu and Atchafalya in Louisiana, were included as shown in Figure M-1. The discharge of the Mississippi was not directly included in this model; it was assumed that the salinity recorded by the moorings along the eastern side of the box model (Figure M-2) would account for the presence of freshwater from the Mississippi. While we recognized that the salinity sensors were 10 m below the surface and probably would miss most of the freshwater, we relied on the fact that the patterns of salinity variability were based on hydrographic data taken to within 3 m of the surface and would include most of the freshwater. This is clearly supported by the dominant mode EOF for salinity on the eastern end of the box model (Figure M-5). Directly including the Mississippi discharge in the box model would be problematic for several reasons. First, it is difficult to determine what percentage of the discharge through the three major passes on the delta ends up on the Texas-Louisiana shelf, and secondly, whether it flows onto the inner or outer shelf. Moreover, the flow out of the delta can proceed eastward under the right wind conditions and thereby miss the Texas-Louisiana shelf entirely. For these reasons we did not directly include river discharge from the Mississippi. Finally, it should be emphasized that the divergence of volume flux for each box is exactly zero by design, while the divergence of freshwater and heat are not zero, but are products of the box model.

We first show five examples of the volume, freshwater, and heat fluxes on the Texas-Louisiana shelf: a summer month without ring impingement on the outer shelf; a summer month with ring impingement; a non-summer month without ring impingement; a non-summer month with ring impingement; and the month having smallest fluxes of any studied. We define a summer month as June, July, or August, when the component of the wind stress is downcoast, and non-summer as the remainder of the year when the wind stress component is upcoast.

Section 2.5.1 discusses Loop Current eddies during the LATEX period and gives a timetable showing when eddies were impinging on the shelf. The presence of rings dramatically affects the fluxes on the outer shelf, but generally has little impact on the inner shelf.

There is no summer month without the presence of an eddy adjacent to the shelf, but July 1994 shows the least impact (Figure H.1-1) on the outer shelf. The northern portion of Eddy eXtra affected the western shelf to some extent, but it helped to drive the flow upcoast; hence, we use this month as the example of a summer month without ring impingement. Figure M-6 shows uniform upcoast flux of volume, freshwater, and heat on the inner shelf and is consistent with our understanding of summer wind-driven circulation on the inner shelf. On the outer shelf, the flow of volume, freshwater, and heat are also consistent with the seasonal pattern, with one exception for the freshwater.

The example of a summer month with ring impingement, July 1993, was chosen because the northern portion of Eddy Vazquez was impacting the western shelf and Eddy Whopper the eastern shelf. Figure M-7 shows uniform upcoast flux of volume, freshwater (except the far western end), and heat on the inner shelf. This is consistent with our understanding of summer wind-driven circulation on the inner shelf and indicates that the inner shelf is unaffected by rings adjacent to the outer shelf. The flow on the outer shelf is not consistent with any seasonal pattern, but shows the impact of Eddy Whopper on the eastern shelf. Eddy Whopper appears to be drawing volume, freshwater and heat off the shelf, even though the 20°C isotherms (Figure H.1-1) appear to be parallel to the shelf break.

The example of a non-summer month without ring impingement on the outer shelf (February 1994, Figure M-8) shows uniform downcoast flux of volume and freshwater on the inner shelf, but upcoast flux of heat. The volume and freshwater fluxes are consistent with our understanding of the non-summer circulation pattern on the shelf, and the heat flux is consistent with a shelf that is losing heat to the atmosphere and would have to replenish it with a flow of heat from the south. The outer shelf flux of volume is uniformly downcoast, the flux of freshwater shows no consistent pattern, and the flux of heat is upshelf.

The example of a non-summer month with ring impingement on the outer shelf, January 1993, was chosen because Eddy Vazquez was adjacent to the western end of the shelf (see Figure H.1-1). Figure M-9 shows the same inner shelf flux pattern as the nonsummer month without ring impingement—uniform downcoast flux of volume and freshwater and upcoast flux of heat. On the outer shelf, the impact of Eddy Vazquez is seen to reverse the volume flux through box 6 to upcoast and possibly to affect the cross-shelf flux over the 200-m isobath.

Finally we show August 1994 (Figure M-10) because it is the month with the least activity of any studied.

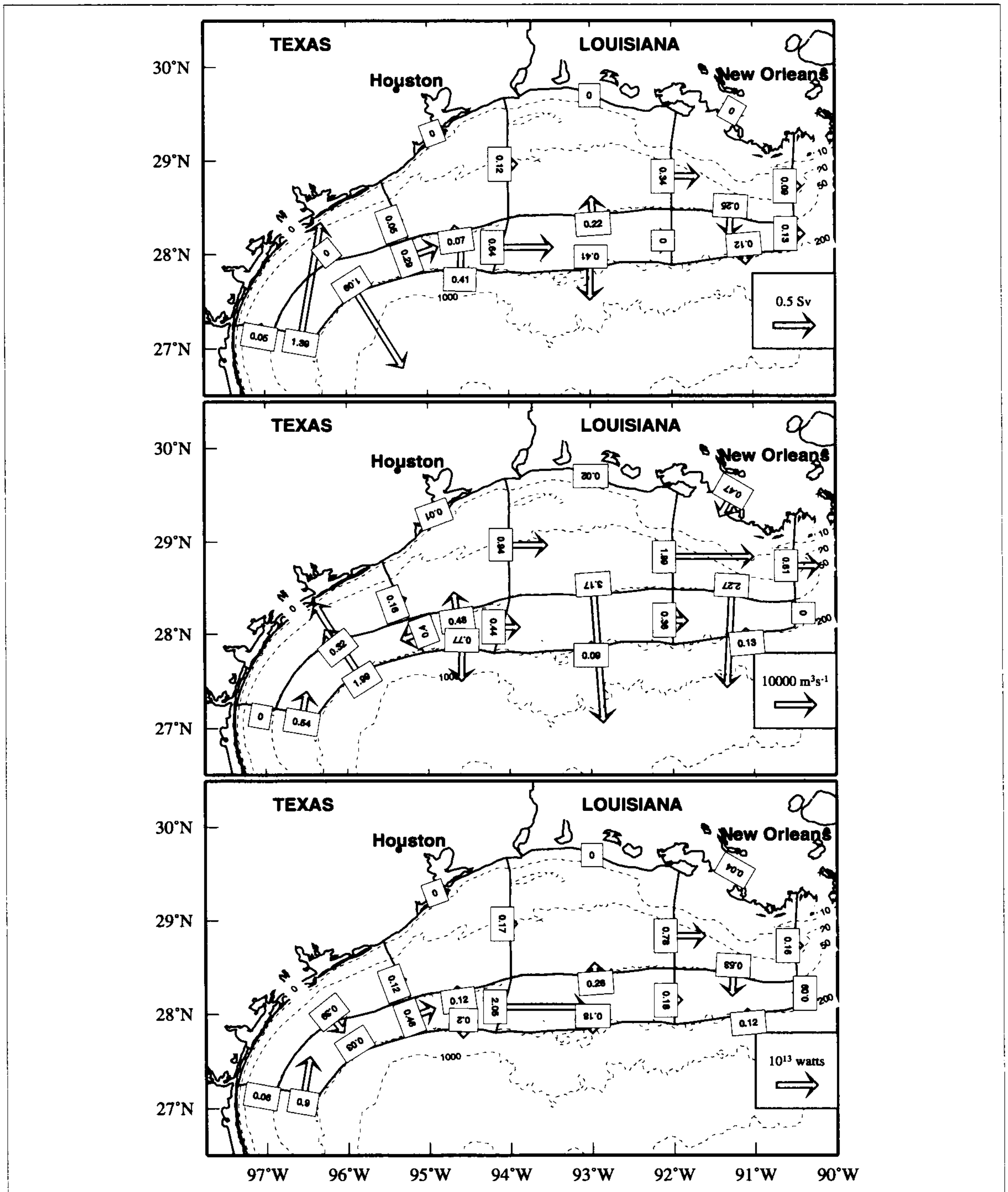

Figure M-6. Box model fluxes for July 1994, a summer month with minimal eddy activity. The upper panel shows the volume flux, the middle panel the fresh water flux relative to a salinity of 35.48, and the lower panel the heat flux relative to a temperature of 21.6°C.

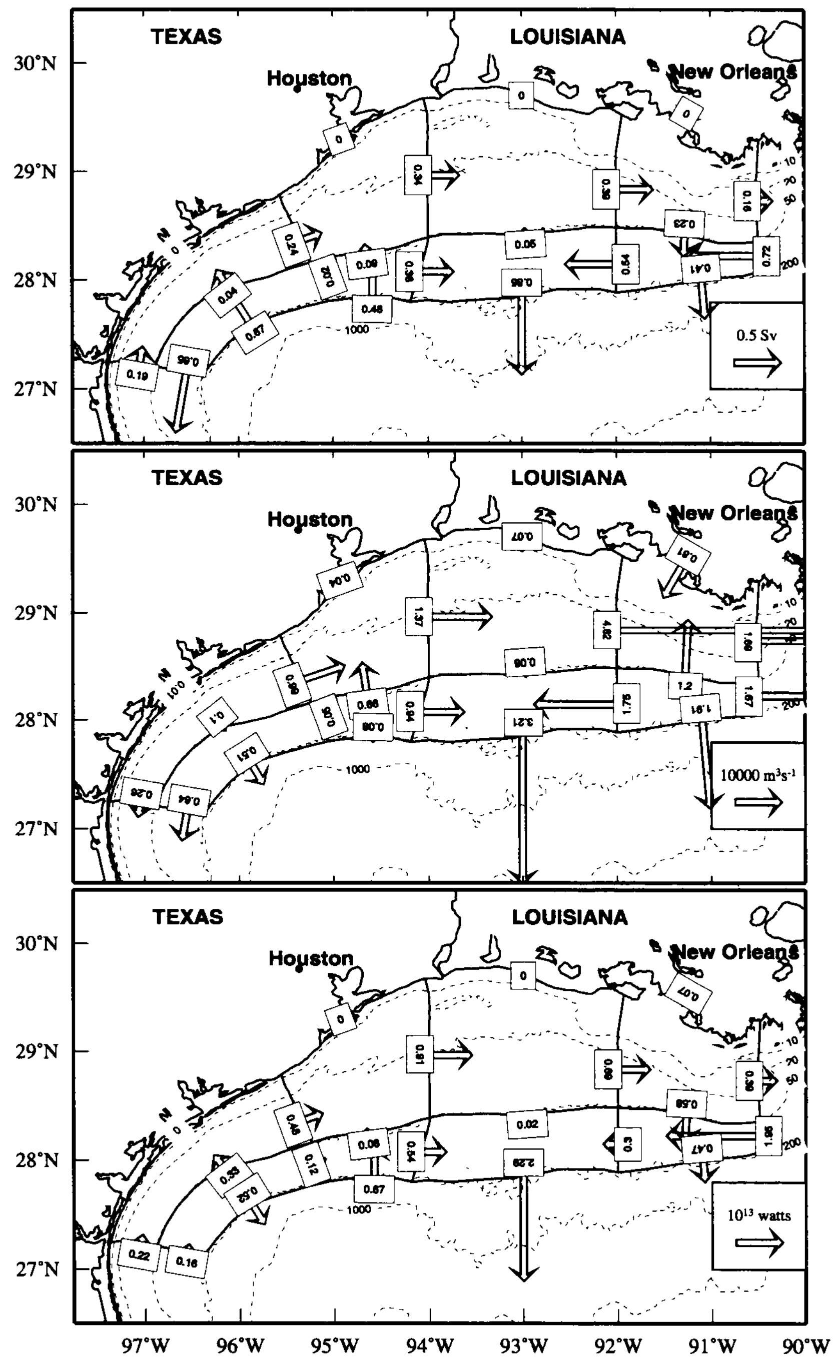

Figure M-7. Box model fluxes for July 1993, a summer month with significant eddy activity. The upper panel shows the volume flux, the middle panel the fresh water flux relative to a salinity of 35.48, and the lower panel the heat flux relative to a temperature of 21.6°C.

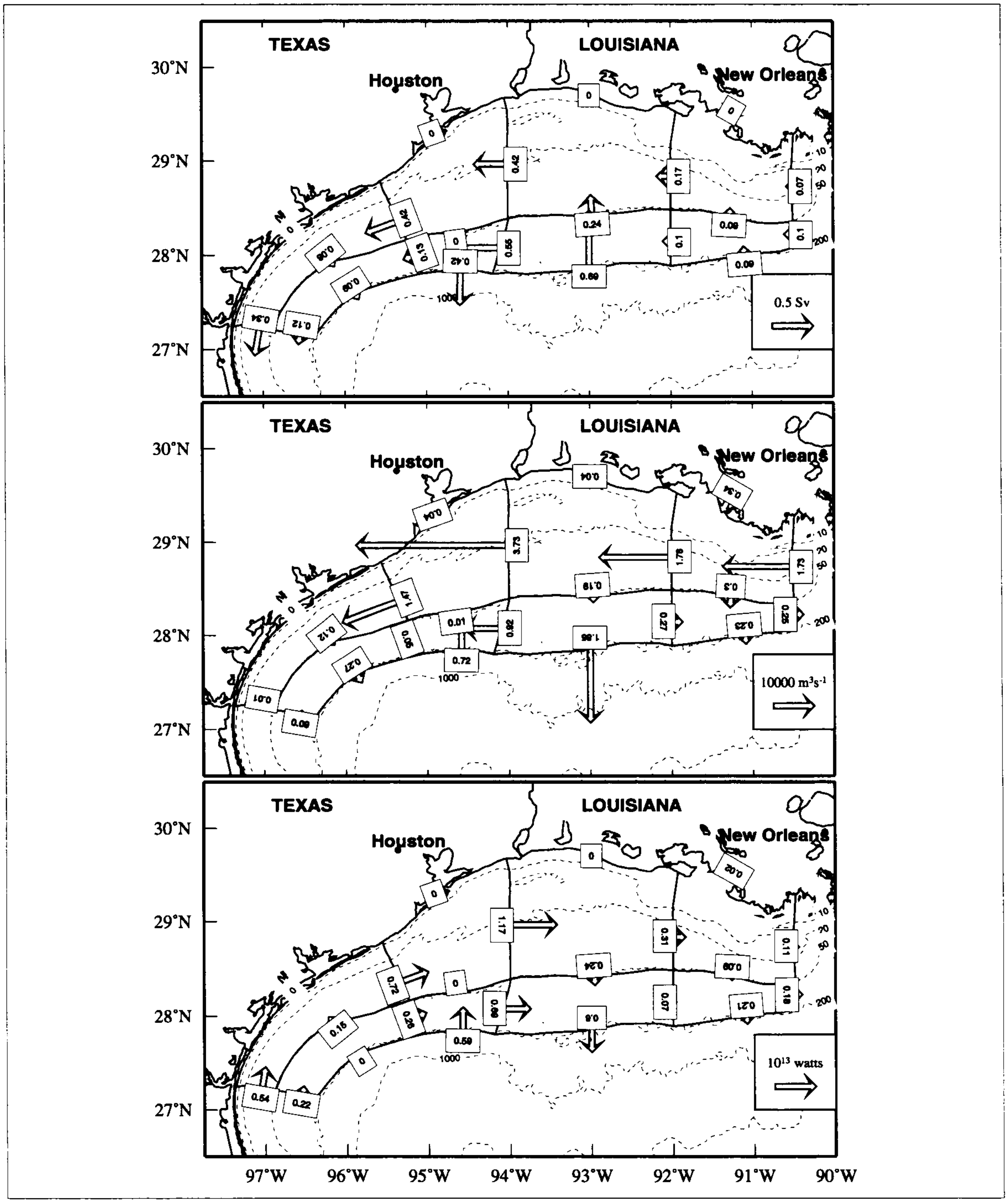

Figure M-8. Box model fluxes for February 1994, a nonsummer month with no eddy activity. The upper panel shows the volume flux, the middle panel the fresh water flux relative to a salinity of 35.48, and the lower panel the heat flux relative to a temperature of 21.6°C.

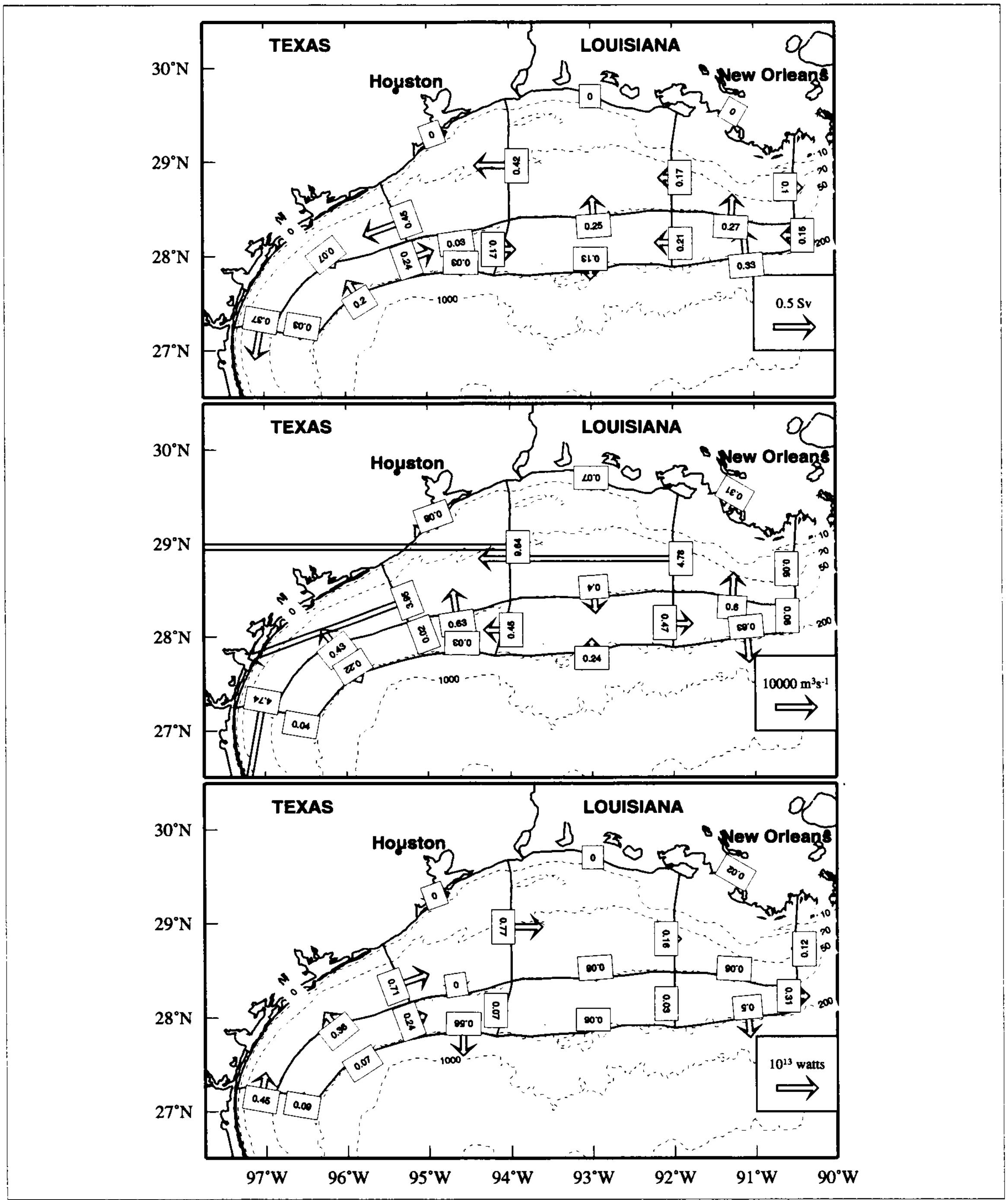

Figure M-9. Box model fluxes for January 1993, a nonsummer month with average eddy activity. The upper panel shows the volume flux, the middle panel the fresh water flux relative to a salinity of 35.48, and the lower panel the heat flux relative to a temperature of 21.6°C.

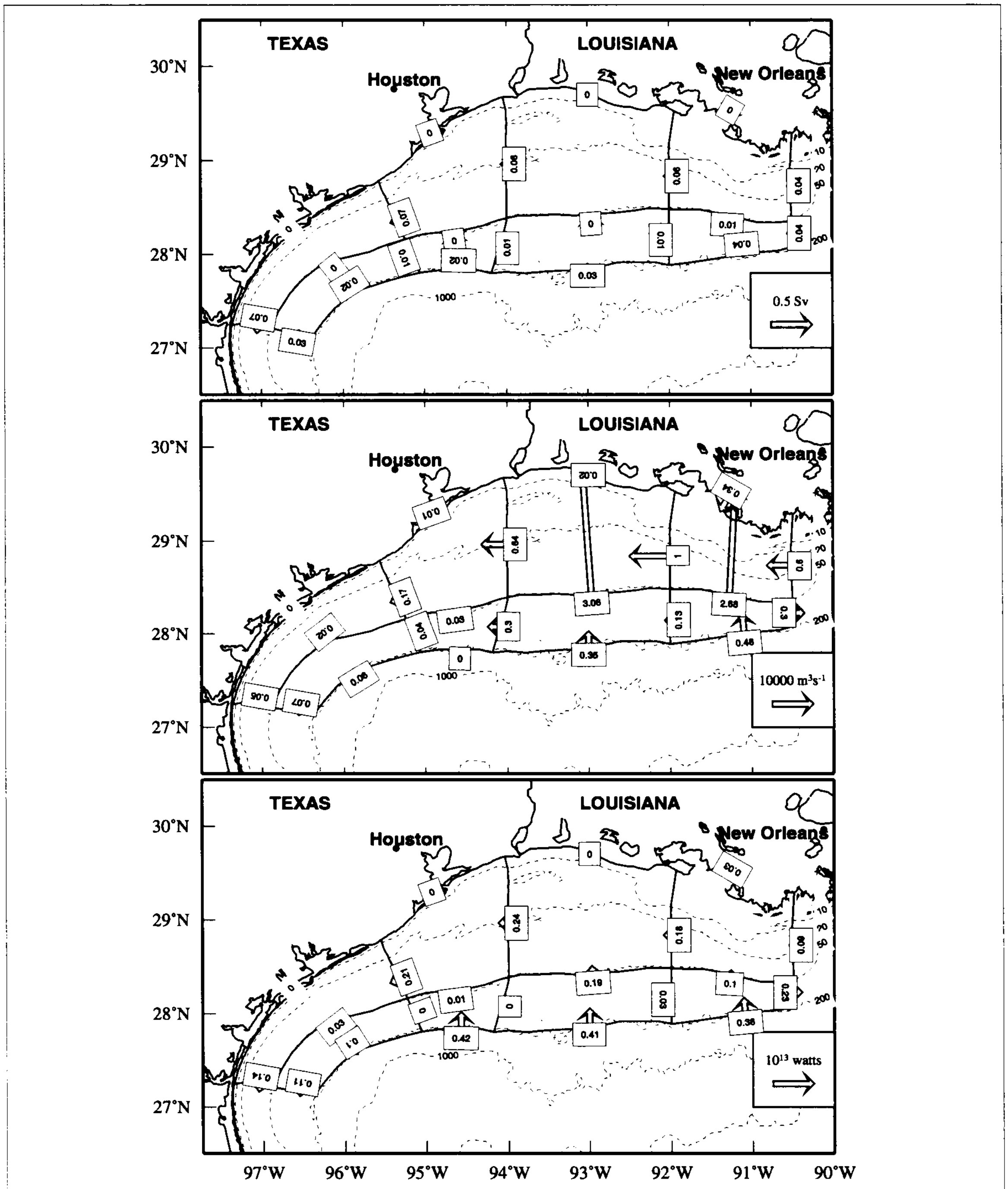

Figure M-10. Box model fluxes for August 1994, the month with the smallest fluxes. The upper panel shows the volume flux, the middle panel the fresh water flux relative to a salinity of 35.48, and the lower panel the heat flux relative to a temperature of 21.6°C.

Volume flux

By examining each of the monthly volume fluxes for the entire period we were able to compile a set of four figures (Figures M-11 through M-14) that show the alongshelf volume flux on the inner and outer shelf and the cross-shelf flux over the 50-m and 200-m isobath.

On the inner shelf, represented by boxes 1 through 4 (Figure M-11), the direction of the alongshelf flux is essentially either upcoast or downcoast over the entire shelf. From August or September through May, the flux is downcoast, and in June through July or August it is upcoast. The strength of the flux, i.e., its magnitude, along the inner shelf varies from box to box and month to month, but it is strongly downcoast (>0.25 Sv) from October through February. Beginning in May, the downcoast flux begins to weaken so that by June the flux reverses direction to upcoast and remains so through July. The strength of this upcoast flux is markedly weaker than the downcoast flux seen the remainder of the year. August is a transition month back to downcoast flux to complete the yearly cycle. We can conclude that, on the inner shelf, the yearly averaged transport of volume is downcoast, from the Mississippi delta toward the Mexican border.

On the outer shelf, represented by boxes 5 through 8 (Figure M-12), the alongshelf flux can be very large, but it has no recognizable seasonal pattern. It appears to be controlled by the presence of eddies along the outer shelf (see Section 2.5.1 for times when rings were adjacent to the shelf). In May, June, and July, there is a relatively uniform upshelf flux through all boxes except the most southerly.

The cross-shelf flux over the 50-m isobath from the inner shelf to the outer shelf (Figure M-13) is typically weaker than the alongshelf fluxes and shows no discernible seasonal pattern. The strength of the flux is markedly stronger at the eastern end of the shelf than it is toward the western end, but it appears that the 50-m isobath acts as an effective barrier to significant cross-shelf volume flux. This is particularly noticeable at the far western end, where fluxes on the outer shelf can be very strong (see July 1993, for example), yet the flux across the 50-m isobath is at least two orders of magnitude smaller.

The cross-shelf flux over the 200-m isobath (Figure M-14) is generally stronger than the outer shelf alongshelf fluxes and shows no discernible seasonal pattern. Unlike the cross-shelf flux over the 50-m isobath, the strength of the flux on the western end of the shelf is the same magnitude as that of the eastern end.

Freshwater flux

By examining each of the monthly freshwater fluxes for the entire period we were able to compile a set of four figures (Figures M-15 through M-18) that show the alongshelf freshwater

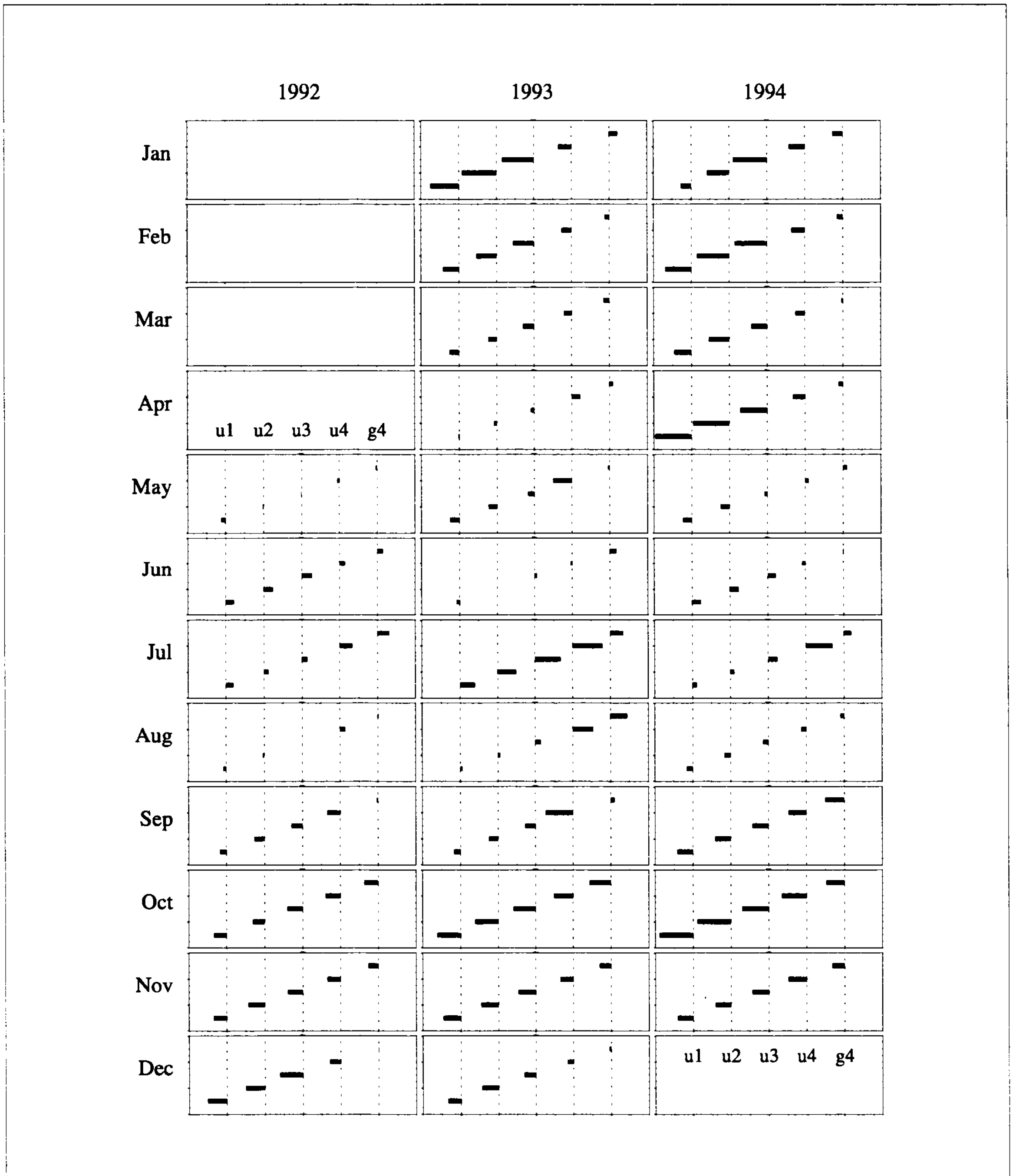

Figure M-11. Alongshelf volume flux on the inner shelf, relative to 0.5 Sv.

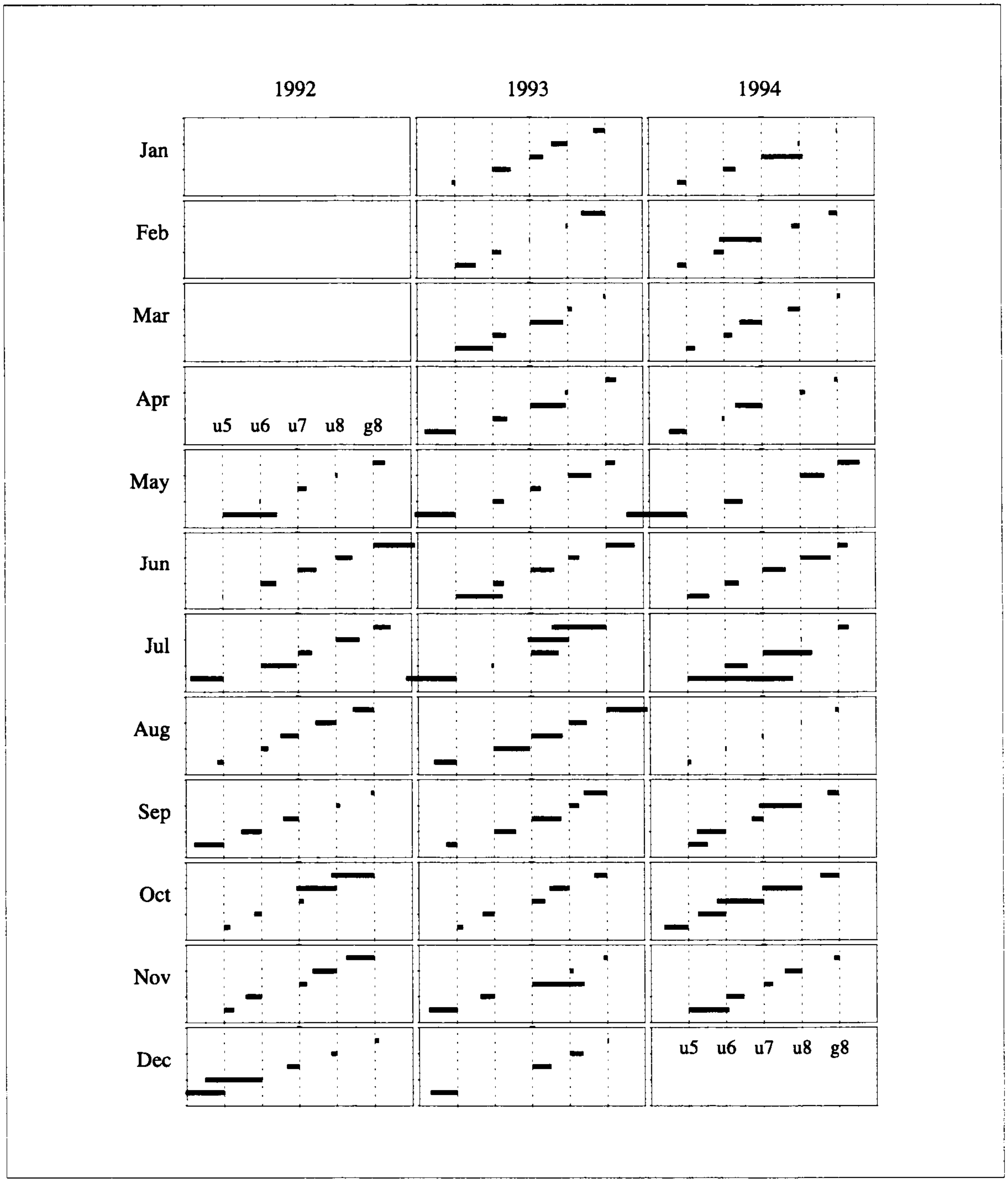

Figure M-12. Alongshelf volume flux on the outer shelf, relative to 0.5 Sv.

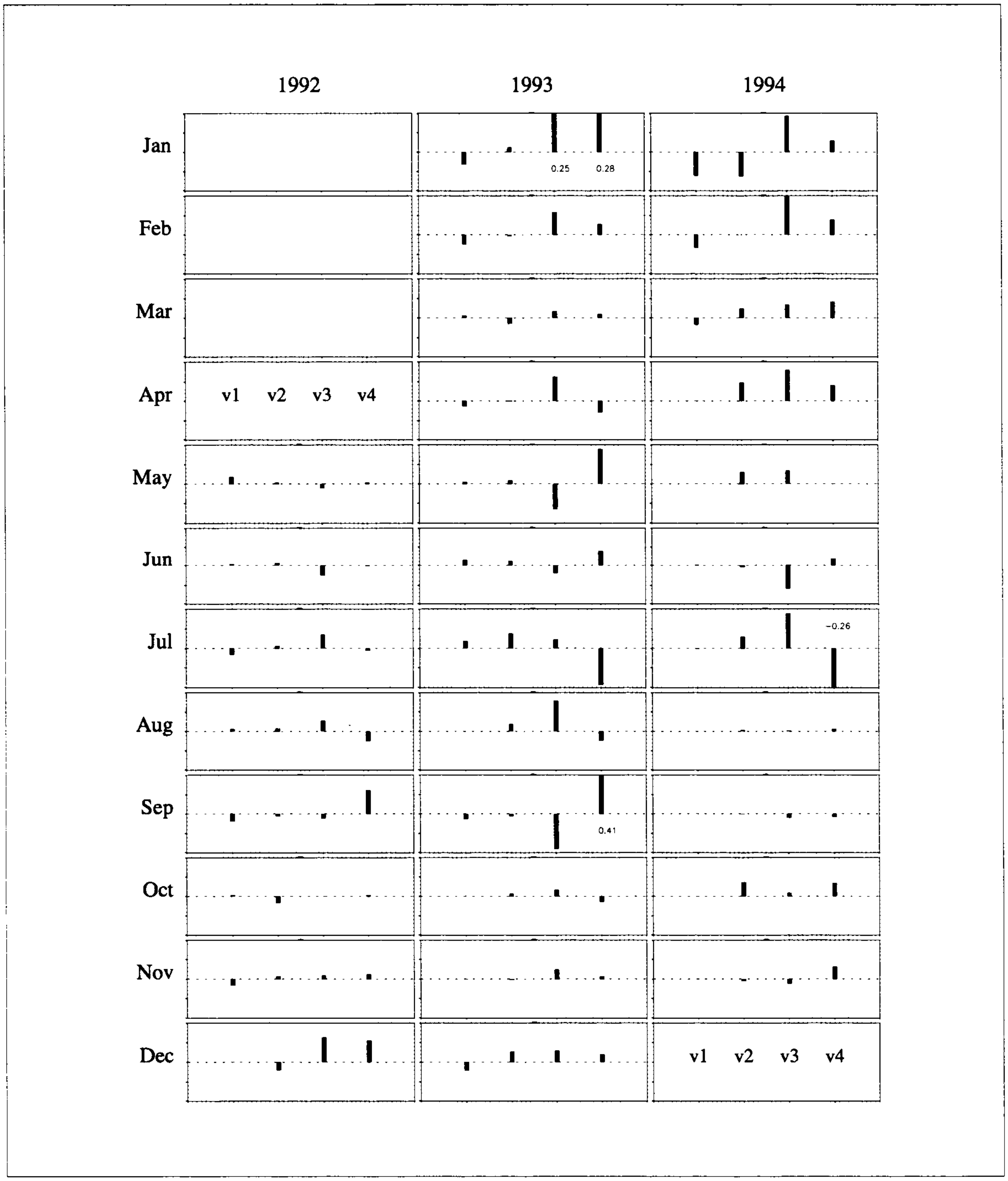

Figure M-13. Cross-shelf volume flux over the 50-m isobath, relative to 0.25 Sv.

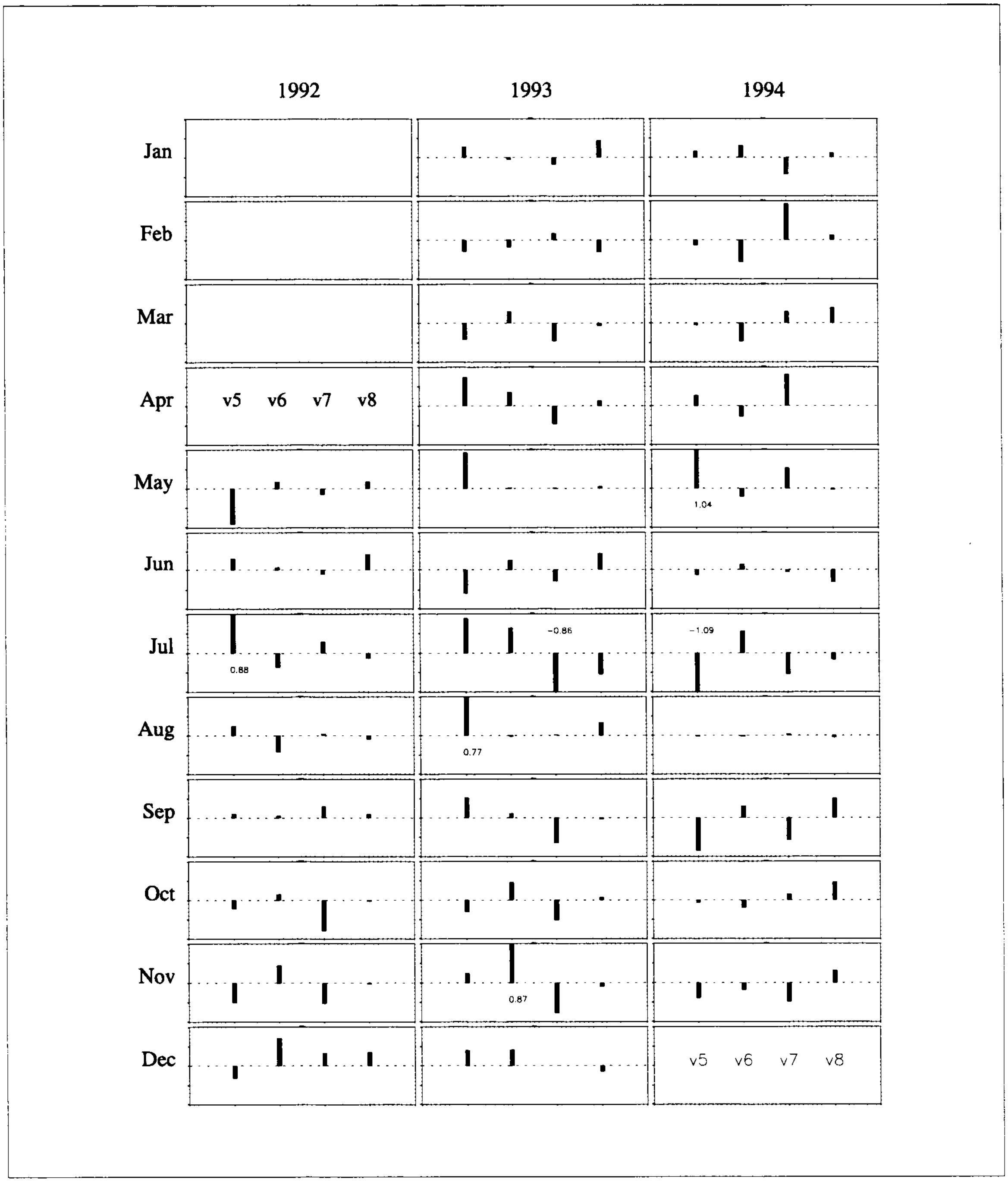

Figure M-14. Cross-shelf volume flux over the 200-m isobath, relative to 0.75 Sv.

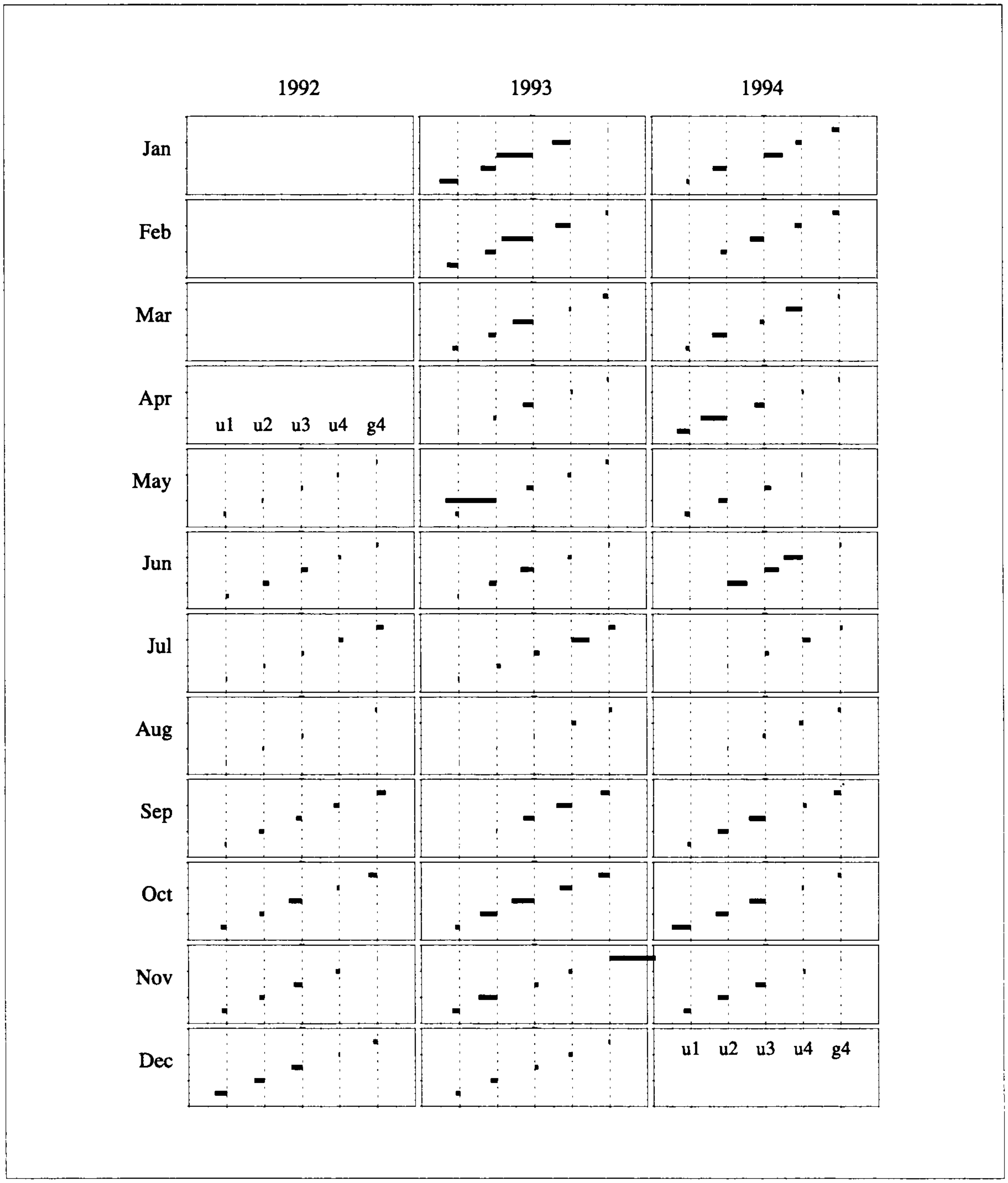

Figure M-15. Alongshelf freshwater flux on the inner shelf, relative to 0.1 Sv.

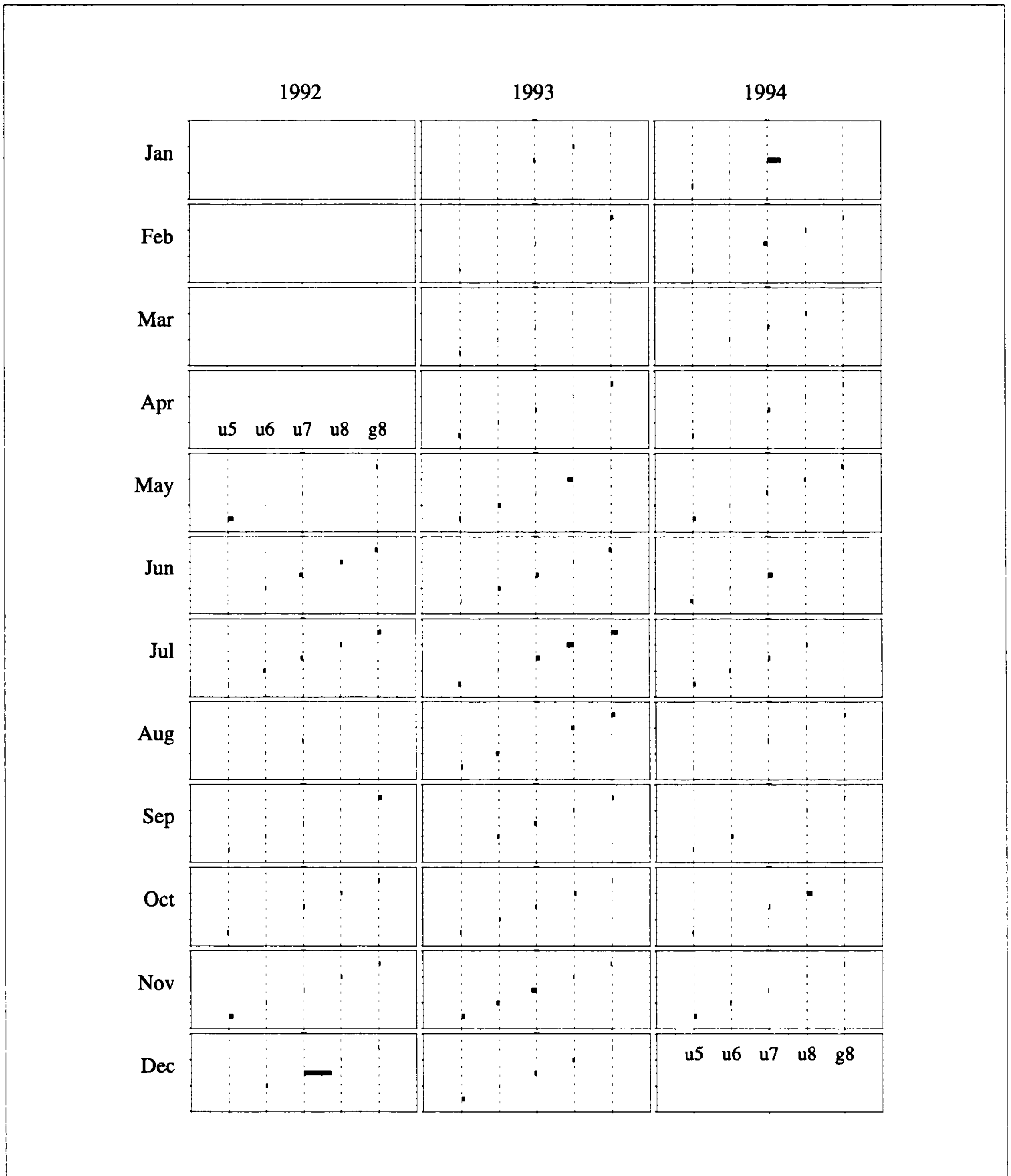

Figure M-16. Alongshelf freshwater flux on the outer shelf, relative to 0.1 Sv.

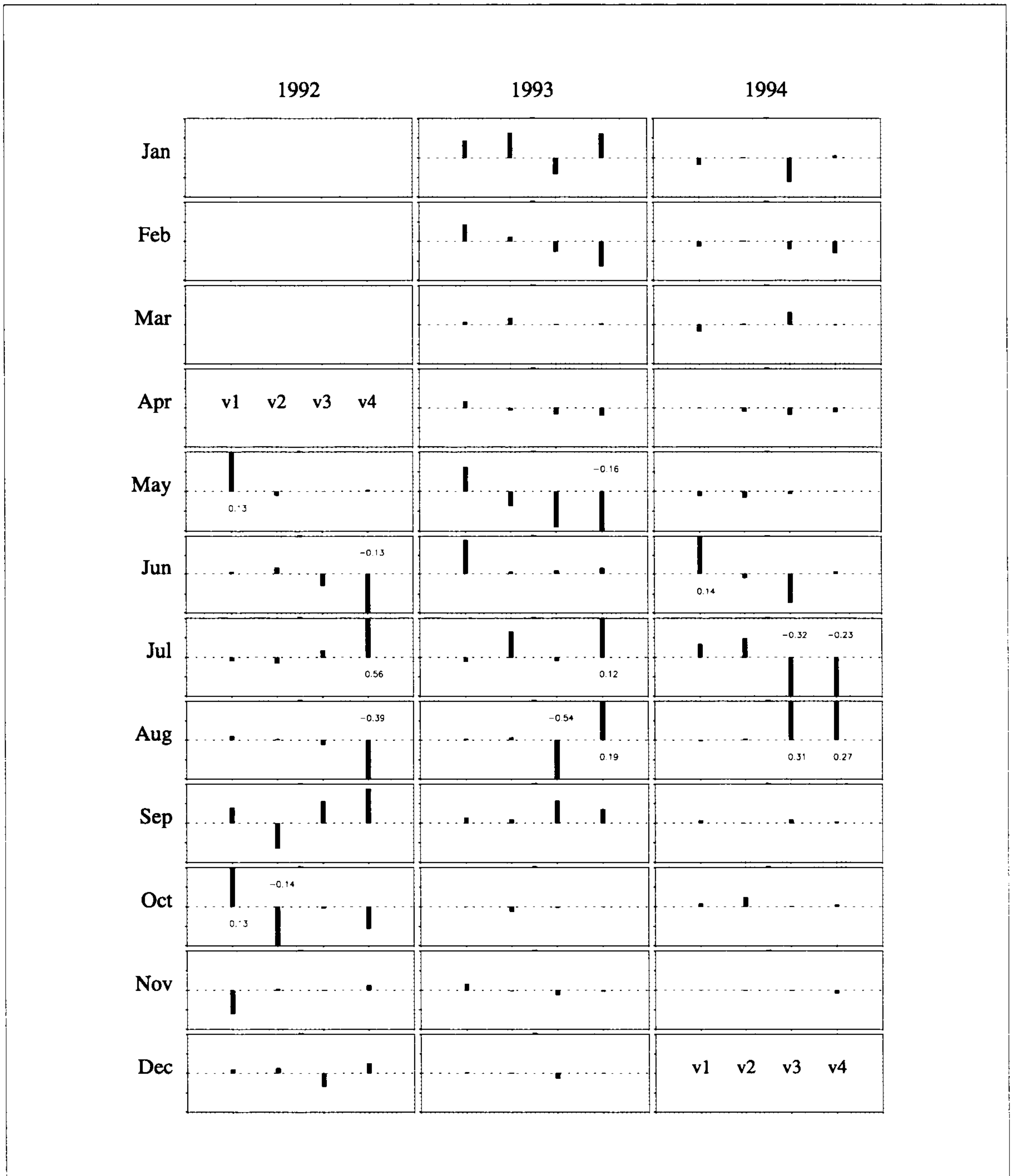

Figure M-17. Cross-shelf freshwater flux over the 50-m isobath, relative to 0.10 Sv.

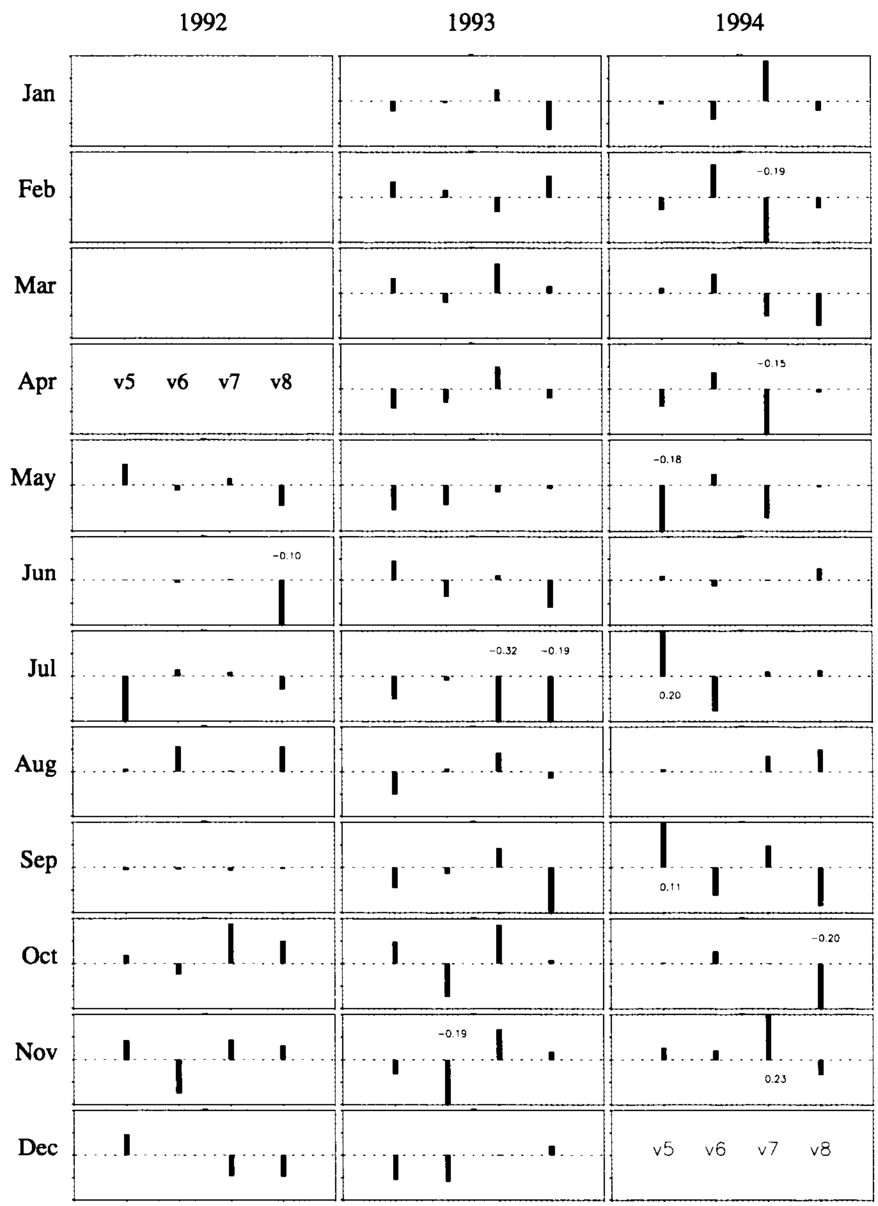

Figure M-18. Cross-shelf freshwater flux over the 200-m isobath, relative to 0.10 Sv.

flux on the inner and outer shelf and the cross-shelf flux over the 50-m and 200-m isobath. We note that it is possible to have a freshwater flux that exceeds the volume flux; e.g., if the volume flux is the combination of an upcoast and downcoast component that are approximately equal but weakly downcoast, then, if the downcoast component is significantly fresher than the upcoast, the freshwater flux will be strongly downcoast and greater than the volume flux. This, in fact, occurred for the alongshelf flux between boxes 2 and 3 during May 1993.

On the inner shelf, represented by boxes 1 through 4 (Figure M-15), the direction of the alongshelf flux generally mirrors that of the volume flux, though there are distinct reversals between the direction of the volume flux and the freshwater flux. In general, from September through April the freshwater flux is downcoast, and from June to July it is upcoast. The strength of this upcoast flux is noticeably weaker than the downcoast flux seen during the remainder of the year. August is the transition month between upcoast and downcoast flux and shows little if any freshwater flux. This indicates that the observed salinity on the inner shelf is close to the shelfwide mean during August. We can conclude that, on the inner shelf, the yearly averaged transport of freshwater, like that of the volume flux, is downcoast, from the Mississippi Delta toward the Mexican border.

On the outer shelf, represented by boxes 5 through 8 (Figure M-16), the flux of alongshelf freshwater is significantly smaller than on the inner shelf. Apparently, the observed salinities of the box sides are nearly always equal to the mean shelfwide salinity, and the alongshelf freshwater flux on the outer shelf is almost nonexistent. This is somewhat surprising given the episodic appearance, and disappearnce, of rings adjacent to the shelf.

The cross-shelf flux over the 50-m isobath (Figure M-17) indicates there are months when there is a siginifcant amount of freshwater being moved between the inner and outer shelf (e.g., May 1993) and months when there is very little (e.g., May 1994). There is no apparent correlation to the times when eddies are adjacent to the shelf.

Cross-shelf freshwater flux over the 200-m isobath (Figure M-18) shows a nearly consistent reversal to that of the volume. This is merely an indication that the observed salinities along the 200-m isobath are nearly always greater than the shelfwide mean. Consequently, freshwater is removed from the outer boxes to increase the mean salinity up to the observed. Of particular interest is July 1993, which shows a significant amount of freshwater flux leaving the outer shelf. As noted above, Eddy Whopper, adjacent to the eastern end of the shelf, had a significant impact during the LATEX period. Even the flux across the 50-m isobath shows an offshelf flux of freshwater.

Though it was possible to use these freshwater fluxes to compute divergences based on the divergence of freshwater within each box, it was not done. The box model results are unavailable because of two contributing factors: the known variance in the velocity fit and the use of month-long averages. Experience with fitting the current meter velocity to the EOF fields showed that the average variance was approximately 2.5 $cm \cdot s^{-1}$. Assuming that the monthly averaged velocities resulted in a net zero horizontal freshwater divergence, then a variance of 2.5 $cm \cdot s^{-1}$ on each of the four sides with an area of 5,000,000 m^2 would result in a divergence of 500,000 $m^3 \cdot s^{-1}$. Over one month this would result in a unrealistic rise of 130 m. This problem can be alleviated by considering the entire shelf, in which case the maximum rise can be shown to be less than 4 m per month. Integrating the monthly averaged flux over the period of a month, while seemingly reasonable, merely compounds the error in the velocity fit. Nevertheless, we believe these freshwater fluxes to be qualitatively reliable as an estimate of the monthly averaged fluxes. Steps are being taken to improve the freshwater flux estimates so that meaningful divergences can be estimated.

Heat flux

By examining each of the monthly heat fluxes for the entire period, we compiled a set of four figures (Figures M-19 through M-22) that show the alongshelf heat flux on the inner and outer shelf and the cross-shelf flux over the 50-m and 200-m isobath.

On the inner shelf, boxes 1 through 4 (Figure M-19), the alongshelf flux shows a remarkable bimodal yearly pattern. From June through October, the heat flux pattern follows that of the volume flux and is consistent with the seasonal circulation pattern. However, beginning in November, the heat flux weakens dramatically and then reverses to upcoast from December through March, opposite to the volume flux. An advective flux of heat against the volume flux, while physically unrealistic, indicates that the observed temperatures on the inner shelf for these time periods are less than the shelfwide mean, and heat would have to be transported into the box to raise its temperature.

On the outer shelf, boxes 5 through 8 (Figure M-20), the alongshelf flux can be very large but in general it follows the volume flux. The cross-shelf flux over the 50-m isobath (Figure M-21) is significantly weaker than the alongshelf fluxes and shows no discernable seasonal pattern. The cross-shelf flux over the 200-m isobath (Figure M-22) is significantly stronger than the flux over the 50-m isobath and shows many months in which the heat flux is opposite to the volume flux.

As for the freshwater fluxes, errors in the divergence of heat within each box result because the known variance in the velocity fit and the use of month-long averages. Nevertheless, we believe these heat fluxes to be qualitatively reliable as an estimate of the monthly averaged fluxes, and steps are being taken to improve the heat flux estimates.

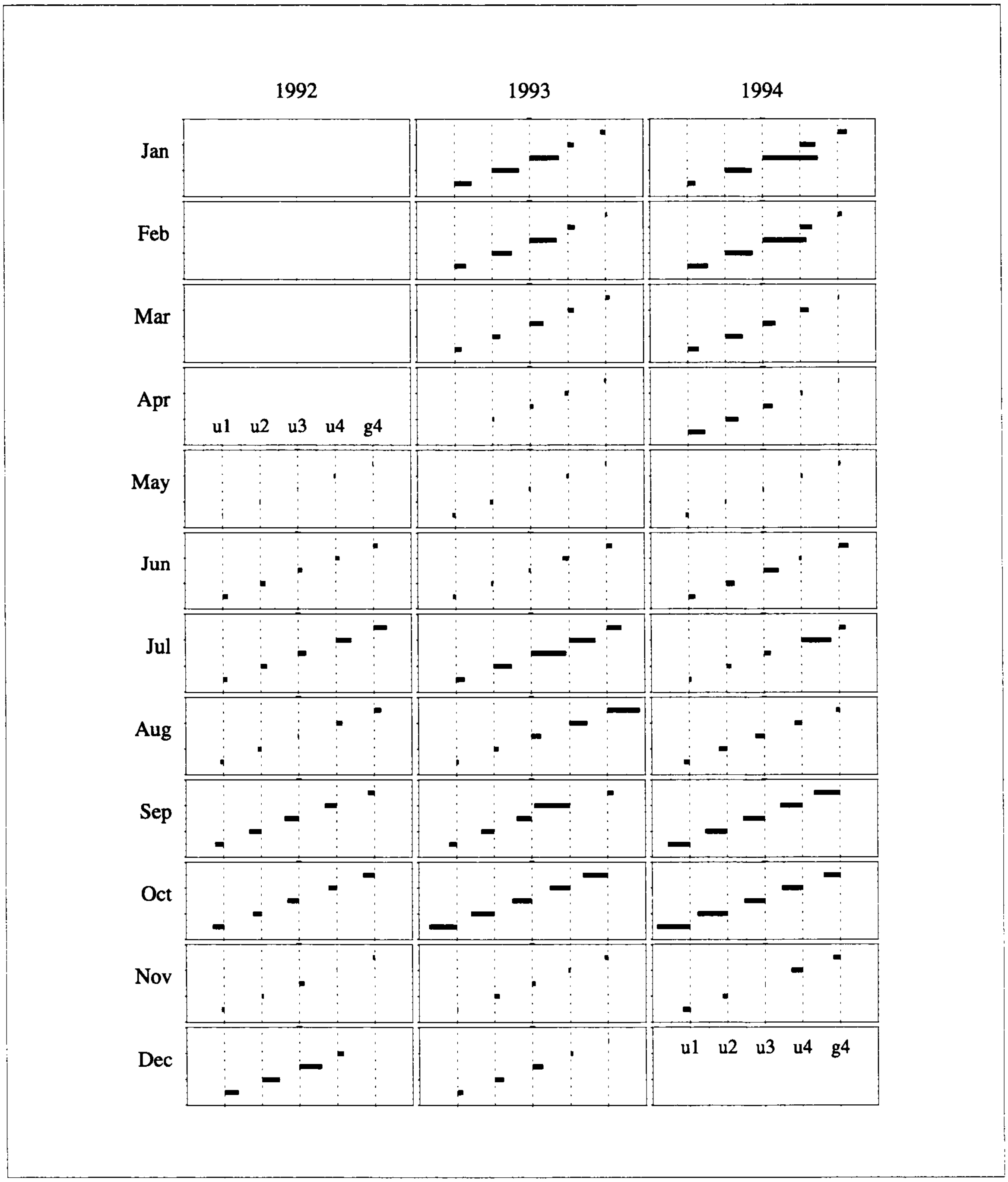

Figure M-19. Alongshelf heat flux on the inner shelf, relative to 10^{13} W.

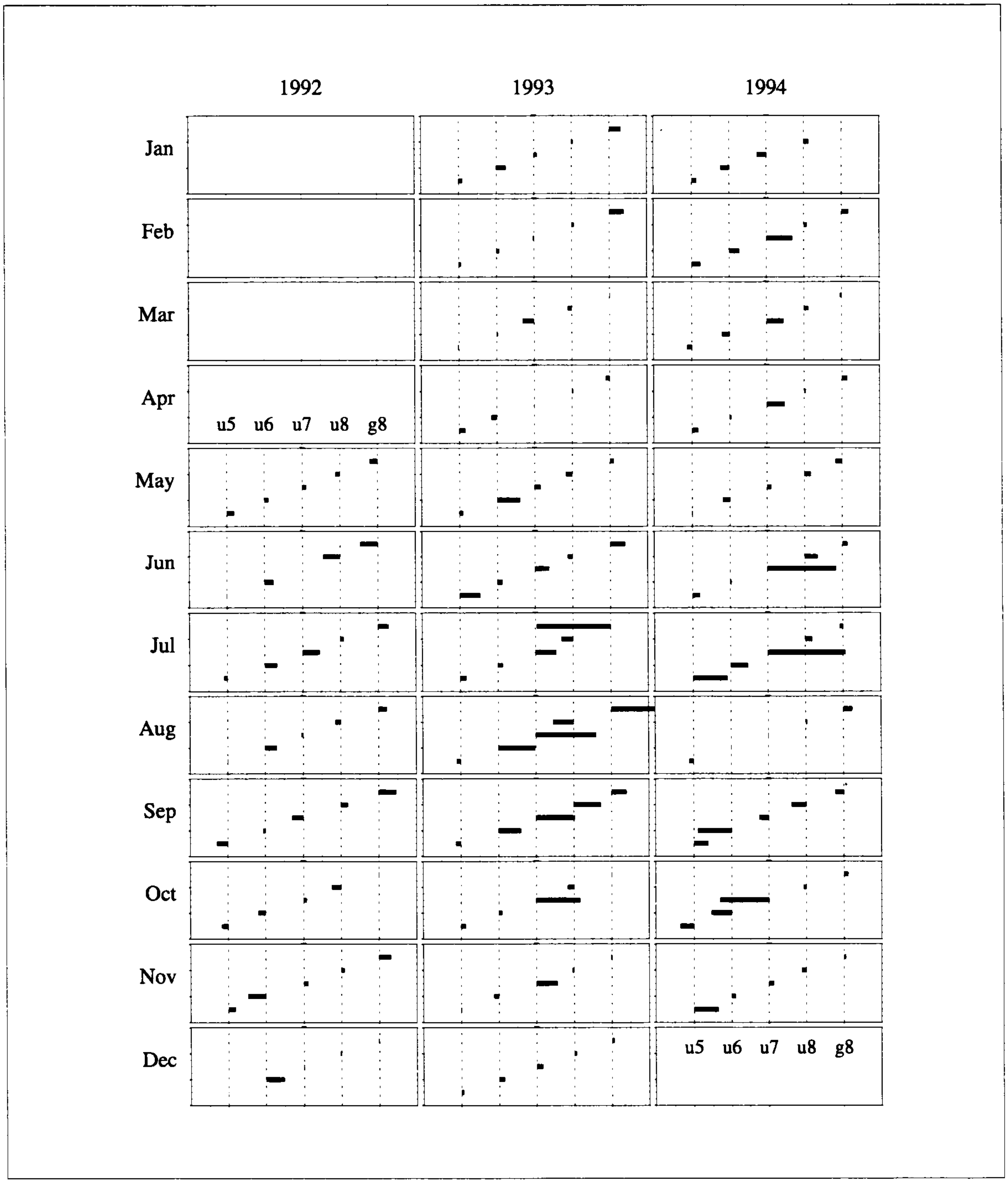

Figure M-20. Alongshelf heat flux on the outer shelf, relative to 10^{13} W.

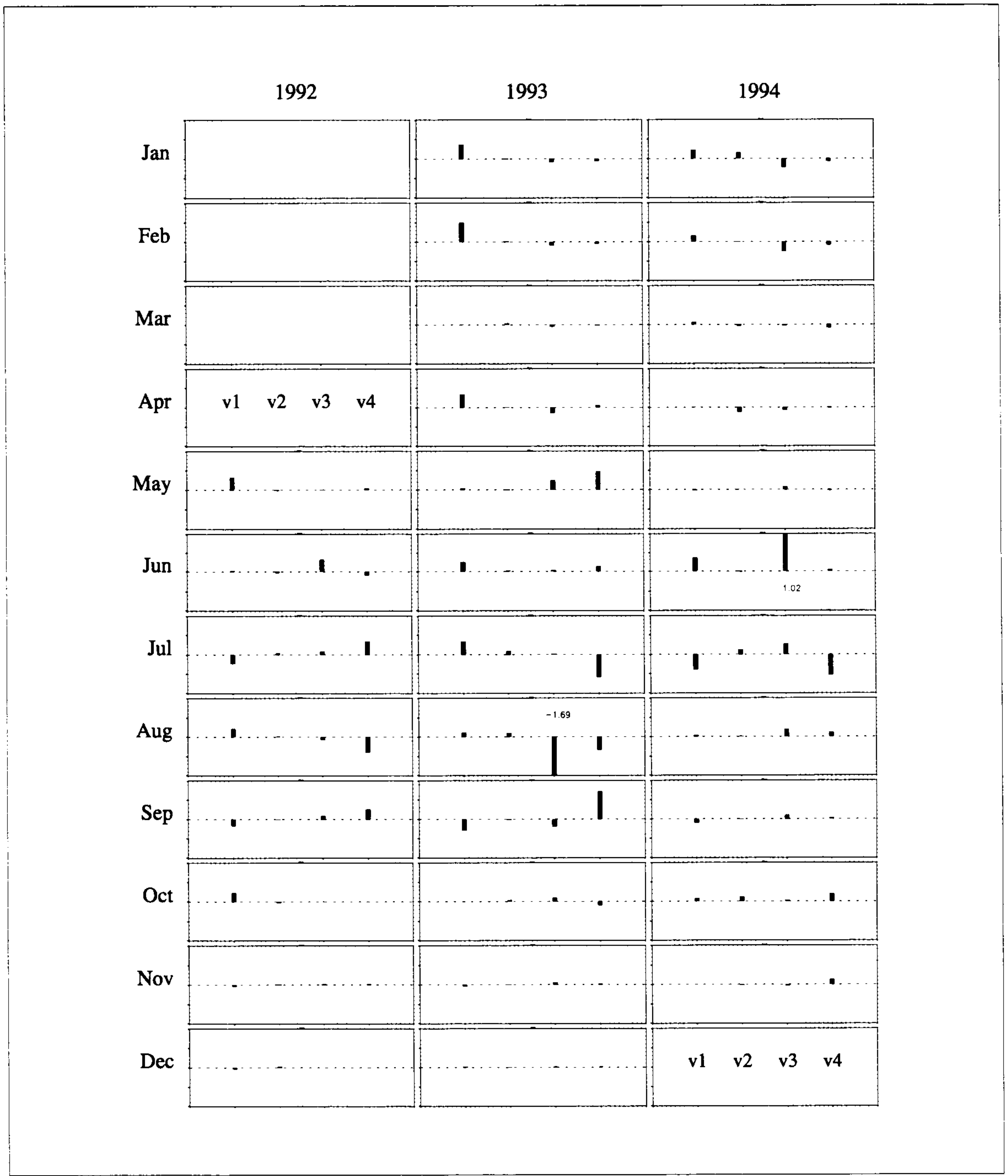

Figure M-21. Cross-shelf heat flux over the 50-m isobath, relative to 10^{13} W.

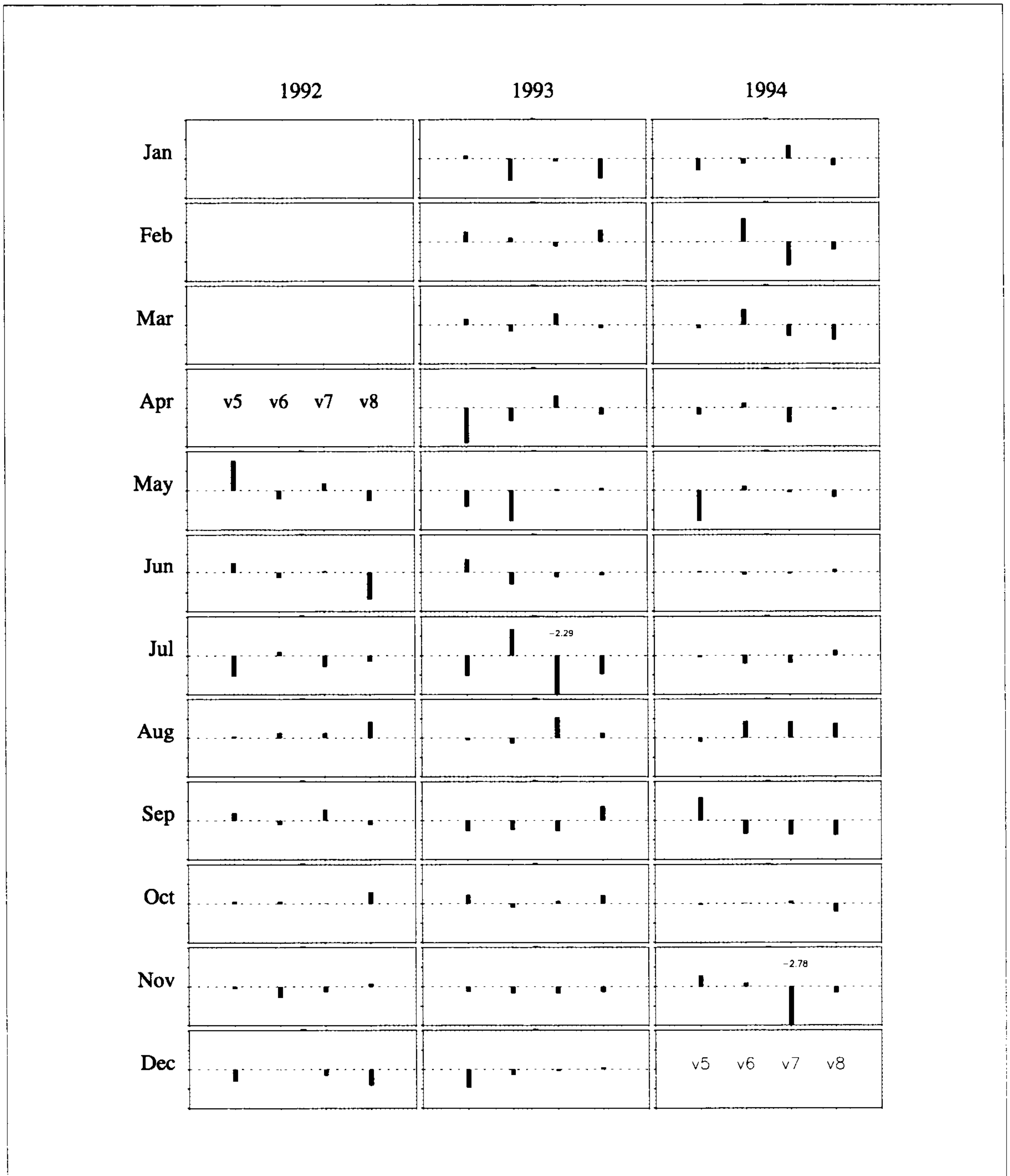

Figure M-22. Cross-shelf heat flux over the 200-m isobath, relative to 10^{13} W.

References

Arango, H.G., and R.O. Reid. 1991. A generalized reduced-gravity ocean model. Atmosphere-Ocean. 29:256-287.

Bender, L.C. III. 1996. Modification of the physics and numerics in a third-generation ocean wave model. J. Atmos. Oceanic Technol. 13(3):726-750.

Bender, L.C. III, and F. Kelly. 1998. LATEX Shelf Data Report: Acoustic Doppler current proiler, May 1992 through November 1994. Texas A&M University, Dept. of Oceanography, College Station, TX. 372 pp.

Berger, T.J., P. Hamilton, J.J. Singer, and R.R. Leben. 1996. Louisiana/Texas Shelf Physical Oceanography Program: Eddy Circulation Study, Final Synthesis Report. OCS Study MMS 96-0051. U.S. Department of the Interior, Minerals Management Service, Gulf of Mexico OCS Region, New Orleans, LA. 324 pp.

Bloomfield, P. 1976. Fourier analysis of time series: An introduction, pp. 22-41 and 118-150. John Wiley & Sons, Inc. New York, NY. 258 pp.

Breaker, L.C., L.D. Burroughs, Y.Y. Chao, J.F. Culp, N.L. Guinasso, Jr, R.L. Teboulle, and C.R. Wong. 1994. The impact of Hurricane Andrew on the near surface marine environment in the Bahamas and the Gulf of Mexico. Weather and Forecasting. 9(4):542-546.

Caplan, P.M. 1995. The 12-14 March 1993 superstorm: Performance of the NMC Global Medium-Range Model. Bull. Amer. Meteor. Soc. 76:201-212.

Capurro, L.R.A., and J.L. Reid, eds. 1972. Contributions on the physical oceanography of the Gulf of Mexico, Volume II, Texas A&M University, Oceanographic Studies. Gulf Publishing Co., Houston, TX. 288 pp.

Chen, C., R.O. Reid, and W.D. Nowlin Jr. 1996. Near-inertial oscillations over the Texas-Louisiana shelf. J. Geophys. Res. 101(C2):3509-3524.

Chen, H.-W. 1995. Variability and structure of currents over the Texas-Louisiana shelf- a view from a shipboard acoustic Doppler current profiler. Ph.D. Dissertation. Texas A&M Univ. College Station, TX. 117 pp.

Church, J.A., N.J. Freeland, and R.L. Smith. 1986a. Coastal-trapped waves on the east Australian continental shelf. Part I: Propagation of modes. J. Phys. Oceanogr. 16: 1929-1943.

Church, J.A., N.J. White, A.J. Clarke, H.J. Freeland, and R.L. Smith. 1986b. Coastal-trapped waves on the east Australian continental shelf. Part II: Model verification. J. Phys. Oceanogr. 16:1945-1957.

Clarke, A.J., and D.S. Battisti. 1981. The effect of continental shelves on tides. Deep-Sea Res. 28A:665-682.

Cochrane, J.D. 1958. The frequency distribution of water characteristics in the Pacific Ocean. Deep-Sea Res. 5:111-127.

Cochrane, J.D., and F.J. Kelly. 1986. Low-frequency circulation on the Texas-Louisiana continental shelf. J. Geophys. Res. 91:10,645-10,659.

Csanady, G.T. 1979. The pressure field along the western margin of the North Atlantic. J. Geophys. Res. 84(C8):4905-4914.

Csanady, G.T. 1981. Circulation in the coastal ocean, pp. 101-183. In Advances in Geophysics, Vol. 23. Academic Press. New York, NY. 279 pp.

Current, C.L. 1996. Spectral model simulation of wind driven subinertial circulation on the inner Texas-Louisiana shelf. PhD Dissertation. Texas A&M University, Dept. of Oceanography, College Station, TX. 144 pp.

DiMarco, S.F. 1998. On the use of the method of cyclic descent to estimate principal tidal constituents. Texas A&M University, Dept. of Oceanography, College Station, TX. Reference No. 98-1-T. 33 pp.

DiMarco, S.F., and L.C. Bender III. 1998. WAM4 model/data comparison in the NW Gulf of Mexico, pp. 334-341. Proceedings of Waves '98 Meeting, 30 Apr - 1 May 1998, Houston, TX. Amer. Soc. Civil Eng., New York, NY.

DiMarco, S.F., and R.O. Reid. 1998. Characterization of the principal tidal current constituents on the Texas-Louisiana shelf. J. Geophys. Res. 103(2):3093-3110.

DiMarco, S.F., A.E. Jochens, and M.K. Howard. 1997. LATEX Shelf Data Report: Current meters, April 1992 through December 1994; 10 volumes. Texas A&M University, Dept. of Oceanography, College Station, TX.

DiMarco, S.F, F.J. Kelly, and N.L. Guinasso, Jr. 1995a. LATEX Shelf Data Report: MiniSpec directional wave gauges. Volume I: April 1992 through August 1993. Texas A&M University, Dept. of Oceanography, College Station, TX. Reference No. 95-4-T. 331 pp.

DiMarco, S.F., F.J. Kelly, J. Zhang, and N.L. Guinasso, Jr.. 1995b. Directional wave spectra on the Louisiana-Texas shelf during Hurricane Andrew. J. Coastal Res. SI-21:217-233.

Dolan, R., and R.E. Davis. 1992. Rating northeasters. Mariners Weather Log. 36(1): 4-10.

Elliott, B.A. 1982. Anticyclonic rings in the Gulf of Mexico. J. Phys. Oceanogr. 12:1292-1309.

Etter, P.C., and J.D. Cochrane. 1975. Water temperature on the Texas-Louisiana shelf. Texas A&M University Sea Grant Program, Mar. Adv. Bull. SG 75-604. 22 pp.

Flierl, G.R. 1979. Baroclinic solitary waves with radial symmetry. Dyn. Atmos. Oceans. 6:15-38.

Glenn, S.M., and C.C. Ebbesmeyer. 1993. Drifting buoy observations of a Loop Current anticyclonic eddy. J. Geophys. Res. 98:20,105-20,119.

Godin, G. 1972. The analysis of tides. University of Toronto Press, Toronto, Canada. 264 pp.

Gonella, J. 1972. A rotary-component method for analyzing meteorolgical and oceanograpic vector time series. Deep-Sea Res. 19: 833-846.

Grymes, J.M. III, and G.W. Stone. 1995. A review of key meteorological and hydrological aspects of Hurricane Andrew. J. Coastal Res. SI-21:6-23.

Hasselmann, S., K. Hasselmann, J.H. Allender, and T.P. Barnett. 1985. Computations and parameterizations of the nonlinear energy transfer in a gravity-wave spectrum. Part II: Parameterizations of the nonlinear energy transfer for application in wave models. J. Phys Oceanogr. 15:1378-1391.

Hayashi, Y. 1979. A generalized method of resolving transient disturbances into standing and traveling waves by space-time spectral analysis. J. Atmos. Sci. 36:1017-1029

Hellerman, S., and M. Rosenstein. 1983. Normal monthly wind stress over the world ocean and error estimates. J. Phys. Oceanogr. 13:1093-1104.

Hsu, S.A. 1994. On the incorporation of wave characteristics into drag coefficient formulation at sea, pp 237-238. Preprint: Second international conference on air-sea interaction, meteorology, and oceanography of the coastal zone, Lisbon, Portugal. Amer. Meteor. Soc., Boston, MA.

Hsu, S.A. 1993. The Gulf of Mexico—a breeding ground for winter storms. Mariners Weather Log. 37(2):4-11.

Hsu, S.A. 1988. Coastal Meteorology. Academic Press. San Diego, CA. 260 pp.

Hsu, S.A. 1972. Coastal air-circulation system: Observations and empirical model. Mon. Weather Rev. 98:487-509.

Ives, D.C., and R.M. Zacharias. 1987. Conformal mapping and orthogonal grid generation, pp. 1-10. AIAA/SAE/ASME/ASEE 23rd Joint Propulsion Conference, San Diego, CA.

Janssen, P.A.E.M. 1989. Wave-induced stress and the drag of airflow over sea waves. J. Phys. Oceanogr. 19:745-754.

Janssen, P.A.E.M. 1991. Quasi-linear theory of wind-wave generation applied to wave forecasting. J. Phys. Oceanogr. 21:1631-1642.

Johnson, G.A., E.A. Meindl, E.B. Mortimer, and J.S. Lynch. 1984. Features associated with repeated strong cyclogenesis in the western Gulf of Mexico during the winter of 1982-83, pp. 110-117. In Postprints, 3rd Conference on Meteorology of the Coastal Zone. Amer. Meteorol. Soc. Boston, MA.

Kanamitsu, M. 1989. Description of the NMC global data assimilation and forecast system. Weather and Forecasting. 4:335-342.

Kanamitsu, M., J.C. Alpert, K.A. Campana, P.M. Caplan, D.G. Deaven, M. Iredell, B. Katz, H.-L. Pan, J. Sela, and G.H. White. 1991. Recent changes implemented into the global forecast system at NMC. Weather and Forecasting. 6:425-435.

Kocin, P.J., P.N. Schumacher, R.F. Morales, Jr., and L.W. Uccellini. 1995. Overview of the 12-14 March 1993 superstorm. Bull. Amer. Meteor. Soc. 76:165-182.

Kosro, and Huyer. 1986. CTD and velocity surveys of seaward jets off northern California, July 1981 and July 1982. J. Geophys. Res. 91:7680-7690.

Kundu, P. J. 1976. Ekman veering observed near the ocean bottom. J. Phys. Oceanogr. 6:238-242.

Leipper, D.F. 1970. A sequence of current patterns in the Gulf of Mexico. J. Geophys. Res. 75(3):637-657.

Lewis, J.K., A.D. Kirwan, Jr., and G.Z. Forristall. 1989. Evolution of a warm-core ring in the Gulf of Mexico: Lagrangian observations. J. Geophys. Res. 94:8163-8178.

Li, Y., W.D. Nowlin, Jr., and M.E. Reap. 1996. LATEX Technical Report: A volumetric temperature-salinity census for the Texas-Louisiana continental shelf. Texas A&M University, Dept. of Oceanography, College Station, TX. Reference No. 96-5-T. 44 pp.

Liscum, F., and J.W. East. 1995. Floods in southeast Texas, October 1994, pp 367-372. Proceedings of Texas Water '95, Texas section of the American Society of Civil Engineers, August 16-17, 1995, San Antonio, Texas. Amer. Soc. Civil Eng., New York, NY.

Longuet-Higgins, M.S., D.E. Cartwright, and N.D. Smith. 1963. Observations of the directional spectrum of sea waves using the motion of a floating buoy, pp. 111-131. In Ocean wave spectra, Proceedings of a conference held at Easton. Prentice Hall, Englewood Cliffs, NJ.

Lott, N. 1993. The big one! A review of the March 12-14, 1993 "Storm of the Century." Natl. Climatic Data Ctr Tech. Rpt 93-01. 5 pp.

Middleton, J.F., and D.G. Wright. 1990. Coastally trapped waves in a stratified ocean. J. Phys. Oceanogr. 20:1521-1527.

Mitchum, G.T., and A.J. Clarke. 1986. Evaluation of frictional, wind-forced long-wave theory on the west Florida shelf. J. Phys. Oceanogr. 16:1029-1037.

MMS. 1994. Hurricane Andrew's impact on natural gas and oil facilities on the outer continental shelf, Interim report as of November 1993. OSC Report/MMS-94-0031, U.S. Dept. of the Interior, Minerals Management Service, Gulf of Mexico OCS Region, New Orleans, LA.

Montgomery, R.B. 1958. Water characteristics of Atlantic Ocean and of world ocean. Deep-Sea Res. 5:134-148.

Montgomery, R.B. 1941. Transport of the Florida Current off Habana. J. Mar. Res. 4(3):198-220.

Murty, T.S., G.A. McBean, and B. McKee. 1983. Explosive cyclogenesis over the northeast Pacific Ocean. Monthly Weather Review. 111:1131-1135.

Nakamoto, S. 1989. Solitonlike solutions in Loop Current eddies. J. Geophys. Res. 94: 14,567-14,574.

Narayanan, S., and I. Webster. 1988. Coastally trapped waves in the presence of a shelf edge density front. J. Geophys. Res. 93:14,025-14,031.

Narayanan, S., and I. Webster. 1987. Coastally trapped waves in the presence of a barotropic shelf edge jet. J. Geophys. Res. 92:9494-9502.

NDBC. 1990. Climatic summaries for the NDBC buoy and stations update 1. National Data Buoy Center Report, US Dept. of Commerce. Stennis Space Center, MS. 454 pp.

NMC Development Division. 1988. Documentation of the research version of the NMC medium-range forecasting model. NMC Development Division, Camp Springs, MD. 504 pp.

NOAA. 1996. Climate diagnostics bulletin, July 1996. Climate Prediction Center, W/NP52. NOAA/NWS/NCEP, NOAA Science Center. Washington D.C.

North, G.R., T.L. Bell, R.F. Cahalan, and F.J. Moeng. 1982. Sampling errors in the estimation of empirical orthogonal functions. Monthly Weather Rev. 110:699-706.

Nowlin, W.D., Jr. 1972. Winter circulation patterns and property distributions, pp. 3-52. In L.R.A. Capurro and J.L. Reid, eds. Contributions on the Physical Oceanography of the Gulf of Mexico. Gulf Publishing Co., Houston, TX.

Ochi, M.K. 1994. On hurricane-generated seas, pp. 374-387. In O.T. Magoon and J.M. Hemsley, eds. Ocean wave measurement and analysis. Amer. Soc. Civil Eng., New York, NY.

Oey, L.-Y. 1995. Eddy- and wind-forced shelf circulation. J. Geophys. Res. 100:8621-8637.

Pandolfo, J.P. 1969. Motions with inertial and diurnal period in a numerical model of the navifacial boundary layer. J. Mar. Res. 27:301-317.

Panofsky, H.A., and G.W. Brier. 1968. Some applications of statistics to meteorology. Penn. St. Univ. Press. University Park, PA.

Pollak, M.J. 1958. Frequency distribution of potential temperatures and salinities in the Indian Ocean. Deep-Sea Res. 5:128-133.

Price, J.F., R.A. Weller, and R. Pinkel. 1986. Diurnal cycling: Observations and models of the upper ocean response to diurnal heating, cooling, and wind mixing. J. Geophys. Res. 91:8411-8427.

Quirox, R.S. 1983. The climate of the El Niño winter of 1982-83—a season of extraordinary climate anomalies. Monthly Weather Review. 111:1685-1706.

Reid, J.L., and A.W. Mantyla. 1976. The effect of the geostrophic flow upon coastal sea elevations in the northern North Pacific ocean. J. Geophys. Res. 81:3100-3110.

Reid, R.O., and R.E. Whitaker. 1981. Numerical model for astronomical tides in the Gulf of Mexico. Volume I: Theory and application. Texas A&M Univ. College Station, TX. 115 pp.

Saucier, W.J. 1949. Texas-West Gulf cyclones. Monthly Weather Review. 77:219-231.

Schumann, S.A., J. Moser, G.A. Johnson, N.D. Walker, and S.A. Hsu. 1995. An overview of a strong winter low in the Gulf of Mexico, 12-13 March 1993. National Weather Digest. 20:11-25.

Shureman, P. 1976. Manual of harmonic analysis and predictions of tides. Coastal and Geodetic Survey special publ. 98, U.S. Dept. of Commerce, Washington DC.

Simpson, R.H., and H. Riehl. 1981. The hurricane and its impact, pp. 366-368. Louisiana State Univ. Press. Baton Rouge, LA.

Smith, W.H.F., and P. Wessel. 1990. Gridding with continuous curvature splines in tension. Geophysics. 55:293-305.

Stone, G.W., J.M. Grymes, III, K.D. Robbins, S.G. Underwood, G.D. Steyer, R.A. Muller. 1993. A chronologic overview of climatological and hydrological aspects associated with Hurricane Andrew and its morphological effects along Louisiana coast, U.S.A. Shore and Beach. 61(2):2-12.

Trenberth, K.E., and T.J. Hoar. 1996. The 1990-1995 El Niño - Southern Oscillation event—longest on record. Geophys. Res. Lttrs. 23(1):57-60.

Uccellini, L.W., P.J. Kocin, P.M. Stokols, and R.A. Door. 1995. Forecasting the 12-14 March 1993 superstorm. Bull. Amer. Meteor. Soc. 76:183-199.

Ulm, W.F. 1983. A volumetric temperature-salinity census for the continental shelf of the northwestern Gulf of Mexico. MS Thesis. Texas A&M University, Dept. of Oceanography, College Station, TX. 56 pp.

Vastano, A.C., and C.N. Barron Jr. 1994. Comparison of satellite and drifter surface flow estimates in the northwestern Gulf of Mexico. Cont. Shelf Res. 14(6):589-605.

Vukovich, F.M., and B.W. Crissman. 1986. Aspects of warm rings in the Gulf of Mexico. J. Geophys. Res. 91:2645-2660.

WAMDI Group: S. Hasselmann, K. Hasselmann, E. Bauer, P.A.E.M. Janssen, G.J. Komen, L. Bertotti, P. Lionello, A. Guillame, V.C. Cardone, J.A. Greenwood, M. Reistad, L. Zambresky, and J.A. Ewing. 1988. The WAM model—A third generation wave prediction model. J. Phys. Oceanogr. 18:1775-1810.

Wessel, P., and W.H.F. Smith. 1993. The GMT-SYSTEM version 2.1.4 technical reference and cookbook. Univ. of Hawaii, Honolulu/Scripps Inst. of Oceanography, UCSD. San Diego, CA. 70 pp.

Wessel, P., and W.H.F. Smith. 1991. Free software helps map and display data. Eos Trans. Am. Geophys. Union. 72:441, 445-446.

Whitaker, R.E. 1971. Seasonal variations of steric and recorded sea level of the Gulf of Mexico. MS Thesis. Texas A&M University, Dept. of Oceanography, College Station, TX. 111 pp.

Wilson, R.J. 1967. Amount and distribution of water masses in February and March 1962 in the Gulf of Mexico. MS Thesis. Texas A&M University, Dept. of Oceanography, College Station, TX. 54 pp.

Wüst, G. 1964. Stratification and circulation in the Antillean-Caribbean basins, Part 1. Columbia University Press. New York, NY. 54 pp.

Zhang, J., R.E. Randall, L. Chen, M. Ye, and J.K. Longridge. 1994. Nonlinear decomposition of a two-dimensional wave field, pp. 150-164. In O.T. Magoon and J.M. Hemsley, eds. Ocean wave measurement and analysis. Amer. Soc. Civil Eng., New York, NY.

Zhang, J., R.E. Randall, and C.A. Spell. 1992. Component wave interactions and irregular wave kinematics. J. Waterway, Port, Coastal, and Ocean Eng. 118(4):401-416.

The Department of the Interior Mission

As the Nation's principal conservation agency, the Department of the Interior has responsibility for most of our nationally owned public lands and natural resources. This includes fostering sound use of our land and water resources; protecting our fish, wildlife, and biological diversity; preserving the environmental and cultural values of our national parks and historical places; and providing for the enjoyment of life through outdoor recreation. The Department assesses our energy and mineral resources and works to ensure that their development is in the best interests of all our people by encouraging stewardship and citizen participation in their care. The Department also has a major responsibility for American Indian reservation communities and for people who live in island territories under U.S. administration.

The Minerals Management Service Mission

As a bureau of the Department of the Interior, the Minerals Management Service's (MMS) primary responsibilities are to manage the mineral resources located on the Nation's Outer Continental Shelf (OCS), collect revenue from the Federal OCS and onshore Federal and Indian lands, and distribute those revenues.

Moreover, in working to meet its responsibilities, the **Offshore Minerals Management Program** administers the OCS competitive leasing program and oversees the safe and environmentally sound exploration and production of our Nation's offshore natural gas, oil and other mineral resources. The MMS **Minerals Revenue Management** meets its responsibilities by ensuring the efficient, timely and accurate collection and disbursement of revenue from mineral leasing and production due to Indian tribes and allottees, States and the U.S. Treasury.

The MMS strives to fulfill its responsibilities through the general guiding principles of: (1) being responsive to the public's concerns and interests by maintaining a dialogue with all potentially affected parties and (2) carrying out its programs with an emphasis on working to enhance the quality of life for all Americans by lending MMS assistance and expertise to economic development and environmental protection.